Exciton Fission and Fusion

Andrew B. Pun

Submitted in partial fulfillment of the
requirements for the degree of Doctor of Philosophy
in the Graduate School of Arts and Sciences

COLUMBIA UNIVERSITY

2019

Abstract

Exciton Fission and Fusion

Andrew B. Pun

One of the most important features of modern semiconductor technology is the exciton, the bound electron-hole pair that drives everything from photovoltaics to light emitting diodes to transistors. This dissertation explores how we can develop materials that are able to control the energetics of excitons, by splitting them and combining them. Also explored are the applications allowed by the control of exciton energetics.

The topics covered in this thesis are singlet exciton fission, and triplet fusion upconversion. Chapter 1 will introduce these concepts, and provide an overview of these fields.

Chapter 2 discusses the singlet fission properties of a fully conjugated tetracene polymer and its derivatives. This chapter includes the synthesis of these materials, their photophysical properties, as well as their incorporation into bilayer semiconducting devices and their properties under an applied magnetic field.

Chapter 3 explores the study of an organic-inorganic hybrid singlet fission triplet acceptor complex. A singlet fission capable pentacene dimer was covalently linked to an iron-oxo cluster with an electron affinity appropriate to accept triplets generated from singlet fission. This chapter explores the synthesis and photophysical properties of this hybrid complex, as well as the nature of the triplet pair state generated from intramolecular singlet fission.

In Chapter 4, a new design rule for intramolecular singlet fission is studied, the energy sink. A series of pentacene dimers spaced by tetracene bridges are synthesized, and their singlet fission properties are explored via transient absorption spectroscopy and time resolved electron spin resonance spectroscopy.

Chapter 5 begins the portion of the thesis focused on triplet fusion upconversion. The lessons learned from previous work in intramolecular singlet fission are applied to synthesize more efficient annihilators for upconversion. A series of tetracene dimers are synthesized, and their upconversion properties are explored. The work demonstrates intramolecular triplet fusion as a method to enhance the performance of existing annihilators.

Chapter 6 details the discovery that diketopyrrolopyrroles can be used as upconversion annihilators. The advantages of these materials relative to existing annihilators are explained. Energetic design rules for upconversion annihilators are also discussed.

Finally, in Chapter 7 a new application of triplet fusion upconversion is explored: infrared light sensitized photoredox catalysis.

Table of Contents

List of Figures

List of Tables

Acknowledgements

I wouldn't be where I am today if it weren't for the love and support of countless people over the years. I can't say enough good things about all the people who have done so much to help me become the person I am, but this is a start.

First off I want to thank Yi. His deciding to take me into his group and personally mentor me absolutely changed my life. He taught me how to be a scientist, and I'll always look up to him for his brilliance, kindness, and poise. Those early days at the Molecular Foundry set me on this path towards a PhD, I learned so much from being around all those scientists, and made a lot of great friends. There are too many people to thank by name, but I have to single out Liana and Teresa for teaching me so much.

I want to thank Luis for taking me on as a grad student in his lab. He displayed a lot of faith in me, even when I just joined the lab, and the freedom he's given me has really allowed me to stay engaged in science, exploring all sorts of ideas. He has also put together an incredible group of people around him. Elango was an incredible scientific resource, but also a mentor for all the non-science related things I had to deal with in grad school, not to mention a great friend. Working together with him and Sam we did a lot of great science, and had a ton of fun along the way. Along with those two, I couldn't ask for a better group of people to spend my days with than Helen, Jess, JLow, Spencer, Anastasia, Sebastian, Lauren, Rachel, Kaia and Emily. I'm happy to call all of you my friends.

I can't imagine making it through the 5 years of grad school with some other great friends. Thanks to Makeda for always putting up with me, and thanks to Trevor and Mike for all those great lunches. Thanks too to some of my closest and oldest friends, Anirudh and Sophia, for your support through the years. And a special thanks to Evan, grad school would have been a

lot more boring without you, not to mention I'd be a lot hungrier. It's been fun going from working in Yi's lab together to becoming roommates and now doctors, you're like a second brother.

Dan I can't thank enough, I've learned so much from you. You took the time to patiently teach this chemist some of the mysteries of upconversion and engineering. But I think all the other lessons you taught me were even more important. Your wisdom and the way you carry yourself are something to be admired, it's still weird to think you're only a couple years older than me. I can't wait to see you become famous and I can tell everyone how I was the first person to ever work for you.

I also want to thank all the other great scientific mentors I've had over the years. Thanks to Bruno and the rest of the Ehrler lab, you were amazing hosts, and I had a great time working at AMOLF and living in Amsterdam. Thanks to Tom, first for the great collaboration, but even more so for all the advice you've passed on, I only wish you were at Columbia earlier so we could have worked together longer. Thanks to Matt Sfeir for all the help with transient absorption over the years. Thanks to Xav, it's been great working with you and getting to know you over the years. Thanks for taking care of so many of my friends too. I also want to thank Colin Nuckolls for serving on my second year and fourth year committees, and Mike Steigerwald for serving on my thesis defense committees.

Last and most importantly I want to thank my family, I could fill a hundred books with words to thank you all for the millions of things you've done for me, but I'll try to keep it short. Nobody has made me angrier in my life than my brother Anthony, but I'm not sure even you know how big of a positive impact you've had on my life. Growing up with you as an older brother was awful, because you were so unbearably good at everything you did. Every day of my

life you pushed me to be better, and I wouldn't be half the person I am today if it weren't for you.

I've been asked a lot about who my heroes are, in life, in science or some combination. I don't know what people expect me to say, but it's an easy answer for me: my parents. In a little over a generation my family has gone from farmers in the farthest corners of rural Peru all the way to where I am now. It wouldn't have happened if it weren't for the brilliance, bravery, and grit my parents showed every day of their lives. They separately moved all the way to America, when they barely spoke the language, and made better lives for themselves and their children. They sacrificed everything for me and Anthony, and taught us how to be exceptional like them. Life could have been tough for two foreign kids growing up in Folsom back then, but that pride in ourselves and where we came from turned me into what I am. I can never thank you enough. Mom and Dad te amo mas que hay estrellas en el cielo (you know the rest).

For my family: Anthony, Mom, Dad,
and everyone that came before

Chapter 1: Singlet Fission and Triplet Fusion Upconversion

1.1 Preface

Section 1.2 of this chapter has been partially adapted from the manuscript entitled "Understanding the Bound Triplet Pair State in Singlet Fission" by Samuel N. Sanders, Andrew B. Pun, Kaia R. Parenti, Elango Kumarasamy, Lauren M. Yablon, Matthew Y. Sfeir, and Luis M. Campos which has been accepted for publication in Chem. Equal contributions to this manuscript were made by Samuel N. Sanders and myself.

1.2 Singlet Fission

Singlet Fission (SF) is a photophysical process in which a lone singlet exciton decays into two triplet excitons.[1,2] A schematic of this process can be seen below in Figure 1.1. Recently, there has been a surge of interest in this photophysical process – a form of multiple exciton generation (MEG) – because of its potential in optolelectronics.[3] For example, SF and other MEG strategies can be used to harness energy that is typically lost to thermalization in a photovoltaic (PV) device.[4–6] Thus, by taking advantage of MEG, the overall incident photon-to-current efficiency of a SF sensitized PV cell could be increased by up to ~10 % absolute.[7–9] As the study of SF continues to mature, one of the areas of great interest is the mechanism of triplet generation. However, SF is not as simple as a transition from the S_1 state to two free triplet states, $2xT_1$, and requires a multiexciton or coupled triplet pair intermediate state to permit the conservation of spin angular momentum.

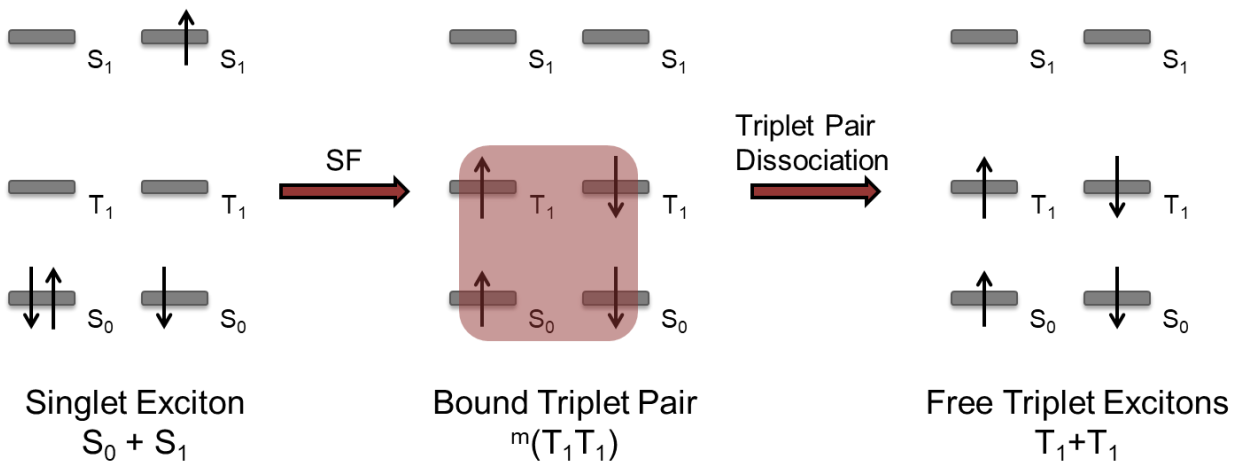

Figure 1.1 Singlet Fission the process by which one singlet exciton becomes two triplet excitons via an intermediate bound triplet pair state.

Traditionally, most singlet fission has been observed as an intermolecular process (xSF) within crystals or solid films containing an ensemble of molecules.[10–16] However, it has recently been shown by our group and others that by covalently linking singlet fission chromophores together, it is possible to observe intramolecular singlet fission (iSF).[17–21] Examples of common xSF chromophores are shown in Figure 1.2A, with example iSF materials shown in Figure 1.2B. Because iSF is a property of each individual molecule, the rate of SF and lifetime of triplets generated is not affected by solid state packing for iSF molecules as it is in compounds that undergo xSF.[10] SF materials need to be combined with existing high performance photovoltaics in order to surpass the existing thermodynamic limit on singlet junction photovoltaics. Rather than having to use expensive crystal deposition techniques, iSF materials are amenable to high throughput solution casting methods such as spin coating.

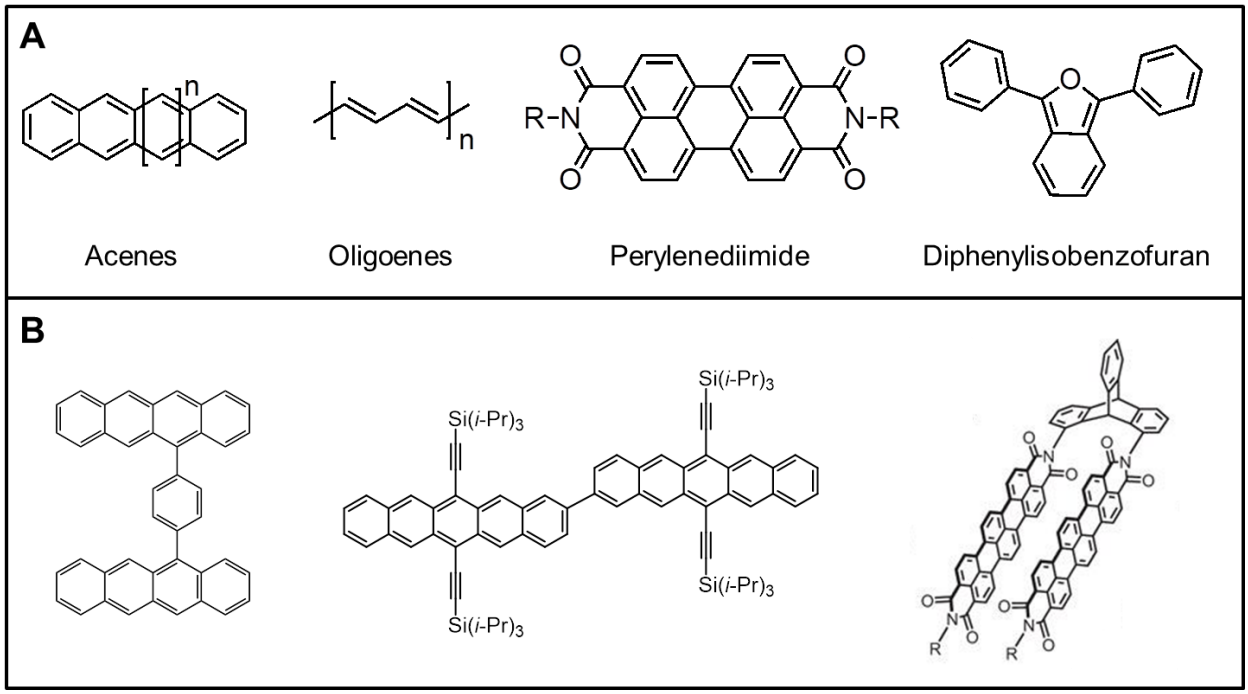

Figure 1.2 Intermolecular and Intramolecular Singlet Fission Compounds A) Example of xSF capable chromophores.[2] B) Examples of iSF capable molecules.[17,21,22]

While iSF materials have these advantages over xSF materials, challenges remain to their incorporation into optoelectronic devices. Most notably, because the two chromophores that undergo SF are linked, the two triplets that are generated from iSF are bound. This bound triplet pair state behaves differently from the free triplets that are typically generated rapidly from xSF. Because the triplet pair state is an overall spin singlet initially, it can rapidly decay to the ground state. This is seen in the very short lifetime of the triplets generated in closely linked acene dimers.[17,23,24] In order for iSF to become competitive with existing xSF materials, this challenge needs to be overcome. Research in the Campos group seeks to solve this problem. By synthesizing new compounds that are capable of undergoing iSF, we can develop design rules for new generations of iSF materials. This effort is directed towards the goal of iSF materials that can undergo sub-ps SF generating a quantitative (200%) yield of free triplets which can readily be extracted at a device interface. In Chapters 2-4 below, I will discuss efforts to optimize iSF

materials towards the goal of synthesizing iSF materials which can be used in high performance optoelectronic devices.

1.3 Triplet Fusion Upconversion

Optical upconversion is the process by which low energy photons are converted into higher energy ones. There are a wide variety of potential applications for upconversion, including biological imaging,[25] chemical sensing,[26] and data storage.[27]

Much work has been done in the field of upconversion involving lanthanide doped nanoparticles, where individual nanoparticles undergo multiple excitations in order to generate one high energy photon.[28,29] While great strides have been made in this field of upconversion, there are a variety of factors that make lanthanide upconversion unsuited for technological applications. The two primary reasons are the scarcity of the materials that are involved, and the very high incident excitations that are required to promote the disallowed transitions necessary for upconversion in lanthanides.[30]

Upconversion can also proceed via a two photon-absorption (TPA) mechanism.[31] In the TPA mechanism, upon high excitation of sub-bandgap photons, a molecule can absorb two photons, allowing the population of its first excited state singlet (S_1). TPA is interesting in the simplicity of the system, but requires a very high incident flux, which limits its use.

Triplet-fusion (TF), also known as triplet-triplet annihilation, stands out as an exciting form of upconversion.[32] It can readily occur at low incident flux, even appearing visible to the human eye when excited with a green laser pointer,[33] and has been demonstrated as a viable mechanism to upconvert incident light across the visible spectrum, as well as near UV and IR radiation.[34–41] TF upconversion also has the added benefit of having a linear dependence on

incident light flux, at least beyond a certain turnover point that is unique to each upconversion system.[42]

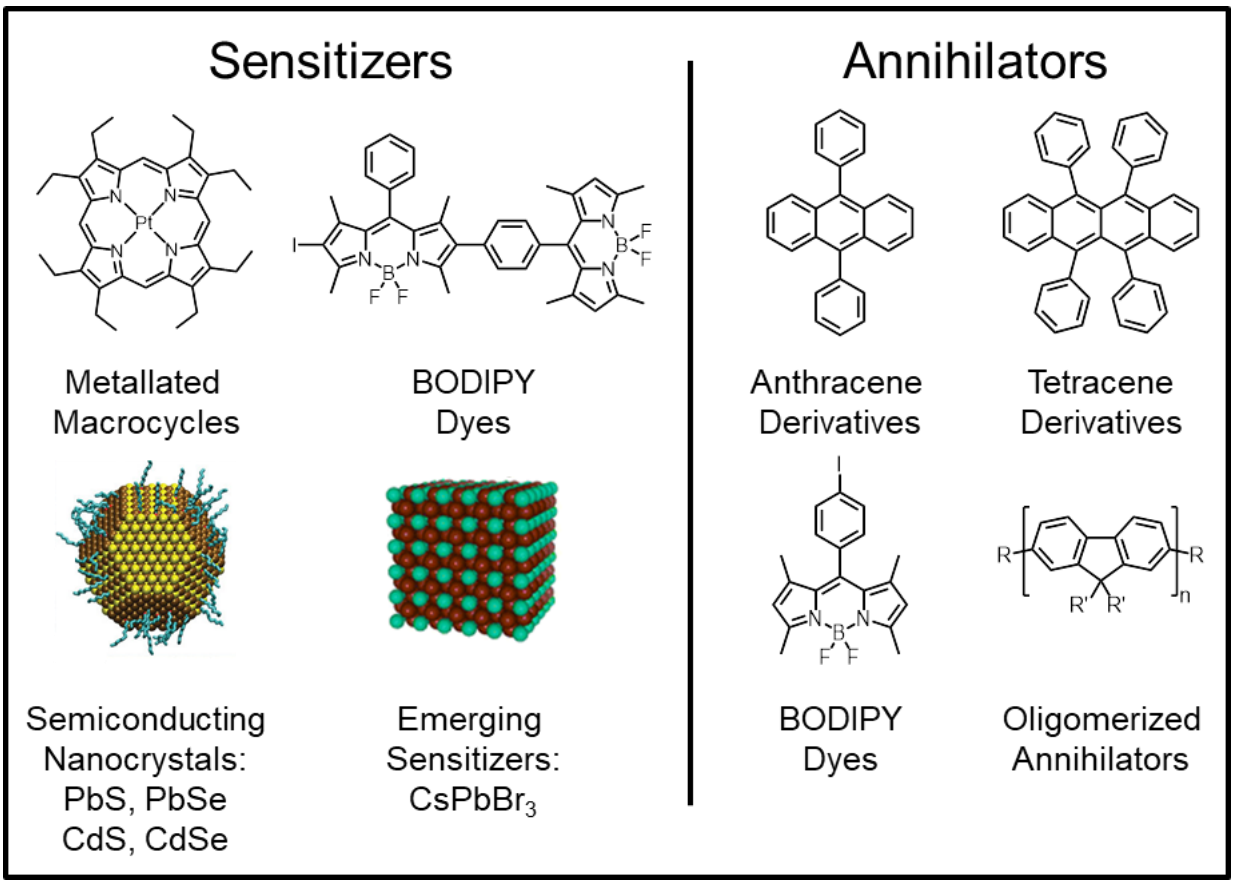

Figure 1.3 TF Upconversion Sensitizers and Annihilators examples of commonly used compounds for TF upconversion.

TF upconversion requires two components, a sensitizer and an annihilator; common examples of these species can be seen in Figure 1.3. The sensitizer absorbs long wavelength light to form a singlet exciton which can transfer to a triplet state on an annihilator due to strong spin-orbit coupling of the sensitizer. Two annihilators which have been sensitized can then meet, and undergo a Dexter energy transfer process, where two triplet excitons combine to form one higher energy singlet exciton. This singlet exciton then rapidly decays via fluorescence, emitting a lower wavelength photon than what was absorbed by the sensitizer. A schematic of this process can be seen in Figure 1.4.

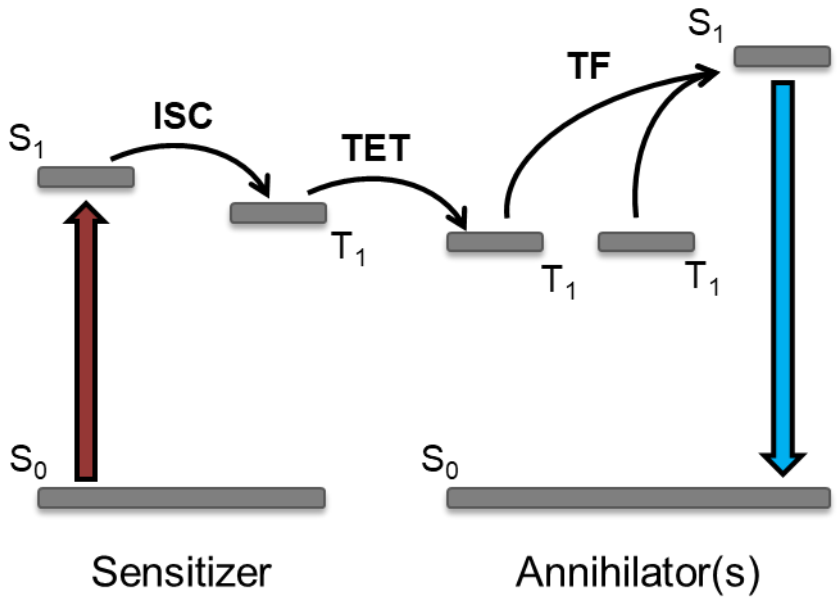

Figure 1.4 Triplet Fusion Upconversion the process by which two low energy photons are converted into one higher energy photon. Upon absorption of low energy light, the sensitizer is promoted from its ground state singlet (S_0) to its first excited state singlet (S_1). The sensitizer then rapidly undergoes rapid intersystem crossing (ISC) to populate its first excited state triplet (T_1). The sensitizer then undergoes triplet energy transfer (TET) upon collision with an annihilator. Two annihilators in the T_1 state can then undergo triplet fusion (TF) to populate an annihilator S_1 state, which decays to the S_0 state via fluorescence, emitting a higher energy photon.

In order to enhance the efficiency of TF upconversion, we can begin by the energetics of the sensitizer and the annihilator. The first excited state triplet energy of the sensitizer (^{3}[Sen]*) must be higher than the first excited state triplet energy of the annihilator (^{3}[An]*). This ensures that the triplet energy transfer from sensitizer to annihilator is exothermic and therefore a favorable process. Finally, the first excited state singlet energy of the annihilator must be less than double the energy of the first excited state triplet energy of the annihilator. This is to ensure that the fusion of two annihilator T_1 states (^{3}[An]*) results in enough energy to populate the annihilator S_1 state (^{1}[An]*). It is desirable that the difference between ^{1}[Sen]* and ^{3}[Sen]* as well as between ^{3}[Sen]* and ^{3}[An]* be very small. Also, ^{1}[An]* should only be slightly less than double ^{3}[An]*. These additional criteria minimize thermalization losses and ensure the largest

anti-Stokes shift possible from the upconversion process. A summary of these energetic requirements as well as desirable energetic properties is summarized below in Figure 1.5.

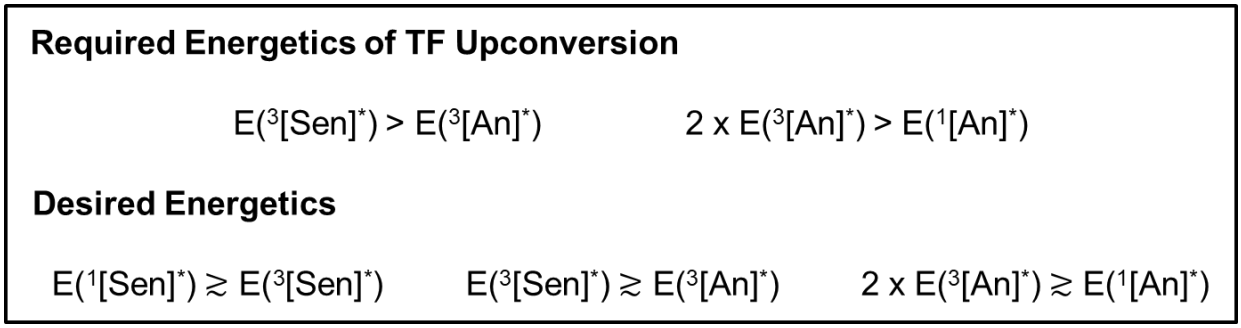

Figure 1.5 Required and Desired Energetics of TF Upconversion Sensitizer (Sen) and annihilator (An) excited states denoted with super script *, with spin state in superscript.

While TF upconversion continues to receive increased attention, several obstacles remain to be overcome before the widespread proliferation of TF upconversion across a variety of applications. On a fundamental level, further advances to TF sensitizers and annihilators are necessary, including the development of new materials as well as the optimization of existing materials. Before TF upconversion can be widely used, it needs to be highly efficient, with robust, chemically tolerant sensitizer and annihilator components. In Chapter 5-7 below, I will discuss efforts towards this, as well as expanding the applications of TF upconversion.

1.4 References

(1) Singh, S.; Jones, W. J.; Siebrand, W.; Stoicheff, B. P.; Schneider, W. G. Laser Generation of Excitons and Fluorescence in Anthracene Crystals. *J. Chem. Phys.* **1965**, *42* (1), 330.

(2) Smith, M. B.; Michl, J. Singlet Fission. *Chem. Rev.* **2010**, *110* (11), 6891.

(3) Semonin, O. E.; Luther, J. M.; Choi, S.; Chen, H.-Y.; Gao, J.; Nozik, A. J.; Beard, M. C. Peak External Photocurrent Quantum Efficiency Exceeding 100% via MEG in a Quantum Dot Solar Cell. *Science* **2011**, *334* (6062), 1530.

(4) Green, M. A. Third Generation Photovoltaics: Ultra-High Conversion Efficiency at Low Cost. *Prog. Photovolt. Res. Appl.* **2001**, *9* (2), 123.

(5) Paci, I.; Johnson, J. C.; Chen, X.; Rana, G.; Popović, D.; David, D. E.; Nozik, A. J.; Ratner, M. A.; Michl, J. Singlet Fission for Dye-Sensitized Solar Cells: Can a Suitable Sensitizer Be Found? *J. Am. Chem. Soc.* **2006**, *128* (51), 16546.

(6) Greyson, E. C.; Stepp, B. R.; Chen, X.; Schwerin, A. F.; Paci, I.; Smith, M. B.; Akdag, A.; Johnson, J. C.; Nozik, A. J.; Michl, J.; et al. Singlet Exciton Fission for Solar Cell

Applications: Energy Aspects of Interchromophore Coupling. *J. Phys. Chem. B* **2010**, *114* (45), 14223.
(7) Hanna, M. C.; Nozik, A. J. Solar Conversion Efficiency of Photovoltaic and Photoelectrolysis Cells with Carrier Multiplication Absorbers. *J. Appl. Phys.* **2006**, *100* (7).
(8) Congreve, D. N.; Lee, J.; Thompson, N. J.; Hontz, E.; Yost, S. R.; Reusswig, P. D.; Bahlke, M. E.; Reineke, S.; Van Voorhis, T.; Baldo, M. A. External Quantum Efficiency Above 100% in a Singlet-Exciton-Fission-Based Organic Photovoltaic Cell. *Science* **2013**, *340* (6130), 334.
(9) Lee, J.; Jadhav, P.; Reusswig, P. D.; Yost, S. R.; Thompson, N. J.; Congreve, D. N.; Hontz, E.; Van Voorhis, T.; Baldo, M. A. Singlet Exciton Fission Photovoltaics. *Acc. Chem. Res.* **2013**, *46* (6), 1300.
(10) Yost, S. R.; Lee, J.; Wilson, M. W. B.; Wu, T.; McMahon, D. P.; Parkhurst, R. R.; Thompson, N. J.; Congreve, D. N.; Rao, A.; Johnson, K.; et al. A Transferable Model for Singlet-Fission Kinetics. *Nat. Chem.* **2014**, *6* (6), 492.
(11) Chan, W.-L.; Ligges, M.; Jailaubekov, A.; Kaake, L.; Miaja-Avila, L.; Zhu, X.-Y. Observing the Multiexciton State in Singlet Fission and Ensuing Ultrafast Multielectron Transfer. *Science* **2011**, *334* (6062), 1541.
(12) Monahan, N. R.; Sun, D.; Tamura, H.; Williams, K. W.; Xu, B.; Zhong, Y.; Kumar, B.; Nuckolls, C.; Harutyunyan, A. R.; Chen, G.; et al. Dynamics of the Triplet-Pair State Reveals the Likely Coexistence of Coherent and Incoherent Singlet Fission in Crystalline Hexacene. *Nat. Chem.* **2016**, *9*, 341.
(13) Busby, E.; Berkelbach, T. C.; Kumar, B.; Chernikov, A.; Zhong, Y.; Hlaing, H.; Zhu, X.-Y.; Heinz, T. F.; Hybertsen, M. S.; Sfeir, M. Y.; et al. Multiphonon Relaxation Slows Singlet Fission in Crystalline Hexacene. *J. Am. Chem. Soc.* **2014**, *136* (30), 10654.
(14) Berkelbach, T. C.; Hybertsen, M. S.; Reichman, D. R. Microscopic Theory of Singlet Exciton Fission. III. Crystalline Pentacene. *J. Chem. Phys.* **2014**, *141* (7), 74705.
(15) Tempelaar, R.; Reichman, D. R. Vibronic Exciton Theory of Singlet Fission. III. How Vibronic Coupling and Thermodynamics Promote Rapid Triplet Generation in Pentacene Crystals. *J. Chem. Phys.* **2018**, *148* (24), 244701.
(16) Zeng, T.; Hoffmann, R.; Ananth, N. The Low-Lying Electronic States of Pentacene and Their Roles in Singlet Fission. *J. Am. Chem. Soc.* **2014**, *136* (15), 5755.
(17) Sanders, S. N.; Kumarasamy, E.; Pun, A. B.; Trinh, M. T.; Choi, B.; Xia, J.; Taffet, E. J.; Low, J. Z.; Miller, J. R.; Roy, X.; et al. Quantitative Intramolecular Singlet Fission in Bipentacenes. *J. Am. Chem. Soc.* **2015**, *137* (28), 8965.
(18) Zirzlmeier, J.; Lehnherr, D.; Coto, P. B.; Chernick, E. T.; Casillas, R.; Basel, B. S.; Thoss, M.; Tykwinski, R. R.; Guldi, D. M. Singlet Fission in Pentacene Dimers. *Proc. Natl. Acad. Sci.* **2015**, *112* (17), 5325.
(19) Lukman, S.; Musser, A. J.; Chen, K.; Athanasopoulos, S.; Yong, C. K.; Zeng, Z.; Ye, Q.; Chi, C.; Hodgkiss, J. M.; Wu, J.; et al. Tuneable Singlet Exciton Fission and Triplet–Triplet Annihilation in an Orthogonal Pentacene Dimer. *Adv. Funct. Mater.* **2015**, *25* (34), 5452.
(20) Korovina, N. V; Das, S.; Nett, Z.; Feng, X.; Joy, J.; Haiges, R.; Krylov, A. I.; Bradforth, S. E.; Thompson, M. E. Singlet Fission in a Covalently Linked Cofacial Alkynyltetracene Dimer. *J. Am. Chem. Soc.* **2016**, *138* (2), 617.
(21) Müller, A. M.; Avlasevich, Y. S.; Müllen, K.; Bardeen, C. J. Evidence for Exciton Fission

and Fusion in a Covalently Linked Tetracene Dimer. *Chem. Phys. Lett.* **2006**, *421* (4), 518.
(22) Margulies, E. A.; Miller, C. E.; Wu, Y.; Ma, L.; Schatz, G. C.; Young, R. M.; Wasielewski, M. R. Enabling Singlet Fission by Controlling Intramolecular Charge Transfer in π-Stacked Covalent Terrylenediimide Dimers. *Nat. Chem.* **2016**, *8* (12), 1120.
(23) Sanders, S. N.; Kumarasamy, E.; Pun, A. B.; Steigerwald, M. L.; Sfeir, M. Y.; Campos, L. M. Intramolecular Singlet Fission in Oligoacene Heterodimers. *Angew. Chem. Int. Ed.* **2016**, *55* (10), 3373.
(24) Fuemmeler, E. G.; Sanders, S. N.; Pun, A. B.; Kumarasamy, E.; Zeng, T.; Miyata, K.; Steigerwald, M. L.; Zhu, X.-Y.; Sfeir, M. Y.; Campos, L. M.; et al. A Direct Mechanism of Ultrafast Intramolecular Singlet Fission in Pentacene Dimers. *ACS Cent. Sci.* **2016**, *2* (5), 316.
(25) Park, Y. Il; Lee, K. T.; Suh, Y. D.; Hyeon, T. Upconverting Nanoparticles: A Versatile Platform for Wide-Field Two-Photon Microscopy and Multi-Modal in Vivo Imaging. *Chem. Soc. Rev.* **2015**, *44* (6), 1302.
(26) Borisov, S. M.; Larndorfer, C.; Klimant, I. Triplet–Triplet Annihilation-Based Anti-Stokes Oxygen Sensing Materials with a Very Broad Dynamic Range. *Adv. Funct. Mater.* **2012**, *22* (20), 4360.
(27) Zhou, Y.; Han, S.-T.; Chen, X.; Wang, F.; Tang, Y.-B.; Roy, V. A. L. An Upconverted Photonic Nonvolatile Memory. *Nat. Commun.* **2014**, *5*, 4720.
(28) Wang, F.; Liu, X. Recent Advances in the Chemistry of Lanthanide-Doped Upconversion Nanocrystals. *Chem. Soc. Rev.* **2009**, *38*, 976.
(29) Boyer, J.-C.; Vetrone, F.; Cuccia, L. A.; Capobianco, J. A. Synthesis of Colloidal Upconverting NaYF4 Nanocrystals Doped with Er3+, Yb3+ and Tm3+, Yb3+ via Thermal Decomposition of Lanthanide Trifluoroacetate Precursors. *J. Am. Chem. Soc.* **2006**, *128* (23), 7444.
(30) Chen, G.; Qiu, H.; Prasad, P. N.; Chen, X. Upconversion Nanoparticles: Design, Nanochemistry, and Applications in Theranostics. *Chem. Rev.* **2014**, *114* (10), 5161.
(31) Ye, C.; Zhou, L.; Wang, X.; Liang, Z. Photon Upconversion: From Two-Photon Absorption (TPA) to Triplet–Triplet Annihilation (TTA). *Phys. Chem. Chem. Phys.* **2016**, *18* (16), 10818.
(32) Singh-Rachford, T. N.; Castellano, F. N. Photon Upconversion Based on Sensitized Triplet–Triplet Annihilation. *Coord. Chem. Rev.* **2010**, *254* (21–22), 2560.
(33) Islangulov, R. R.; Kozlov, D. V; Castellano, F. N. Low Power Upconversion Using MLCT Sensitizers. *Chem. Commun.* **2005**, No. 30, 3776.
(34) Singh-Rachford, T. N.; Castellano, F. N. Triplet Sensitized Red-to-Blue Photon Upconversion. *J. Phys. Chem. Lett.* **2010**, *1* (1), 195.
(35) McCusker, C. E.; Castellano, F. N. Efficient Visible to Near-UV Photochemical Upconversion Sensitized by a Long Lifetime Cu(I) MLCT Complex. *Inorg. Chem.* **2015**, *54* (12), 6035.
(36) Gray, V.; Xia, P.; Huang, Z.; Moses, E.; Fast, A.; Fishman, D. A.; Vullev, V. I.; Abrahamsson, M.; Moth-Poulsen, K.; Lee Tang, M. CdS/ZnS Core-Shell Nanocrystal Photosensitizers for Visible to UV Upconversion. *Chem. Sci.* **2017**, *8* (8), 5488.
(37) Sasaki, Y.; Amemori, S.; Kouno, H.; Yanai, N.; Kimizuka, N. Near Infrared-to-Blue Photon Upconversion by Exploiting Direct S-T Absorption of a Molecular Sensitizer. *J. Mater. Chem. C* **2017**, *5* (21), 5063.

(38) Amemori, S.; Yanai, N.; Kimizuka, N. Metallonaphthalocyanines as Triplet Sensitizers for Near-Infrared Photon Upconversion beyond 850 Nm. *Phys. Chem. Chem. Phys.* **2015**, *17* (35), 22557.
(39) Moor, K.; Kim, J.-H.; Snow, S.; Kim, J.-H. [C70] Fullerene-Sensitized Triplet-Triplet Annihilation Upconversion. *Chem. Commun.* **2013**, *49* (92), 10829.
(40) Di, D.; Yang, L.; Richter, J. M.; Meraldi, L.; Altamimi, R. M.; Alyamani, A. Y.; Credgington, D.; Musselman, K. P.; MacManus-Driscoll, J. L.; Friend, R. H. Efficient Triplet Exciton Fusion in Molecularly Doped Polymer Light-Emitting Diodes. *Adv. Mater.* **2017**, *29* (13), 1605987.
(41) Singh-Rachford, T. N.; Castellano, F. N. Pd(II) Phthalocyanine-Sensitized Triplet−Triplet Annihilation from Rubrene. *J. Phys. Chem. A* **2008**, *112* (16), 3550.
(42) Haefele, A.; Blumhoff, J.; Khnayzer, R. S.; Castellano, F. N. Getting to the (Square) Root of the Problem: How to Make Noncoherent Pumped Upconversion Linear. *J. Phys. Chem. Lett.* **2012**, *3* (3), 299.

Chapter 2: Singlet Fission in Polytetracene

2.1 Preface

This chapter is based on manuscript entitled "Triplet Harvesting from Intramolecular Singlet Fission in Polytetracene" by Andrew B. Pun, Samuel N. Sanders, Elango Kumarasamy, Matthew Y. Sfeir, Daniel N. Congreve, and Luis M. Campos published in Advanced Materials.[1]

I synthesized and characterized all the materials studied. I fabricated and tested the bilayer devices and took EQE measurements with Daniel N. Congreve. Samuel N. Sanders and Matthew Y. Sfeir carried out transient absorption measurements and analysis. Daniel Congreve measured magnetic field dependence of photocurrent.

2.2 Introduction

Since the observation of ultrafast electron transfer between a conjugated polymer and C_{60},[2,3] we have witnessed 25 years of development in second-generation photovoltaic (PV) devices, reaching efficiencies above 10%.[4–6] Moreover, the efficiency of single-junction PVs incorporating CdTe, copper indium gallium selenide, crystalline Si, and hybrid perovskites have all exceeded 20% in recent years.[7] But even as processing and fabrication techniques continue to improve, the efficiency of first and second-generation devices will never exceed the Shockley–Queisser limit of 33%.[8] In order to push device efficiencies further, third-generation photovoltaics offer an attractive alternative through nonconventional mechanisms of photocurrent generation, including tandem devices, hot carrier extraction, and multiple exciton generation (MEG).[9,10] Singlet fission (SF), the process by which an excited singlet exciton generates two triplet excitons in molecular materials, is one such MEG process.[11] It has been calculated that the maximum power conversion efficiency of a single-junction photovoltaic

device incorporating a SF layer is 44.4%.[10] This SF process has been observed in intermolecularly coupled singlet fission chromophores (xSF),[12–15] and intramolecularly in individual molecules and polymers (intramolecular singlet fission, iSF).[16–21]

Practical singlet fission devices are still in their infancy due to the need for new SF chromophores and schemes capable of efficiently dissociating and extracting SF-generated triplet pairs. In fact, the few devices that have extracted more than one exciton per incident photon have all relied on xSF.[22–31] In such devices,[32] solid-state packing interactions of the SF chromophore are crucial to generate triplet pairs, and any perturbations can have a drastic effect on both the rate and yield of xSF.[12,33] As a result, the active layer must be carefully deposited, hampering high-throughput processing and limiting the types of device architectures to bilayers. iSF materials can overcome these technical challenges because their SF process is an intrinsic property of each molecule. iSF chromophores allow for conventional solution-processing techniques, as highly oriented crystalline domains are not a prerequisite for singlet fission. Additionally, iSF materials also have the potential to be used in bulk heterojunctions[3] and nanostructured active layers,[34] among other high-performance device architectures. However, it should be noted that iSF materials tend to produce primarily spin-coupled triplet pairs[35,36] with shorter lifetimes than free triplets due to geminal recombination. These properties have so far been a major roadblock to the application of iSF materials in devices. These highly coupled triplet pairs with short lifetimes are localized and bound upon generation,[37] posing a barrier to efficient extraction of multiple charge carriers per incident photon—the signature of singlet fission photovoltaic (SF-PV) devices. Should these drawbacks to iSF be addressed, it is clear that iSF is a desirable process to increase power conversion efficiency in 3rd generation PVs.

To this end, we sought to synthesize a solution-processable iSF material that would undergo ultrafast iSF to generate high-energy triplets. Although pentacene has been the prototypical SF chromophore because the SF process is exoergic, with $E(S_1) > 2E(T_1)$,[23,38–40] the triplet energy is not well matched for use as a sensitizer in an idealized tandem solar cell.[10] In addition to limiting the achievable maximum V_{oc} to a level below the ideal 0.95 V level,[23,26,41] the triplet energy is also well below the bandgap of the most widely used conventional solar cell materials, including Si (Figure 2.1A), GaAs, and CdTe. While unsubstituted tetracene has a higher T_1 energy (≈1.2 eV, Figure 2.1A) that is better matched to conventional solar cells, xSF is slightly endoergic, which results in a rate of SF that is nearly three orders of magnitude slower in tetracene than in pentacene.[42–46] This slow rate of SF causes parasitic processes such as singlet exciton dissociation and fluorescence to compete with the SF process in a device.[47,48] However, it has recently been reported that functionalized tetracene derivatives can exhibit an ultrafast xSF rate constant, potentially suggesting a route to achieve high solubility, high triplet energy, and rapid singlet fission in a single material.[49]

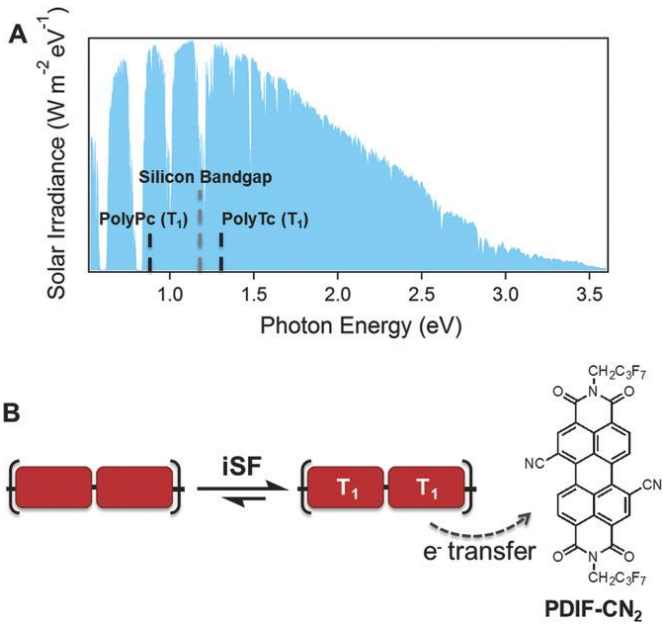

Figure 2.1 PolyTc Overview A) Approximate triplet energies of pentacene and tetracene polymers relative to the bandgap of silicon. B) Representative diagram of the generation of triplet pairs upon iSF in PolyTc, and their extraction to an acceptor.

In order to investigate various aspects of SF in tetracene-based materials, we synthesized a soluble polytetracene (PolyTc) and characterized the excited state dynamics in solution and thin-films, in addition to fabricating SF-PV devices incorporating various acceptors of different electron affinities ($PC_{70}BM$, C_{60}, and PDIF-CN2) that have been shown to harvest the triplets generated from xSF.[41,47,50] We found that PolyTc undergoes iSF in dilute solution and in the solid-state to generate high-energy triplets on the sub-picosecond timescale. Solid-state measurements show that in a thin film, the correlated triplet pairs that are initially generated from iSF evolve into a decoupled state over time. Finally, magnetic field modulation of photocurrent measurements strongly show evidence that the triplets generated by iSF can be extracted in a device. This occurs when PolyTc is interfaced with an acceptor having a suitable lowest unoccupied molecular orbital (LUMO) level (Figure 2.1B). This report showcases our ability to tune intermolecular interactions to extract the tightly-bound triplet pairs from iSF, demonstrating the utility of iSF materials in next-generation optoelectronic devices, where we will be able to combine high-performing PVs with a SF sensitizer to push the efficiency of these devices past the Shockley–Queisser limit.

2.3 Synthesis and Characterization

While pentacene dimers, oligomers, and polymers have shown remarkably high yields of triplet pairs by singlet fission, until recently, tetracene dimers have featured negligible triplet pair yields.[51] Korovina et al. cleverly designed tetracene dimers with varying levels of orbital overlap controlled by a linker moiety, which led to iSF, as inclusion of alkynyl groups on the tetracene can make SF energetically more favorable than in unsubstituted tetracene.[18] However, in this case, the tetracene–tetracene coupling was highly dependent on the spatial arrangement of

individual chromophores relative to one another in a dimer, making iterative modification challenging. In our design of PolyTc, we avoid fine-tuning through-bond and through-space overlap, focusing only on extending conjugation. This choice allows us to install two solubilizing and stabilizing triisopropylsilylacetylene groups (TIPS) per tetracene monomer, which lower the triplet energy to facilitate iSF and allow the requisite solubility for polymerization.[52]

The synthesis of PolyTc was carried out by Suzuki step-growth polymerization of bis-functionalized tetracenes, as previously reported for the synthesis of polypentacene.[53] Phenyl and biphenyl spaced alternating copolymers, Poly(Tc-*alt*-Ph) and Poly(Tc-*alt*-BiPh) respectively, were also synthesized. These polymers were synthesized in order to both slow down the dynamics of iSF and decouple the triplet pairs generated, as shown in our previous work.[21,36] This decoupling results in triplet pairs with photoinduced absorption nearly identical to that of individual triplet excitons, definitively confirming the iSF process in our tetracene polymers. Trialkylsilylacetylene substitution of the acenes is used to impart solubility and stability in air and light (Figure 2.9-2.11) and modifies the driving force for singlet fission.[49,54] This synthetic pathway yields regiorandom polymers, stemming from a mixture of regioisomers in the monomer synthesis. However, synthesis of regiopure monomers was not undertaken because previous work in our group had shown negligible differences in the rates of iSF and triplet decay between *syn* and *anti* isomers of a pentacene trimer.[37] Gel permeation chromatography reveals this polymer to consist of, on average, 7 repeat units. Both crystal structures[21] and calculations[55] on directly linked pentacene dimers show a relatively planar interacene geometry with a small barrier to rotation about the biaryl bond. We expect PolyTc to behave similarly, and for through-bond interactions between tetracenes to provide the interchromophore coupling for SF in solution, but through-space interactions in the solid state could also facilitate SF.

We determined the electronic properties of PolyTc using cyclic voltammetry measurements (Figure 2.6) and assigned the highest occupied molecular orbital (HOMO) at −5.2 eV and LUMO at −3.1 eV. Measurement of the steady-state absorption (Figure 2.2) shows that the lowest energy optical transition of solution phase PolyTc is redshifted from the Tc monomer by ≈25 nm. This design also opens an additional absorption band between 400 and 500 nm that is not present in the monomer, TIPS-Tc, and can be beneficial as it provides a wide range of light absorption in an active layer of a SF-PV. The origin of this new high-energy absorption is tied to the specific linkage of these acenes allowing orbital mixing across multiple acene units, and is being further explored by our group. The optical absorption of PolyTc thin films shows additional broadening and a tail to the red of the absorption maxima that is typically attributed to interchain interactions from aggregation in conjugated polymers (Figure 2.2). To explore this further, we studied the topology of these films with atomic force microscopy (AFM), which revealed a collection of nanocrystalline domains (Figure 2.7-8).

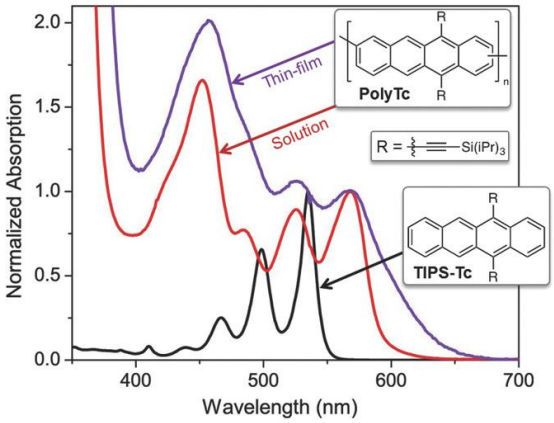

Figure 2.2 PolyTc UV/Vis Steady-state absorption profiles of TIPS-Tc dissolved in chloroform (black), PolyTc dissolved in chloroform (red) and in a thin film (purple).

Previous work has shown the free triplet energy (T_1) of TIPS-Tc to be ≈1.2 eV[49] while studies in our group have suggested that minimal changes in the triplet energy result from covalent linkage of TIPS acenes.[20,21,37] In the first approximation, $2 \times T_1 > S_1$ (2.4 eV > 2.1 eV),

which suggests endoergic SF. However, as is discussed below, our measurements, including the ultrafast rate of iSF and the presence of delayed PL,[56,57] suggest that singlet fission is roughly isoergic in these compounds. Taken together, this evidence implies either a slightly smaller triplet energy in the polymer, or the formation of a triplet pair that, because of intertriplet interactions, has a total energy that is less than twice that of a free triplet.

2.4 Solution Transient Absorption Spectroscopy

We employed transient absorption spectroscopy (TAS) to assign and characterize iSF in PolyTc. TAS has been the most common technique to establish the presence of SF in a material due to its ability to distinguish the dynamics of a material on a timescale down to tens of femtoseconds and to observe non-emissive species such as triplet excitons. Using TAS we can observe the change from an initial photoexcited singlet state to the triplet pair state generated from SF. The assignment of iSF in these materials was accomplished following our previously established criteria in a family of similar compounds, which we discuss below.[20,21,35–37,55] TAS (Figure 2.3A) and ultrafast photoluminescence (Figure 2.23) measurements on dilute PolyTc in toluene reveal that the photoexcited singlet state decays in ≈150 fs. Singlet features in the TA spectra are identified by their temporal correspondence to the decay of the prompt fluorescence signal (Figure 2.22) and are characterized by a broad photoinduced absorption between 400 and 600 nm (Figure 2.3 and 2.14). Based on the ultrafast singlet fission kinetics and lack of a parasitic decay channel, we infer that triplet pair generation is quantitative in these materials. The singlet fission dynamics in these materials are qualitatively similar to our recent report of singlet fission in polypentacene.[37]

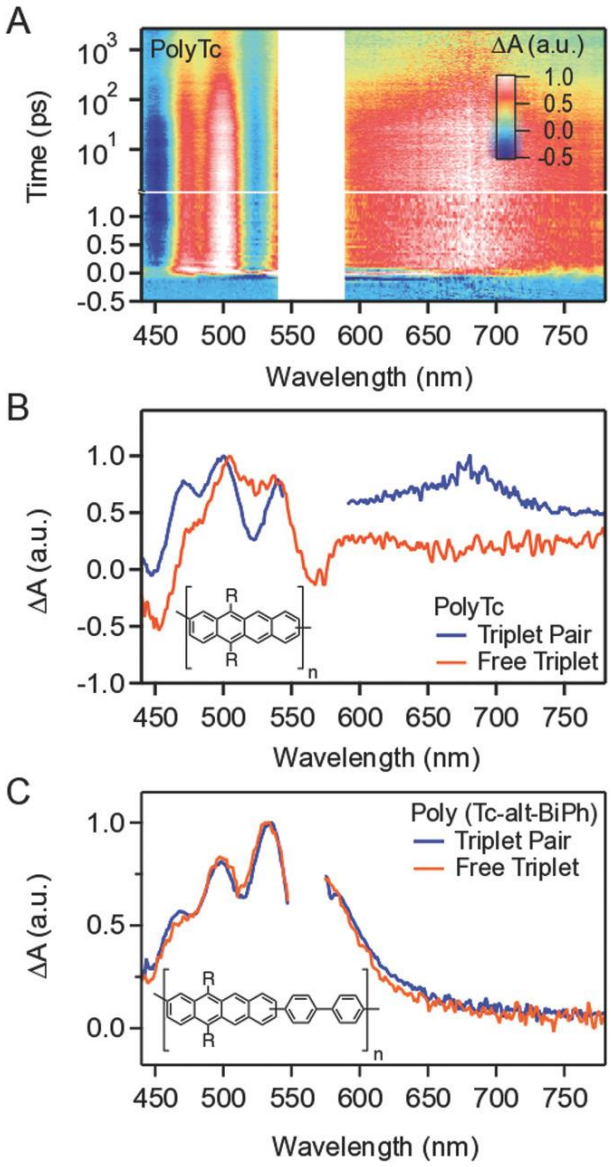

Figure 2.3 Solution PolyTc Transient Absorption Spectroscopy A) Transient absorption spectrum of PolyTc as a function of time and wavelength excited at 560 nm (~25 μJ cm^{-2}) as a dilute solution in toluene. B,C) Comparison of transient spectra of triplet pairs (blue, generated via direct excitation at 560 nm followed by singlet fission) and free triplets (orange, generated from sensitization with anthracene) for PolyTc (triplet pair at 2 ns) and individual triplet from sensitization (60 μs) (B) and Poly(Tc-*alt*-BiPh) (triplet pair at 2.2 ns) and individual triplet from sensitization (17 μs) (C).

The singlet decays to a spin-coupled triplet pair with multiplicity m, ^{m}(TT), which we identify by its characteristic transient spectra and distinct recombination dynamics. The spectral signature of triplet pairs is assigned by comparing the transient absorption spectra of triplet pairs

formed via singlet fission (photoexcitation) to triplets populated via sensitization experiments, in which an individual free triplet is populated on the molecule by collisional transfer with a triplet sensitizer. The free triplet and triplet pair transient spectra are dominated by a strong and narrow excited state absorption feature spanning 460–520 nm (Figure 3A). We observe small spectral differences between the free triplet and triplet pair (Figure 3B), most notably the appearance of an additional near-infrared absorption feature (≈675 nm) and a net blue-shift of the $T_1 \rightarrow T_n$ photoinduced absorption signal near 500 nm in the ^{m}(TT) state. We have observed similar discrepancies in other acene oligomers and polymers.[20,21,35–37,55] These differences tend to be most visible in directly linked chromophores, where intertriplet proximity is at a maximum, but become less prominent with increasing chromophore separation.[37] We have verified that adding a conjugated spacer leads to the convergence of the triplet pair and free triplet spectra in tetracene polymers. For example, the triplet pair (via iSF) and free triplet (via sensitization), are identical in an alternating copolymer of TIPS-Tc and para-biphenylene, Poly(Tc-*alt*-BiPh) (Figure 2.3C), in agreement with our previous results on other bridged acene compounds.

In addition to their spectral signatures, the recombination dynamics of the triplets indicate that they remain spin coupled. In all iSF compounds, transient absorption spectroscopy has shown that geminate, spin-correlated triplet pair recombination occurs orders of magnitude faster than decay of free triplets. Here, the triplet pair decay is multiexponential, with a dominant time constant of ≈8 ns, orders of magnitude shorter than the >40 μs free triplet lifetime in solution. An additional 150 ps fast decay is observed with an identical transient spectrum to the 8 ns component. The fast geminate decay is likely due to the partial singlet multiplicity of triplet pairs, which can couple to the ground state without necessitating a change in angular momentum.

In addition, in photoluminescence measurements, after ultrafast decay of the prompt fluorescence signal, we observe a residual long-lived delayed fluorescence signal (Figure 2.23), similar to what is observed in tetracene molecular crystals, conjugated tetracene–pentacene heterodimers, and cofacial tetracene dimers.[18,36,58,59] The delayed fluorescence results from the interconversion of the nearly degenerate singlet state and the (net singlet) spin-coupled triplet pair state and persists until the spin coupling of the triplet pair is broken or the ground state is fully repopulated. As such, it confirms that triplet pairs remain spin coupled for several nanoseconds. The dynamics of delayed fluorescence (Figure 2.23) rule out a detectable contribution from residual singlets that are unable to undergo singlet fission. We see that the long lived fluorescence decay is shorter in PolyTc and longer in Poly(Tc-*alt*-BiPh) than TIPS-Tc. This reflects the lifetime of the spin-coupled triplet pairs, which increases with increasing chromophore separation. As singlet fission is much faster than radiative recombination, this dynamical process lowers the overall fluorescence quantum yield of PolyTc in solution to ≈30% of monomeric TIPS-Tc (23% overall for PolyTc, based on the reported absolute fluorescence quantum yield of TIPS-Tc).[49] These results are consistent with recent electron spin resonance measurements that show that triplet pairs remain spin coupled for several hundred nanoseconds, even across a biphenylene bridge.[35] Together, these data point to the generation of triplet pairs at room temperature in solution, without significant dissociation into free triplets.

2.5 Thin Film Transient Absorption Spectroscopy

In contrast to dilute solution, thin films of PolyTc exhibit signatures of free triplets. Using TAS, we observe a rapid SF process in thin films of PolyTc (Figure 2.4A) with a time constant of ≈100 fs. The triplet pair spectrum is similar to what is observed in solution, with a narrow triplet excited state absorption feature between 500 and 550 nm and an additional broad NIR

absorption. Differences in the vibronic structure (e.g., changes in the relative intensity of peaks at ≈520, 500, and 470 nm) suggest interchain interactions emerge upon film formation.[60,61] These relative changes in intensity can also be seen in the linear absorption data (Figure 2.15). Analogous to what is done for the solution phase dynamics, assignment of the triplet pair state is made by comparison to solid-state triplet sensitization measurements, which we obtain by mixing a palladium phthalocyanine sensitizer into the PolyTc solution prior to spin-coating, at ≈5 wt%.[18,47,62,63] Excitation of the sensitizer at 730 nm, dispersed in the PolyTc film, followed by intersystem crossing and triplet transfer, populates free triplet excitons on PolyTc. We note that we independently measure the transient spectra of both the thin film and solution, and also compare to sensitization experiments performed on films and in solution for PolyTc. As such, we account for small differences in the transient spectra of PolyTc solution and PolyTc film in our analysis.

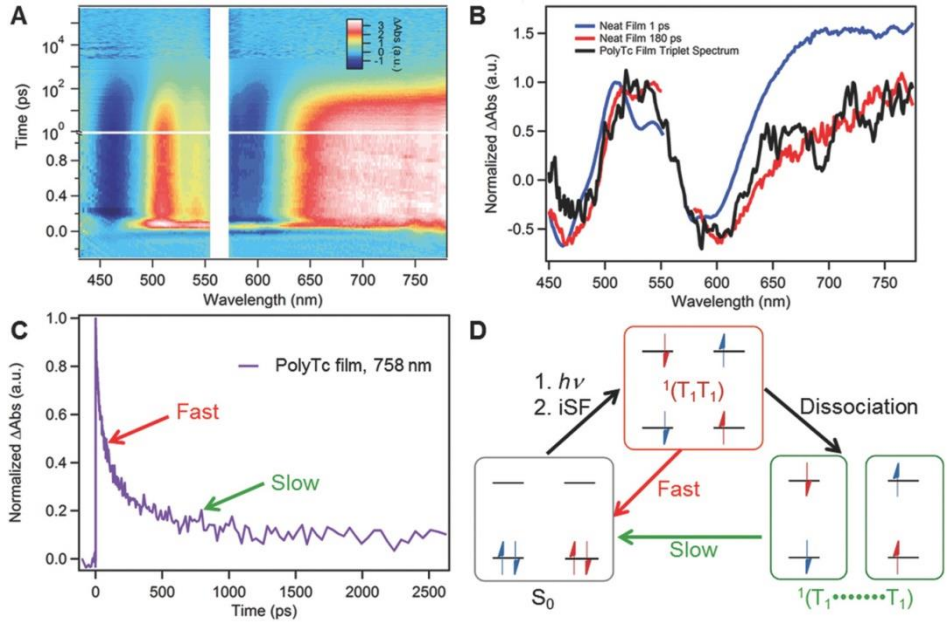

Figure 2.4 Solid State PolyTc Transient Absorption Spectroscopy A) Transient absorption spectrum of PolyTc as a function of time and wavelength excited at 560 nm deposited on a glass slide (≈150 μJ cm^{-2}). B) Spectra of triplets generated from SF at early times (blue) and late times (red) against those generated from triplet photosensitization (black). C) Lifetime of triplets generated in the solid state. D) Representative diagram of the possible decay of the triplet

pair(^{1}[TT]) generated from singlet fission to either the ground state singlet (S_0) or dissociated triplets(^{1}(T…T)).

In thin films, the transient spectrum of PolyTc evolves significantly within the first hundred picoseconds (Figure 2.4B), in stark contrast to what is observed in solution, existing as a coupled triplet pair before evolving into free triplets. This can be clearly seen by inspection of the transient absorption spectrum immediately after singlet fission (blue trace in Figure 2.4B), which contains the characteristic enhanced NIR absorption feature of triplet pairs. In contrast, the transient absorption spectrum at long delay times (red trace in Figure 2.4B) is identical to the free triplet spectrum (black trace in Figure 2.4B) obtained by solid-state sensitization. A similar spectral evolution was recently observed in aggregates of TIPS-pentacene.[64] By fitting the decay kinetics of the broad NIR absorption feature between 650 and 750 nm, we obtain a time constant of ≈140 ps for spin-coupled triplet pairs, and a free triplet lifetime of ≈60 ns. From our observation that triplet pairs are tightly bound in these materials, it may be important to investigate the design and synthesis of iSF chromophores that can efficiently generate free triplets immediately after SF, as it is known that longer charge carrier lifetimes promote extraction and lead to higher-performance devices. We note that the triplet pairs are nearly 100 times shorter lived in films than in solution, consistent with recent reports of enhanced mobility in materials where singlets and triplet pairs are able to interconvert.[56,57] These mobile triplet pairs, no longer constrained along the backbone of one polymer chain, are more readily able to sample sites that promote recombination or dissociation. Despite the shorter triplet pair lifetime, a significant free triplet population forms from the triplet pair in the solid-state, in contrast to a negligible free triplet yield in solution. From these data, which are summarized in Figure 2.4D, it is clear that interchain interactions promote free triplet formation.

2.6 Bilayer Device Characterization

To further confirm the viability of iSF materials for triplet harvesting applications, we sought to investigate the key factors that could lead to the breakup of triplet excitons into charge carriers in a working PV device. Given the lack of precedent for triplet pair extraction from iSF, we fabricated active layers composed of PolyTc and a series of acceptor molecules (see Figure 2.5A). Out of various SF device architectures, for a prototypical case exploring a new concept, we chose an active layer fabricated by making a bilayer, where one is the iSF chromophore (donor) and the other is the acceptor.[19,22,41,65,66] For optimal performance, the donor should undergo fast iSF quantitatively, and generate free, high-energy triplets with long lifetimes to allow for diffusion at the interface to be extracted by the acceptor. As with other PV devices, these devices would also benefit from materials with high electron and hole mobilities to enable diffusion of the charge carriers to the electrodes.

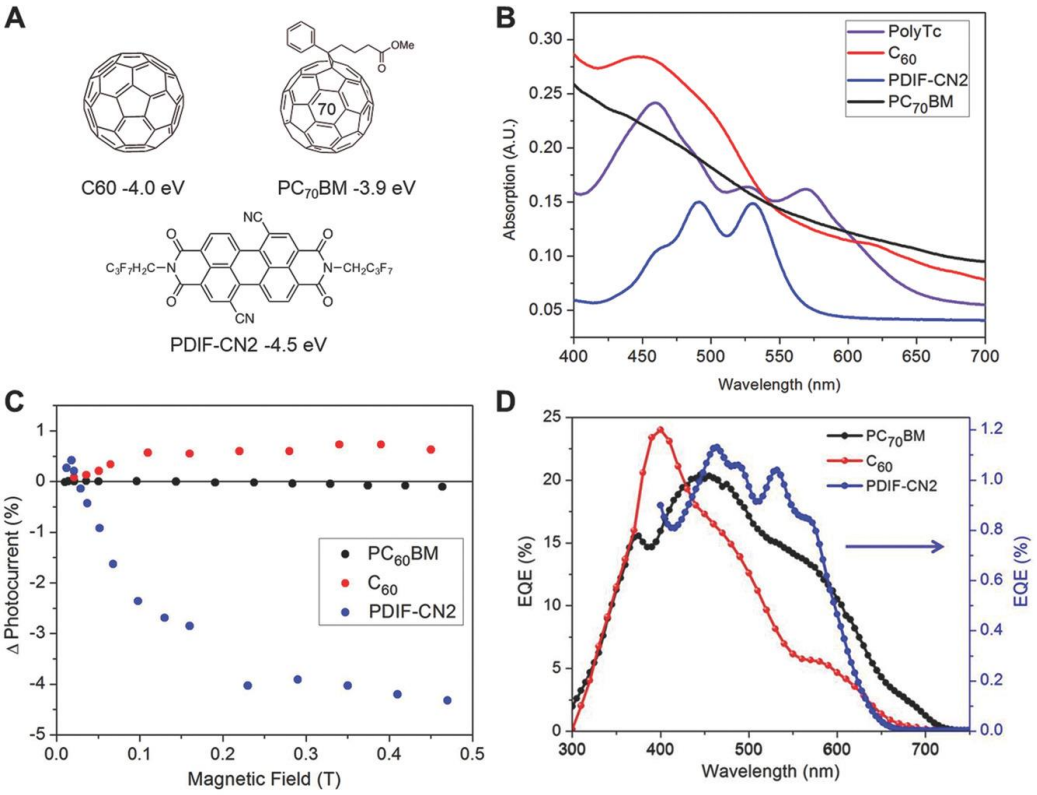

Figure 2.5 PolyTc MFE and EQE A) Structures of the acceptors used in this work, with their LUMO levels relative to vacuum. B) Steady-state absorption profiles of the individual layers of

acceptors and of PolyTc. C) Change in photocurrent with an applied magnetic field on PolyTc OPVs incorporating PC60BM (black) C60 (red) or PDIF-CN2 (blue) as the electron acceptor. Error bars for these points are 0.25% absolute ΔPhotocurrent and can be seen in Figure S20 (Supporting Information). D) EQE characteristics of PolyTc OPVs incorporating PC70BM (black) C60 (red) or PDIF-CN2 (blue) as the electron acceptor. EQE values for the PDIF-CN2 containing device have been scaled by 20 for clarity.

A device in which the harvesting of SF-generated triplets is the dominant charge transport mechanism can be distinguished from direct singlet harvesting by monitoring the change in photocurrent as a function of applied magnetic field. A PV device that harvests primarily triplets from the SF material should show an increase in photocurrent at small magnetic fields, followed by a decrease and eventual saturation as the magnetic field is increased.[23,41] This feature arises because at low magnetic field, the number of triplet–triplet pairs with singlet character increases from three. At higher magnetic field, the number of triplet–triplet pairs with singlet character decreases down to two. This change increases, then decreases the rate of singlet fission, which leads to a positive and then negative change in photocurrent if the device operates via majority triplet transport as a result of singlet fission. Figure 2.5C shows this characteristic effect of photocurrent enhancement at low magnetic field, as seen in Figure 2.24, and reduction at high magnetic field for the acceptor PDIF-CN2, but not for C_{60} or $PC_{60}BM$. This result stems from the much lower LUMO of PDIF-CN2 in comparison to the fullerenes, which provides a suitable driving force for the dissociation of the triplets generated.[66]

Precedent exists for the need for low-LUMO acceptors in some situations to harvest SF-generated triplets.[30] While majority triplet harvesting is seen for bilayers of C_{60} and pentacene,[23] it is not seen in films of C_{60} and diphenyl pentacene, which has an identical HOMO to that of PolyTc.[66] Work by Jadhav et al. also shows that small differences, such as edge-on vs face-on acene-fullerene interactions can lead to a change from triplet to singlet dominated charge extraction. This arises from the edge-on acene-fullerene geometry giving a low enough CT state

energy to allow for triplet exciton dissociation. A similar effect is likely occurring in our system, which is why we do not observe triplet dominated charge transport when using the fullerenes as acceptors, in spite of the higher triplet energy of tetracene relative to pentacene.

Within these three types of devices, the external quantum efficiency (EQE) as a function of excitation wavelength was obtained in order to test whether PolyTc was contributing to the photocurrent generation (Figure 2.5D). When PDIF-CN2 is the acceptor we see an enhanced EQE contribution from PolyTc, and we can see peaks at 530 and 570 nm that correspond to peaks in the steady-state absorption of PolyTc (Figure 2.5B). Taken alone, the enhanced EQE contribution seen for PDIF-CN2 is not conclusive evidence of triplet extraction. But combined with the characteristic behavior of the photocurrent as a function of magnetic field, shown in Figure 2.5C, this EQE contribution from the donor confirms the extraction of multiple charge carriers generated from iSF in PolyTc when PDIF-CN2 is used as the acceptor.

In the case of the fullerene-based devices, we believe the photocurrent comes primarily from singlets generated and extracted from the acceptor layer. Because of the ultrafast rate of iSF for PolyTc and the fact that these devices do not show the characteristic magnetic field dependence that indicates triplet breakup, it is evident that PolyTc is not contributing significantly to photocurrent. The EQE of the fullerene-based devices also lacks the longer wavelength peaks characteristic of PolyTc contribution, instead showing EQE that roughly matches the absorption of the particular fullerene acceptor used.

Observing the extraction of triplets generated from iSF is an important finding because it had been postulated that these triplet pairs were too strongly coupled, which could only lead to recombination rather than dissociation and extraction. Unfortunately, the overall performance of our triplet extracting device remains low, likely due to the high crystallinity of PDIF-CN2 which

has been shown to lead to difficulties in fabricating a rectifying contact.[26] It must be noted that these devices could be improved by optimizing various parameters that improve breakup of the triplet pairs and improve the charge carrier mobilities of the materials. Furthermore, there is room for improvement with utilization of different architectures such as bulk heterojunctions, where interpenetrating networks of donor and acceptor lead to shorter diffusion lengths to the donor-acceptor interface.

This work is the first example of the dissociation and extraction of triplets generated from iSF, and will lead toward the development of new device architectures and other processing techniques to efficiently extract multiple charge carriers from these iSF materials. We are currently taking advantage of the facile synthesis of PolyTc to explore derivatives of the compound, where our synthetic modifications will alter the energy levels of PolyTc in order to expand the number of available acceptors. Future work points to the interfacing of iSF materials onto already high-performing solar materials such as silicon, GaAs CdTe, or inorganic–organic perovskites. At such early stages, the potential of iSF materials in third-generation photovoltaic devices continues to blossom.

2.7 Conclusion

In conclusion we have synthesized PolyTc, the first fully conjugated all-tetracene polymer. Ultrafast dynamics revealed by TAS show that PolyTc undergoes ultrafast iSF yielding high-energy triplet excitons which are confirmed by sensitization experiments. These triplets have a lifetime of ≈8 ns in solution. In the solid state, recombination is biexponential, and features spectral evolution from a strongly correlated triplet pair state to a state resembling free triplets. Previous efforts to incorporate tetracene in optoelectronic devices had been hampered by the slow rate of SF, which could be outcompeted by parasitic processes such as singlet charge

transfer. In stark contrast, PolyTc generates high-energy triplets as seen in tetracene, but undergoes iSF three orders of magnitude faster than crystalline tetracene, allowing us to incorporate these materials into devices. Magnetic field effect measurements demonstrate that given an acceptor with a suitably depressed LUMO, photovoltaic devices can operate by majority triplet carrier transport, and showcase for the first time that it is possible to extract the triplets generated from iSF. This first conclusive evidence of charge extraction from iSF materials will allow for future studies to optimize device performance, including studying ideal rates of iSF and triplet lifetime, and ideal morphology. Due to the high-energy triplets generated by PolyTc, in the future we should be able to find a suitable acceptor molecule which is also solution processable in order to fabricate higher-performing devices via high-throughput deposition, including dual bandgap single-junction PVs, and interfacing iSF materials with existing high-performance PV technologies to exceed the Shockley–Queisser limit.

2.8 Methods

Solution Transient Absorption Spectroscopy: Solution state transient absorption spectroscopy was performed on the compounds dissolved in 1 or 2 mm quartz cuvettes in less than 100×10^{-6} m concentration of tetracene repeat unit after bubbling argon through the solution to displace oxygen. These solutions were interrogated using a transient absorption spectroscopy system previously described by our group.[20] Briefly, a commercial Ti:sapphire laser system (SpectraPhysics) operating at a repetition rate of 1 kHz was used to seed a commercial optical parametric amplifier (LightConversion) which generated resonant pump pulses with ≈100 fs time duration. A small portion of the 800 nm fundamental was focused into a sapphire disk to generate supercontinuum probe light. Shot to shot detection of these pump and probe beams was accomplished by a fiber-coupled silicon (visible) or InGaAs (infrared) diode

array. A mechanical delay stage was used to control pump probe delay for high time resolution data. Longer, microsecond timescale data was collected using an electronically synchronized delay between pump and probe. Excitation fluence in each measurement was ≈25 μJ cm^{-2} except where otherwise noted.

Solution Triplet Photosensitization: In solution, the compound of interest was dissolved along with a large excess of anthracene. Photoexcitation at 360 nm preferentially excites the anthracene, which undergoes intersystem crossing to form the anthracene triplet. Collisions in solution between anthracene triplet excitons and the tetracene derivative populate individual triplets on the tetracene chromophores which are then interrogated optically to reveal the lifetime and spectrum of the free triplet exciton in these systems.

Film Transient Absorption Spectroscopy: A film of PolyTc was spin-cast onto a glass slide at 3000 RPM from a 5 mg mL^{-1} in chloroform solution. The glass slide was sealed in an argon environment, and then interrogated using the same transient absorption setup described above.

Film Triplet Photosensitization: PolyTc was mixed with $PdPc(OBu)_8$ (5 wt%) and drop cast on a glass slide from chloroform. Excitation at 730 nm, using the transient absorption spectroscopy setup described above, was used to selectively excite the sensitizer, which undergoes subsequent intersystem crossing and triplet transfer.

Magnetic-Field-Effect Measurements: Measurements of the change in photocurrent with application of magnetic field were performed using a mechanically chopped 530 nm LED coupled to a lock-in amplifier. While the device was under illumination, an electromagnet was cycled on and off approximately every 5 s. The delta was calculated by taking the difference between the two values and normalizing it by the current at zero field.

Solar-Cell Fabrication: Conventional geometry bilayer OPVs were fabricated using a device architecture of ITO/MoO_3/PolyTc/(C_{60} or PDIF-CN2)/bathocuproine (BCP)/Al. Indium tin oxide (ITO)-coated glass substrates were cleaned by successive sonication in soap solution, deionized water, acetone, and isopropyl alcohol for 15 min at 40 °C and UV ozone cleaned for 10 min before being transferred to a N_2 glovebox. When C_{60} was used as the acceptor, a 12 nm thick MoO_3 layer was then thermally evaporated under a high vacuum (≈4 × 10^{-6} mbar). PolyTc was then spincast at a rate of 3000 RPM followed by subsequent thermal evaporation of C_{60} (35 nm), BCP (10 nm), and Al (80 nm) under high vacuum (≈4 × 10^{-6} mbar). The device was fabricated the same when PDIF-CN2 was the acceptor, but with 20 nm of PDIF-CN2, and 5 nm BCP. The Al electrodes defined the devices with a shadow mask of 0.03 cm^2 in area for all measurements.

Inverted bulk heterojunction OPVs were fabricated with a device architecture of ITO/ZnO/(1:2 PolyTc:PC_{70}BM blend)/MoO_3/Ag. ITO-coated glass substrates were cleaned as above. ZnO nanoparticles were synthesized as previously reported,[67] spin-coated onto the glass substrate at 3000 rpm for 60 s and baked at 200 °C for 60 min then transferred to a N2 glovebox. The PolyTc:PC_{70}BM blend was then spincast at a rate of 2000 RPM with 0.5% DIO followed by subsequent deposition of MoO_3 (15 nm) and Ag (100 nm) by thermal evaporation under high vacuum (≈4 × 10^{-6} mbar). The Ag electrodes defined the devices with a shadow mask of 0.03 cm2 in area.

Solar-Cell Testing: A Thermal-Oriel 300W solar simulator provided an AM 1.5G solar illumination at 100 mW cm^{-2} for OPV device testing. A Keithley 236 source-measure unit was used to measure current density−voltage (J−V) curves. EQE spectra were measured with a monochromator and calibrated with a silicon photodiode up to 800 nm.

General Methods: All commercially obtained reagents/solvents were used as received; chemicals were purchased from Alfa Aesar®, Sigma-Aldrich®, Acros organics®, TCI America®, Mallinckrodt®, and Oakwood® Products, and were used as received without further purification. Unless stated otherwise, reactions were conducted in oven-dried glassware under argon atmosphere. ^{1}H-NMR and ^{13}C-NMR spectra were recorded on Bruker 400 MHz (100 MHz for ^{13}C) and on 500 MHz (125 MHz for ^{13}C) spectrometers. Data from the 1H-NMR and ^{13}C-NMR are reported as chemical shift (δ ppm) with the corresponding integration values. Coupling constants (J) are reported in hertz (Hz). Standard abbreviations indicating multiplicity were used as follows: s (singlet), b (broad), d (doublet), t (triplet), q (quartet), m (multiplet) and virt (virtual).

The mass spectral data for the compounds were obtained from XEVO G2-XS Waters® equipped with a QTOF detector with multiple inlet and ionization capabilities including electrospray ionization (ESI), atmospheric pressure chemical ionization (APCI), and atmospheric solids analysis probe (ASAP). The base peaks were usually obtained as $[M]^{+}$ or $[M^{+}H]^{+}$ ions.

Absorption spectra were obtained on a Shimadzu UV 1800 UV-Vis spectrophotometer. The TGA analysis was carried out in q500-2210 TA instrument. Emission spectra were obtained on a Horiba Fluoromax-4. Differential Scanning Calorimetry (DSC) was performed on a TA Instruments DSC Q2000 fitted with a RCS90 refrigerated cooling system to determine the glass transition temperatures. DSC measurements were taken at a sampling rate of 10 °C/min in the temperature range of 0°C to 140°C.

Anhydrous solvents were obtained from a Schlenk manifold with purification columns packed with activated alumina and supported copper catalyst (Glass Contour, Irvine, CA). All

reactions were carried out under argon unless otherwise noted. Atomic Force Microscopy (AFM) measurements were carried out using a Bruker Dimension Icon AFM.

Gel permeation chromatography (GPC) analyses were carried out using an Agilent PL GPC 50 integrated system (2 x PL gel Mini-MIX C columns, 5 micron, 4.6 mm ID) equipped with UV and refractive index detectors. The GPC columns were eluted at a rate of 1.0 mL/min with 1,2,4-trichlorobenzene (150 °C) and were calibrated relative to monodisperse polyethylene standards.

2.9 Synthesis of Polytetracenes

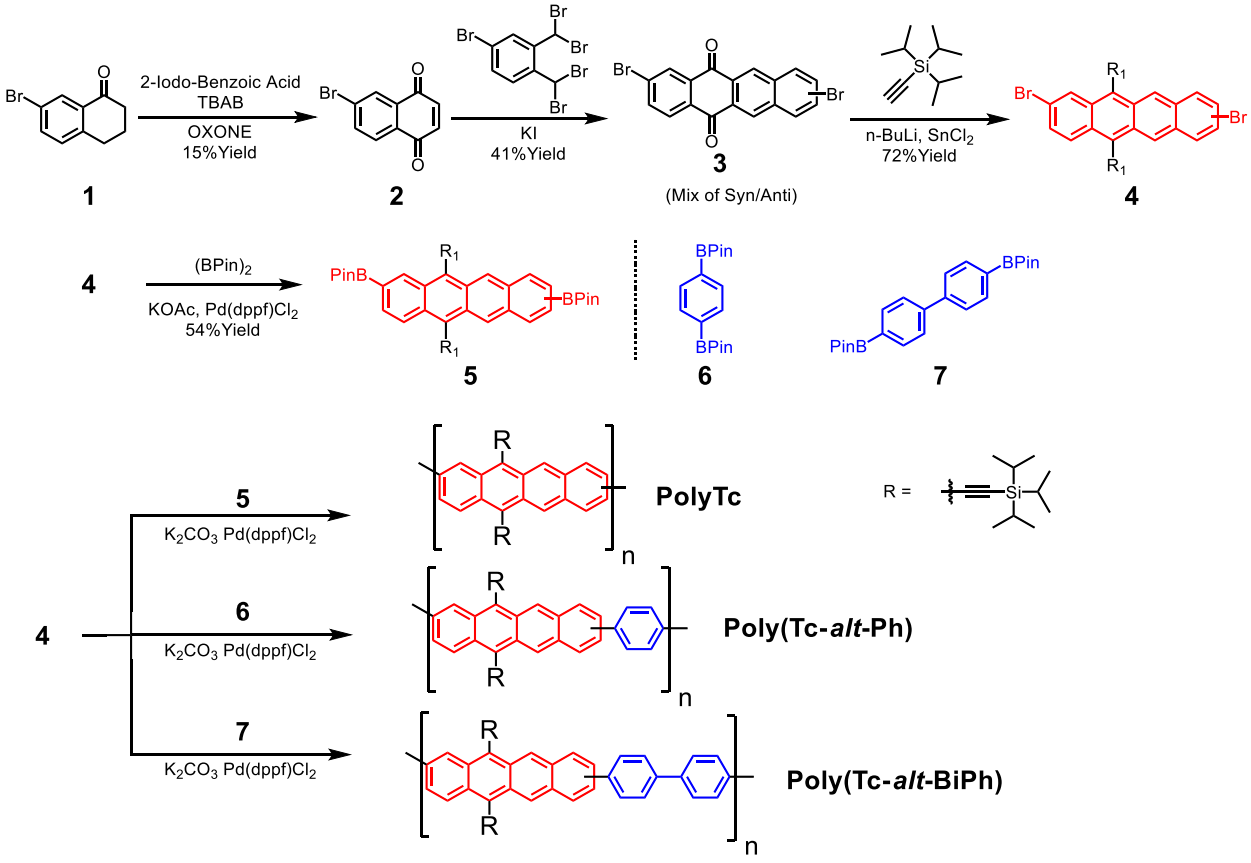

Compound **2** was synthesized according to a procedure reported in the literature.[68]

Synthesis of 3

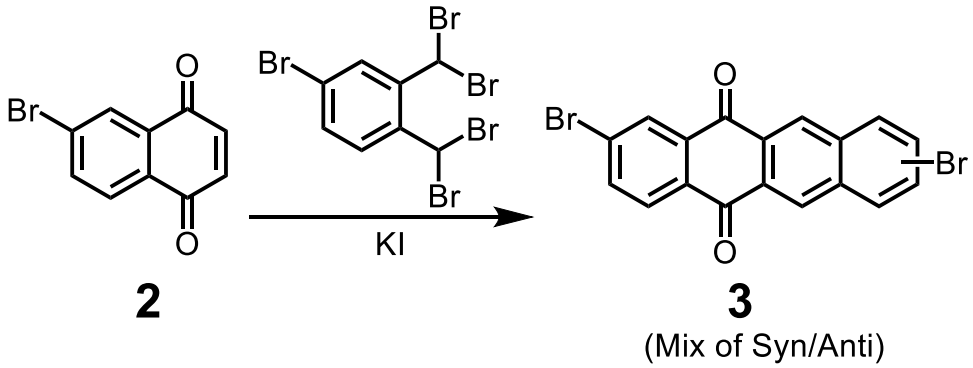

2 (1.4 g, 5.9 mmol), 4-bromo-1,2-bis(dibromomethyl)benzene (3.07 g, 6.14 mmol) and potassium iodide (3.921g, 23.6 mmol) were added to a round bottom flask. Sequential vacuum and argon was used to degas the mixture followed by the addition of dry and degassed DMF (32 mL). The reaction was brought to 110 °C and allowed to stir overnight. The reaction was then brought to room temperature and precipitated in methanol (50 mL). This mixture was then filtered and the solids were washed with water, methanol, and DCM (100 mL each). The solid was then collected and dried to obtain **3** as a pale yellow solid (1.0 g, 41% Yield).

^{1}H-NMR (400 MHz, $CDCl_3$, δ ppm): 8.84 (s, 1H), 8.77 (s, 1H), 8.53 (s, 1H), 8.29-8.25 (m, 2H), 8.00-7.95 (m, 2H), 7.90 (d, 1H).

Limited solubility of material prevented the acquisition of a ^{13}C-NMR.

MS (ESI): Calculated $[M^{+}H]^{+}$: 416.8950; Observed: 416.8955.

Synthesis of 4

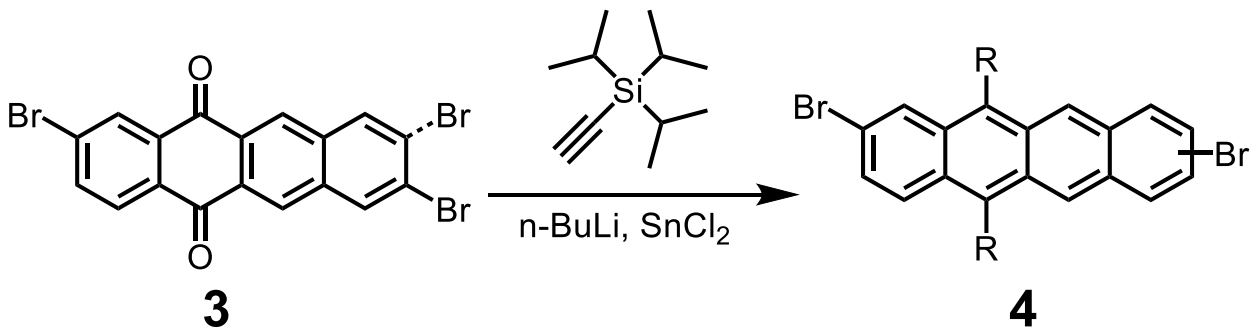

3 **4**

(Triisopropylsilyl)acetylene (638.3 mg, 3.5 mmol) was combined with 4 mL of dry THF in a schlenk flask. Sequential vacuum and argon was used to degas the mixture followed by the dropwise addition of n-butyllithium (3.2 mmol) at 0 °C. The solution was allowed to warm to room temperature and stirred for 1 h. **3** (416 mg, 1 mmol) was then added to the flask, followed by sequential vacuum and argon to degas the mixture. The reaction was allowed to stir for 4 h before being quenched by the addition of wet ether (2 mL). The solvent was evaporated, and purified by column chromatography using pure hexanes to remove excess (triisopropylsilyl)acetylene followed by pure DCM as the eluent to isolate the crude diol. This diol was then dissolved in 1:1 THF:MeCN (12 mL), and $SnCl_2 \cdot 2(H_2O)$ was added (2.25 g, 10 mmol). The resulting mixture was stirred at room temperature for 1 h in the dark, then washed with water (50 mL). The mixture was extracted with hexanes (2 x 50 mL) and the combined organic layers were washed with brine (30 mL), dried over sodium sulfate, filtered and concentrated. The crude was purified by column chromatography using hexanes as eluent to obtain **4** as a deep red solid (536 mg, 72% yield).

^{1}H-NMR (400 MHz, $CDCl_3$, δ ppm): 9.24 (s, 1H), 9.15 (s, 1H), 8.84 (dd, 1H), 8.48 (dd, 1H), 8.17 (d, 1H), 7.88 (dd, 1H), 7.60 (dt, 1H), 7.51 (d, 1H), 1.33-1.30 (m, 42H).

^{13}C-NMR (125 MHz, $CDCl_3$, δ ppm): 133.6, 133.0, 131.3, 131.0, 130.7, 130.6, 130.5, 130.4, 130.3, 130.0, 129.6, 129.3, 127.1, 125.7, 122.1, 120.8, 119.4, 118.0, 107.2, 103.2, 19.1, 11.7.

MS (ESI): Calculated $[M^+H]^+$: 747.1880; Observed: 747.1904.

Synthesis of **5**

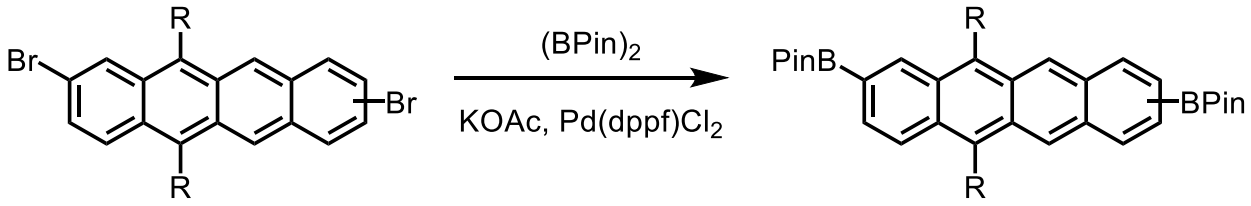

4 **5**

4 (150 mg, 0.2 mmol), bis(pinacolato)diboron (153 mg, 0.6 mmol), potassium acetate (60 mg, 0.6 mmol) and Pd(dppf)Cl_2·DCM (16.5 mg, 0.02 mmol) were added to a reaction vial, followed by sequential vacuum and argon to degas the solids. Dry, degassed 1,4-dioxane (5 mL) was then added, and the mixture was then allowed to stir at 100 °C in the dark overnight. The reaction was then brought to room temperature, and the solvent was evaporated. The crude was then purified by column chromatography using 25% to 40% DCM in hexanes as the eluent to obtain **5** as a deep red solid (91 mg, 54% yield).

^{1}H-NMR (400 MHz, $CDCl_3$, δ ppm): 9.32 (d, 1H), 9.27 (t, 2H), 8.61 (t, 1H), 8.56 (d, 1H), 7.97 (dd, 1H), 7.84 (dd, 1H), 7.78 (dd, 1H), 1.42 (d, 24H), 1.36-1.31 (m, 42H).

^{13}C-NMR (125 MHz, $CDCl_3$, δ ppm): 137.9, 137.0, 134.0, 133.2, 132.4, 131.8, 130.9, 130.4, 129.9, 128.0, 127.6, 126.4, 126.1, 120.1, 118.5, 106.8, 106.0, 104.0, 84.2, 84.1, 25.1, 19.2, 11.8.

MS (ESI): Calculated $[M^+H]^+$: 841.5408; Observed: 841.5399.

General synthesis of PolyTc, Poly(Tc-alt-Ph), and Poly(Tc-alt-BiPh)

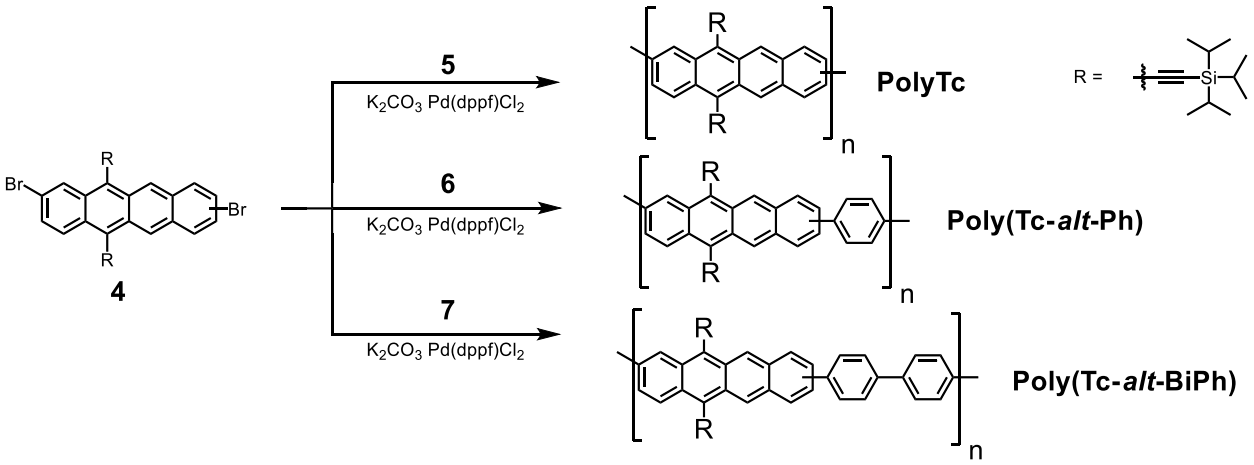

4 (1 eq) is combined with **5**, **6**, or **7**, (1 eq) and $Pd(dppf)Cl_2$·DCM (.1 eq) in a reaction vial followed by sequential vacuum and argon to degas the solids. K_2CO_3 (5 eq) was then dissolved in H_2O and degassed. The solids were then dissolved in a mixture of 9:1 THF:K_2CO_3 in H_2O solution, and allowed to stir at 45 °C for 15 h in the dark. 0.1 mL bromobenzene was then added and the reaction was allowed to stir for a further 2 h at 45 °C before the addition of phenylboronic acid pinacol ester. The reaction was allowed to stir at 45 °C for 2 h before being brought to room temperature and precipitated into methanol. The solids were then filtered directly into a cellulose thimble and purified by sequential soxhlet extraction in acetone, hexanes, and finally chloroform. The chloroform fraction was collected, evaporated, and reprecipitated into methanol. The solid was then collected and used for measurements.

2.10 Thermogravimetric Analysis of Polytetracenes

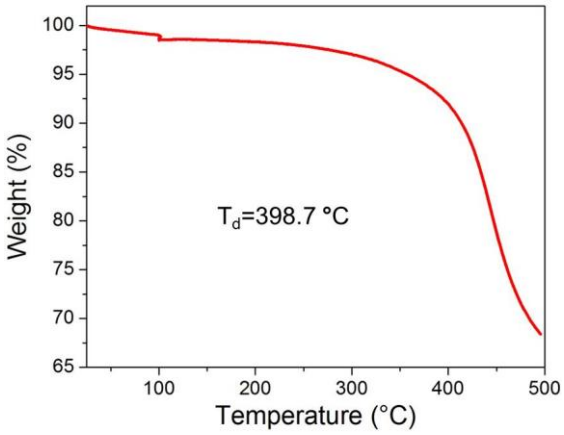

PolyTc

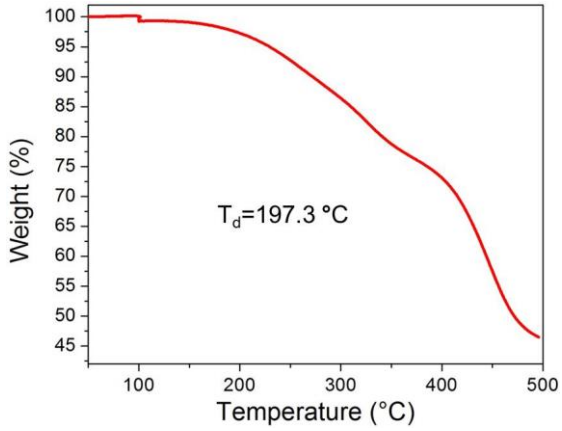

Poly(Tc-*alt*-Ph)

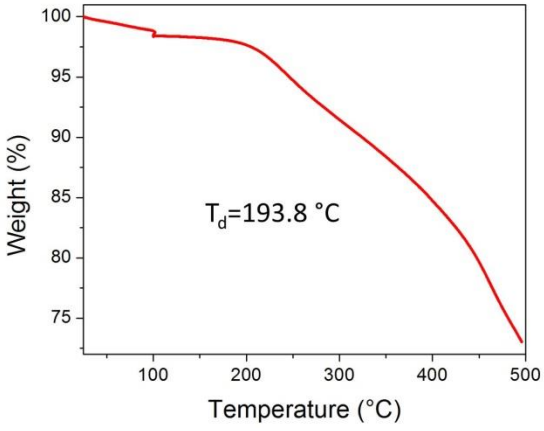

Poly(Tc-*alt*-BiPh)

2.11 Differential Scanning Calometric Analysis of Polytetracenes

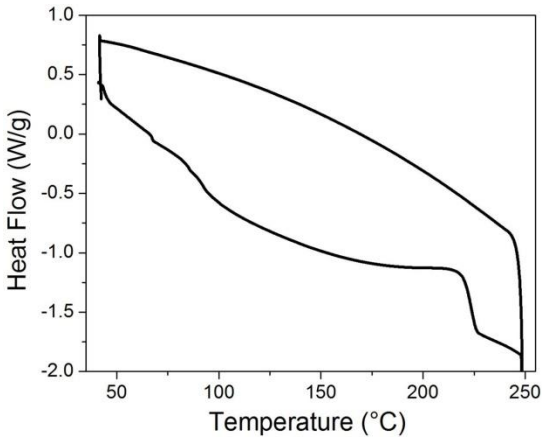

PolyTc

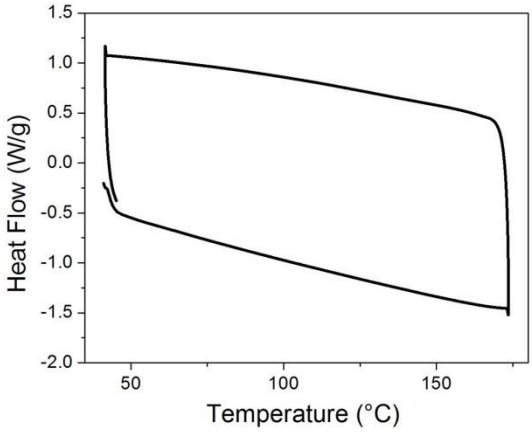

Poly(Tc-*alt*-Ph)

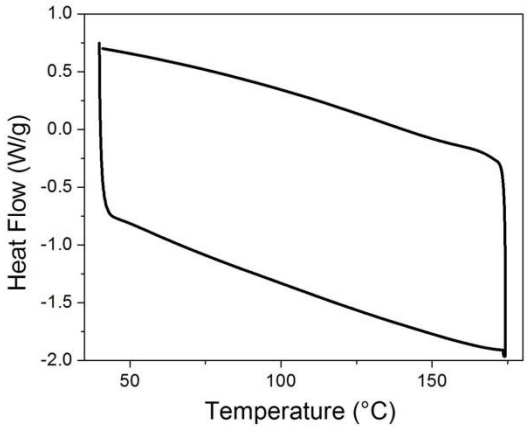

Poly(Tc-*alt*-BiPh)

2.12 Gel Permeation Chromatography of Polytetracenes

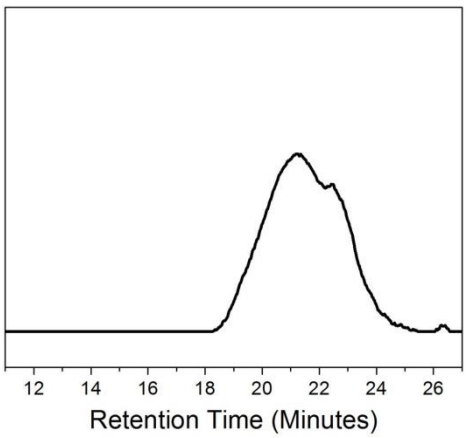

PolyTc (M_n= 3725 g/mol Đ= 3.20)

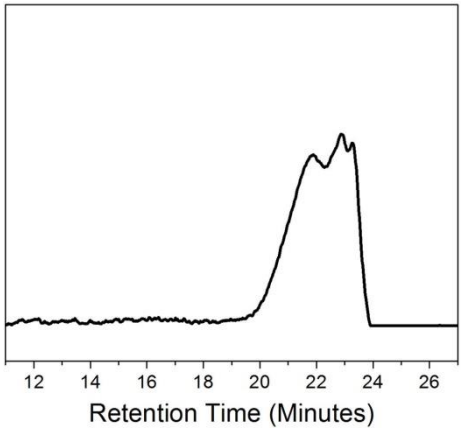

Poly(Tc-*alt*-Ph) (M_n= 2562 g/mol Đ= 1.92)

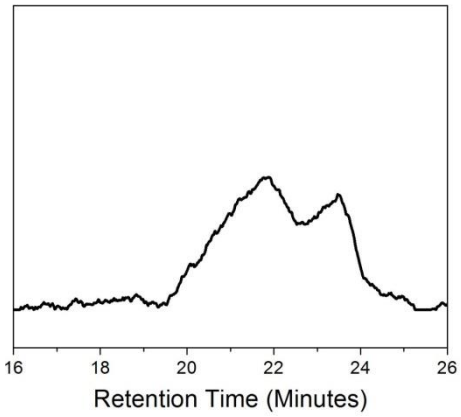

Poly(Tc-*alt*-BiPh) (M_n= 2902 g/mol Đ= 2.69)

2.13 Cyclic Voltammetry

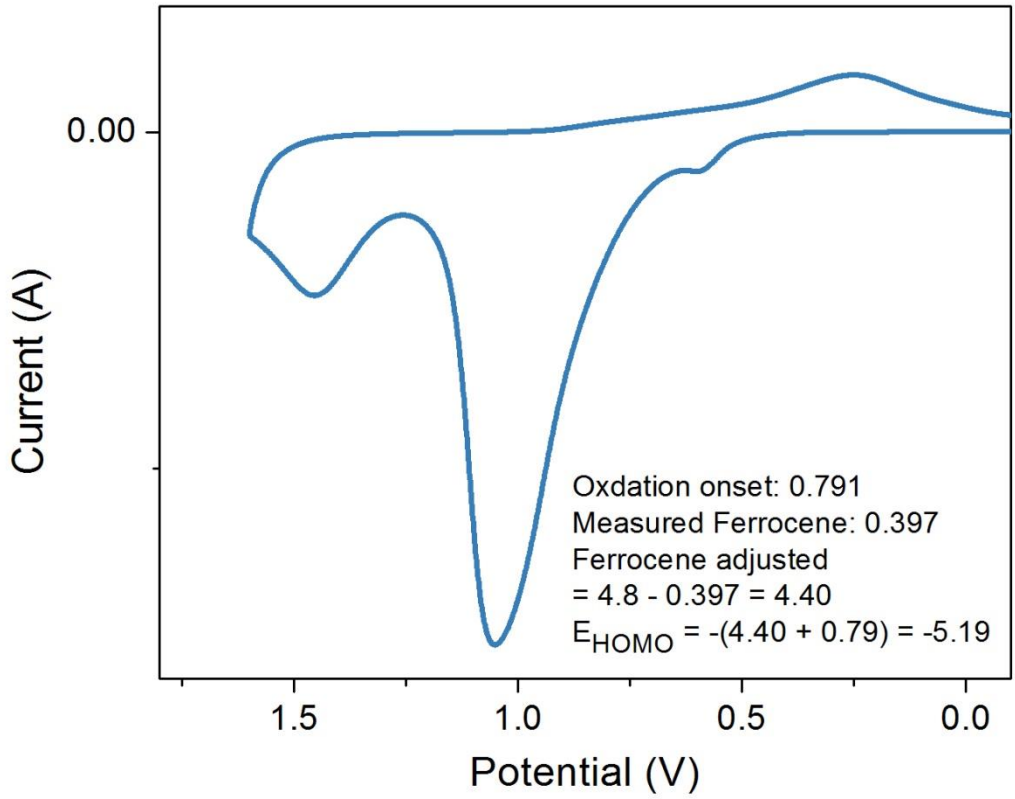

Figure 2.6 Cyclic Voltammogram of PolyTc plotted against the ferrocene oxidation potential

2.14 Atomic Force Microscopy

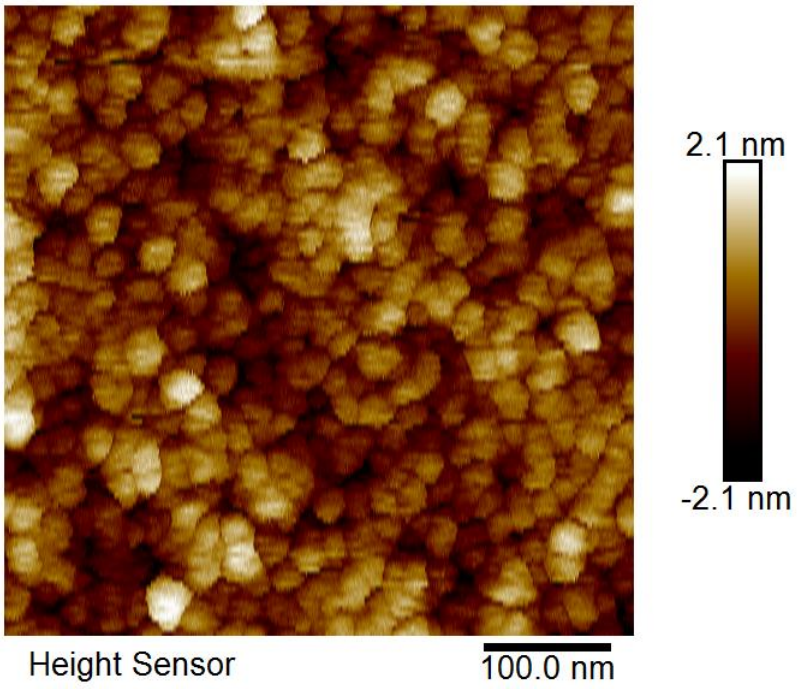

Figure 2.7 Atomic Force Microscopy Image of PolyTc (5 mg/mL in Chloroform, spun at 2,000 RPM on Si/SiO_2)

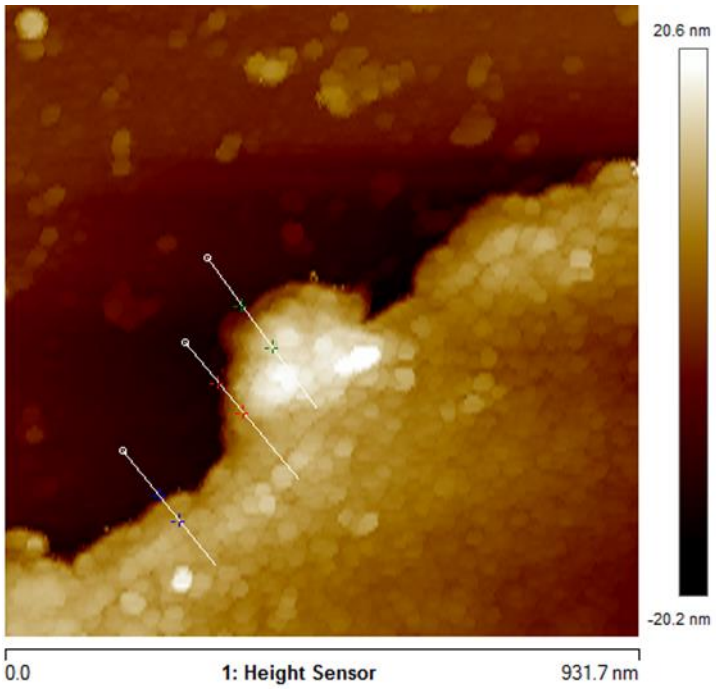

Figure 2.8 Atomic Force Microscopy Image of PolyTc (5 mg/mL in Chloroform, spun at 2,000 RPM on Si/SiO_2). Film cut to measure height of film (24.3 nm)

2.15 UV-Vis Stability Study

5 µg/mL solutions of TIPS-Tc and PolyTc were exposed to 365 nm radiation over a period of 30 minutes in air. Evolution of the spectra overtime is shown below.

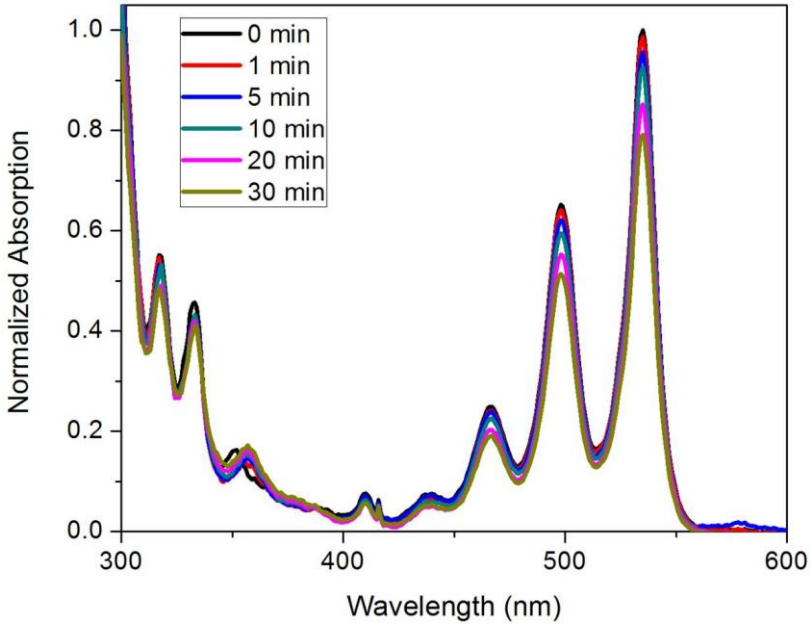

Figure 2.9 Decay of TIPS-Tc

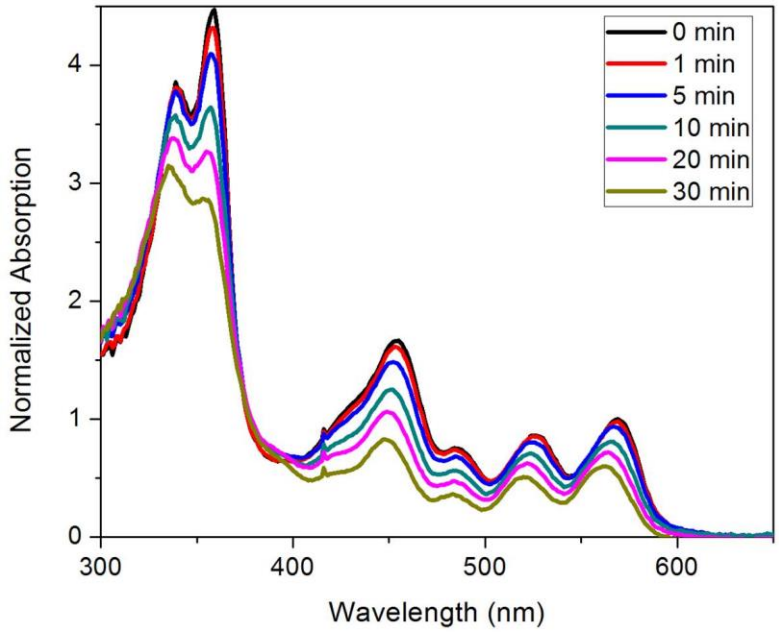

Figure 2.10 Decay of PolyTc

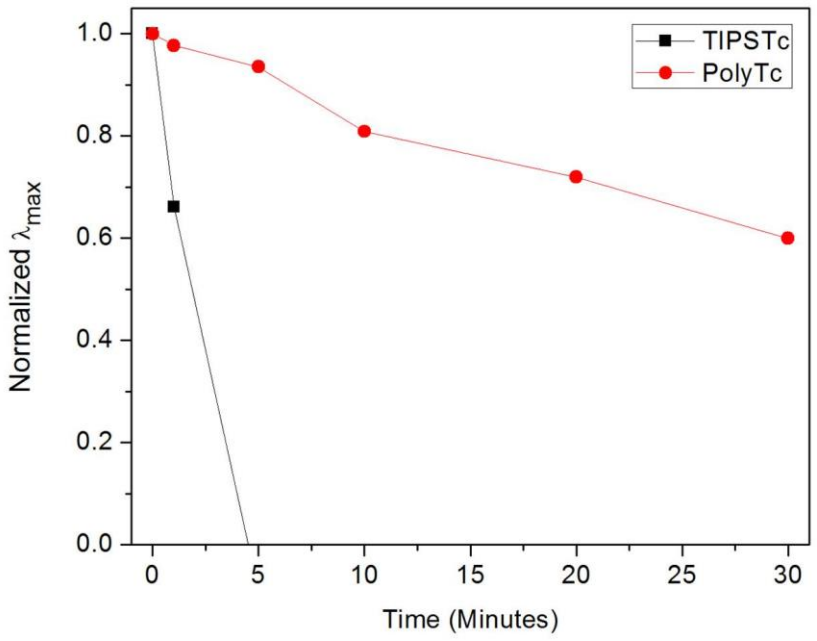

Figure 2.11 Change in λ_{max} over time for TIPS-TC and PolyTc normalized per absorbed photon from 345-385 nm.

2.16 NMR Spectra

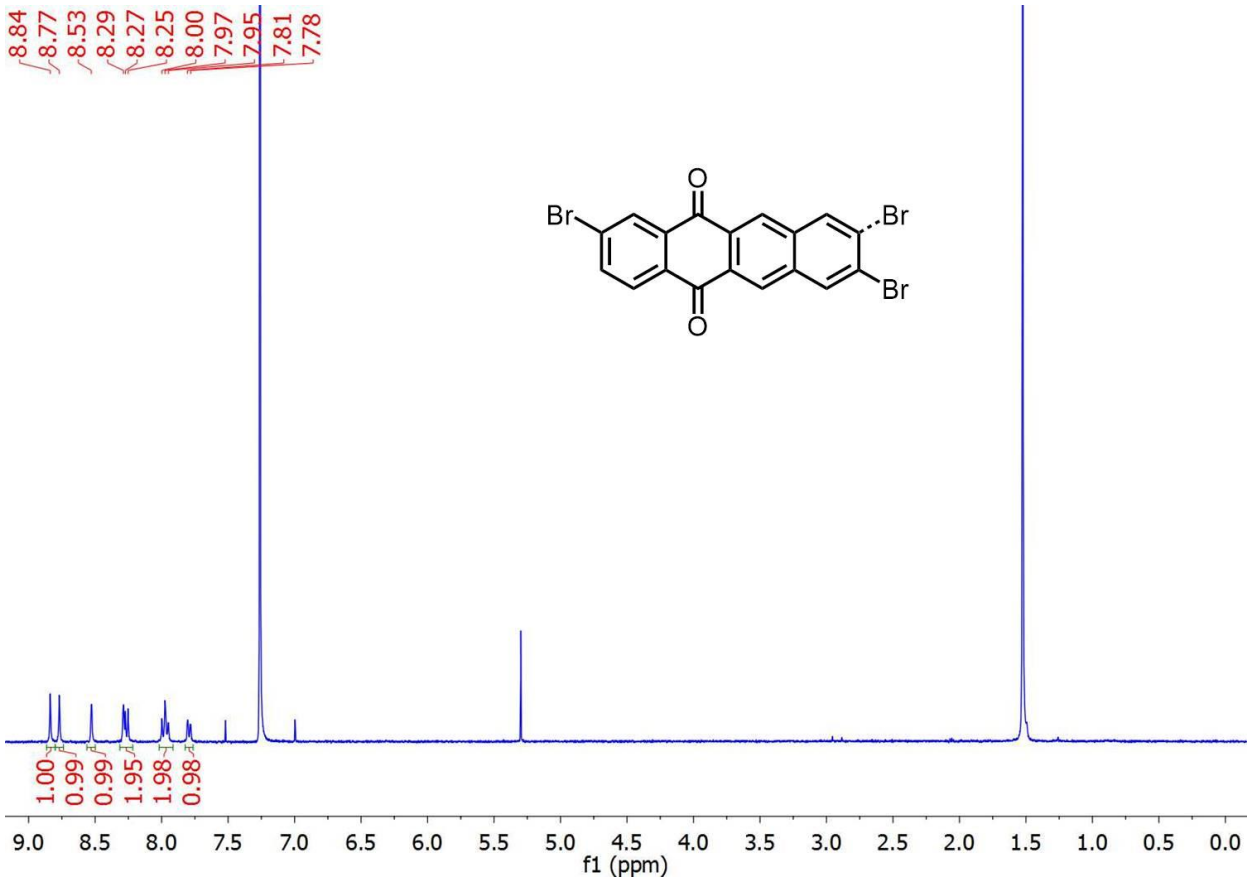
8.84
8.77
8.53
8.29
8.27
8.25
8.00
7.97
7.95
7.81
7.78
Br
Br
Br
O
O
1.00
0.99
0.99
1.95
1.98
0.98
9.0
8.5
8.0
7.5
7.0
6.5
6.0
5.5
5.0
4.5
4.0
3.5
3.0
2.5
2.0
1.5
1.0
0.5
0.0
f1 (ppm)

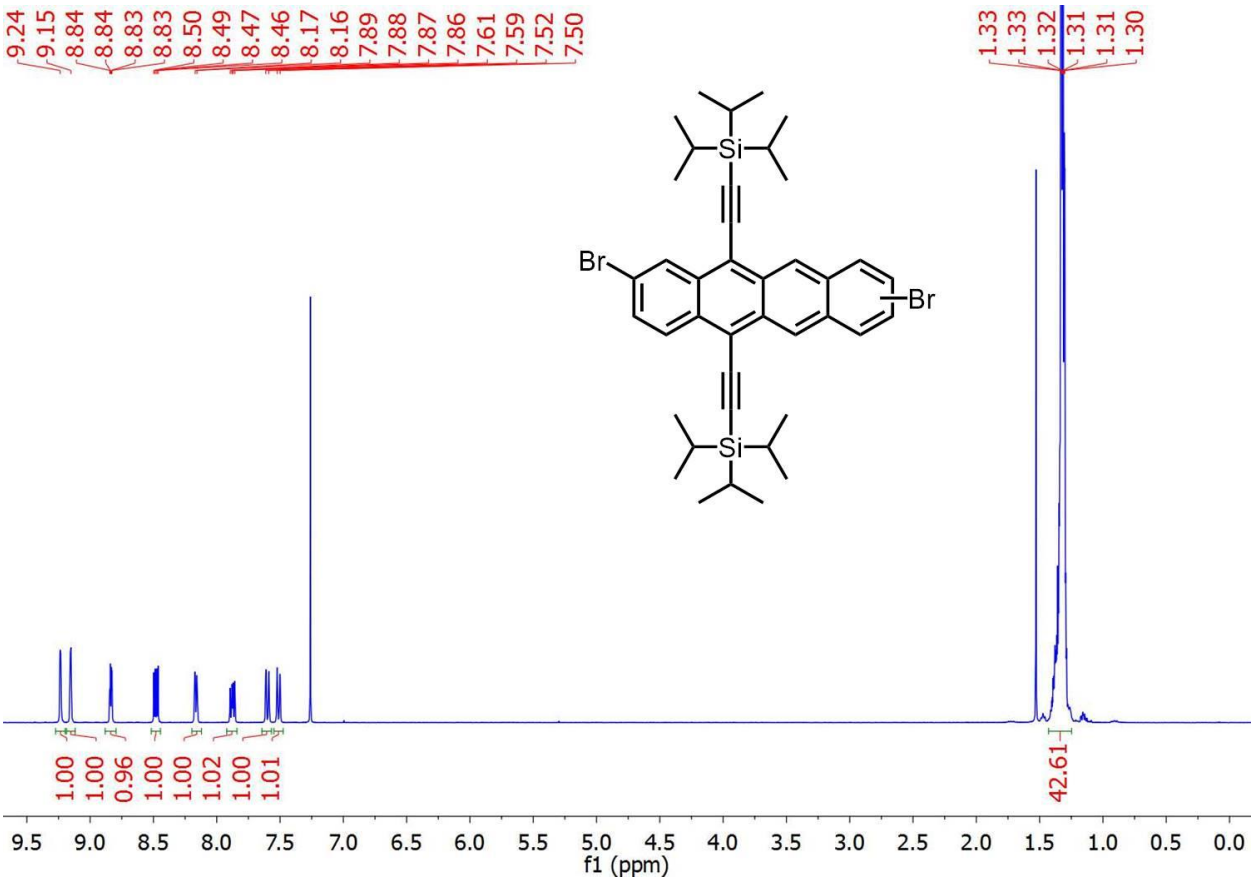
9.24
9.15
8.84
8.84
8.83
8.83
8.50
8.49
8.47
8.46
8.17
8.16
7.89
7.88
7.87
7.86
7.61
7.59
7.52
7.50
1.33
1.33
1.32
1.31
1.31
1.30
Si
Br
Br
Si
1.00
1.00
0.96
1.00
1.00
1.02
1.00
1.01
42.61
9.5
9.0
8.5
8.0
7.5
7.0
6.5
6.0
5.5
5.0
4.5
4.0
3.5
3.0
2.5
2.0
1.5
1.0
0.5
0.0
f1 (ppm)

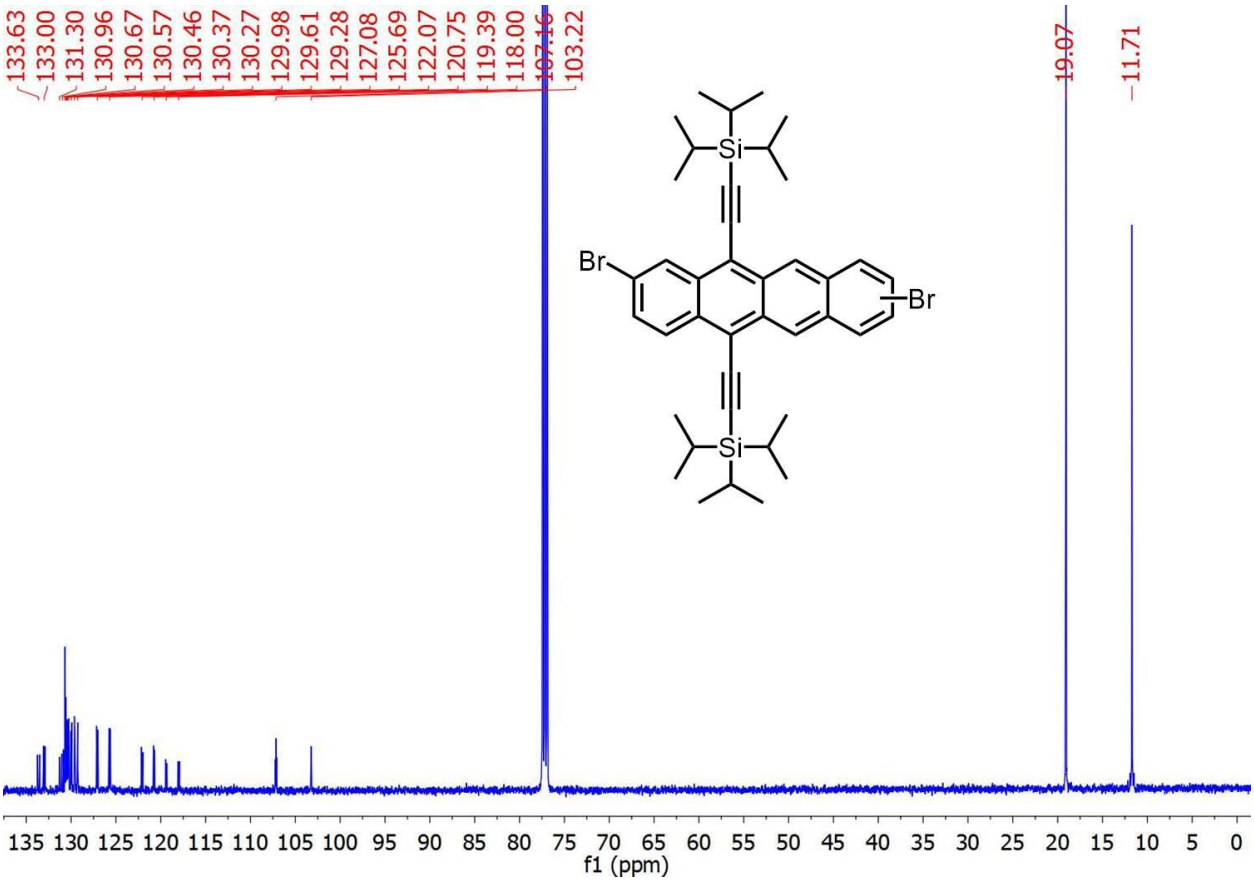
133.63
133.00
131.30
130.96
130.67
130.57
130.46
130.37
130.27
129.98
129.61
129.28
127.08
125.69
122.07
120.75
119.39
118.00
107.16
103.22
19.07
11.71
Si
Si
Br
Br
135 130 125 120 115 110 105 100 95 90 85 80 75 70 65 60 55 50 45 40 35 30 25 20 15 10 5 0
f1 (ppm)

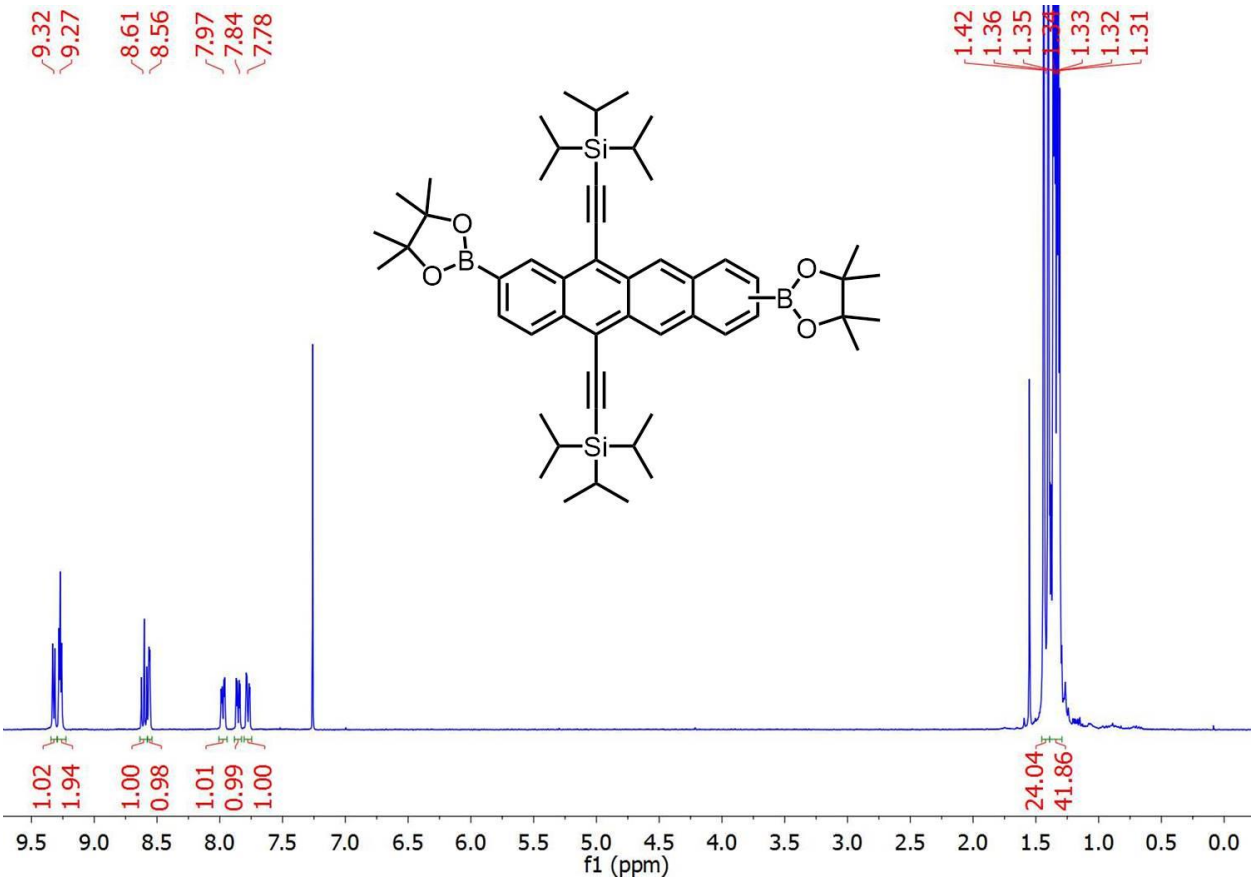
9.32
9.27
8.61
8.56
7.97
7.84
7.78
1.42
1.36
1.35
1.33
1.32
1.31
Si
Si
B
B
O
O
O
O
1.02
1.94
1.00
0.98
1.01
0.99
1.00
24.04
41.86
9.5 9.0 8.5 8.0 7.5 7.0 6.5 6.0 5.5 5.0 4.5 4.0 3.5 3.0 2.5 2.0 1.5 1.0 0.5 0.0
f1 (ppm)

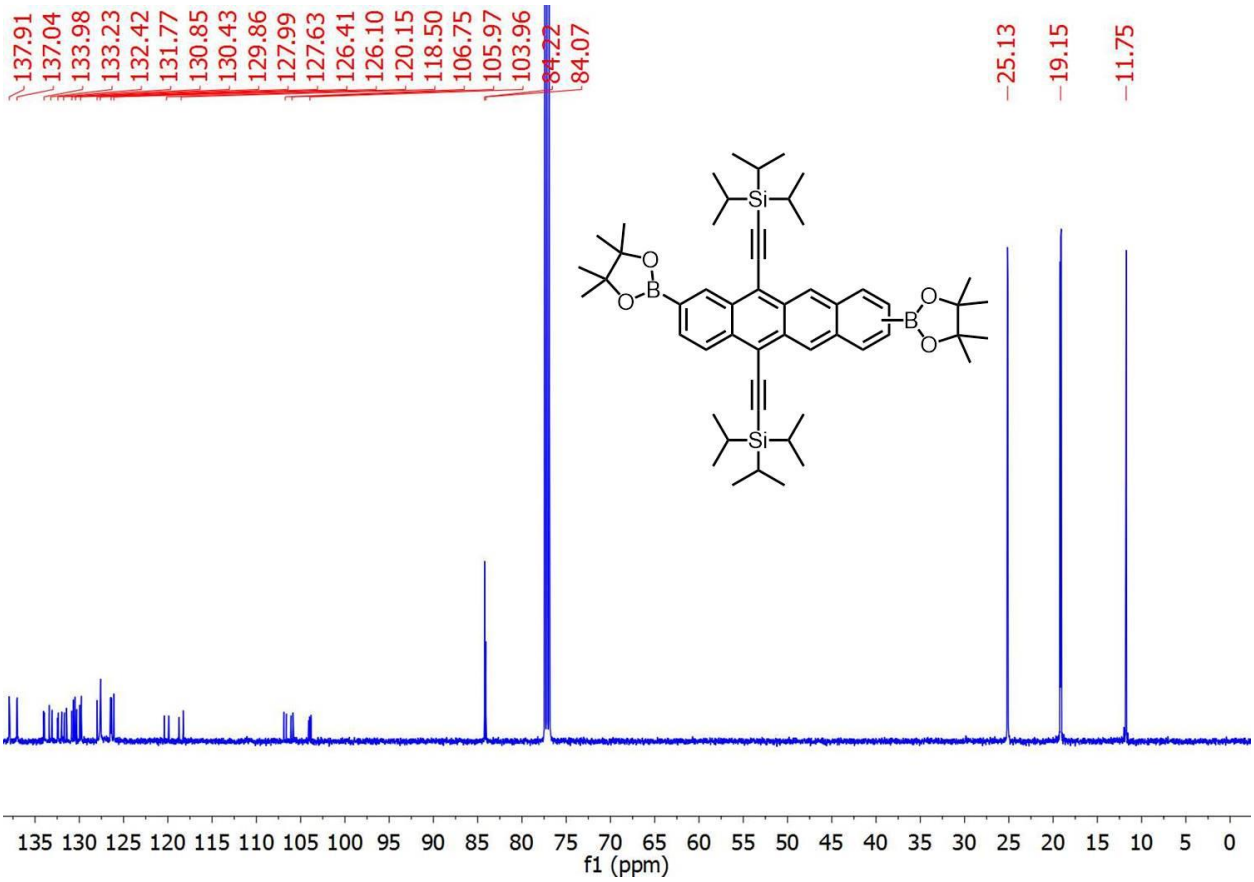

2.17 OPV J-V Curves

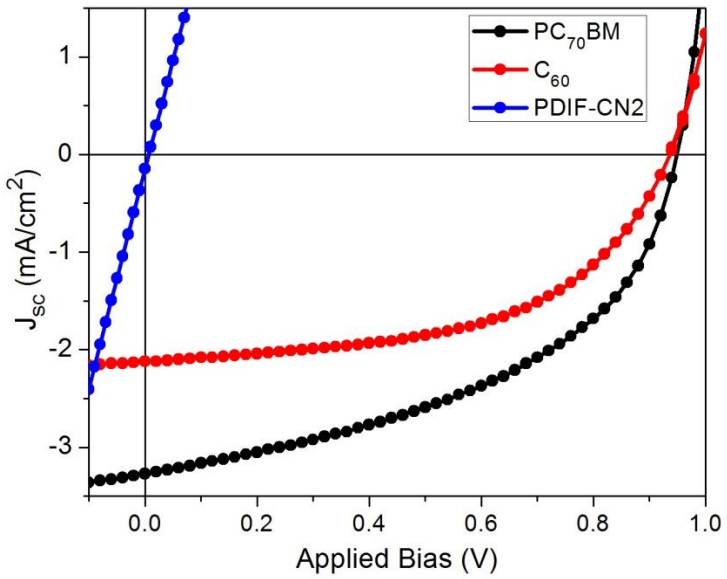

Figure 2.12 J-V characteristics of OPVs fabricated using PolyTc as the donor material and $PC_{70}BM$ (Black) C_{60} (Red) and PDIF-CN2 (Blue) as the acceptor material.

2.18 OPV Figures of Merit

Acceptor		J_{sc} (mA/cm^2)	V_{oc} (V)	FF	PCE (%)
C_{60}	Average	1.99	0.93	0.54	1.00
	Maximum	2.05	0.93	0.54	1.07
$PC_{70}BM$	Average	3.05	0.95	0.46	1.34
	Maximum	3.27	0.95	0.46	1.46

Average figures of merit from 20 pixels across 3 substrates

2.19 Transient Absorption Spectroscopy

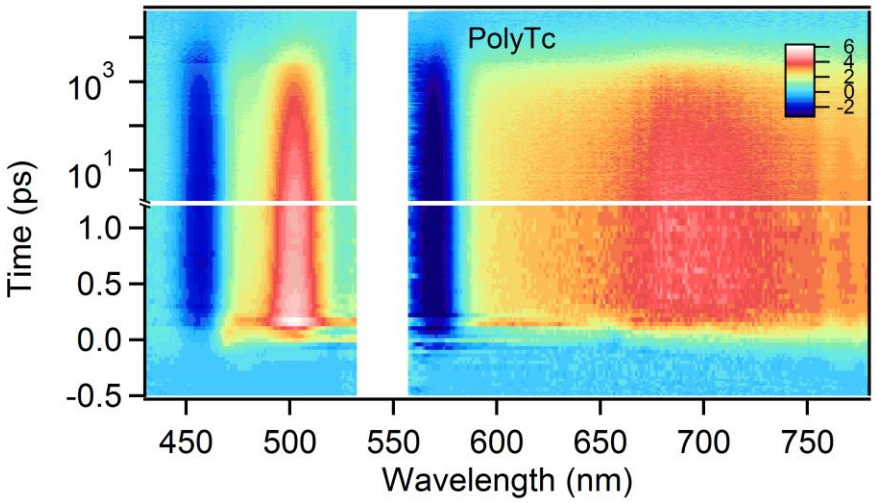

Figure 2.13 Dilute Transient Absorption Spectrum of PolyTc collected as a dilute (<100 µM) solution in toluene and excited at 545 nm (~25 µJ/cm^2).

Photoexcitation of PolyTc in toluene results in a rapid decay of the photoexcited singlet exciton into a new state which we assign as the correlated triplet pair on timescales similar to

that of our instrument response function. Singlet exciton-associated features can most clearly be observed near 450 nm, where photoinduced absorption overwhelms the strong ground state bleach (GSB), resulting in almost no net photoinduced change in absorption (PIA), as well as near 530 nm where enhanced PIA is present in the singlet exciton relative to the triplet pair. Similar to previous work on singlet fission in polypentacene, we find that the correlated triplet pair decays on timescales much faster than an individual triplet exciton (tens of μs), and we do not detect separation of the triplet pair along the polymer backbone, which would be evidenced by a longer-lived component with a spectrum more closely matched to the triplet spectrum produced in sensitization experiments (see below).

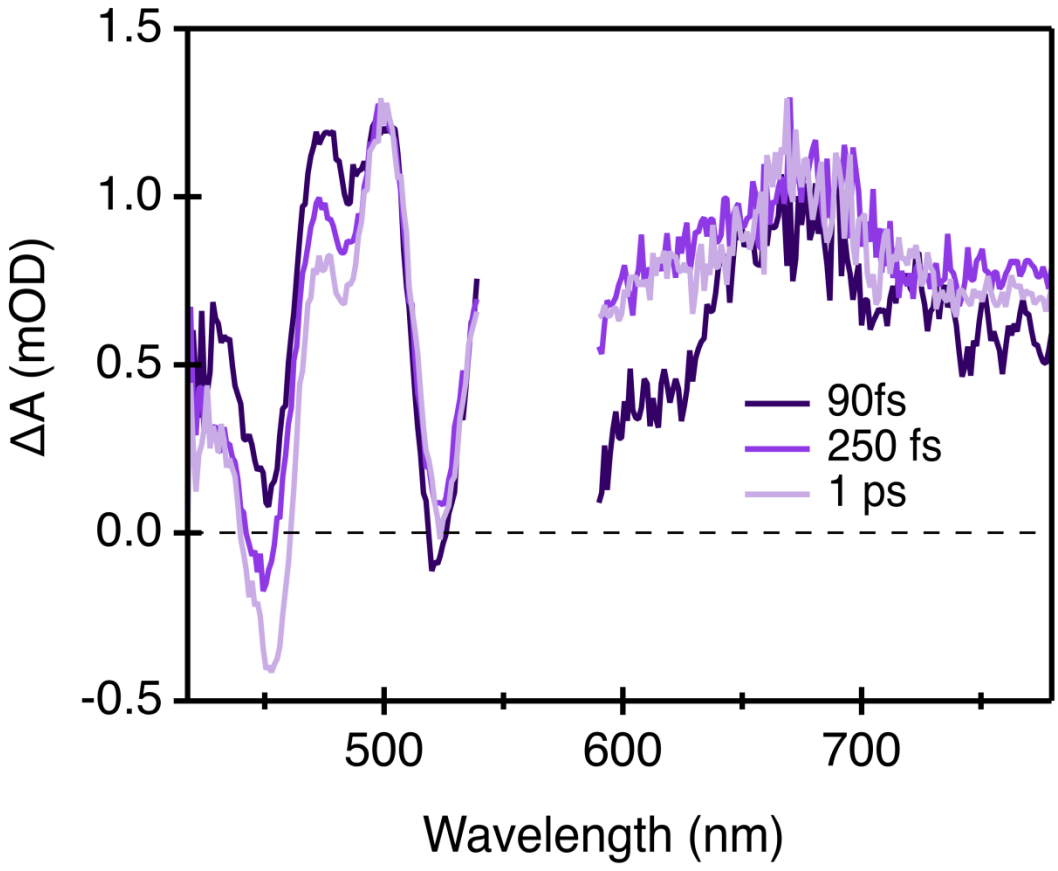

Figure 2.14 Traces Taken at Different Times Showing the Evolution of the Excited State Absorption of PolyTc.

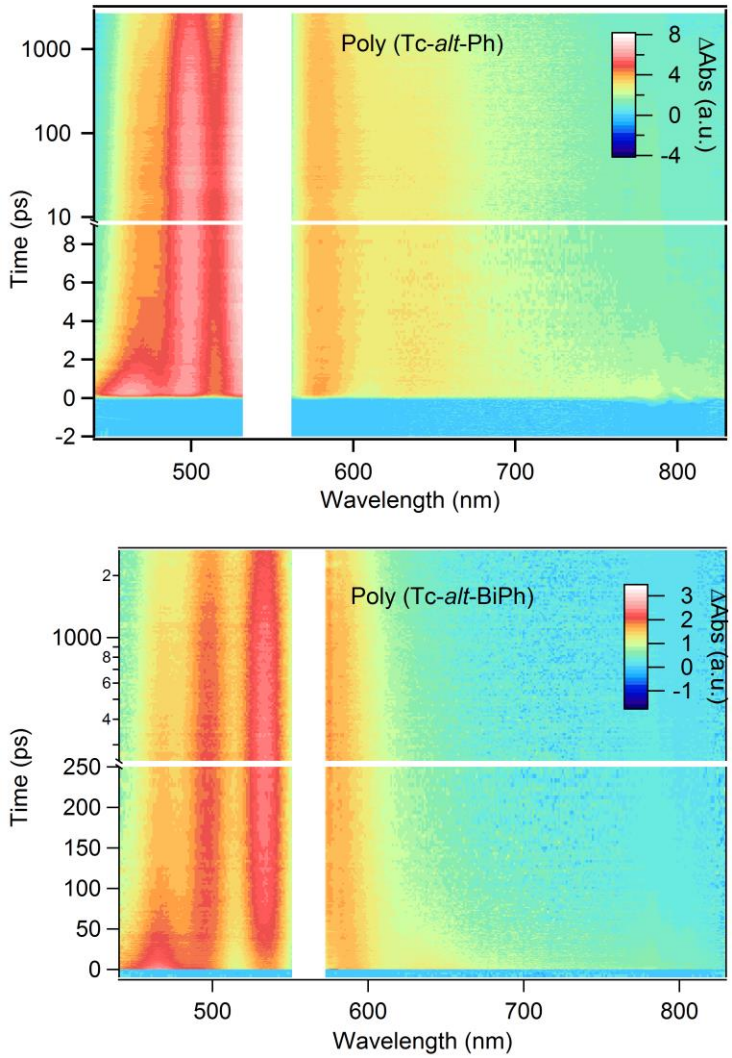

Figure 2.15 Transient Absorption Spectroscopy of PolyTc Derivatives Transient absorption spectra of Poly (Tc-*alt*-Ph) excited at 545 nm, and Poly (Tc-*alt*-BiPh), excited at 560 nm, both collected as a dilute solution in toluene (<100 µM), with a fluence of ~25 µJ/cm^2.

We have previously employed phenylene bridges to spatially separate the correlated triplet pairs produced by iSF. The use of these spacers tends to slow the rate of SF, with SF rates of 3.3 and 77 ps for Poly (Tc-*alt*-Ph) and Poly (Tc-*alt*-BiPh), respectively, as addition of one or even two benzene rings between chromophores reduces coupling. In addition to the effects on the dynamics, the introduction of spacer groups affects the spectrum of the resulting correlated triplet pairs. By reducing the triplet-triplet coupling, the triplet pair state begins to more closely match those of individual triplets produced in sensitization experiments (see sensitization

experiments below). The convergence of these spectra suggests that spectral differences between the correlated triplet pair in PolyTc, which does not have any spacers, and the sensitized PolyTc triplet spectrum, are simply caused by coupling between the two triplet excitons and not indicative of another state or occurrence of another process parasitic to SF in these compounds.

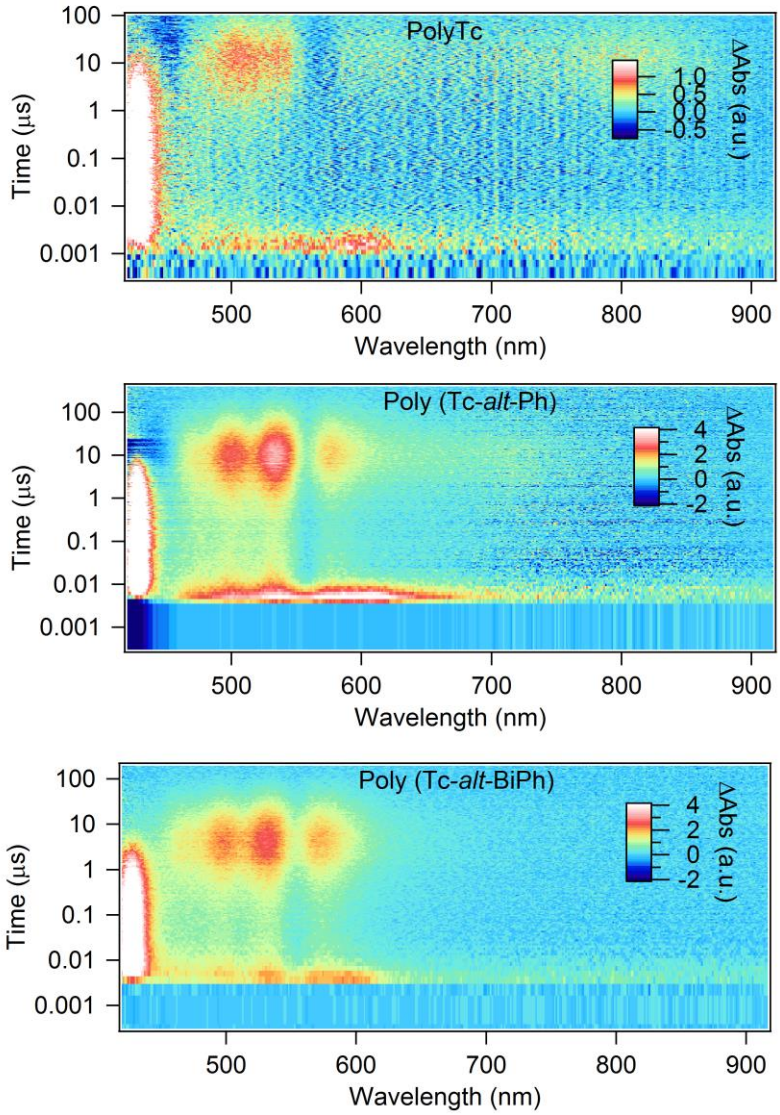

Figure 2.16 Triplet Photosensitization Experiments where anthracene is dissolved at ~15 mM in toluene, along with tetracene polymer (<100 µM tetracene repeat unit), and excitation at 360 nm (~50 µJ/cm2) preferentially excites the anthracene.

Triplet photosensitization experiments were performed to deduce the triplet spectra and lifetime in the tetracene polymers. We have described these experiments previously. In this case,

we dissolved anthracene at ~15mM in toluene, along with the polymer of interest and photoexcited at 360 nm. This primarily excites the anthracene, which undergoes intersystem crossing to populate anthracene triplets, which feature a prominent PIA near 420 nm. Collisions between these anthracene triplets and the polymer result in triplet excitons on the polymer, evidenced by decay of the anthracene triplet signal and rise of a new feature, revealing the individual polymer triplet spectra and kinetics.

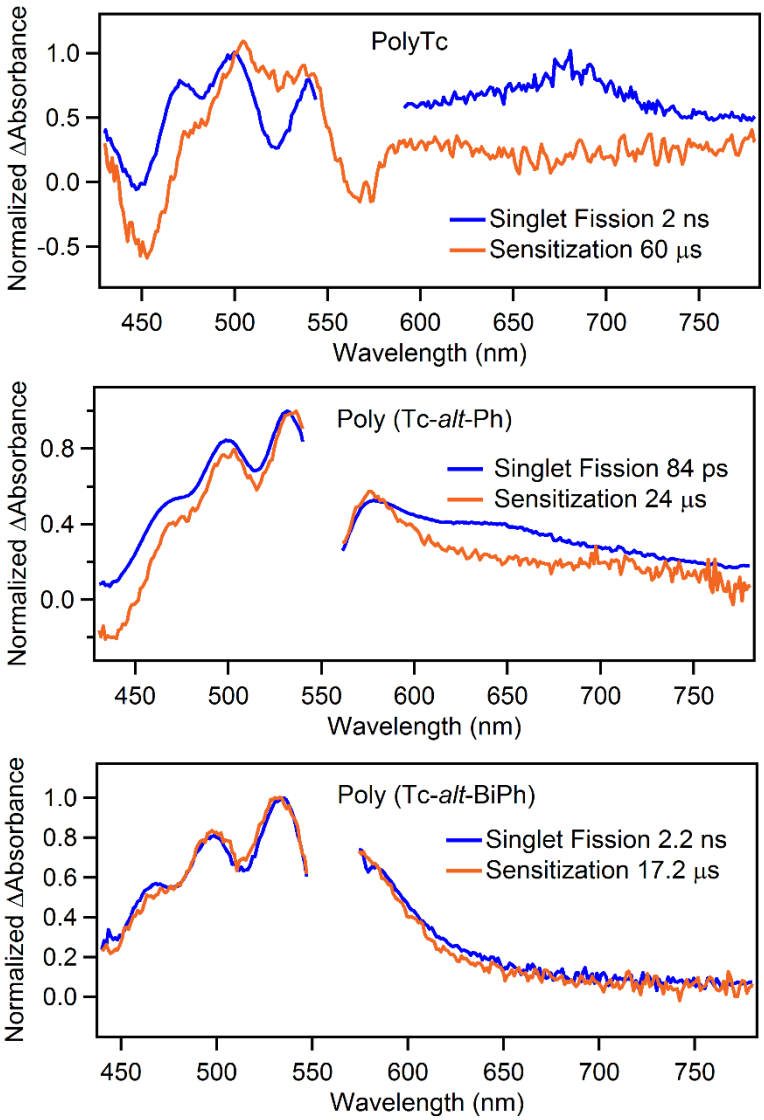

Figure 2.17 SF vs Sensitization of PolyTcs Comparison of the spectra produced after photoexcitation and subsequent singlet fission in solution (blue traces) and the spectra produced following triplet transfer from anthracene in photosensitization experiments (orange traces).

Comparison of the correlated triplet pair spectra, in blue, produced from direct photoexcitation, and the sensitized (individual triplet) spectrum in orange. In the case of PolyTc, significant spectral differences are clear, particularly near 700 nm, indicating a strongly correlated triplet pair. Introduction of a spacer in Poly(Tc-*alt*-Ph) results in a better matched spectrum. Biphenyl spacers between tetracene repeat units in Poly(Tc-*alt*-BiPh) are sufficient to result in well-matched individual triplet and triplet pair spectra.[21] These results are similar to pentacene dimers and pentacene-tetracene heterodimers reported previously by our group, and demonstrated that spectral differences in PolyTc are the result of strong triplet exciton correlations.

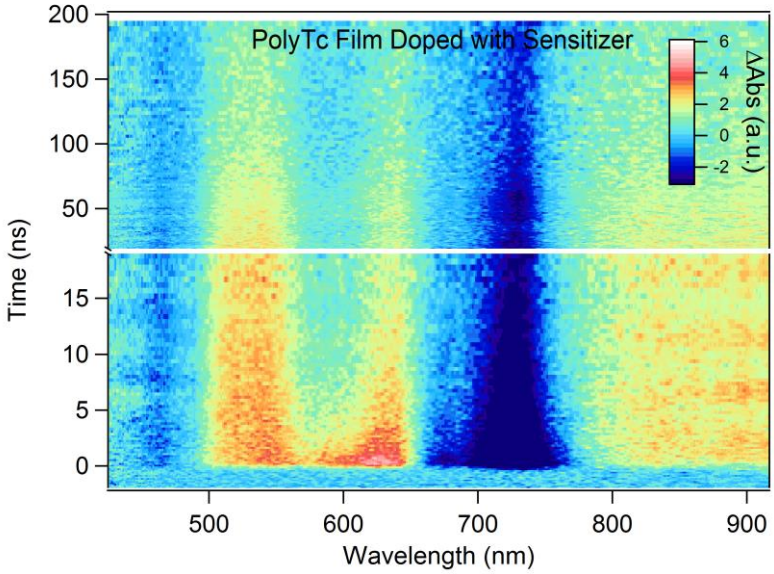

Figure 2.18 Sensitized Solid State Transient Absorption Spectroscopy Transient absorption spectrum produced by photoexcitation at 730 nm (250 μJ/cm^2) of a drop cast thin film of ~5 wt% $PdPc(OBu)_8$ in PolyTc on a glass slide under argon atmosphere

The PolyTc film doped with palladium sensitizer features a prominent GSB near 730 nm shortly after photoexcitation. This ground state bleach is diminished and a feature near 520 nm is enhanced as transfer to the PolyTc occurs. On the timescale of our measurement, the transfer is

incomplete, as evidenced by the persistence of ground state bleach signal at 730 nm at the end of the measurement. The results of this measurement are discussed in more detail below.

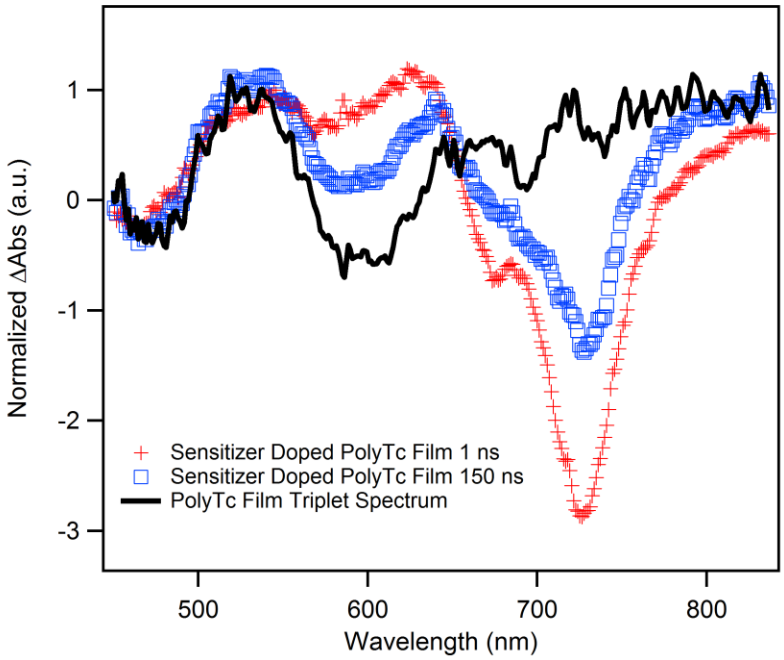

Figure 2.19 Spectral Comparison of Sensitized PolyTc Film Comparison of the spectrum at early times in the film sensitization spectrum, where the signal is dominated by the sensitizer triplet (red), and the spectrum at later times where a mixture of sensitizer triplet and PolyTc triplet coexist (blue), as well as a subtraction of the early time spectrum from the late time spectrum (black), where the spectra were normalized to remove the bleach at 730 nm (extrapolation of the PolyTc triplet spectrum).

The advantage of $PdPc(OBu)_8$ is that it features rapid ISC and a well-defined resonance at 730 nm which is well-separated from absorption of the PolyTc film, allowing selective excitation of the sensitizer. We photoexcite at 730 nm, rapidly populating sensitizer triplet excitons at early times. The spectrum at 1 ns is shown above (red markers) and primarily represents triplet excitons on the sensitizer, with a large 730 nm ground-state bleach. Over time, the spectrum changes and the 730 nm ground state bleach is reduced and ground state bleach near 590 nm is enhanced as triplet transfer from the sensitizer to the PolyTc occurs. Even at late times in our measurement, a prominent ground state bleach near 730 nm persists, suggesting

incomplete triplet transfer from the sensitizer. Following a procedure by Wasielewski et al., we subtract the early-time spectrum (representing the sensitizer triplet spectrum) from the final spectrum (a mixture of sensitizer triplet spectrum and PolyTc triplet spectrum), normalizing the subtraction such that there is no remaining bleach near 730 nm. This spectrum, shown in black, is the extrapolated pure PolyTc triplet spectrum,[63] which can be compared to the spectrum produces by SF in films of PolyTc, as shown below.

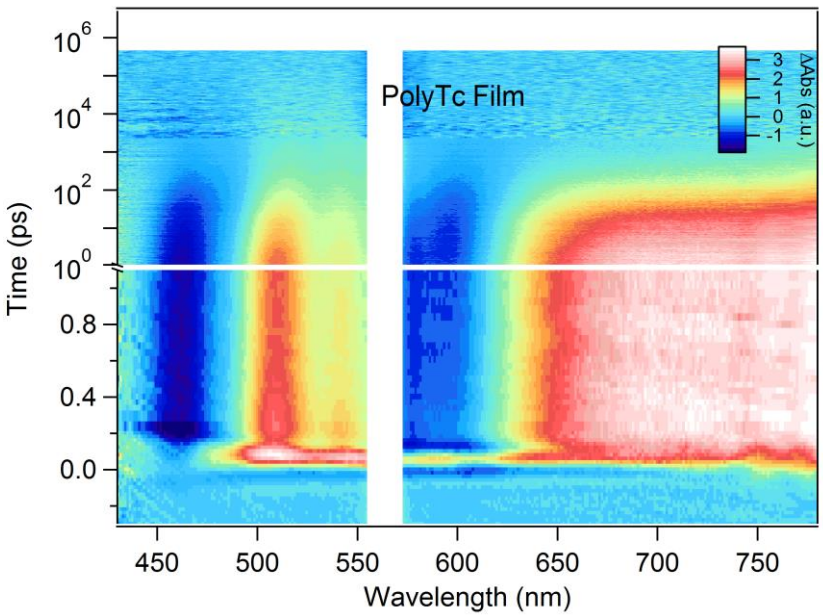

Figure 2.20 Solid State Transient Absorption Spectroscopy of PolyTc produced by photoexcitation of a PolyTc film deposited from a 5mg/mL chloroform solution by spin coating on a glass slide at 3000 RPM. Photoexcitation of the sample under argon at 560 nm (~150 $\mu J/cm^2$) produced the spectrum shown.

Photoexcitation at 560 nm of a PolyTc spin-coated film results in rapid singlet fission, similar to the behavior observed in solution. Most prominently, enhanced photoinduced absorption near 455 and 545 nm are reduced as the singlet exciton decays and the triplet pair spectrum rises. Unlike the solution data, photoexcitation of the film produces a correlated triplet pair spectrum which does not decay monoexponentially to the ground state, and changes spectrally as a function of time. This spectral evolution is discussed in more detail below.

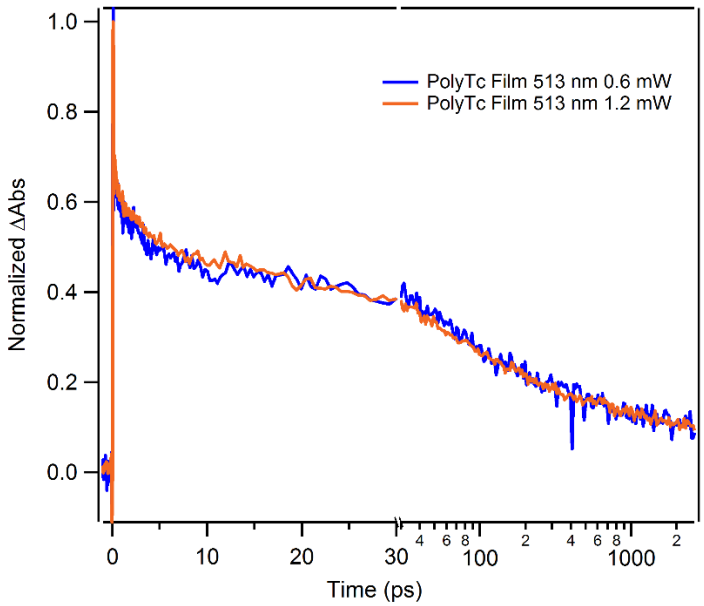

Figure 2.21 Normalized Comparison of the Kinetics at 513 nm, where features of both singlet and triplet PIA are present, for photoexcitation of the PolyTc thin film at ~75 µJ/cm2 and ~150 µJ/cm2 reveal indistinguishable behavior, indicating absence of power dependent effects at the fluences considered

Thin film measurements were also conducted at multiple fluences to ensure experiments were conducted below the regime of fluence-dependent kinetics. As shown above, the kinetics are not dependent on the pump fluences. We have chosen to monitor at 513 nm as it features prominent singlet and triplet excited state absorption. The data at higher and lower power are superimposable.

2.20 Photoluminescence Spectroscopy

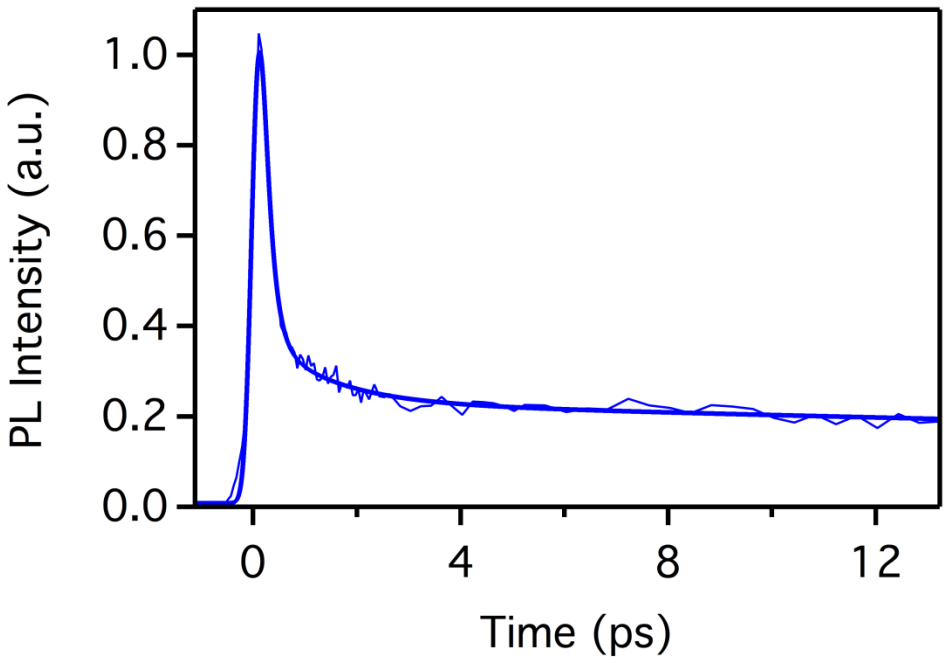

Figure 2.22 Ultrafast Photoluminescence Upconversion studies show that the prompt emission decays with a time constant that is faster than the instrument response function (< 250 fs). By correlating these measurements to transient absorption studies, we determine that the singlet fission occurs in ~ 150 fs. A residual delayed emission signal has an amplitude that is ~ 20% of the prompt signal (from fitting) and corresponds to interconversion between the coupled triplet pair and the singlet state.

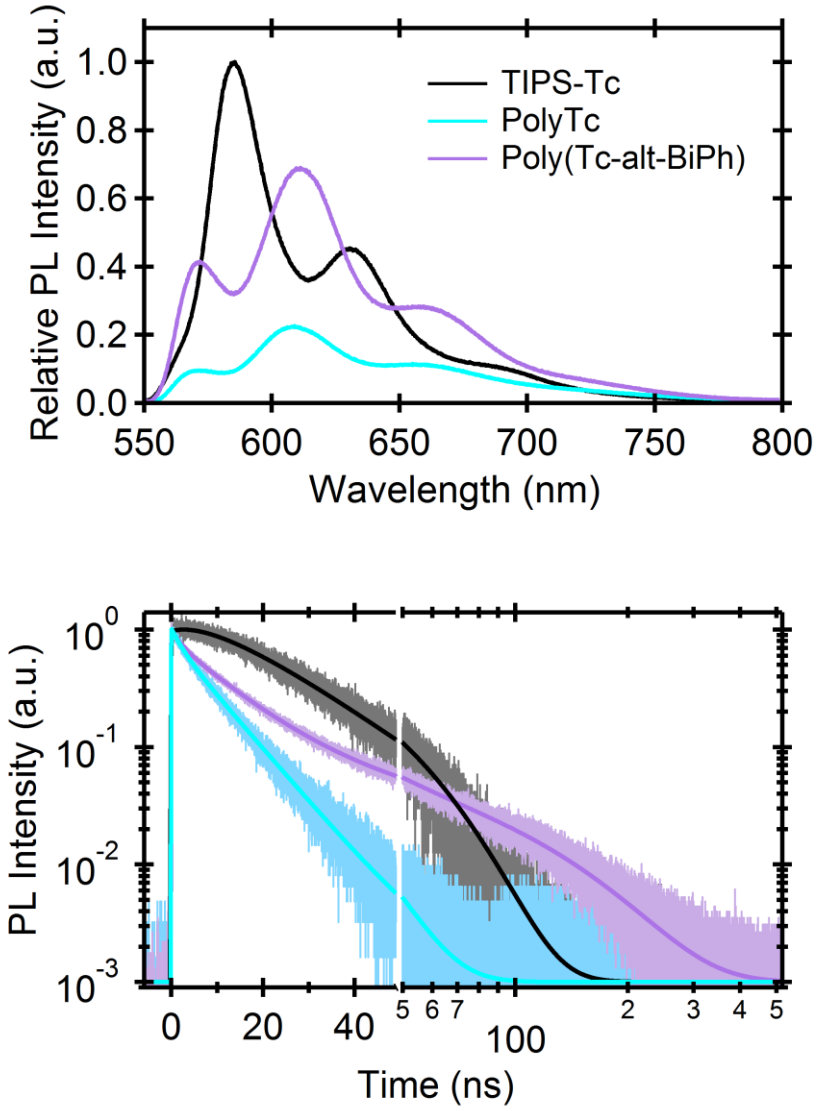

Figure 2.23 Photoluminescence of PolyTcs (Top) Steady-state photoluminescence showing the spectra and intensities of PolyTc and Poly(Tc-alt-BiPh) relative to monomeric TIPS-Tc. The integrated PL quantum yield of PolyTc is approximately 30% of TIPS-Tc. (Bottom) Time resolved photoluminescence from time correlated single photon counting (below) spectra of TIPS-Tc (black), PolyTc (Cyan) and Poly(Tc-alt-BiPh) (fuchsia). The shorter PL lifetime in PolyTc coupled with the longer lifetime in Poly(Tc-alt-BiPh) compared to TIPS-Tc is a signature of delayed PL and reflects the lifetime of the spin coupled triplet pair.

2.21 Magnetic Field Effect on Photocurrent

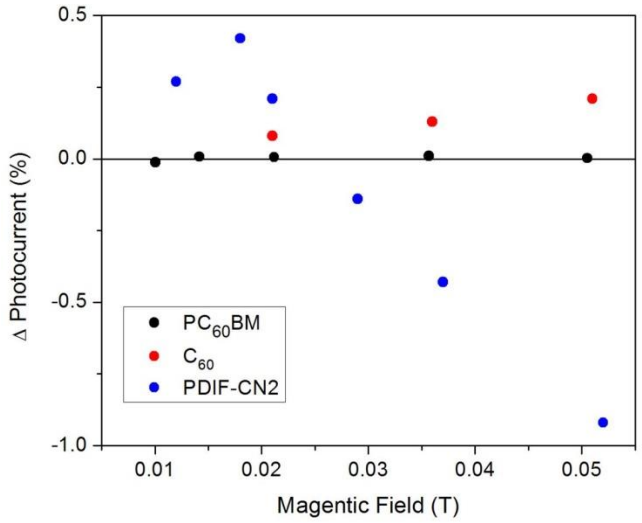

Figure 2.24 Low Field Magnetic Field Effect Zoom in of the low magnetic field region of the change in photocurrent with an applied magnetic field on PolyTc OPVs incorporating PC60BM (black) C60 (red) or PDIF-CN2 (blue) as the acceptor. This shows the characteristic increase in photocurrent at low magnetic fields, followed by a decrease in photocurrent indicating majority triplet charge transport when PDIF-CN2 is used as the acceptor.

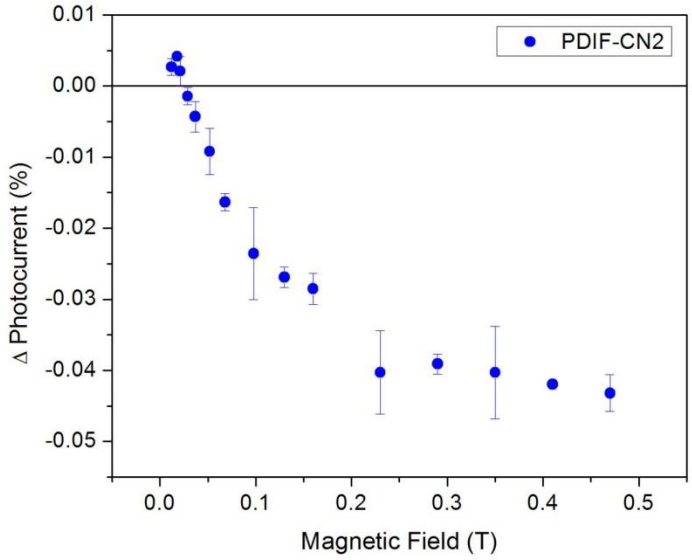

Figure 2.25 Magnetic Field Effect with Error Bars Change in photocurrent with an applied magnetic field on PolyTc OPVs

2.22 Outlook

Since the work above was published, we have tried to build on it and use PolyTc in optoelectronic devices. We had hoped PolyTc would be a useful material for application in devices because so much is already known about making polymer based organic photovoltaics

(OPVs), but attempts at Brookhaven, Berkeley, MIT and AMOLF have all been unsuccessful. OPVs using PolyTc as a donor and fullerenes as acceptors can be made with decent power conversion efficiencies. However, MFE measurements show that these devices are just working via singlet charge extraction.

Combining the energy sink motif from Chapter 4, I also made an alternating tetracene-anthracene copolymer (PolyTA) and took that with me to Amsterdam to try to make iSF OPVs at AMOLF in Bruno Ehrler's lab. I also brought model oligomers of these compounds, a directly linked tetracene dimer BT0, and a tetracene dimer spaced with an anthracene bridge TAT. None of these compounds exhibited triplet charge extraction in devices, either as OPVs with fullerenes, or when interfaced with PbS nanocrystals. In both cases it seems that most of the photocurrent is coming from the non-iSF material.

From this, I believe there are a couple factors that need to be addressed before PolyTc or any other iSF material can be applied in devices. First, with all the large TIPS groups in an amorphous material, it is a fair assumption that the mobility of the iSF materials when spincast is quite low. Mobility measurements could be done, ideally in a field effect transistor, to determine spin coating conditions that produce films with reasonable mobilities. Synthetic modifications could also be made to the TIPS sidechains to increase mobility, but that poses a synthetic challenge because the polymerization of PolyTc already seems to be limited by solubility issues. Carefully engineering a comonomer to impart flexibility and therefore solubility to the polymer chain could be a possibility.

Another issue with these materials is the fact that they are generating tightly bound triplet pairs. PolyTA was synthesized to get around that, but they are still likely a problem, especially in these relatively short oligomer chains that we have in hand. This relates to the last issue, which is

the exact energetics of the triplets generated. Endothermic singlet fission is consistently invoked for tetracene based materials, but does not make sense to me in the context of PolyTc. It is said that endothermic SF can occur because of an entropic gain, going from one exciton to two. But we have shown that iSF readily occurs in PolyTc, even in dilute solution where there are no interchain interactions. In this case we generate tightly bound triplet pairs which do not dissociate before decaying to the ground state, in which case there is no energy gain to be had from entropy. UV-Vis also shows that the S_1 state of PolyTc is redshifted by about 0.15 eV relative to TIPS-Tc. This would mean that even though SF in PolyTc is about 0.3 eV endothermic, it occurs faster than SF in tetracene crystals. To me this is more indicative of a change in triplet energy for PolyTc which allows iSF to occur so rapidly. More accurate measurements of triplet energy need to be done, which will allow device structures to be designed more rationally.

2.23 References

(1) Pun, A. B.; Sanders, S. N.; Kumarasamy, E.; Sfeir, M. Y.; Congreve, D. N.; Campos, L. M. Triplet Harvesting from Intramolecular Singlet Fission in Polytetracene. *Adv. Mater.* **2017**, *29* (41), 1701416.

(2) Sariciftci, N. S.; Smilowitz, L.; Heeger, A. J.; Wudl, F. Photoinduced Electron Transfer from a Conducting Polymer to Buckminsterfullerene. *Science* **1992**, *258* (5087), 1474 LP.

(3) Yu, G.; Gao, J.; Hummelen, J. C.; Wudl, F.; Heeger, A. J. Polymer Photovoltaic Cells: Enhanced Efficiencies via a Network of Internal Donor-Acceptor Heterojunctions. *Science* **1995**, *270* (5243), 1789 LP.

(4) He, Z.; Xiao, B.; Liu, F.; Wu, H.; Yang, Y.; Xiao, S.; Wang, C.; Russell, T. P.; Cao, Y. Single-Junction Polymer Solar Cells with High Efficiency and Photovoltage. *Nat. Photonics* **2015**, *9*, 174.

(5) Nian, L.; Zhang, W.; Zhu, N.; Liu, L.; Xie, Z.; Wu, H.; Würthner, F.; Ma, Y. Photoconductive Cathode Interlayer for Highly Efficient Inverted Polymer Solar Cells. *J. Am. Chem. Soc.* **2015**, *137* (22), 6995.

(6) Huang, J.; Carpenter, J. H.; Li, C.-Z.; Yu, J.-S.; Ade, H.; Jen, A. K.-Y. Highly Efficient Organic Solar Cells with Improved Vertical Donor–Acceptor Compositional Gradient Via an Inverted Off-Center Spinning Method. *Adv. Mater.* **2016**, *28* (5), 967.

(7) Green, M. A.; Emery, K.; Hishikawa, Y.; Warta, W.; Dunlop, E. D. Solar Cell Efficiency Tables (Version 47). *Prog. Photovolt. Res. Appl.* **2016**, *24* (1), 3.

(8) Shockley, W.; Queisser, H. J. Detailed Balance Limit of Efficiency of P-n Junction Solar

Cells. *J. Appl. Phys.* **1961**, *32* (3), 510.
(9) Green, M. A. Third Generation Photovoltaics: Ultra-High Conversion Efficiency at Low Cost. *Prog. Photovolt. Res. Appl.* **2001**, *9* (2), 123.
(10) Hanna, M. C.; Nozik, A. J. Solar Conversion Efficiency of Photovoltaic and Photoelectrolysis Cells with Carrier Multiplication Absorbers. *J. Appl. Phys.* **2006**, *100* (7).
(11) Singh, S.; Jones, W. J.; Siebrand, W.; Stoicheff, B. P.; Schneider, W. G. Laser Generation of Excitons and Fluorescence in Anthracene Crystals. *J. Chem. Phys.* **1965**, *42* (1), 330.
(12) Yost, S. R.; Lee, J.; Wilson, M. W. B.; Wu, T.; McMahon, D. P.; Parkhurst, R. R.; Thompson, N. J.; Congreve, D. N.; Rao, A.; Johnson, K.; et al. A Transferable Model for Singlet-Fission Kinetics. *Nat. Chem.* **2014**, *6* (6), 492.
(13) Walker, B. J.; Musser, A. J.; Beljonne, D.; Friend, R. H. Singlet Exciton Fission in Solution. *Nat. Chem.* **2013**, *5* (12), 1019.
(14) Johnson, J. C.; Nozik, A. J.; Michl, J. The Role of Chromophore Coupling in Singlet Fission. *Acc. Chem. Res.* **2013**, *46* (6), 1290.
(15) Schrauben, J. N.; Ryerson, J. L.; Michl, J.; Johnson, J. C. Mechanism of Singlet Fission in Thin Films of 1,3-Diphenylisobenzofuran. *J. Am. Chem. Soc.* **2014**, *136* (20), 7363.
(16) Lukman, S.; Musser, A. J.; Chen, K.; Athanasopoulos, S.; Yong, C. K.; Zeng, Z.; Ye, Q.; Chi, C.; Hodgkiss, J. M.; Wu, J.; et al. Tuneable Singlet Exciton Fission and Triplet–Triplet Annihilation in an Orthogonal Pentacene Dimer. *Adv. Funct. Mater.* **2015**, *25* (34), 5452.
(17) Zirzlmeier, J.; Lehnherr, D.; Coto, P. B.; Chernick, E. T.; Casillas, R.; Basel, B. S.; Thoss, M.; Tykwinski, R. R.; Guldi, D. M. Singlet Fission in Pentacene Dimers. *Proc. Natl. Acad. Sci.* **2015**, *112* (17), 5325.
(18) Korovina, N. V; Das, S.; Nett, Z.; Feng, X.; Joy, J.; Haiges, R.; Krylov, A. I.; Bradforth, S. E.; Thompson, M. E. Singlet Fission in a Covalently Linked Cofacial Alkynyltetracene Dimer. *J. Am. Chem. Soc.* **2016**, *138* (2), 617.
(19) Busby, E.; Xia, J.; Wu, Q.; Low, J. Z.; Song, R.; Miller, J. R.; Zhu, X.-Y.; Campos, L. M.; Sfeir, M. Y. A Design Strategy for Intramolecular Singlet Fission Mediated by Charge-Transfer States in Donor–acceptor Organic Materials. *Nat. Mater.* **2015**, *14* (4), 426.
(20) Sanders, S. N.; Kumarasamy, E.; Pun, A. B.; Steigerwald, M. L.; Sfeir, M. Y.; Campos, L. M. Intramolecular Singlet Fission in Oligoacene Heterodimers. *Angew. Chem. Int. Ed.* **2016**, *55* (10), 3373.
(21) Sanders, S. N.; Kumarasamy, E.; Pun, A. B.; Trinh, M. T.; Choi, B.; Xia, J.; Taffet, E. J.; Low, J. Z.; Miller, J. R.; Roy, X.; et al. Quantitative Intramolecular Singlet Fission in Bipentacenes. *J. Am. Chem. Soc.* **2015**, *137* (28), 8965.
(22) Lee, J.; Jadhav, P.; Reusswig, P. D.; Yost, S. R.; Thompson, N. J.; Congreve, D. N.; Hontz, E.; Van Voorhis, T.; Baldo, M. A. Singlet Exciton Fission Photovoltaics. *Acc. Chem. Res.* **2013**, *46* (6), 1300.
(23) Congreve, D. N.; Lee, J.; Thompson, N. J.; Hontz, E.; Yost, S. R.; Reusswig, P. D.; Bahlke, M. E.; Reineke, S.; Van Voorhis, T.; Baldo, M. A. External Quantum Efficiency Above 100% in a Singlet-Exciton-Fission-Based Organic Photovoltaic Cell. *Science* **2013**, *340* (6130), 334.
(24) Ehrler, B.; Walker, B. J.; Böhm, M. L.; Wilson, M. W. B.; Vaynzof, Y.; Friend, R. H.; Greenham, N. C. In Situ Measurement of Exciton Energy in Hybrid Singlet-Fission Solar Cells. *Nat. Commun.* **2012**, *3*, 1019.

(25) Yang, L.; Tabachnyk, M.; Bayliss, S. L.; Böhm, M. L.; Broch, K.; Greenham, N. C.; Friend, R. H.; Ehrler, B. Solution-Processable Singlet Fission Photovoltaic Devices. *Nano Lett.* **2015**, *15* (1), 354.
(26) Kawata, S.; Pu, Y.-J.; Saito, A.; Kurashige, Y.; Beppu, T.; Katagiri, H.; Hada, M.; Kido, J. Singlet Fission of Non-Polycyclic Aromatic Molecules in Organic Photovoltaics. *Adv. Mater.* **2016**, *28* (8), 1585.
(27) Wilson, M. W. B.; Rao, A.; Ehrler, B.; Friend, R. H. Singlet Exciton Fission in Polycrystalline Pentacene: From Photophysics toward Devices. *Acc. Chem. Res.* **2013**, *46* (6), 1330.
(28) Lee, J.; Jadhav, P.; Baldo, M. A. High Efficiency Organic Multilayer Photodetectors Based on Singlet Exciton Fission. *Appl. Phys. Lett.* **2009**, *95* (3), 3.
(29) Ehrler, B.; Musselman, K. P.; Böhm, M. L.; Friend, R. H.; Greenham, N. C. Hybrid Pentacene/a-Silicon Solar Cells Utilizing Multiple Carrier Generation via Singlet Exciton Fission. *Appl. Phys. Lett.* **2012**, *101* (15), 103.
(30) Reusswig, P. D.; Congreve, D. N.; Thompson, N. J.; Baldo, M. A. Enhanced External Quantum Efficiency in an Organic Photovoltaic Cell via Singlet Fission Exciton Sensitizer. *Appl. Phys. Lett.* **2012**, *101* (11), 113304.
(31) Pazos-Outón, L. M.; Lee, J. M.; Futscher, M. H.; Kirch, A.; Tabachnyk, M.; Friend, R. H.; Ehrler, B. A Silicon–Singlet Fission Tandem Solar Cell Exceeding 100% External Quantum Efficiency with High Spectral Stability. *ACS Energy Lett.* **2017**, *2* (2), 476.
(32) Thompson, N. J.; Congreve, D. N.; Goldberg, D.; Menon, V. M.; Baldo, M. A. Slow Light Enhanced Singlet Exciton Fission Solar Cells with a 126% Yield of Electrons per Photon. *Appl. Phys. Lett.* **2013**, *103* (26), 263302.
(33) Roberts, S. T.; McAnally, R. E.; Mastron, J. N.; Webber, D. H.; Whited, M. T.; Brutchey, R. L.; Thompson, M. E.; Bradforth, S. E. Efficient Singlet Fission Discovered in a Disordered Acene Film. *J. Am. Chem. Soc.* **2012**, *134* (14), 6388.
(34) Treat, N. D.; Campos, L. M.; Dimitriou, M. D.; Ma, B.; Chabinyc, M. L.; Hawker, C. J. Nanostructured Hybrid Solar Cells: Dependence of the Open Circuit Voltage on the Interfacial Composition. *Adv. Mater.* **2010**, *22* (44), 4982.
(35) Tayebjee, M. J. Y.; Sanders, S. N.; Kumarasamy, E.; Campos, L. M.; Sfeir, M. Y.; McCamey, D. R. Quintet Multiexciton Dynamics in Singlet Fission. *Nat. Phys.* **2017**, *13* (2), 182.
(36) Sanders, S. N.; Kumarasamy, E.; Pun, A. B.; Appavoo, K.; Steigerwald, M. L.; Campos, L. M.; Sfeir, M. Y. Exciton Correlations in Intramolecular Singlet Fission. *J. Am. Chem. Soc.* **2016**, *138* (23), 7289.
(37) Sanders, S. N.; Kumarasamy, E.; Pun, A. B.; Steigerwald, M. L.; Sfeir, M. Y.; Campos, L. M. Singlet Fission in Polypentacene. *Chem* **2017**, *1* (3), 505.
(38) Zeng, T.; Hoffmann, R.; Ananth, N. The Low-Lying Electronic States of Pentacene and Their Roles in Singlet Fission. *J. Am. Chem. Soc.* **2014**, *136* (15), 5755.
(39) Chan, W.-L.; Ligges, M.; Jailaubekov, A.; Kaake, L.; Miaja-Avila, L.; Zhu, X.-Y. Observing the Multiexciton State in Singlet Fission and Ensuing Ultrafast Multielectron Transfer. *Science* **2011**, *334* (6062), 1541 LP.
(40) Chan, W.-L.; Berkelbach, T. C.; Provorse, M. R.; Monahan, N. R.; Tritsch, J. R.; Hybertsen, M. S.; Reichman, D. R.; Gao, J.; Zhu, X.-Y. The Quantum Coherent Mechanism for Singlet Fission: Experiment and Theory. *Acc. Chem. Res.* **2013**, *46* (6), 1321.

(41) Jadhav, P. J.; Mohanty, A.; Sussman, J.; Lee, J.; Baldo, M. A. Singlet Exciton Fission in Nanostructured Organic Solar Cells. *Nano Lett.* **2011**, *11* (4), 1495.
(42) Chan, W.-L.; Ligges, M.; Zhu, X.-Y. The Energy Barrier in Singlet Fission Can Be Overcome through Coherent Coupling and Entropic Gain. *Nat. Chem.* **2012**, *4*, 840.
(43) Wilson, M. W. B.; Rao, A.; Johnson, K.; G??linas, S.; Di Pietro, R.; Clark, J.; Friend, R. H. Temperature-Independent Singlet Exciton Fission in Tetracene. *J. Am. Chem. Soc.* **2013**, *135* (44), 16680.
(44) Stern, H. L.; Musser, A. J.; Gelinas, S.; Parkinson, P.; Herz, L. M.; Bruzek, M. J.; Anthony, J.; Friend, R. H.; Walker, B. J. Identification of a Triplet Pair Intermediate in Singlet Exciton Fission in Solution. *Proc. Natl. Acad. Sci.* **2015**, *112* (25), 7656.
(45) Burdett, J. J.; Müller, A. M.; Gosztola, D.; Bardeen, C. J. Excited State Dynamics in Solid and Monomeric Tetracene: The Roles of Superradiance and Exciton Fission. *J. Chem. Phys.* **2010**, *133* (14), 144506.
(46) Margulies, E. A.; Wu, Y. L.; Gawel, P.; Miller, S. A.; Shoer, L. E.; Schaller, R. D.; Diederich, F.; Wasielewski, M. R. Sub-Picosecond Singlet Exciton Fission in Cyano-Substituted Diaryltetracenes. *Angew. Chem. Int. Ed.* **2015**, *54* (30), 8679.
(47) Wu, T. C.; Thompson, N. J.; Congreve, D. N.; Hontz, E.; Yost, S. R.; Van Voorhis, T.; Baldo, M. A. Singlet Fission Efficiency in Tetracene-Based Organic Solar Cells. *Appl. Phys. Lett.* **2014**, *104* (19), 193901.
(48) Smith, M. B.; Michl, J. Singlet Fission. *Chem. Rev.* **2010**, *110* (11), 6891.
(49) Stern, H. L.; Cheminal, A.; Yost, S. R.; Broch, K.; Bayliss, S. L.; Chen, K.; Tabachnyk, M.; Thorley, K.; Greenham, N.; Hodgkiss, J. M.; et al. Vibronically Coherent Ultrafast Triplet-Pair Formation and Subsequent Thermally Activated Dissociation Control Efficient Endothermic Singlet Fission. *Nat. Chem.* **2017**, *9*, 1205.
(50) Chu, C.-W.; Shao, Y.; Shrotriya, V.; Yang, Y. Efficient Photovoltaic Energy Conversion in Tetracene-C60 Based Heterojunctions. *Appl. Phys. Lett.* **2005**, *86* (24), 243506.
(51) Müller, A. M.; Avlasevich, Y. S.; Müllen, K.; Bardeen, C. J. Evidence for Exciton Fission and Fusion in a Covalently Linked Tetracene Dimer. *Chem. Phys. Lett.* **2006**, *421* (4), 518.
(52) Northrop, B. H.; Houk, K. N.; Maliakal, A. Photostability of Pentacene and 6,13-Disubstituted Pentacene Derivatives: A Theoretical and Experimental Mechanistic Study. *Photochem. Photobiol. Sci.* **2008**, *7* (12), 1463.
(53) Kumarasamy, E.; Sanders, S. N.; Pun, A. B.; Vaselabadi, S. A.; Low, J. Z.; Sfeir, M. Y.; Steigerwald, M. L.; Stein, G. E.; Campos, L. M. Properties of Poly- and Oligopentacenes Synthesized from Modular Building Blocks. *Macromolecules* **2016**, *49* (4), 1279.
(54) Chen, J.; Subramanian, S.; Parkin, S. R.; Siegler, M.; Gallup, K.; Haughn, C.; Martin, D. C.; Anthony, J. E. The Influence of Side Chains on the Structures and Properties of Functionalized Pentacenes. *J. Mater. Chem.* **2008**, *18* (17), 1961.
(55) Fuemmeler, E. G.; Sanders, S. N.; Pun, A. B.; Kumarasamy, E.; Zeng, T.; Miyata, K.; Steigerwald, M. L.; Zhu, X.-Y.; Sfeir, M. Y.; Campos, L. M.; et al. A Direct Mechanism of Ultrafast Intramolecular Singlet Fission in Pentacene Dimers. *ACS Cent. Sci.* **2016**, *2* (5), 316.
(56) Tong, Z.; Yan, W.; Zhi, G.; Justin, J.; Libai, H. Two Birds with One Stone: Tailoring Singlet Fission for Both Triplet Yield and Exciton Diffusion Length. *Adv. Mater.* **2016**, *28* (34), 7539.
(57) Wan, Y.; Guo, Z.; Zhu, T.; Yan, S.; Johnson, J.; Huang, L. Cooperative Singlet and

Triplet Exciton Transport in Tetracene Crystals Visualized by Ultrafast Microscopy. *Nat. Chem.* **2015**, *7*, 785.
(58) Burdett, J. J.; Bardeen, C. J. The Dynamics of Singlet Fission in Crystalline Tetracene and Covalent Analogs. *Acc. Chem. Res.* **2013**, *46* (6), 1312.
(59) Tayebjee, M. J. Y.; Clady, R. G. C. R.; Schmidt, T. W. The Exciton Dynamics in Tetracene Thin Films. *Phys. Chem. Chem. Phys.* **2013**, *15* (35), 14797.
(60) Spano, F. C. The Spectral Signatures of Frenkel Polarons in H- and J-Aggregates. *Acc. Chem. Res.* **2010**, *43* (3), 429.
(61) Spano, F. C. Modeling Disorder in Polymer Aggregates: The Optical Spectroscopy of Regioregular Poly(3-Hexylthiophene) Thin Films. *J. Chem. Phys.* **2005**, *122* (23), 234701.
(62) Singh-Rachford, T. N.; Castellano, F. N. Pd(II) Phthalocyanine-Sensitized Triplet−Triplet Annihilation from Rubrene. *J. Phys. Chem. A* **2008**, *112* (16), 3550.
(63) Mauck, C. M.; Hartnett, P. E.; Margulies, E. A.; Ma, L.; Miller, C. E.; Schatz, G. C.; Marks, T. J.; Wasielewski, M. R. Singlet Fission via an Excimer-Like Intermediate in 3,6-Bis(Thiophen-2-Yl)Diketopyrrolopyrrole Derivatives. *J. Am. Chem. Soc.* **2016**, *138* (36), 11749.
(64) Pensack, R. D.; Tilley, A. J.; Parkin, S. R.; Lee, T. S.; Payne, M. M.; Gao, D.; Jahnke, A. A.; Oblinsky, D. G.; Li, P.-F.; Anthony, J. E.; et al. Exciton Delocalization Drives Rapid Singlet Fission in Nanoparticles of Acene Derivatives. *J. Am. Chem. Soc.* **2015**, *137* (21), 6790.
(65) Busby, E.; Xia, J.; Low, J. Z.; Wu, Q.; Hoy, J.; Campos, L. M.; Sfeir, M. Y. Fast Singlet Exciton Decay in Push-Pull Molecules Containing Oxidized Thiophenes. *J. Phys. Chem. B* **2015**, *119* (24), 7644.
(66) Jadhav, P. J.; Brown, P. R.; Thompson, N.; Wunsch, B.; Mohanty, A.; Yost, S. R.; Hontz, E.; Van Voorhis, T.; Bawendi, M. G.; Bulović, V.; et al. Triplet Exciton Dissociation in Singlet Exciton Fission Photovoltaics. *Adv. Mater.* **2012**, *24* (46), 6169.
(67) Sun, Y.; Seo, J. H.; Takacs, C. J.; Seifter, J.; Heeger, A. J. Inverted Polymer Solar Cells Integrated with a Low-Temperature-Annealed Sol-Gel-Derived ZnO Film as an Electron Transport Layer. *Adv. Mater.* **2011**, *23* (14), 1679.
(68) Ren, J.; Lu, L.; Xu, J.; Yu, T.; Zeng, B.-B. Selective Oxidation of 1-Tetralones to 1,2-Naphthoquinones with IBX and to 1,4-Naphthoquinones with Oxone® and 2-Iodobenzoic Acid. *Synthesis (Stuttg).* **2015**, *47* (15), 2270.

Chapter 3: Pentacene-Iron-Oxo Cluster Hybrids

3.1 Preface

This chapter is based on manuscript entitled "Distinct Properties of the Triplet Pair State from Singlet Fission" by M. Tuanh Trinh, Andrew Pinkard, Andrew B. Pun, Samuel N. Sanders, Elango Kumarasamy, Matthew Y. Sfeir, Luis M. Campos, Xavier Roy, and Xiao-Yang Zhu published in Science Advances.[1]

I synthesized and characterized all the materials studied along with Andrew Pinkard with input from Elango Kumarasamy. M. Tuanh Trinh carried out transient absorption measurements and analysis with input from Samuel N. Sanders and Matthew Y. Sfeir. Equal contributions to this paper were made by M. Tuanh Trinh, Andrew Pinkard, and myself.

3.2 Introduction

Singlet fission is a many-body photophysical process in molecules where the photoexcited singlet (S_1) splits into two triplets (2 x T_1) with spin conservation.[2,3] Since its discovery, efficient singlet fission has been reported mostly for solids and aggregates of conjugated molecules,[2,3] and a dominant mechanistic picture is the molecular dimer model[4,5]

$$S_0 + S_1 \leftrightarrows {}^1(TT) \leftrightarrows 2T_1$$

where S_0 is the ground state and the intermediate ^{1}(TT) is the correlated triplet pair with both singlet spin and double-excitation characters. Despite its prevalent use, Monahan et al.[6,7] pointed out the inadequacy of the dimer model in describing inherently delocalized excitons in the solid state. Exciton delocalization has been cited as an important driving force for singlet fission.[8–11] This problem is circumvented in recent demonstrations of efficient singlet fission in single molecules (particularly in dimers of acenes[12–17]) that allow for accurate application of the dimer model and for closely connecting experiment with theory.[18] The isolation of the transient ^{1}(TT)

state in a single molecule leads to a much longer lifetime than that in the condensed phase, thus allowing spectroscopic characterization of this ambiguous and poorly understood state. This is exemplified in the detection by electron spin resonance spectroscopy in pentacene dimers of the quintet state, ^{5}(TT), which is mixed with the ^{1}(TT) state as predicted by the spin Hamiltonian.[19]

The ^{1}(TT) state is a singlet excited state with double-excitation characters and differs from 2 x T_1 not only by the electronic and spin entangled nature of the former but also by the presence of orbital overlap, which changes its excitation energy from the sum of two triplet energies. Scholes[20] recently clarified some persistent confusion on the ^{1}(TT) state in theoretical descriptions. The energetic difference between the correlated triplet pair state and two individual triplets, that is, the triplet pair binding energy, can be as large as 1 eV, as is known for the excited states of oligoenes,[21–23] including carotenoids,[24] where the tightly bound triplet pair has been called the "dark" S1 state serving as a sink for nonradiative recombination and a less tightly bound triplet pair (S*) has been associated with singlet fission.[16,25–27] In contrast, in prototypical model systems of pentacene or tetracene dimers (both covalent and van der Waals), computational analysis predicted little, if any, triplet pair binding energy.[18,28–33] However, a recent finding of similar ^{1}(TT) lifetimes in polypentacene and bipentacene indicates that the triplet pair does not dissociate even in a long conjugated chain,[34] suggesting that the correlated triplet pair state is more strongly bound than previously thought.

A major obstacle to a clear understanding of the ^{1}(TT) state is the lack of spectroscopic signatures from experiments. Zhu and co-workers applied time-resolved two-photon photoemission spectroscopy to quantitatively determine the energetic position of the ^{1}(TT) state from its ionization potential (IP) in crystalline pentacene,[35] tetracene,[11] and hexacene.[7] This approach is unambiguous only for hexacene[7] where the ^{1}(TT) state is energetically well

separated from S_1 but is difficult for other singlet fission systems where the ^{1}(TT) states are in close energetic resonance with S_1. The most widely used technique to probe singlet fission has been transient absorption (TA) spectroscopy, but most studies to date have only identified spectral features assigned to S_1 and T_1 states, and there has been little explanation as to why these TA peaks nearly always overlap.[13–17,36,37] Exceptions to this prevalent practice can be found in the recent work of Sanders et al.[12] who found, in pentacene dimers, an excited-state absorption (ESA) peak at ~690 nm whose magnitude is strongly correlated with the strength of intertriplet electronic coupling and in the work of Pensack et al.[38] who observed near-infrared (IR) (1200 to 1400 nm) ESA in pentacene aggregates assigned to ^{1}(TT) but not to the triplet pair labeled ^{1}(T…T), which has lost electronic coherence but retained spin coherence. These two examples reveal the presence of spectroscopic signatures for the ^{1}(TT) state in TA, but the origins of these transitions and their relationships to the energetics of the 1(TT) state remain unknown.

The distinct electronic structure of the ^{1}(TT) state should be reflected not only in its spectroscopic signature but also in its chemical and physical properties. The oft-cited motivation for nearly every recent paper on this subject has been the potential "usefulness" of singlet fission to solar energy conversion. The basic argument was put forward initially by Dexter[39] for the sensitization of conventional solar cells by singlet fission chromophores in 1979, but a more recent paper by Hanna and Nozik[40] on using singlet fission to increase the solar cell efficiency above the Shockley-Queisser limit really energized the field. A number of research groups have explored the harvesting of triplet pairs from intermolecular singlet fission using solid interfaces between a singlet fission material and an electron or triplet acceptor material.[35,41–44] These efforts have also led to the successful demonstration of singlet fission–based solar cells with quantum efficiencies exceeding 100%.[45] The recent demonstration of efficient intramolecular singlet

fission in single molecules[12–17,37] opens the door to new opportunities for the realization of singlet fission–sensitized solar cells.[46] A more exciting opportunity is the potential for the harvesting of two electron-hole pairs for photocatalysis, for example, by coupling a singlet fission molecule to a molecular or cluster-based catalytic center[47] to enable two-electron redox reactions. Unlike intermolecular singlet fission in the solid state in which electronic delocalization[6,48] and entropy[11] are driving forces to split the ^{1}(TT) state to two electronically decoupled triplets (which can nonetheless retain spin coherence) on ultrafast time scales,[20] the confinement in a molecular dimer or oligomer traps the two triplets in the ^{1}(TT) state in a single molecule.[19,34] Thus, instead of individual triplets at solid-state interfaces, the harvesting of triplets in intramolecular singlet fission would likely come from the ^{1}(TT) state. However, the two triplets in the ^{1}(TT) state from intramolecular singlet fission can be tightly bound, and charge or energy transfer from each triplet may be inhibited.

Here, we use triisopropylsilylethynyl-functionalized pentacene (TIPS-Pc) dimers, each coupled at the 2-position without or with a phenylene spacer, BP0 or BP1 (Figure 3.1),[12] as well as pentacene dimers with different dihedral angles,[18] as model systems to quantitatively probe the nature of the tightly bound ^{1}(TT) state from the ESA spectra. Molecules of this type allow for the systematic tuning of electronic coupling between the two pentacene units and between the S_1 and the ^{1}(TT) states, as reflected in the singlet fission time constants of τ_{SF} = 0.76, 20, and 220 ps and triplet recombination time constants of τ_{AN} = 0.45, 16.5, and 270 ns for dimers with zero, one, and two phenylene spacers (BP0, BP1, and BP2), respectively, obtained from an analysis of TA spectra in the visible region.[12] Here, we focus on the distinct ESA peak in the near-IR region ($h\nu \sim 1$ eV), which is a signature of the ^{1}(TT) state from singlet fission in BP0. Its intensity diminishes as the intertriplet electronic coupling is lowered in BP1 or significantly decreases in

bipentacene with different dihedral angles.[18] The ESA peak of ^{1}(TT) in BP0 closely resembles that of the S1 state in the near-IR region; both show vibronic progressions of the aromatic ring breathing mode and can be assigned to the ^{1}(TT)→S_n and S_1→$S_{n'}$ transitions, respectively. This finding unambiguously establishes that ^{1}(TT) is spectroscopically distinct from 2 x T_1, and such a spectroscopic signature enables one to quantitatively follow the dynamics of this critical intermediate in singlet fission.

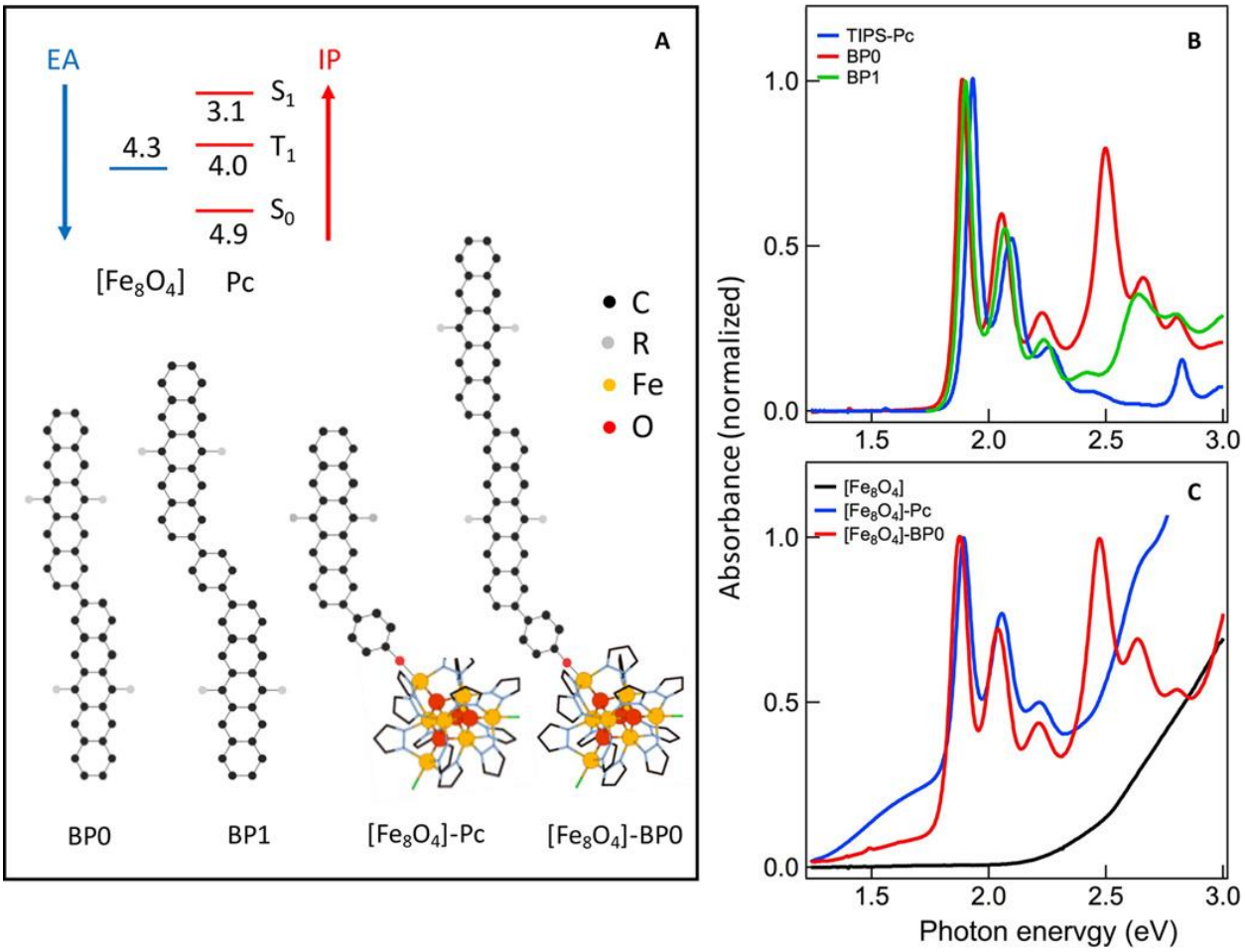

Figure 3.1 The Model Systems for Intramolecular Singlet Fission and Triplet Harvesting A) Schematics of BP0, BP1, $[Fe_8O_4]$-Pc, and $[Fe_8O_4]$-BP0. R = (triisopropylsilyl)ethynyl (TIPS) for $[Fe_8O_4]$-Pc and (n-octyldiisopropyl)silylethynyl (NODIPS) for $[Fe_8O_4]$-BP0 and $[Fe_8O_4]$-BP1. The inset shows estimated IP and EA (electron affinity) from electrochemical oxidation/reduction potentials of $[Fe_8O_4]$ and TIPS-pentacene. B and C) Optical absorption spectra of B) TIPS-Pc, BP0, and BP1 in toluene and C) $[Fe_8O_4]$, $[Fe_8O_4]$-Pc, and $[Fe_8O_4]$-BP0 in dichloromethane solutions.

To establish the distinct chemical properties of the ^{1}(TT) state, we use the redox-active molecular cluster $Fe_8O_4pz_{12}C_{l4}$ (pz, pyrazolate), which we label [Fe_8O_4], as an electron acceptor[49,50] and tether BP_0 to [Fe_8O_4] through a Fe-phenoxide bond (schematically illustrated in Figure 3.1A). As a control, we replace the pentacene dimer BP0 with a pentacene monomer (Pc). Note that the formation of the Fe-phenoxide bond in both [Fe_8O_4]-Pc and [Fe_8O_4]-BP0 introduces a low-energy absorption tail (~1.3 to 1.8 eV; Figure 3.1C). This spectral feature has been assigned to the phenolate-to-Fe(III) ligand-to-metal charge transfer (LMCT) transition[51] but may also have contributions from pentacene-to-[Fe_8O_4] charge transfer (CT) transitions. We show that electron transfer from pentacene to [Fe_8O_4] occurs efficiently from an individual T_1 state in pentacene ([Fe_8O_4]-Pc), but not from the tightly bound triplet pair state in [Fe_8O_4]-BP0. This finding establishes that the chemical property of the ^{1}(TT) state is distinctly different from that of an individual triplet and suggests that reducing intertriplet electronic coupling in ^{1}(TT) might be needed for the harvesting of triplets from intramolecular singlet fission.

3.3 Spectroscopic Signature of the ^{1}(TT) State

We use TA spectroscopy to probe singlet fission in BP0 and BP1.[12] We excite the S_1 state of each pentacene dimer at $h\nu_1$ = 2.1 eV and probe the subsequent dynamics from the TA of a white-light continuum (Figure 3.2). Figure 3.2A and B shows TA spectra at selected pump-probe delays, Δt = 0.1 ps (red), 10 ps (purple), and 100 ps (blue) for BP0. The visible parts of the TA spectra have been discussed extensively before, and the broad positive TA features at $\Delta t < 1$ ps and $\Delta t > 2$ ps are assigned to the ESA of S_1 and T_1, respectively.[12] The latter is confirmed by the ESA spectrum of T_1 obtained from sensitization (black). On the basis of the calculated triplet energies in pentacene (T3 and T4 are close in energy and are not distinguished here),[52] we assign the ESA peak at 2.42 eV to the $T_1 \rightarrow T_3$ transition. For the triplet pair from singlet fission, this

transition corresponds to $^1(T_1T_1) \rightarrow ^1(T_1T_3)$. In each case, the ESA transition also shows vibronic progression ($h\nu_{vib}$ ~ 0.17 eV) similar to those in the ground-state absorption spectrum.[12] The singlet decay and triplet formation can be clearly seen from kinetic profiles at probe photon energies of $h\nu_2$ = 2.13 eV (gray) and 2.42 eV (green), respectively (Figure 3.2C), with τ_{SF} = 0.7 ps (11); note that there is an overlapping contribution to ESA signal at $h\nu_2$ = 2.42 eV from the singlet at short time scales. The two triplets confined to the pentacene dimer can be assigned to ^{1}(TT), which decays on the time scale of τ_{TT1} = 450 ps (see the green curve at long pump-probe delays in Figure 3.2C), much shorter than the 30-μs lifetime of an individual triplet.[12] Here, we focus on the near-IR region, which provides key spectroscopic insight into the triplet pair state.

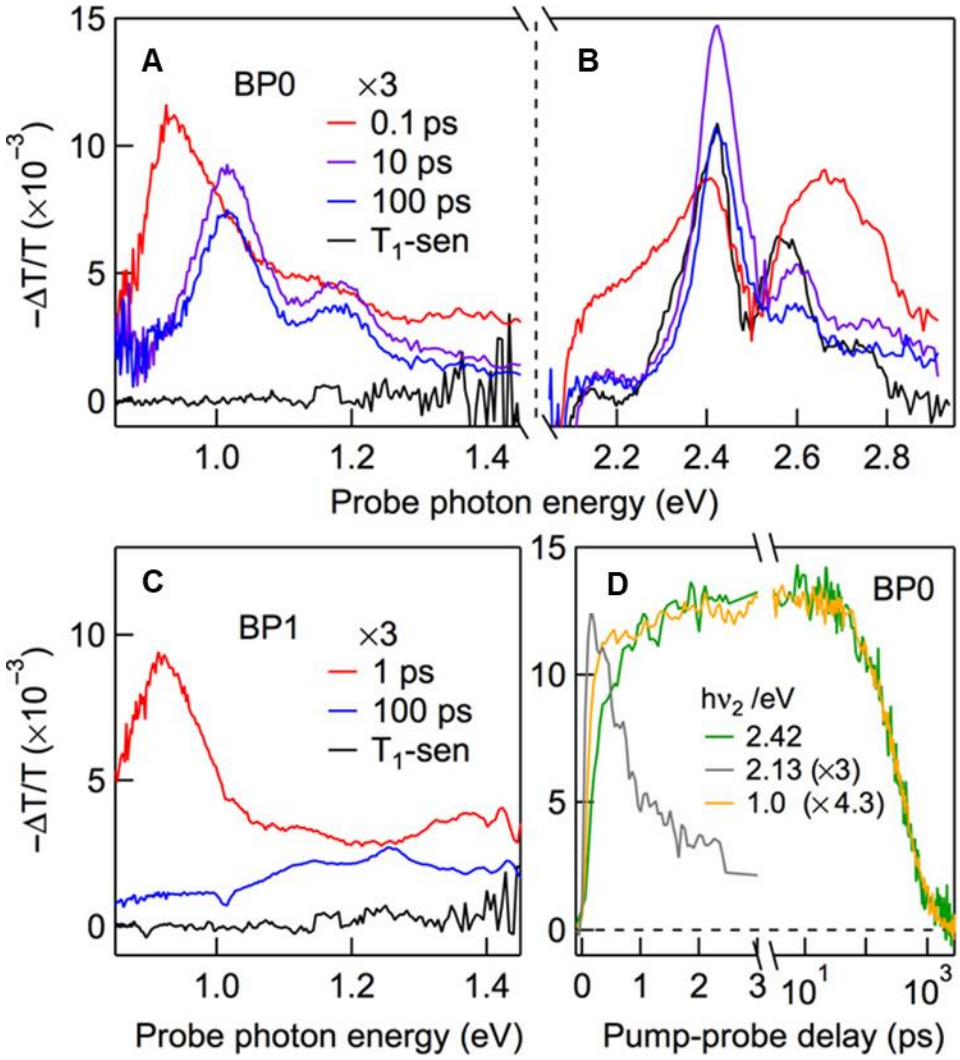

Figure 3.2 TA in the Near-IR and Visible Regions Reveal Singlet and Triplet Characters of ^{1}(TT) TA spectra in A) the near-IR and B) the visible regions for BP0 at different pump-probe delays, Δt = 0.1 ps (red), 10 ps (purple), and 100 ps (blue), following excitation at time zero by $h\nu_1$ = 2.1 eV. The triplet TA spectrum from sensitization (black) is also shown in A) and B). C) Kinetic profiles from TA spectra for BP0 at the indicated probe photon energies. (D) TA spectra at Δt = 1 ps (red) and 100 ps (blue) for BP1 following excitation at time zero by $h\nu_1$ = 2.1 eV. The corresponding triplet spectrum (black) from sensitization is also shown.

There is a distinct ESA peak at 0.922 ± 0.005 eV when the singlet dominates at Δt = 0.1 ps (red) (Figure 3.2A); this peak is also accompanied by a vibronic feature on the higher energy side, with $h\nu_{vib}$ ~ 0.17 eV, similar to the vibronic progressions of $S_0 \rightarrow S_1$, $T_1 \rightarrow T_n$, and $^1(T_1T_1) \rightarrow 1(T_1T_n)$ discussed above. This ESA is assigned to an $S_1 \rightarrow S_{n'}$ transition, with transition energy close to the $S_1 \rightarrow S_2$ transition for a single pentacene molecule. In the absorption spectrum of TIPS-Pc in Figure 3.1B (blue), there is a weakly allowed $S_0 \rightarrow S_2$ peak at 2.82 eV, in agreement with the two-photon absorption spectrum of the same molecule.[53] Given the $S_0 \rightarrow S_1$ peak at 1.93 eV (blue spectrum in Figure 3.1B), we obtain the $S_1 \rightarrow S_2$ transition energy at 0.89 eV. In conjugated bipentacene dimers, the singlet states are described by linear combinations of two localized states on each pentacene chromophore.[18] Although both symmetric and antisymmetric linear combinations are possible, the optically bright S_1 state in BP0 is of odd parity (u). Therefore, excited state transitions must occur to $S_{n'}$ states of even parity (g). We assign the 0.92-eV peak to a transition from S_1 to the symmetric linear combination of the monomer S2 states.

At longer pump-probe delays, for example, Δt = 10 ps (purple) or 100 ps (blue), when there is only the triplet pair state, the ESA spectrum blue-shifts to 1.012 ± 0.005 eV and the vibronic signature becomes better resolved. This ESA peak does not originate from a $T_1 \rightarrow T_n$ transition as it is completely absent in the triplet absorption spectrum (black) from sensitization. On the basis of the similarity of this ESA peak to that of the $S_1 \rightarrow S_{n'}$ transition at early times, we

assign the former to a $^1(TT) \rightarrow S_n$ transition. The $^1(TT)$ state in BP0 is expected to correspond to the totally symmetric representation, as shown theoretically by Fuemmeler et al.;[18] it will be of opposite parity to the S1 state and will exhibit a distinct set of excited state transitions to states of odd parity.[18] Sn is expected to be close in energy to $S_{n'}$, because the difference in the $S_1 \rightarrow S_{n'}$ and $^1(TT) \rightarrow S_n$ transition energies, $\Delta E = 90$ meV, is close to the predicted exoergicity of ~100 to 150 meV for singlet fission in bipentacene.[18,28,30–33] The small energy spacing implies that both S_n and $S_{n'}$ likely originate from different linear combinations of the S_2 monomer state of different parity. Note that, unlike the results shown here for the pentacene dimer, the near-IR ESA assigned to $^1(TT)$ in pentacene aggregates does not show vibronic features.[38]

The ESA spectrum of the $^1(TT)$ state reveals its delocalized singlet and localized triplet characters in the near-IR and the visible regions, respectively. We use "delocalized singlet" or "delocalization" to emphasize $^1(TT)$ in a single electronic state, which can be approximately viewed as two T_1 states (on two pentacene units) that are electronically coupled and coherent. Likewise, the term "localized triplet" or "localization" refers to a T_1 state on an individual pentacene unit with physical properties that are insensitive to the presence or absence of electronic coupling and coherence with a neighboring T_1 state. Spectroscopically, delocalization and localization are reflected in the transitions $^1(TT) \rightarrow S_n$ and $^1(T_1T_1) \rightarrow {}^1(T_1T_n)$, respectively. Note that the two notations, $^1(TT)$ and $^1(T_1T_1)$, describe the same triplet pair state. The kinetic profiles (Figure 3.2C) for the $^1(TT) \rightarrow S_n$ (orange) and $^1(T_1T_1) \rightarrow {}^1(T_1T_n)$ (green) transitions are similar; the difference at short time scales (<1 ps) can be attributed to the different overlapping contributions from ESA of S_1. Note that transitions to Sn are allowed from $^1(TT)$ but spin-forbidden from $^3(TT)$ or $^5(TT)$. The perfect agreement between the decays of $^1(TT) \rightarrow$Sn and the $^1(T_1T_1) \rightarrow {}^1(T_1T_n)$ signals suggests that there are negligible transitions within the triplet pair

manifold, for example, ^{1}(TT)→^{5}(TT) or ^{1}(TT)→^{3}(TT), during the lifetime (450 ps) of the triplet pair state. Transitions within the triplet pair manifold are expected to occur on much longer time scales.[19,54]

Supporting the conclusion that delocalization or intertriplet electronic coupling in the ^{1}(TT) state is reflected in the ^{1}(TT)→Sn transition strength, we find that, in BP1, the weakening of the inter-T_1 electronic coupling diminishes its delocalized character as reflected in the ^{1}(TT)→S_n transition strength (Figure 3.2D) where the near-IR peak for ^{1}(TT) at long times, for example, Δt = 100 ps (blue), becomes nonresolvable from the broad background, in distinct contrast to the S_1→S_n peak at Δt = 1 ps. In contrast, the localized character represented by the $^1(T_1T_1)$→$^1(T_1T_n)$ transition in the visible region remains.[12]

To more quantitatively isolate the S_1 spectrum from that of the ^{1}(TT), we carry out global analysis based on a sequential kinetic model, S_1→^{1}(TT)→S_0.[12] The resulting S1 (red) and ^{1}(TT) (blue) spectra are shown in Figure 3.3. The global analysis yields time constants of 0.75 ± 0.05 ps and 460 ± 10 ps for singlet fission and triplet pair annihilation, respectively, in agreement with the previous report.[12] Similar to the S_1-$S_{n'}$ transition, the ^{1}(TT)-S_n transition is also characterized by vibronic peaks assigned to 0-0 and 0-1 transitions, with a vibrational energy spacing of 0.16 to 0.17 eV, which corresponds to the ring breathing mode of pentacene along the short molecular axis.[55] In addition to the near-IR peak, the ^{1}(TT) state in BP0 also features a distinct peak at 1.810 ± 0.005 eV. Similar to the transition at 1.012 ± 0.003 eV, the peak at 1.810 ± 0.005 eV diminishes as the intertriplet coupling weakens in BP1 and BP2.[12] Thus, the peak at 1.810 ± 0.005 also reflects the singlet character of the ^{1}(TT) state and can be assigned to a ^{1}(TT)→$S_{n''}$ transition. Because of the overlapping bleaching feature (S_0→S_1), we are not able to resolve vibronic progression for this transition.

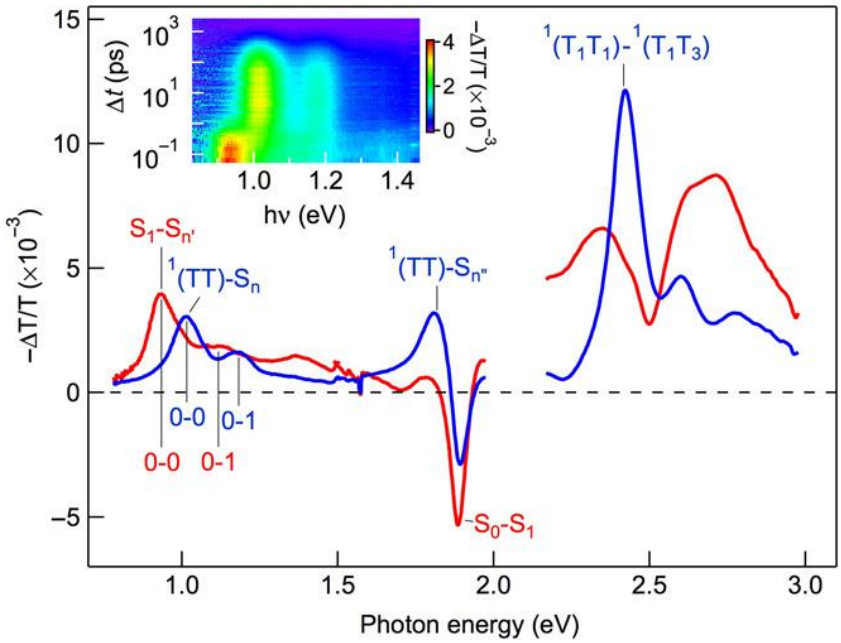

Figure 3.3 TA Spectra of BP0 for the S_1 and ^{1}(TT) States from Global Analysis Red: Singlet state. Blue: Triplet pair state. Inset: 2D pseudocolor (intensity) plot of TA spectra following excitation at time zero by $h\nu_1$ = 2.1 eV. The transitions, along with vibronic progressions, are shown on each spectrum.

Further supporting the conclusion that the near-IR $^1(TT) \rightarrow S_{n''}$ transition is a spectroscopic signature of the tightly bound triplet pair state, we turn to modified BP0 molecules with different dihedral angles. In this approach, we control the dihedral angle twist by steric hindrance from the phenyl group attached to the 1-position of one or both pentacene units in the bipentacene molecule, as shown schematically in the insets in Figure 3.4.[18] Computational analysis gives dihedral angles between the two pentacene molecules of 42° and 57°, and these two molecules are therefore labeled as BP-42 and BP-57, respectively.[18] For comparison, the dihedral angle in BP0 is 37°; thus, BP0 ≡ BP-37. Theoretical analysis showed that the intertriplet electronic coupling decreases with increasing dihedral angle.[18] The singlet fission time constants are τ_{SF} = 0.76, 1.69, and 3.38 ps, and the corresponding triplet-triplet annihilation time constants are τ_{SF} = 0.45, 1.6, and 5.2 ns for BP-37, BP-42, and BP-57, respectively.[18] Figure 3.4 shows the near-IR region of the S_1 (red) and ^{1}(TT) (blue) ESA spectra for BP-42 (top) and BP-57 (bottom).

We multiply the ^{1}(TT) spectra by factors of 2.5 and 4.6 for BP-42 and BP-57, respectively, to normalize the ^{1}(TT)-S_n peak intensity to the S_1-$S_{n'}$ intensity in each case. For comparison, the normalization factor would be 1.25 for BP-37 in Figure 3.3. Thus, relative to the S1-Sn′ transition, the ^{1}(TT)-S_n transition strength is 80, 40, and 22% for BP-37, BP-42, and BP-57, respectively. This confirms the correlation between the ^{1}(TT)-S_n ESA transition strength and the intertriplet electronic coupling in the ^{1}(TT) state.

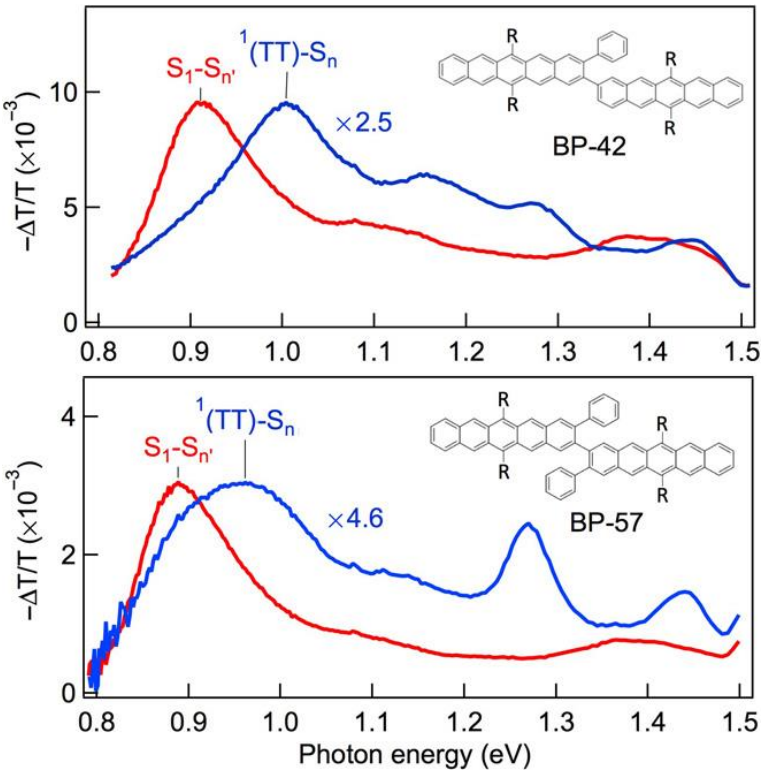

Figure 3.4 TA of the ^{1}(TT) State in the Near-IR Region Depends on Electronic Coupling Near-IR TA spectra of BP-42 (top) and BP-57 (bottom). The ^{1}(TT) spectra (blue) have been multiplied by factors of 2.5 and 4.6 for BP-42 and BP-57, respectively, to normalize the peak intensities of 1(TT) to those of S_1 (red).

In all the pentacene dimers investigated here, the decay rate of the triplet pair state is also found to be strongly correlated with the extent of delocalization in the ^{1}(TT) state, which is reflected in the ^{1}(TT)-S_n transition strength. This is understood as the rate of T_1-T_1 annihilation is determined by the inter-pentacene electronic coupling strength, as addressed in detail

elsewhere.[12,18]

The relative amplitudes of the 0-0 and 0-1 transitions allow us to estimate the Huang-Rhys factor (S) in each case and, thus, the relative shifts in the potential energy surfaces (PESs) involved. The Huang-Rhys factor is related to the offset (ΔQ_e) in the equilibrium positions of the two PESs in an optical transition: $S = 0.5\alpha (\Delta Q_e)^2$, where $\alpha = \mu\omega/\hbar$; μ is the reduced mass, and ω is the angular frequency of the vibration.[56] In the harmonic oscillator and low-temperature approximation appropriate for the pentacene ring breathing mode at room temperature, the ratio in the Franck-Condon factors (and the ratio in peak intensities) between the 0-1 and 0-0 transition is equal to the Huang-Rhys factor.[56] Thus, we obtain $S = 0.36 \pm 0.05$ and 0.45 ± 0.05 for the $S_1 \rightarrow S_3$ and $^1(TT) \rightarrow S_3$ transitions, respectively, from the near-IR ESA spectra for BP0 in Figure 3.3. For comparison, we obtain from the optical absorption spectrum a value of $S = 0.55 \pm 0.05$ for the S0-S1 transition.[12] For the pentacene ring breathing mode, we neglect the difference in equilibrium geometries between Sn′ and Sn, because they both likely come from the linear combination of S_2 in each pentacene chromophore. The spectroscopic results obtained above allow us to construct PESs for singlet fission in BP0. Although there are four possible arrangements of the PES from experimental ΔQ values, Figure 3.5 shows the scenario that is more consistent with the expectation of increasing nuclear displacement with excitation energy. The offset in equilibrium positions of the S_1 PES and the $^1(TT)$ PES ($\Delta Qe \sim 0.081$ Å) is also consistent with theoretical results on the covalent dimer.[18] The barrierless nature of the crossing point between S_1 and $^1(TT)$ explains the fast singlet fission rate for BP0. Furthermore, the PES of $^1(TT)$ crosses that of S0 with only two vibrational quanta on the former; this opens up an efficient nonradiative decay pathway. The nonradiative lifetime of $^1(TT)$ (450 ps in BP0) is shorter than that of the radiative lifetime (~13 ns) of S_1 in TIPS-pentacene.[12,57] Although Figure

3.5 is only an approximation given the uncertainties in the spectroscopic determination of Huang-Rhys factors, it represents the first estimation of PES for singlet fission from experimental data.

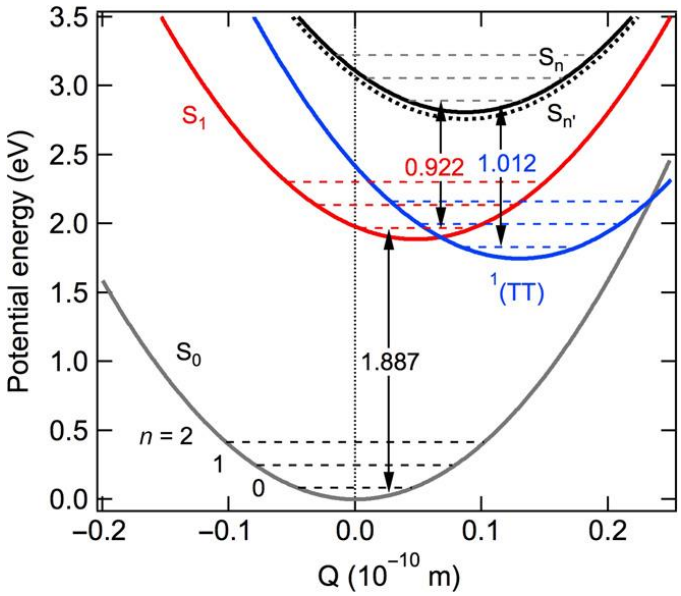

Figure 3.5 Estimated PES for BP0 Molecule The barrier-less nature for the crossing from S_1 (red) to ^{1}(TT) (blue) facilitates the fast singlet fission for BP0. The near-IR transition for BP0 can be explained by the transition from ^{1}(TT) to S_n, which is similar to the transition from S_1 to $S_{n'}$.

3.4 Distinct Chemical Property of the ^{1}(TT) State

The above spectroscopic analysis of singlet fission in BP0 provides evidence for a strong coupled triplet pair state, ^{1}(TT), whose delocalized and localized characters are revealed in ESA in the near-IR and visible regions, respectively. Here, we show that the tightly bound triplet pair state exhibits chemical properties that are different from those of an individual triplet.

The inset in Figure 3.1A shows the estimated values for the IP and EA for TIPS-Pc and [Fe_8O_4], respectively. These values are obtained from the electrochemical oxidation potentials for TIPS-Pc[58] and [Fe_8O_4],[59] respectively, based on the reference value of the Ag/AgCl electrochemical potential at 4.4 eV below vacuum energy (EV).[60] Also shown are the estimated

IPs of S_1 and T_1 states from the excitation energies of TIPS-Pc. The use of IPs and EAs of both ground and excited states allows us to accurately put all relevant energy levels on the same single-particle diagram, as discussed in detail by Zhu.[61] Note that the energy levels obtained from electrochemistry are adiabatic single-particle energies and can be used to approximate the vertical single-particle energies, that is, highest occupied molecular orbital and lowest unoccupied molecular orbital, when the reorganization energies are negligible.[61] Given this approximate energy level diagram, we expect efficient electron transfer from either the T_1 or the S_1 in pentacene to the [Fe_8O_4] cluster. Figure 3.1C compares the optical absorption spectra of the [Fe_8O_4] cluster (black) and those of compounds [Fe_8O_4]-Pc (red) and [Fe_8O_4]-BP0 (blue). The absorption spectra of both [Fe_8O_4]-Pc and [Fe_8O_4]-BP0 primarily arise from the sum of the absorption spectra of [Fe_8O_4] and that of pentacene or bipentacene. An additional broad feature below 1.75 could contain a CT state from the Pc-PhO-ligand or the BP0-PhO-ligand to the [Fe_8O_4] cluster, in addition to the more local LMCT transition.[51]

The energy level alignment in Figure 3.1A suggests that, in addition to direct photoexcitation of the CT state, electron transfer can occur from T_1 in pentacene to [Fe_8O_4] to indirectly form the CT state. We find that CT and T_1 are strongly coupled resonantly. When we directly excite the CT state in [Fe_8O_4]-Pc or [Fe_8O_4]-BP0 at $h\nu$ = 1.65 eV (Figure 3.6A), we observe in each case a TA spectrum characteristic of the T_1 state in pentacene, including an ESA peak at ~2.4 eV and a ground-state bleaching at 1.88 and 2.05 eV (see Figure 3.8 for complete TA data for [Fe_8O_4]-Pc). Although we observe small differences in the TA spectra for [Fe_8O_4]-Pc (green) and [Fe_8O_4]-BP0 (red), they all match their T_1 spectra obtained by sensitization very well. For clarity, here, we only present the T_1 spectrum of [Fe_8O_4]-BP0 (gray); see the Figure 3.10 for T_1 spectra of the other molecules. Note that neither the isolated [Fe_8O_4] nor the

uncoupled pentacene molecules absorb light below ~1.75 eV. Excitation of isolated [Fe_8O_4] at higher photon energies results in completely different TA spectra (Figure 3.9). The ultrafast formation of T_1 within experimental time resolution (~100 fs) from the selective excitation of CT indicates that the cluster and pentacene ligands are strongly electronically coupled. Supporting this conclusion, we found in a triplet sensitization experiment that the observable T_1 signal from [Fe_8O_4]-Pc is an order of magnitude lower than that from TIPS-Pc (Figure 3.10).

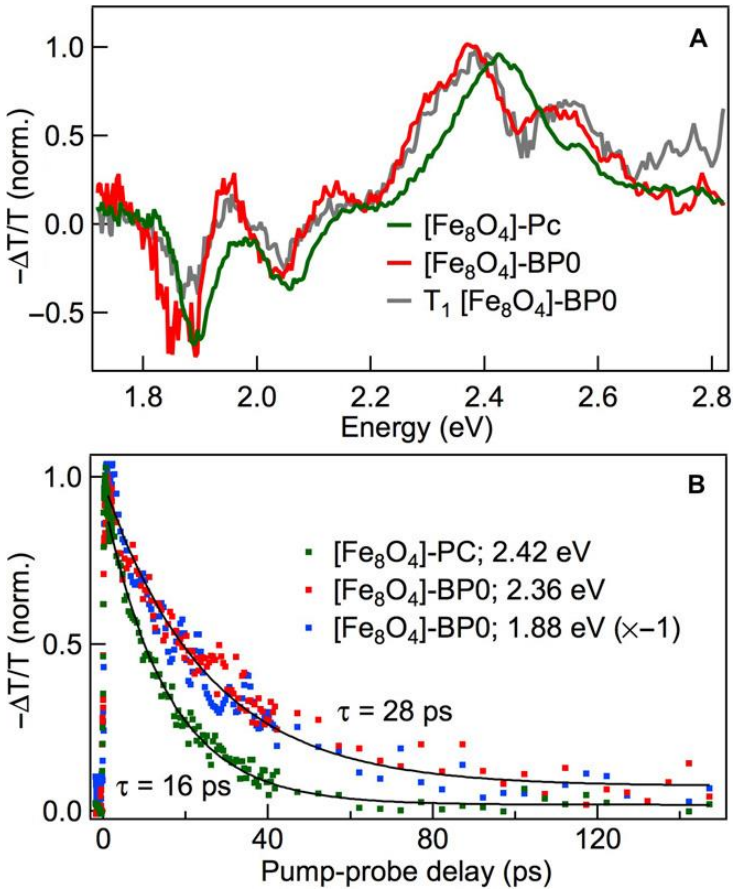

Figure 3.6 TA reveals the strong coupling of CT states to T_1 A) TA spectra at 1 ps for [Fe_8O_4]-Pc (green) and [Fe_8O_4]-BP0 (red) upon CT excitation of 1.65 eV. The gray curve is the triplet spectrum of [Fe_8O_4]-BP0 from triplet sensitization. B) Triplet decay dynamics for [Fe_8O_4]-Pc (green) and [Fe8O4]-BP0 (red and blue for ESA and ground-state bleaching, respectively). The solid curves are single-exponential fits with the indicated lifetimes ($\tau = 16 \pm 2$ ps for [Fe_8O_4]-Pc and 28 ± 3 ps for [Fe_8O_4]-BP0).

The coupled T_1-CT state features first-order decay kinetics well described by single-

exponential decays (solid curves in Figure 3.6B), with time constants of $\tau_{CT\text{-}T1}$ = 28 ± 3 ps and 16 ± 2 ps for $[Fe_8O_4]$-BP0 and $[Fe_8O_4]$-Pc, respectively. The simple first-order kinetics is reflected in both the decay in T_1-like ESA signal (red dots) and the recovery in ground-state bleaching (blue dots) for $[Fe_8O_4]$-BP0 in Figure 3.6B. The T_1-CT decay constant is five orders of magnitude shorter than that of an individual T_1 state in pentacene or bipentacene molecules.[12] Because no fluorescence emission is observed for any of the cluster-pentacene complexes, we assign the fast decay in the T_1-CT state to nonradiative recombination. Both CT across the pentacene-cluster interface and the presence of paramagnetic Fe atoms can couple to electron spins, thus facilitating recombination.[62]

Unlike the strong coupling of individual T_1 in pentacene or bipentacene to the CT state at their interfaces to $[Fe_8O]$, we find that the triplet state in the tightly bound ^{1}(TT) in BP0 does not undergo CT to the electron accepting cluster. Figure 3.7A shows TA spectra for $[Fe_8O_4]$-BP0 as a function of pump-probe delay, following initial photoexcitation at $h\nu_1$ = 2.1 eV. Figure 3.7B shows horizontal cuts at selected pump-probe delays (Δt = 0, 10, and 100 ps), along with a T_1 spectrum obtained from sensitization of $[Fe_8O_4]$-BP0. At this excitation photon energy, BP0 is known to undergo efficient singlet fission,[12] and the results for $[Fe_8O_4]$-BP0 are nearly identical to those in BP0. Initially (Δt = 0 ps; red spectrum in Figure 3.7B), the TA spectrum is that of S_1 characterized by the broad ESA in the visible region and a vibronically resolved ESA in the near-IR region. The singlet exciton decay and triplet rise in $[Fe_8O_4]$-BP0 are both characterized by a single-exponential lifetime of τ_{SF} = 0.55 ± 0.02 ps, which is slightly shorter than the corresponding process in BP0 (τ_{SF} = 0.76 ps).[12] Figure 3.7D compares the ^{1}(TT) decay dynamics in $[Fe_8O_4]$-BP0, as monitored by the decays of ESA signals attributed to both triplet (2.36 eV, red) and singlet (0.97 eV, green) characters. For comparison, we also show in Fig. 3.7D the

^{1}(TT) decay dynamics in BP0 (2.36 eV, blue). The three decay traces are superimposable. The data for [Fe_8O_4]-BP0 are well described by a single-exponential decay with a time constant of τ_{TT} = 0.42 ± 0.03 ns, which is, within experimental uncertainty, identical to that of BP0. In stark contrast to the efficient CT from an individual T_1 state in [Fe_8O_4]-Pc, there is no measurable CT from the tightly bound ^{1}(TT) state in [Fe_8O_4]-BP0.

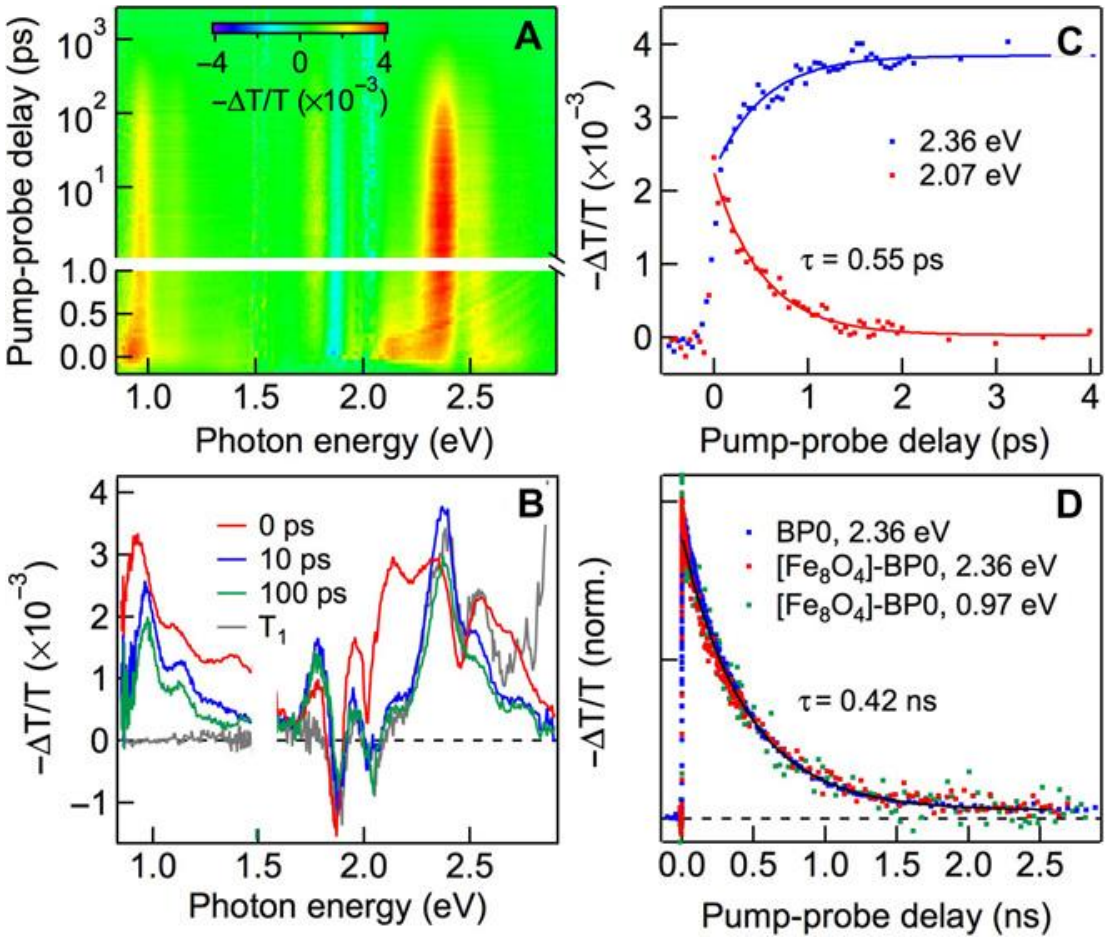

Figure 3.7 TA Spectra and Dynamics of [Fe_8O_4]-BP0 under 2.1 eV excitation A) 2D pseudocolor plot of TA (= −ΔT/T; T, transmission) as a function of pump-probe delay (Δt) and probe photon energy. B) TA spectra at Δt = 0 ps (red), 10 ps (blue), and 100 ps (green), along with T_1 spectrum from sensitization (gray). (C) Singlet fission dynamics, as represented by S_1 decay at 2.07 eV (red) or ^{1}(TT) buildup at 2.36 eV (blue). (D) Comparison of ^{1}(TT) decay dynamics for [Fe_8O_4]-BP0 and BP0.

In summary, using covalently linked pentacene dimers as model systems, we show evidence for a tightly bound triplet pair state, which reveals its delocalized ^{1}(TT) and localized

T_1 characters in the near-IR and visible ESA spectra, respectively. The near-IR ESA spectra can be assigned the $^1(TT)\rightarrow Sn$ transition, which is similar to the $S_1\rightarrow S_{n'}$ transition, with vibrational progression corresponding to the well-known aromatic ring breathing mode. The $^1(TT)\rightarrow S_n$ transition is an indicator of the intertriplet coupling strength; when a phenylene spacer is inserted between the pentacene moieties (BP1) or varies the angle between the pentacene moieties (BP45, BP90, and 1,2-BP) to decrease this coupling, we find that the $^1(TT)\rightarrow S_n$ ESA peak decreases. This is in contrast to the spectrum in the visible region, assigned to the $^1(T_1T_1)\rightarrow 1(T_1T_3)$ transition present with similar intensities for all bipentacene molecules. Using an electron-accepting iron oxide molecular cluster [Fe_8O_4] linked to pentacene and bipentacene (BP0), we find that electron transfer to the cluster occurs efficiently from an individual T1 but not from the $^1(TT)$ state. Thus, the tightly bound $^1(TT)$ state exhibits a distinctively different chemical reactivity from that of an individual T_1 state. A viable strategy to efficiently harvest triplets from intramolecular singlet fission is to control the intertriplet electronic coupling via molecular design.

3.5 Synthesis

The synthesis of TIPS-Pc, BP0, and BP1 molecules (11); BP0 with different dihedral angles;[18] and the [Fe_8O_4] cluster[50] has been previously described. To install the pentacene-based ligands on [Fe_8O_4], we first deprotonated the pendent phenol group with an excess of sodium hydride in tetrahydrofuran (THF). The reaction mixture was filtered through a 0.2-μm syringe filter and added dropwise to a solution of [Fe_8O_4] in THF. We used a 1:1 stoichiometric ratio of the ligand to [Fe_8O_4] to prepare the monosubstituted clusters, which were purified by reversed-phase chromatography. Additional synthetic details and characterization data can be found below.

3.6 Optical Absorption Experimental

The TIPS-Pc, BP0, and BP1 samples were dissolved in dry toluene (with a concentration of <100 μM) and kept free from oxygen and moisture for optical measurements on a Shimadzu UV 1800 UV-Vis Spectrophotometer. Ultraviolet-visible (UV-Vis) absorption spectra of BP0 and BP1 (Figure 3.1B) showed a slight red shift from that of TIPS-Pc but contained otherwise nearly identical vibronic features near the absorption threshold ($S_0 \rightarrow S_1$) (11). Solutions of [Fe_8O_4], [Fe_8O_4]-Pc, or [Fe_8O_4]-BP0 in chloroform were used for absorption measurements. Optical absorption spectra of [Fe_8O_4], [Fe_8O_4]-Pc, and [Fe_8O_4]-BP0 in Figure 3.1C will be discussed later.

3.7 Transient Absorption Experimental

To investigate singlet fission and triplet transfer, we used femtosecond TA (fs-TA) spectroscopy. The samples were dissolved in dry toluene and kept free from oxygen and moisture. The pump pulse came from an optical parametric amplifier (tunable from UV to the near-IR, 100-fs pulse width, 1 kHz rep rate). The probe pulse was a white-light supercontinuum (from 450 to 850 nm and from 850 to 1600 nm for the visible and near-IR range, respectively). The delay between pump and probe pulses was controlled by a translational stage with a delay time up to 3 ns. The detection consisted of a pair of multichannel detector arrays coupled to a high-speed data acquisition system (HELIOS, Ultrafast System Inc.). The sample solution was at room temperature during measurement. The nanosecond-microsecond TA measurements were carried out on the same setup as fs-TA with the same pump pulse. The probe pulse was a white-light supercontinuum (from 400 to 1600 nm) generated by a supercontinuum laser (Leukos). The laser pulse width was ≤1 ns at 2 kHz. The pump-probe delay was controlled electrically.

The triplet-sensitizing experiment was carried out on the same setup except for the fact

that the white-light probe beams were generated by a picosecond laser and the pump-probe delay was controlled electrically. A mixture of a (bi)pentacene compound and an excess of anthracene was dissolved in toluene with the concentration of anthracene ~100x that of (bi)pentacene. Photoexcitation at 3.35 eV created singlets in anthracene, which underwent intersystem crossing to form triplets. The triplets in anthracene subsequently transferred to (bi)pentacene molecules via diffusional collisions on a time scale of 1 to 2 μs (see the section 3.10).

3.8 Charge Transfer Excitation for [Fe_8O_4]-Pc

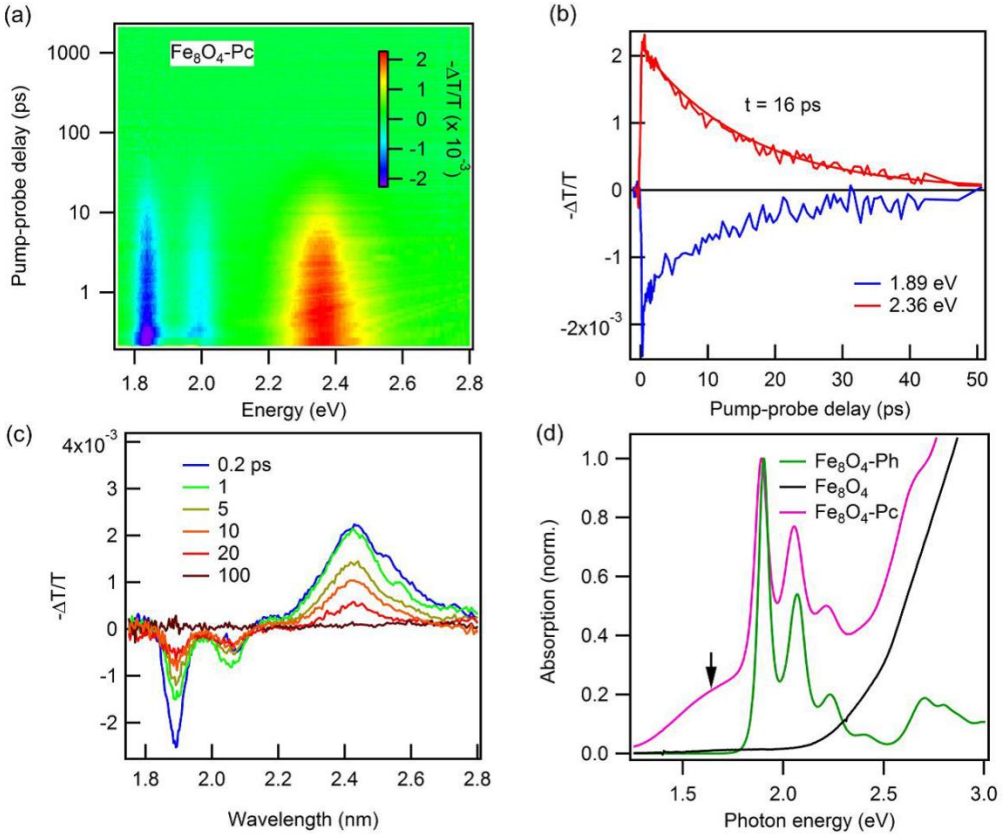

Figure 3.8 Transient Absorption (TA) Spectra and Ddynamics of [Fe_8O_4]-Pc A) 2D pseudocolor plot of TA (-ΔT/T, T: transmission) as a function of pump-probe delay (Δt) and probe photon energy upon CT excitation of 1.65 eV (arrow in D)). B) Decay dynamics at probe photon energy of 1.89 eV (bleaching) and 2.36 eV (ESA). C) TA spectra at several pump-probe delay. D) Absorption spectra of TIPS-pentacene-phenol (Pc-Ph, green); $Fe_8O4pz_{12}C_{l4}$ cluster, i.e., [Fe_8O_4] (black); and [Fe_8O_4]-Pc (purple). Note that at this excitation energy, there is no absorbance by the [Fe_8O_4] only.

3.9 Transient Absorption for the [Fe_8O_4] Cluster

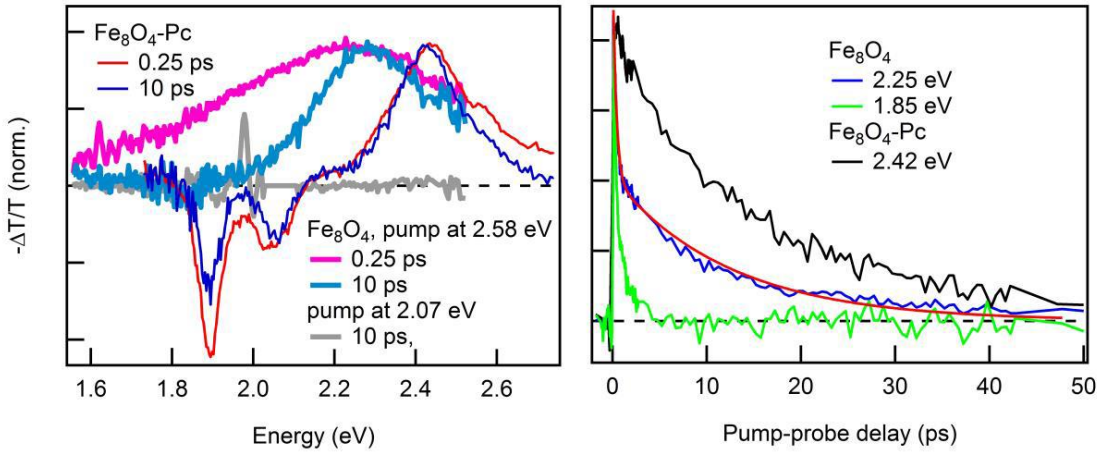

Figure 3.9 Comparison between $Fe_8O_4pz_{12}Cl_4$ Cluster only (pumped at 2.58 and 2.07 eV) and [Fe_8O_4]-Pc (pumped at 1.65 eV) Left: The normalized spectra at 0.25 and 10 ps for both samples, the data for $Fe_8O_4pz_{12}Cl_4$ cluster above 2.53 eV was omitted due to strong scattering from the pump pulse. The grey curve is from the cluster pumped at 2.07 eV showing no pump-induced absorption signal. Right: Dynamics for the cluster at 1.85 and 2.25 eV. The biexponential fit to the dynamics at 2.25 eV (blue) gives the time constants of 0.36 (54 %) and 12.4 ps (46%). The dynamics for [Fe_8O_4]-Pc decay mono-exponentially with a constant of 16 ps (black).

3.10 Triplet Sensitization Experiments

The triplet sensitization experiment was carried out on the same setup as the femtosecond transient absorption setup except the white-light probe beams were generated by a supercontinuum laser from Leukos. The laser pulse width is < 1 ns runs at 2 kHz. The pump-probe delay was controlled electrically. A mixture of the compound and anthracene was dissolved in toluene and kept free from oxygen to avoid oxygen triplet quenching. Photoexcitation at 3.44 eV creates singlets in anthracene which undergo intersystem crossing to form triplets. The triplets in anthracene subsequently transfer to pentacene molecules via diffusional collisions in time scale of ~1-2 μs.

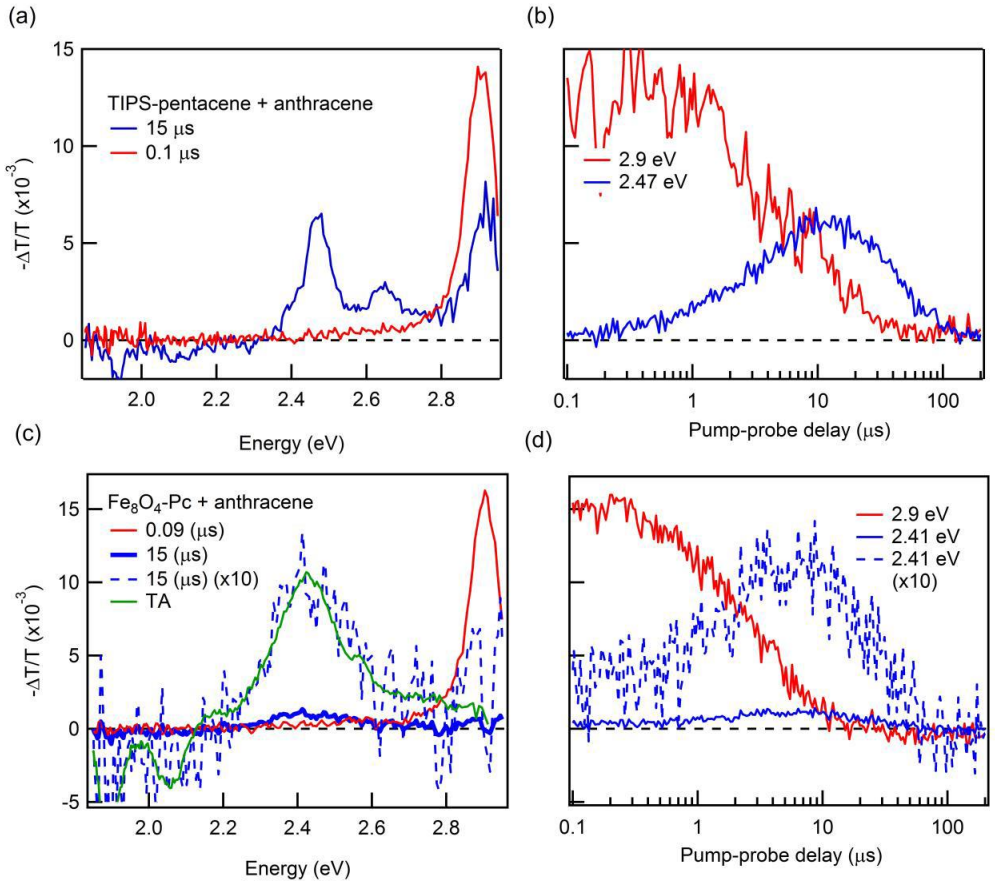

Figure 3.10 Triplet-Sensitizing Experiments A,B) Spectra and dynamics for the mixed solution of anthracene and TIPS-pentacene. C,D) Mixed solution of Fe_8O_4-Pc and anthracene. The peaks at 2.47 (in A,B) and 2.41 eV (in C,D) are assigned to triplet absorption in pentacene, the peak at 2.9 eV is triplet absorption from anthracene. The TA spectrum for [Fe_8O_4]-Pc excited at 1.65 eV (Fig. 2 in the main text) was plotted in C) for comparison. The molar concentration for anthracene is 50 mM, for TIPS-Pentacene is 15 μM, and for [Fe8O_4]-Pc is 36 μM. Note that the small T1 signal observed from sensitization of [Fe_8O_4]-Pc may come from a small population of free TIPS-Pc molecules that has broken off the cluster from laser irradiation.

3.11 General Methods

All commercially obtained reagents/solvents were used as received; chemicals were purchased from Alfa Aesar®, Sigma-Aldrich®, Acros organics®, TCI America®, Mallinckrodt®, Strem Chemicals® and Oakwood® Products, and were used as received without further purification. Synthesis of **1**, Dibromo NODIPS Pentacene, **4**, **5** and $Fe_8O_4pz_{12}C_{l4}$ (Iron Oxo Cluster) were synthesized as previously reported.[12,50] Unless stated otherwise, reactions

were conducted in oven-dried glassware under argon atmosphere. ^{1}H-NMR and ^{13}C-NMR spectra were recorded on Bruker 400 MHz (100 MHz for ^{13}C) and on 500 MHz (125 MHz for ^{13}C) spectrometers. Data from the ^{1}H-NMR and ^{13}C spectroscopy are reported as chemical shift (δ ppm) with the corresponding integration values. Coupling constants (*J*) are reported in hertz (Hz). Standard abbreviations indicating multiplicity were used as follows: s (singlet), b (broad), d (doublet), t (triplet), q (quartet), m (multiplet) and virt (virtual).

The mass spectral data for the compounds were obtained from (1) XEVO G2-XS Waters® equipped with a QTOF detector with multiple inlet and ionization capabilities including electrospray ionization (ESI), atmospheric pressure chemical ionization (APCI), and atmospheric solids analysis probe (ASAP) or (2) a Bruker UltrafleXtreme MALDI TOF/TOF instrument using a dithranol matrix. The base peaks were usually obtained as $[M]^{+}$ or $[M+H]^{+}$ ions. Infrared (IR) spectra were obtained using a Perkin Elmer Spectrum 400 FTIR spectrometer using a PIKE ATR attachment.

Absorption spectra were obtained on a Shimadzu UV 1800 UV-Vis spectrophotometer. Anhydrous solvents were obtained from a Schlenk manifold with purification columns packed with activated alumina and supported copper catalyst (Glass Contour, Irvine, CA). All reactions were carried out under argon unless otherwise noted. Reactions and sample preparations requiring an inert atmosphere were carried out under nitrogen using standard Schlenk techniques or in a nitrogen-filled glovebox.

3.12 Compound Synthesis

Synthesis of 2

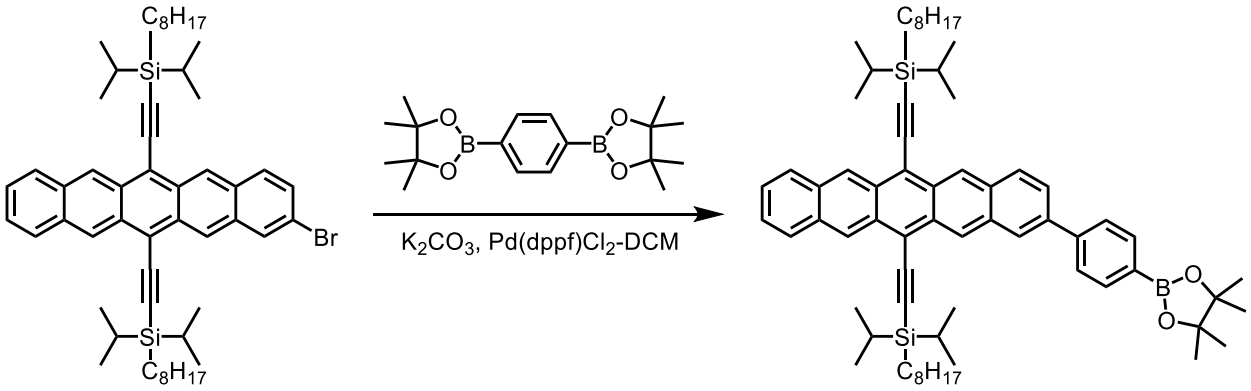

1 **2**

1 (1.5 g, 1.75 mmol), 1,4-Benzenediboronic acid bis(pinacol) ester (1.73 g, 5.25 mmol) and Pd(dppf)Cl_2·DCM (71.1 mg, 0.09 mmol) were added to a reaction vial, followed by sequential vacuum and argon to degas the solids. K_2CO_3 (1.2 g, 8.75 mmol) was then dissolved in 4.5 mL H_2O and degassed. The solids were then dissolved in 45 mL of a mixture of 9:1 THF:K_2CO_3 in H_2O solution, and allowed to stir at 70 °C overnight in the dark. The reaction was then brought to room temperature and extracted with DCM and the combined organic layers were washed with DI water and brine, dried over sodium sulfate, filtered and concentrated. The crude was then purified by column chromatography using 25% to 50% DCM in hexanes as the eluent to obtain **2** as a deep blue solid (973 mg, 56.7% yield).

^{1}H-NMR (500 MHz, $CDCl_3$, δ ppm): 9.36 (s, 1H), 9.32 (s, 3H) 8.20 (s, 1H), 8.09 (d, 1H), 8.03-8.00 (m, 4H), 7.84 (d, 2H), 7.76 (d, 1H), 7.46-7.42 (m, 2H), 1.80 (m, 4H), 1.56 (m, 6H), 1.45-1.35 (m, 54H), 0.99 (m, 4H), 0.83 (m, 6H).

^{13}C-NMR (125 MHz, $CDCl_3$, δ ppm): 143.47, 138.19, 136.40, 135.43, 132.39, 132.35, 132.32, 131.55, 130.93, 130.78, 130.69, 130.62, 129.34, 129.19, 128.68, 126.77, 126.54, 126.33, 126.29, 126.12, 126.02, 125.57, 118.44, 118.32, 107.66, 107.51, 104.54, 104.51, 83.89, 34.05, 34.02,

33.97, 31.97, 31.92, 29.50, 29.47, 29.39, 29.37, 25.01, 24.96, 24.92, 24.74, 22.64, 18.71, 18.44, 14.08, 14.06, 12.18, 10.47.

MS (ESI): Calculated $[M]^+$: 980.6505; Observed: 980.6499.

Synthesis of Pc-Phenol

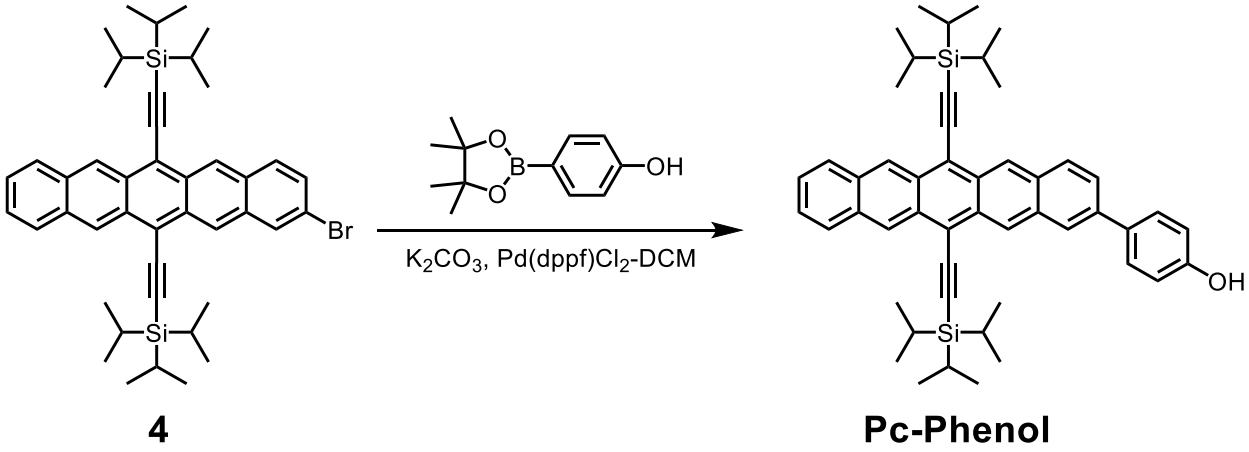

4 **Pc-Phenol**

4 (300 mg, 0.42 mmol), 4-Hydroxyphenylboronic acid pinacol ester (110 mg, 0.50 mmol) and Pd(dppf)Cl_2·DCM (17.1 mg, 0.021 mmol) were added to a reaction vial, followed by sequential vacuum and argon to degas the solids. K_2CO_3 (577 mg, 4.2 mmol) was then dissolved in 1 mL H_2O and degassed. The solids were then dissolved in 10 mL of a mixture of 9:1 THF:K_2CO_3 in H_2O solution, and allowed to stir at 70 °C overnight in the dark. The reaction was then brought to room temperature and extracted with DCM and the combined organic layers were washed with DI water and brine, dried over sodium sulfate, filtered and concentrated. The crude was then purified by column chromatography using 35% to 50% DCM in hexanes as the eluent to obtain **Pc-Phenol** as a teal solid (226 mg, 74.0% yield).

^{1}H-NMR (500 MHz, $CDCl_3$, δ ppm): 9.33 (s, 4H), 8.07 (t, 2H), 8.00 (m, 2H), 7.71 (m, 3H), 7.44 (m, 2H), 7.03 (d, 2H), 4.90 (s, 1H), 1.48-1.39 (m, 42H).

^{13}C-NMR (125 MHz, $CDCl_3$, δ ppm): 155.58, 137.93, 133.74, 132.41, 129.42, 128.83, 128.71, 126.53, 126.18, 126.15, 116.04, 19.16, 11.86.

MS (ESI): Calculated $[M]^+$: 730.4026; Observed: 730.4038.

Synthesis of BP0-Phenol

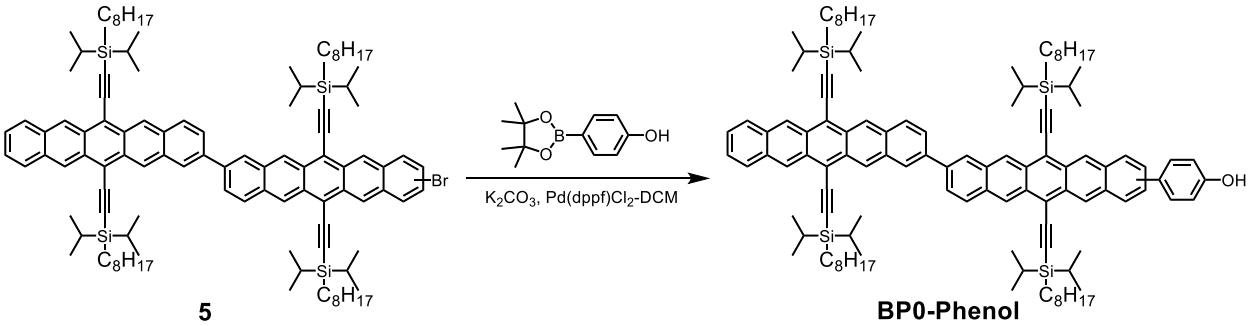

5 (100 mg, 0.06 mmol), 4-Hydroxyphenylboronic acid pinacol ester (16 mg, 0.07 mmol) and Pd(dppf)Cl_2·DCM (2.5 mg, 0.003 mmol) were added to a reaction vial, followed by sequential vacuum and argon to degas the solids. K_2CO_3 (84.3 mg, 0.61 mmol) was then dissolved in 1 mL H_2O and degassed. The solids were then dissolved in 10 mL of a mixture of 9:1 THF:K_2CO_3 in H_2O solution, and allowed to stir at 70 °C overnight in the dark. The reaction was then brought to room temperature and extracted with DCM and the combined organic layers were washed with DI water and brine, dried over sodium sulfate, filtered and concentrated. The crude was then purified by column chromatography using 50% to 75% DCM in hexanes as the eluent to obtain **BP0-Phenol** as a green solid (53 mg, 52.7% yield).

^{1}H-NMR (500 MHz, $CDCl_3$, δ ppm): 9.40 (s, 2H), 9.33 (m, 6H), 8.36 (s, 2H), 8.15 (d, 2H), 8.10 (s, 1H), 8.06 (d, 2H), 8.00 (m, 2H), 7.94 (m, 2H), 7.70 (m, 3H), 7.43 (m, 2H), 7.01 (d, 2H), 4.84 (s, 1H), 1.80 (m, 8H), 1.45-1.21 (m, 90H), 0.99 (m, 9H), 0.84 (m, 9H), 0.74 (m, 8H).

^{13}C-NMR (125 MHz, $CDCl_3$, δ ppm): 155.47, 137.85, 133.60, 132.36, 131.60, 130.66, 129.61, 128.70, 128.57, 126.37, 126.20, 126.06, 125.95, 124.86, 115.90, 107.55, 104.53, 34.08, 34.03,

31.98, 31.91, 29.53, 29.47, 29.39, 29.37, 25.04, 24.97, 22.66, 22.61, 18.76, 18.74, 18.48, 14.10, 14.01, 12.21, 10.50.

MS (ESI): Calculated $[M+H]^+$: 1649.0870; Observed: 1649.0900.

Synthesis of BP1-Phenol

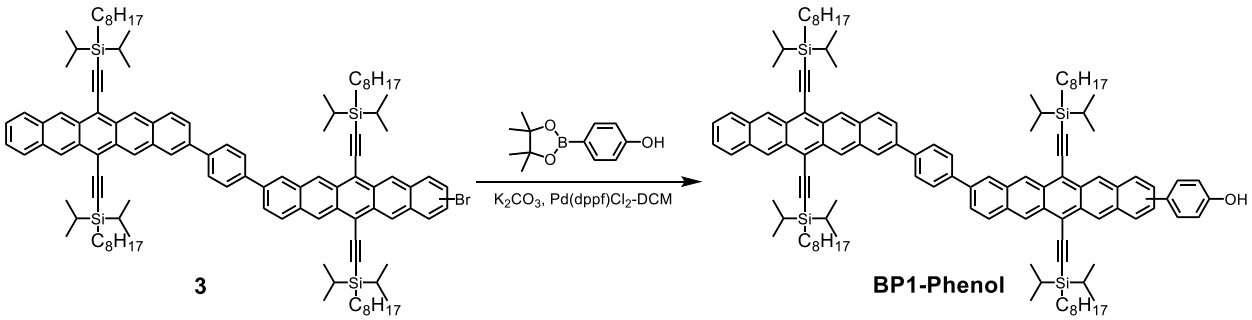

3 (325 mg, 0.2 mmol), 4-Hydroxyphenylboronic acid pinacol ester (50.6 mg, 0.23 mmol) and Pd(dppf)Cl_2·DCM (8.16 mg, 0.01 mmol) were added to a reaction vial, followed by sequential vacuum and argon to degas the solids. K_2CO_3 (263 mg, 1.9 mmol) was then dissolved in 1 mL H_2O and degassed. The solids were then dissolved in 10 mL of a mixture of 9:1 THF:K_2CO_3 in H_2O solution, and allowed to stir at 70 °C overnight in the dark. The reaction was then brought to room temperature and extracted with DCM and the combined organic layers were washed with DI water and brine, dried over sodium sulfate, filtered and concentrated. The crude was then purified by column chromatography using 50% DCM in hexanes as the eluent to obtain **BP1-Phenol** as a green solid (121 mg, 37.0% yield).

^{1}H-NMR (400 MHz, $CDCl_3$, δ ppm): 9.37 (s, 2H), 9.32 (d, 6H), 8.26 (s, 2H), 8.13-8.04 (m, 4H), 7.99 (m, 6H), 7.81 (d, 2H), 7.70 (m, 3H), 7.43 (m, 2H), 7.01 (d, 2H), 4.83 (s, 1H), 1.79 (m, 8H), 1.43-1.20 (m, 100H), 0.82 (m, 18H).

^{13}C-NMR (125 MHz, $CDCl_3$, δ ppm): 155.59, 140.52, 140.13, 137.83, 133.72, 132.62, 132.52, 132.48, 131.69, 131.12, 130.91, 130.78, 129.61, 129.42, 128.84, 128.70, 127.87, 127.32, 126.82, 126.50, 126.32, 126.20, 125.95, 124.97, 118.64, 118.45, 116.03, 107.80, 107.68, 104.75, 34.23,

34.19, 32.14, 32.11, 29.67, 29.64, 29.59, 29.56, 29.53, 25.18, 25.13, 22.81, 18.91, 18.89, 18.86, 18.64, 18.62, 14.26, 14.23, 12.36, 10.65.

MS (ESI): Calculated $[M+H]^+$: 1725.1184; Observed: 1725.1183

Synthesis of Pentacene-Cluster Adducts Fe-Pc, Fe-BP0, and Fe-BP1

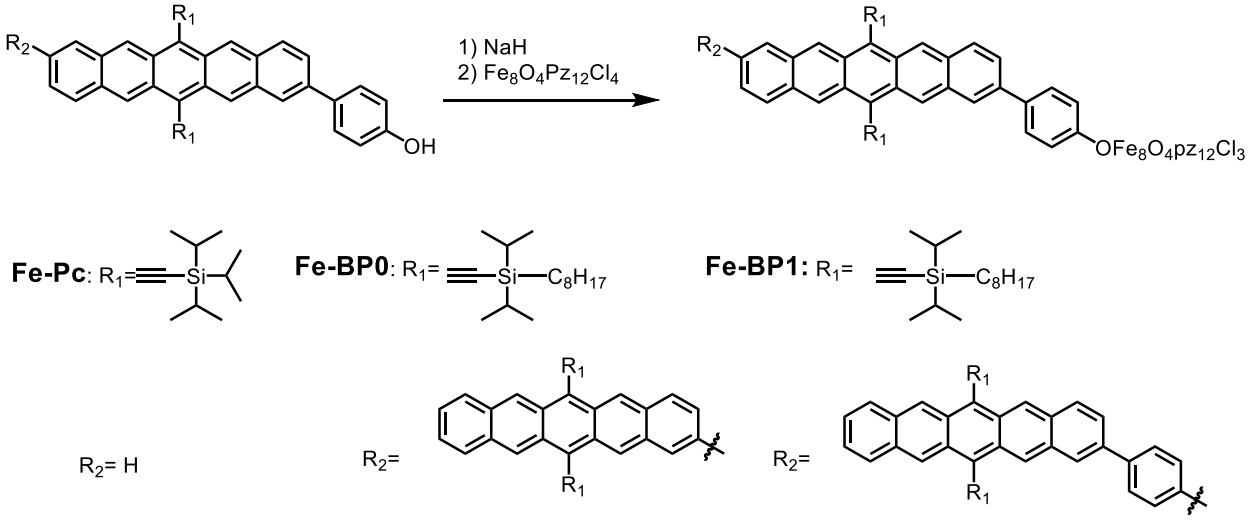

In a nitrogen-filled glovebox, $Fe_8O_4pz_{12}Cl_4$ (1 eq) was dissolved in approximately 10 mL of anhydrous THF. In a separate vial, NaH (10 eq) was suspended in THF to which **Pc**, **BP0**, or **BP1** Phenol (1 eq.) was added and stirred for about 1 h, turning the suspension from dark green to a dark violet. This mixture was then filtered through a syringe filter (0.2 mm PTFE) to give a dark violet solution. This solution was slowly added dropwise to the solution of $Fe_8O_4pz_{12}Cl_4$ and stirred for 16 h at room temperature. The solvent was then removed under vacuum. The residue was removed from the glovebox and purified via flash chromatography using a RediSep® Rf Reversed-phase C18 column and gradient elution (10% to 50% DCM in MeCN). Fractions containing the desired product were collected and concentrated to give the products as dark green solids.

Upon reaction of the sodium salt of Pc-PhOH with Fe8O4pz12Cl4, a chloride is displaced from the cluster, substituted with a Pc-PhO-, BP0-PhO-, and BP1-PhO-, giving rise to [Fe8O4]-Pc, [Fe8O4]- BP0, and [Fe8O4]-BP1, respectively. The high-spin Fe3+ centers of the cluster give rise to large paramagnetic shifting and signal broadening of the resulting adducts, making complete characterization by NMR a challenge. However, the position of the aromatic protons of the pentacenes shifts from the usual 6-8 ppm region upon addition to the cluster. In the case of the simplest adduct, [Fe8O4]-Pc, upon treatment with anhydrous HCl, the aromatic resonances associate with the pentacene moiety return to the 6-8 ppm region, evidence that the pentacene moiety goes from being directly covalently linked to the cluster to the free Pc-PhOH and Fe8O4pz12Cl4 molecules. Mass spectrometry of the [Fe8O4]-Pc adduct shows the molecular ion of the desired compound (m/z = 2152), as well as fragments corresponding to Fe8O4pz12Cl3 (m/z = 1420) and Pc-PhOH (m/z = 730). Taken in context of the NMR and IR data, we use this as evidence for formation of the desired product. The larger size of [Fe8O4]-BP0 and [Fe8O4]-BP1 fragment more quickly upon ionization into the BP0/BP1 and Fe8O4pz12Cl4, but the distinct electronic absorption and IR spectra, as well as the ability to separate the material from any remaining starting material using RP-chromatography, indicate that monosubstituted adducts have formed.

Fe-Pc: (15 mg, 20% yield)

MS (ESI): Calculated $[M]^+$: 2152.1179; Observed: 2152.1206

Fe-BP0: (23 mg, 22% yield)

Fe-BP1: (18 mg, 17% yield)

3.13 Infrared Spectrum

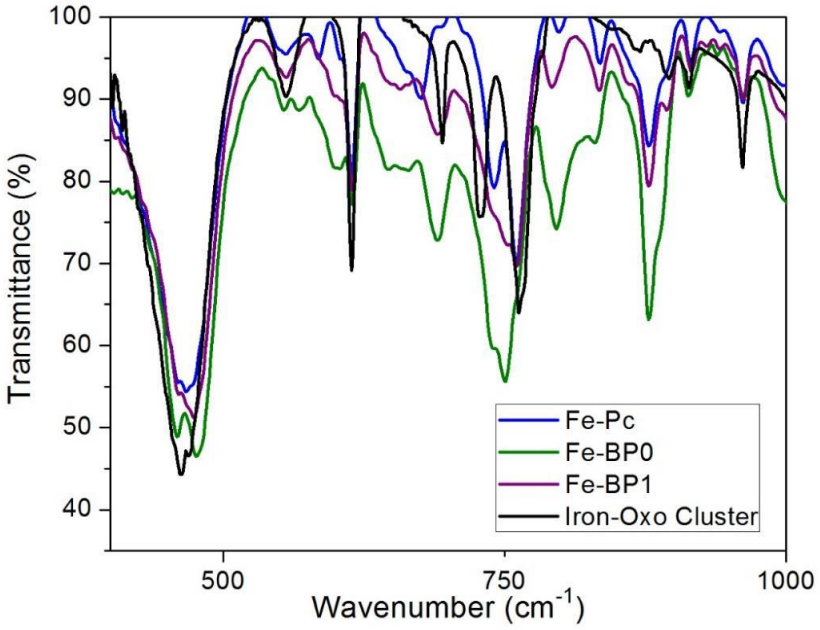

Figure 3.11 Infrared Spectrum Infrared spectrum of the chloride terminated Iron-oxo cluster (black), Fe-Pc (blue), Fe-BP0 (green), Fe-BP1 (purple). The stretch peak at 460 cm^{-1} corresponds to the Fe-O stretch of the cluster cubane structure. The persistence of this peak after the ligand exchange demonstrates the cluster remains intact.

3.14 UV-Vis Spectra

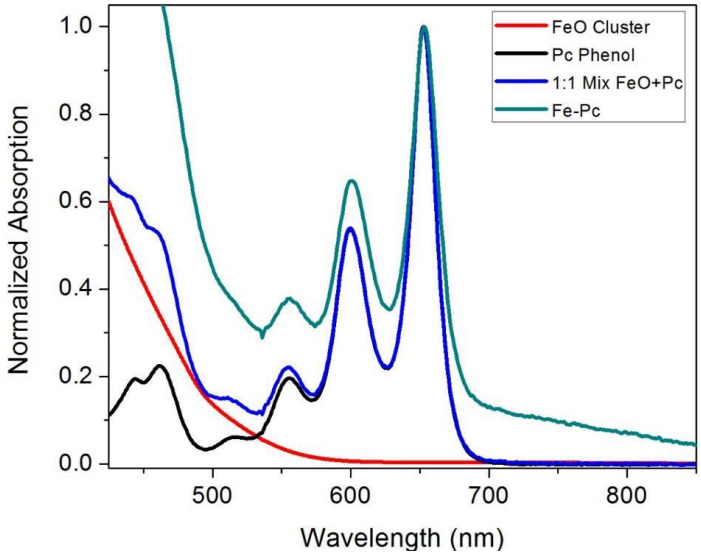

Figure 3.12 Pc-Phenol Absorption Spectra Normalized UV-Vis spectra of Pc-Phenol (black), Iron-Oxo cluster (red), a 1:1 mixture of the two in solution (blue) and the 1:1 adduct Fe-Pc (green).

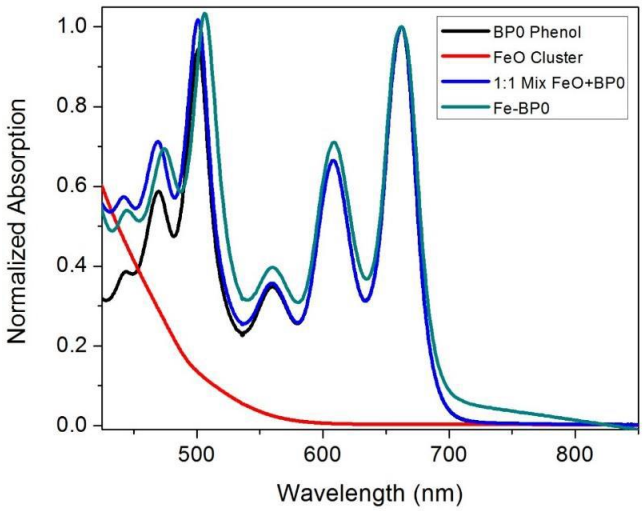

Figure 3.13 BP0-Phenol Absorption Spectra Normalized UV-Vis spectra of BP0-Phenol (black), Iron-Oxo cluster (red), a 1:1 mixture of the two in solution (blue) and the 1:1 adduct Fe-BP0 (green).

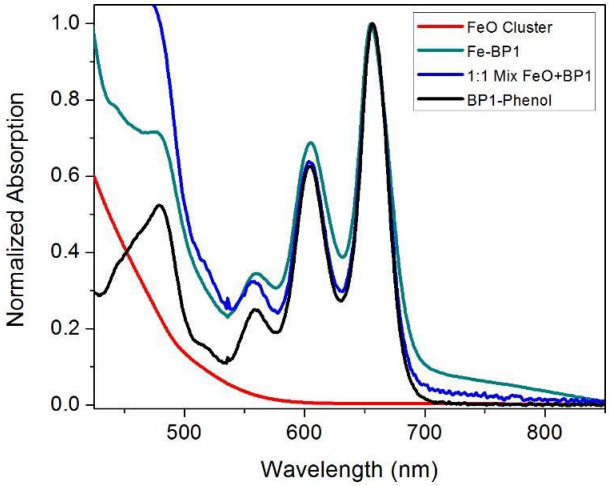

Figure 3.14 BP1-Phenol Absorption Spectra Normalized UV-Vis spectra of BP1-Phenol (black), Iron-Oxo cluster (red), a 1:1 mixture of the two in solution (blue) and the 1:1 adduct Fe-BP1 (green).

3.15 NMR Spectra

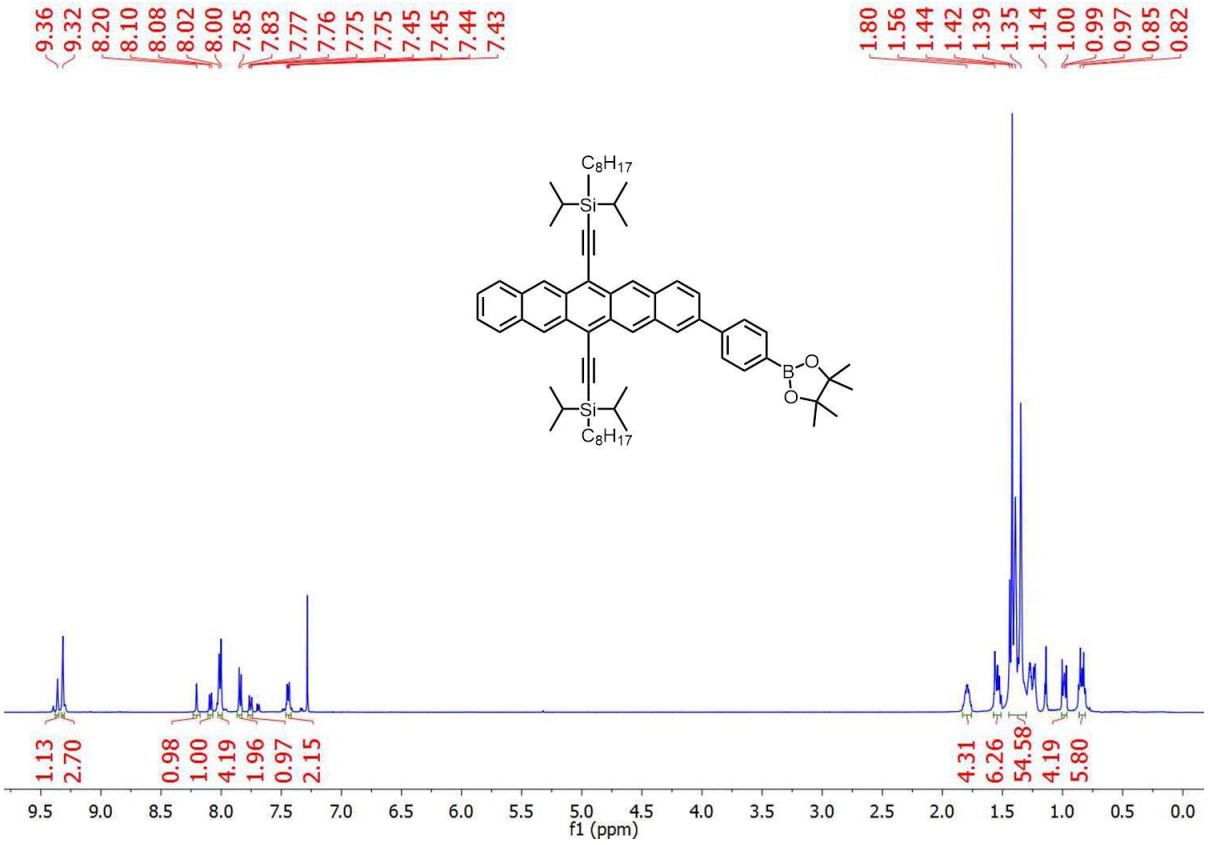
9.36
9.32
8.20
8.10
8.08
8.02
8.00
7.85
7.83
7.77
7.76
7.75
7.75
7.45
7.45
7.44
7.43
1.80
1.56
1.44
1.42
1.39
1.35
1.14
1.00
0.99
0.97
0.85
0.82
1.13
2.70
0.98
1.00
4.19
1.96
0.97
2.15
4.31
6.26
54.58
4.19
5.80
f1 (ppm)

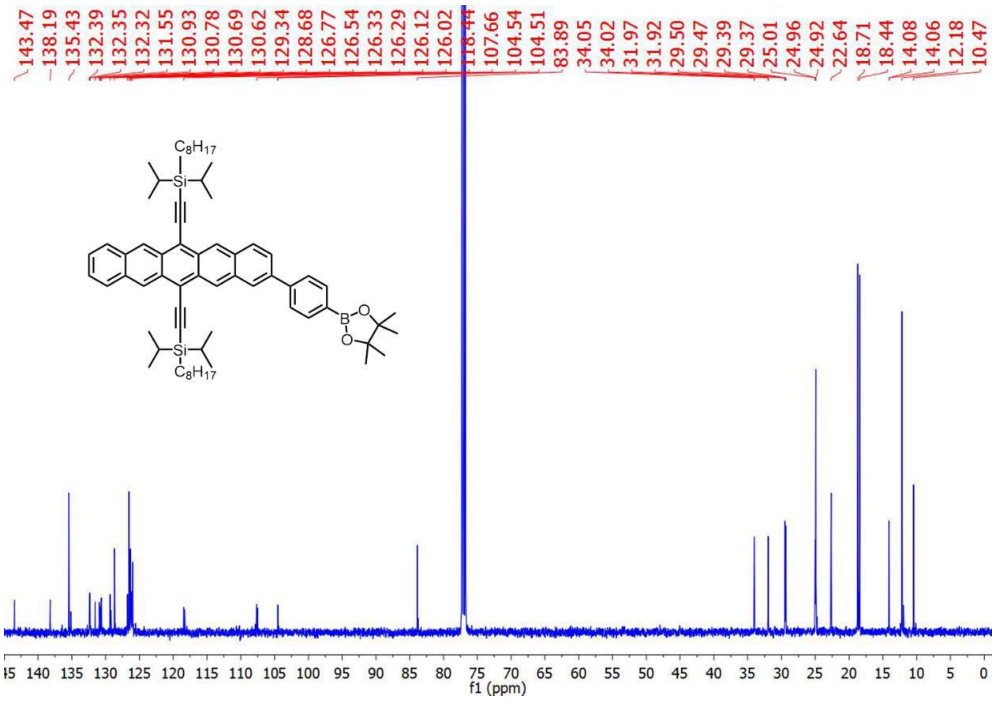
143.47
138.19
135.43
132.39
132.35
132.32
131.55
130.93
130.78
130.69
130.62
129.34
128.68
126.77
126.54
126.33
126.29
126.12
126.02
118.44
107.66
104.54
104.51
83.89
34.05
34.02
31.97
31.92
29.50
29.47
29.39
29.37
25.01
24.96
24.92
22.64
18.71
18.44
14.08
14.06
12.18
10.47
f1 (ppm)

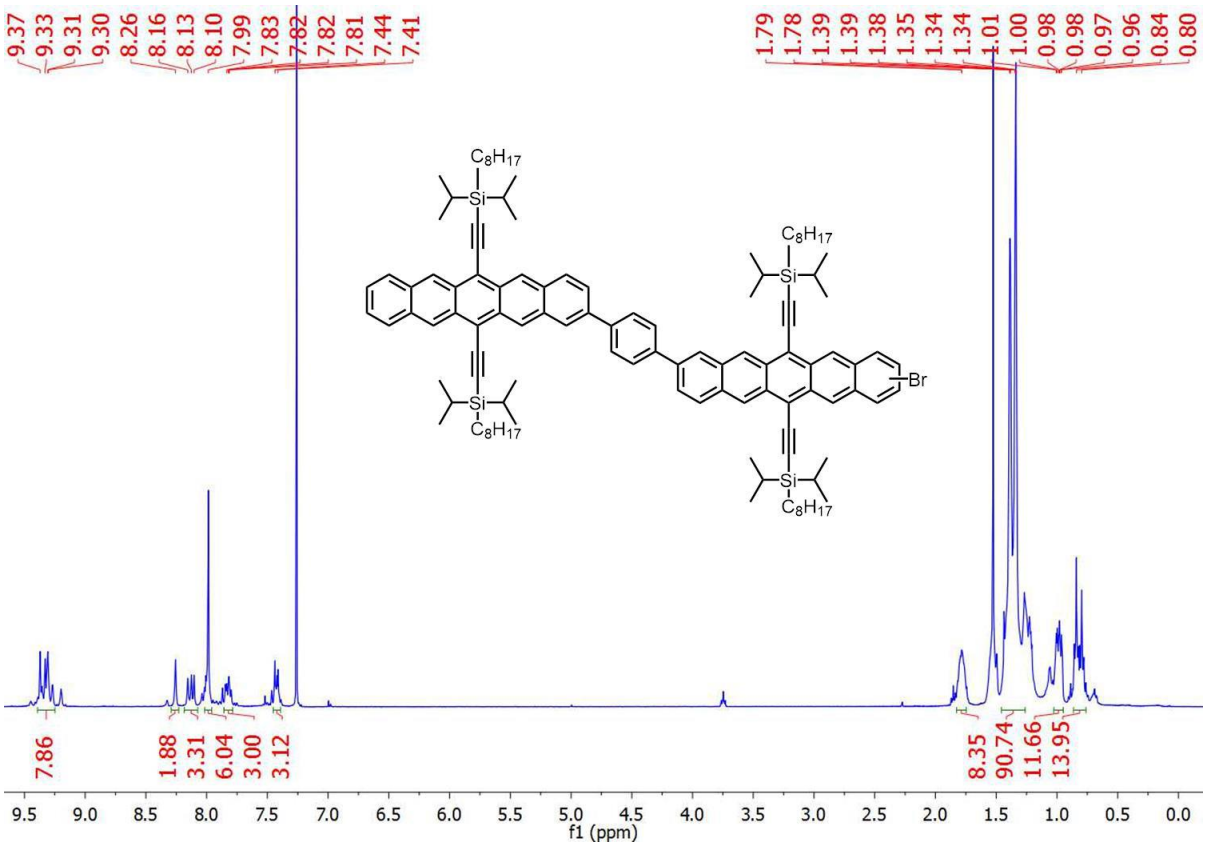
9.37
9.33
9.31
9.30
8.26
8.16
8.13
8.10
7.99
7.83
7.82
7.82
7.81
7.44
7.41
1.79
1.78
1.39
1.39
1.38
1.35
1.34
1.34
1.01
1.00
0.98
0.98
0.97
0.96
0.84
0.80
C8H17
Si
Br
7.86
1.88
3.31
6.04
3.00
3.12
8.35
90.74
11.66
13.95
9.5 9.0 8.5 8.0 7.5 7.0 6.5 6.0 5.5 5.0 4.5 4.0 3.5 3.0 2.5 2.0 1.5 1.0 0.5 0.0
f1 (ppm)

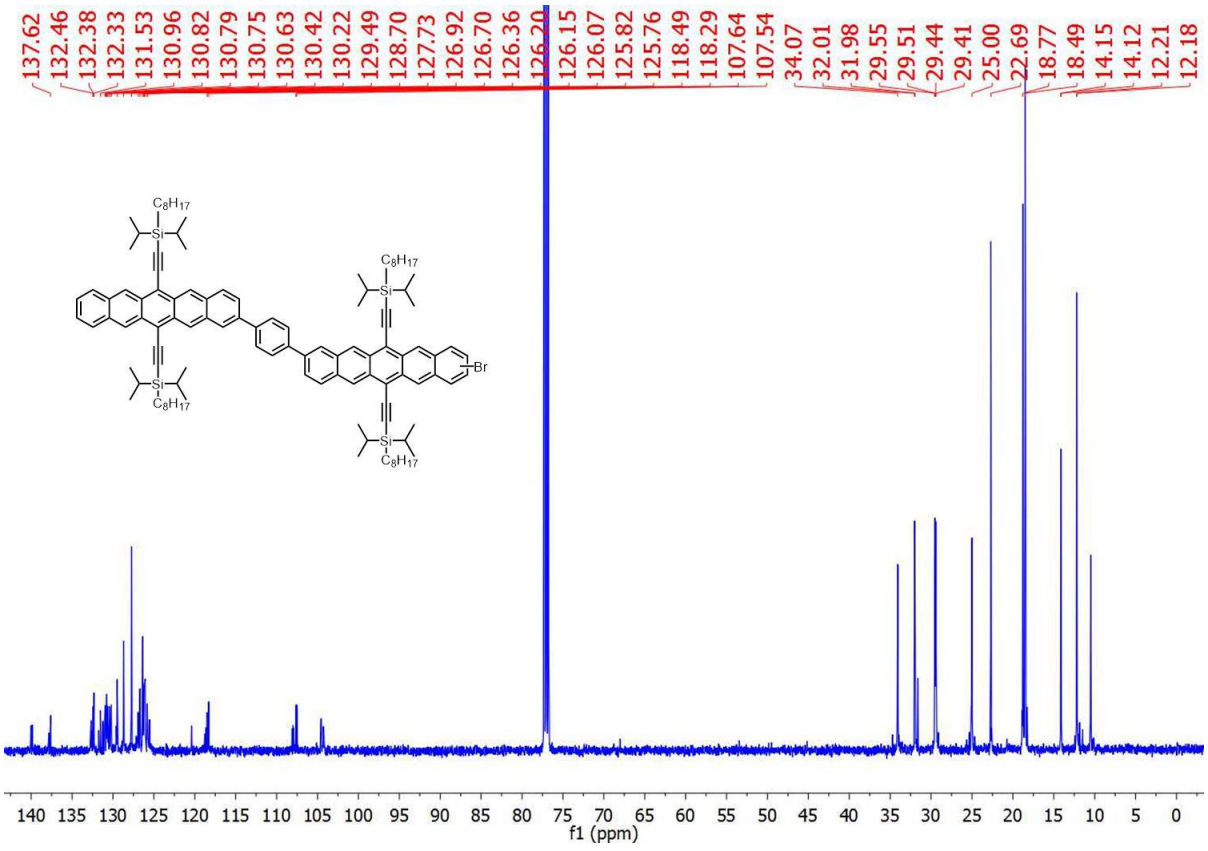
137.62
132.46
132.38
132.33
131.53
130.96
130.82
130.79
130.75
130.63
130.42
130.22
129.49
128.70
127.73
126.92
126.70
126.36
126.20
126.15
126.07
125.82
125.76
118.49
118.29
107.64
107.54
34.07
32.01
31.98
29.55
29.51
29.44
29.41
25.00
22.69
18.77
18.49
14.15
14.12
12.21
12.18
C8H17
Si
Br
140 135 130 125 120 115 110 105 100 95 90 85 80 75 70 65 60 55 50 45 40 35 30 25 20 15 10 5 0
f1 (ppm)

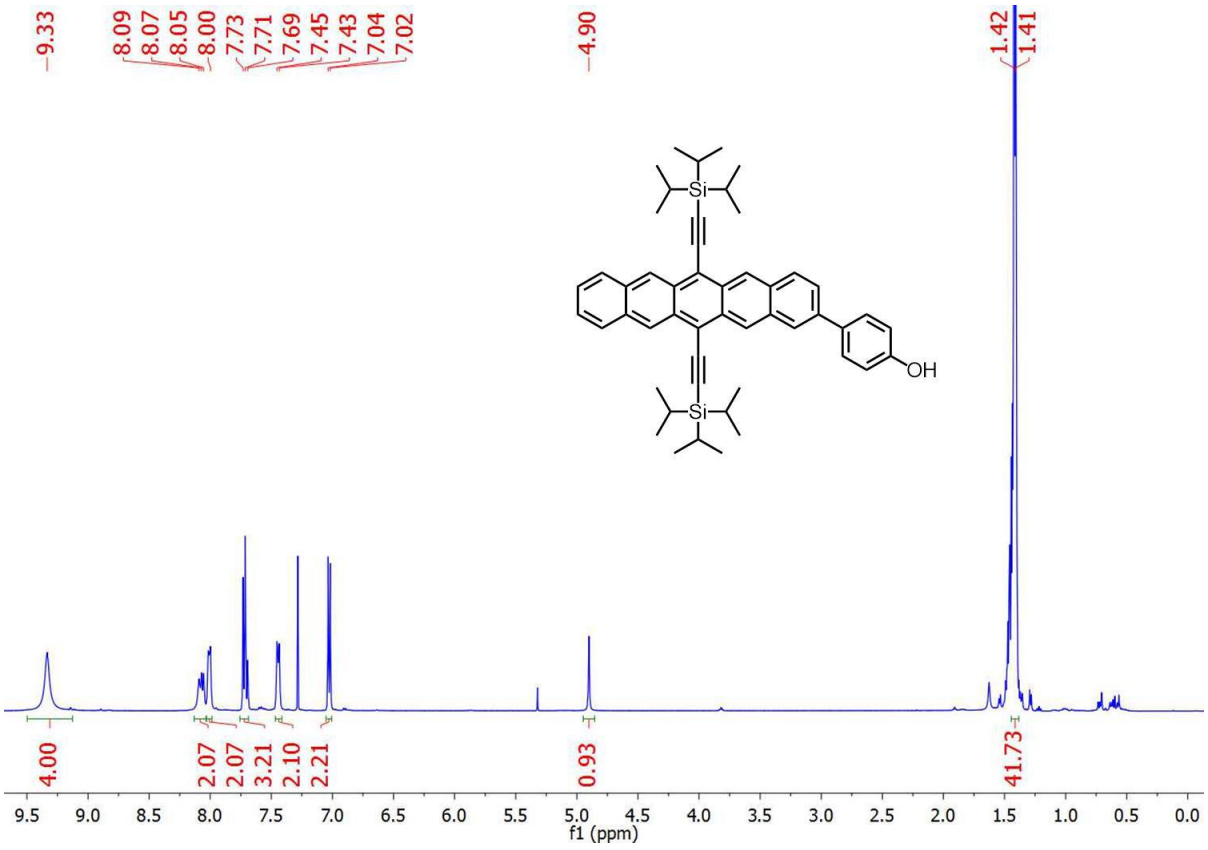
9.33
8.09
8.07
8.05
8.00
7.73
7.71
7.69
7.45
7.43
7.04
7.02
4.90
1.42
1.41
Si
Si
OH
4.00
2.07
2.07
3.21
2.10
2.21
0.93
41.73
9.5 9.0 8.5 8.0 7.5 7.0 6.5 6.0 5.5 5.0 4.5 4.0 3.5 3.0 2.5 2.0 1.5 1.0 0.5 0.0
f1 (ppm)

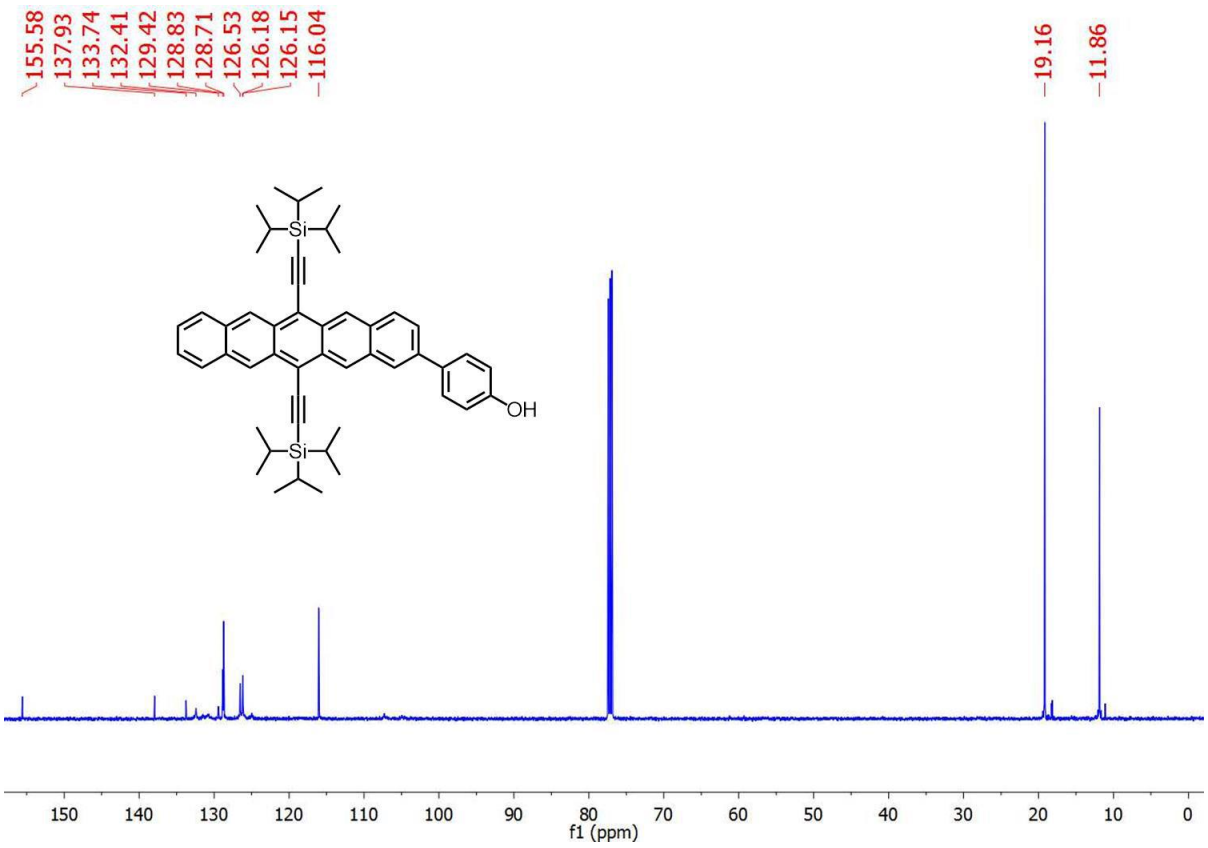
155.58
137.93
133.74
132.41
129.42
128.83
128.71
126.53
126.18
126.15
116.04
19.16
11.86
OH
Si
150 140 130 120 110 100 90 80 70 60 50 40 30 20 10 0
f1 (ppm)

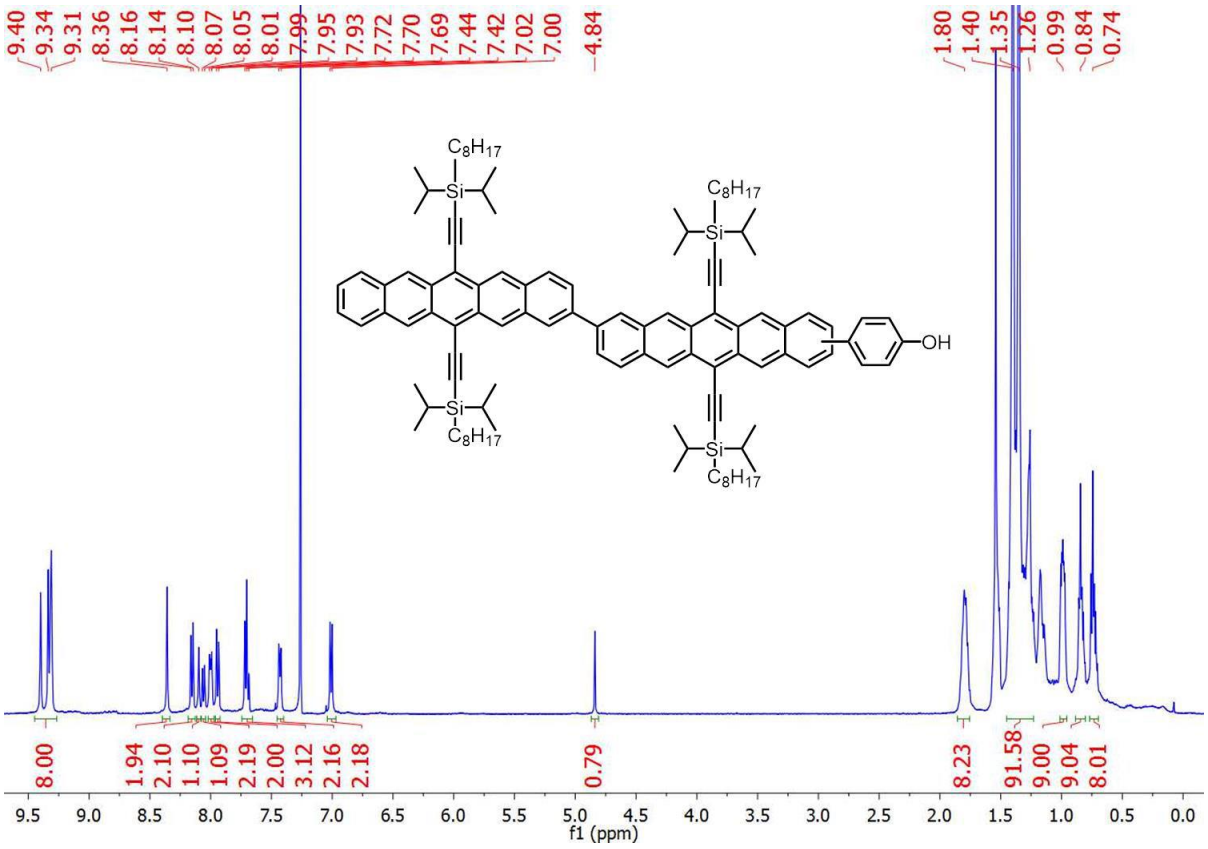
9.40
9.34
9.31
8.36
8.16
8.14
8.10
8.07
8.05
8.01
7.99
7.95
7.93
7.72
7.70
7.69
7.44
7.42
7.02
7.00
4.84
1.80
1.40
1.35
1.26
0.99
0.84
0.74
C8H17
Si
OH
8.00
1.94
2.10
1.10
1.09
2.19
2.00
3.12
2.16
2.18
0.79
8.23
91.58
9.00
9.04
8.01
9.5 9.0 8.5 8.0 7.5 7.0 6.5 6.0 5.5 5.0 4.5 4.0 3.5 3.0 2.5 2.0 1.5 1.0 0.5 0.0
f1 (ppm)

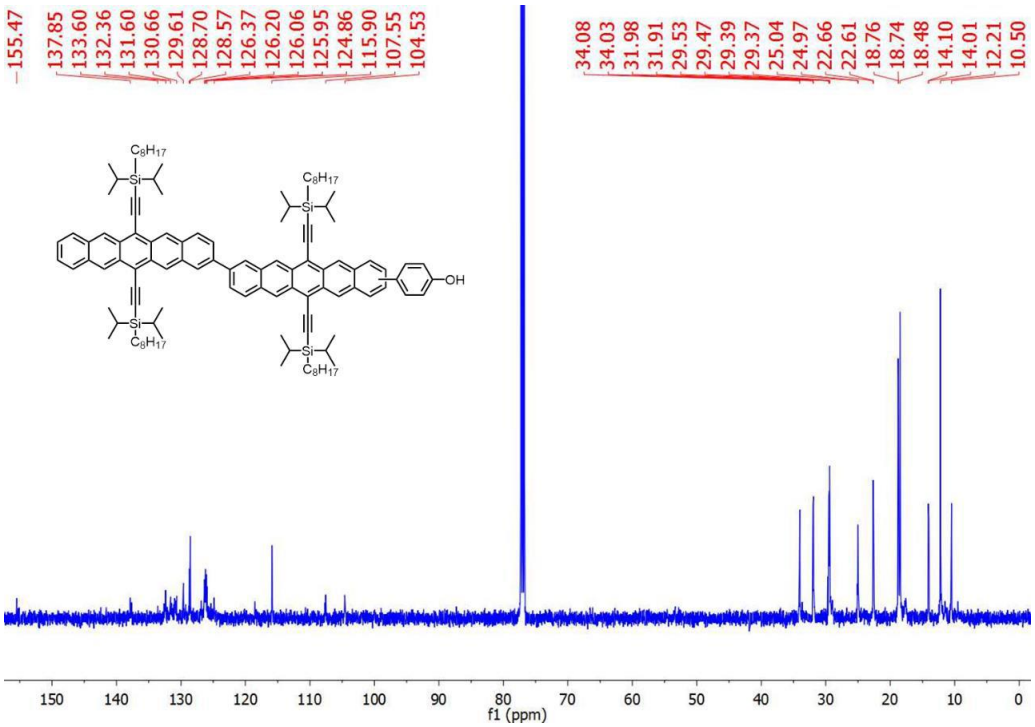
155.47
137.85
133.60
132.36
131.60
130.66
129.61
128.70
128.57
126.37
126.20
126.06
125.95
124.86
115.90
107.55
104.53
34.08
34.03
31.98
31.91
29.53
29.47
29.39
29.37
25.04
24.97
22.66
22.61
18.76
18.74
18.48
14.10
14.01
12.21
10.50
OH
f1 (ppm)

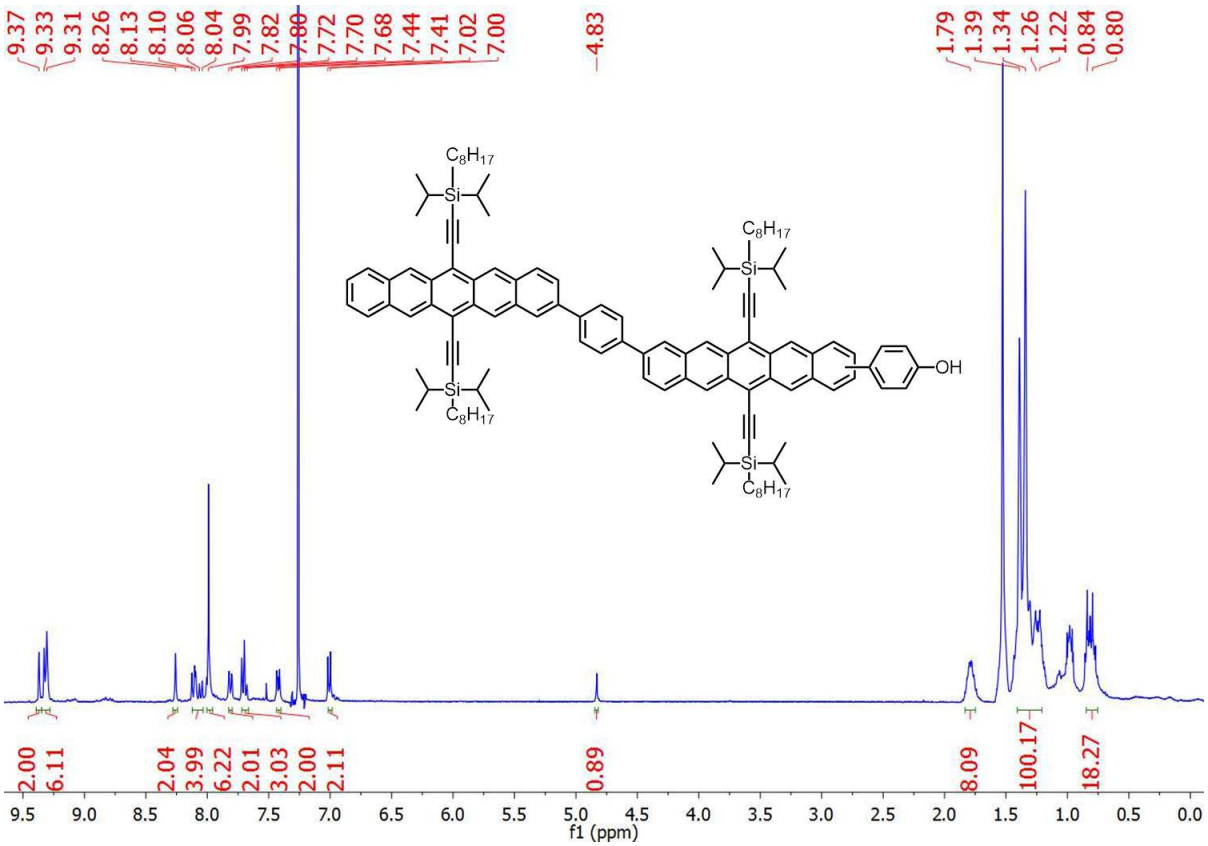
9.37
9.33
9.31
8.26
8.13
8.10
8.06
8.04
7.99
7.82
7.80
7.72
7.70
7.68
7.44
7.41
7.02
7.00
4.83
1.79
1.39
1.34
1.26
1.22
0.84
0.80
OH
2.00
6.11
2.04
3.99
6.22
2.01
3.03
2.00
2.11
0.89
8.09
100.17
18.27
f1 (ppm)

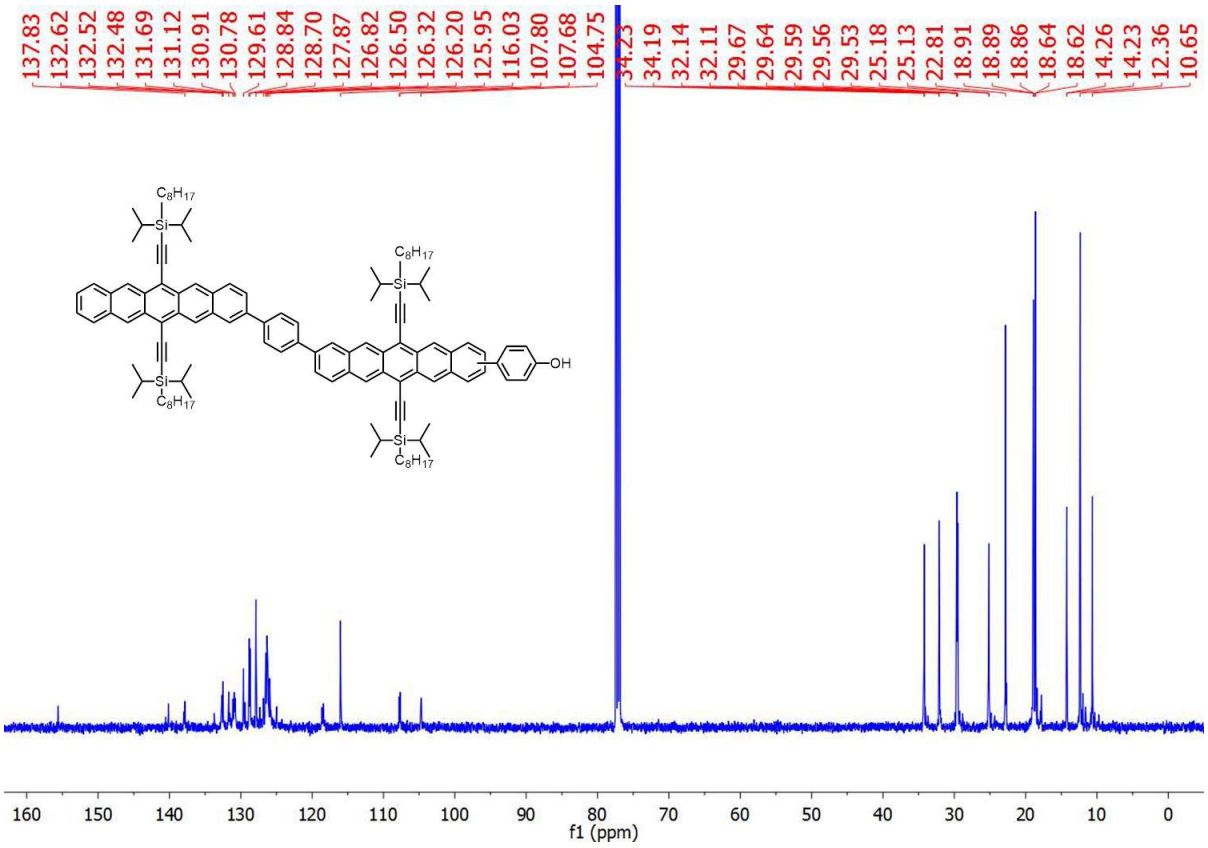
137.83
132.62
132.52
132.48
131.69
131.12
130.91
130.78
129.61
128.84
128.70
127.87
126.82
126.50
126.32
126.20
125.95
116.03
107.80
107.68
104.75
34.23
34.19
32.14
32.11
29.67
29.64
29.59
29.56
29.53
25.18
25.13
22.81
18.91
18.89
18.86
18.64
18.62
14.26
14.23
12.36
10.65
C8H17
Si
OH
160
150
140
130
120
110
100
90
80
70
60
50
40
30
20
10
0
f1 (ppm)

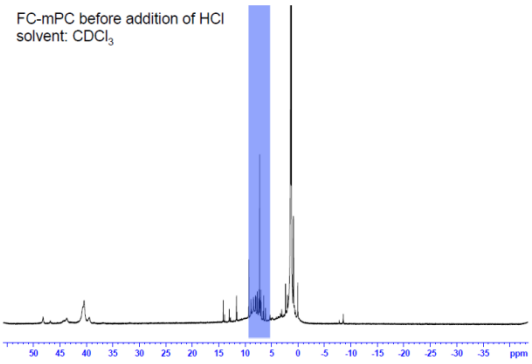

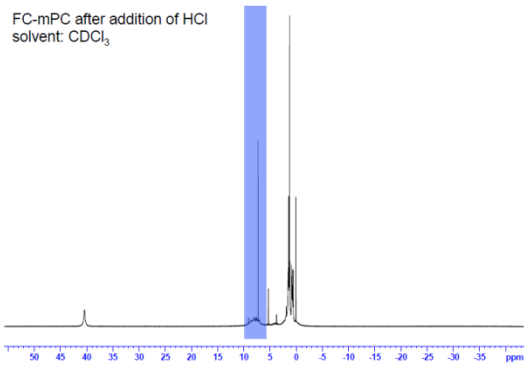

3.16 Mass Spectra

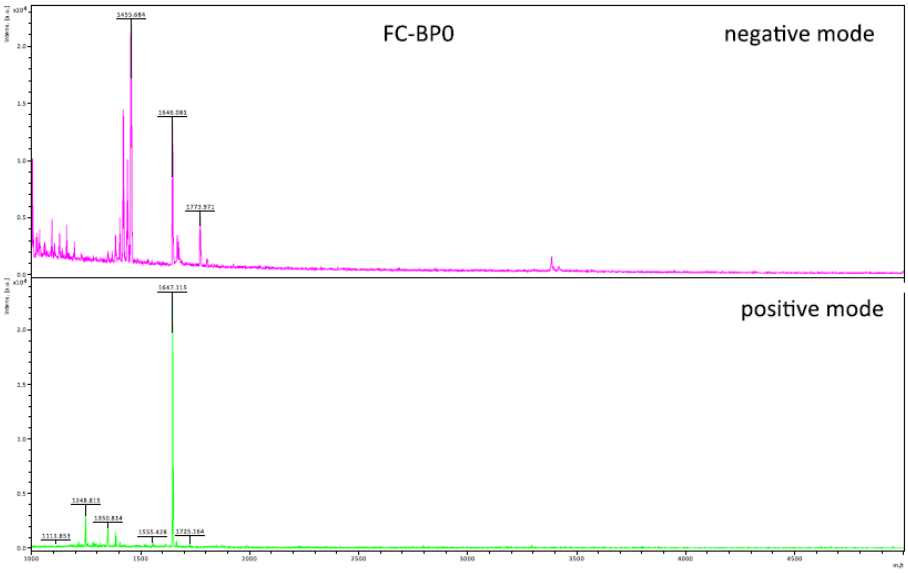

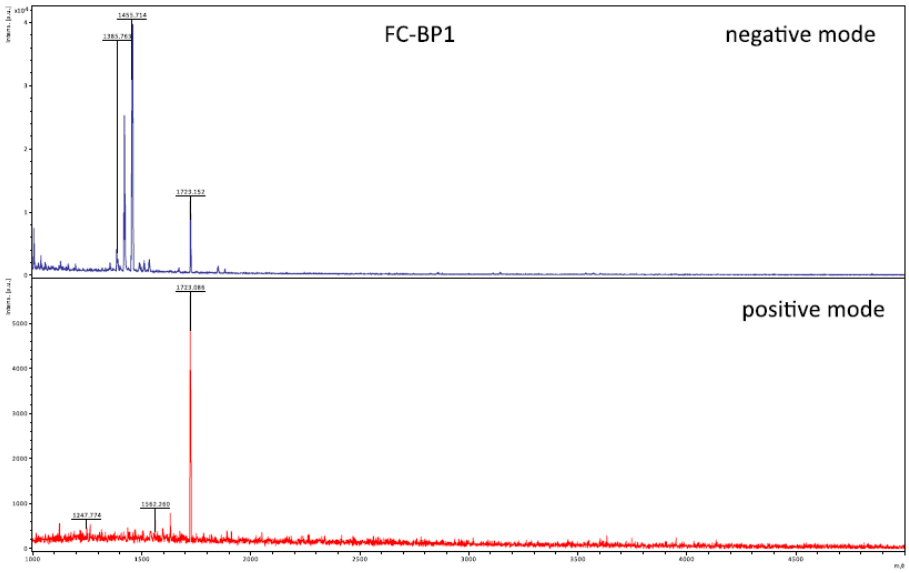

3.17 Outlook

This organic-inorganic system that we synthesized here was one of my favorite projects that I got to work on. One of the biggest issues moving forward with this project involves the purification of these hybrid compounds. If that issue can be overcome, given the amount of literature on inorganic clusters, I think there are many different hybrids that could be studied.

Besides new materials, in this project in particular, a large impact could be made if the triplets from iSF could be extracted to the iron-oxo cluster, and then the dream would be for that excited cluster to perform some sort of chemical work, either catalysis or charge extraction in a device. Of course the bound triplet pair state gives us problems in all our iSF work, but the energy sink motif from Chapter 4 could potentially be applied here. We also have learned a lot more chemistry involving tetracenes. Given that I have made a tetracene dimer ligand for Akshay Rao that has a thiol on one side, it should be possible to make this into a phenoxy and link it to the iron-oxo cluster or another cluster. The higher triplet energy of tetracene may reveal different dynamics.

On a somewhat related note, it would be nice to see if the inorganic clusters from the Roy lab could be used as sensitizers. We spoke about this a couple times, but the tungsten clusters did not upconvert when mixed in solution with anthracenes. This would be a very interesting system to explore and I hope someone takes it up at some point. A hybrid sensitizer-annihilator system could also be synthesized, similar to the work of Ming Lee Tang, except with a cleaner system since you would know how many annihilators are attached to each sensitizer.

3.18 References

(1) Trinh, M. T.; Pinkard, A.; Pun, A. B.; Sanders, S. N.; Kumarasamy, E.; Sfeir, M. Y.; Campos, L. M.; Roy, X.; Zhu, X.-Y. Distinct Properties of the Triplet Pair State from Singlet Fission. *Sci. Adv.* **2017**, *3* (7).

(2) Smith, M. B.; Michl, J. Singlet Fission. *Chem. Rev.* **2010**, *110* (11), 6891–6936.

(3) Smith, M. B.; Michl, J. Recent Advances in Singlet Fission. *Annu. Rev. Phys. Chem.* **2013**, *64* (1), 361–386.

(4) Johnson, R. C.; Merrifield, R. E. Effects of Magnetic Fields on the Mutual Annihilation of Triplet Excitons in Anthracene Crystals. *Phys. Rev. B* **1970**, *1* (2), 896–902.

(5) Suna, A. Kinematics of Exciton-Exciton Annihilation in Molecular Crystals. *Phys. Rev. B* **1970**, *1* (4), 1716–1739.

(6) Monahan, N.; Zhu, X.-Y. Charge Transfer–Mediated Singlet Fission. *Annu. Rev. Phys. Chem.* **2015**, *66* (1), 601–618.

(7) Monahan, N. R.; Sun, D.; Tamura, H.; Williams, K. W.; Xu, B.; Zhong, Y.; Kumar, B.; Nuckolls, C.; Harutyunyan, A. R.; … Zhu, X.-Y. Dynamics of the Triplet-Pair State

Reveals the Likely Coexistence of Coherent and Incoherent Singlet Fission in Crystalline Hexacene. *Nat. Chem.* **2016**, *9*, 341.
(8) Pensack, R. D.; Tilley, A. J.; Parkin, S. R.; Lee, T. S.; Payne, M. M.; Gao, D.; Jahnke, A. A.; Oblinsky, D. G.; Li, P.-F.; … Scholes, G. D. Exciton Delocalization Drives Rapid Singlet Fission in Nanoparticles of Acene Derivatives. *J. Am. Chem. Soc.* **2015**, *137* (21), 6790–6803.
(9) Wang, R.; Zhang, C.; Zhang, B.; Liu, Y.; Wang, X.; Xiao, M. Magnetic Dipolar Interaction between Correlated Triplets Created by Singlet Fission in Tetracene Crystals. *Nat. Commun.* **2015**, *6*, 8602.
(10) Teichen, P. E.; Eaves, J. D. Collective Aspects of Singlet Fission in Molecular Crystals. *J. Chem. Phys.* **2015**, *143* (4), 44118.
(11) Chan, W.-L.; Ligges, M.; Zhu, X.-Y. The Energy Barrier in Singlet Fission Can Be Overcome through Coherent Coupling and Entropic Gain. *Nat. Chem.* **2012**, *4*, 840.
(12) Sanders, S. N.; Kumarasamy, E.; Pun, A. B.; Trinh, M. T.; Choi, B.; Xia, J.; Taffet, E. J.; Low, J. Z.; Miller, J. R.; … Campos, L. M. Quantitative Intramolecular Singlet Fission in Bipentacenes. *J. Am. Chem. Soc.* **2015**, *137* (28), 8965–8972.
(13) Busby, E.; Xia, J.; Wu, Q.; Low, J. Z.; Song, R.; Miller, J. R.; Zhu, X.-Y.; Campos, L. M.; Sfeir, M. Y. A Design Strategy for Intramolecular Singlet Fission Mediated by Charge-Transfer States in Donor–acceptor Organic Materials. *Nat. Mater.* **2015**, *14* (4), 426–433.
(14) Margulies, E. A.; Miller, C. E.; Wu, Y.; Ma, L.; Schatz, G. C.; Young, R. M.; Wasielewski, M. R. Enabling Singlet Fission by Controlling Intramolecular Charge Transfer in π-Stacked Covalent Terrylenediimide Dimers. *Nat. Chem.* **2016**, *8* (12), 1120–1125.
(15) Zirzlmeier, J.; Lehnherr, D.; Coto, P. B.; Chernick, E. T.; Casillas, R.; Basel, B. S.; Thoss, M.; Tykwinski, R. R.; Guldi, D. M. Singlet Fission in Pentacene Dimers. *Proc. Natl. Acad. Sci.* **2015**, *112* (17), 5325–5330.
(16) Trinh, M. T.; Zhong, Y.; Chen, Q.; Schiros, T.; Jockusch, S.; Sfeir, M. Y.; Steigerwald, M.; Nuckolls, C.; Zhu, X. Intra- to Intermolecular Singlet Fission. *J. Phys. Chem. C* **2015**, *119* (3), 1312–1319.
(17) Korovina, N. V; Das, S.; Nett, Z.; Feng, X.; Joy, J.; Haiges, R.; Krylov, A. I.; Bradforth, S. E.; Thompson, M. E. Singlet Fission in a Covalently Linked Cofacial Alkynyltetracene Dimer. *J. Am. Chem. Soc.* **2016**, *138* (2), 617–627.
(18) Fuemmeler, E. G.; Sanders, S. N.; Pun, A. B.; Kumarasamy, E.; Zeng, T.; Miyata, K.; Steigerwald, M. L.; Zhu, X.-Y.; Sfeir, M. Y.; Campos, L. M.; Ananth, N. A Direct Mechanism of Ultrafast Intramolecular Singlet Fission in Pentacene Dimers. *ACS Cent. Sci.* **2016**, *2* (5), 316–324.
(19) Tayebjee, M. J. Y.; Sanders, S. N.; Kumarasamy, E.; Campos, L. M.; Sfeir, M. Y.; McCamey, D. R. Quintet Multiexciton Dynamics in Singlet Fission. *Nat. Phys.* **2017**, *13* (2), 182–188.
(20) Scholes, G. D. Correlated Pair States Formed by Singlet Fission and Exciton–Exciton Annihilation. *J. Phys. Chem. A* **2015**, *119* (51), 12699–12705.
(21) Koutecky, J.; Paldus, J. Quantum Chemical Studies on Transannular Interaction. *Tetrahedron* **1963**, *19*, 201–221.
(22) Hosteny, R. P.; Dunning, T. H.; Gilman, R. R.; Pipano, A.; Shavitt, I. Ab Initio Study of the Π-electron States of Trans-butadiene. *J. Chem. Phys.* **1975**, *62* (12), 4764–4779.
(23) Tavan, P.; Schulten, K. Electronic Excitations in Finite and Infinite Polyenes. *Phys. Rev. B*

1987, *36* (8), 4337–4358.
(24) Polívka, T.; Sundström, V. Dark Excited States of Carotenoids: Consensus and Controversy. *Chem. Phys. Lett.* **2009**, *477* (1), 1–11.
(25) Gradinaru, C. C.; Kennis, J. T. M.; Papagiannakis, E.; van Stokkum, I. H. M.; Cogdell, R. J.; Fleming, G. R.; Niederman, R. A.; van Grondelle, R. An Unusual Pathway of Excitation Energy Deactivation in Carotenoids: Singlet-to-Triplet Conversion on an Ultrafast Timescale in a Photosynthetic Antenna. *Proc. Natl. Acad. Sci.* **2001**, *98* (5), 2364 LP-2369.
(26) Papagiannakis, E.; Kennis, J. T. M.; van Stokkum, I. H. M.; Cogdell, R. J.; van Grondelle, R. An Alternative Carotenoid-to-Bacteriochlorophyll Energy Transfer Pathway in Photosynthetic Light Harvesting. *Proc. Natl. Acad. Sci.* **2002**, *99* (9), 6017 LP-6022.
(27) Antognazza, M. R.; Lüer, L.; Polli, D.; Christensen, R. L.; Schrock, R. R.; Lanzani, G.; Cerullo, G. Ultrafast Excited State Relaxation in Long-Chain Polyenes. *Chem. Phys.* **2010**, *373* (1), 115–121.
(28) Berkelbach, T. C.; Hybertsen, M. S.; Reichman, D. R. Microscopic Theory of Singlet Exciton Fission. II. Application to Pentacene Dimers and the Role of Superexchange. *J. Chem. Phys.* **2013**, *138* (11), 114103.
(29) Feng, X.; Casanova, D.; Krylov, A. I. Intra- and Intermolecular Singlet Fission in Covalently Linked Dimers. *J. Phys. Chem. C* **2016**, *120* (34), 19070–19077.
(30) Coto, P. B.; Sharifzadeh, S.; Neaton, J. B.; Thoss, M. Low-Lying Electronic Excited States of Pentacene Oligomers: A Comparative Electronic Structure Study in the Context of Singlet Fission. *J. Chem. Theory Comput.* **2015**, *11* (1), 147–156.
(31) Zeng, T.; Hoffmann, R.; Ananth, N. The Low-Lying Electronic States of Pentacene and Their Roles in Singlet Fission. *J. Am. Chem. Soc.* **2014**, *136* (15), 5755–5764.
(32) Aryanpour, K.; Shukla, A.; Mazumdar, S. Theory of Singlet Fission in Polyenes, Acene Crystals, and Covalently Linked Acene Dimers. *J. Phys. Chem. C* **2015**, *119* (13), 6966–6979.
(33) Feng, X.; Luzanov, A. V; Krylov, A. I. Fission of Entangled Spins: An Electronic Structure Perspective. *J. Phys. Chem. Lett.* **2013**, *4* (22), 3845–3852.
(34) Sanders, S. N.; Kumarasamy, E.; Pun, A. B.; Steigerwald, M. L.; Sfeir, M. Y.; Campos, L. M. Singlet Fission in Polypentacene. *Chem* **2017**, *1* (3), 505–511.
(35) Chan, W.-L.; Ligges, M.; Jailaubekov, A.; Kaake, L.; Miaja-Avila, L.; Zhu, X.-Y. Observing the Multiexciton State in Singlet Fission and Ensuing Ultrafast Multielectron Transfer. *Science* **2011**, *334* (6062), 1541 LP-1545.
(36) Yost, S. R.; Lee, J.; Wilson, M. W. B.; Wu, T.; McMahon, D. P.; Parkhurst, R. R.; Thompson, N. J.; Congreve, D. N.; Rao, A.; … Van Voorhis, T. A Transferable Model for Singlet-Fission Kinetics. *Nat. Chem.* **2014**, *6* (6), 492–497.
(37) Lukman, S.; Musser, A. J.; Chen, K.; Athanasopoulos, S.; Yong, C. K.; Zeng, Z.; Ye, Q.; Chi, C.; Hodgkiss, J. M.; … Greenham, N. C. Tuneable Singlet Exciton Fission and Triplet–Triplet Annihilation in an Orthogonal Pentacene Dimer. *Adv. Funct. Mater.* **2015**, *25* (34), 5452–5461.
(38) Pensack, R. D.; Ostroumov, E. E.; Tilley, A. J.; Mazza, S.; Grieco, C.; Thorley, K. J.; Asbury, J. B.; Seferos, D. S.; Anthony, J. E.; Scholes, G. D. Observation of Two Triplet-Pair Intermediates in Singlet Exciton Fission. *J. Phys. Chem. Lett.* **2016**, *7* (13), 2370–2375.
(39) Dexter, D. L. Two Ideas on Energy Transfer Phenomena: Ion-Pair Effects Involving the

OH Stretching Mode, and Sensitization of Photovoltaic Cells. *J. Lumin.* **1979**, *18–19*, 779–784.
(40) Hanna, M. C.; Nozik, A. J. Solar Conversion Efficiency of Photovoltaic and Photoelectrolysis Cells with Carrier Multiplication Absorbers. *J. Appl. Phys.* **2006**, *100* (7).
(41) Chan, W.-L.; Tritsch, J. R.; Zhu, X.-Y. Harvesting Singlet Fission for Solar Energy Conversion: One- versus Two-Electron Transfer from the Quantum Mechanical Superposition. *J. Am. Chem. Soc.* **2012**, *134* (44), 18295–18302.
(42) Tritsch, J. R.; Chan, W.-L.; Wu, X.; Monahan, N. R.; Zhu, X.-Y. Harvesting Singlet Fission for Solar Energy Conversion via Triplet Energy Transfer. *Nat. Commun.* **2013**, *4*, 1–7.
(43) Thompson, N. J.; Wilson, M. W. B.; Congreve, D. N.; Brown, P. R.; Scherer, J. M.; Bischof, T. S.; Wu, M.; Geva, N.; Welborn, M.; … Baldo, M. A. Energy Harvesting of Non-Emissive Triplet Excitons in Tetracene by Emissive PbS Nanocrystals. *Nat. Mater.* **2014**, *13*, 1039.
(44) Tabachnyk, M.; Ehrler, B.; Gélinas, S.; Böhm, M. L.; Walker, B. J.; Musselman, K. P.; Greenham, N. C.; Friend, R. H.; Rao, A. Resonant Energy Transfer of Triplet Excitons from Pentacene to PbSe Nanocrystals. *Nat. Mater.* **2014**, *13*, 1033.
(45) Congreve, D. N.; Lee, J.; Thompson, N. J.; Hontz, E.; Yost, S. R.; Reusswig, P. D.; Bahlke, M. E.; Reineke, S.; Van Voorhis, T.; Baldo, M. A. External Quantum Efficiency Above 100% in a Singlet-Exciton-Fission-Based Organic Photovoltaic Cell. *Science* **2013**, *340* (6130), 334–337.
(46) Paci, I.; Johnson, J. C.; Chen, X.; Rana, G.; Popović, D.; David, D. E.; Nozik, A. J.; Ratner, M. A.; Michl, J. Singlet Fission for Dye-Sensitized Solar Cells: Can a Suitable Sensitizer Be Found? *J. Am. Chem. Soc.* **2006**, *128* (51), 16546–16553.
(47) Esswein, A. J.; Nocera, D. G. Hydrogen Production by Molecular Photocatalysis. *Chem. Rev.* **2007**, *107* (10), 4022–4047.
(48) Bardeen, C. J. The Structure and Dynamics of Molecular Excitons. *Annu. Rev. Phys. Chem.* **2014**, *65* (1), 127–148.
(49) Turkiewicz, A.; Paley, D. W.; Besara, T.; Elbaz, G.; Pinkard, A.; Siegrist, T.; Roy, X. Assembling Hierarchical Cluster Solids with Atomic Precision. *J. Am. Chem. Soc.* **2014**, *136* (45), 15873–15876.
(50) Baran, P.; Boča, R.; Chakraborty, I.; Giapintzakis, J.; Herchel, R.; Huang, Q.; McGrady, J. E.; Raptis, R. G.; Sanakis, Y.; Simopoulos, A. Synthesis, Characterization, and Study of Octanuclear Iron-Oxo Clusters Containing a Redox-Active Fe4O4-Cubane Core. *Inorg. Chem.* **2008**, *47* (2), 645–655.
(51) Alhashmialameer, D.; Collins, J.; Hattenhauer, K.; Kerton, F. M. Iron Amino-Bis(Phenolate) Complexes for the Formation of Organic Carbonates from CO2 and Oxiranes. *Catal. Sci. Technol.* **2016**, *6* (14), 5364–5373.
(52) Chakraborty, H.; Shukla, A. Theory of Triplet Optical Absorption in Oligoacenes: From Naphthalene to Heptacene. *J. Chem. Phys.* **2014**, *141* (16), 164301.
(53) Kamada, K.; Ohta, K.; Kubo, T.; Shimizu, A.; Morita, Y.; Nakasuji, K.; Kishi, R.; Ohta, S.; Furukawa, S.; … Nakano, M. Strong Two-Photon Absorption of Singlet Diradical Hydrocarbons. *Angew. Chem. Int. Ed.* **2007**, *46* (19), 3544–3546.
(54) Piland, G. B.; Burdett, J. J.; Dillon, R. J.; Bardeen, C. J. Singlet Fission: From Coherences to Kinetics. *J. Phys. Chem. Lett.* **2014**, *5* (13), 2312–2319.

(55) Bakulin, A. A.; Lovrincic, R.; Yu, X.; Selig, O.; Bakker, H. J.; Rezus, Y. L. A.; Nayak, P. K.; Fonari, A.; Coropceanu, V.; … Cahen, D. Mode-Selective Vibrational Modulation of Charge Transport in Organic Electronic Devices. *Nat. Commun.* **2015**, *6*, 7880.
(56) de Jong, M.; Seijo, L.; Meijerink, A.; Rabouw, F. T. Resolving the Ambiguity in the Relation between Stokes Shift and Huang–Rhys Parameter. *Phys. Chem. Chem. Phys.* **2015**, *17* (26), 16959–16969.
(57) Walker, B. J.; Musser, A. J.; Beljonne, D.; Friend, R. H. Singlet Exciton Fission in Solution. *Nat. Chem.* **2013**, *5* (12), 1019–1024.
(58) Payne, M. M.; Delcamp, J. H.; Parkin, S. R.; Anthony, J. E. Robust, Soluble Pentacene Ethers. *Org. Lett.* **2004**, *6* (10), 1609–1612.
(59) Raptis, R. G.; Georgakaki, I. P.; Hockless, D. C. R. A FeIII/Oxo Cubane Contained in an Octanuclear Complex of T Symmetry That Is Stable Over Five Oxidation States. *Angew. Chem. Int. Ed.* **1999**, *38* (11), 1632–1634.
(60) Janietz, S.; Bradley, D. D. C.; Grell, M.; Giebeler, C.; Inbasekaran, M.; Woo, E. P. Electrochemical Determination of the Ionization Potential and Electron Affinity of Poly(9,9-Dioctylfluorene). *Appl. Phys. Lett.* **1998**, *73* (17), 2453–2455.
(61) Zhu, X.-Y. How to Draw Energy Level Diagrams in Excitonic Solar Cells. *J. Phys. Chem. Lett.* **2014**, *5* (13), 2283–2288.
(62) Lower, S. K.; El-Sayed, M. A. The Triplet State and Molecular Electronic Processes in Organic Molecules. *Chem. Rev.* **1966**, *66* (2), 199–241.

Chapter 4: Free Triplets via Intramolecular Singlet Fission

4.1 Preface

This chapter is based on manuscript entitled "Ultrafast Intramolecular Singlet Fission to Persistent Multiexcitons" by Andrew B. Pun, Amir Asadpoordarvish, Elango Kumarasamy, Murad J.Y. Tayebjee, Daniel Niesner, Dane R. McCamey, Samuel N. Sanders, Luis M. Campos, and Matthew Y. Sfeir which has been accepted for publication in Nature Chemistry.

I designed the molecules with Samuel N. Sanders, Elango Kumarasamy, and Luis M. Campos. I synthesized the molecules with Elango Kumarasamy. Samuel N. Sanders, Daniel Niesner and Matthew Y. Sfeir performed transient absorption measurements and analyzed the data. Amir Asadpoordarvish, Murad J. Y. Tayebjee, and Samuel N. Sanders performed the time-resolved electron spin resonance measurements, with data analyzed by them along with Dane R. McCamey and Matthew Y. Sfeir. Equal contributions to this paper were made by Amir Asadpoordarvish, Samuel N. Sanders, and myself.

4.2 Introduction

In both natural light harvesting complexes and synthetic materials, molecular assemblies rely on marked energy gradients to convert light into usable forms of energy, e.g., funneling of excitons in light harvesting complexes or in artificial electron transfer complexes, such as occurs in the generation of long-lived charge separated states in donor-bridge-acceptor molecules and at molecular interfaces.[1–3] In excitonic amplification systems, where one photon leads to two or more excitons, there is a grand challenge to control and dictate the fate of the multiexciton state.[4–6] While inorganic materials yield weakly correlated excitons, competition from carrier cooling and remarkably fast rates of multiexciton recombination inhibit the formation of a stable multiexciton population.[7,8] On the other hand, organic singlet fission chromophores are highly

tunable and can form long-lived multiexcitons rapidly at the ideal energy threshold, i.e., quantitatively producing two excitons from one photon at the point when the total energy conservation requirement is reached. But SF chromophores have been observed to yield highly localized triplet pairs that exhibit strong coupling interactions.[9–14] In this vein, little is known about trapped triplet pairs that are forced to cohabit individual molecules, particularly the relationship between the population (number of triplets) and magnetization dynamics.[15,16] Thus, we postulate that molecular engineering with precise selection and arrangement of building blocks can be used to tune energy gradients that can quantitatively split and direct the migration of correlated triplet pairs into individual free triplet excitons.

To date, families of intramolecular singlet fission (iSF) chromophores have been reported, including heterodimers, oligomers, and polymers of tetracene and pentacene (Figure 4.1A).[17–31] While structure-property relationship studies have led to profound information about multiexciton dynamics in various materials, molecular design guidelines to tune the interactions between triplets and the triplet pair dissociation dynamics are still in their infancy.[20] The primary bottleneck for the design of iSF materials is that it has been a challenge to independently optimize triplet formation and triplet decay rates. Importantly, simultaneous fast formation and slow decay has not been observed within the same system in individual molecules.

Early studies established that strongly coupled contiguous chromophores, in which spin-coupled triplet pairs, $^{m}(T_1T_1)$, residing on adjacent molecular units undergo ultrafast iSF rates (Figure 4.1B). However, these materials exhibit a correspondingly fast decay rate from the triplet pair state.[26,28,32] Studies of singlet fission polymers have revealed that this problem cannot be overcome by simply extending the conjugated backbone (e.g., from a dimer to a polymer) due to the large biexciton binding energies.[18,29,33] As the energy of the biexciton is not exactly twice the

energy of the free triplet, determining the exact nature of the triplet pair is important for chromophore design, resolving controversies regarding the energy conservation criteria, including the role of entropy, and for developing appropriate exciton harvesting schemes.[33–35] The most successful approach to enhance triplet pair lifetimes involves using bridges to separate chromophores, as the bonding motif (e.g., conjugated, cross-conjugated, and homo-/non-conjugated bridges) can be used to modulate electronic coupling between triplets in the pair (Figure 4.1C).[15,17,24,27,32,36,37] In these compounds, a sub-population of triplet pair species can dissociate into free triplets with lifetimes comparable to molecular crystals. However, increasing the lifetime of the triplets comes at the cost of iSF yields, as excited state population is readily lost by radiative recombination and other parasitic deactivation processes.[15,17,24,36]

Thus, the question remains – how can chromophores be designed such that rates of iSF are fast while quantitatively yielding persistent multiexcitons? Addressing this fundamental question can lead to important information about the nature of the triplet pair, the behavior of multiexcitons in individual molecules and new molecular design guidelines – all of which are essential to optoelectronic devices, photophysical processes, and reactivity. Here, we introduce a general "energy cleft" design (Figure 4.1D) that produces strongly coupled triplet pairs on ultrafast timescales, and then breaks them into weakly coupled triplet pairs. This strategy leverages the inequivalent triplet energies of pentacene (P) and tetracene (T) building blocks (Figure 4.1A), arranged in order to create a corrugated potential energy surface that drives the spatial separation of the two triplets, thus reducing their electronic coupling. It is important to note that these systems do not rely on conventional donor/acceptor interactions, or intermolecular assemblies to break short-lived correlated triplet pairs. The resulting molecules

based on the connectivity of pentacene and tetracene derivatives undergo ultrafast iSF, and near unity generation of free triplets that live for ~20 µs.

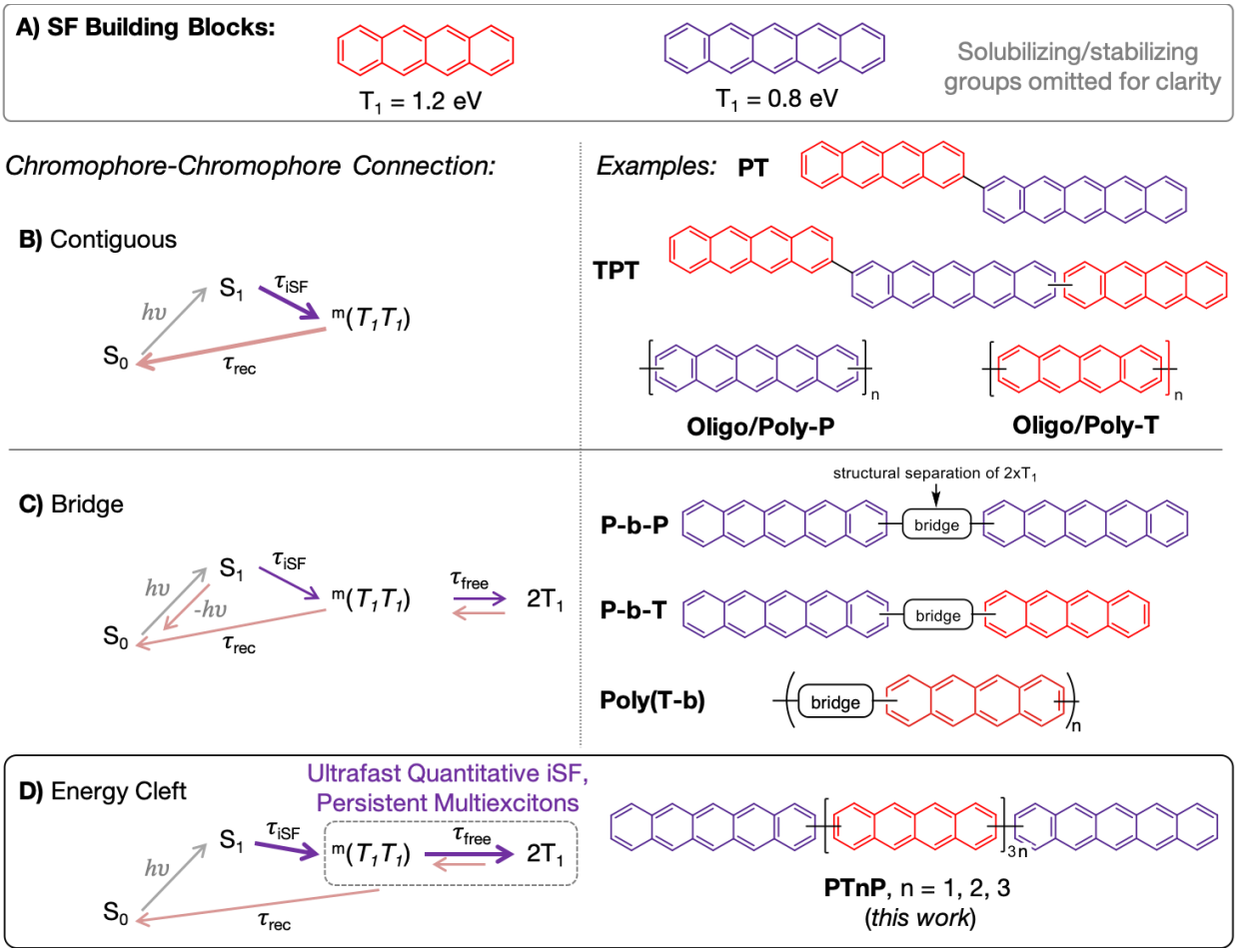

Figure 4.1 PTnP Design Strategy A) Tetracene and pentacene building blocks for singlet fission compounds. Comparison of iSF material designs such as: B) Contiguous iSF compounds have triplets localized on adjacent molecules. They exhibit rapid SF (green arrow) and rapid triplet decay (red arrow). (C) Bridge compounds in which both the triplet pair generation and triplet pair decay rates can be reduced. This results in a lower overall yield but allows some free triplets to form. Triplet decay occurs primarily from the spin-coupled triplet pair. In all panels, a thicker line weight for connecting arrows indicates a faster rate constant. (D) The energy cleft design, which promotes rapid singlet fission and slow triplet pair recombination. Here, decay of triplets occurs after rapid interconversion of different spin states. In all panels, an increased line weight of connecting arrows indicates a faster rate constant.

4.3 Results and Discussion

To demonstrate that the energy cleft design is capable of simultaneous amplification and migration of excitons within individual molecules, we have designed and synthesized a representative series of chromophores based on the **PTnP** motif, featuring **n**=1, 2, and 3 consecutive tetracene chromophores with pentacenes flanking the molecule. We note that while several possible isomers exist for each PTnP compound (*cis*- or *trans*- connectivity between chromophores plus variations in the relative location of the TIPS group along the tetracene backbone), we have previously shown that these variations will not affect the SF dynamics.[25,29] Each of the energy cleft materials contains a contiguous pentacene-tetracene (**PT**) unit that has previously been found to undergo iSF.[38] In **PTnP,** the lowest energy triplet pair state is localized on the two non-contiguous terminal pentacenes, driving the dynamic relaxation process to spatially separated triplets (energy cleft). The electronic characteristics of the P-T building block have been well characterized and serve as the basis for our design. While the transition energy of the lowest singlet state is nearly identical to the pentacene monomer, exciton correlations result in a singlet state with some tetracene character, but minimal CT character (Figure 4.15).[39,40] As such, singlet fission occurs for all excitation wavelengths, even those well below the absorption onset of the tetracene monomer. In this way, the net energy losses in the **PTnP** compounds are equivalent to all other pentacene-based singlet fission materials. Rather, the energy cleft simply introduces energetic potential along the conjugated backbone, dictating the spatial dynamics of the overall relaxation process. For comparison, we have also synthesized and characterized the inverted design of a multichromophore compound with terminal tetracenes (**TPT**). This compound does not feature the energy cleft design as the lowest energy triplet pair configuration is located on contiguous chromophores, with no subsequent relaxation/spatial separation. Details of the synthesis and characterization of these materials are found below in section 4.14.

The optical properties of the **PTnP** compounds are highly similar to each other and to the **PT** dimer, and feature characteristic absorptions corresponding to the P and T subunits. Similar to other contiguous dimer materials, we have found that the strongly coupled contiguous **PT** iSF dimer exhibits rapid (<1 ps) singlet fission upon photoexcitation of the S_1 state and a correspondingly fast rate of recombination (τ_{iSF} and τ_{rec}, respectively, Figure 4.1B). We reiterate that explicit excitation of the tetracene unit (hot exciton excitation) is not required to observe the SF dynamics reported here. Here we present data for pumping the vibrationally excited S_1 state (600 nm) so the ground state bleach dynamics (~ 660 nm) can be clearly observed. Identical dynamics for direct pumping with 660 nm excitation are observed. Following well-established procedures, we find that rapid singlet fission also occurs in **PTnP** materials with quantitative yields (Section 4.8). We briefly summarize this procedure: the lifetime of the photoexcited singlet state is measured *via* the decay of the ultrafast prompt fluorescence and used to assign spectral features that decay with the same time constant in transient absorption measurements (Figure 4.2A,B). The triplet population dynamics that result from singlet fission are tracked using the strong pentacene triplet-triplet excited state absorption feature at ~ 520 nm (Figure 4.2C). This transition is unambiguously assigned to the triplet state, based on comparisons to triplet sensitization measurements.[24,30,32]

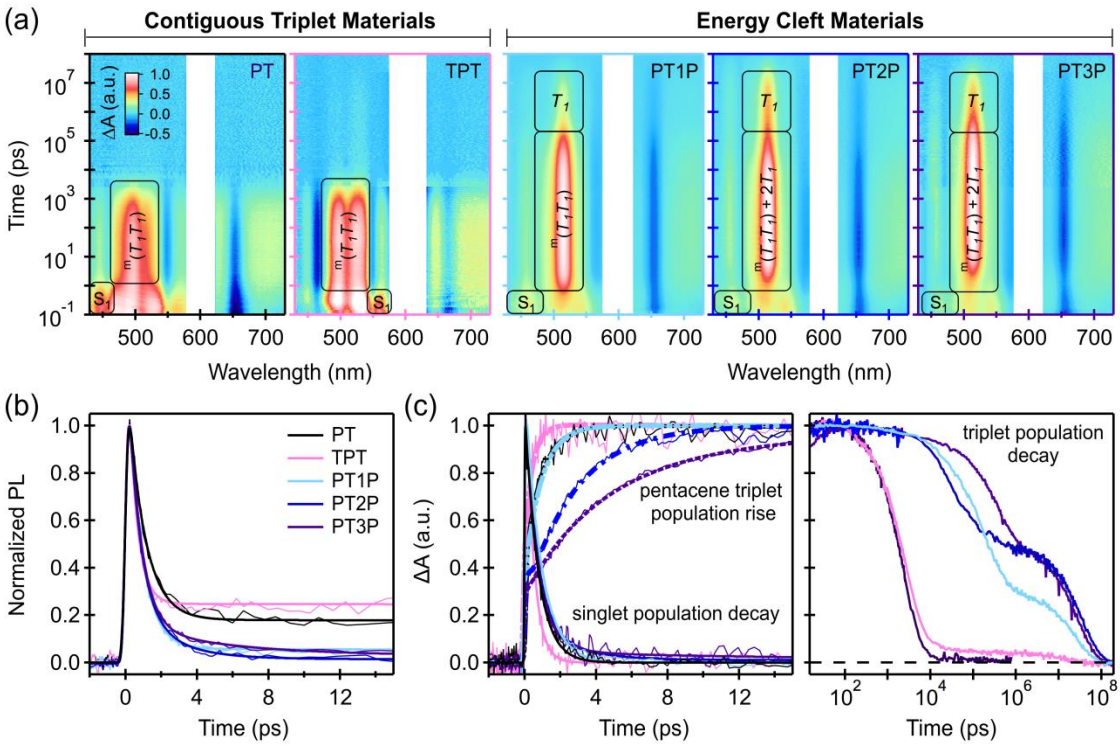

Figure 4.2 Dynamics of Singlet Fission and Energy Transfer. A) Transient absorption in dilute toluene with excitation at 600 nm (~25μJ/cm^2) as a function of time and wavelength where prominent photoinduced absorption features from singlet (S_1), triplet pair $^m(T_1T_1)$ and individual triplet (T_1) are annotated. In B), photoluminescence under the same conditions revealing singlet fission as prompt decay, and a plateau corresponding to delayed photoluminescence for the contiguous **PT** and **TPT** materials. In C), we plot single wavelength kinetics selective for singlet decay from the transient absorption data shown in A) as well as pentacene triplet rise as a function of time, where some overlap with singlet photoinduced absorption results in non-zero signal at the start of the experiment.

A detailed analysis of the data obtained reveals a valuable piece of information - it is possible to observe the dynamics of the exciton migration from tetracene to pentacene (Figure 4.3). We find that in the **PTnP** energy cleft compounds, the formation and migration of the multiexciton state is occurring independently from one another, on distinct picosecond timescales. First, the singlet fission time constant is determined from the decay of the bright singlet state using transient emission measurements (Figure 4.2B). We find that the singlet decays with nearly an identical rate in the contiguous triplet materials (**PT**, **TPT**) and the energy

cleft materials (**PTnP**). The singlet fission time constants derived from the decay of the singlet are summarized in Table 4.1, and range from 600 – 880 fs for the **PTnP** series, nearly identical to the **PT** dimer (885 fs). The nearly identical time constants indicate that a similar electronic configuration leads to singlet fission, since the rate constant is intimately sensitive to electronic coupling between chromophores.[30]

Second, we resolve the migration and splitting of the triplet pair by comparing the overall population of triplets on the pentacene units to the singlet population. In the **PTnP** compounds with **n** = 2 and 3, we observe an additional time constant for populating the pentacene-pentacene $^{m}(T_{1[\mathbf{P}]}T_{1[\mathbf{P}]})$ state (Figure 4.3; $T_{1[\mathrm{P}]}$ refers to a triplet on pentacene) that is slower than the singlet fission time constant. This discrepancy between the singlet decay (amplification via singlet fission) and the rise of the triplet population on pentacene, $T_{1[\mathbf{P}]}$, can be attributed to the exciton migration from the high-energy tetracene, $T_{1[\mathbf{T}]}$, to the lower energy pentacene as a result of the energy cleft. By transient absorption spectroscopy, we selectively monitor the excited state absorption signal that is proportional to the total pentacene triplet population (sharp peak at ~520 nm) as well as the distinct NIR excited state absorption (~ 1500 nm, assigned to $T_1 \rightarrow S_n$) feature that is a marker for strongly bound triplet pairs on contiguous chromophores. in the NIR (Figure 4.11).[33,40,41] While the rise and subsequent decay of the tetracene triplet absorption signal is not independently observable, since the overall triplet absorption coefficient is ~ 50x smaller than pentacene,[16] the time scales for decay of the NIR transient signal exactly correlates to the slower rise of the pentacene triplet population after SF. Using global analysis, we determine the time scales for the conversion of the $^{m}(T_{1[\mathbf{P}]}T_{1[\mathbf{T}]})$ pentacene-tetracene coupled triplet pair (~ 1.9 eV) to a lower energy (but longer range) $^{m}(T_{1[\mathbf{P}]}T_{1[\mathbf{P}]})$ pentacene-pentacene triplet pair state (~ 1.6 eV). Interestingly, we find that the multiexciton migration occurs with a time constant of 2.6 ps in

PT2P and 5.7 ps in **PT3P**, reflecting the increase in pentacene-pentacene distance from **PT2P** to **PT3P**. The fact that these dynamics are resolvable indicates that triplet pair generation primarily occurs across contiguous units (**PT**), with minimal contribution from the longer-range pentacene-pentacene interactions. The energy cleft dynamics are too fast to be resolved in **PT1P**, in which the singlet fission and pentacene population dynamics are identical.

In the **PTnP** series, the energy cleft design, in which the triplet pair state is spatially separated across non-contiguous chromophores, severely frustrates triplet-triplet recombination. As in other strongly coupled dimer systems, the triplet pair in the stand-alone **PT** dimer decays rapidly with a triplet pair lifetime of ~2.4 ns, as the triplets are spatially constrained to nearest-neighbor chromophores. In **TPT**, energy conservation ensures a spatially contiguous configuration within the molecule, i.e., conversion to the non-contiguous tetracene-tetracene triplet pair is energetically uphill by ~ 0.4 eV. Since the triplet pair remains on continuous chromophores, the triplet pair decay dynamics are nearly identical to the isolated **PT** dimer, with a time constant of ~ 2.5 ns. In contrast, the triplet pair lifetime in the **PTnP** energy cleft compounds is approximately 2 orders of magnitude longer as a result of the spatial separation of the pentacene-pentacene triplet pair generated. Moreover, a large population of an additional long-lived triplet species is observed with a time constant exceeding 20 μs (Table 4.1 – $T_{1[\mathbf{P}]}$). While similarly slow triplet recombination dynamics were achieved in pentacene dimers separated by a terphenylene bridge, the long spacer results in slow iSF rates insufficient to outcompete parasitic radiative decay processes from the bright singlet.[32] Here, the **PTnP** compounds retain the sub-ps triplet generation times of directly linked dimers, yielding quantitative formation of persistent multiexcitons, without loss to parasitic processes.

	PT	**TPT**	**PT1P**	**PT2P**	**PT3P**	**PADTP**
S_1	830 fs	510 fs	880 fs	540 fs	605 fs	760 fs
$^{m}(T_{1[\mathbf{P}]}T_{1[\mathbf{T}]})$ or $^{m}(T_{1[\mathbf{P}]}T_{1[\mathbf{ADT}]})$	2.4 ns	2.5 ns	not resolvable	2.6 ps	5.7 ps	not resolvable
$^{m}(T_{1[\mathbf{P}]}T_{1[\mathbf{P}]})$	-	-	172 ns	53 ns	376 ns	46 ns
$T_{1[\mathbf{P}]}$	-	-	23 µs	33 µs	27 µs	8.6 µs

Table 4.1 PTnP Excited State Time Constants Decay times of the singlet (S_1), pentacene-tetracene triplet pair $^{m}(T_{1[P]}T_{1[T]})$, pentacene-pentacene triplet pair $^{m}(T_{1[P]}T_{1[P]})$ and pentacene free triplet ($T_{1[P]}$) as determined from global analysis of transient absorption spectroscopy measurements shown in Figure 4.2A,C.

Using time-resolved electron spin resonance experiments (tr-ESR, Figure 4.3), we observe that a large intertriplet spacing in the final energy cleft configuration promotes rapid interconversion between the various two triplet spin configurations. As in previous measurements on iSF compounds, we identify triplet pairs coupled into an overall quintet (S=2) as well as free triplets (S=1).[11,15] In agreement with previous results, the net quintet state forms rapidly (Figure 4.3, right panel, black plot line), such that the mechanism of its formation cannot be readily identified within the time resolution of this technique (~ 100 ns). However, within the **PTnP** series, the formation rate of the free triplet signal increases with increasing separation of the terminal pentacenes (Figure 4.3, right panel, red plot line). In fact, for **PT3P** (largest separation), both the quintet and free triplets are formed faster than the instrument response. The rapid interconversion of spin states in the energy cleft molecules likely results from decreased interchromophore exchange coupling. The decreased coupling results in a smaller energy level spacing between the different triplet pairs, which enhances the degree of mixing between triplet pair states of different multiplicities and the rate of dephasing (Figure 4.4A).[42] Crucially, our

data shows the formation time constant of free triplets in **PT3P** (< 100 ns, determined by tr-ESR) is faster than any significant loss channels for the triplet population (~ 400 ns in **PT3P**, determined by TAS). This disparity implies that the time scales for dephasing and population loss are not necessarily equivalent.

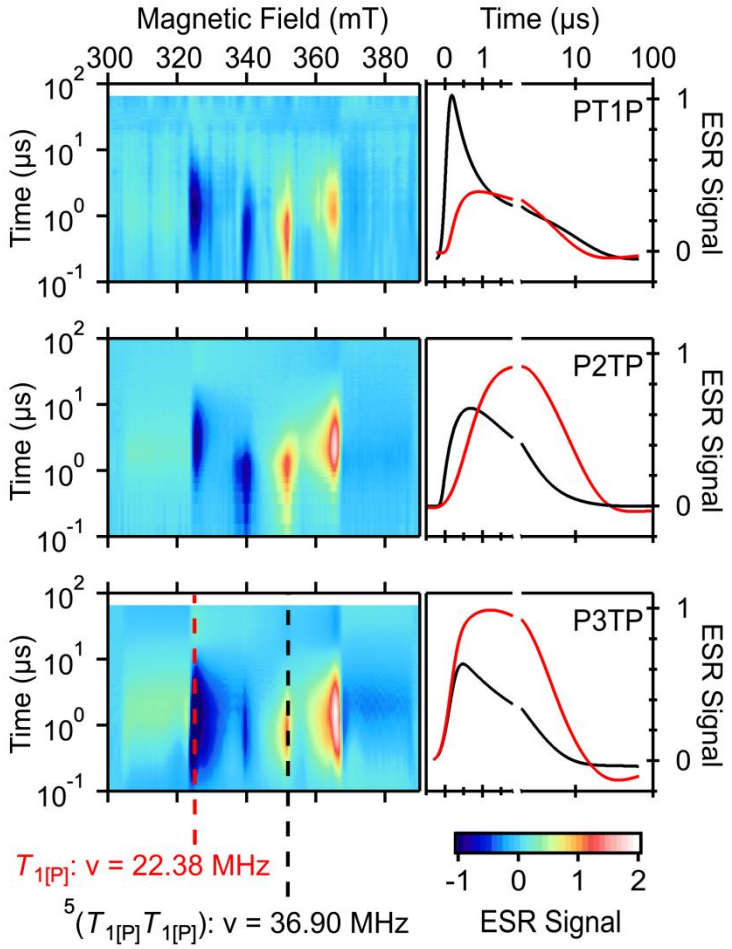

Figure 4.3 Time Resolved ESR Spectroscopy of PTnP Time resolved electron spin resonance spectroscopy of the energy cleft materials A) PT1P, B) PT2P, and V) PT3P. Left panels show the microwave absorption as a function of time and magnetic field. The nutation frequencies for the quintet and triplet associated peaks are listed, and the kinetics of these peaks are shown on the right for the different molecules, with quintet denoted in black, and free triplet in red. Molecules were embedded in toluene at 80K and excited at 599 nm.

Correlating the population and magnetization dynamics we identify the two dominant processes that repopulate the ground state directly from the triplet pair, resulting in the loss of either one or both of the triplets in the pair[43,44]:

$$^1(T_1T_1) \rightarrow S_0 + S_0 \text{ (loss of both triplets concurrently)}$$

$$^3(T_1T_1) \rightarrow T_2 + S_0 \text{ (loss of one triplet)}$$

In the population dynamics (Figure 4.2C), we observe a clear signature of decay *via* the $^3(T_1T_1)$ channel that uniquely results in the net loss of one triplet for each molecule in the excited state. Experimentally, this manifests as the rapid (~ 1 μs) loss of 50% of the total triplet population, with the remaining decaying at the individual triplet lifetime (~ 20 μs). There is no direct path to generate $^3(T_1T_1)$ because it has opposite parity to $^1(T_1T_1)$ and, unlike $^5(T_1T_1)$, cannot directly mix via dipolar interactions.[43] Instead, the rapid dephasing observed using tr-ESR (Figure 4.3) suggests that the $^3(T_1T_1)$ may form by rephasing of free triplets.[45] If $^3(TT)$ can only form by rephrasing of free triplets, then the fraction of the population that has decayed through the $^3(TT)$ channel can be used to determine the overall singlet to free triplet yield, by quadrupling (200% full scale) the relative amplitude of the triplet population that decays with the free triplet lifetime (a_{T_1}). The 50% amplitude asymptote is unambiguously observed in **PT2P** and **PT3P**, indicating that decay via $^3(T_1T_1)$ is the primary loss mechanism and that the free triplet yields are quantitative**.** However, in **PT1P** the process involving $^3(T_1T_1)$ is less favorable because the triplet pairs do not rapidly dephase into free triplets. As such, direct decay of $^1(T_1T_1)$ is favored, leading to suboptimal asymptote (~ 30%), and overall triplet yield of ~ 120%. We note that this model describing the origin of the biexponential decay in the population dynamics contains subtle but important differences from other reports that assign the fast component to coupled triplet pairs and the slower component to free triplets.[15,17,23,24,32,36,37,39,46,47] When we consider simultaneously

the population and magnetization dynamics, it is clear that the first decay component corresponds to two triplets per molecule (coupled and uncoupled are possible) and the second corresponds to just one triplet per molecule. We note that no significant buildup of a polarized $^3(T_1T_1)$ is likely to occur due to rapid decay (spin allowed), precluding their direct observation by tr-ESR.

By all metrics, our energy cleft compounds are performance outliers compared to other iSF connectivity designs (see Figure 4.1), including contiguous triplet pair compounds (CONTIG) and bridged compounds with conjugated (B: CON), cross-conjugated (B: XCON), and homo-/non-conjugated (B: HOMO/NON) units (Figure 4.4). By comparing the triplet pair formation and decay rate constants (Figure 4.4B), we can identify distinct families of compounds that exhibit a fixed relationship between the triplet formation and decay rate that depends on chromophore coupling (roughly linear on a log-log plot, lines are guides to the eye). The energy cleft compounds are clear outliers from these simple trends, with constant ultrafast singlet decay as the triplet pair lifetime is tuned. In comparing the singlet decay to free triplet yield (Figure 4.4C), the effect of the energy cleft design is even more striking, as the energy cleft compounds are the only materials with singlet exciton lifetimes < 50 ps that yield any measurable free triplets at all.

In order to standardize the quantification and comparison of the relative performance of all iSF chromophores, here we introduce the triplet evolution parameter (TEP). The TEP metric allows us to evaluate the parameters most important to device implementation - ultrafast singlet decays and high free triplet yield - within a simple metric. Considering the formation rates *and* yields is preferable to evaluating yields alone, since ultrafast singlet decay is essential to

outcompete other parasitic processes, preserving the designed iSF dynamics in thin films (Figure 4.13,14) or in a device architecture that harvests the triplets:

$$TEP = \left[{}^{k_{SF}}\!/_{k_{AD}} \right] \cdot \left[{}^{\Phi_{max}}\!/_{4 * a_{T_1}} \right]$$

In equation 1, a_{T_1} is the amplitude of the triplet population that decays with the free triplet lifetime, the maximum free triplet yield (Φ_{max}) is 200%, and the maximum triplet pair formation rate constant (k_{AD}) is dictated by the adiabatic limit (~ 1/80 fs). Using this metric, the impact of the energy cleft design is readily apparent, as PTnP materials perform more than 100x better than the best materials using other design schemes (Figure 4D). Importantly, the performance of these materials is comparable to the best SF molecular crystals, with sub-ps generation times, quantitative free triplet yields, and microsecond triplet lifetimes.

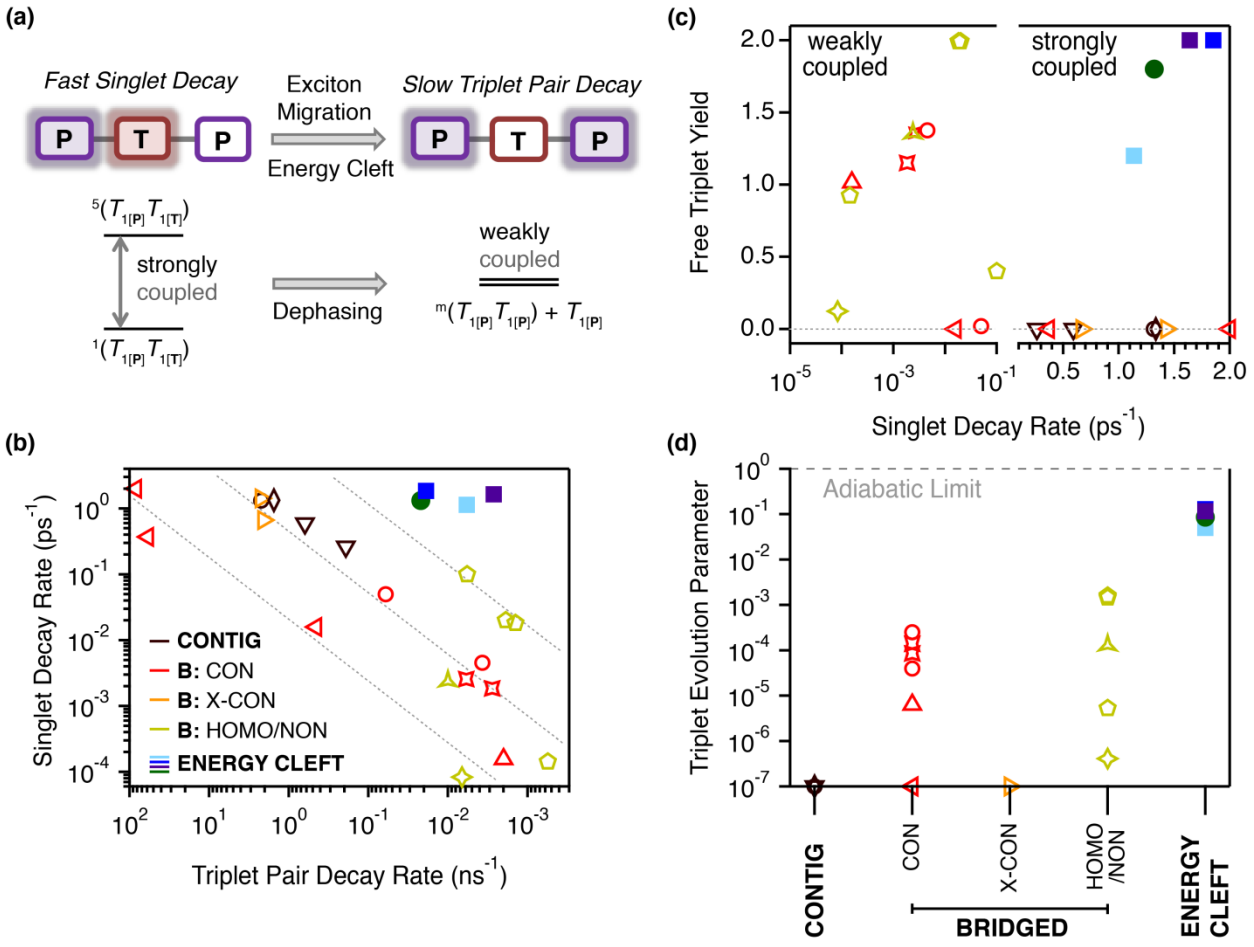

Figure 4.4 Comparison of PTnP to Existing iSF Materials A) Schematic showing the migration of excitons from a contiguous pentacene-tetracene triplet pair to a further separated pentacene-pentacene triplet pair. The increased spatial separation leads to a corresponding reduction in the exchange coupling between triplet pairs, reducing the energy spacing between triplet pairs of different multiplicity and enhancing the dynamics of dephasing. B) – D) Comparison of the PTnP energy funnel compounds to all other pentacene based iSF materials. B) Previous compounds have exhibited a direct relationship between the triplet pair generation and decay rates, such that slowing down decay necessitates slowing down generation. PTnP materials break this relationship, exhibiting fast generation and slow decay of triplet pairs. C) The lifetime of the triplet pair directly affects the free triplet yield. PTnP compounds generate triplet pairs 100x faster than other materials with high free triplet yields. D) Performance according to the triplet evolution parameter for various design schemes. Here, 80 fs is used as the adiabatic limit. PTnP compounds exhibit nearly ideal free triplet generation behavior. For graphs B) – D), the colors correspond to the design scheme: contiguous (CONTIG) = maroon, conjugated bridged (B: CON) = red, cross-conjugated bridged (B: X-CON) = orange, homoconjugated and nonconjugated bridged (B: HOMO/NON) = yellow, PT1P = light blue, PT2P = blue, PT3P = purple, PADTP = filled green circle. Previously published data is represented as open circles,[32] up arrows,[15] down arrows,[30] left arrows,[28] right arrows,[37] diamond,[26] pentagon,[24] vertical four pointed star,[36] rotated four pointed star,[46] and three pointed star.[17]

To further show that this is a general design scheme, we have synthesized and characterized pentacene-anthraditiophene-pentacene (**PADTP**) as an intramolecular singlet fission compound based on the energy cleft design. Details of the synthesis and transient absorption data and analysis are found below. Similar to the role of tetracene in **PTnP** compounds, anthradithiophene is a singlet fission active bridge[14] such that photoexcitation results in a contiguous triplet pair with the neighboring pentacene chromophore. This compound allows us to evaluate the relative importance of the energy alignment in the energy cleft design. In **PTnP,** the $^{m}(T_{1[\mathbf{P}]}T_{1[\mathbf{T}]})$ triplet pair is isoergic with the singlet and the difference between the intermediate and final triplet pair states is large (~ 0.4 eV). In **PADTP**, the $^{m}(T_{1[\mathbf{P}]}T_{1[\mathbf{ADT}]})$ intermediate pair is equally offset in energy from both the singlet and final $^{m}(T_{1[\mathbf{P}]}T_{1[\mathbf{T}]})$ triplet pair (~ 0.2 eV).[14] Not surprisingly, we find that **PADTP** behaves similarly to **PTnP**, showing rapid singlet fission and a high free triplet yield, underlining the generality of the energy cleft design for other chromophores (Table 4.1). While the triplet pair and free triplet lifetimes are slightly shorter, presumably due to the presence of heteroatoms in the ADT bridge, the overall free triplet yield, as determined using the biexponential analysis for the triplet population decay described above, is higher (green circles, Figure 4.4). As such, the overall TEP falls in a range between **PT1P** and **PT2P**.

4.4 Conclusions

In conclusion, we have designed and characterized a series of compounds with an energy cleft motif that allows rapid singlet fission and triplet-pair dissociation, efficiently generating long lived multiexciton states. The energy cleft design may serve as a model for analogous processes in molecular crystals, where structural disorder can serve to promote spatial separation of triplets causing rapid dephasing of triplet pairs. Moving forward, energy cleft materials

provide viable singlet fission and triplet pair recombination rates for incorporation into optoelectronic devices.

4.5 Methods

Synthesis of Energy Cleft Compounds

All commercially obtained reagents/solvents were used as received; chemicals were purchased from Alfa Aesar®, Sigma-Aldrich®, Acros organics®, TCI America®, Mallinckrodt®, and Oakwood® Products, and were used as received without further purification. Unless stated otherwise, reactions were conducted in oven-dried glassware under argon atmosphere. Bromo-TIPS-Tetracene **1**, BisBpin-NODIPS-Pentacene **2**, Bpin-NODIPS-Pentacene **3**, Bpin-TIPS-Pentacene **4**, Dibromo-TIPS-Tetracene **7, PT**, Dibromo-NODIPS-tetracene, Dibromo-NODIPS pentacene and dibromo-TIPS-anthradithiophene were synthesized according to literature procedure.[18,25,29,38] ^{1}H-NMR and ^{13}C-NMR spectra were recorded on Bruker 400 MHz (100 MHz for ^{13}C) and on 500 MHz (125 MHz for ^{13}C) spectrometers. Data from the ^{1}H-NMR and ^{13}C spectroscopy are reported as chemical shift (δ ppm) with the corresponding integration values. Coupling constants (*J*) are reported in hertz (Hz). Standard abbreviations indicating multiplicity were used as follows: s (singlet), b (broad), d (doublet), t (triplet), q (quartet), m (multiplet) and virt (virtual). The mass spectral data for the compounds were obtained from XEVO G2-XS Waters® equipped with a QTOF detector with multiple inlet and ionization capabilities including electrospray ionization (ESI), atmospheric pressure chemical ionization (APCI), and atmospheric solids analysis probe (ASAP). The base peaks were usually obtained as $[M]^{+}$ or $[M+H]^{+}$ ions. Anhydrous solvents were obtained from a Schlenk manifold with purification columns packed with activated alumina and supported copper catalyst (Glass Contour, Irvine, CA). All reactions were carried out under argon unless otherwise noted.

Ultrafast Optical Measurements

Details of the transient absorption experiments have been described previously.19 Briefly, a 1 kHz amplified Ti:Sapphire system with an optical parametric amplifier is generates resonant pump pulses of ~ 100 fs. This laser is also used to generate a femtosecond supercontinuum probe in a thin sapphire plate, where delay is controlled mechanically with respect to the pump pulse. A nanosecond supercontinuum probe pulse is generated in a fiber laser (Leukos) and employed using an electronically delayed configuration to investigate longer delayed times. The pump pulse is the same for both probe measurements. The measurements are conducted at concentrations below 100 μM, and typically ~50 μM unless otherwise noted. Photoluminescence upconversion measurements were acquired using a 90 kHz Yb:KGW amplified laser (Light Conversion) equipped with an optical parametric amplifier. The 1030 nm fundamental was used as the gate pulse and a pulse centered at 600 nm was used for excitation. Upconversion was achieved in a noncollinear arrangement with type-II BBO crystal and detected with a photomultiplier tube.

Time-Resolved Electron Spin Resonance Measurements

Pulsed laser, continuous microwave and pulsed laser, pulsed microwave measurements were carried out using the method described in our previous report.[15] Briefly, compounds were dissolved in toluene and transferred to a sealed quartz ESR tube under nitrogen. UV-visible absorption spectroscopy was employed to ensure that no aggregation occurred. Experiments were undertaken using a Bruker Elexsys E580. Samples were transferred to a cryogenically cooled (Oxford Instruments, CF935) resonator (Bruker, MD5) attached to an X-band microwave source (Bruker, Super X FT-ESR Bridge). A ~7 ns 660 nm laser pulse was used to excite the sample (Opotek, OPOLETTE). In nutation frequency measurements, the nutation pulse was

applied 1.0 μs after the laser pulse at 340 mT (9.7047 GHz) and 325 mT (9.7062 GHz), respectively. The data from pulsed laser, pulsed microwave measurements was fit with a damped sine wave to establish the nutation frequency of a given transition.

4.6 UV-Visible Absorption Spectra

UV-visible absorption spectra were obtained as dilute solutions in toluene for all new compounds investigated in this report (Figure 4.5). Notably, the materials all feature clear absorption features for pentacene, with an onset of vibronic progression near 660 nm, and features for tetracene, with an onset of absorption near 550 nm. The coupling at the 2 position of these acenes also results in a new absorption peak near 470 nm, as reported previously. The data have been normalized at the pentacene associated absorption near 660 nm to facilitate comparison. This normalization reveals that PTP features a relatively larger magnitude pentacene absorption than tetracene relative to PT2P. We ascribe this reduction in peak height the larger number of regioisomers in PT2P, resulting in peak broadening increasing the area but reducing the height of the tetracene peak. PT3P has a larger magnitude and broader tetracene feature, as it has even more regioisomers, and also more tetracenes for each pentacene. Finally, TPT features a similar number of regioisomers to PTP, and therefore has a tetracene feature that is relatively sharp, but with a significantly larger tetracene absorption relative to pentacene, as expected.

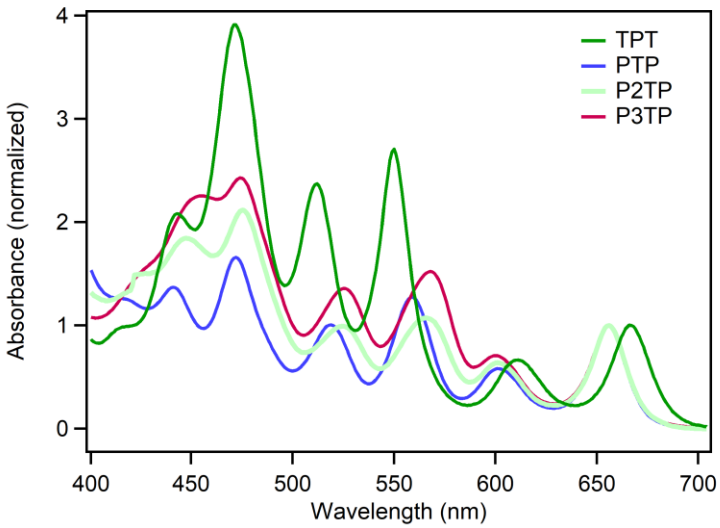

Figure 4.5 UV-Visible Absorption Spectra of PTP, PT2P, PT3P and TPT, the new molecules reported here, as dilute (<100 µM) solutions in toluene.

4.7 Global Analysis

Global analysis was crucial for accurate assignment of distinct species and their respective lifetimes in transient absorption spectroscopy experiments, and was performed using the Glotaran software package.[48] This technique reproduces a dataset as a series of unique spectra with associated lifetimes. Because it treats the data set in aggregate, it provides especially accurate time constants, and because it creates a reproduced model of the data, we can compare the raw data to our model to ensure we have accurately captured the dynamics and spectra of the system. Below, we show examples of our fitting for PT3P, a representative compound discussed in this paper. In Figure 4.6, we show the three species isolated from fitting the fs TA data exciting at 600 nm in toluene for PT3P. Interestingly, the splitting of the pentacene-tetracene to pentacene-pentacene triplet pair slightly more than doubles the value of the pentacene photoinduced absorption peak near 520 nm. We would expect this signal to roughly double going from one pentacene triplet to two, but this triplet pair splitting process also involves loss of tetracene associated ground state bleach in this region, resulting in an even larger signal increase.

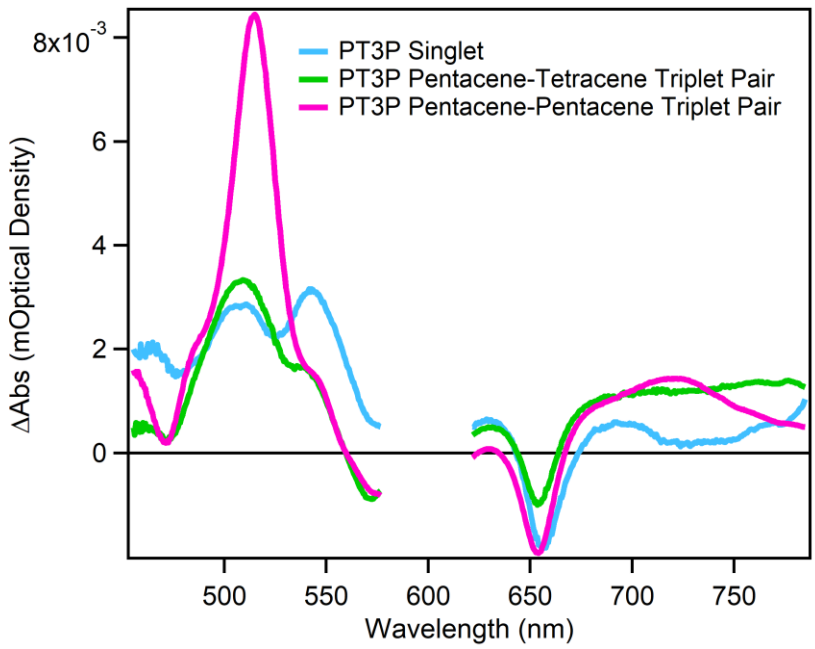

Figure 4.6 Spectra Isolated by Global Analysis of the femtosecond transient absorption spectroscopy for the singlet exciton, the pentacene-tetracene triplet pair and the final pentacene-pentacene triplet pair state.

In Figure 4.7, we compare kinetics at 560 nm in the raw data to fits. The global fitting agrees well with the data, and shows the decay of the singlet associated signal in this region is completed for PT3P around 2 ps. We also show the kinetics at 730 nm, where there is minimal singlet photoinduced absorption (Figure 4.6). In this region, we can see a fast rise, also completed around 2 ps corresponding to singlet fission, but a secondary, slower rise as well corresponding to the rise of the second pentacene triplet as the triplet pair splitting occurs to populate the final pentacene-pentacene triplet pair state.

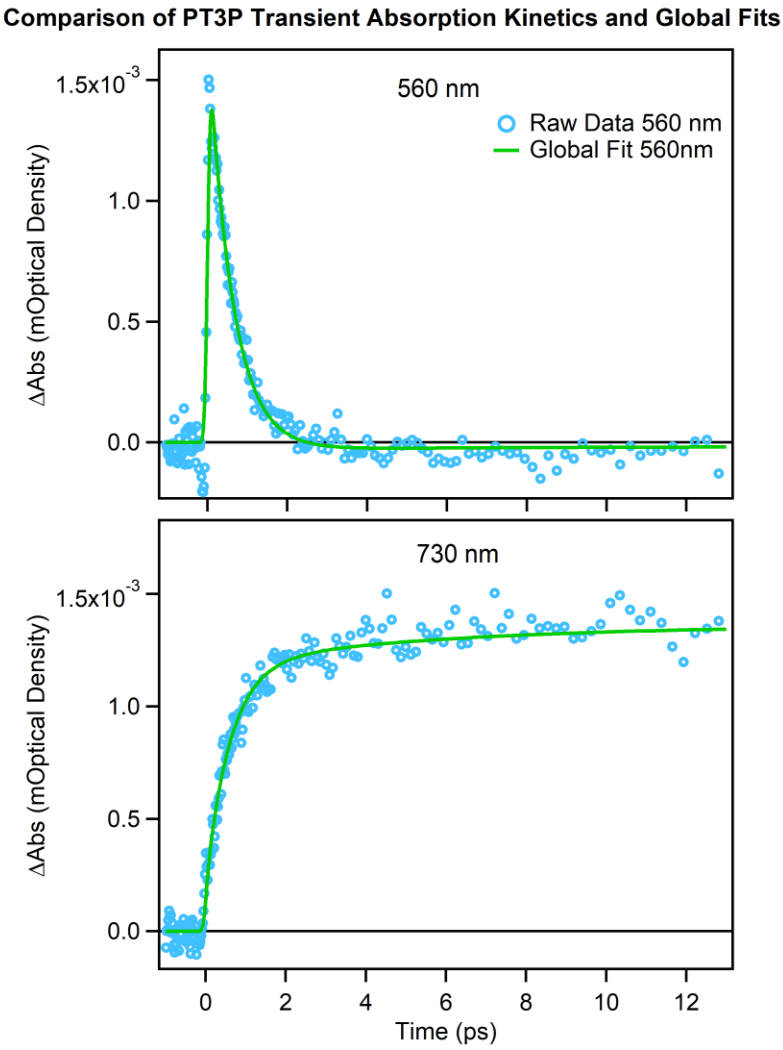

Figure 4.7 Comparison of Global Analysis Fits to Raw Data at 560 nm, where only singlet exciton has significant photoinduced absorption, and at 730 nm, where photoinduced absorption is dominated by triplet signal.

In Figure 4.8, we compare spectra from raw data to those obtained by global fitting. The green trace shows a near-zero residual throughout, indicating a good fit for the data at times corresponding mostly to singlet (180 fs), pentacene-tetracene triplet pair (1.5 ps), and the pentacene-pentacene triplet pair (25 ps).

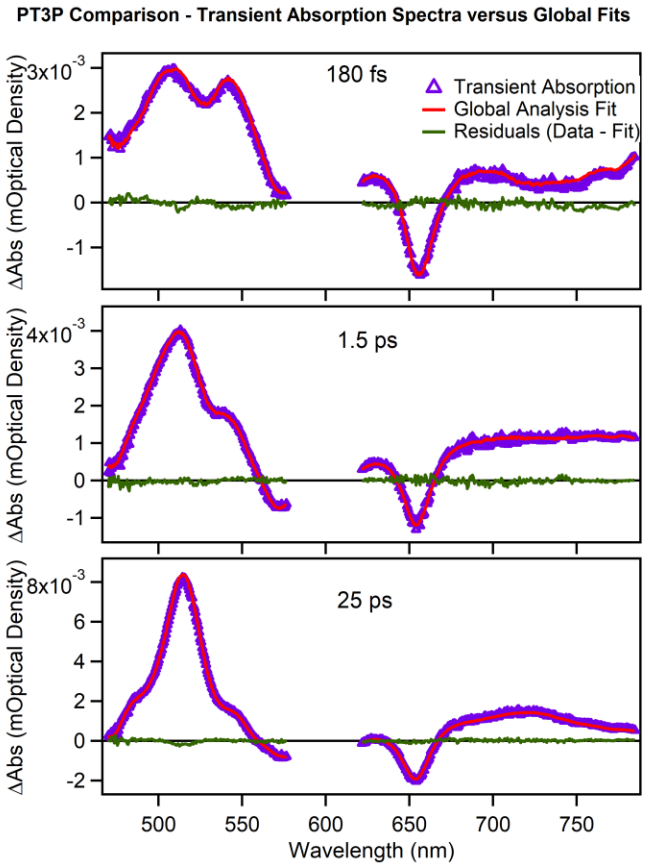

Figure 4.8 Spectral Comparison of Raw Data and Global Fitting at time scales dominated by singlet (180 fs), pentacene-tetracene triplet (1.5 ps), and pentacene-pentacene triplet (25 ps), as well as residuals (green).

In Figure 4.9, we compile the isolated spectra from global analysis for TPT, PTP, PT2P and PT3P, all of the new compounds reported here.

In every case, the singlet exciton lineshapes are reasonably similar, with differences primarily defined by differences in ground state bleach signal among the different compounds. The singlet exciton decays in all cases concurrent with rise of a new state. For TPT, PT2P and PT3P, this new state is the pentacene-tetracene triplet pair state. In PTP, that state is not resolved. In the case of TPT, this state represents the final state, as there is no energy cleft built in to separate this pentacene-tetracene triplet pair. In the case of PT2P and PT3P, we see this pentacene-tetracene triplet pair state decay and the rise of a third state, the pentacene-pentacene

triplet pair state, seen as an increase in pentacene ground state bleach and an approximate doubling of the pentacene triplet signal with a maximum around 520 nm. In PTP, we do not resolve the intermediate, so this pentacene-pentacene triplet pair lineshape evolves directly from the singlet isolated spectrum.

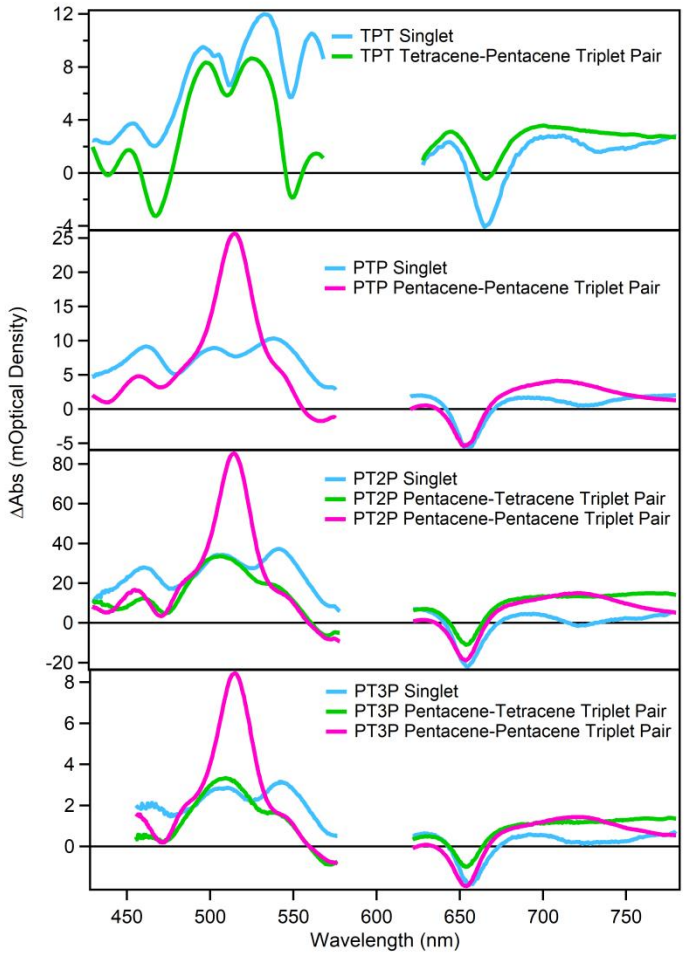

Figure 4.9 Global Analysis Isolated Spectra for all new compounds reported here, measured as dilute solutions in toluene with excitation at 600 nm.

4.8 Singlet Fission Yield Determination

The normal triplet yield determination using triplet sensitization methods must be modified slightly to account for the heterogeneous nature of the compounds studied here. We

determine all yields to be quantitative, i.e., > 199%. Detailed analysis is shown here for PT3P, but similar results were obtained for all compounds.

First, we determine the relationship between singlet exciton concentration and the magnitude of the ground state bleach signal observed in transient optical experiments. In our procedure, we avoid two potentially problematic assumptions. First, we do not simply assume that the molar extinction coefficient measured in linear measurements can be directly mapped onto the transient optical experiments. Second, we have avoided the assumption that 100% of the population of triplets from the sensitizer is transferred to the pentacene sub-ensemble since tetracene chromophores are also energetically accessible. The GSB near 660 nm is specific for pentacene occupation and the triplet-triplet absorption peak at 520 nm is dominated by pentacene. So even in an ensemble with mixed occupation, we have specific optical markers that can be used to isolate the pentacene contribution.

To determine the molar extinction coefficient associated with the ground state bleach signal, we measure the attenuated power by a PT3P solution in toluene from a stabilized 600 nm pump beam. The spot size is determined to be 0.94 mm using a CCD based beam profiler, giving a total incident fluence of 1.76×10^{14} photons/cm^2 for our experiment. To verify this method, solutions of TIPS-pentacene (TPc) and a bridged bipentacene (BP2) with known molar extinction coefficients are measured for comparison.[4]

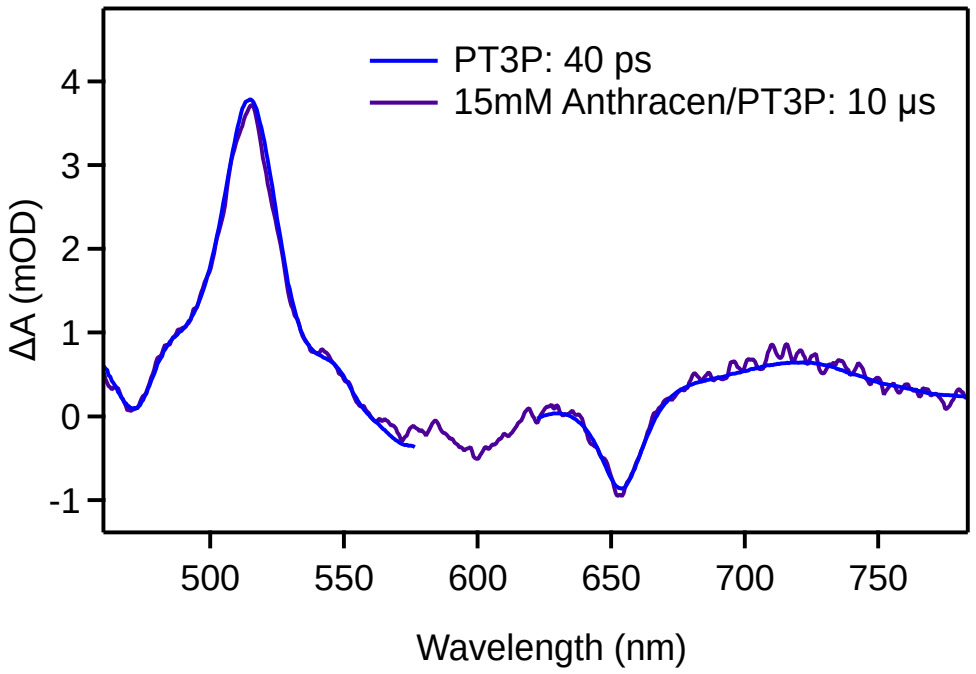

Figure 4.10 PT3P Fission vs Triplet Sensitization

The absorbed fluence is calculated using the linear optical density at 600 nm solutions of TPc, BP2, and PT3P and is defined as (incident fluence)*(1 – 10^{-OD}).

We determine the GSB amplitude from fitting transient spectra at a fixed time (40 ps) using a linear background to account for overlapping excited state absorptions. Using the relation that one absorbed photon yields one exciton, we calculate the molar extinction coefficient for the GSB signal using the equation:

$\varepsilon_{GSB} = OD_{GSB} / (\text{Absorbed Fluence}) * 10^{-3} * N_A$

	OD @ 600 nm	Absorbed Fluence [cm^{-2}]	GSB Amplitude	ε_{GSB} [M^{-1} cm^{-1}]
TPc	0.165	5.56×10^{13}	2.3×10^{-3}	24900
BP2	0.136	4.73×10^{13}	3.3×10^{-3}	42000
PT3P	0.043	1.66×10^{13}	1.1×10^{-3}	31200

To determine the molar extinction coefficient associated with the triplet-triplet excited state absorption, we use triplet sensitization measurements. We analyze the transient spectra near the peak of the triplet population (~ 10 μs) and analyze only the signals that can be uniquely identified with occupation on the pentacene chromophores. Again, we avoid assuming that all the triplet population generated by the sensitizer is transferred to the pentacene chromophores. This also allows us to scale the sensitization spectra to match the amplitudes of the SF spectra.

Using the fitting procedure described above to extract the GSB amplitude and directly reading off the magnitude of the transient signal at 515 nm, we can determine the molar extinction coefficient associated with the triplet-triplet excited state absorption:

$$\varepsilon_{triplet} = (OD_{triplet} / OD_{GSB}) * \varepsilon_{GSB} = (0.0037/0.0011) * (31200/2) = 52500\ M^{-1}\ cm^{-1}$$

In the above calculation, we halve the GSB extinction coefficient by a factor of 2 in response to the fact that only half the molecule is bleached after triplet sensitization, as compared to direct photoexcitation in which the entire molecule is bleached. This assumption can be validated by comparing the ratios of the triplet to GSB peaks in the graph above. As both SF and triplet sensitization yield the same peak ratios, and our other data has confirmed that SF is indeed

occurring, then this assumption is valid. This factor of two is further validated by global analysis, which shows that the bleach magnitude at 660 nm is halved when the pentacene-tetracene triplet pair is transiently occupied (Figure S5). We note that this value is nearly identical to that obtained in bipentacene compounds, further supporting our approach.

From this, we can readily calculate our singlet fission yield:

$[triplet]/[singlet] = (OD_{triplet} / OD_{GSB}) * \varepsilon_{GSB} / \varepsilon_{triplet} = (3.7/1.1)*(31200/52500) = 1.99$

4.9 NIR Transient Data

The NIR spectral region contains specific spectral markers for the correlated triplet pair that can be used to reinforce the conclusions drawn from the analysis of the visible TA data. Specifically, it has been found that a distinct NIR excited state absorption feature is a marker for strongly bound triplet pairs on contiguous chromophores, in which significant mixing of the singlet and triplet electronic manifolds occurs. This feature, which can be seen here near 1500 nm for PT2P and PT3P is present in our data, has been assigned to a transition of the triplet pair state to a high energy singlet state ($(TT)_1 \rightarrow S_n$). The higher energy transition seen at earlier times is the direct $S_1 \rightarrow S_n$ transition.

The $(TT)_1 \rightarrow S_n$ spectral feature appears with the singlet fission time constant and decays on the same picosecond timescales that has been assigned as the relaxation from the P-T triplet pair to the P-P triplet pair in PT2P and PT3P. As in our previous analysis, the lifetime in the pentacene-tetracene triplet pair is unresolved in PTP due to ultrafast relaxation to the pentacene triplet pair. In PT dimer and TPT, the contiguous triplet pair state persists during the entire triplet pair population lifetime.

	PT	**TPT**	**PT1P**	**PT2P**	**PT3P**
S_1	0.93 ps	0.49 ps	0.90 ps	0.51 ps	0.52 ps
$^{m}(T_{1[\mathbf{P}]}T_{1[\mathbf{T}]})$	2600 ps	2500 ps	not resolvable	3.0 ps	5.3 ps

Table 4.2 Summary of Time Constants Extracted from Global Analysis of NIR transient absorption spectra.

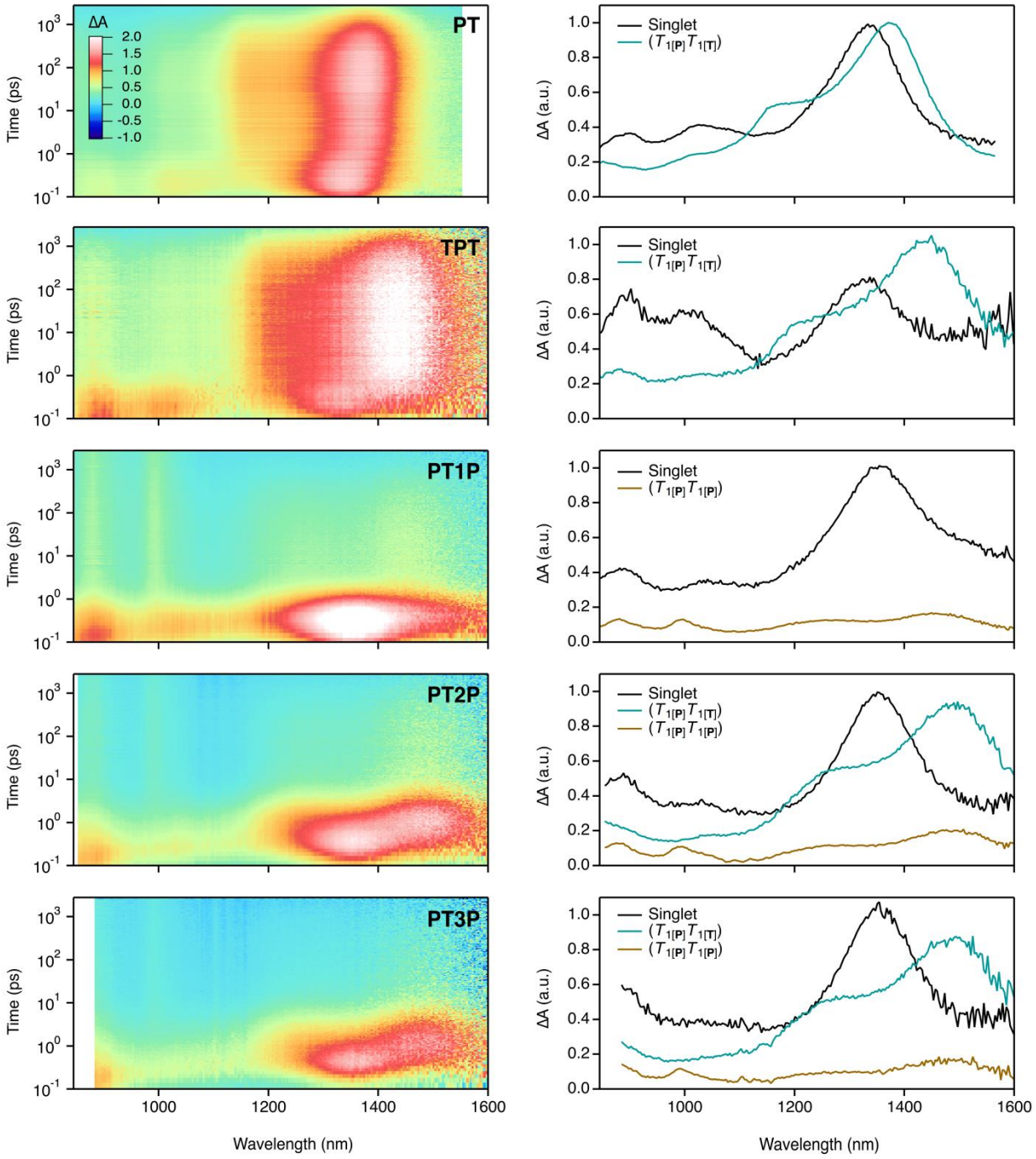

Figure 4.11 NIR Transient Absorption Spectra and Global Analysis left and right respectively for PT, TPT,PT1P, PT2P, and PT3P.

4.10 Pulsed Electron Spin Resonance

In Figure 4.12, we show the results of pulsed laser pulsed microwave electron spin resonance experiments for PT3P in toluene at 80K. We have described these experiments before, but briefly, we photoexcite to populate excited states, and then use pulsed microwave to nutate these states. The spin of the state affects the rate of nutation, helping to identify quintets, triplets or other species. Figure 4.12 (above) shows the echo amplitude as a function of nutation pulse length at 340 mT, while Figure 4.12 (below) shows the same data at 325 mT.

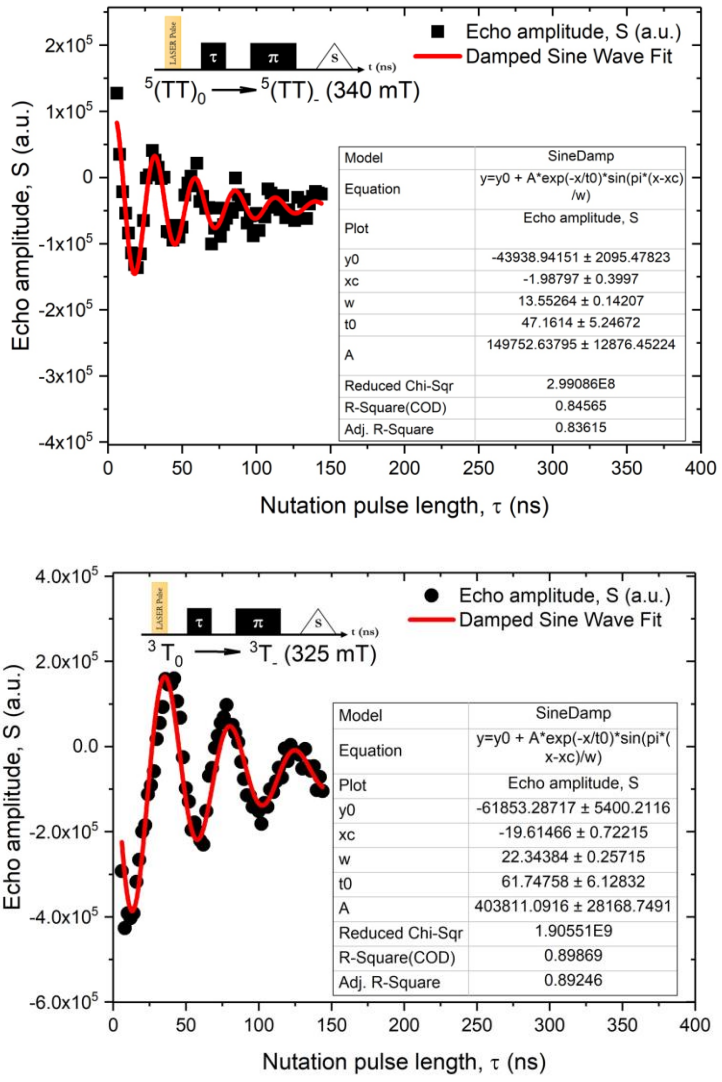

Figure 4.12 Nutation Data of the $^5(TT)_0 \leftrightarrow {}^5(TT)_{-1}$ (solid black squares) (Top) and $^3T_0 \leftrightarrow {}^3T_{-1}$ (solid black circles) (Bottom) at microwave frequencies of 9.7047 GHz and 9.7062 GHz and magnetic fields of 340 mT and 325 mT, respectively, 1 μs after the laser pulse illuminated a PT3P solution in toluene at 80K. The schematic inset shows the pulse sequence used, where π-

pulse corresponds to a complete inversion of the spin. Solid red lines are Damped Sine Wave fits and the inset tables are showing the fitting information.

4.11 Thin Film Data

In general, intermolecular interactions become important in thin films and intermolecular SF can kinetically compete with intramolecular fission. However, in these particular compounds, intermolecular interactions are extremely weak in the solid state and the energy cleft design still holds.

Here, we show that the time scales extracted from transient absorption data in solution are nearly identical in the solid state, with SF time constants on the order of 500 fs for all PTnP compounds. Furthermore, only in PT2P and PT3P do we clearly resolve an intermediate state that corresponds to the strongly bound, contiguous triplet pair.

	PT1P	**PT2P**	**PT3P**
S_1	0.45 ps	0.3 ps	0.5 ps
$^{m}(T_{1[\mathbf{P}]}T_{1[\mathbf{T}]})$	not resolvable	2.8 ps	7.0 ps

Table 4.3 Summary of Time Constants Extracted from Global Analysis of Thin Films.

In addition, we have found that the recombination dynamics follow the solution phase trend, with a distinct biexponential decay dynamics featuring the 50% amplitude distribution. As is expected for an intrinsically intramolecular decay process, the recombination kinetics are independent of laser fluence.

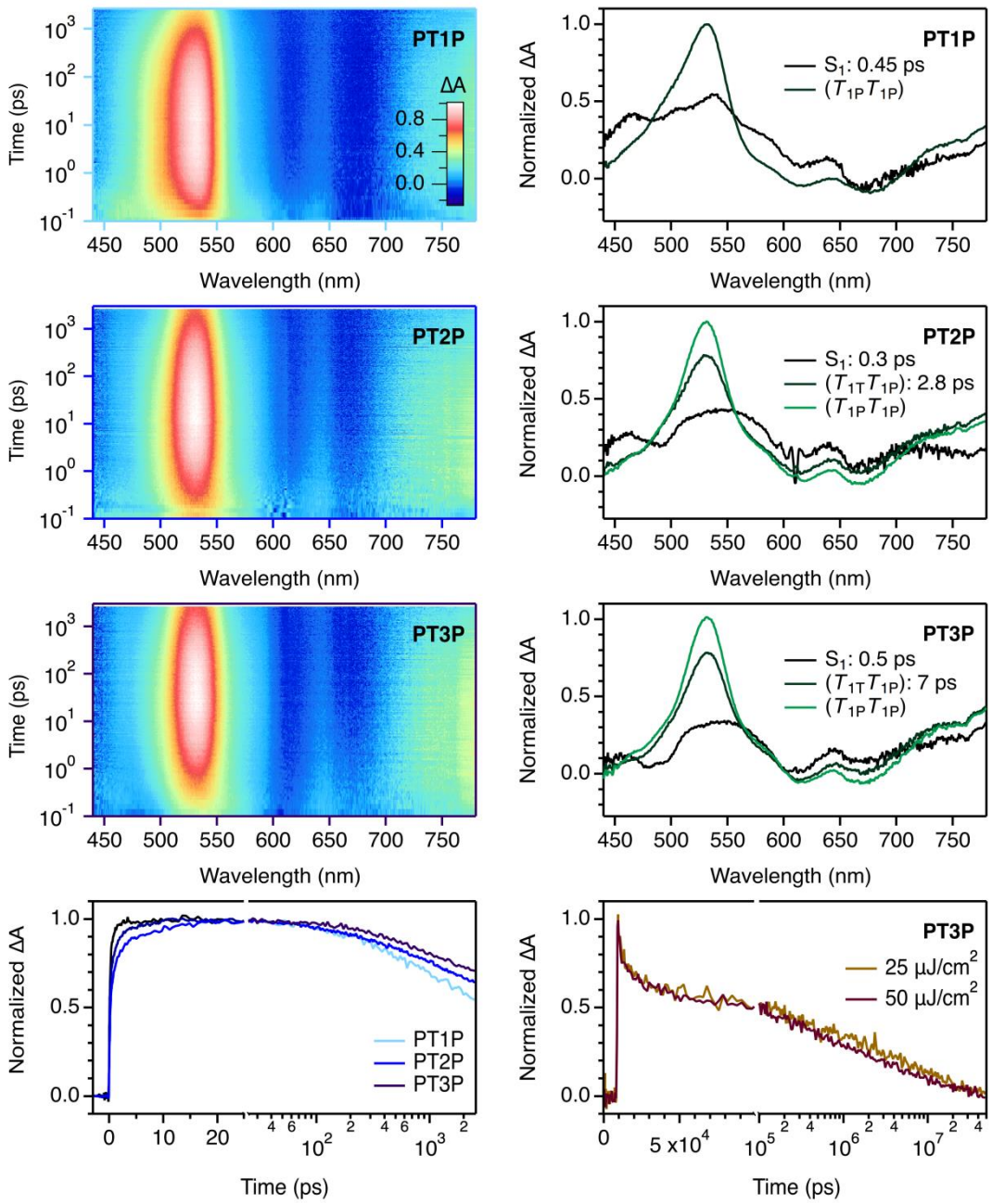

Figure 4.13 Thin Film Transient Absorption Spectra The first three rows show the raw transient absorption (left) and global analysis (right) of thin films of PTnP compounds. The bottom row shows (left) a kinetic cut corresponding to the maximum of the triplet excited state absorption signal at ~ 515 nm and (right) full population dynamics exhibiting the characteristic biexponential decay and power independence of an intramolecular decay process.

In addition, time-resolved ESR measurements on thin films that clearly shows the faster rise of the free triplet signal in going from PT1P to PT3P, as was observed in solution. This

effect can be alternatively seen by plotting spectral slices taken at a time after formation but before significant population decay occurs (chosen here to be ~ 1 us). Figure 4.14 A-C shows that the net quintet state (S=2) as well as free triplets (S=1) are forming rapidly in PTnP films analogous to PTnP compounds isolated in a frozen toluene matrix (Figure 4.4). In Figure S9 D-C, we compare the spectral slices of tr-ESR on PTnP aggregated films 1 μs after the laser pulse. The ratio of the free triplet signal (~ 365 mT) compared to the correlated triplet signal (~ 350 mT) monotonically increases as the length of the tetracene bridge increases, reflecting the more favorable kinetics to form free triplet pairs that do not readily undergo parasitic triplet pair recombination.

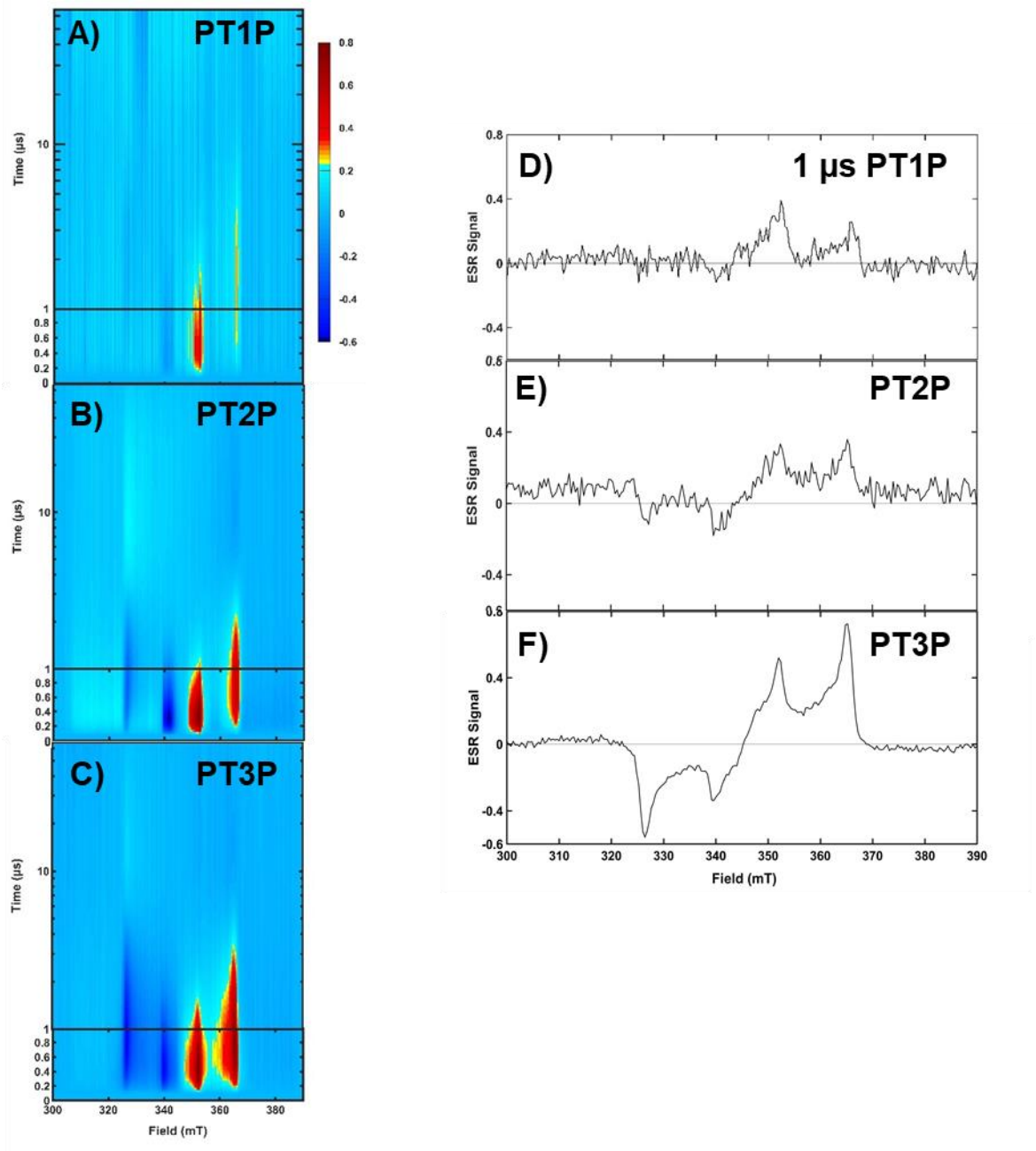

Figure 4.14 Thin Film tr-ESR Spectra Transient ESR spectral 2D maps and 1µs delayed after flash slices of (A,D) PT1P, (B,E) PT2P, and (C,F) PT3P thin films after excitation by a pulsed laser at 599 nm (3 mW). The thin-film samples were kept at 80 K in a 9.6-9.7 GHz microwave resonator.

4.12 Cyclic Voltammograms

Cyclic voltammetry measurements taken using a Bio-Logic VSP-300 potentiostat, using a glassy carbon working electrode, Ag wire reference electrode, and Pt wire counter electrode.

Measurements were done with a scan rate of 75 mV/s in DCM with 0.1 M tetrabutylammonium hexafluorophosphate as the electrolyte after sparging with argon. All measurements were calibrated with a ferrocene/ferrocenium (Fc/Fc+) redox couple.

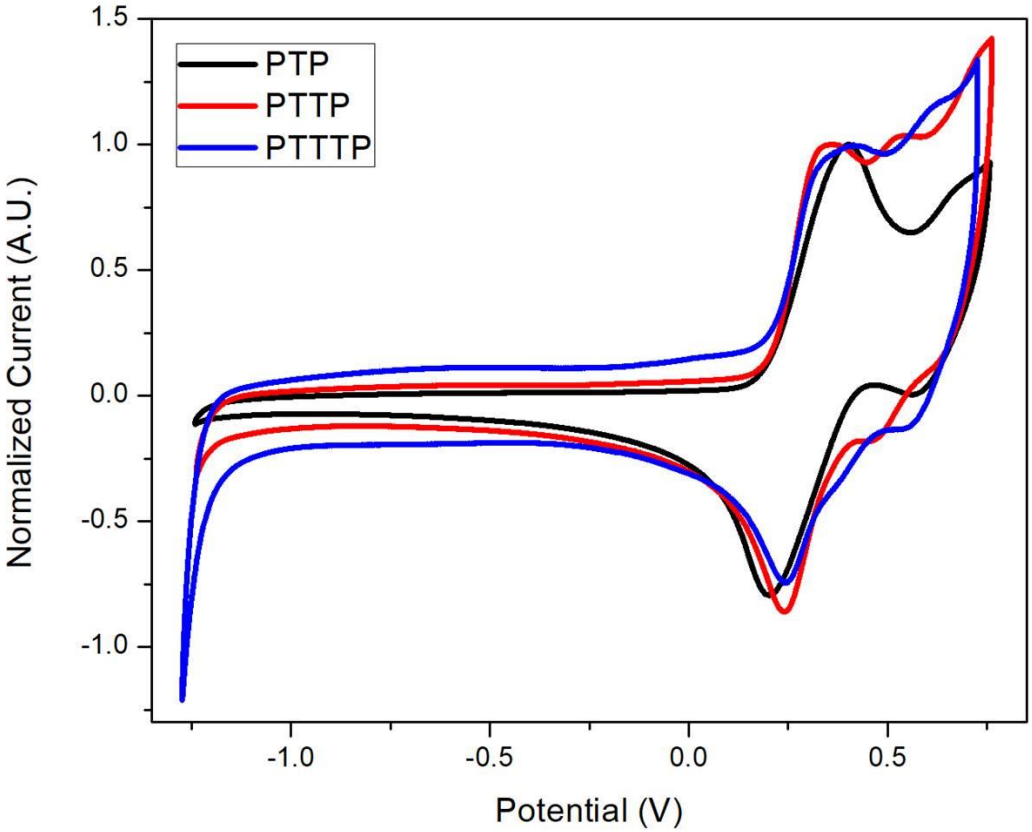

Figure 4.15 Cyclic Voltammograms of PTnP Compounds PTP (black), PTTP (red), and PTTTP (blue). Normalized to the first oxidation peak in the forward direction. For reference, tips pentacene has been reported in literature.[49]

4.13 Singlet Fission in Pentacene-Anthradithiophene-Pentacene (PADTP)

PADTP behaves similarly to PT1P, showing rapid singlet fission and a high free triplet yield, validating the energy cleft design for other chromophore systems.

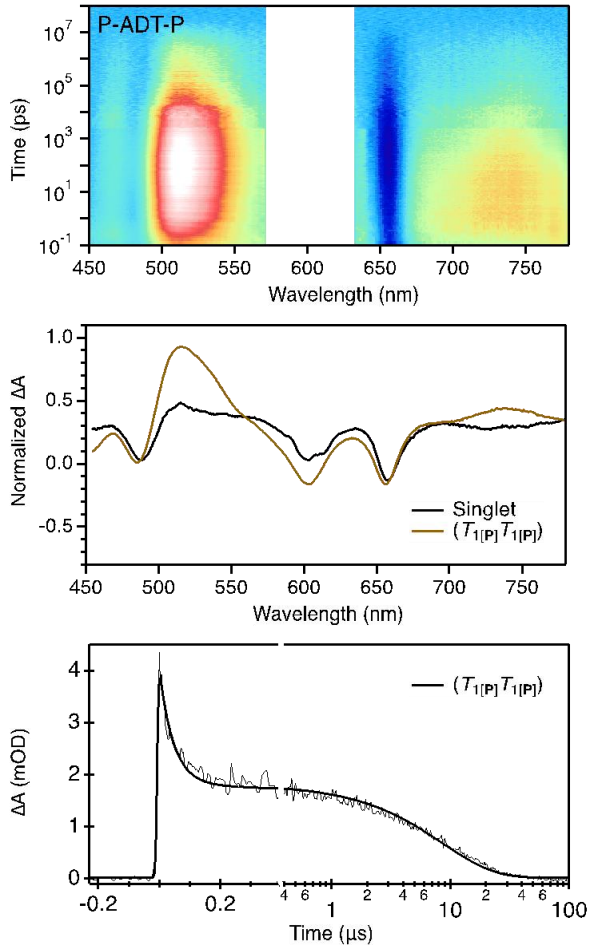

Figure 4.16 Transient Absorption and Excited State Dynamics of PADTP (Top) Raw transient absorption data and (middle) global analysis of **PADTP** in dilute toluene solution. (Bottom) The triplet recombination dynamics are very similar to **PT1P**, with a ~50 ns fast component dominating until the 45% amplitude threshold is reached, followed by decay at the one triplet lifetime.

Transient absorption measurements reveal that the excited state dynamics of **PADTP** are nearly identically to those of **PTP** (Figure 4.18). **PADTP** exhibits a singlet fission time constant of ~ 700 fs and an unresolvable relaxation to a set of weakly coupled pentacene triplets. Long lived population of the ADT triplet is not observed, and ruled out by spectral analysis (Figure 4.19). The transient spectra corresponding to the ADT triplet is determined by sensitization of an ADT monomer in solution. The decay of pentacene triplets follows the expected behavior and

are distinguished by their extremely long-lived triplet population and ~ 45% population sub-ensemble that decay at the mono triplet exciton lifetime. These data show that a significant reduction of the energetic offset between the intermediate and final triplet pair state is possible while maintaining the favorable triplet exciton dynamics seen in previously studied energy cleft compounds (**PTnP**). These results confirm the generality of the energy cleft design.

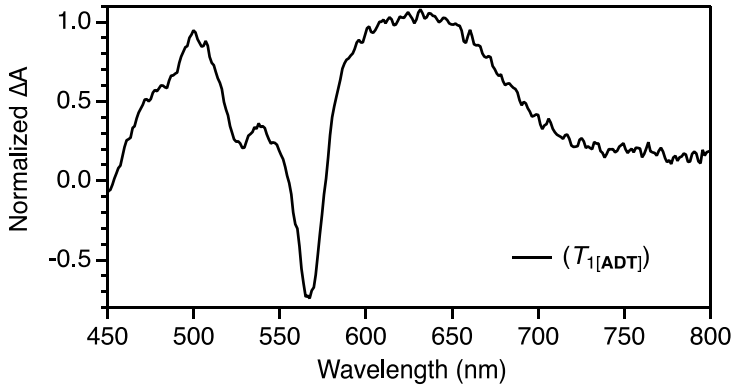

Figure 4.17 Triplet Sensitization of an ADT Monomer in dilute toluene solution.

4.14 Synthesis

Throughout the synthetic procedure described below, R_1 denotes (Triisopropylsilyl)acetylene, R_2 denotes (n-octyl,diisopropylsilyl) acetylene.

Synthesis of PT-Br

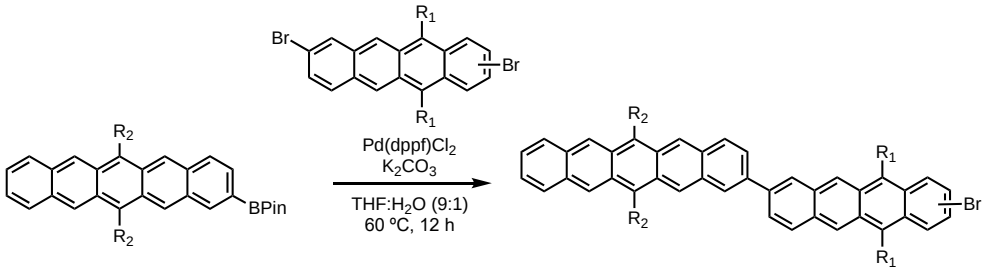

Bpin-NODIPS-Pentacene (322 mg, 0.36 mmol), Dibromo-TIPS-tetracene (797 mg, 1.07 mmol), K_2CO_3 (249 mg, 1.8 mmol) and Pd(dppf)Cl_2·DCM (29 mg, 0.04 mmol) were added to a reaction

vial. Sequential vacuum and argon was used to degas the mixture. The solids were then dissolved in a 15 mL of a 9:1 mixture of dry THF: degassed water. The reaction was brought to 60 °C and allowed to stir for 12 h. The reaction was cooled to room temperature. The crude reaction mixture was concentrated and purified by 3% neutral alumina (3-7% $CHCl_3$ in Hexanes) to obtain **PT-Br** as a burgundy solid. (300 mg, 58% Yield).

^{1}H-NMR (400 MHz, $CDCl_3$, δ ppm): 9.39-9.32 (m, 5H), 9.24 (s, 1H), 9.10-9.09 (m, 1H), 8.82-8.79 (m, 1H), 8.39 (s, 1H), 8.22-8.21 (m, 1H), 8.14-8.09 (m, 2H), 8.03-8.00 (m, 2H), 7.98-7.92 (m, 2H), 7.56-7.53 (m, 1H), 7.47-7.44 (m, 2H), 1.84-1.78 (m, 4H), 1.46-1.35 (m, 77H), 1.30-1.25 (m, 9H), 1.18-1.15 (m, 4H), 1.03-0.99 (m, 4H), 0.87-0.83 (m, 3H) and 0.76-0.72 (m, 3H).

^{13}C-NMR (100 MHz, $CDCl_3$, δ ppm): 138.90, 138.78, 137.73, 133.37, 133.13, 132.80, 132.73, 132.51, 132.42, 132.38, 132.18, 131.64, 131.01, 130.97, 130.88, 130.70, 130.48, 130.36, 130.18, 129.65, 129.62, 129.52, 128.69, 128.33, 126.95, 126.87, 126.68, 126.40, 126.28, 126.16, 126.08, 125.57, 125.44, 120.42, 120.36, 118.95, 118.81, 118.56, 118.42, 107.78, 107.60, 106.84, 106.30, 104.57, 103.82, 103.61, 34.11, 34.02, 31.98, 31.90, 29.53, 29.47, 29.39, 25.03, 24.98, 22.68, 22.60, 19.05, 19.01, 18.77, 18.49, 14.09, 13.99, 12.24, 11.66, 10.57, 10.50.

MS (APCI+): Calculated $[M+H]^+$: 1443.7963; Observed: 1443.953.2310.

Synthesis of TPT

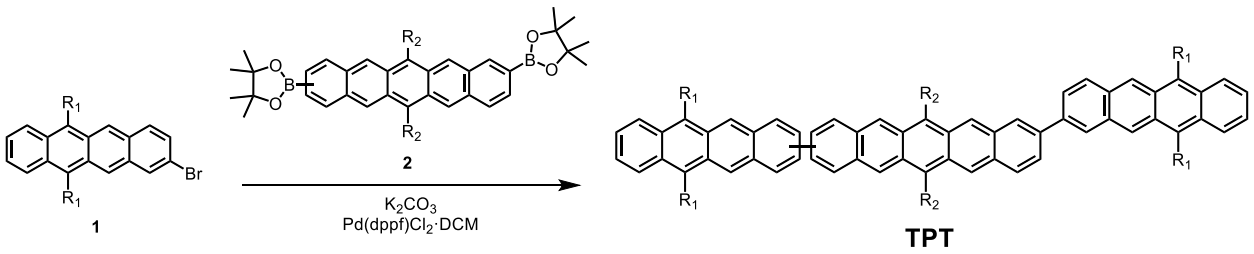

1 (70 mg, .098 mmol)**, 2** (42 mg, .045 mmol), K_2CO_3 (31 mg, 0.22 mmol) and Pd(dppf)Cl_2·DCM (3.64 mg, 0.004 mmol) were added to a reaction vial. Sequential vacuum and argon was used to degas the mixture. The solids were then dissolved in a 8 mL of a 9:1 mixture of dry THF: degassed water. The reaction was brought to 65 °C and allowed to stir overnight. The reaction was cooled to room temperature. The crude reaction mixture was concentrated and purified by chromatography on silica gel (5% DCM in Hexanes) to obtain **TPT** as a burgundy solid. (29 mg, 34% Yield).

^{1}H-NMR (400 MHz, $CDCl_3$, δ ppm): 9.43 (s, 4H), 9.36 (m, 4H), 8.66 (m, 4H), 8.38 (m, 4H), 8.18 (t, 4H), 7.99 (d, 2H), 7.95 (d, 2H), 7.57 (m, 4H), 1.82 (m, 6H), 1.45-0.6 (m, 140H).

^{13}C-NMR (125 MHz, $CDCl_3$, δ ppm): 137.94, 137.88, 137.83, 132.96, 132.85, 132.51, 131.76, 131.62, 131.29, 130.93, 130.77, 129.77, 129.65, 127.58, 127.02, 126.95, 126.91, 126.37, 126.22, 126.05, 118.89, 118.75, 106.19, 106.07, 104.12, 104.06, 34.30, 34.25, 34.20, 32.13, 32.06, 31.98, 29.74, 29.69, 29.64, 29.56, 29.54, 29.52, 25.28, 25.21, 25.15, 22.82, 22.76, 22.71, 19.16, 19.14, 18.96, 18.95, 18.93, 18.66, 18.65, 14.27, 14.18, 14.07, 12.37, 11.79, 10.67.

MS (ESI): Calculated $[M+H]^+$: 1953.2336; Observed: 1953.2310.

Synthesis of PTP

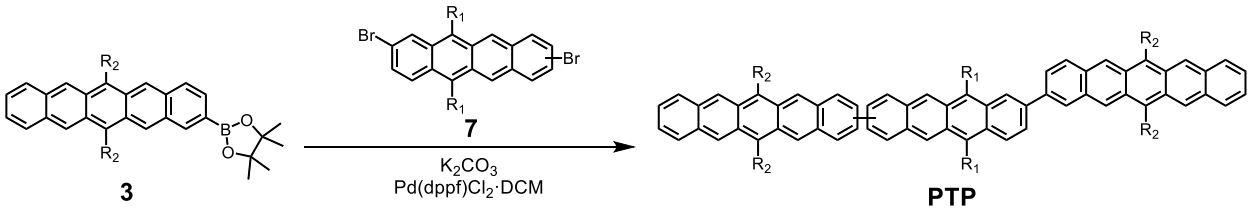

3 (60 mg, .066 mmol)**, 7** (22 mg, .03 mmol), K_2CO_3 (21 mg, .15 mmol) and Pd(dppf)Cl_2·DCM (2.5 mg, .003 mmol) were added to a reaction vial. Sequential vacuum and argon was used to degas the mixture. The solids were then dissolved in a 8 mL of a 9:1 mixture of dry THF: degassed water. The reaction was brought to 65 °C and allowed to stir overnight. The reaction was cooled to room temperature. The crude reaction mixture was concentrated and purified by chromatography on silica gel (25% DCM in Hexanes) to obtain **PTP** as a burgundy solid. (39 mg, 61% Yield).

^{1}H-NMR (400 MHz, $CDCl_3$, δ ppm): 9.45 (s, 1H), 9.39 (m, 3H), 9.33 (m, 6H), 9.11 (s, 1H), 8.82 (dd, 1H), 8.41 (s, 1H), 8.38 (d, 2H), 8.19 (dd, 2H), 8.10 (t, 2H), 7.97 (m, 7H), 7.43 (m, 4H), 1.80 (m, 8H), 1.54 (m, 8H), 1.45-0.70 (m, 150H).

Limited solubility and large number of unique carbons of material prevented the acquisition of a ^{13}C-NMR.

MS (ESI): Calculated $[M]^+$: 2143.3999; Observed: 2143.3999.

Synthesis of PT2P

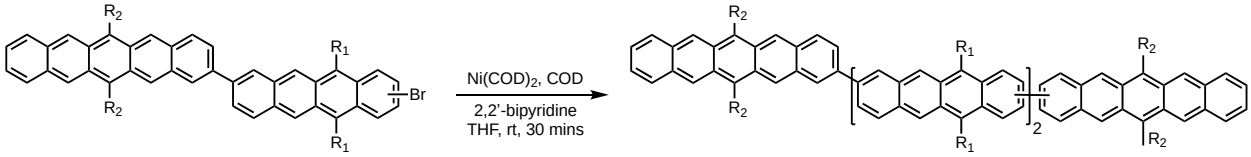

To a dry vial in a glove box, added $Ni(COD)_2$ (9.5 mg, 0.035 mmol, 1.0 equiv), COD (7.6 mg, 0.07 mmol), 2,2'-bipyridine (5.5 mg, 0.035 mmol) and THF (3 mL). The mixture immediately turned purple and to this solution added a solution of **PT-Br** (50 mg, 0.035 mmol) in THF (2 mL) slowly. The resulting solution was stirred at room temperature under dark for 30 mins. The solution was concentrated and purified on a alumina column (packed on a 20 mL syringe) using first hexanes to remove COD and 10% DCM:hexanes to elute the product as a burgundy solid. (36 mg, 45% Yield).

^{1}H-NMR (400 MHz, $CDCl_3$, δ ppm): 9.48-9.34 (m, 13H), 9.22 (s, 1H), 9.14 (m, 2H), 8.86-8.81 (m, 3H), 8.47-8.41 (3, 5H), 8.28-8.19 (m, 5H), 8.04-7.97 (m, 13H), 7.47-7.44 (m, 4H), 1.82-1.79 (m, 13H), 1.44-1.36 (m, 163H), 1.29 (m, 32H), 1.19-1.17 (m, 13H), 1.04-0.99 (m, 13H), 0.93-0.86 (m, 27H) and 0.77-0.75 (m, 9H).

Limited solubility and large number of unique carbons prevented the acquisition of a ^{13}C-NMR.

MS (MALDI+): Calculated $[M]^+$: 3457.2483; Observed: 3457.1240.

Synthesis of PT3P

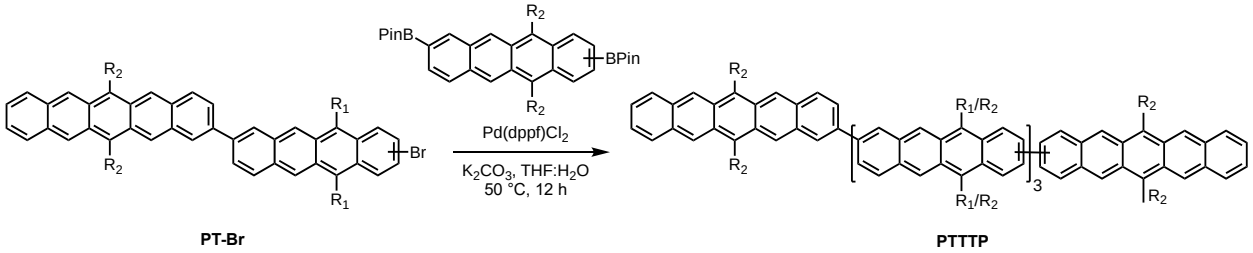

PT-Br (60 mg, 0.042 mmol, 2.2 equiv)**, Bis-Bpin NODIPS tetracene** (17 mg, 0.019 mmol, 1.0 equiv), K_2CO_3 (29 mg, 0.21 mmol) and $Pd(dppf)Cl_2 \cdot DCM$ (3.4 mg, 0.0042 mmol) were added to a reaction vial. Sequential vacuum and argon was used to degas the mixture. The solids were then dissolved in a 4 mL of a 9:1 mixture of dry THF: degassed water. The reaction was brought to 50 °C and allowed to stir overnight under dark. The reaction was cooled to room temperature. The crude reaction mixture was concentrated and purified by chromatography on silica gel (25% DCM in Hexanes) to obtain **PT3P** as a burgundy solid. (30 mg, 45% Yield).

^{1}H-NMR (400 MHz, $CDCl_3$, δ ppm): 9.39-9.32 (m, 10H), 9.24 (s, 2H), 9.09-9.09 (m, 2H), 8.82-8.79 (m, 2H), 8.39 (s, 2H), 8.22 (s, 2H), 8.14-8.09 (m, 4H), 8.04-8.01 (m, 4H), 7.97-7.92 (m, 4H), 7.56-7.54 (m, 2H), 7.47-7.44 (m, 4H), 1.82-1.79 (m, 8H), 1.42-1.36 (m, 142H), 1.28 (m, 23H), 1.18-1.15 (m, 9H), 1.03-0.99 (m, 9H), 0.87-0.84 (m, 9H) and 0.76-0.72 (m, 8H).

Limited solubility and large number of unique carbons of material prevented the acquisition of a ^{13}C-NMR.

MS (MALDI+): Calculated $[M]^+$: 2729.7447; Observed: 2730.7471.

Synthesis of Bis-Bpin ADT

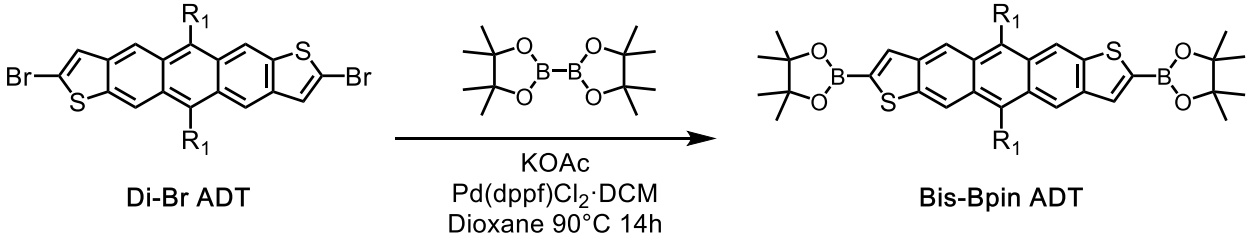

Di-Br ADT (300 mg, 0.37 mmol)**,** Bis(pinacolato)diboron (282 mg, 1.11 mmol), KOAc (109 mg, 1.11 mmol) and Pd(dppf)Cl_2·DCM (30 mg, 0.037 mmol) were added to a reaction vial. Sequential vacuum and argon was used to degas the mixture. The solids were then dissolved in 4 mL of dry dioxane. The reaction was brought to 90 °C and allowed to stir overnight under dark. The reaction was cooled to room temperature. The crude reaction mixture was concentrated and purified by chromatography on silica gel to obtain **Bis-Bpin ADT** as a burgundy solid. (250 mg, 75% Yield).

^{1}H-NMR (500 MHz, $CDCl_3$, δ ppm): 9.24-9.19 (m, 4H), 8.01-7.97 (m, 2H), 1.47-1.41 (m, 24H), 1.39-1.31 (m, 42H).

^{13}C NMR (125 MHz, $CDCl_3$, δ ppm): δ 142.45, 142.13, 141.28, 141.08, 134.58, 130.73, 130.40, 130.29, 129.95, 122.77, 119.99, 118.12, 106.36, 104.28, 84.97, 84.95, 25.01, 19.13, 19.09, 11.76.

MS (ESI+): Calculated $[M]^+$: 902.4614; Observed: 902.4621.

Synthesis of PADTP

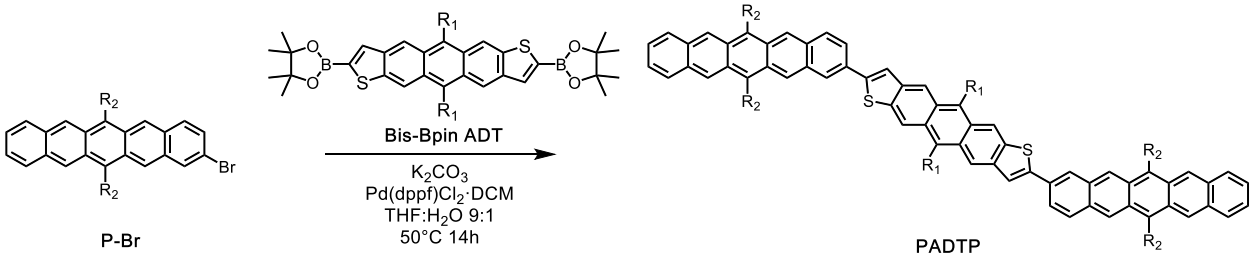

P-Br (112 mg, 0.13 mmol)**, Bis-Bpin ADT** (50 mg, 0.06 mmol), K_2CO_3 (39 mg, 0.3 mmol) and Pd(dppf)Cl_2·DCM (4.6 mg, 0.006 mmol) were added to a reaction vial. Sequential vacuum and argon was used to degas the mixture. The solids were then dissolved in a 4 mL of a 9:1 mixture of dry THF: degassed water. The reaction was brought to 50 °C and allowed to stir overnight under dark. The reaction was cooled to room temperature. The crude reaction mixture was concentrated and purified by chromatography on alumina to obtain **PADTP** as a black solid. (34 mg, 28% Yield).

^{1}H-NMR (400 MHz, $CDCl_3$, δ ppm): 9.40-8.87 (m, 12H), 8.14- 7.82 (m, 8H), 7.80-7.66 (m, 2H), 7.61-7.27 (m, 5H), 7.25-7.13 (m, 1H), 1.85-1.76 (m 6H), 1.58-1.53 (m, 6H), 1.49-1.14 (m, 130H), 1.09-0.94 (m, 12H), 0.87-0.81 (m, 6H), 0.78-0.72 (m, 6H).

Limited solubility and large number of unique carbons prevented the acquisition of a ^{13}C-NMR.

MS (MALDI+): Calculated $[M]^+$: 2205.328; Observed: 2205.408.

4.15 NMR Spectra

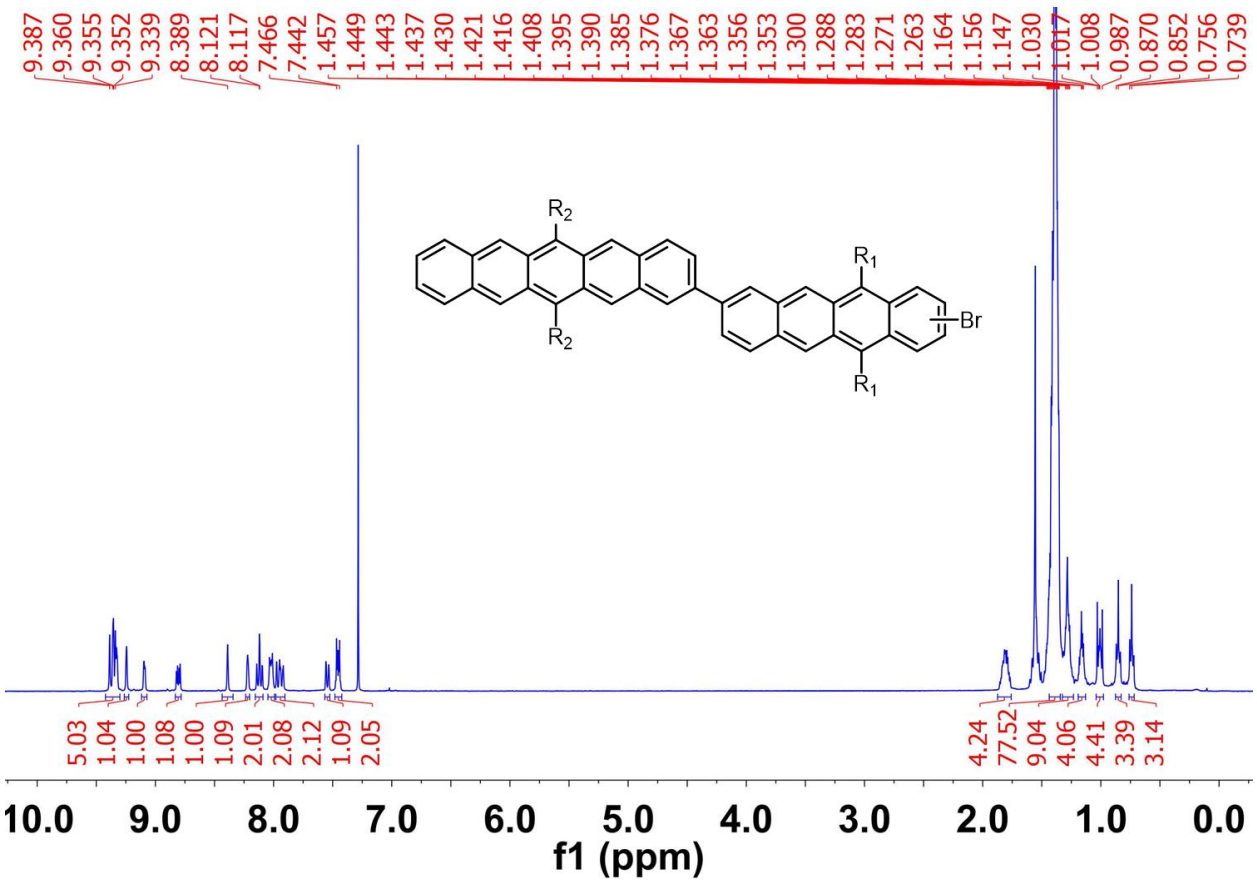
9.387
9.360
9.355
9.352
9.339
8.389
8.121
8.117
7.466
7.442
1.457
1.449
1.443
1.437
1.430
1.421
1.416
1.408
1.395
1.390
1.385
1.376
1.367
1.363
1.356
1.353
1.300
1.288
1.283
1.271
1.263
1.164
1.156
1.147
1.030
1.017
1.008
0.987
0.870
0.852
0.756
0.739
R2
R2
R1
R1
Br
5.03
1.04
1.00
1.08
1.00
1.09
2.01
2.08
2.12
1.09
2.05
4.24
77.52
9.04
4.06
4.41
3.39
3.14
10.0
9.0
8.0
7.0
6.0
5.0
4.0
3.0
2.0
1.0
0.0
f1 (ppm)

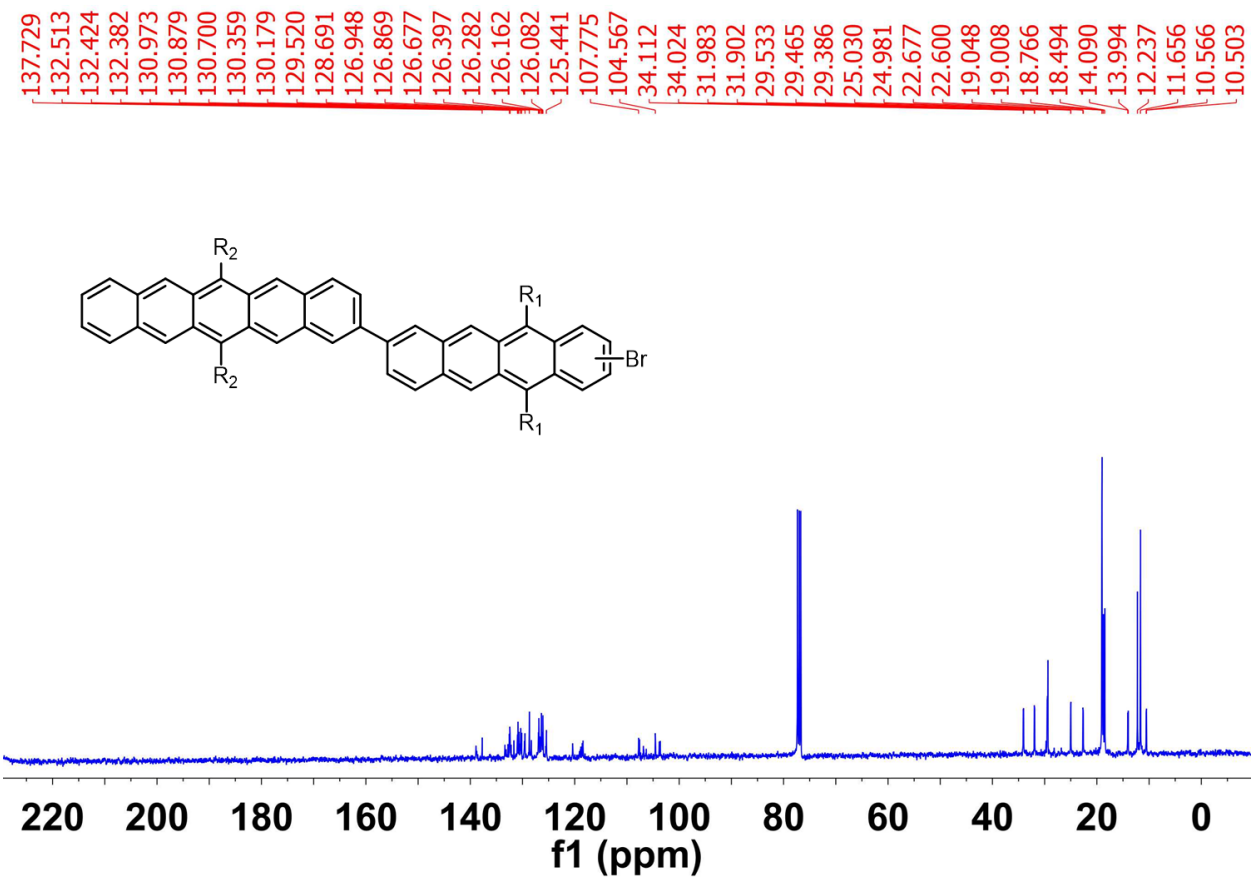
137.729
132.513
132.424
132.382
130.973
130.879
130.700
130.359
130.179
129.520
128.691
126.948
126.869
126.677
126.397
126.282
126.162
126.082
125.441
107.775
104.567
34.112
34.024
31.983
31.902
29.533
29.465
29.386
25.030
24.981
22.677
22.600
19.048
19.008
18.766
18.494
14.090
13.994
12.237
11.656
10.566
10.503
R2
R2
R1
R1
Br
220
200
180
160
140
120
100
80
60
40
20
0
f1 (ppm)

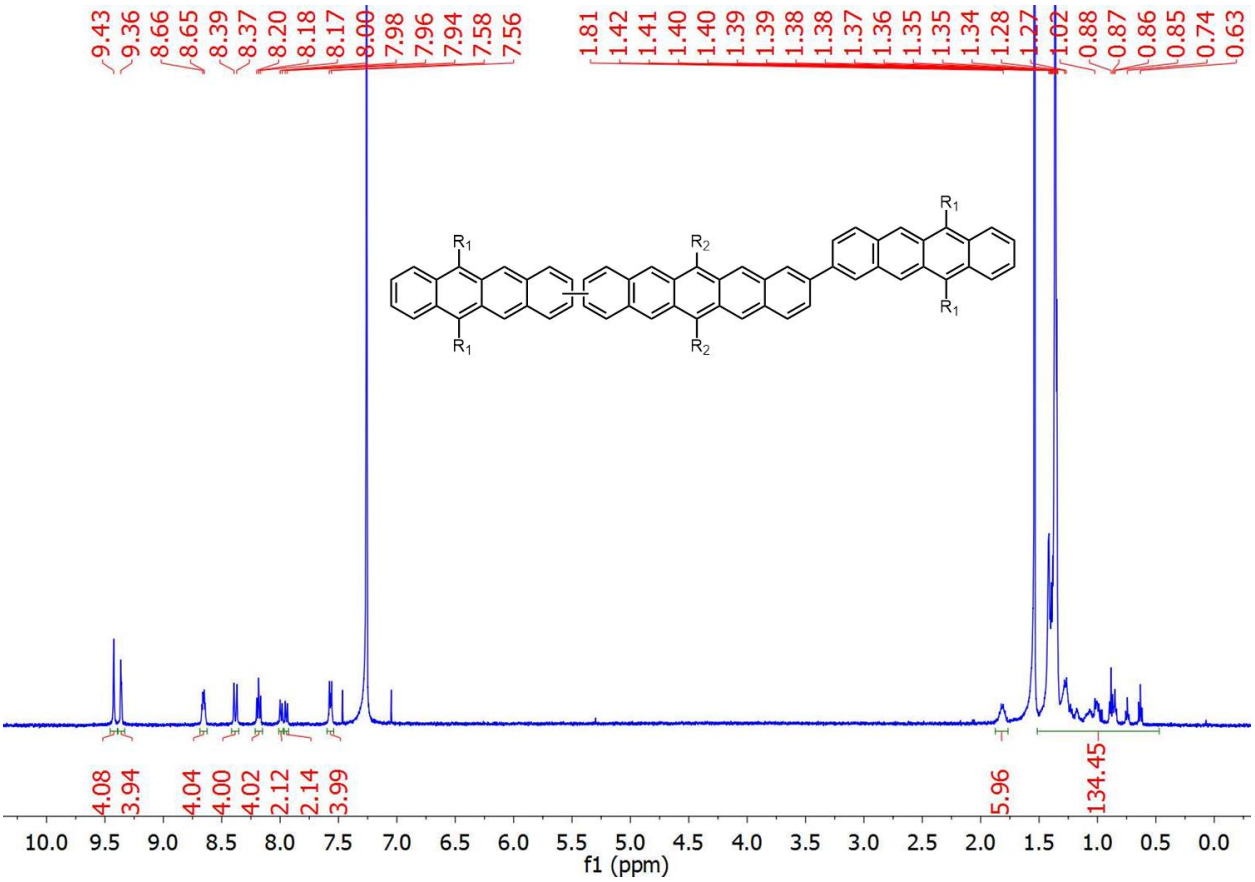
9.43
9.36
8.66
8.65
8.39
8.37
8.20
8.18
8.17
8.00
7.98
7.96
7.94
7.58
7.56
1.81
1.42
1.41
1.40
1.40
1.39
1.39
1.38
1.38
1.37
1.36
1.35
1.35
1.34
1.28
1.27
1.02
0.88
0.87
0.86
0.85
0.74
0.63
R1
R2
4.08
3.94
4.04
4.00
4.02
2.12
2.14
3.99
5.96
134.45
10.0 9.5 9.0 8.5 8.0 7.5 7.0 6.5 6.0 5.5 5.0 4.5 4.0 3.5 3.0 2.5 2.0 1.5 1.0 0.5 0.0
f1 (ppm)

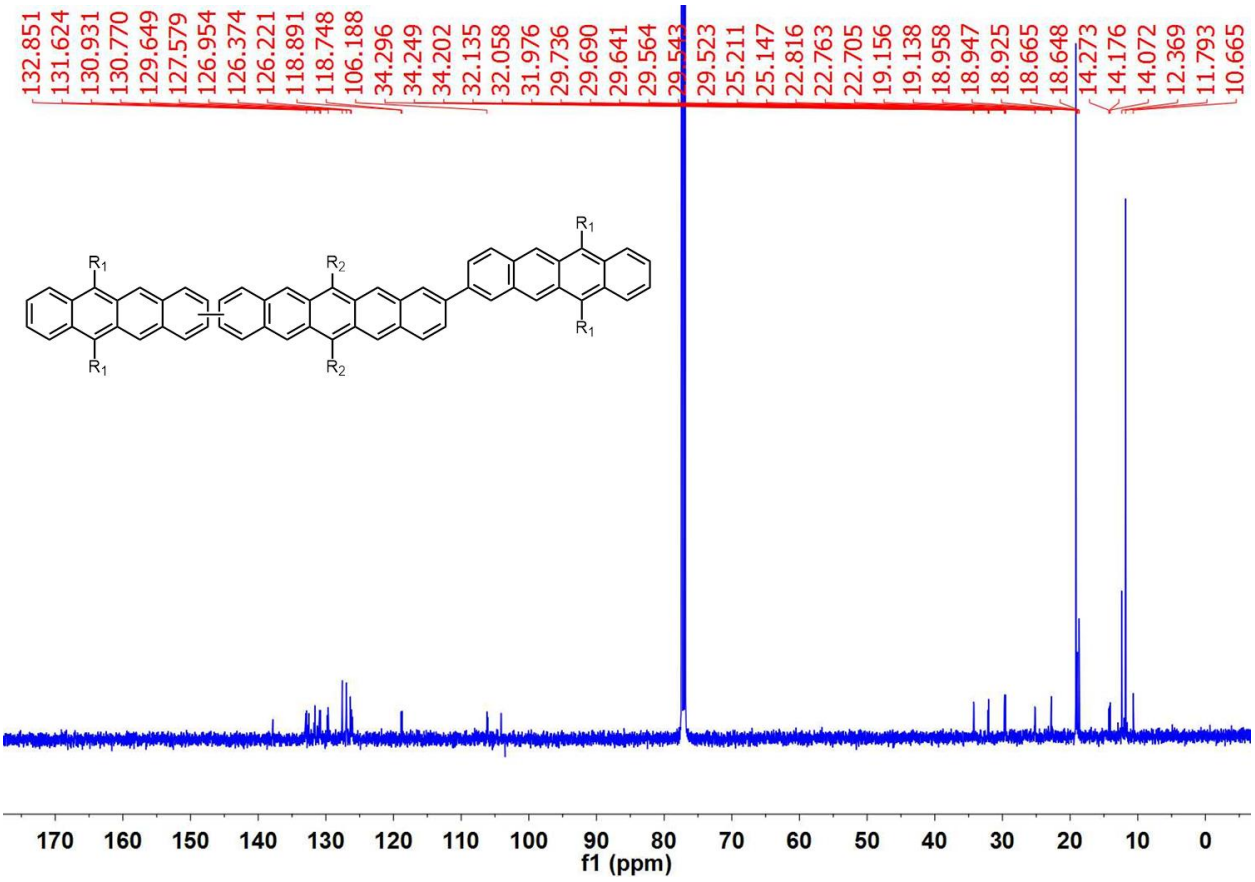
132.851
131.624
130.931
130.770
129.649
127.579
126.954
126.374
126.221
118.891
118.748
106.188
34.296
34.249
34.202
32.135
32.058
31.976
29.736
29.690
29.641
29.564
29.543
29.523
25.211
25.147
22.816
22.763
22.705
19.156
19.138
18.958
18.947
18.925
18.665
18.648
14.273
14.176
14.072
12.369
11.793
10.665
R1
R2
170 160 150 140 130 120 110 100 90 80 70 60 50 40 30 20 10 0
f1 (ppm)

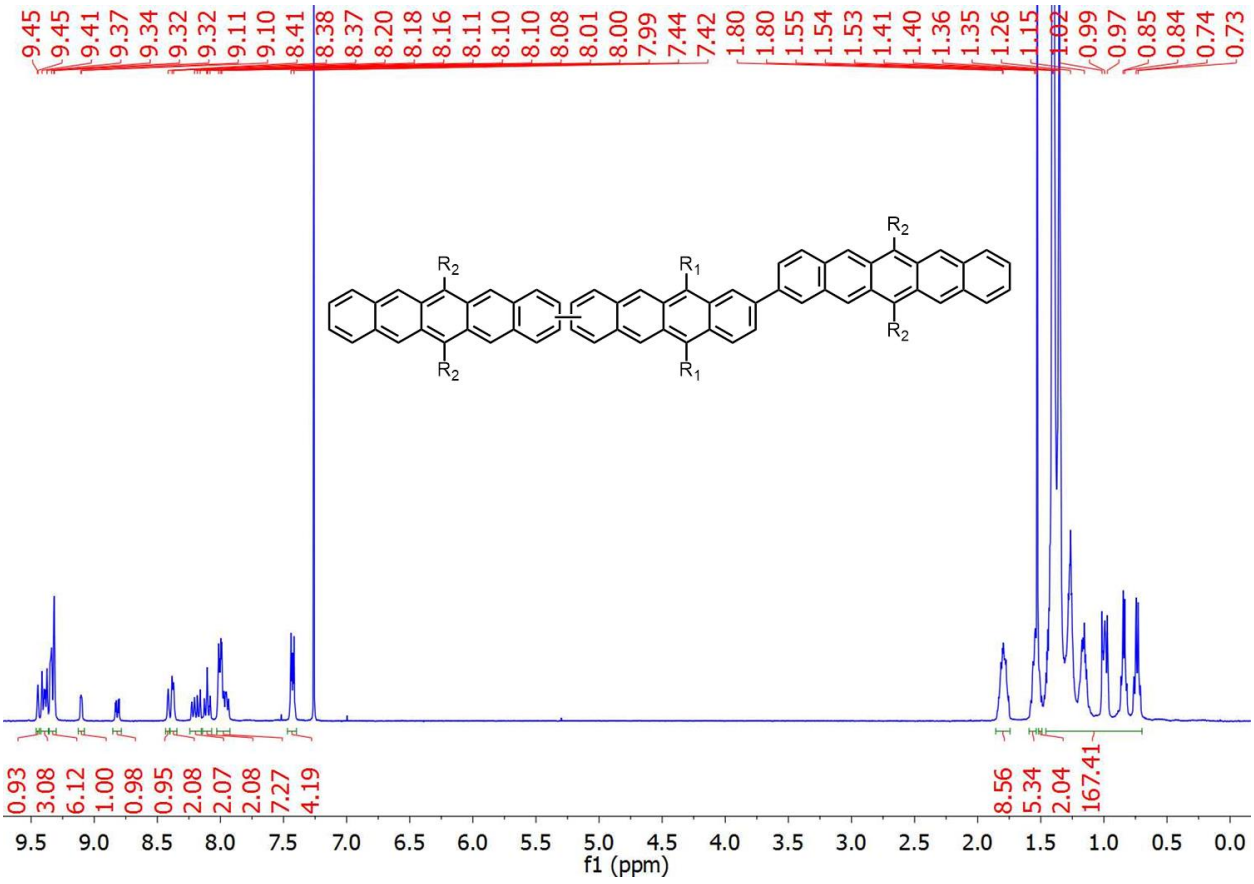
9.45 9.45 9.41 9.37 9.34 9.32 9.32 9.11 9.10 8.41 8.38 8.37 8.20 8.18 8.16 8.11 8.10 8.10 8.08 8.01 8.00 7.99 7.44 7.42 1.80 1.80 1.55 1.54 1.53 1.41 1.40 1.36 1.35 1.26 1.15 1.02 0.99 0.97 0.85 0.84 0.74 0.73
R2
R1
R2
R2
R1
R2
0.93 3.08 6.12 1.00 0.98 0.95 2.08 2.07 2.08 7.27 4.19 8.56 5.34 2.04 167.41
9.5 9.0 8.5 8.0 7.5 7.0 6.5 6.0 5.5 5.0 4.5 4.0 3.5 3.0 2.5 2.0 1.5 1.0 0.5 0.0
f1 (ppm)

.

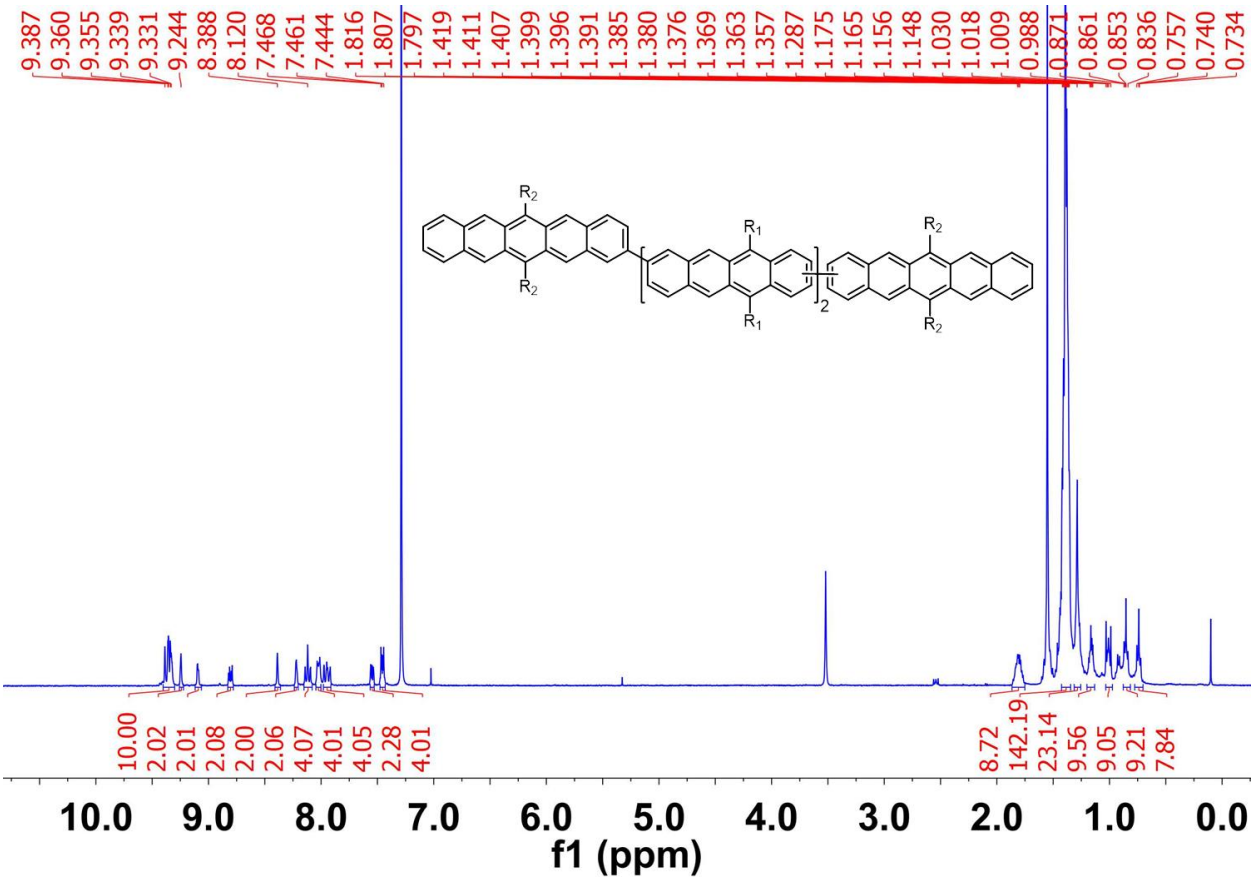
9.387
9.360
9.355
9.339
9.331
9.244
8.388
8.120
7.468
7.461
7.444
1.816
1.807
1.797
1.419
1.411
1.407
1.399
1.396
1.391
1.385
1.380
1.376
1.369
1.363
1.357
1.287
1.175
1.165
1.156
1.148
1.030
1.018
1.009
0.988
0.871
0.861
0.853
0.836
0.757
0.740
0.734
R2
R1
R2
R1
2
R2
10.00
2.02
2.01
2.08
2.00
2.06
4.07
4.01
4.05
2.28
4.01
8.72
142.19
23.14
9.56
9.05
9.21
7.84
10.0
9.0
8.0
7.0
6.0
5.0
4.0
3.0
2.0
1.0
0.0
f1 (ppm)

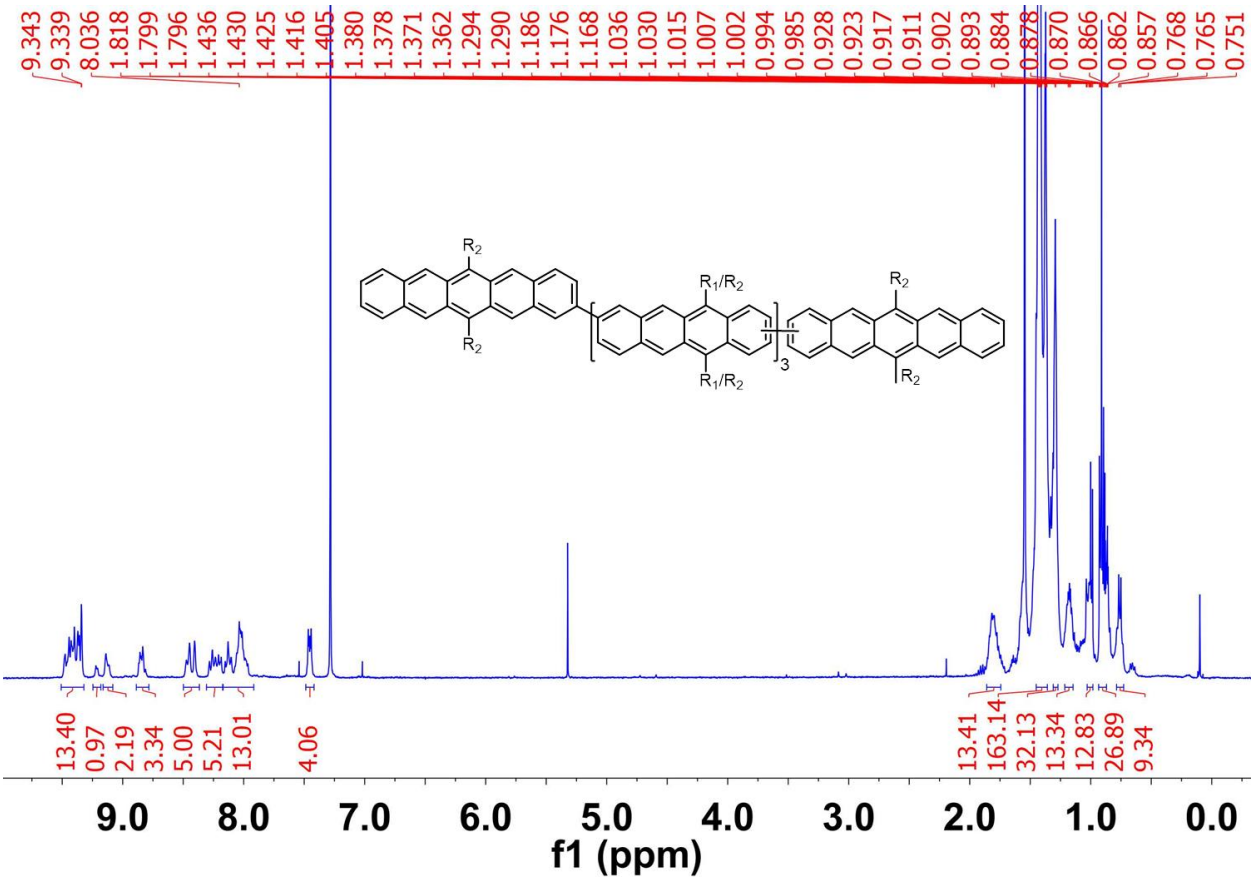
9.343
9.339
8.036
1.818
1.799
1.796
1.436
1.430
1.425
1.416
1.405
1.380
1.378
1.371
1.362
1.294
1.290
1.186
1.176
1.168
1.036
1.030
1.015
1.007
1.002
0.994
0.985
0.928
0.923
0.917
0.911
0.902
0.893
0.884
0.878
0.870
0.866
0.862
0.857
0.768
0.765
0.751
R2
R1/R2
R2
R2
R1/R2
R2
3
13.40
0.97
2.19
3.34
5.00
5.21
13.01
4.06
13.41
163.14
32.13
13.34
12.83
26.89
9.34
9.0
8.0
7.0
6.0
5.0
4.0
3.0
2.0
1.0
0.0
f1 (ppm)

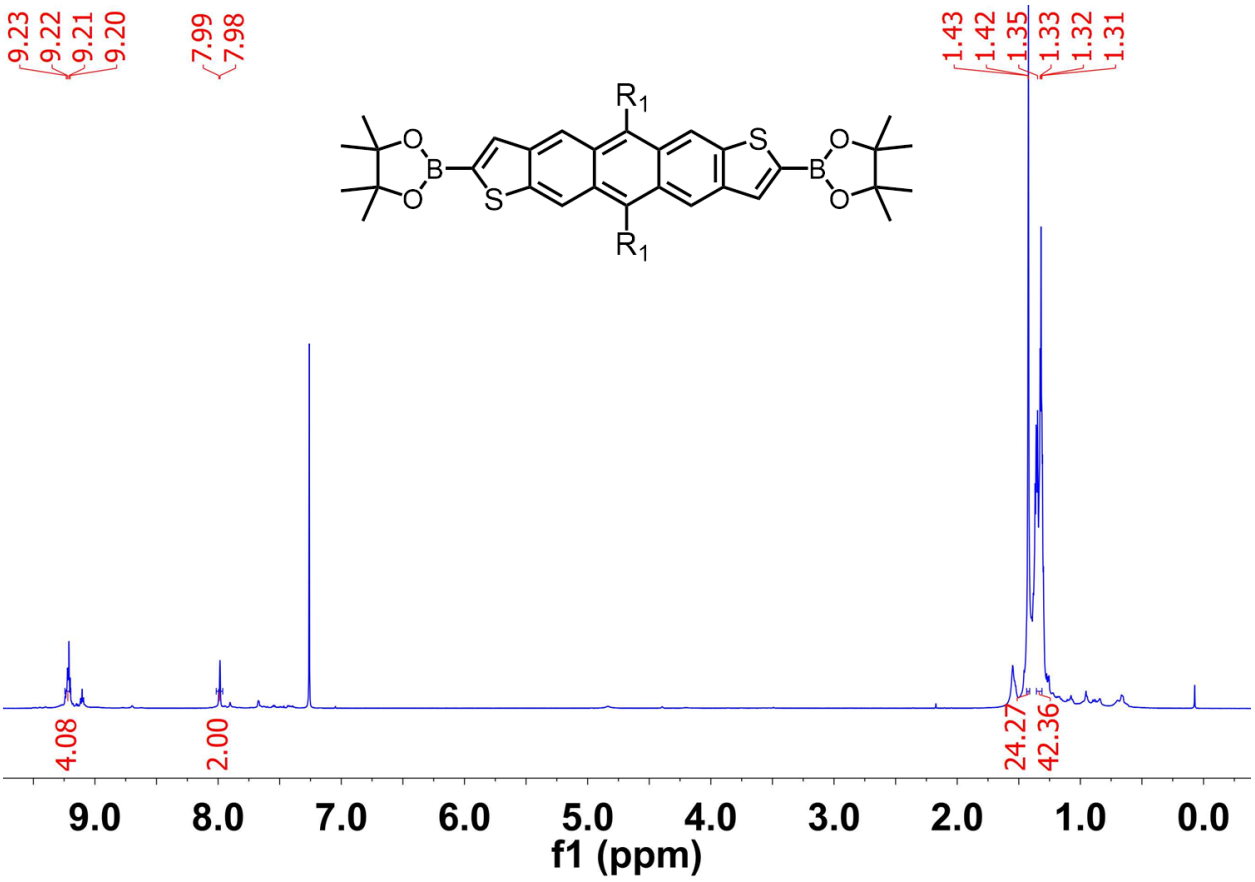
9.23
9.22
9.21
9.20
7.99
7.98
1.43
1.42
1.35
1.33
1.32
1.31
R1
R1
O
B
O
S
S
O
B
O
4.08
2.00
24.27
42.36
9.0
8.0
7.0
6.0
5.0
4.0
3.0
2.0
1.0
0.0
f1 (ppm)

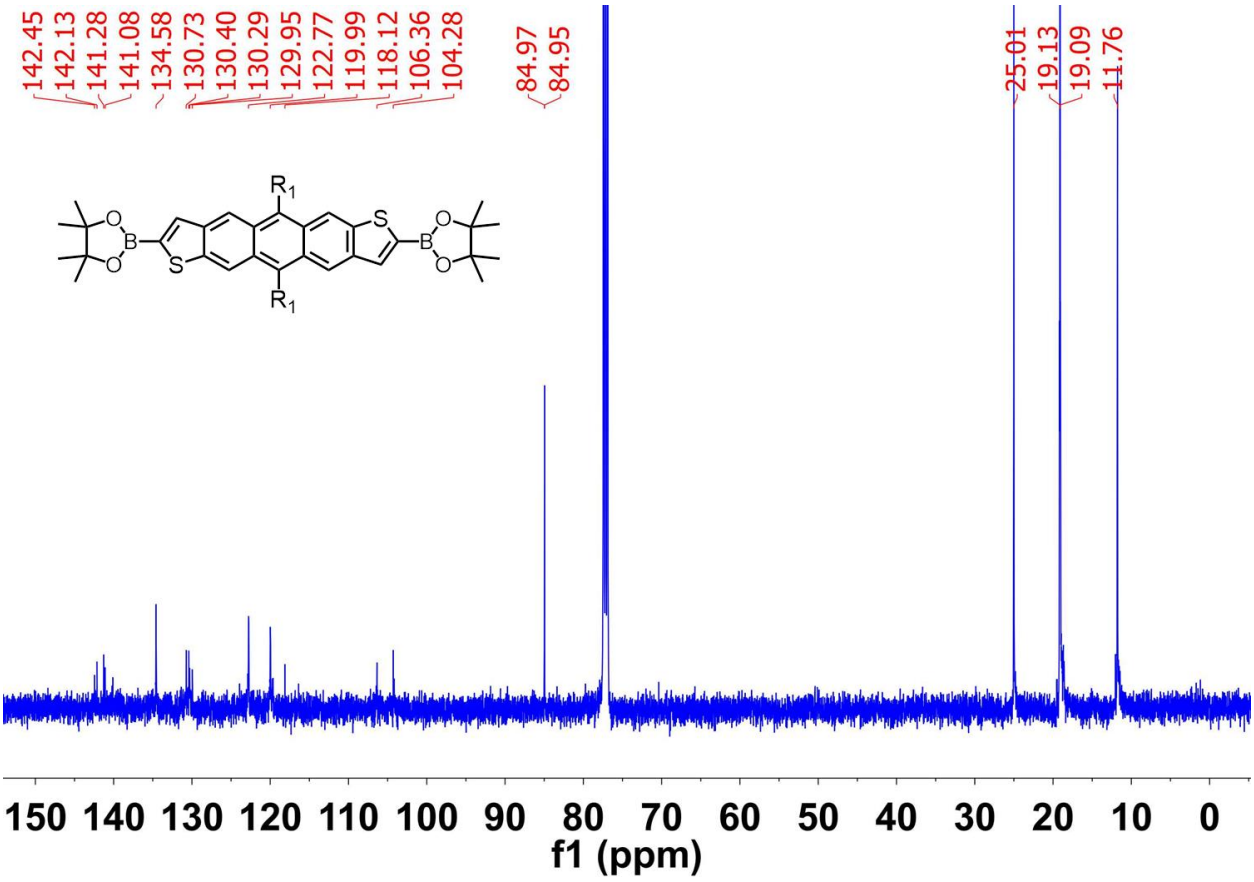
142.45
142.13
141.28
141.08
134.58
130.73
130.40
130.29
129.95
122.77
119.99
118.12
106.36
104.28
84.97
84.95
25.01
19.13
19.09
11.76
R1
R1
O
B
O
S
S
O
B
O
150 140 130 120 110 100 90 80 70 60 50 40 30 20 10 0
f1 (ppm)

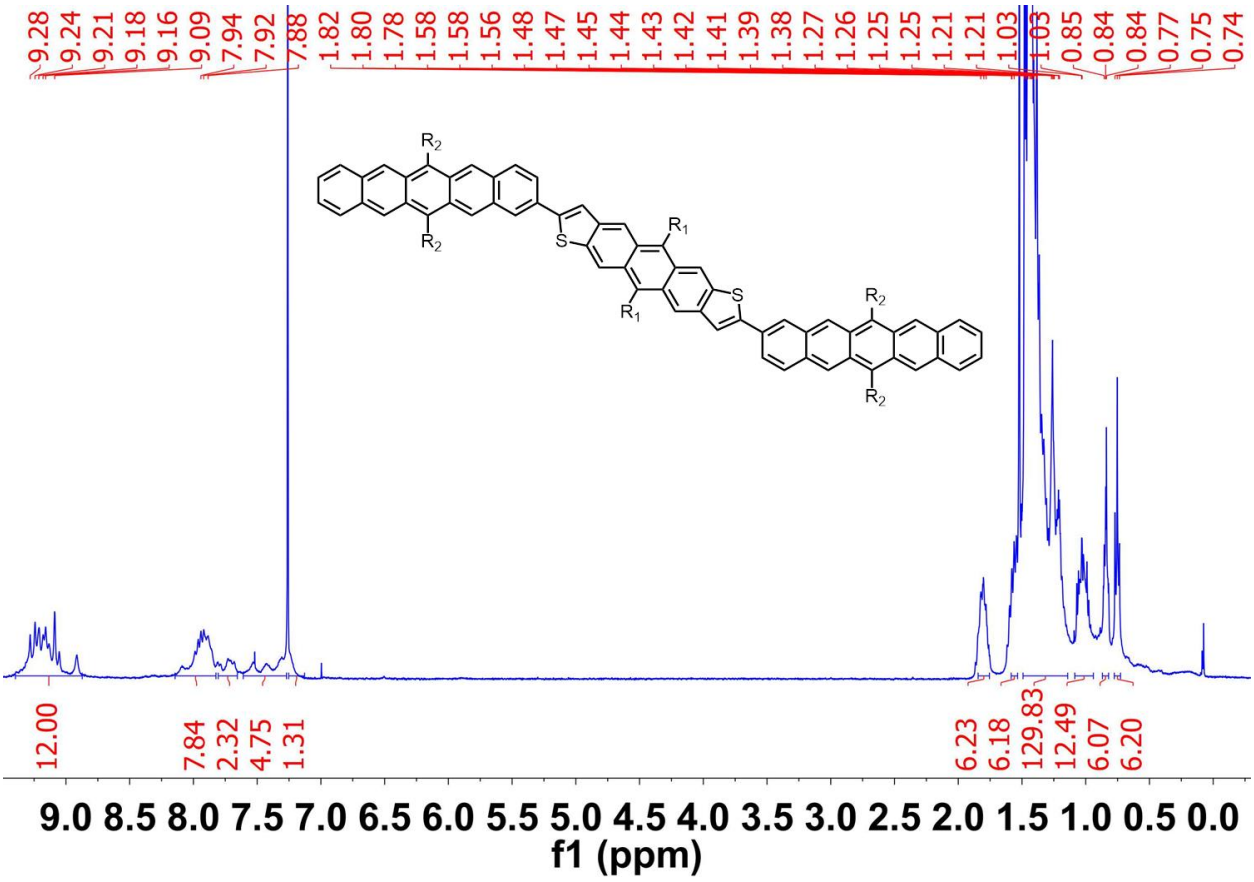

4.16 Outlook

The work in this chapter represents work that has gone on since my very first year of grad school. It started out when I synthesized a fully conjugated pentacene-tetracene copolymer (PolyPT). Sam took TA measurements on this polymer and noticed the compound had a much longer triplet lifetime than either the model heterodimer PT or polypentacene. Based on this I synthesized PTP, and noticed a similar triplet lifetime to PolyPT, and we have been refining the story ever since. We talk at great length about the energy sink (cleft) motif, whereby triplets will move to occupy lower energy triplet states (pentacene vs tetracene) if possible, which can lead to spatial separation and therefore extended triplet lifetimes. However we do not talk about bridge resonance, a term that Sam and I coined to describe a separate phenomenon. The rate of iSF in dimers slows down as the pentacenes are spaced, but the rate also speeds up if the frontier

orbitals of the bridge are close in energy of the SF chromophores. We believe this is the reason why an anthracene spaced pentacene dimer (PAP) actually undergoes iSF faster than a naphthalene spaced dimer (PNP). As expected PAP generates longer lived triplets than PNP, but this decoupling of SF rate from triplet lifetime via bridge resonance is a powerful design rule that can be exploited in conjunction with the energy sink motif.

As I spoke about in the outlook of Chapter 2, we also tried to make photovoltaic devices using some materials that have an energy sink to increase free triplet yield. However none of these devices operated via triplet charge carrier extraction. While these design rules allow us to synthesize materials with idealized rates of iSF and triplet lifetimes, further design still needs to go into the materials to ensure they can be interfaced into high performance optoelectronics.

4.17 References

(1) Huber, R. C.; Ferreira, A. S.; Thompson, R.; Kilbride, D.; Knutson, N. S.; Devi, L. S.; Toso, D. B.; Challa, J. R.; Zhou, Z. H.; Rubin, Y.; et al. Long-Lived Photoinduced Polaron Formation in Conjugated Polyelectrolyte-Fullerene Assemblies. *Science* **2015**, *348* (6241), 1340–1343.

(2) Scholes, G. D.; Rumbles, G. Excitons in Nanoscale Systems. *Nat. Mater.* **2006**, *5* (9), 683–696.

(3) Albinsson, B.; Mårtensson, J. Long-Range Electron and Excitation Energy Transfer in Donor–Bridge–Acceptor Systems. *J. Photochem. Photobiol. C Photochem. Rev.* **2008**, *9* (3), 138–155.

(4) Hanna, M. C.; Nozik, A. J. Solar Conversion Efficiency of Photovoltaic and Photoelectrolysis Cells with Carrier Multiplication Absorbers. *J. Appl. Phys.* **2006**, *100* (7).

(5) Tayebjee, M. J. Y.; McCamey, D. R.; Schmidt, T. W. Beyond Shockley–Queisser: Molecular Approaches to High-Efficiency Photovoltaics. *J. Phys. Chem. Lett.* **2015**, *6* (12), 2367–2378.

(6) Semonin, O. E.; Luther, J. M.; Beard, M. C. Quantum Dots for Next-Generation Photovoltaics. *Mater. Today* **2012**, *15* (11), 508–515.

(7) Klimov, V. I.; Mikhailovsky, A. A.; McBranch, D. W.; Leatherdale, C. A.; Bawendi, M. G. Quantization of Multiparticle Auger Rates in Semiconductor Quantum Dots. *Science* **2000**, *287* (5455), 1011 LP – 1013.

(8) Padilha, L. A.; Stewart, J. T.; Sandberg, R. L.; Bae, W. K.; Koh, W.-K.; Pietryga, J. M.; Klimov, V. I. Carrier Multiplication in Semiconductor Nanocrystals: Influence of Size, Shape, and Composition. *Acc. Chem. Res.* **2013**, *46* (6), 1261–1269.

(9) Lukman, S.; Richter, J. M.; Yang, L.; Hu, P.; Wu, J.; Greenham, N. C.; Musser, A. J.

Efficient Singlet Fission and Triplet-Pair Emission in a Family of Zethrene Diradicaloids. *J. Am. Chem. Soc.* **2017**, *139* (50), 18376–18385.
(10) Pensack, R. D.; Ostroumov, E. E.; Tilley, A. J.; Mazza, S.; Grieco, C.; Thorley, K. J.; Asbury, J. B.; Seferos, D. S.; Anthony, J. E.; Scholes, G. D. Observation of Two Triplet-Pair Intermediates in Singlet Exciton Fission. *J. Phys. Chem. Lett.* **2016**, *7* (13), 2370–2375.
(11) Weiss, L. R.; Bayliss, S. L.; Kraffert, F.; Thorley, K. J.; Anthony, J. E.; Bittl, R.; Friend, R. H.; Rao, A.; Greenham, N. C.; Behrends, J. Strongly Exchange-Coupled Triplet Pairs in an Organic Semiconductor. *Nat. Phys.* **2016**, *13*, 176.
(12) Stern, H. L.; Cheminal, A.; Yost, S. R.; Broch, K.; Bayliss, S. L.; Chen, K.; Tabachnyk, M.; Thorley, K.; Greenham, N.; Hodgkiss, J. M.; et al. Vibronically Coherent Ultrafast Triplet-Pair Formation and Subsequent Thermally Activated Dissociation Control Efficient Endothermic Singlet Fission. *Nat. Chem.* **2017**, *9*, 1205.
(13) Folie, B. D.; Haber, J. B.; Refaely-Abramson, S.; Neaton, J. B.; Ginsberg, N. S. Long-Lived Correlated Triplet Pairs in a π-Stacked Crystalline Pentacene Derivative. *J. Am. Chem. Soc.* **2018**, *140* (6), 2326–2335.
(14) Yong, C. K.; Musser, A. J.; Bayliss, S. L.; Lukman, S.; Tamura, H.; Bubnova, O.; Hallani, R. K.; Meneau, A.; Resel, R.; Maruyama, M.; et al. The Entangled Triplet Pair State in Acene and Heteroacene Materials. *Nat. Commun.* **2017**, *8*, 15953.
(15) Tayebjee, M. J. Y.; Sanders, S. N.; Kumarasamy, E.; Campos, L. M.; Sfeir, M. Y.; McCamey, D. R. Quintet Multiexciton Dynamics in Singlet Fission. *Nat. Phys.* **2017**, *13* (2), 182–188.
(16) Stern, H. L.; Musser, A. J.; Gelinas, S.; Parkinson, P.; Herz, L. M.; Bruzek, M. J.; Anthony, J.; Friend, R. H.; Walker, B. J. Identification of a Triplet Pair Intermediate in Singlet Exciton Fission in Solution. *Proc. Natl. Acad. Sci.* **2015**, *112* (25), 7656–7661.
(17) Basel, B. S.; Zirzlmeier, J.; Hetzer, C.; Phelan, B. T.; Krzyaniak, M. D.; Reddy, S. R.; Coto, P. B.; Horwitz, N. E.; Young, R. M.; White, F. J.; et al. Unified Model for Singlet Fission within a Non-Conjugated Covalent Pentacene Dimer. *Nat. Commun.* **2017**, *8*, 15171.
(18) Kumarasamy, E.; Sanders, S. N.; Pun, A. B.; Vaselabadi, S. A.; Low, J. Z.; Sfeir, M. Y.; Steigerwald, M. L.; Stein, G. E.; Campos, L. M. Properties of Poly- and Oligopentacenes Synthesized from Modular Building Blocks. *Macromolecules* **2016**, *49* (4), 1279–1285.
(19) Xia, J.; Sanders, S. N.; Cheng, W.; Low, J. Z.; Liu, J.; Campos, L. M.; Sun, T. Singlet Fission: Progress and Prospects in Solar Cells. *Adv. Mater.* **2017**, *29* (20), 1601652.
(20) Low, J. Z.; Sanders, S. N.; Campos, L. M. Correlating Structure and Function in Organic Electronics: From Single Molecule Transport to Singlet Fission. *Chem. Mater.* **2015**, *27* (16), 5453–5463.
(21) Liu, H.; Wang, R.; Shen, L.; Xu, Y.; Xiao, M.; Zhang, C.; Li, X. A Covalently Linked Tetracene Trimer: Synthesis and Singlet Exciton Fission Property. *Org. Lett.* **2017**, *19* (3), 580–583.
(22) Wang, X.; Wang, R.; Shen, L.; Tang, Z.; Wen, C.; Dong, B.; Liu, H.; Zhang, C.; Li, X. Intramolecular Singlet Fission in a Face-to-Face Stacked Tetracene Trimer. *Phys. Chem. Chem. Phys.* **2018**, *20* (9), 6330–6336.
(23) Hetzer, C.; Guldi, D. M.; Tykwinski, R. R. Pentacene Dimers as a Critical Tool for the Investigation of Intramolecular Singlet Fission. *Chem. - A Eur. J.* **2018**, *24* (33), 8245–8257.

(24) Kumarasamy, E.; Sanders, S. N.; Tayebjee, M. J. Y.; Asadpoordarvish, A.; Hele, T. J. H.; Fuemmeler, E. G.; Pun, A. B.; Yablon, L. M.; Low, J. Z.; Paley, D. W.; et al. Tuning Singlet Fission in π-Bridge-π Chromophores. *J. Am. Chem. Soc.* **2017**, *139* (36), 12488–12494.
(25) Pun, A. B.; Sanders, S. N.; Kumarasamy, E.; Sfeir, M. Y.; Congreve, D. N.; Campos, L. M. Triplet Harvesting from Intramolecular Singlet Fission in Polytetracene. *Adv. Mater.* **2017**, *29* (41), 1701416.
(26) Lukman, S.; Musser, A. J.; Chen, K.; Athanasopoulos, S.; Yong, C. K.; Zeng, Z.; Ye, Q.; Chi, C.; Hodgkiss, J. M.; Wu, J.; et al. Tuneable Singlet Exciton Fission and Triplet–Triplet Annihilation in an Orthogonal Pentacene Dimer. *Adv. Funct. Mater.* **2015**, *25* (34), 5452–5461.
(27) Korovina, N. V; Das, S.; Nett, Z.; Feng, X.; Joy, J.; Haiges, R.; Krylov, A. I.; Bradforth, S. E.; Thompson, M. E. Singlet Fission in a Covalently Linked Cofacial Alkynyltetracene Dimer. *J. Am. Chem. Soc.* **2016**, *138* (2), 617–627.
(28) Zirzlmeier, J.; Lehnherr, D.; Coto, P. B.; Chernick, E. T.; Casillas, R.; Basel, B. S.; Thoss, M.; Tykwinski, R. R.; Guldi, D. M. Singlet Fission in Pentacene Dimers. *Proc. Natl. Acad. Sci.* **2015**, *112* (17), 5325–5330.
(29) Sanders, S. N.; Kumarasamy, E.; Pun, A. B.; Steigerwald, M. L.; Sfeir, M. Y.; Campos, L. M. Singlet Fission in Polypentacene. *Chem* **2017**, *1* (3), 505–511.
(30) Fuemmeler, E. G.; Sanders, S. N.; Pun, A. B.; Kumarasamy, E.; Zeng, T.; Miyata, K.; Steigerwald, M. L.; Zhu, X.-Y.; Sfeir, M. Y.; Campos, L. M.; et al. A Direct Mechanism of Ultrafast Intramolecular Singlet Fission in Pentacene Dimers. *ACS Cent. Sci.* **2016**, *2* (5), 316–324.
(31) Lukman, S.; Chen, K.; Hodgkiss, J. M.; Turban, D. H. P.; Hine, N. D. M.; Dong, S.; Wu, J.; Greenham, N. C.; Musser, A. J. Tuning the Role of Charge-Transfer States in Intramolecular Singlet Exciton Fission through Side-Group Engineering. *Nat. Commun.* **2016**, *7*, 13622.
(32) Sanders, S. N.; Kumarasamy, E.; Pun, A. B.; Trinh, M. T.; Choi, B.; Xia, J.; Taffet, E. J.; Low, J. Z.; Miller, J. R.; Roy, X.; et al. Quantitative Intramolecular Singlet Fission in Bipentacenes. *J. Am. Chem. Soc.* **2015**, *137* (28), 8965–8972.
(33) Trinh, M. T.; Pinkard, A.; Pun, A. B.; Sanders, S. N.; Kumarasamy, E.; Sfeir, M. Y.; Campos, L. M.; Roy, X.; Zhu, X.-Y. Distinct Properties of the Triplet Pair State from Singlet Fission. *Sci. Adv.* **2017**, *3* (7), e1700241.
(34) Buchanan, E. A.; Havlas, Z.; Michl, J. Chapter Seven - Singlet Fission: Optimization of Chromophore Dimer Geometry. In *Advances in Quantum Chemistry: Ratner Volume*; Sabin, J. R., Brändas, E. J. B. T.-A. in Q. C., Eds.; Academic Press, 2017; Vol. 75, pp 175–227.
(35) Kim, H.; Zimmerman, P. M. Coupled Double Triplet State in Singlet Fission. *Phys. Chem. Chem. Phys.* **2018**, *20* (48), 30083–30094.
(36) Basel, B. S.; Zirzlmeier, J.; Hetzer, C.; Reddy, S. R.; Phelan, B. T.; Krzyaniak, M. D.; Volland, M. K.; Coto, P. B.; Young, R. M.; Clark, T.; et al. Evidence for Charge-Transfer Mediation in the Primary Events of Singlet Fission in a Weakly Coupled Pentacene Dimer. *Chem* **2018**, *4* (5), 1092–1111.
(37) Zirzlmeier, J.; Casillas, R.; Reddy, S. R.; Coto, P. B.; Lehnherr, D.; Chernick, E. T.; Papadopoulos, I.; Thoss, M.; Tykwinski, R. R.; Guldi, D. M. Solution-Based Intramolecular Singlet Fission in Cross-Conjugated Pentacene Dimers. *Nanoscale* **2016**, *8*

(19), 10113–10123.
(38) Sanders, S. N.; Kumarasamy, E.; Pun, A. B.; Steigerwald, M. L.; Sfeir, M. Y.; Campos, L. M. Intramolecular Singlet Fission in Oligoacene Heterodimers. *Angew. Chem. Int. Ed.* **2016**, *55* (10), 3373–3377.
(39) Sanders, S. N.; Kumarasamy, E.; Pun, A. B.; Appavoo, K.; Steigerwald, M. L.; Campos, L. M.; Sfeir, M. Y. Exciton Correlations in Intramolecular Singlet Fission. *J. Am. Chem. Soc.* **2016**, *138* (23), 7289–7297.
(40) Khan, S.; Mazumdar, S. Optical Probes of the Quantum-Entangled Triplet-Triplet State in a Heteroacene Dimer. *Phys. Rev. B* **2018**, *98* (16), 165202.
(41) Khan, S.; Mazumdar, S. Theory of Transient Excited State Absorptions in Pentacene and Derivatives: Triplet–Triplet Biexciton versus Free Triplets. *J. Phys. Chem. Lett.* **2017**, *8* (23), 5943–5948.
(42) Bayliss, S. L.; Chepelianskii, A. D.; Sepe, A.; Walker, B. J.; Ehrler, B.; Bruzek, M. J.; Anthony, J. E.; Greenham, N. C. Geminate and Nongeminate Recombination of Triplet Excitons Formed by Singlet Fission. *Phys. Rev. Lett.* **2014**, *112* (23), 238701.
(43) Smith, M. B.; Michl, J. Singlet Fission. *Chem. Rev.* **2010**, *110* (11), 6891–6936.
(44) Merrifield R E. Magnetic Effects on Triplet Exciton Interactions . *Pure and Applied Chemistry* . 1971, p 481.
(45) Burdett, J. J.; Bardeen, C. J. Quantum Beats in Crystalline Tetracene Delayed Fluorescence Due to Triplet Pair Coherences Produced by Direct Singlet Fission. *J. Am. Chem. Soc.* **2012**, *134* (20), 8597–8607.
(46) Sakuma, T.; Sakai, H.; Araki, Y.; Mori, T.; Wada, T.; Tkachenko, N. V; Hasobe, T. Long-Lived Triplet Excited States of Bent-Shaped Pentacene Dimers by Intramolecular Singlet Fission. *J. Phys. Chem. A* **2016**, *120* (11), 1867–1875.
(47) Kuroda, K.; Yazaki, K.; Tanaka, Y.; Akita, M.; Sakai, H.; Hasobe, T.; Tkachenko, N. V; Yoshizawa, M. A Pentacene-Based Nanotube Displaying Enriched Electrochemical and Photochemical Activities. *Angew. Chem. Int. Ed.* **2019**, *58* (4), 1115–1119.
(48) Snellenburg, J. J.; Laptenok, S.; Seger, R.; Mullen, K. M.; van Stokkum, I. H. M. Glotaran: A Java-Based Graphical User Interface for the R Package TIMP. *J. Stat. Software; Vol 1, Issue 3* **2012**.
(49) Kazim, S.; Ramos, F. J.; Gao, P.; Nazeeruddin, M. K.; Grätzel, M.; Ahmad, S. A Dopant Free Linear Acene Derivative as a Hole Transport Material for Perovskite Pigmented Solar Cells. *Energy Environ. Sci.* **2015**, *8* (6), 1816–1823.

Chapter 5: Upconversion in Tetracene Dimers

5.1 Preface

This chapter is based on manuscript entitled "Annihilator Dimers Enhance Triplet Fusion Upconversion" by Andrew B. Pun, Samuel N. Sanders, Matthew Y. Sfeir, Luis M. Campos, and Daniel N. Congreve published in Chemical Science.[1]

I synthesized and characterized all the materials studied. I characterized the upconversion properties of these materials with help from Daniel N. Congreve. Daniel Congreve developed the kinetic model. Samuel N. Sanders and Matthew Y. Sfeir measured the triplet lifetimes of the materials studied.

5.2 Introduction

The ability to design and synthesize materials that convert infrared light into visible light is remarkably important due to widespread potential applications, including solar energy capture,[2] photocatalysis,[3] data storage,[4] night vision,[5] and biological imaging.[6] In this vein, the process by which low energy photons are converted to a single high energy photon is known as optical upconversion.[7,8] In recent years this process has received a surge of interest for its potential in solar energy applications.[9] As a result, much work has been done to optimize upconversion in highly ordered and condensed systems, where there are large numbers of annihilators in very close proximity, thus leading to high upconversion efficiencies.[10] Considering that upconversion can also greatly benefit other areas, such as imaging[11] and photochemistry,[3,12] where lower concentrations are required, a major challenge remains to find efficient upconverting materials that are robust with respect to concentration level. Thus, it is imperative to investigate how structural modifications to annihilators can be exploited to tune the process of upconversion.

One promising approach to exhibit efficient upconversion is using mixed conjugated organic systems operating via triplet fusion (TF) upconversion, also known as triplet–triplet annihilation upconversion (Figure 5.1A).[13,14] In such systems, an organometallic sensitizer absorbs long wavelength light, exciting the sensitizer to a singlet state, which then rapidly undergoes intersystem crossing to a long lived triplet state, shown in Figure 5.1B. This triplet can then be transferred from the sensitizer to an organic annihilator via collisional triplet energy transfer (TET), provided the triplet energy level of the annihilator is lower than that of the sensitizer. Two annihilators in their excited triplet states (T_1) can then come together and undergo intermolecular triplet fusion (xTF), populating the excited singlet (S_1) state of one of the annihilators. This S1 then decays to the ground state singlet (S_0) via fluorescence, giving off a photon of higher energy than the incident light. In order for the xTF process to occur, it must conserve energy, such that the energy of the singlet state is less than twice the energy of the triplet state, i.e. $E(S_1) < 2 \times E(T_1)$. A schematic of the xTF process can be seen in Figure 5.1C.

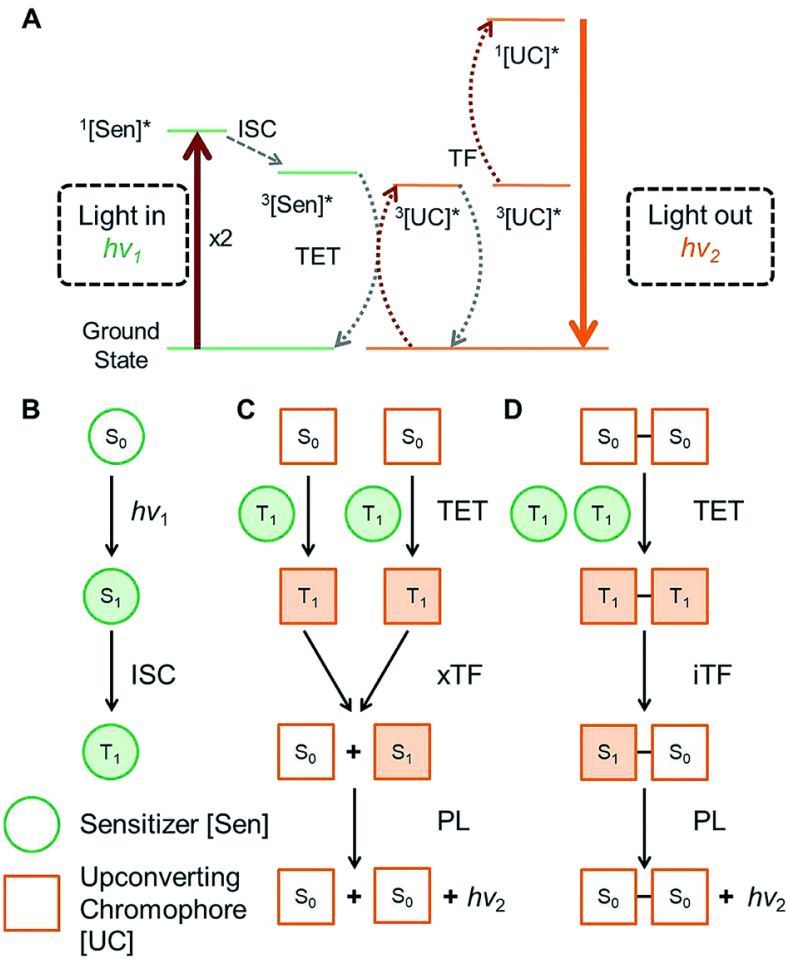

Figure 5.1 Triplet Fusion Upconversion Diagrams A) Qualitative energy level diagram of the full triplet fusion upconversion mechanism. *Denotes first excited state ([Sen] = sensitizer, [UC] = upconverting chromophore) B) mechanism by which triplet states are populated in a molecular sensitizer by photoexcitation ($h\nu_1$), followed by intersystem crossing (ISC). C) Mechanism of conventional intermolecular triplet fusion upconversion (xTF) giving off a high energy photon ($h\nu_2$). (D) Proposed mechanism for intramolecular triplet fusion upconversion (iTF). Unfilled and filled shapes represent ground state and excited state molecules, respectively. S and T denote singlet and triplet states respectively.

In order for TF to be a technically viable process, it is necessary to absorb low energy photons (such as IR and near infrared, NIR) that are inaccessible to many optoelectronic materials. Thus, a major focus in the field of TF upconversion has been on finding sensitizers which can absorb sufficiently low energy. Great strides have been made in recent years to this end, including the use of lead and cadmium chalcogenide nanocrystals as sensitizers to complement existing molecular annihilators.[15–18] While much focus has been given to improving

the sensitizer, comparatively little work has been done on the annihilator.[19,20] Novel and exciting methods focusing on the structure of the materials to assemble the annihilators have been explored by the Simon and Kimizuka groups.[21–23] But to date, there has been very little work to modify the annihilator itself to intrinsically enhance upconversion, especially operating at low concentrations in solution. Thus far, most work in the field of optical upconversion has employed common acene derivatives, such as diphenyl anthracene and rubrene, or perylene as the organic upconverter.[24–26] In this work, we investigate how covalently coupling two upconverting chromophores to form an annihilator dimer affects the efficiency of upconversion. In contrast to previously studied polymeric systems, which focus on large assemblies,[27–29] we sought to investigate interactions between two individual chromophores. Thus, we synthesized a series of tetracene dimers linked by 0, 1, 2, and 4 p-phenylene spacers (BTn; n = 0, 1, 2, 4), which were designed to undergo intramolecular triplet fusion upconversion (iTF, Figure 5.1D), in addition to the typical xTF caused by collisions between chromophores.

5.3 Optical Characterization Experimental

Solutions of BT0,1,2,4 or TIPS–tetracene (TIPS–Tc) with $PdPc(OBu)_8$ were prepared from anhydrous toluene in a nitrogen glovebox. Solutions were made in 1 cm x 1 cm cuvettes from Spectrocell and were degassed by sparging with nitrogen for 30 seconds then sealed before removing from glovebox for measurement. Solutions were excited with a 730 nm laser diode purchased from Thorlabs, focused to a beam diameter of 0.15 mm. Unless otherwise noted, the excitation density in all experiments was 113 W cm^{-2}. All upconverted PL spectra were measured with a QEPro spectrometer purchased from Ocean Optics through a 700 nm shortpass filter. Power intensity dependence measurements were taken by varying the beam intensity using neutral density filters.

5.4 PLQY Experimental

PLQY measurements were made using an integrating sphere purchased from Labsphere following de Mello et al.[30] 29 Briefly, the 10 mm cuvette was placed inside the sphere and excited with either 730 nm or 445 nm light focused from a laser diode. The upconversion quantum yield was determined by comparing the quantum yields when excited at 730 nm and 445 nm, with the upconversion yield defined such that it is the number of excitations leading to a singlet exciton on the annihilator. The cited yields are for annihilator concentrations of 5×10^{-4} M. The sphere and all optical equipment were calibrated against a calibrated silicon photodetector from Newport Corp.

5.5 Results and Discussion

Our approach in designing annihilators for upconversion is rooted in our fundamental understanding of how the platform of acene dimers operates in intramolecular singlet fission (iSF) – the reverse process of iTF.[31] In all reported acene dimers, the spatial proximity of the generated triplet pairs leads to extremely rapid recombination.[32] Even in the case of acene chromophores spaced by up to two p-phenylene spacers, the lifetime of a pair of triplets on one acene dimer is no more than 270 ns,[31,33] ensuring us that iTF can occur with a relatively long bridge between the chromophores. However, it should be noted that when the energetic criteria for iSF is not met, the dimeric system is ideal to undergo iTF, because of the aforementioned rapid triplet recombination. Considering that the energy of the singlet state in tetracene is roughly less than twice the energy of the triplet state – an observation that is not favorable for iSF but good for iTF – we investigate the upconversion process in a series of tetracene dimers shown in Figure 5.2A. The tetracene dimer BT0 does not contain a bridge, but BT1 and BT2

contain a phenylene and biphenylene bridge, respectively. These bridges effectively separate the triplets after sensitization, but maintain electronic communication between them. We also synthesized a tetracene dimer with a quaterphenylene bridge, BT4, to observe the effects of dimerization in a system where the two tetracene chromophores are too distant to be in good electronic communication. BT4 was chosen as it is the longest *p*-phenylene spaced dimer we could readily synthesize. These compounds were chosen due to the presence of the triisopropylsilylacetylene (TIPS) groups which impart stability and solubility, as well as facilitating iterative synthesis.[34] These compounds were compared to a monomeric TIPS–Tc annihilator. $PdPc(OBu)_8$ was chosen as the sensitizer, as it has been previously shown that this compound can efficiently donate triplets to tetracene derivatives upon absorption of near IR light.[35]

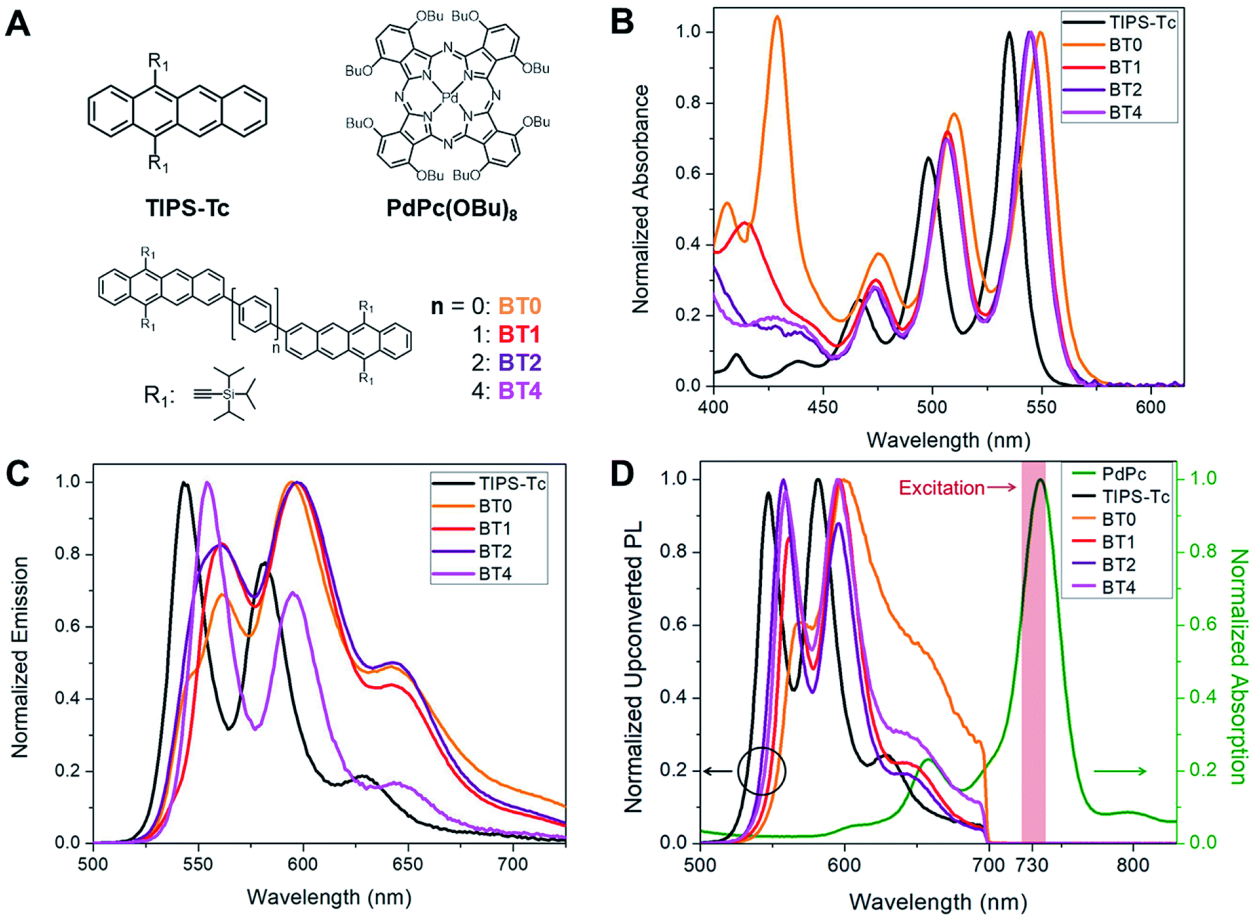

Figure 5.2 Optical Properties of BTn and TIPS-Tc A) Structures of the compounds used in this work. B) Normalized steady state absorbance spectra of the annihilators used. C) Normalized photoluminescence spectra of the annihilators used, excited at 490 nm. D) Normalized upconverted photoluminescence spectra at 5×10^{-4} M annihilator and 2.5×10^{-5} M $PdPc(OBu)_8$ (700 nm short pass filter used). Normalized steady state absorbance of $PdPc(OBu)_8$ shown in green. The shaded red region represents excitation wavelength from 730 nm diode.

The absorption and emission spectra of the annihilators used in this work can be seen in Figure 5.2B and C, respectively. The absorption of the tetracene dimers exhibits a modest redshift in the onset of absorption relative to TIPS–Tc. This is characteristic of the extension of a π system typically seen in conjugated organic molecules. The emission spectra of the upconverting chromophores are similar to one another, with TIPS–Tc and BT4 exhibiting a more pronounced peak at 550 nm relative to the peak at 600 nm, and vice versa for BT0–BT2. The normalized absorption spectra of $PdPc(OBu)_8$ can be seen in green in Figure 5.2D, exhibiting strong absorption in the near IR. Upon excitation with a 730 nm laser diode (shaded red Figure 5.2D), optical upconversion was observed for TIPS–Tc as well as all four tetracene dimers. The normalized upconversion photoluminescence (UCPL) of these compounds can be seen in Figure 5.2D.

To confirm that iTF was possible, we performed DFT calculations of the T_1 states of BT0, BT1, BT2, and BT4.[36] Figure 5.3 shows the T_1 orbitals of BT0, BT1, BT2, and BT4. In the case of closely linked dimers such as BT0, BT1, and BT2, the T_1 state is generally localized on one of the tetracene chromophores, but spills onto the second chromophore. This mixing of triplet states across multiple chromophores facilitates iTF. In the case of BT4, the two tetracene chromophores are too far apart to allow the T_1 state to be shared. As a result, BT4 should not be able to undergo iTF, and instead we would expect it to behave similarly to TIPS–Tc as an upconversion annihilator.

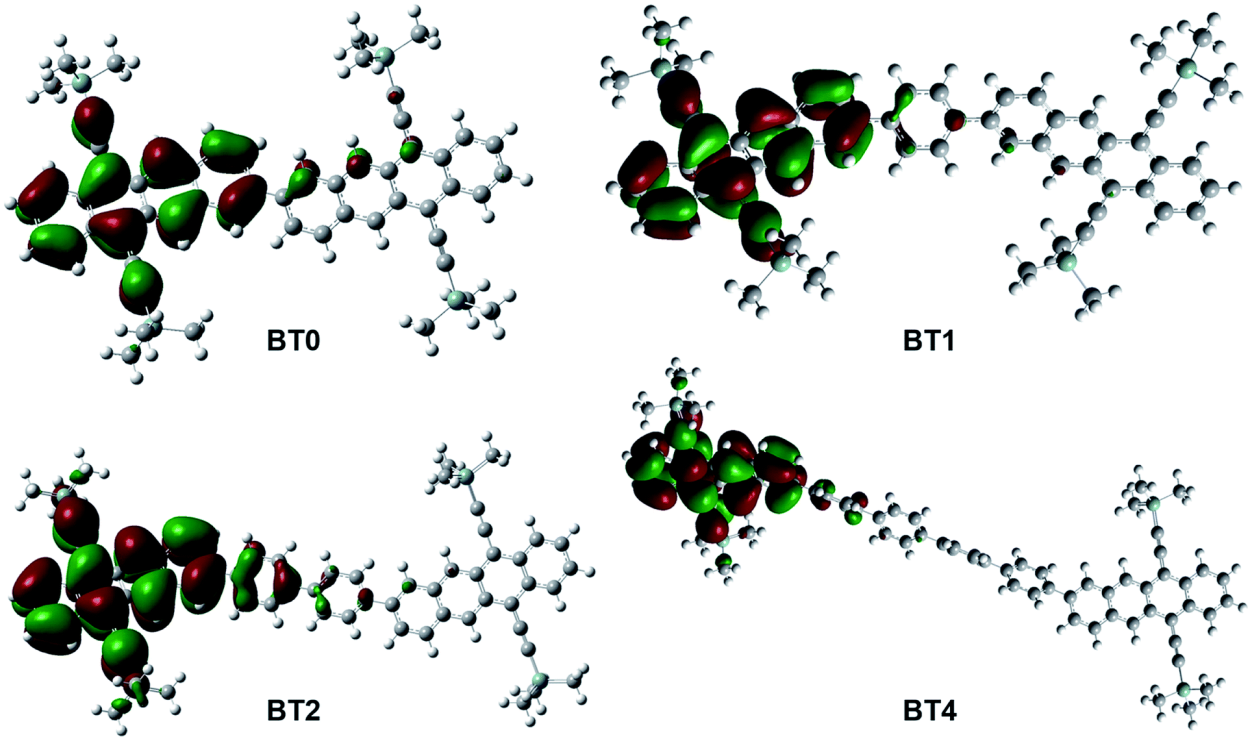

Figure 5.3 T_1 Orbitals of Tetracene Dimers generated via DFT calculations

After establishing the presence of upconversion when using tetracene dimers as annihilators, we explored the dependence of upconversion photoluminescence intensity on the concentration of these materials. We began with a sensitizer concentration of 2.5 x 10^{-5} M, and an annihilator concentration of 5 x 10^{-4} M, these being typical of solution state measurements of upconversion.[20,35] We then lowered the concentration of the annihilator down to 3.75 x 10^{-5} M while holding the amount of sensitizer constant in order to study the effects of iTF on concentration. The dependence of upconversion PL as a function of concentration of the annihilator can be seen in Figure 5.4A. BT4 decays nearly identically to the monomeric TIPS–Tc, as we would expect in a system where the two tetracene chromophores are electronically independent of one another and lack the iTF upconversion pathway. BT0 exhibits the lowest upconversion PL across all concentrations, which is likely due to its low photoluminescence quantum yield (PLQY) as a result of singlet fission, a competing pathway for singlet decay.[37,38]

In stark contrast, BT1 and BT2 both exhibit higher upconversion PL compared to TIPS–Tc, across all concentrations. This is even in spite of the significantly lower PLQYs of BT1 and BT2, a result of the fact that these compounds undergo singlet fission as well. In fact, the overall upconversion yield (defined as the percentage of absorbed photons that become a singlet on the annihilator) is significantly higher in BT1 than in TIPS–Tc, at 4.2% vs. 0.70%, respectively. This upconversion yield is equivalent to that of a previously reported tetracene dimer[20] but we note that we are using a phosphor that absorbs lower energy light and lower concentrations of sensitizer. Calculations show that the T_1 energies of the annihilators studied in this work vary by only 7 meV (Table 5.1), ruling out changes in T_1 energy as the source of our enhanced upconversion performance in these materials. Indeed, the robustness of the BT1 upconverting chromophore to these non-ideal conditions proves its usefulness in a wide variety of demanding upconversion applications where lower concentrations are required.

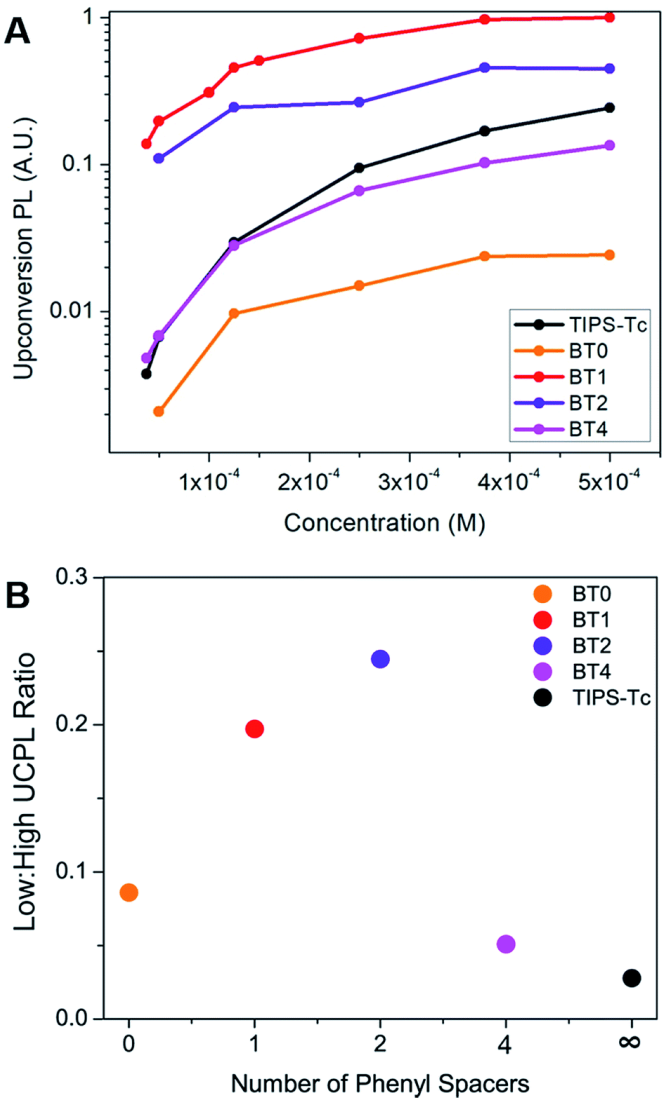

Figure 5.4 Upconversion Dependence on Annihilator Concentration A) Change in upconversion PL of compounds studied as a function of annihilator concentration at 2.5 x 10−5 M $PdPc(OBu)_8$. B) UCPL at 5 x 10^{-4} M divided by UCPL at 5 x 10−5 M annihilator concentration plotted as a function of the number of phenyl spacers in the annihilator used.

We then performed Stern–Volmer quenching experiments on our system to measure the rate of triplet energy transfer (k_{TET}) from sensitizer to annihilator. This was done to rule out an increase in k_{TET} as the source of enhanced UCPL in our tetracene dimers (Figure 5.14, Table 5.2). These measurements showed a slight enhancement in k_{TET} of the dimers relative to TIPS–Tc. The change in k_{TET} is small relative to the overall enhancement in UCPL for these materials, but in order to provide further evidence of iTF, we constructed a kinetic model of our system.

The details of this model can be found in Figure 5.16. Using this model, we are able to fit the rate of triplet fusion (k_{TF}) to our experimental data in Figure 5.4A. Using the values of k_{TET} extracted from our Stern–Volmer measurements, we find the only way to fit our data using the model is with an enhanced rate of kTF (Table 5.6). TIPS–Tc has a k_{TF} of 2.3 x 10^6 (M^{-1} s^{-1}), compared to 250 x 10^6 (M^{-1} s^{-1}) for BT1. We believe this enhancement in k_{TF} is additional supporting evidence of iTF, which leads to enhanced UPCL yields of our BT dimers.

In the case of classical xTF, a high concentration of annihilator molecules has been considered crucial for efficient upconversion, despite the fact that this high concentration can lead to fluorescence quenching via aggregation.[8,39,40] At high annihilator concentrations, we expect xTF to dominate (that is, excited annihilator molecules are much more likely to collide with one another than with a sensitizer). This is demonstrated by the fact that TIPS–Tc is competitive with both BT1 and BT2 at higher concentrations. At low concentrations, however, excited annihilators are as likely to collide with sensitizers as they are with another annihilator, and thus the ability to hold two triplets is greatly advantageous, and the dimeric materials dominate, suggesting that iTF is occurring. This is exhibited by the greater than an order of magnitude reduction of UCPL for TIPS–Tc, while BT1 and BT2 only see a modest decrease in UCPL at low concentrations (Figure 5.4A). For this reason, most demonstrations of upconversion in solution do so with an annihilator concentration of ~1 mM, whereas we can see bright upconversion even at annihilator concentrations as low as 3.75 x 10^{-5} M. The benefit of the extra iTF pathway can clearly be seen in its high upconversion PL seen at very low concentrations. This is further demonstrated in Figure 5.4B, where we compare the UCPL of these annihilators and low and high concentration. This opens the door for the use of iTF capable upconversion materials in photochemical or imaging applications, where high concentrations of

extrinsic materials are undesirable. For example, it is known that a high concentration of annihilators will reduce the propagation of the upconverted PL in solution.[41] This is disadvantageous for imaging applications where it is crucial that the upconverted PL be detectable throughout the species. Photochemical reactions where the photocatalyst is excited by upconverted PL[12] would also benefit from a low concentration of annihilator, because a high concentration of these extra species could easily lead to undesirable side reactions.

Because it requires two initial species, upconversion PL has a quadratic dependence on light intensity at low fluence. This dependence on light intensity then exhibits a change from quadratic to linear once TF becomes the dominant recombination mechanism.[42]Figure 5.5 shows the dependence of upconversion PL intensity on incident power density for TIPS–Tc and BT1 (BT0, BT2, and BT4 shown in Figure 5.6, 5.7 and 5.8 respectively). The crossover point of BT1, 4.3 W cm^{-2} is an order of magnitude lower than that of TIPS–Tc at 44.5 W cm^{-2}. This crossover point reduction is a crucial benefit for BT1, as it ensures that upconversion is occurring at maximum efficiency even at low photon flux.

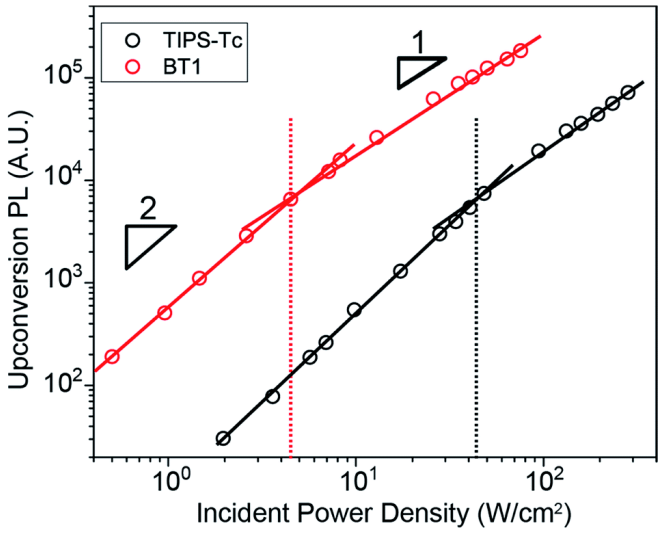

Figure 5.5 BT1 vs TIPS-Tc Turnover Points Dependence of upconverted PL on incident light intensity at 2.5 x 10^{-4} M TIPS–Tc and BT1 concentration. The transition between quadratic and linear dependences occurs at 44.5 and 4.3 W cm^{-2} for TIPS–Tc and BT1 respectively.

5.6 Conclusions

In conclusion, we have synthesized a new series of tetracene dimers that suggest that intramolecular triplet fusion is occurring in these materials. Dimerization is an attractive strategy towards enhanced upconversion because it offers intrinsic benefits to upconversion, rather than relying on complex processing or assembly techniques. This should ease the transition of these materials into non-ideal media where they could be widely applicable, such as in biological systems or photochemical reactions, where a greater number of exogenous species can reduce the efficiency of xTF. As compared to monomeric TIPS–Tc, a tetracene dimer exhibits greater upconversion yield, less sensitivity to concentration, and reduced power thresholds. These improvements pave the way towards upconversion as a viable candidate for a host of applications, especially when a high concentration of outside species is either unfavorable or untenable.

5.7 General Methods

All commercially obtained reagents/solvents were used as received; chemicals were purchased from Alfa Aesar®, Sigma-Aldrich®, Acros organics®, TCI America®, Mallinckrodt®, and Oakwood® Products, and were used as received without further purification. Unless stated otherwise, reactions were conducted in oven-dried glassware under argon atmosphere. Bromo-TIPS-Tetracene was synthesized according to literature procedure.[32] ^{1}H-NMR and ^{13}C-NMR spectra were recorded on a Bruker 400 MHz (100 MHz for ^{13}C) NMR and on a 500 MHz (125 MHz for ^{13}C) NMR spectrometer. Data from the ^{1}H-NMR and ^{13}C-NMR spectroscopy are reported as chemical shift (δ ppm) with the corresponding integration values. Standard abbreviations indicating multiplicity were used as follows: s (singlet), b (broad), d (doublet), t (triplet), q (quartet), m (multiplet) and virt (virtual).

The mass spectral data for the compounds were obtained from XEVO G2-XS Waters® equipped with a QTOF detector with multiple inlet and ionization capabilities including electrospray ionization (ESI), atmospheric pressure chemical ionization (APCI), and atmospheric solids analysis probe (ASAP). The base peaks were usually obtained as $[M]^+$ or $[M+H]^+$ ions.

Absorption spectra were obtained on a Shimadzu UV 1800 UV-Vis spectrophotometer. Emission spectra were obtained on a Horiba Fluoromax-4.

Anhydrous solvents were obtained from a Schlenk manifold with purification columns packed with activated alumina and supported copper catalyst (Glass Contour, Irvine, CA).

5.8 Synthesis

Synthesis of TIPS-Bpin-Tetracene

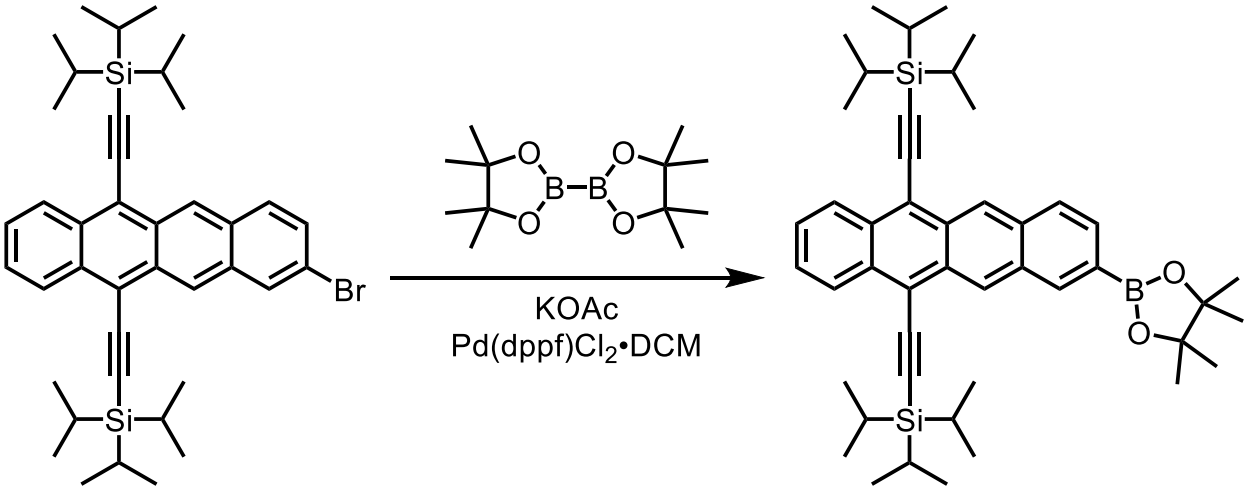

TIPS-Bromo-Tetracene (1.00 g, 1.5 mmol)**,** bis(pinacolato)diboron (571 mg, 2.25 mmol), KOAc (311 mg, 2.25 mmol) and Pd(dppf)Cl_2·DCM (61.3 mg, 0.075 mmol) were added to a reaction vial. Sequential vacuum and argon was used to degas the mixture. The solids were then dissolved in 20 mL degassed dioxane. The reaction was brought to 100 °C and allowed to stir overnight. The reaction was cooled to room temperature. The crude reaction mixture was concentrated and

purified by chromatography on silica gel (25% DCM in Hexanes) to obtain **TIPS-Bpin-Tetracene** as an orange solid. (600 mg, 56% Yield).

^{1}H-NMR (400 MHz, $CDCl_3$, δ ppm): 9.30 (d, J= 22.0 Hz, 2H), 8.70-8.58 (m, 2H), 8.55 (s, 1H), 7.96 (d, J= 8.7 Hz, 1H), 7.82-7.71 (m, 1H), 7.64-7.44 (m, 2H), 1.45-1.39 (m, 12H), 1.37-1.29 (m, 42H).

^{13}C-NMR (125 MHz, $CDCl_3$, δ ppm): 137.77, 133.02, 132.85, 132.76, 131.64, 130.91, 130.30, 129.69, 127.56, 127.47, 127.41, 126.82, 126.66, 126.06, 119.01, 118.56, 106.12, 105.90, 103.91, 103.80, 84.08, 24.97, 19.01, 18.97, 11.61.

MS (ESI): Calculated $[M+H]^+$: 715.4547; Observed: 715.4487

Synthesis of TIPS-Tetracene-Ph-Ph-Br

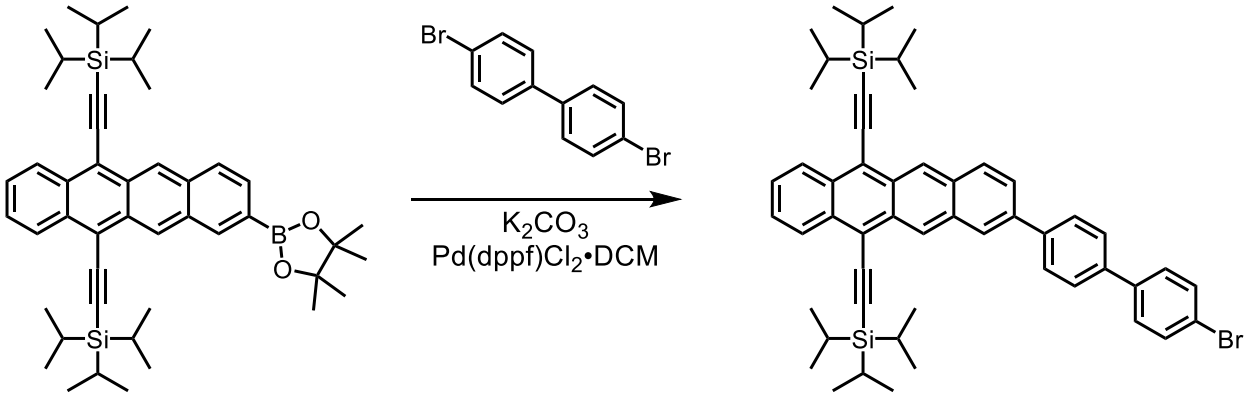

TIPS-Bpin-Tetracene (200 mg, 0.28 mmol)**,** 4,4'-dibromobiphenyl (284 mg, 0.7 mmol), K_2CO_3 (194 mg, 1.4 mmol) and $Pd(dppf)Cl_2 \cdot DCM$ (11.4 mg, 0.014 mmol) were added to a reaction vial. Sequential vacuum and argon was used to degas the mixture. The solids were then dissolved in

12 mL of a 9:1 mixture of THF: degassed water. The reaction was brought to 70 °C and allowed to stir overnight. The reaction was cooled to room temperature. The crude reaction mixture was concentrated and purified by chromatography on silica gel (10% DCM in hexanes) to obtain **TIPS-Tetracene-Ph-Ph-Br** as a red solid. (151 mg, 66% Yield).

^{1}H-NMR (500 MHz, $CDCl_3$, δ ppm): 9.35 (d, J= 14.9 Hz, 2H), 8.82-8.54 (m, 2H), 8.21 (s, 1H), 8.11 (d, J= 8.9 Hz, 1H) 7.88 (d, J= 8.3 Hz, 2H), 7.79 (dd, J= 8.9, 1.7 Hz, 1H), 7.73 (d, J= 8.3 Hz, 2H), 7.61 (d, J= 8.5 Hz, 2H), 7.58-7.48 (m, 4H), 1.41-1.29 (m, 42H).

^{13}C-NMR (125 MHz, $CDCl_3$, δ ppm): 140.19, 139.54, 139.21, 137.64, 132.78, 132.66, 132.29, 132.00, 131.37, 130.72, 130.52, 129.38, 128.63, 127.82, 127.50, 127.42, 126.81, 126.76, 126.65, 126.18, 126.08, 125.83, 121.74, 118.72, 118.54, 106.01, 105.94, 103.92, 103.88, 18.98, 11.62.

MS (ESI): Calculated $[M]^+$: 820.3331; Observed: 820.3345

Synthesis of TIPS-Tetracene-Ph-Ph-Bpin

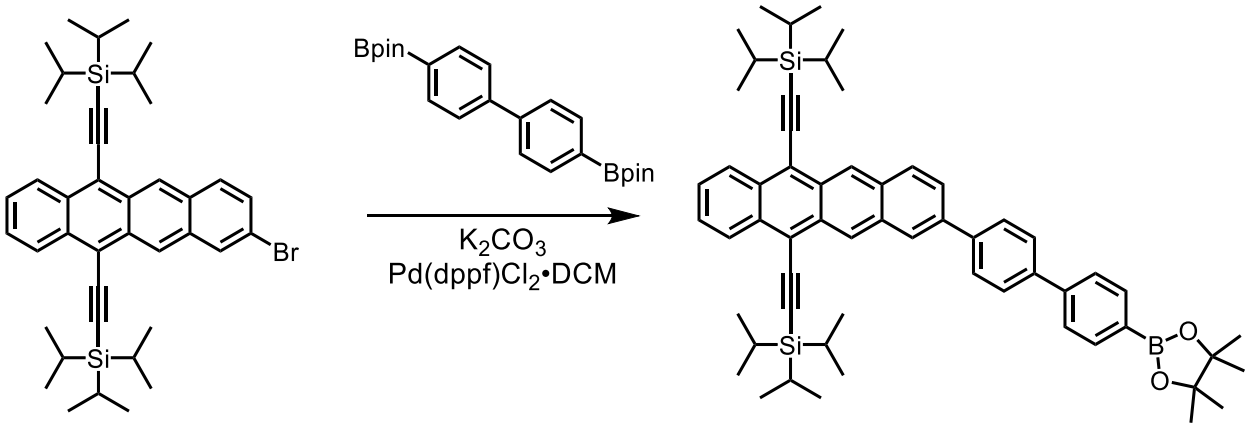

TIPS-Bromo-Tetracene (500 mg, 0.75 mmol)**,** 4,4′-Biphenyldiboronic acid bis(pinacol) ester (762 mg, 1.88 mmol), K_2CO_3 (518 mg, 3.75 mmol) and $Pd(dppf)Cl_2 \cdot DCM$ (30.6 mg, 0.0375 mmol) were added to a reaction vial. Sequential vacuum and argon was used to degas the mixture. The solids were then dissolved in 16 mL of a 9:1 mixture of THF: degassed water. The reaction was brought to 70 °C and allowed to stir overnight. The reaction was cooled to room temperature. The crude reaction mixture was concentrated and purified by chromatography on silica gel (50% DCM in hexanes) to obtain **TIPS-Tetracene-Ph-Ph-Bpin** as a red solid. (260 mg, 40% Yield).

^{1}H-NMR (500 MHz, $CDCl_3$, δ ppm): 9.35 (d, J= 17.4 Hz, 2H), 8.80-8.51 (m, 2H), 8.23 (dd, J= 1.8, 0.9 Hz, 1H), 8.14-8.09 (m, 1H) 7.94 (d, J= 8.1 Hz, 2H), 7.89 (d, J= 8.3 Hz, 2H), 7.81 (d, J= 8.5 Hz, 3H), 7.72 (d, J= 8.1 Hz, 2H), 7.63-7.52 (m, 2H), 1.42-1.38 (m, 12H), 1.37-1.30 (m, 42H).

^{13}C-NMR (125 MHz, $CDCl_3$, δ ppm): 143.40, 140.40, 140.22, 137.93, 135.52, 132.89, 132.78, 132.46, 131.52, 130.85, 130.64, 129.46, 127.93, 127.85, 127.56, 126.91, 126.86, 126.77, 126.50, 126.31, 126.29, 125.93, 118.84, 118.69, 106.14, 106.03, 104.07, 104.04, 84.02, 25.05, 19.12, 11.75.

MS (ESI): Calculated $[M]^+$: 866.5096; Observed: 866.5104

Synthesis of BT0

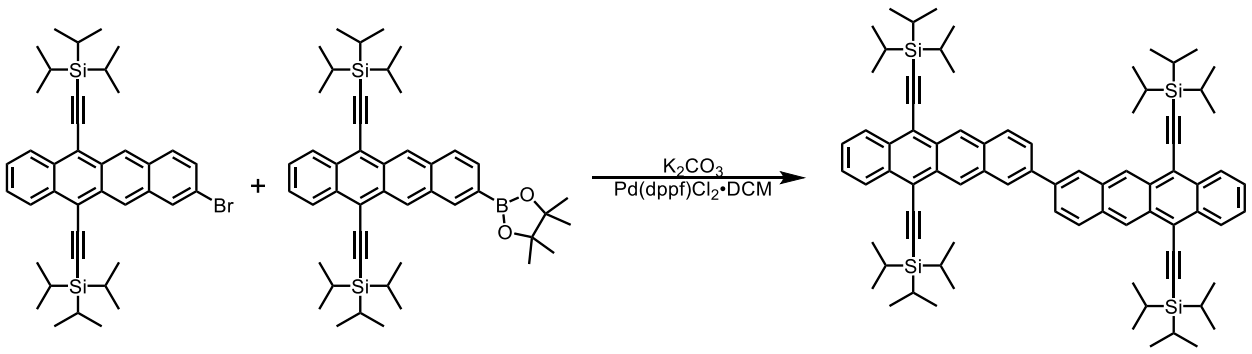

TIPS-Bromo-Tetracene (93.4 mg, 0.14 mmol)**,** TIPS-Bpin-Tetracene (100 mg, 0.14 mmol), K_2CO_3 (194 mg, 1.4 mmol) and $Pd(dppf)Cl_2 \cdot DCM$ (11.4 mg, 0.014 mmol) were added to a reaction vial. Sequential vacuum and argon was used to degas the mixture. The solids were then dissolved in 10 mL of a 9:1 mixture of THF: degassed water. The reaction was brought to 65 °C and allowed to stir overnight. The reaction was cooled to room temperature. The crude reaction mixture was concentrated and purified by chromatography on silica gel (5% chloroform in hexanes) to obtain **BT0** as a red solid. (27 mg, 16% Yield).

^{1}H-NMR (400 MHz, $CDCl_3$, δ ppm): 9.39 (d, J= 23.1 Hz, 4H), 8.65 (dd, J= 8.4, 4.0 Hz, 4H), 8.38 (s, 2H), 8.19 (d, J= 9.1 Hz, 2H), 7.97 (d, J= 9.0 Hz, 2H), 7.60-7.53 (m, 4H), 1.45-1.29 (m, 84H).

^{13}C-NMR (125 MHz, $CDCl_3$, δ ppm): 138.06, 132.97, 132.85, 132.52, 132.47, 131.60, 130.97, 130.95, 130.76, 129.69, 127.59, 126.96, 126.94, 126.37, 126.21, 118.90, 118.76, 106.21, 106.09, 104.10, 104.05, 19.14, 11.77.

MS (ESI): Calculated $[M]^+$: 1175.7085; Observed: 1175.7090.

Synthesis of BT1

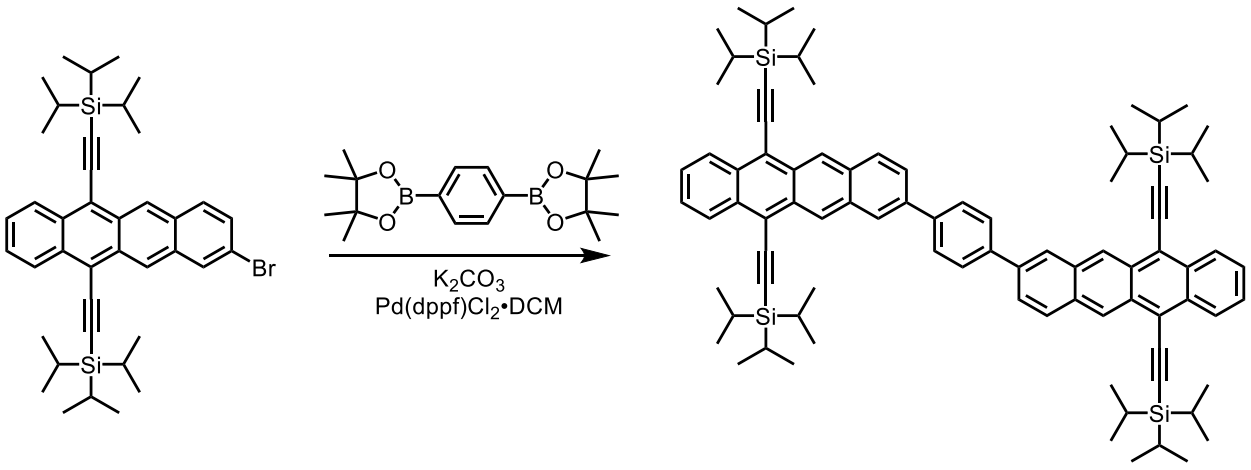

TIPS-Bromo-Tetracene (120 mg, 0.18 mmol)**,** 1,4-Benzenedibronic acid Bis(Pinacol) Ester (25.8 mg, 0.078 mmol), K_2CO_3 (108 mg, 0.78 mmol) and $Pd(dppf)Cl_2$·DCM (6.5 mg, 0.008 mmol) were added to a reaction vial. Sequential vacuum and argon was used to degas the mixture. The solids were then dissolved in 10 mL of a 9:1 mixture of THF: degassed water. The reaction was brought to 65 °C and allowed to stir overnight. The reaction was cooled to room temperature. The crude reaction mixture was concentrated and purified by chromatography on silica gel (10% chloroform in hexanes) to obtain **BT1** as a red solid. (39 mg, 40% Yield).

^{1}H-NMR (400 MHz, $CDCl_3$, δ ppm): 9.37 (d, J= 15.4 Hz, 4H), 8.70-8.60 (m, 4H), 8.28 (s, 2H), 8.15 (m, 2H), 7.99 (s, 4H), 7.86 (dd, J= 8.9, 1.7 Hz, 2H), 7.61-7.51 (m, 4H), 1.43-1.30 (m, 84H).

^{13}C-NMR (125 MHz, $CDCl_3$, δ ppm): 140.29, 137.93, 132.95, 132.82, 132.51, 131.56, 130.89, 130.68, 129.54, 128.10, 128.05, 127.58, 126.94, 126.89, 126.80, 126.34, 125.96, 118.88, 118.71, 106.17, 106.07, 104.10, 104.06, 19.13, 11.78.

MS (ESI): Calculated $[M+H]^+$: 1252.7477; Observed: 1252.7462.

Synthesis of BT2

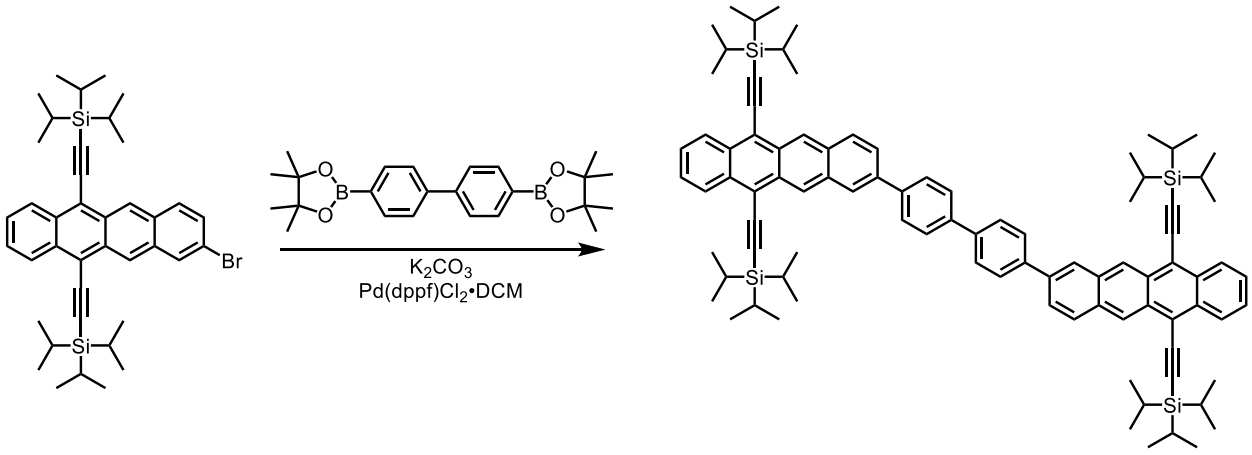

TIPS-Bromo-Tetracene (200 mg, 0.3 mmol)**,** 4,4'-Biphenyldibronic acid Bis(Pinacol) Ester (52.8 mg, 0.13 mmol), K_2CO_3 (180 mg, 1.3 mmol) and $Pd(dppf)Cl_2$·DCM (10.6 mg, 0.013 mmol) were added to a reaction vial. Sequential vacuum and argon was used to degas the mixture. The solids were then dissolved in 10 mL of a 9:1 mixture of THF: degassed water. The reaction was brought to 65 °C and allowed to stir overnight. The reaction was cooled to room temperature. The crude reaction mixture was concentrated and purified by chromatography on silica gel (10% chloroform in hexanes) to obtain **BT2** as a red solid. (78 mg, 45% Yield).

^{1}H-NMR (400 MHz, $CDCl_3$, δ ppm): 9.36 (d, J= 15.0 Hz, 4H), 8.70-8.63 (m, 4H), 8.26 (s, 2H), 8.14 (m, 2H), 8.00-7.82 (m, 10H), 7.62-7.54 (m, 4H), 1.42-1.27 (m, 84H).

^{13}C-NMR (125 MHz, $CDCl_3$, δ ppm): 139.95, 139.85, 137.79, 132.79, 132.66, 132.36, 131.41, 130.74, 130.52, 129.36, 127.80, 127.61, 127.44, 126.80, 126.74, 126.64, 126.18, 125.77, 118.73, 118.56, 106.01, 105.91, 103.96, 103.92, 19.01, 18.99, 11.63.

MS (ESI): Calculated $[M+H]^+$: 1328.7791; Observed: 1328.7792.

Synthesis of BT4

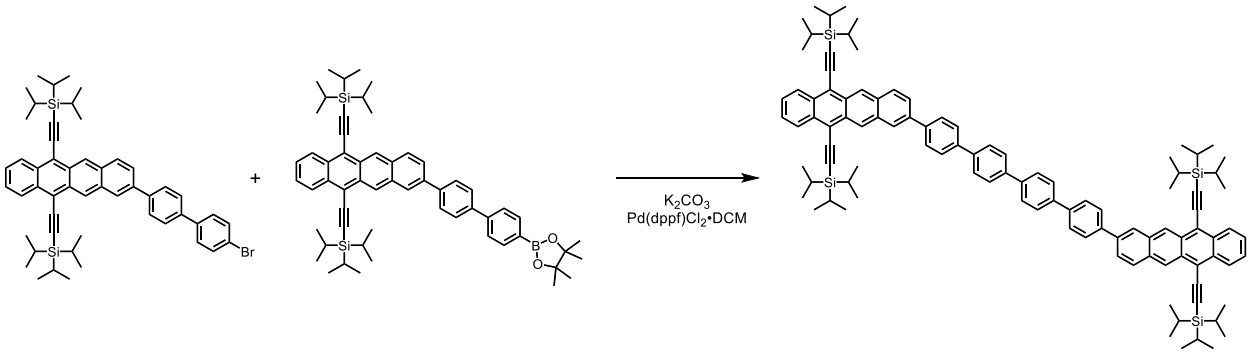

TIPS-Tetracene-Ph-Ph-Bpin (55.5 mg, 0.064 mmol)**,** TIPS-Tetracene-Ph-Ph-Br (50 mg, 0.061 mmol), K_2CO_3 (42.2 mg, 0.3 mmol) and $Pd(dppf)Cl_2$·DCM (2.5 mg, 0.003 mmol) were added to a reaction vial. Sequential vacuum and argon was used to degas the mixture. The solids were then dissolved in 8 mL of a 9:1 mixture of THF: degassed water. The reaction was brought to 70 °C and allowed to stir overnight. The reaction was cooled to room temperature. The crude reaction mixture was concentrated and purified by chromatography on silica gel (20% chloroform in hexanes) to obtain **BT4** as a red solid. (27 mg, 16% Yield).

^{1}H-NMR (500 MHz, $CDCl_3$, δ ppm): 9.36 (d, J= 17.9 Hz, 4H), 8.64 (dt, J=7.3, 2.9Hz 4H), 8.25 (s, 2H), 8.13 (d, J=8.9 Hz 2H), 7.95-7.89 (m, 4H), 7.89-7.74 (m, 14H), 7.59-7.51 (m, 4H), 1.40-1.25 (m, 84H).

Limited solubility prevented the acquisition of a ^{13}C NMR.

MS (ESI): Calculated $[M]^+$: 1479.8339; Observed: 1479.8326

5.9 Power Dependence Measurements

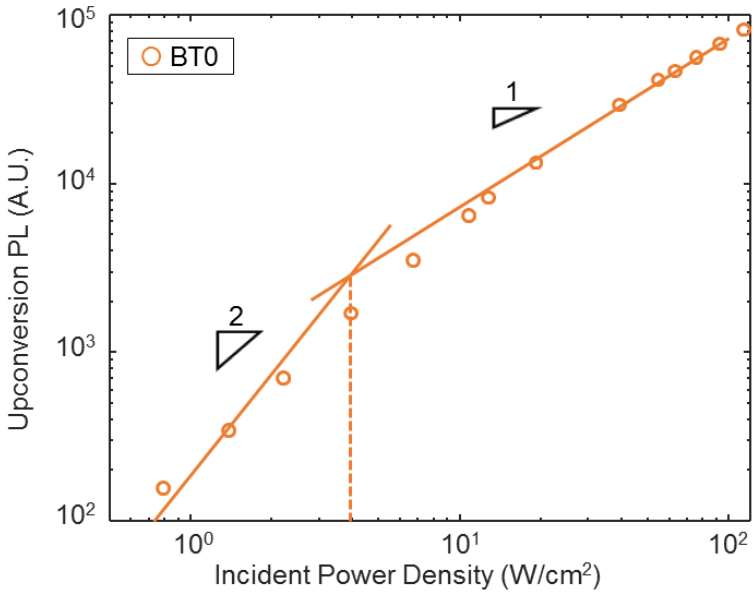

Figure 5.6 BT0 Turnover Point Dependence of upconverted PL on incident light intensity at $2.5x10^{-4}$ M BT0 concentration. The transition between quadratic and linear dependences occurs at 3.9 W/cm^2.

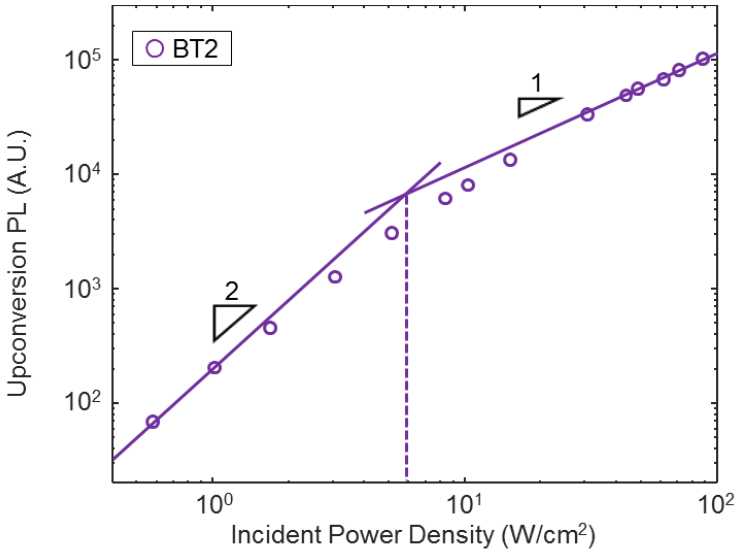

Figure 5.7 BT2 Turnover Point Dependence of upconverted PL on incident light intensity at 2.5×10^{-4} M BT2 concentration. The transition between quadratic and linear dependences occurs at 5.7 W/cm^2.

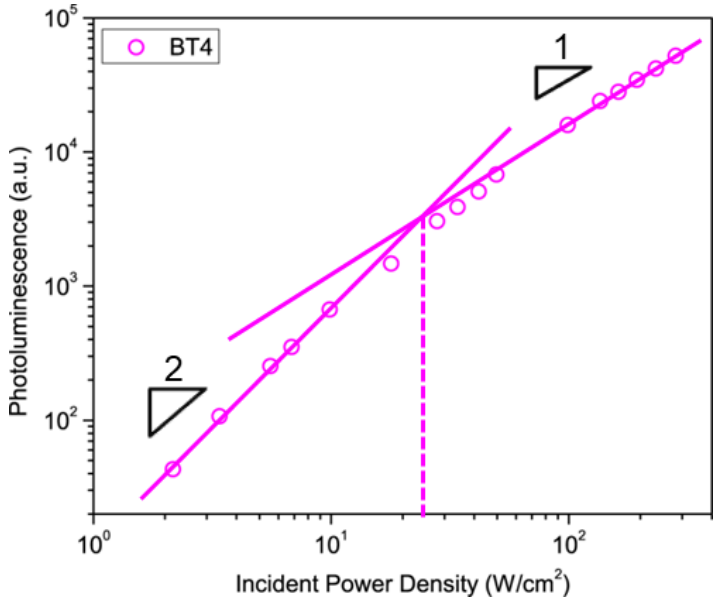

Figure 5.8 BT4 Turnover Point Dependence of upconverted PL on incident light intensity at 2.5×10^{-4} M BT4 concentration. The transition between quadratic and linear dependences occurs at 25.7 W/cm^2.

5.10 Computational Methods

Calculations were done using density functional theory (DFT) within the Gaussian 09 Suite, all geometries were optimized using the B3LYP functional and the 6-31G** basis set. To

simplify the computation, the (triisopropylsilyl)acetylene groups were simplified to (trimethylsilyl)acetylene groups.

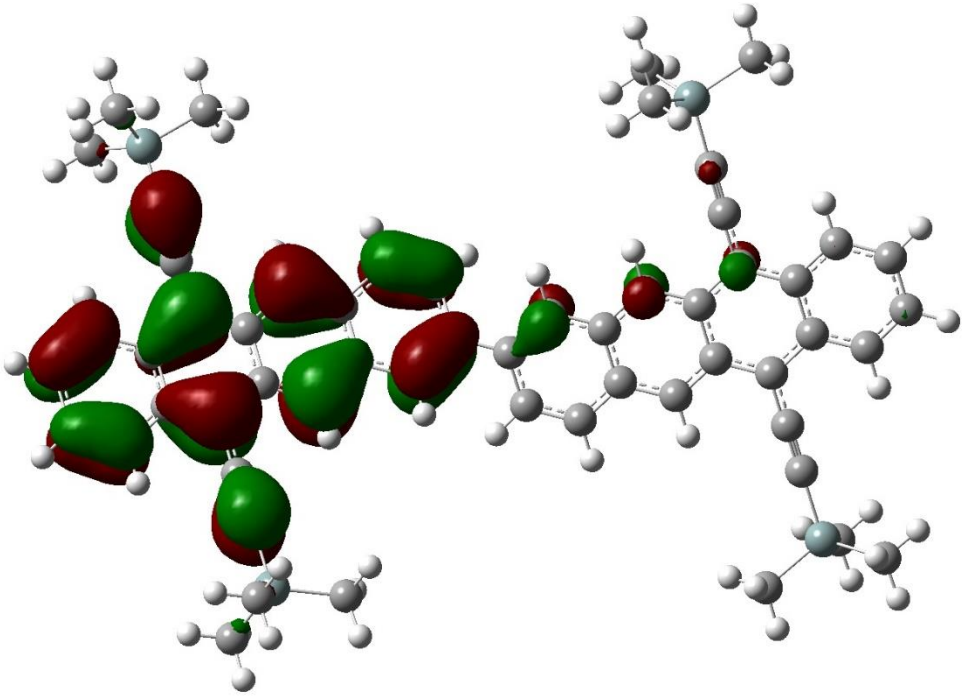

Figure 5.9 Zoom in of T_1 Orbital of BT0

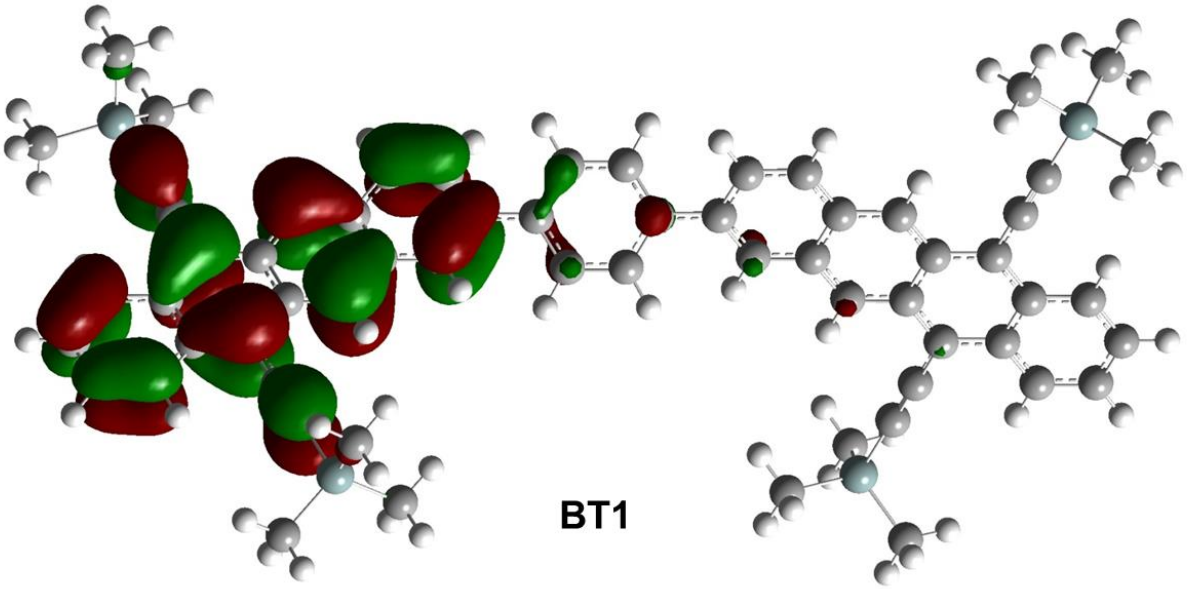

Figure 5.10 Zoom in of T_1 Orbital of BT1

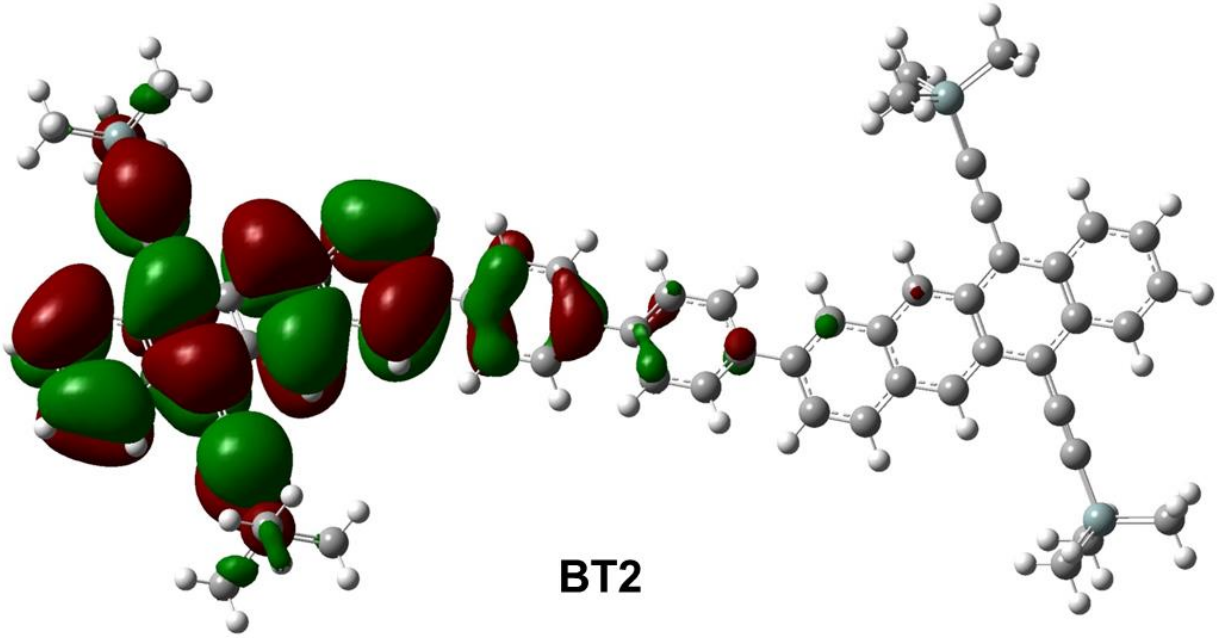

Figure 5.11 Zoom in of T_1 Orbital of BT2

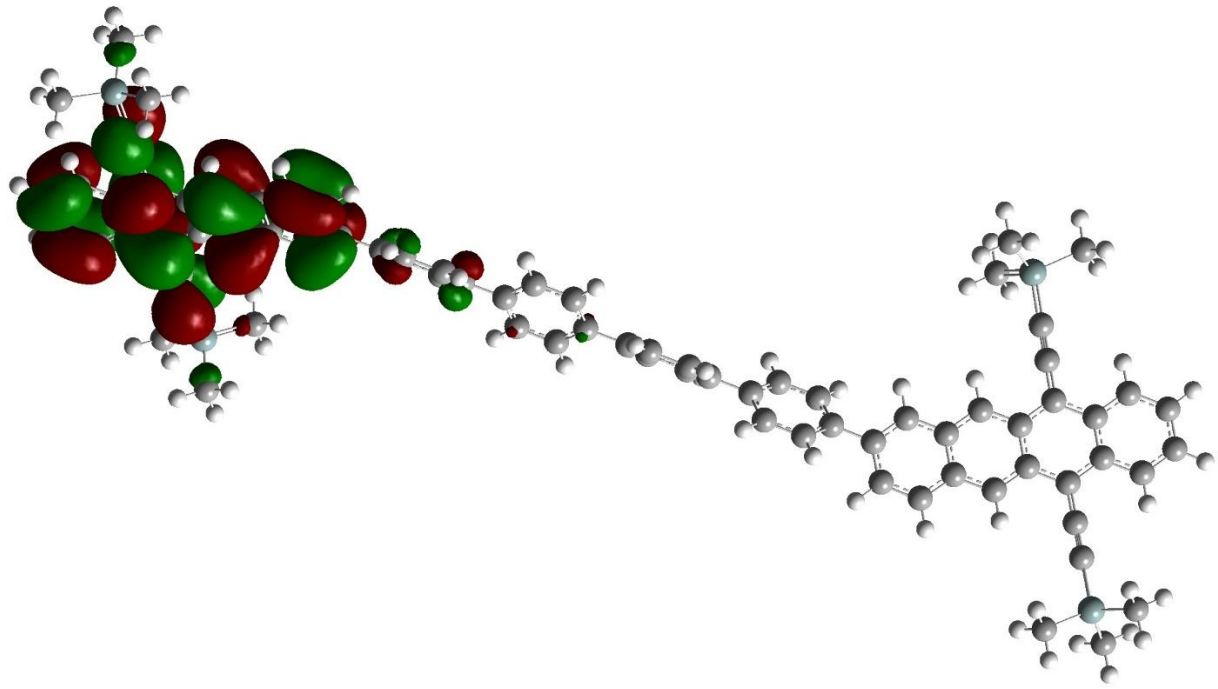

Figure 5.12 Zoom in of T_1 Orbital of BT4

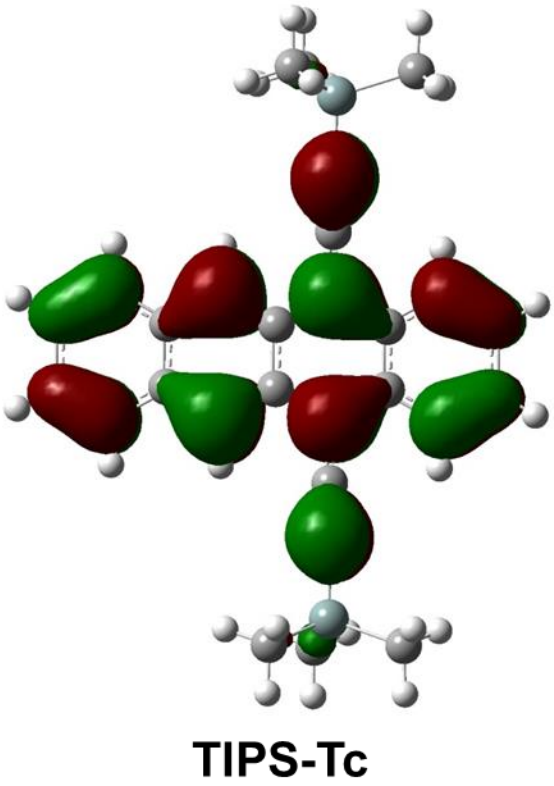

Figure 5.13 Zoom in of T_1 Orbital of TIPS-Tc

5.11 Annihilator Photophysical Properties

Annihilator	T_1 Energy (eV)
TIPS-Tc	0.946
BT0	0.941
BT1	0.940
BT2	0.939
BT4	0.939

Table 5.1 Calculated T_1 Energies of Annihilators

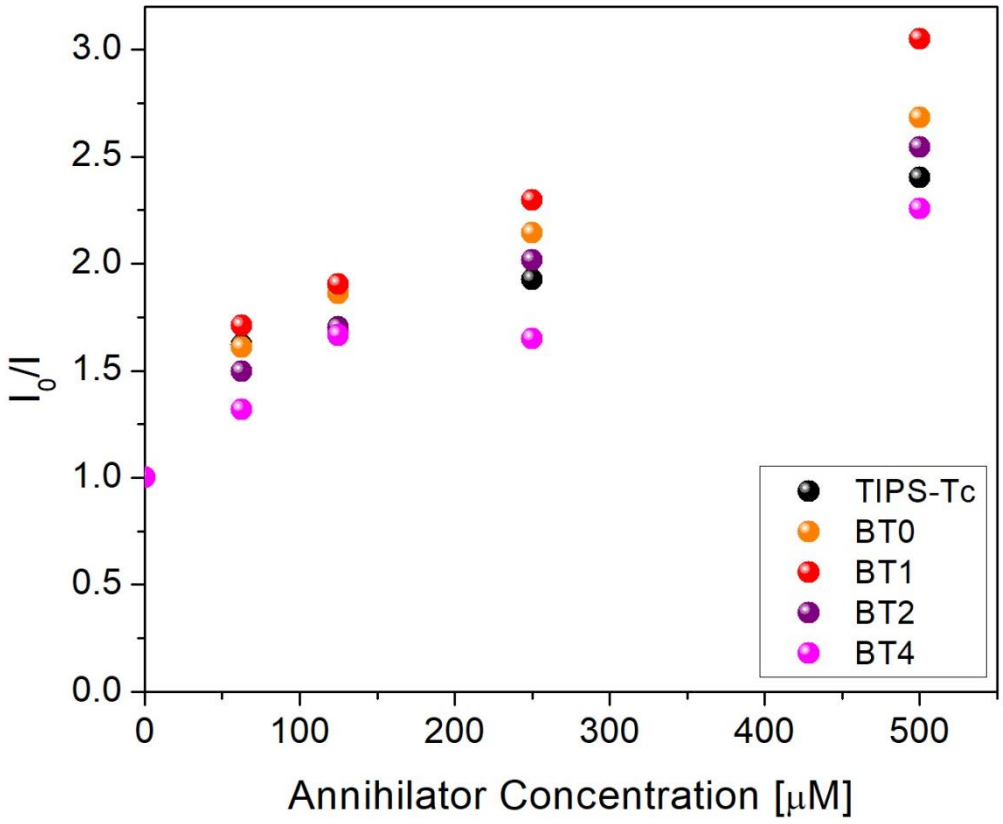

Figure 5.14 Stern-Volmer Plot of PdPc quenching by annihilators used in this work

Annihilator	K_{TET} ($M^{-1}*s^{-1}$)
TIPS-Tc	$7.89*10^8$
BT0	$9.83*10^8$
BT1	$1.21*10^9$
BT2	$9.26*10^8$
BT4	$7.40*10^8$

Table 5.2 K_{TET} Values for PdPc to Annihilators Studied, extracted from Stern-Volmer plot. Phosphorescence lifetime of PdPc is 3.04 μs.

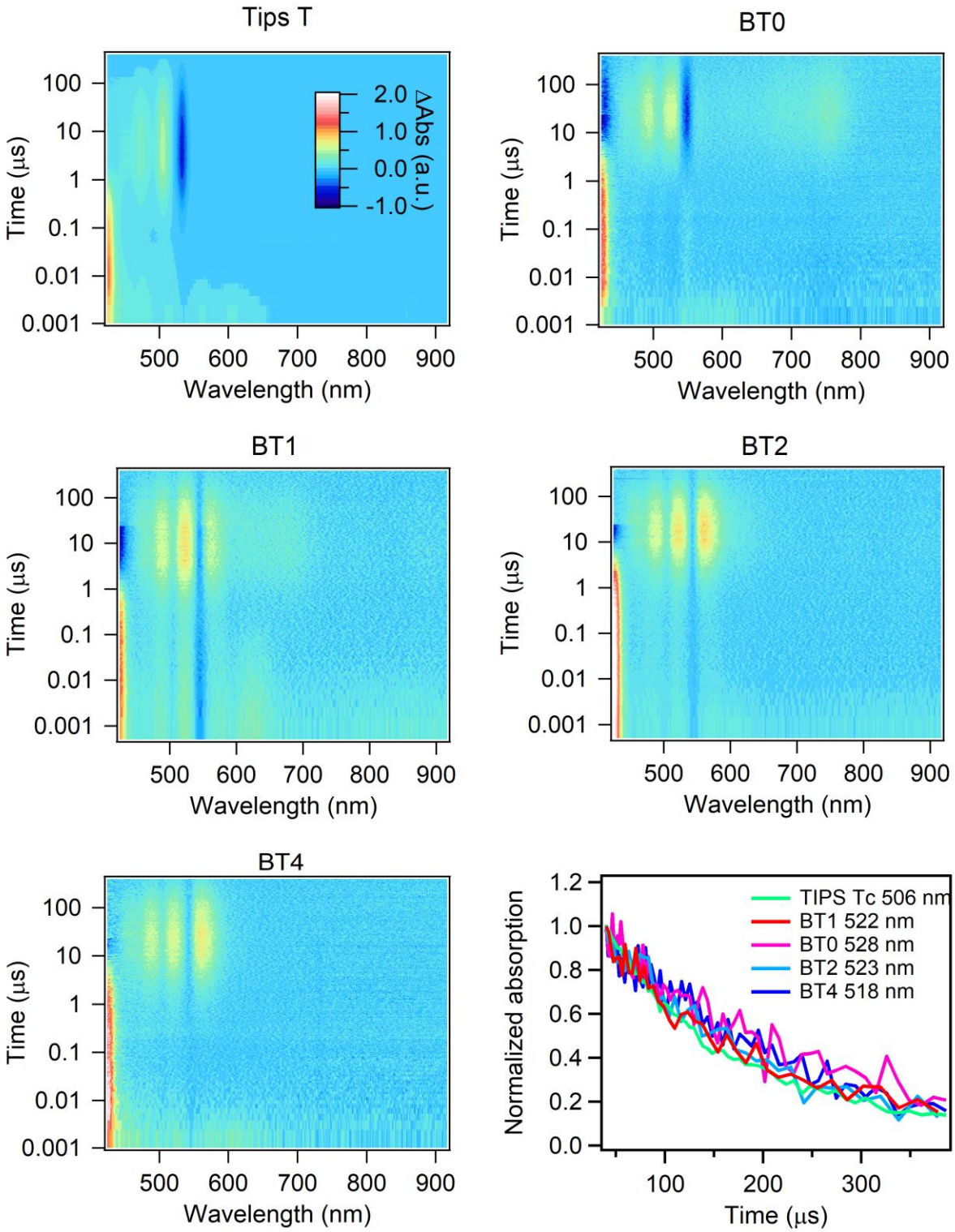

Figure 5.15 Triplet Lifetime TAS 2D transient absorption color plots of triplet sensitization experiments done on annihilators used in this work. Also included are kinetic traces of T_1 decay, from which triplet lifetimes were extracted.

Anthracene was dissolved at ~15 mM in toluene along with the compound of interest (typically ~50 μM) and placed in a 1 mL cuvette. Argon flow was used to degas the solution, and 360 nm pump pulses (~25 μJ/cm2) were used to excite the anthracene. Anthracene undergoes intersystem crossing to produce a triplet absorption with a prominent peak near 415 nm which is quenched by transfer to the triplet state of the tetracene material. The excited state absorption was probed at the peak to extract kinetics of this state in each case. Because the kinetics at early times are convoluted by the signals from anthracene and the fact that rise of the signal via transfer occurs over several microseconds, the lifetimes of the triplet state are most clearly seen by fitting the data after anthracene decay is complete. By fitting the data after that decay is complete we obtained lifetimes for the triplet in each case. Overall these lifetimes are similar and suggest that the dynamics of an individual triplet is similar throughout these systems and not significantly altered by dimerization.

Annihilator	T_1 Lifetime (μs)
TIPS-Tc	119
BT0	233
BT1	118
BT2	150
BT4	250

Table 5.3 T_1 Lifetimes of Annihilators

Annihilator	PLQY
TIPS-Tc	57.0%
BT0	0.3%
BT1	12.5%
BT2	10.1%
BT4	18.9%

Table 5.4 Photoluminescence Quantum Yields (PLQYs) of Annihilators

Annihilator	Upconversion Yield
TIPS-Tc	0.70%
BT0	N/A
BT1	4.2%
BT2	3.3%
BT4	0.33%

Table 5.5 Upconversion Yields of Annihilators

5.12 Kinetic Modeling

To begin we set the following equations:

$$\frac{d^3S^*}{dt} = 0 = {}^1S * k_\phi - k_{TET} * {}^3S^* * {}^1A - k_{Phos} * {}^3S^* - k_{TET2} * {}^3S^* * {}^3A^*$$

$$\frac{d^3A^*}{dt} = 0 = k_{TET} * {}^3S^* * {}^1A - k_{NR} * {}^3A^* - 2 * k_{TF} * ({}^3A^*)^2 - k_{TET2} * {}^3S^* * {}^3A^*$$

Where ^{3}S* and ^{3}A* are the concentration of the sensitizer and annihilator first excited state triplets, respectively, and ^{1}S and ^{1}A are the ground state singlets of sensitizer and annihilator respectively. Intersystem crossing of the sensitizer is assumed to be rapid. The final term (k_{TET2})x(^{3}S*)x(^{3}A*) represents a second triplet added to a dimer which is already populated with one triplet which then proceeds to do triplet fusion, fluoresce, and return to the ground state, and is set to zero for TIPS-Tc. We can then plot the efficiency defined as:

$$eff = \frac{2 * k_{TF} * ({}^3A^*)^2 + 2 * k_{TET} * {}^3S^* * {}^3A^*}{{}^1S * k_\phi}$$

We note that this is certainly an over-simplification of the final TF process, but without a detailed spin dynamics study, we believe this to be a reasonable approximation. This leaves us with a single fit parameter k_{TF} for each material, with the following values for the remaining constants:

Rate	Value (TIPs;BT1;BT2;BT4)	Source
k_{ϕ}	Sets light intensity	Independent Variable
k_{TET}	(7.9; 12.1; 9.3; 7.4) *10^{8} (M^{-1}*S^{-1})	Stern-Volmer (Figure S9, Table S2)
k_{Phos}	3.3*10^{5} (s^{-1})	Literature[43]
k_{TET2}	Same as k_{TET}	Stern-Volmer (Figure S9, Table S2)
k_{NR}	(8400; 8500; 6700; 4000) (s^{-1})	TA Measurements (Figure S10, Table S3)
k_{TF}	Fit	Fit

We assume the second triplet transfer rate to be equal to the initial triplet transfer. We can fit the data for TIPS, BT1, and BT2 as shown below. We were unable to adequately fit BT4, likely due to our simplistic iTF model approximations, and BT0 was not fit due to its ability to rapidly undergo singlet fission.

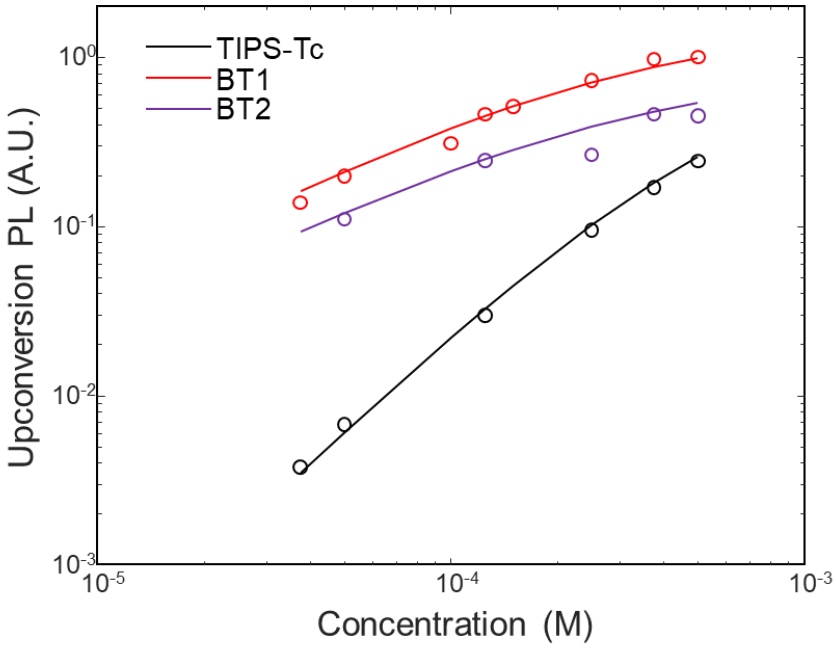

Figure 5.16 Kinetic Modelling of our experimental data from main text Figure 4A (open circles), with solid fit lines for TIPS-Tc (black), BT1 (red) and BT2 (purple).

This fit yields the following values for k_{TF}:

Material	k_{TF} ($M^{-1}*s^{-1}$)
TIPS-Tc	$2.3*10^6$
BT1	$250*10^6$
BT2	$23*10^6$

Table 5.6 k_{TF} values extracted from fit lines in Figure 5.16

We can further model the performance of these systems using intensity dependence, observing a decent qualitative fit:

Material	Modelled Threshold (W/cm^2)	Experimental Threshold (W/cm^2)
TIPS-Tc	76.1	44.5
BT1	11.5	4.3
BT2	44.9	5.7

Table 5.7 Modelled Threshold Values from the fit in Figure 5.16. The threshold is defined as the power density where there is a transition between quadratic and linear dependence on UCPL.

5.13 DFT Optimized Coordinates

TIPS-Tc S_0

Atom	X	Y	Z
C	0.720605	-4.32611	0.001309
C	-0.70407	-4.32883	0.001223
C	-1.39736	-3.14962	0.001495
C	-0.71838	-1.89018	0.001903
C	0.725555	-1.88744	0.001794
C	1.409427	-3.14427	0.001566
C	-1.42832	-0.66668	0.002172
C	-0.72479	0.579729	0.001757
C	0.72259	0.582474	0.00178
C	1.430843	-0.66124	0.001727
C	-1.40521	1.811544	0.001103
C	-0.72926	3.030009	0.000788
C	0.717689	3.032761	0.0012
C	1.398242	1.816877	0.001621
C	-1.41778	4.286379	-5E-06
C	-0.72534	5.465513	-0.00016
C	0.704474	5.468233	0.000425

C	1.401406	4.29175	0.001041
C	2.852617	-0.65892	0.001162
C	-2.85009	-0.66928	0.002816
C	4.076389	-0.65363	0.000409
C	-4.07387	-0.66719	0.003253
Si	5.918169	-0.65515	-0.00138
Si	-5.91562	-0.66439	-0.00047
C	6.529365	0.235276	1.548758
C	6.517888	-2.44663	-0.00213
C	6.526164	0.235694	-1.55254
C	-6.53195	-0.723	1.7845
C	-6.51369	0.915514	-0.84645
C	-6.52025	-2.18188	-0.94944
H	1.259508	-5.26891	0.001101
H	-1.23936	-5.27369	0.000788
H	-2.48158	-3.1449	0.001107
H	2.493619	-3.13558	0.001547
H	-2.49029	1.804784	0.000568
H	2.483341	1.814126	0.001758
H	-2.50442	4.280984	-0.00061
H	-1.25857	6.411584	-0.00079
H	1.234103	6.416331	0.00031
H	2.48807	4.290537	0.001399
H	7.624847	0.253759	1.577851
H	6.17627	1.270978	1.580365
H	6.177923	-0.26489	2.456784
H	7.613003	-2.48747	-0.00308
H	6.162837	-2.985	-0.88676
H	6.164365	-2.98514	0.883028
H	6.172934	-0.26427	-2.45998
H	6.172895	1.271366	-1.58315
H	7.621583	0.254289	-1.58385
H	-7.62753	-0.71948	1.814788
H	-6.18526	-1.6271	2.295024
H	-6.17756	0.140177	2.356807
H	-7.60875	0.948293	-0.8757
H	-6.1489	0.976912	-1.87667
H	-6.16753	1.807769	-0.31476
H	-6.17449	-3.10891	-0.48076
H	-7.61551	-2.21004	-0.97722
H	-6.15874	-2.1742	-1.9826

TIPS-Tc T_1

Atom	X	Y	Z

C	0.693547	-4.35084	0.001314
C	-0.7004	-4.34973	0.001708
C	-1.39298	-3.13836	0.001941
C	-0.7147	-1.90962	0.001888
C	0.711723	-1.91076	0.001728
C	1.388045	-3.14057	0.00133
C	-1.43902	-0.64374	0.001761
C	-0.72572	0.60952	0.00168
C	0.726705	0.608366	0.001526
C	1.438034	-0.64604	0.001859
C	-1.39431	1.82936	0.001527
C	-0.71286	3.079324	0.001095
C	0.71775	3.078185	0.000698
C	1.397222	1.827143	0.000948
C	-1.39748	4.313818	0.000919
C	-0.69894	5.512062	0.000332
C	0.70774	5.510938	-0.00012
C	1.404356	4.311573	0.000063
C	2.842064	-0.65451	0.002104
C	-2.84306	-0.65016	0.001201
C	4.071483	-0.66456	0.001904
C	-4.07248	-0.65891	0.000432
Si	5.911734	-0.68122	-0.00063
Si	-5.91274	-0.6771	-0.00148
C	6.531606	-0.21807	1.723639
C	6.498426	-2.4172	-0.46056
C	6.528938	0.572946	-1.27228
C	-6.53462	0.211809	1.545842
C	-6.53103	0.205778	-1.5537
C	-6.49683	-2.4738	0.00169
H	1.243156	-5.28725	0.000925
H	-1.25151	-5.28526	0.001734
H	-2.47759	-3.13274	0.00211
H	2.472671	-3.13664	0.0008
H	-2.47975	1.828856	0.001674
H	2.482653	1.824957	0.000463
H	-2.48422	4.312348	0.001231
H	-1.23864	6.454301	0.00019
H	1.248962	6.452308	-0.00063
H	2.491093	4.308342	-0.00034
H	7.627271	-0.21868	1.753655
H	6.188742	0.779909	2.014678
H	6.174622	-0.92669	2.477647
H	7.593241	-2.46503	-0.47184
H	6.140343	-2.70675	-1.45362

H	6.139174	-3.16265	0.256207
H	6.170135	0.328546	-2.27707
H	6.188102	1.585332	-1.03276
H	7.624436	0.587114	-1.30096
H	-7.63034	0.221733	1.571721
H	-6.18179	-0.2837	2.45585
H	-6.1898	1.250338	1.576102
H	-7.62667	0.21496	-1.58262
H	-6.17539	-0.29272	-2.46098
H	-6.18672	1.244398	-1.58666
H	-6.13882	-3.00709	0.888197
H	-7.59156	-2.52423	0.000688
H	-6.13697	-3.01117	-0.88159

BT0 S_0

Atom	X	Y	Z
C	-10.5181	-0.83024	0.553284
C	-10.1267	-2.15621	0.8962
C	-8.8078	-2.5182	0.862009
C	-7.79198	-1.58402	0.484916
C	-8.18889	-0.24021	0.137229
C	-9.57873	0.094302	0.186308
C	-6.42588	-1.95032	0.449106
C	-5.42902	-0.99546	0.070759
C	-5.82777	0.351182	-0.27964
C	-7.21133	0.710877	-0.24055
C	-4.06302	-1.33141	0.031198
C	-3.08441	-0.40779	-0.33418
C	-3.48461	0.936932	-0.68229
C	-4.83326	1.277716	-0.64939
C	-1.69613	-0.74521	-0.36592
C	-0.72962	0.172975	-0.71244
C	-1.14697	1.506433	-1.0646
C	-2.46197	1.869664	-1.05141
C	-7.60105	2.035141	-0.58163
C	-6.03413	-3.27364	0.790493
C	-7.92978	3.176878	-0.87474
C	-5.69008	-4.41129	1.08218
Si	-8.41488	4.899242	-1.31228
Si	-5.15946	-6.12098	1.515965
C	-9.76255	4.835232	-2.63441
C	-9.05931	5.762909	0.239452
C	-6.89179	5.798754	-1.97624
C	-6.13556	-7.34757	0.46154

C	-3.31144	-6.28262	1.15849
C	-5.49793	-6.41909	3.350631
C	10.49621	0.826164	0.555697
C	10.10393	2.1517	0.899149
C	8.784949	2.513222	0.863934
C	7.769897	1.578828	0.485203
C	8.167601	0.235352	0.137298
C	9.55759	-0.09863	0.187317
C	6.403646	1.944712	0.448025
C	5.407443	0.989205	0.069896
C	5.806915	-0.35737	-0.28017
C	7.190618	-0.71612	-0.2415
C	4.041294	1.324295	0.030386
C	3.063128	0.400031	-0.33439
C	3.463907	-0.94477	-0.68168
C	4.812786	-1.28465	-0.64898
C	1.674729	0.736773	-0.36625
C	0.708513	-0.18194	-0.71214
C	1.126318	-1.51561	-1.06295
C	2.441491	-1.87824	-1.04959
C	7.583504	-2.03905	-0.58418
C	6.012695	3.26871	0.787761
C	7.921303	-3.17788	-0.87829
C	5.673508	4.40812	1.078311
Si	8.450714	-4.88779	-1.31269
Si	5.170063	6.125178	1.515878
C	7.476044	-6.11399	-0.25641
C	8.108642	-5.18629	-3.14673
C	10.2992	-5.04975	-0.95864
C	3.523277	6.057322	2.438957
C	6.505099	6.881709	2.617679
C	4.9872	7.130491	-0.07349
H	-11.5682	-0.55515	0.584113
H	-10.8816	-2.88114	1.185825
H	-8.50361	-3.52585	1.122166
H	-9.86991	1.10515	-0.07625
H	-3.76951	-2.34183	0.296194
H	-5.13489	2.286304	-0.91244
H	-1.41316	-1.7516	-0.07141
H	-0.3937	2.223252	-1.37498
H	-2.75586	2.877204	-1.33309
H	-10.0735	5.846765	-2.91966
H	-9.40881	4.326124	-3.53652
H	-10.6485	4.301798	-2.27541
H	-9.35727	6.793129	0.013549

H	-8.29321	5.798439	1.020467
H	-9.93135	5.24437	0.65046
H	-6.49291	5.300352	-2.86554
H	-7.14056	6.829388	-2.25345
H	-6.09482	5.837851	-1.22665
H	-5.84623	-8.37758	0.699489
H	-7.21251	-7.25438	0.634173
H	-5.95304	-7.1857	-0.60556
H	-2.95718	-7.29082	1.401426
H	-2.72696	-5.57183	1.751525
H	-3.09426	-6.09761	0.10158
H	-4.95154	-5.70547	3.975398
H	-6.56317	-6.3179	3.581512
H	-5.18602	-7.42858	3.641915
H	11.54633	0.551401	0.587403
H	10.8582	2.876697	1.190239
H	8.480255	3.52048	1.124983
H	9.849773	-1.10917	-0.07523
H	3.747461	2.334637	0.295359
H	5.115229	-2.29324	-0.91112
H	1.391322	1.743208	-0.07232
H	0.3733	-2.23314	-1.37229
H	2.735626	-2.88602	-1.33015
H	7.765494	-7.14407	-0.49389
H	7.659783	-5.95122	0.810337
H	6.398806	-6.02148	-0.4277
H	8.419764	-6.19595	-3.43828
H	8.654149	-4.47304	-3.77271
H	7.043086	-5.08487	-3.37606
H	10.51859	-4.86381	0.097613
H	10.65284	-6.05818	-1.20158
H	10.88266	-4.33922	-1.55296
H	3.196802	7.064682	2.721237
H	2.736729	5.612798	1.820678
H	3.605383	5.462442	3.354085
H	6.23694	7.905269	2.903091
H	7.471022	6.92086	2.103861
H	6.637454	6.301684	3.53653
H	4.224034	6.700802	-0.73015
H	4.693385	8.161902	0.152765
H	5.927734	7.164262	-0.63242

BT0 T_1

Atom	X	Y	Z

C	-10.544	-0.78487	0.512154
C	-10.1619	-2.10403	0.889752
C	-8.84422	-2.47191	0.87867
C	-7.82042	-1.55075	0.491429
C	-8.20785	-0.21364	0.109127
C	-9.59663	0.127386	0.134885
C	-6.45559	-1.92356	0.477925
C	-5.45076	-0.98198	0.087225
C	-5.83992	0.358768	-0.29542
C	-7.22206	0.725025	-0.27871
C	-4.08648	-1.32569	0.065217
C	-3.10008	-0.41518	-0.31316
C	-3.49042	0.92502	-0.68968
C	-4.8375	1.273114	-0.67422
C	-1.71434	-0.76127	-0.33164
C	-0.74086	0.143769	-0.69481
C	-1.14727	1.474948	-1.06737
C	-2.46032	1.846016	-1.06733
C	-7.6026	2.042928	-0.65316
C	-6.07328	-3.23994	0.854744
C	-7.92389	3.178982	-0.97518
C	-5.73817	-4.37166	1.178268
Si	-8.39951	4.892632	-1.45533
Si	-5.22409	-6.07243	1.663892
C	-9.72581	4.803294	-2.79745
C	-9.06804	5.787745	0.06817
C	-6.86503	5.777497	-2.11258
C	-6.21205	-7.32072	0.646628
C	-3.37744	-6.2633	1.313278
C	-5.56637	-6.31125	3.506445
C	10.54079	0.836238	0.535529
C	10.15543	2.125413	0.900972
C	8.805814	2.4776	0.881447
C	7.81654	1.557446	0.499591
C	8.21096	0.238679	0.125587
C	9.574261	-0.09397	0.15232
C	6.406005	1.925096	0.479915
C	5.403521	0.965694	0.087617
C	5.806573	-0.37772	-0.29151
C	7.200565	-0.73424	-0.27416
C	4.051881	1.29287	0.062049
C	3.042902	0.361597	-0.3197
C	3.441451	-0.96242	-0.68517
C	4.822493	-1.2917	-0.66338
C	1.677037	0.700836	-0.33921

C	0.692619	-0.22489	-0.69925
C	1.10538	-1.53111	-1.06158
C	2.441302	-1.88873	-1.05453
C	7.597181	-2.03008	-0.64503
C	6.025019	3.22547	0.848841
C	7.946686	-3.16291	-0.96958
C	5.696879	4.365066	1.17282
Si	8.472305	-4.85789	-1.45803
Si	5.218524	6.073895	1.662341
C	7.062291	-6.05917	-1.08508
C	8.863841	-4.86876	-3.30681
C	10.00861	-5.325	-0.46266
C	4.28868	6.003621	3.305703
C	6.790525	7.105769	1.846391
C	4.111458	6.806289	0.31749
H	-11.5932	-0.50506	0.524754
H	-10.923	-2.81923	1.187334
H	-8.54727	-3.4746	1.165001
H	-9.88056	1.133111	-0.15395
H	-3.80036	-2.33209	0.3527
H	-5.13176	2.277763	-0.9597
H	-1.43605	-1.76271	-0.01621
H	-0.3879	2.182778	-1.38391
H	-2.7468	2.850752	-1.36615
H	-10.032	5.80921	-3.10678
H	-9.35776	4.277129	-3.68392
H	-10.6176	4.276715	-2.44265
H	-9.36231	6.813066	-0.1834
H	-8.3142	5.839274	0.860128
H	-9.94647	5.277534	0.47597
H	-6.45284	5.261452	-2.98561
H	-7.10831	6.802683	-2.4138
H	-6.07981	5.83064	-1.35155
H	-5.92914	-8.34585	0.911802
H	-7.28774	-7.21522	0.82015
H	-6.03206	-7.18947	-0.42508
H	-3.03282	-7.26579	1.591213
H	-2.78667	-5.53803	1.882044
H	-3.15788	-6.11682	0.250842
H	-5.01417	-5.58386	4.109845
H	-6.63087	-6.19366	3.73292
H	-5.26354	-7.31411	3.828601
H	11.58838	0.551056	0.547122
H	10.89892	2.857673	1.200885
H	8.50178	3.479373	1.165018

H	9.869182	-1.09806	-0.13258
H	3.753065	2.297312	0.344663
H	5.123281	-2.29589	-0.94487
H	1.38961	1.702707	-0.03338
H	0.359179	-2.25261	-1.37843
H	2.73596	-2.89298	-1.34718
H	7.34284	-7.0821	-1.36082
H	6.808946	-6.05679	-0.02019
H	6.158467	-5.79885	-1.64539
H	9.183472	-5.86659	-3.62854
H	9.667139	-4.16525	-3.54757
H	7.986974	-4.58991	-3.89974
H	9.806577	-5.30361	0.612915
H	10.34465	-6.33567	-0.72107
H	10.83661	-4.63698	-0.6616
H	3.989488	7.009205	3.622813
H	3.383121	5.39378	3.226329
H	4.912261	5.573981	4.09603
H	6.547132	8.135302	2.13261
H	7.353185	7.143529	0.908148
H	7.44951	6.692224	2.616622
H	3.20166	6.212706	0.181913
H	3.809117	7.826625	0.57962
H	4.630761	6.846942	-0.64518

BT1 S_0

Atom	X	Y	Z
C	-12.3375	1.33996	-0.77721
C	-11.724	2.352374	-1.56961
C	-10.3656	2.375912	-1.73033
C	-9.52862	1.393691	-1.11273
C	-10.1506	0.367661	-0.3096
C	-11.5741	0.381275	-0.16917
C	-8.12312	1.41169	-1.27403
C	-7.30807	0.418588	-0.64296
C	-7.9325	-0.60973	0.162165
C	-9.35442	-0.62023	0.316574
C	-5.90782	0.414356	-0.78339
C	-5.10554	-0.54684	-0.16933
C	-5.73181	-1.57534	0.630882
C	-7.11597	-1.57928	0.775424
C	-3.6833	-0.55313	-0.31047
C	-2.89508	-1.50623	0.294576
C	-3.53548	-2.52389	1.087979

C	-4.89019	-2.55515	1.249274
C	-9.96609	-1.63303	1.105275
C	-7.51068	2.420079	-2.06737
C	-10.4868	-2.50801	1.784107
C	-6.97815	3.285079	-2.74995
Si	-11.2614	-3.83181	2.803935
Si	-6.17029	4.583238	-3.77717
C	-12.0925	-3.03983	4.304299
C	-12.5392	-4.74204	1.751023
C	-9.90793	-5.02536	3.362893
C	-6.85538	6.270102	-3.27285
C	-4.30753	4.516921	-3.46904
C	-6.54486	4.243146	-5.59733
C	12.32478	1.344815	0.779835
C	11.70908	2.354744	1.573691
C	10.35048	2.376271	1.732929
C	9.515528	1.394317	1.112045
C	10.13973	0.370709	0.307563
C	11.56342	0.386357	0.168827
C	8.109814	1.410233	1.271682
C	7.296646	0.418702	0.635784
C	7.923264	-0.60738	-0.17055
C	9.345514	-0.61712	-0.3214
C	5.896126	0.413718	0.772674
C	5.095513	-0.54594	0.154175
C	5.723863	-1.57227	-0.64719
C	7.108375	-1.57545	-0.78829
C	3.672997	-0.55285	0.292045
C	2.88628	-1.50459	-0.31701
C	3.528638	-2.52005	-1.11164
C	4.88372	-2.55053	-1.27006
C	9.960961	-1.6292	-1.1081
C	7.495923	2.41442	2.069244
C	10.48845	-2.50289	-1.78337
C	6.963348	3.275371	2.756895
Si	11.29179	-3.81725	-2.79339
Si	6.165021	4.569266	3.796781
C	10.34018	-4.00359	-4.41465
C	13.07672	-3.30305	-3.13755
C	11.25702	-5.43849	-1.82369
C	4.631108	5.208395	2.897354
C	5.680261	3.804221	5.454609
C	7.397653	5.976368	4.059932
C	-1.42092	-1.50403	0.142374
C	-0.69537	-2.705	0.064114

C	0.686812	-2.70463	-0.09113
C	1.411912	-1.50326	-0.16696
C	0.68587	-0.30183	-0.08914
C	-0.69539	-0.3022	0.065937
H	-13.4168	1.332006	-0.65728
H	-12.3406	3.10799	-2.04722
H	-9.89266	3.143876	-2.33204
H	-12.0348	-0.39196	0.435374
H	-5.44466	1.187352	-1.38784
H	-7.58707	-2.3494	1.377368
H	-3.23032	0.207637	-0.93981
H	-2.9168	-3.26128	1.589516
H	-5.35271	-3.32355	1.862843
H	-12.566	-3.80346	4.932006
H	-11.3662	-2.5013	4.921273
H	-12.8672	-2.32793	4.001849
H	-13.0179	-5.54081	2.328953
H	-12.0745	-5.19676	0.870428
H	-13.3249	-4.06438	1.402125
H	-9.15004	-4.51252	3.963813
H	-10.3301	-5.83093	3.974241
H	-9.40416	-5.4849	2.506428
H	-6.39441	7.067805	-3.86642
H	-7.93818	6.323428	-3.42514
H	-6.65572	6.479047	-2.21711
H	-3.78824	5.274777	-4.06649
H	-3.89436	3.53951	-3.73842
H	-4.07246	4.702479	-2.41607
H	-7.62167	4.26629	-5.79275
H	-6.07157	4.997248	-6.23652
H	-6.17092	3.261035	-5.90346
H	13.40417	1.338631	0.660932
H	12.32417	3.110209	2.053503
H	9.875961	3.142549	2.33559
H	12.02602	-0.38463	-0.43711
H	5.431472	1.185241	1.377809
H	7.58138	-2.34355	-1.39133
H	3.218422	0.206105	0.922427
H	2.911196	-3.25632	-1.61636
H	5.347682	-3.3172	-1.88472
H	10.79033	-4.78298	-5.03993
H	9.296558	-4.28097	-4.23476
H	10.34451	-3.07023	-4.98639
H	13.58915	-4.06194	-3.73965
H	13.64055	-3.17869	-2.20739

H	13.11937	-2.35625	-3.68528
H	11.79825	-5.34455	-0.87693
H	10.23152	-5.74438	-1.59335
H	11.72601	-6.24395	-2.40041
H	4.136338	5.989525	3.48566
H	4.891601	5.635783	1.923899
H	3.904521	4.407263	2.72789
H	5.198965	4.548668	6.099118
H	6.556567	3.417723	5.984605
H	4.978948	2.974677	5.319512
H	7.7067	6.417178	3.106784
H	6.952394	6.771932	4.668151
H	8.297675	5.626211	4.575559
H	-1.22201	-3.65359	0.104309
H	1.213826	-3.65295	-0.1328
H	1.212109	0.64469	-0.16648
H	-1.22198	0.644014	0.144566

BT1 T_1

Atom	X	Y	Z
C	-12.3461	1.398926	-0.78861
C	-11.7387	2.382291	-1.56839
C	-10.3528	2.383377	-1.7271
C	-9.54704	1.410127	-1.11531
C	-10.1686	0.404053	-0.3176
C	-11.5644	0.421874	-0.17171
C	-8.09857	1.411699	-1.28073
C	-7.28577	0.4096	-0.63707
C	-7.92016	-0.61525	0.174366
C	-9.35144	-0.61732	0.327414
C	-5.90137	0.39629	-0.77228
C	-5.07725	-0.58217	-0.14438
C	-5.70458	-1.59342	0.649016
C	-7.11835	-1.57639	0.785833
C	-3.67684	-0.588	-0.28709
C	-2.87764	-1.55719	0.326329
C	-3.51551	-2.55199	1.107532
C	-4.89	-2.56838	1.26457
C	-9.97144	-1.61037	1.104104
C	-7.49303	2.398618	-2.07546
C	-10.5164	-2.47899	1.781907
C	-6.96273	3.261048	-2.77284
Si	-11.333	-3.78155	2.793922
Si	-6.16281	4.543492	-3.82341

C	-12.7348	-2.99075	3.783829
C	-12.0194	-5.11235	1.641112
C	-10.0498	-4.5284	3.962427
C	-7.26196	6.079772	-3.84831
C	-4.47445	4.961213	-3.08453
C	-5.95738	3.860563	-5.57345
C	12.32689	1.372894	0.770556
C	11.70798	2.379294	1.566382
C	10.34979	2.393028	1.730012
C	9.518515	1.406251	1.111869
C	10.14599	0.386104	0.305541
C	11.56908	0.409998	0.162091
C	8.113214	1.414308	1.27578
C	7.303748	0.417967	0.642693
C	7.933734	-0.60522	-0.1647
C	9.355455	-0.60657	-0.32049
C	5.903654	0.405523	0.783306
C	5.106656	-0.55929	0.168132
C	5.738519	-1.58364	-0.63305
C	7.12256	-1.57896	-0.77846
C	3.684552	-0.57328	0.309074
C	2.901535	-1.53074	-0.29595
C	3.547433	-2.545	-1.08924
C	4.902235	-2.56818	-1.25124
C	9.974126	-1.61481	-1.10959
C	7.496119	2.415103	2.075124
C	10.50441	-2.48482	-1.78742
C	6.960792	3.272922	2.764551
Si	11.312	-3.79276	-2.80241
Si	6.158799	4.562012	3.807624
C	10.36014	-3.97679	-4.42378
C	13.09481	-3.27074	-3.14579
C	11.28376	-5.41752	-1.83844
C	4.62378	5.199961	2.909268
C	5.675002	3.791177	5.463054
C	7.388016	5.971228	4.075307
C	-1.40531	-1.54903	0.167016
C	-0.67371	-2.74704	0.093332
C	0.708178	-2.74074	-0.06094
C	1.427641	-1.53601	-0.14327
C	0.695728	-0.33781	-0.07277
C	-0.68574	-0.34396	0.080831
H	-13.424	1.388275	-0.65793
H	-12.3371	3.147717	-2.0531
H	-9.87566	3.146452	-2.33251

H	-12.0326	-0.34474	0.436084
H	-5.42898	1.16263	-1.3786
H	-7.59279	-2.34273	1.390581
H	-3.21686	0.168766	-0.91615
H	-2.91074	-3.29614	1.615934
H	-5.3573	-3.33396	1.878171
H	-13.2473	-3.74151	4.396044
H	-12.3567	-2.21214	4.453881
H	-13.4792	-2.53276	3.124597
H	-12.5148	-5.90378	2.215288
H	-11.2225	-5.57451	1.049971
H	-12.753	-4.69442	0.944379
H	-9.63138	-3.76783	4.629227
H	-10.5008	-5.30889	4.585742
H	-9.22164	-4.98172	3.408128
H	-6.81424	6.864626	-4.46849
H	-8.25215	5.855349	-4.25784
H	-7.39954	6.486074	-2.84128
H	-3.96838	5.726436	-3.68404
H	-3.82513	4.080381	-3.05138
H	-4.57179	5.34481	-2.06396
H	-6.92461	3.597133	-6.013
H	-5.48338	4.603779	-6.22486
H	-5.33208	2.962178	-5.57868
H	13.4059	1.372933	0.648127
H	12.32027	3.138303	2.044173
H	9.872809	3.156601	2.334156
H	12.03416	-0.35837	-0.44527
H	5.436396	1.175261	1.38871
H	7.598195	-2.34521	-1.38179
H	3.227217	0.184847	0.938463
H	2.932741	-3.28602	-1.59034
H	5.368897	-3.33371	-1.86528
H	10.81288	-4.75211	-5.05224
H	9.31768	-4.25878	-4.24431
H	10.36058	-3.04128	-4.99202
H	13.60979	-4.02583	-3.75047
H	13.65863	-3.14708	-2.21553
H	13.13359	-2.32213	-3.69068
H	11.82538	-5.32504	-0.89175
H	10.25954	-5.72794	-1.60845
H	11.75522	-6.2192	-2.4184
H	4.126726	5.978057	3.499666
H	4.883673	5.630937	1.937236
H	3.899307	4.397506	2.737034

H	5.191865	4.53278	6.109464
H	6.551889	3.405015	5.992331
H	4.975469	2.960562	5.325312
H	7.696501	6.415436	3.123554
H	6.940621	6.764054	4.685529
H	8.288584	5.621694	4.590403
H	-1.19716	-3.69726	0.135885
H	1.239775	-3.68665	-0.09915
H	1.217264	0.610736	-0.15673
H	-1.21587	0.60091	0.151688

BT2 S_0

Atom	X	Y	Z
C	-14.7002	-1.11635	0.461266
C	-14.1986	-2.39816	0.828158
C	-12.8509	-2.63121	0.854099
C	-11.914	-1.60406	0.516353
C	-12.4225	-0.30497	0.144202
C	-13.839	-0.10586	0.131148
C	-10.519	-1.83788	0.540132
C	-9.60282	-0.79361	0.195572
C	-10.1131	0.508522	-0.17821
C	-11.5253	0.734682	-0.19743
C	-8.21098	-0.99968	0.207806
C	-7.31075	0.008973	-0.13329
C	-7.82205	1.309809	-0.50292
C	-9.19727	1.52364	-0.5158
C	-5.89714	-0.20026	-0.12575
C	-5.01058	0.796733	-0.46559
C	-5.53667	2.087484	-0.82949
C	-6.87933	2.331368	-0.84759
C	-12.0264	2.014141	-0.5635
C	-10.0175	-3.11718	0.905074
C	-12.4556	3.116122	-0.8781
C	-9.57873	-4.21628	1.216711
Si	-13.1143	4.771948	-1.3445
Si	-8.90496	-5.86747	1.677103
C	-13.1462	4.908214	-3.22852
C	-14.8613	4.94027	-0.6456
C	-11.9887	6.10027	-0.61108
C	-9.53748	-7.14934	0.441745
C	-7.01862	-5.78075	1.616322
C	-9.48265	-6.29906	3.423243
C	14.69749	1.124745	0.433066

C	14.19566	2.407096	0.797732
C	12.84775	2.638762	0.827717
C	11.91101	1.609438	0.496167
C	12.4197	0.309772	0.126382
C	13.8364	0.112166	0.109131
C	10.51581	1.841682	0.524271
C	9.599724	0.795941	0.183824
C	10.11023	-0.50687	-0.18729
C	11.52255	-0.73214	-0.20835
C	8.207806	1.000952	0.197771
C	7.307609	-0.00904	-0.13932
C	7.819144	-1.31065	-0.50583
C	9.194478	-1.52359	-0.5202
C	5.893928	0.199489	-0.13094
C	5.007478	-0.79892	-0.46685
C	5.533765	-2.09058	-0.82716
C	6.876542	-2.33379	-0.84613
C	12.02358	-2.01343	-0.56796
C	10.01466	3.120337	0.892037
C	12.45196	-3.11773	-0.87556
C	9.577656	4.21866	1.208959
Si	13.10714	-4.7784	-1.32947
Si	8.919315	5.869716	1.691953
C	12.22205	-6.08414	-0.28977
C	12.7896	-5.07799	-3.16773
C	14.96181	-4.81061	-0.97258
C	7.791091	5.656491	3.1925
C	10.37246	6.99688	2.121851
C	7.944085	6.583935	0.239494
C	-3.54683	0.564722	-0.46307
C	-2.64752	1.578528	-0.09008
C	-1.27424	1.358302	-0.08262
C	-0.73338	0.114869	-0.45102
C	-1.63235	-0.89849	-0.826
C	-3.0049	-0.67827	-0.83433
C	0.730183	-0.11785	-0.45126
C	1.628629	0.893915	-0.83179
C	3.001207	0.673885	-0.84042
C	3.543668	-0.56731	-0.46399
C	2.644905	-1.5796	-0.08564
C	1.271583	-1.35954	-0.07781
H	-15.7722	-0.94361	0.444621
H	-14.8923	-3.19219	1.088005
H	-12.4626	-3.60456	1.132299
H	-14.2146	0.871858	-0.14901

H	-7.83366	-1.97739	0.488859
H	-9.58303	2.498817	-0.7945
H	-5.52809	-1.17377	0.184125
H	-4.8438	2.86971	-1.12295
H	-7.25602	3.308452	-1.13786
H	-13.5347	5.884672	-3.53962
H	-12.1432	4.796078	-3.6525
H	-13.7838	4.136551	-3.67133
H	-15.2864	5.91917	-0.89483
H	-14.8627	4.842588	0.444674
H	-15.5287	4.173417	-1.0518
H	-11.943	6.023226	0.479861
H	-10.9673	6.015404	-0.99561
H	-12.3579	7.10122	-0.86187
H	-9.15267	-8.1458	0.687157
H	-10.6309	-7.20227	0.446048
H	-9.21888	-6.90819	-0.57734
H	-6.57749	-6.74787	1.88292
H	-6.63161	-5.03281	2.315804
H	-6.66592	-5.51788	0.613807
H	-9.13805	-5.55634	4.149701
H	-10.5748	-6.34339	3.483131
H	-9.0903	-7.27561	3.729057
H	15.76961	0.953263	0.413071
H	14.88935	3.202769	1.052597
H	12.45958	3.612664	1.104142
H	14.21227	-0.86592	-0.16948
H	7.830585	1.979296	0.476668
H	9.580451	-2.49926	-0.79682
H	5.524603	1.173771	0.176213
H	4.840897	-2.87406	-1.11731
H	7.253408	-3.31155	-1.1339
H	12.58445	-7.08801	-0.53892
H	12.39295	-5.92136	0.779109
H	11.14107	-6.06685	-0.4616
H	13.16888	-6.06057	-3.47093
H	13.28628	-4.32175	-3.78383
H	11.71997	-5.04639	-3.39834
H	15.16529	-4.62034	0.086079
H	15.38731	-5.78858	-1.22465
H	15.49404	-4.05404	-1.55808
H	7.382504	6.622419	3.510776
H	6.94857	4.995087	2.966448
H	8.334685	5.226598	4.039748
H	10.01629	7.990667	2.415812

H	11.04565	7.122142	1.267726
H	10.95706	6.591667	2.953953
H	7.107149	5.933935	-0.03508
H	7.534164	7.567731	0.495099
H	8.577865	6.70365	-0.64488
H	-3.02978	2.541857	0.233611
H	-0.61107	2.152968	0.245698
H	-1.24701	-1.85911	-1.15427
H	-3.66799	-1.46971	-1.1699
H	1.242765	1.852911	-1.16417
H	3.663873	1.46379	-1.18042
H	3.027685	-2.54141	0.24195
H	0.608867	-2.1528	0.254766

BT2 T_1

Atom	X	Y	Z
C	-14.715	-1.09014	0.440732
C	-14.2196	-2.3738	0.809541
C	-12.8729	-2.61218	0.839717
C	-11.931	-1.58884	0.504512
C	-12.4332	-0.28788	0.130397
C	-13.8488	-0.08316	0.112964
C	-10.537	-1.82817	0.532744
C	-9.61566	-0.78801	0.189367
C	-10.1196	0.516167	-0.18585
C	-11.5308	0.748168	-0.20865
C	-8.22476	-1.00004	0.204192
C	-7.31953	0.004735	-0.1351
C	-7.82454	1.307903	-0.50522
C	-9.19881	1.5275	-0.52116
C	-5.90686	-0.2106	-0.12522
C	-5.01543	0.782901	-0.4625
C	-5.53523	2.076208	-0.82633
C	-6.8768	2.325719	-0.84721
C	-12.0257	2.029811	-0.57546
C	-10.042	-3.10869	0.902318
C	-12.4499	3.133714	-0.89028
C	-9.6099	-4.20893	1.219338
Si	-13.1018	4.792513	-1.35558
Si	-8.953	-5.86382	1.690949
C	-13.131	4.93142	-3.23944
C	-14.849	4.96607	-0.65839
C	-11.9724	6.115733	-0.61892
C	-10.0736	-7.19351	0.952829

C	-7.20233	-6.03128	1.000353
C	-8.92925	-5.99805	3.575104
C	14.72787	1.180943	0.411771
C	14.2303	2.432752	0.771412
C	12.85232	2.64698	0.806874
C	11.94597	1.624067	0.486097
C	12.45507	0.343403	0.118008
C	13.84491	0.149924	0.089365
C	10.50603	1.848378	0.522401
C	9.58981	0.788683	0.1809
C	10.10929	-0.51556	-0.19359
C	11.53189	-0.73409	-0.21987
C	8.21257	0.981969	0.19899
C	7.287497	-0.0471	-0.14109
C	7.8007	-1.33176	-0.50403
C	9.207809	-1.52651	-0.51922
C	5.895439	0.160147	-0.12597
C	4.995006	-0.85555	-0.46025
C	5.520175	-2.12264	-0.81443
C	6.884299	-2.35339	-0.83508
C	12.04071	-1.99481	-0.57407
C	10.01054	3.109214	0.89265
C	12.48903	-3.09727	-0.88159
C	9.577078	4.212592	1.218223
Si	13.1647	-4.74802	-1.33583
Si	8.923084	5.860848	1.711742
C	12.29856	-6.06689	-0.296
C	12.84834	-5.05451	-3.17367
C	15.02045	-4.75724	-0.98268
C	7.799044	5.64314	3.215313
C	10.37867	6.984808	2.141929
C	7.941917	6.584945	0.267618
C	-3.55272	0.544683	-0.45745
C	-2.65003	1.553658	-0.07953
C	-1.27773	1.327757	-0.06987
C	-0.74111	0.083298	-0.44128
C	-1.64358	-0.92527	-0.82101
C	-3.01519	-0.69946	-0.83128
C	0.721334	-0.15525	-0.44046
C	1.624746	0.855822	-0.81058
C	2.996611	0.631093	-0.81625
C	3.533588	-0.61594	-0.45036
C	2.629573	-1.62659	-0.07873
C	1.257452	-1.40174	-0.07393
H	-15.7862	-0.91319	0.42069

H	-14.9173	-3.16504	1.067343
H	-12.4894	-3.58707	1.119092
H	-14.2197	0.895935	-0.1687
H	-7.85233	-1.97951	0.485624
H	-9.57985	2.504329	-0.80056
H	-5.54249	-1.18599	0.184313
H	-4.83837	2.855706	-1.11763
H	-7.24877	3.30456	-1.13765
H	-13.5151	5.909952	-3.54959
H	-12.1281	4.815614	-3.66251
H	-13.7715	4.16311	-3.68402
H	-15.2706	5.946694	-0.90683
H	-14.8519	4.867046	0.431761
H	-15.5186	4.201942	-1.06616
H	-11.928	6.036627	0.47193
H	-10.9508	6.027996	-1.00258
H	-12.3379	7.118382	-0.86831
H	-9.70703	-8.19403	1.209108
H	-11.0979	-7.10669	1.329216
H	-10.1109	-7.11933	-0.13864
H	-6.7778	-7.00991	1.251578
H	-6.53728	-5.26415	1.410064
H	-7.19594	-5.9337	-0.08994
H	-8.29501	-5.2247	4.019903
H	-9.93434	-5.88725	3.994316
H	-8.54032	-6.97346	3.88903
H	15.79845	1.002563	0.38085
H	14.90813	3.242401	1.024235
H	12.46056	3.619155	1.085871
H	14.22783	-0.82534	-0.19107
H	7.826368	1.956686	0.479603
H	9.596305	-2.50125	-0.79685
H	5.519828	1.132414	0.179864
H	4.839597	-2.91688	-1.10427
H	7.265272	-3.33004	-1.12145
H	12.67398	-7.06543	-0.54742
H	12.4691	-5.90346	0.772821
H	11.21717	-6.06379	-0.46608
H	13.23741	-6.0339	-3.47498
H	13.33661	-4.29455	-3.79188
H	11.77819	-5.03444	-3.40317
H	15.22392	-4.56596	0.075781
H	15.45756	-5.72946	-1.23712
H	15.54188	-3.99324	-1.56826
H	7.392043	6.608465	3.537562

H	6.95542	4.983004	2.989673
H	8.344876	5.210415	4.059647
H	10.0241	7.977259	2.442272
H	11.04873	7.114105	1.285955
H	10.96613	6.575055	2.969768
H	7.103919	5.936807	-0.00811
H	7.532978	7.566874	0.531984
H	8.572147	6.711027	-0.61839
H	-3.02907	2.51755	0.24628
H	-0.61215	2.118675	0.262541
H	-1.26162	-1.88641	-1.1517
H	-3.68089	-1.48714	-1.17051
H	1.243704	1.81912	-1.13594
H	3.661906	1.422607	-1.14732
H	3.009051	-2.59062	0.24604
H	0.591057	-2.1943	0.252913

BT4 S_0

Atom	X	Y	Z
C	18.8907	-1.1159	1.062595
C	18.30392	-2.1958	1.782806
C	16.94457	-2.34578	1.817708
C	16.07968	-1.43094	1.13803
C	16.67472	-0.33681	0.407695
C	18.10026	-0.21828	0.398464
C	14.67292	-1.57897	1.169836
C	13.83008	-0.64923	0.481294
C	14.42764	0.447493	-0.25063
C	15.85076	0.587551	-0.27692
C	12.42819	-0.77188	0.49647
C	11.59916	0.130504	-0.16925
C	12.19859	1.222863	-0.90269
C	13.584	1.352728	-0.92248
C	10.17519	0.006997	-0.15758
C	9.361106	0.897242	-0.82115
C	9.975004	1.979844	-1.54653
C	11.33015	2.135587	-1.58344
C	16.43656	1.66398	-0.99812
C	14.08731	-2.65571	1.890237
C	16.93683	2.5912	-1.62067
C	13.57995	-3.58083	2.51028
Si	17.69343	3.985163	-2.55721
Si	12.81655	-4.96865	3.450422
C	16.67512	5.545773	-2.24544

C	19.46502	4.228987	-1.94868
C	17.68806	3.557263	-4.39746
C	13.48222	-4.93968	5.218384
C	10.94217	-4.73234	3.452994
C	13.26568	-6.59913	2.608597
C	-18.8861	1.095292	1.097968
C	-18.2962	2.143507	1.861106
C	-16.9362	2.28424	1.906605
C	-16.0738	1.391287	1.195263
C	-16.672	0.329331	0.421293
C	-18.0981	0.219392	0.40265
C	-14.6665	1.530581	1.237196
C	-13.8263	0.625119	0.51399
C	-14.4268	-0.44007	-0.26086
C	-15.8505	-0.57229	-0.29596
C	-12.4241	0.742361	0.534944
C	-11.5976	-0.13634	-0.16457
C	-12.1997	-1.19844	-0.93906
C	-13.5856	-1.3224	-0.96561
C	-10.1734	-0.01666	-0.14836
C	-9.36129	-0.883	-0.84515
C	-9.97766	-1.93654	-1.61025
C	-11.3332	-2.08742	-1.65309
C	-16.4396	-1.61663	-1.06034
C	-14.0779	2.574067	2.002735
C	-16.9443	-2.51493	-1.7206
C	-13.5685	3.46993	2.662794
Si	-17.7086	-3.8608	-2.71906
Si	-12.8057	4.818459	3.659011
C	-18.3732	-5.18695	-1.54935
C	-19.1154	-3.1284	-3.74591
C	-16.3877	-4.5918	-3.8549
C	-11.024	5.061949	3.080479
C	-13.8003	6.402597	3.393687
C	-12.8386	4.322091	5.481748
C	7.885526	0.760209	-0.8048
C	7.112562	1.087951	-1.932
C	5.72856	0.953242	-1.92177
C	5.049368	0.489508	-0.78242
C	5.821967	0.163869	0.345752
C	7.206002	0.297499	0.335439
C	3.573503	0.353926	-0.77261
C	2.754706	1.269876	-1.45493
C	1.370226	1.140912	-1.45315
C	0.736736	0.089338	-0.76903

C	1.555211	-0.82454	-0.08351
C	2.940097	-0.6954	-0.08519
C	-0.73893	-0.05131	-0.77406
C	-1.4965	0.273728	-1.91205
C	-2.8807	0.141468	-1.91963
C	-3.5747	-0.32453	-0.79005
C	-2.81733	-0.64972	0.34815
C	-1.43294	-0.51553	0.356226
C	-5.05007	-0.46859	-0.80125
C	-5.82004	-0.1935	0.342033
C	-7.20359	-0.33164	0.330717
C	-7.8855	-0.74718	-0.826
C	-7.11507	-1.02646	-1.96774
C	-5.73128	-0.88875	-1.9561
H	19.97101	-1.00739	1.042791
H	18.9418	-2.90195	2.306009
H	16.49231	-3.16565	2.364333
H	18.54048	0.606183	-0.1511
H	11.98557	-1.59596	1.046393
H	14.03477	2.173645	-1.47046
H	9.74069	-0.83597	0.372237
H	9.336738	2.700368	-2.04808
H	11.77293	2.966824	-2.12554
H	17.10139	6.400327	-2.78315
H	15.64084	5.421829	-2.58233
H	16.6517	5.797441	-1.18044
H	19.94889	5.052424	-2.48612
H	20.06731	3.328413	-2.10618
H	19.48967	4.466161	-0.88032
H	18.26245	2.64672	-4.59535
H	16.66986	3.395796	-4.76548
H	18.13238	4.369103	-4.98461
H	13.04799	-5.75373	5.809955
H	14.57043	-5.05764	5.235244
H	13.24075	-3.99598	5.717584
H	10.45105	-5.53977	4.007843
H	10.5402	-4.73473	2.434661
H	10.66139	-3.78452	3.923331
H	12.89531	-6.62874	1.579002
H	14.3498	-6.74767	2.578046
H	12.82626	-7.44587	3.148229
H	-19.9669	0.993855	1.069962
H	-18.9322	2.832841	2.408496
H	-16.4813	3.080134	2.485573
H	-18.5408	-0.58041	-0.18033

H	-11.9792	1.5434	1.116166
H	-14.0386	-2.11947	-1.54603
H	-9.73716	0.805317	0.412065
H	-9.34111	-2.63917	-2.13865
H	-11.778	-2.89634	-2.22643
H	-18.8368	-6.00391	-2.11411
H	-17.5721	-5.61357	-0.93757
H	-19.129	-4.77701	-0.87185
H	-19.594	-3.90399	-4.35464
H	-18.748	-2.34988	-4.42199
H	-19.885	-2.6818	-3.10821
H	-15.9788	-3.83098	-4.52743
H	-15.5568	-5.01489	-3.28104
H	-16.8087	-5.393	-4.47279
H	-10.5375	5.86093	3.651477
H	-10.4335	4.149771	3.214316
H	-10.9834	5.335244	2.021277
H	-13.371	7.230558	3.96919
H	-14.8406	6.279076	3.711616
H	-13.8058	6.694721	2.338814
H	-12.2796	3.396433	5.651718
H	-12.39	5.104723	6.104241
H	-13.8634	4.161815	5.83148
H	7.604764	1.41745	-2.84193
H	5.166861	1.179874	-2.82293
H	5.327238	-0.16069	1.256214
H	7.768593	0.075487	1.237136
H	3.208189	2.114643	-1.96455
H	0.767701	1.887948	-1.96097
H	1.101894	-1.66931	0.426307
H	3.542883	-1.44199	0.423129
H	-0.99177	0.61789	-2.80966
H	-3.4352	0.420135	-2.81058
H	-3.31889	-1.0296	1.233153
H	-0.88132	-0.75917	1.259263
H	-5.32826	0.147755	1.248002
H	-7.76574	-0.13094	1.237688
H	-7.60761	-1.33792	-2.88382
H	-5.16699	-1.13022	-2.85174

BT4 T_1

Atom	X	Y	Z
C	18.88389	-1.14043	1.106666
C	18.2889	-2.22112	1.81892

C	16.9289	-2.3671	1.843929
C	16.07162	-1.44696	1.161685
C	16.67488	-0.35173	0.43978
C	18.1008	-0.23782	0.440596
C	14.66431	-1.59106	1.183002
C	13.82902	-0.65587	0.49267
C	14.43474	0.441415	-0.23171
C	15.85838	0.577801	-0.24688
C	12.42676	-0.77365	0.498789
C	11.60496	0.133378	-0.16943
C	12.21247	1.225081	-0.89716
C	13.59845	1.350651	-0.90749
C	10.18058	0.015302	-0.16555
C	9.373395	0.909665	-0.8319
C	9.995148	1.99056	-1.55302
C	11.3511	2.141514	-1.58202
C	16.45235	1.656428	-0.95801
C	14.07094	-2.6704	1.893102
C	16.96041	2.585918	-1.57078
C	13.55714	-3.59871	2.502996
Si	17.72934	3.981513	-2.49494
Si	12.79075	-4.99677	3.42538
C	16.57745	4.475428	-3.90853
C	17.97617	5.434637	-1.31302
C	19.39365	3.407084	-3.17985
C	14.08136	-5.72144	4.598968
C	11.31443	-4.33852	4.403877
C	12.22132	-6.30598	2.188086
C	-18.9051	1.080376	1.185793
C	-18.3247	2.11294	1.921187
C	-16.9371	2.255986	1.939811
C	-16.1029	1.377986	1.229837
C	-16.6969	0.322027	0.476949
C	-18.0948	0.19657	0.472582
C	-14.6527	1.527253	1.249581
C	-13.8113	0.615325	0.514955
C	-14.4177	-0.45985	-0.25148
C	-15.8501	-0.60126	-0.26971
C	-12.4256	0.73708	0.519214
C	-11.5736	-0.15323	-0.19658
C	-12.1732	-1.20855	-0.95311
C	-13.5885	-1.33047	-0.95484
C	-10.172	-0.02121	-0.18858
C	-9.34556	-0.89482	-0.90124
C	-9.95616	-1.93434	-1.64509

C	-11.3311	-2.0866	-1.66916
C	-16.4426	-1.63468	-1.01449
C	-14.0747	2.569339	1.992691
C	-16.9633	-2.53646	-1.66762
C	-13.5724	3.482756	2.644427
Si	-17.7438	-3.88106	-2.65265
Si	-12.8278	4.854573	3.620142
C	-19.1616	-3.14823	-3.66437
C	-16.4387	-4.61981	-3.80205
C	-18.4005	-5.20401	-1.47409
C	-11.681	4.120254	4.930584
C	-11.8517	5.973527	2.451237
C	-14.2194	5.828136	4.447197
C	7.897287	0.777947	-0.82183
C	7.129825	1.105236	-1.95288
C	5.745445	0.973249	-1.94823
C	5.060527	0.513216	-0.81079
C	5.82766	0.189374	0.321641
C	7.211947	0.319945	0.31682
C	3.584547	0.378495	-0.80658
C	2.768347	1.291481	-1.49595
C	1.383767	1.162808	-1.49838
C	0.747753	0.114732	-0.81127
C	1.563637	-0.7964	-0.11908
C	2.94849	-0.66776	-0.11688
C	-0.72788	-0.02584	-0.81949
C	-1.48261	0.290625	-1.96177
C	-2.86665	0.156493	-1.97234
C	-3.56318	-0.30237	-0.84136
C	-2.80867	-0.61799	0.30147
C	-1.42452	-0.48236	0.312339
C	-5.03795	-0.45068	-0.85532
C	-5.81175	-0.16777	0.283362
C	-7.19487	-0.31029	0.269838
C	-7.87243	-0.7419	-0.8839
C	-7.09812	-1.02447	-2.02264
C	-5.7152	-0.88215	-2.00871
H	19.96466	-1.03543	1.094312
H	18.92101	-2.93112	2.343908
H	16.47044	-3.18755	2.384521
H	18.54733	0.586943	-0.1034
H	11.97809	-1.59763	1.043896
H	14.05547	2.171007	-1.45115
H	9.739921	-0.8267	0.360692
H	9.362197	2.713686	-2.05759

H	11.79994	2.971618	-2.12085
H	17.00419	5.304947	-4.4837
H	16.41343	3.640028	-4.59651
H	15.60083	4.797675	-3.53307
H	18.43485	6.283251	-1.83339
H	18.62939	5.160226	-0.47864
H	17.02332	5.773118	-0.89386
H	20.07362	3.108497	-2.37547
H	19.27255	2.551073	-3.85121
H	19.87781	4.211397	-3.74533
H	13.65814	-6.55169	5.175683
H	14.94825	-6.10393	4.050572
H	14.43854	-4.96874	5.308981
H	10.83703	-5.1441	4.973364
H	10.55846	-3.90539	3.740944
H	11.62171	-3.56306	5.112653
H	11.48268	-5.89857	1.490465
H	13.061	-6.68898	1.599537
H	11.76036	-7.1539	2.707456
H	-19.9839	0.959274	1.164118
H	-18.9453	2.806907	2.47988
H	-16.4814	3.057709	2.510752
H	-18.5419	-0.60796	-0.10117
H	-11.9746	1.541476	1.091591
H	-14.0416	-2.13282	-1.52841
H	-9.73198	0.802293	0.366555
H	-9.33095	-2.64107	-2.1814
H	-11.7776	-2.89785	-2.23792
H	-19.6515	-3.92518	-4.26243
H	-19.9207	-2.69569	-3.01827
H	-18.801	-2.37442	-4.34936
H	-16.8695	-5.42158	-4.41249
H	-15.6026	-5.04385	-3.23657
H	-16.0354	-3.86234	-4.48163
H	-17.5943	-5.63473	-0.87196
H	-19.1462	-4.79033	-0.78773
H	-18.8749	-6.01845	-2.03358
H	-11.2178	4.91468	5.526862
H	-12.2293	3.464158	5.614021
H	-10.878	3.532278	4.474769
H	-11.3922	6.80237	3.001837
H	-12.4997	6.401538	1.679793
H	-11.0514	5.422472	1.947193
H	-14.802	5.192145	5.121311
H	-13.8131	6.657199	5.037574

H	-14.9056	6.250204	3.706065
H	7.626634	1.431772	-2.8614
H	5.18812	1.198815	-2.85237
H	5.328432	-0.13159	1.230908
H	7.770329	0.099144	1.221428
H	3.223757	2.13383	-2.00784
H	0.78308	1.907509	-2.01181
H	1.108292	-1.63869	0.393012
H	3.549314	-1.41239	0.396578
H	-0.97565	0.629053	-2.86032
H	-3.41899	0.427846	-2.8669
H	-3.31231	-0.99208	1.18775
H	-0.87506	-0.71898	1.218548
H	-5.32348	0.184073	1.187172
H	-7.75865	-0.10204	1.174115
H	-7.58867	-1.34245	-2.93751
H	-5.148	-1.12729	-2.90151

5.14 NMR Spectra

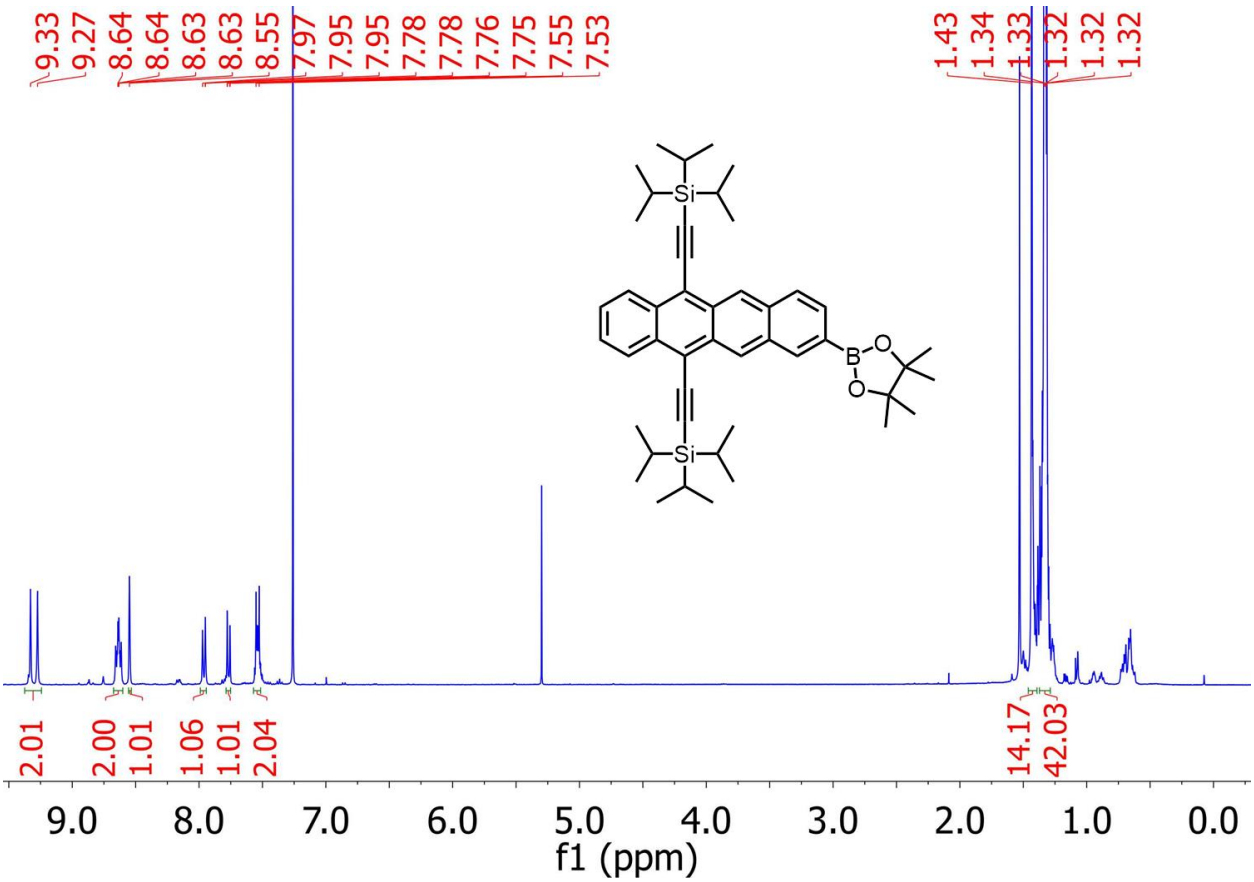

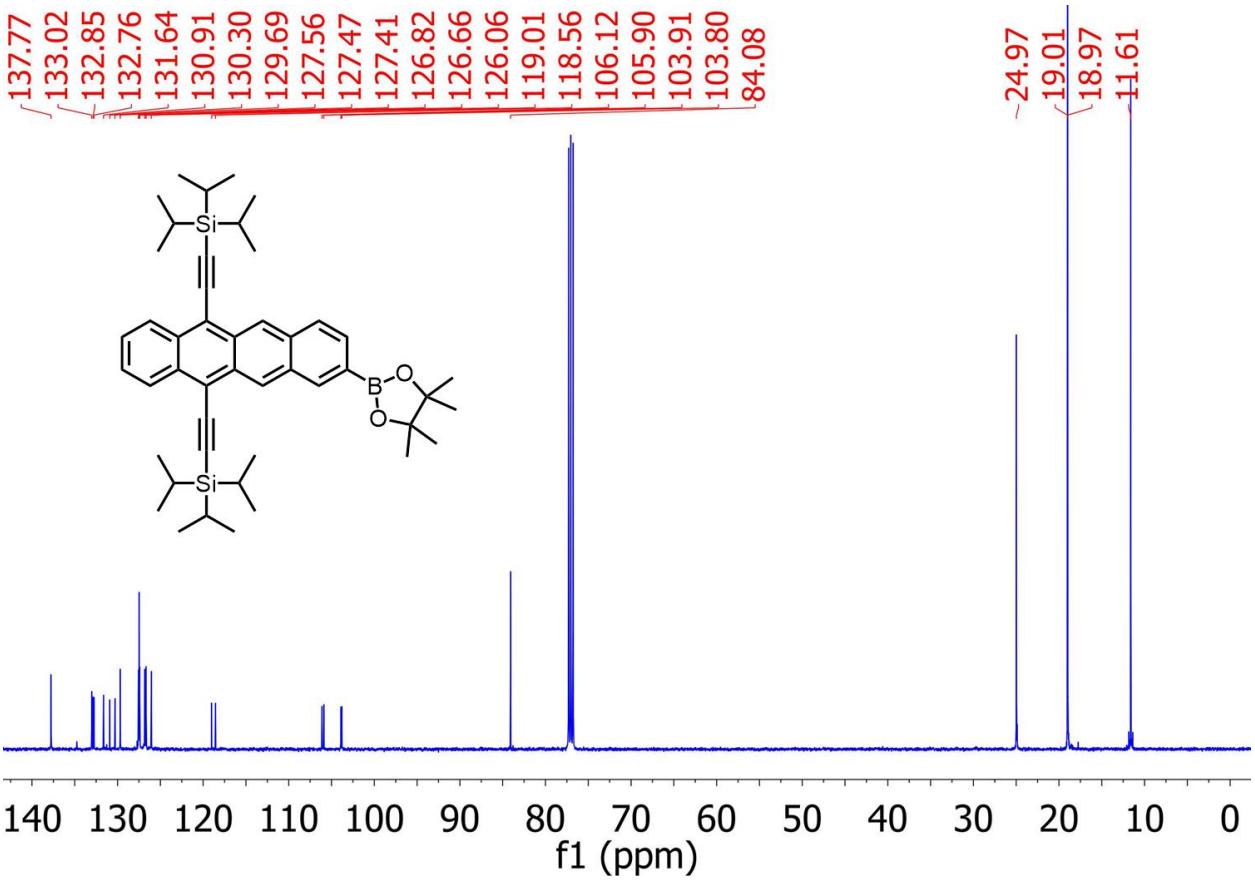
137.77
133.02
132.85
132.76
131.64
130.91
130.30
129.69
127.56
127.47
127.41
126.82
126.66
126.06
119.01
118.56
106.12
105.90
103.91
103.80
84.08
24.97
19.01
18.97
11.61
Si
Si
B
O
O
140 130 120 110 100 90 80 70 60 50 40 30 20 10 0
f1 (ppm)

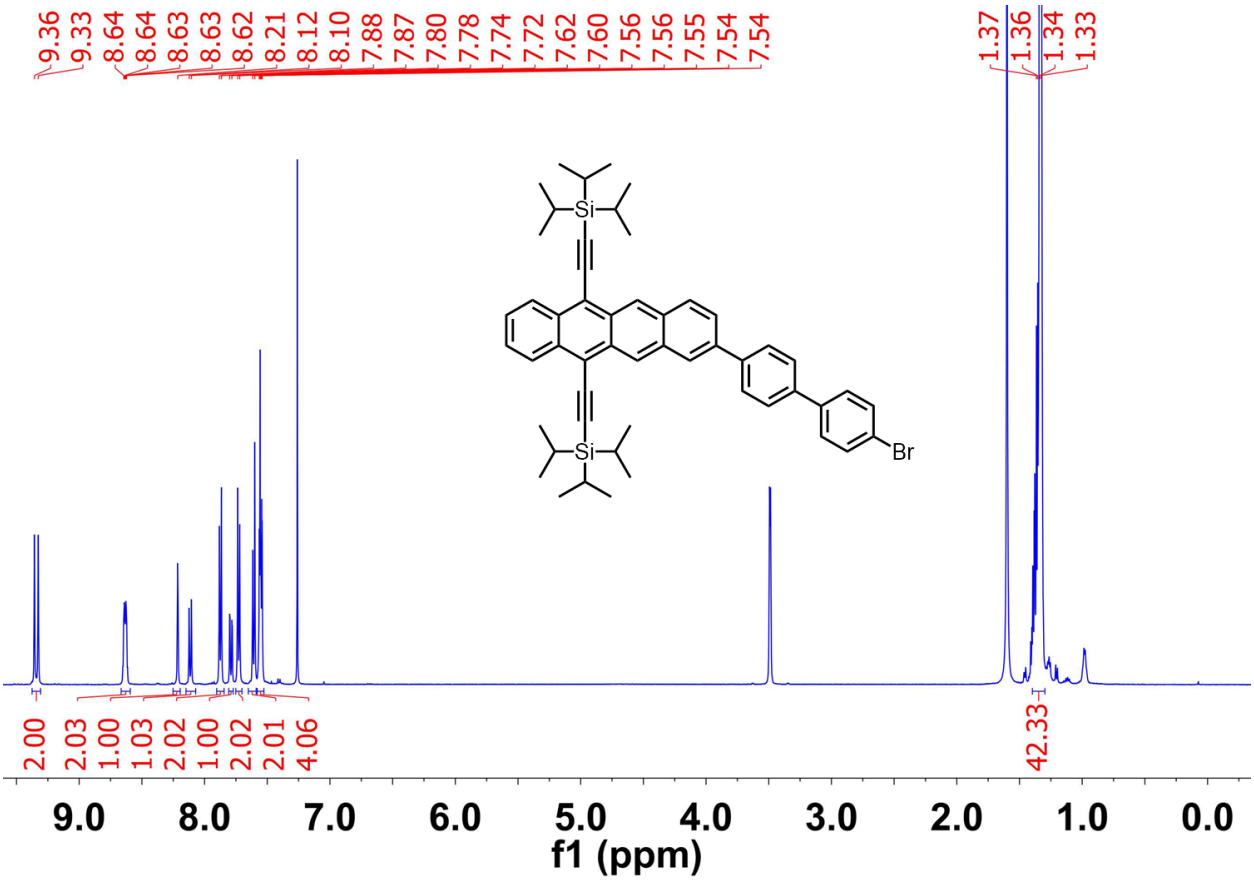
9.36
9.33
8.64
8.64
8.63
8.63
8.62
8.21
8.12
8.10
7.88
7.87
7.80
7.78
7.74
7.72
7.62
7.60
7.56
7.56
7.55
7.54
7.54
1.37
1.36
1.34
1.33
Si
Si
Br
2.00
2.03
1.00
1.03
2.02
1.00
2.02
2.01
4.06
42.33
9.0
8.0
7.0
6.0
5.0
4.0
3.0
2.0
1.0
0.0
f1 (ppm)

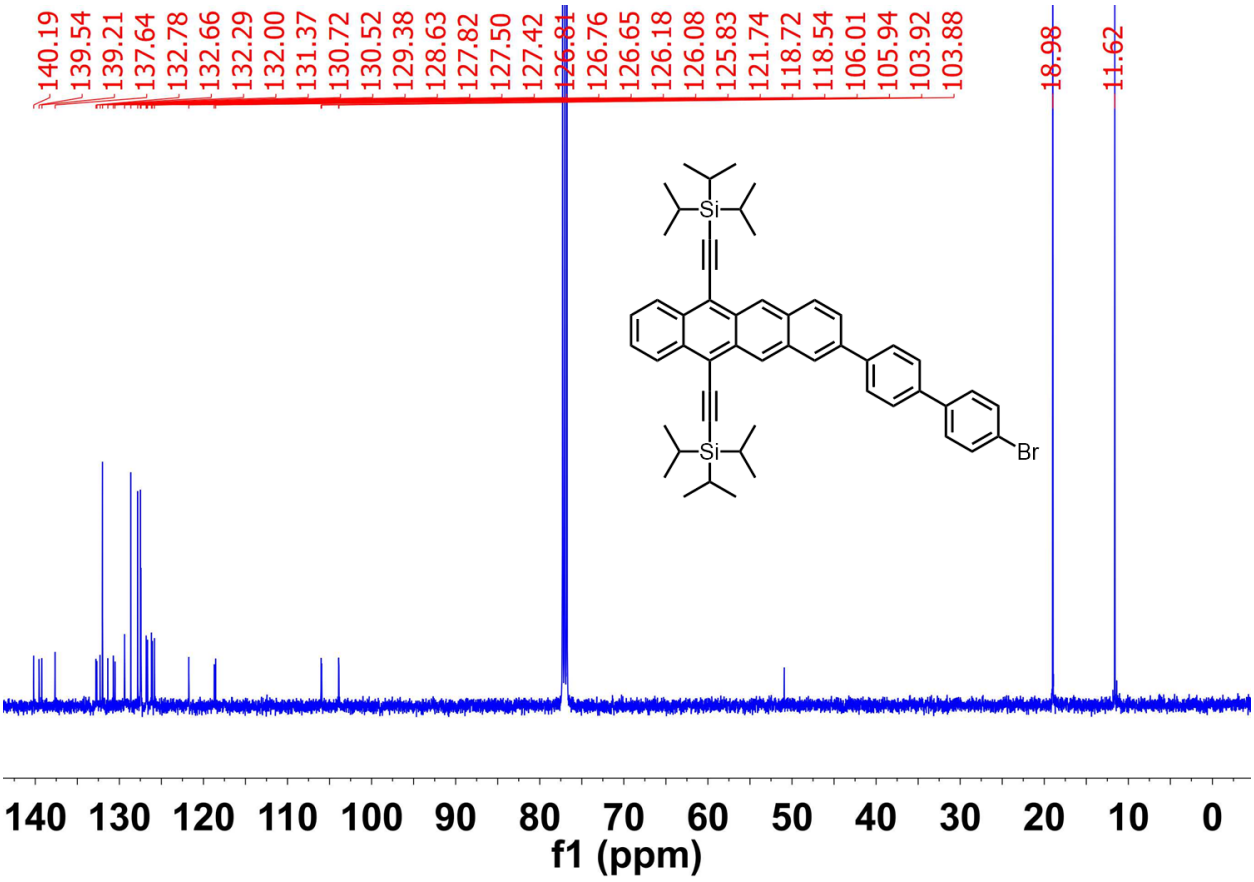
140.19
139.54
139.21
137.64
132.78
132.66
132.29
132.00
131.37
130.72
130.52
129.38
128.63
127.82
127.50
127.42
126.81
126.76
126.65
126.18
126.08
125.83
121.74
118.72
118.54
106.01
105.94
103.92
103.88
18.98
11.62
Si
Si
Br
140 130 120 110 100 90 80 70 60 50 40 30 20 10 0
f1 (ppm)

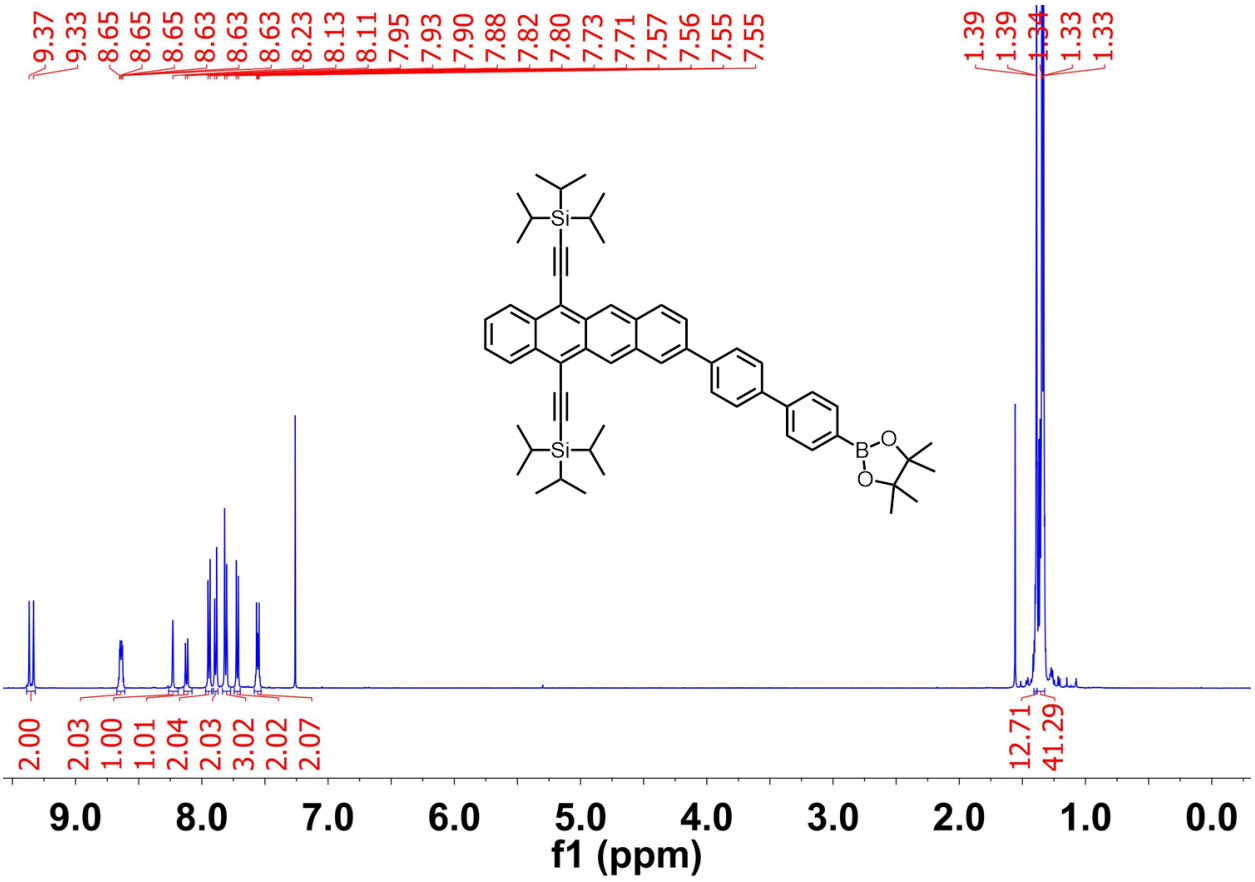
9.37
9.33
8.65
8.65
8.65
8.63
8.63
8.63
8.23
8.13
8.11
7.95
7.93
7.90
7.88
7.82
7.80
7.73
7.71
7.57
7.56
7.55
7.55
1.39
1.39
1.34
1.33
1.33
Si
Si
B
O
O
2.00
2.03
1.00
1.01
2.04
2.03
3.02
2.02
2.07
12.71
41.29
9.0
8.0
7.0
6.0
5.0
4.0
3.0
2.0
1.0
0.0
f1 (ppm)

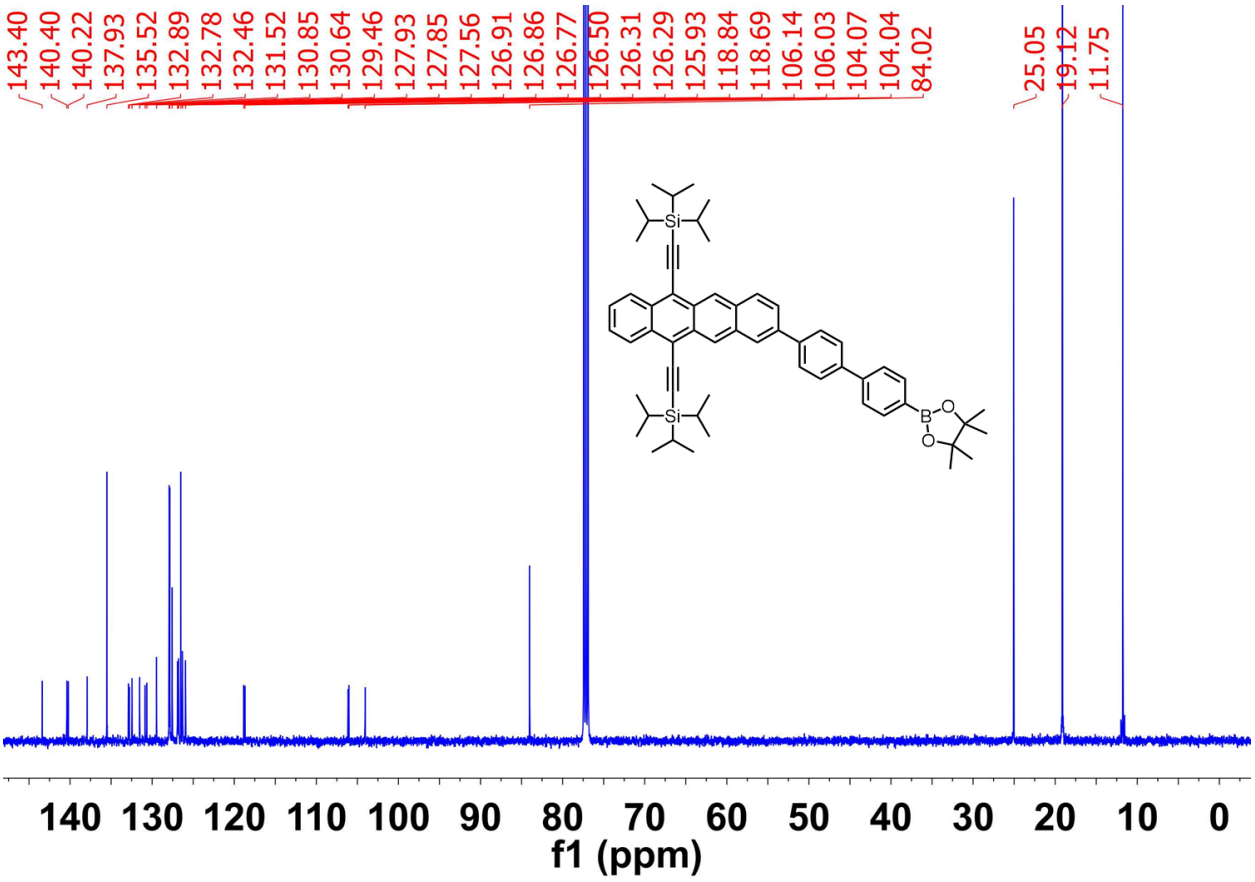
143.40
140.40
140.22
137.93
135.52
132.89
132.78
132.46
131.52
130.85
130.64
129.46
127.93
127.85
127.56
126.91
126.86
126.77
126.50
126.31
126.29
125.93
118.84
118.69
106.14
106.03
104.07
104.04
84.02
25.05
19.12
11.75
Si
Si
B
O
O
140 130 120 110 100 90 80 70 60 50 40 30 20 10 0
f1 (ppm)

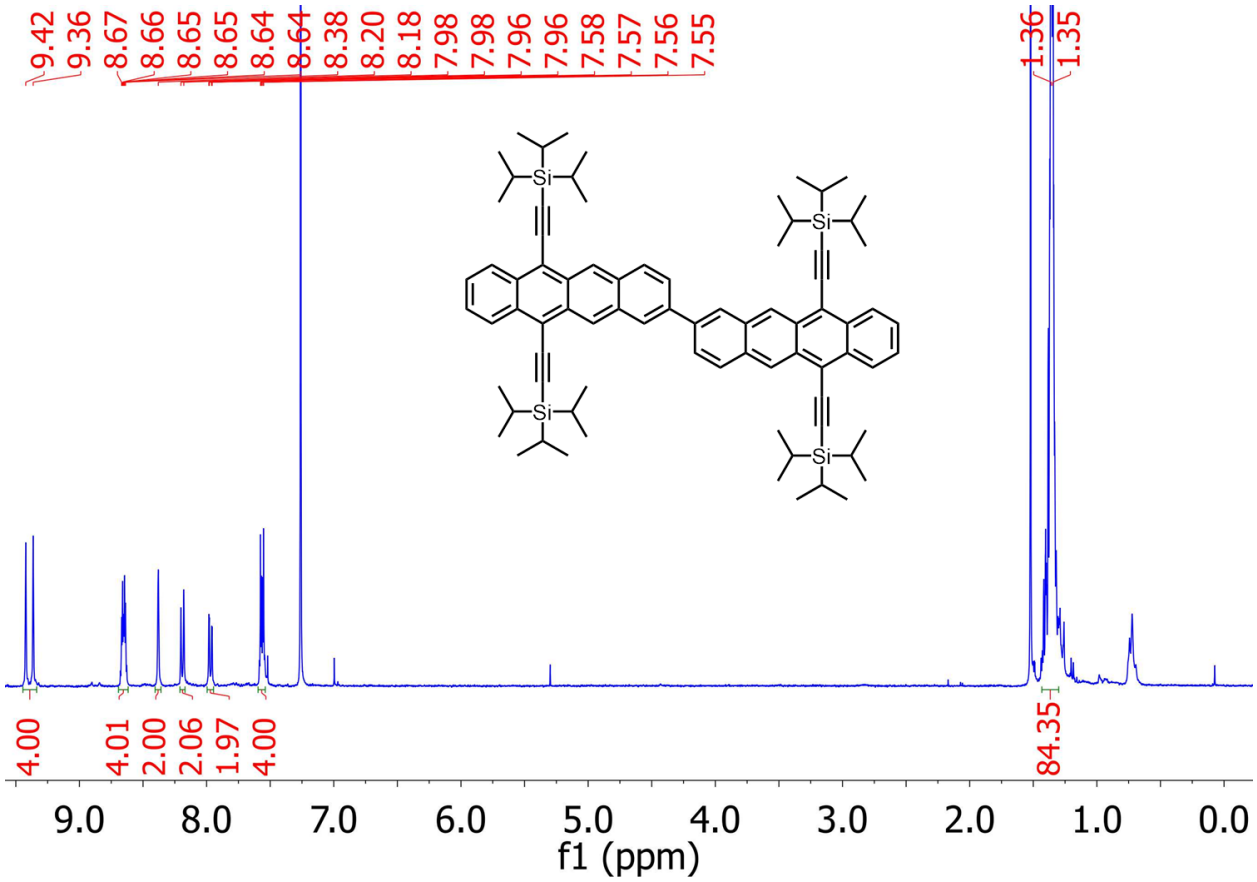
9.42
9.36
8.67
8.66
8.65
8.65
8.64
8.64
8.38
8.20
8.18
7.98
7.98
7.96
7.96
7.58
7.57
7.56
7.55
1.36
1.35
Si
Si
Si
Si
4.00
4.01
2.00
2.06
1.97
4.00
84.35
9.0
8.0
7.0
6.0
5.0
4.0
3.0
2.0
1.0
0.0
f1 (ppm)

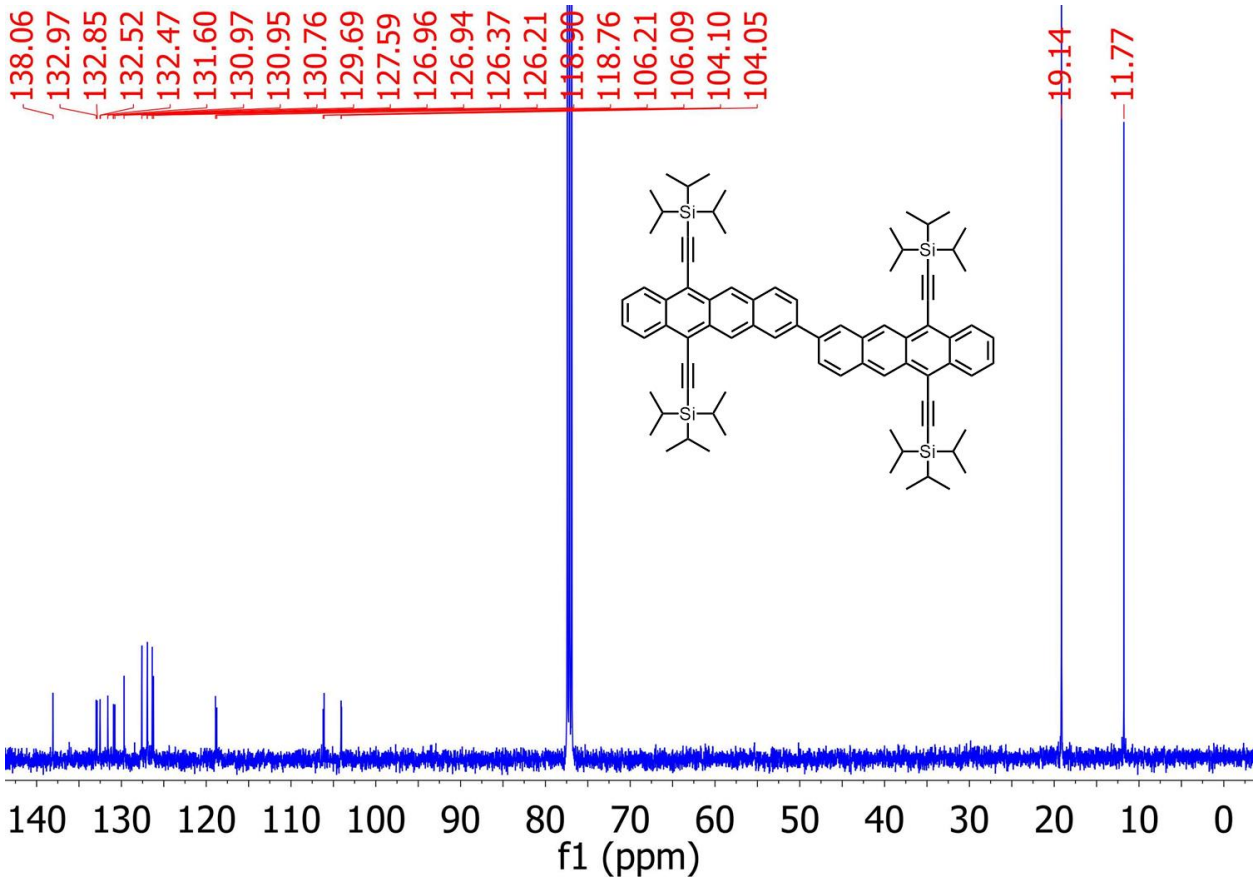
138.06
132.97
132.85
132.52
132.47
131.60
130.97
130.95
130.76
129.69
127.59
126.96
126.94
126.37
126.21
118.90
118.76
106.21
106.09
104.10
104.05
19.14
11.77
Si
Si
Si
Si
140 130 120 110 100 90 80 70 60 50 40 30 20 10 0
f1 (ppm)

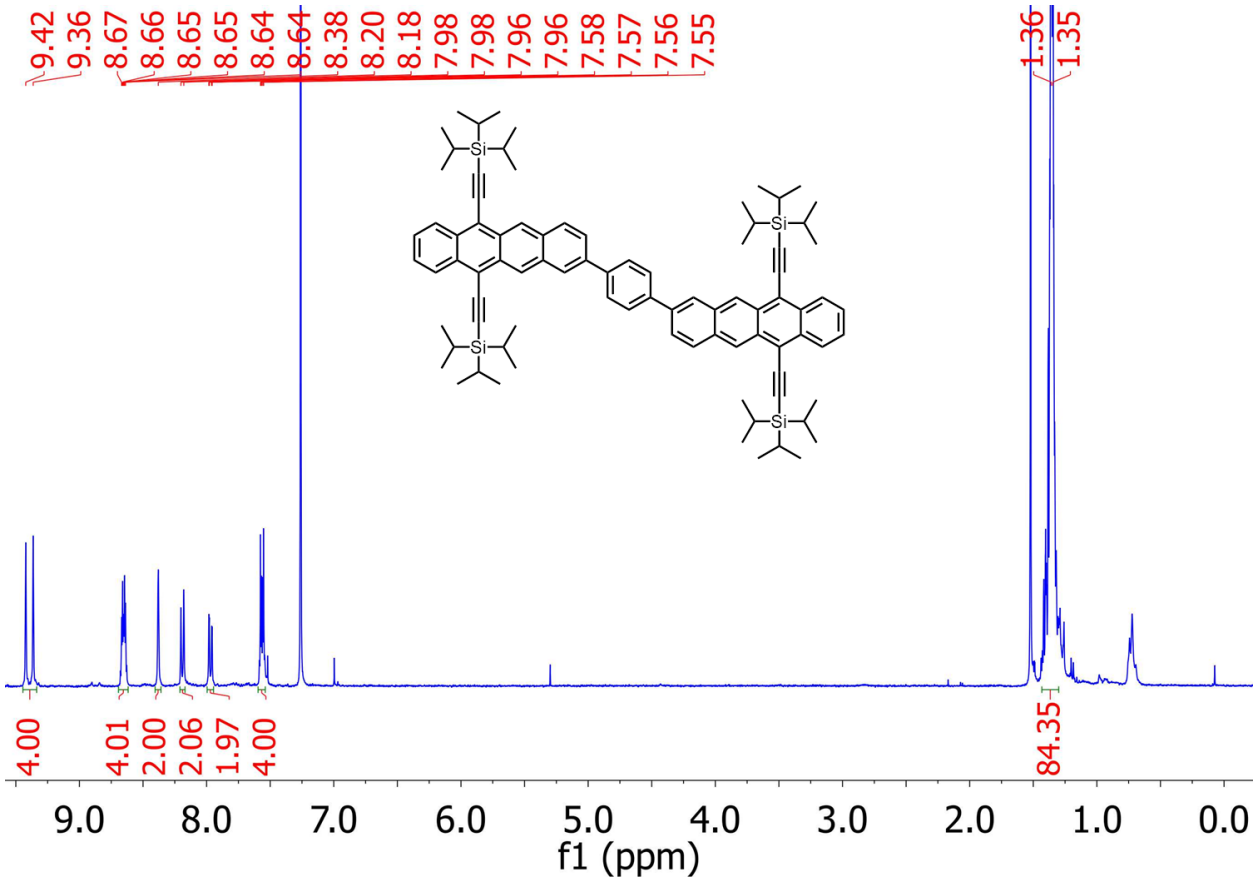
9.42
9.36
8.67
8.66
8.65
8.65
8.64
8.64
8.38
8.20
8.18
7.98
7.98
7.96
7.96
7.58
7.57
7.56
7.55
1.36
1.35
Si
Si
Si
Si
4.00
4.01
2.00
2.06
1.97
4.00
84.35
9.0
8.0
7.0
6.0
5.0
4.0
3.0
2.0
1.0
0.0
f1 (ppm)

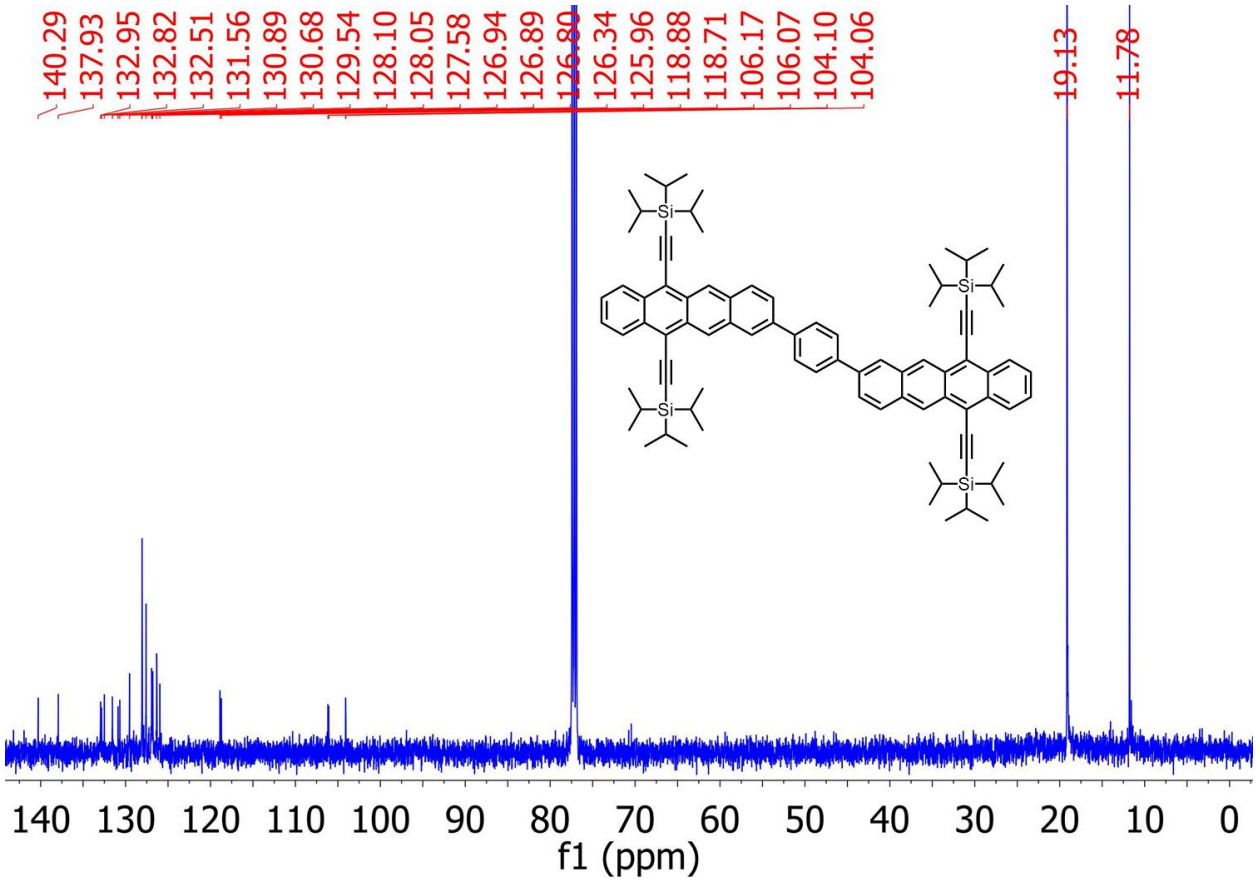
140.29
137.93
132.95
132.82
132.51
131.56
130.89
130.68
129.54
128.10
128.05
127.58
126.94
126.89
126.80
126.34
125.96
118.88
118.71
106.17
106.07
104.10
104.06
19.13
11.78
Si
Si
Si
Si
140 130 120 110 100 90 80 70 60 50 40 30 20 10 0
f1 (ppm)

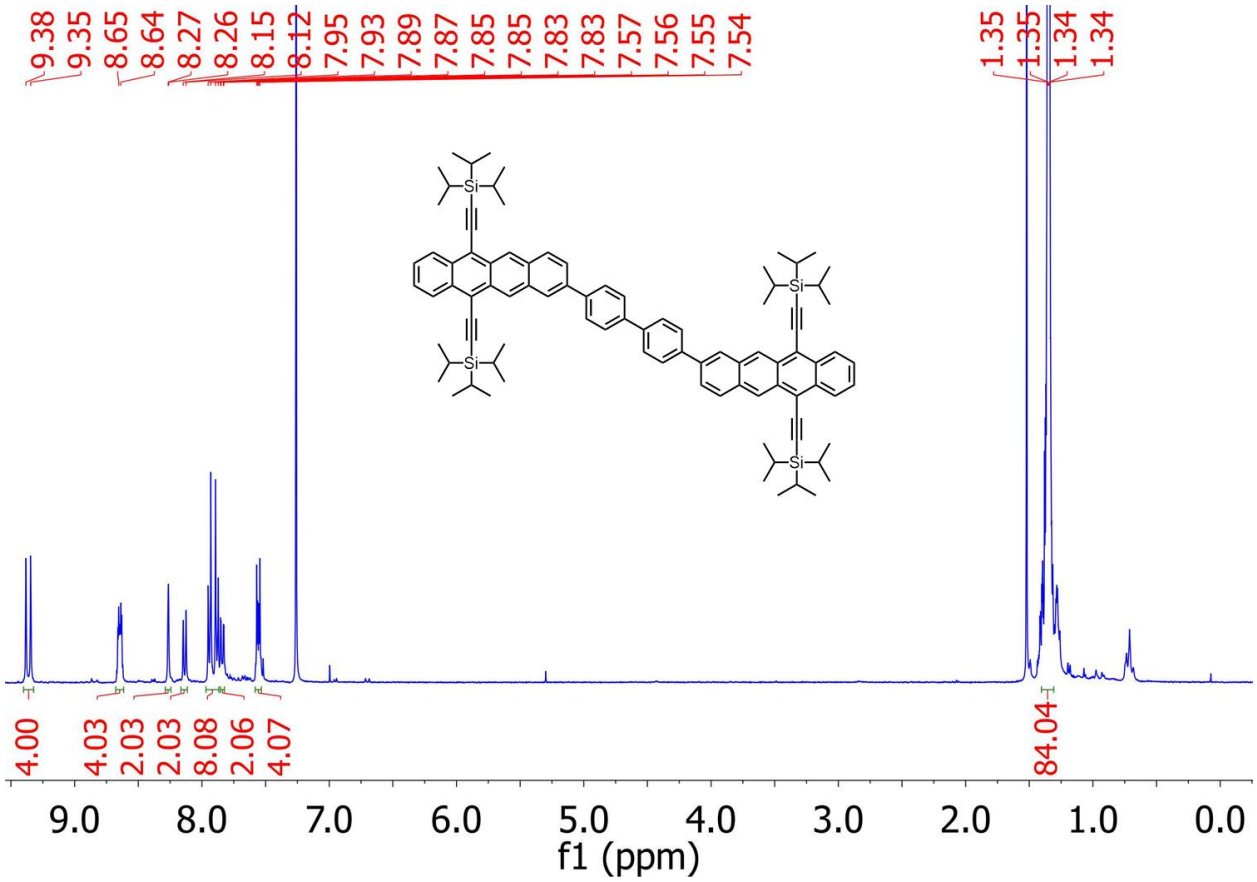
9.38
9.35
8.65
8.64
8.27
8.26
8.15
8.12
7.95
7.93
7.89
7.87
7.85
7.85
7.83
7.83
7.57
7.56
7.55
7.54
1.35
1.35
1.34
1.34
Si
Si
Si
Si
4.00
4.03
2.03
2.03
8.08
2.06
4.07
84.04
9.0
8.0
7.0
6.0
5.0
4.0
3.0
2.0
1.0
0.0
f1 (ppm)

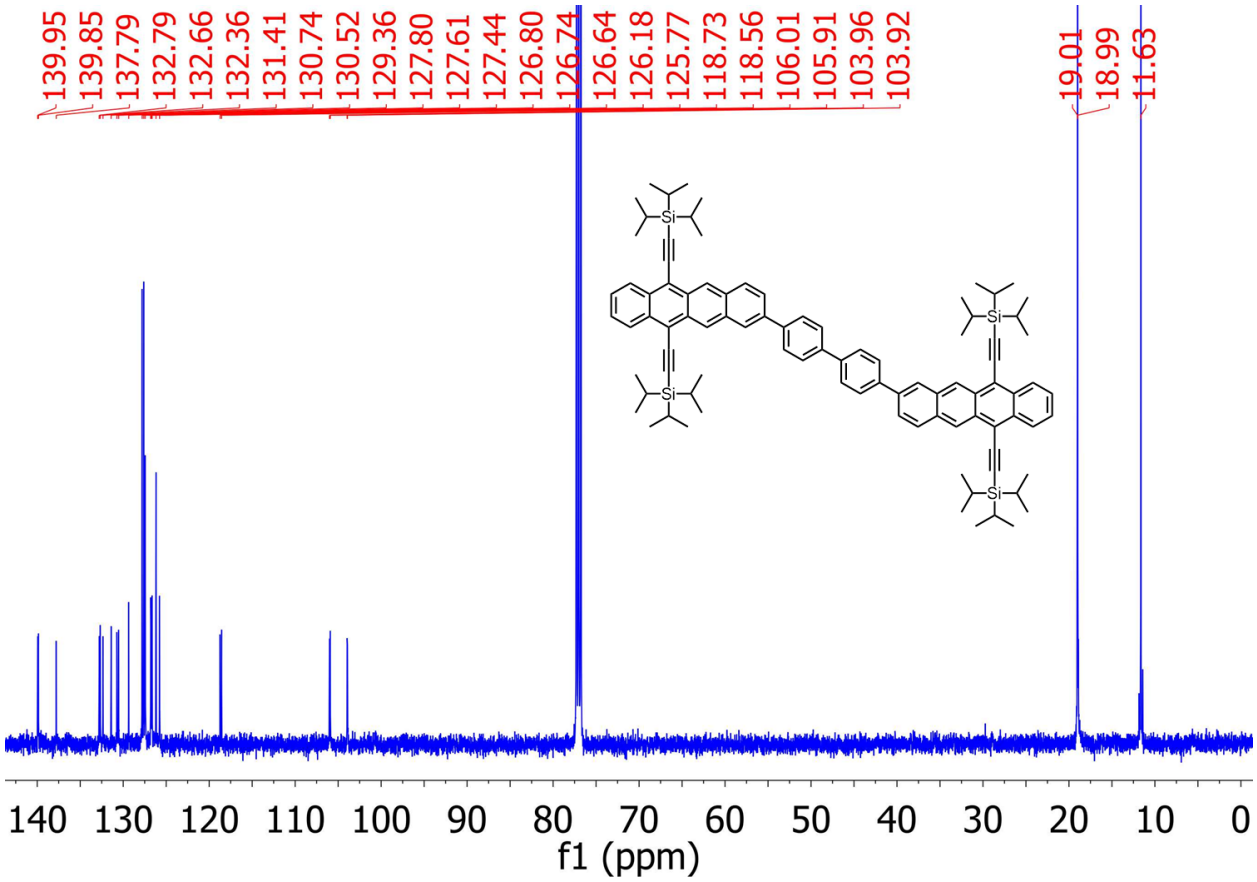
139.95
139.85
137.79
132.79
132.66
132.36
131.41
130.74
130.52
129.36
127.80
127.61
127.44
126.80
126.74
126.64
126.18
125.77
118.73
118.56
106.01
105.91
103.96
103.92
19.01
18.99
11.63
Si
Si
Si
Si
140 130 120 110 100 90 80 70 60 50 40 30 20 10 0
f1 (ppm)

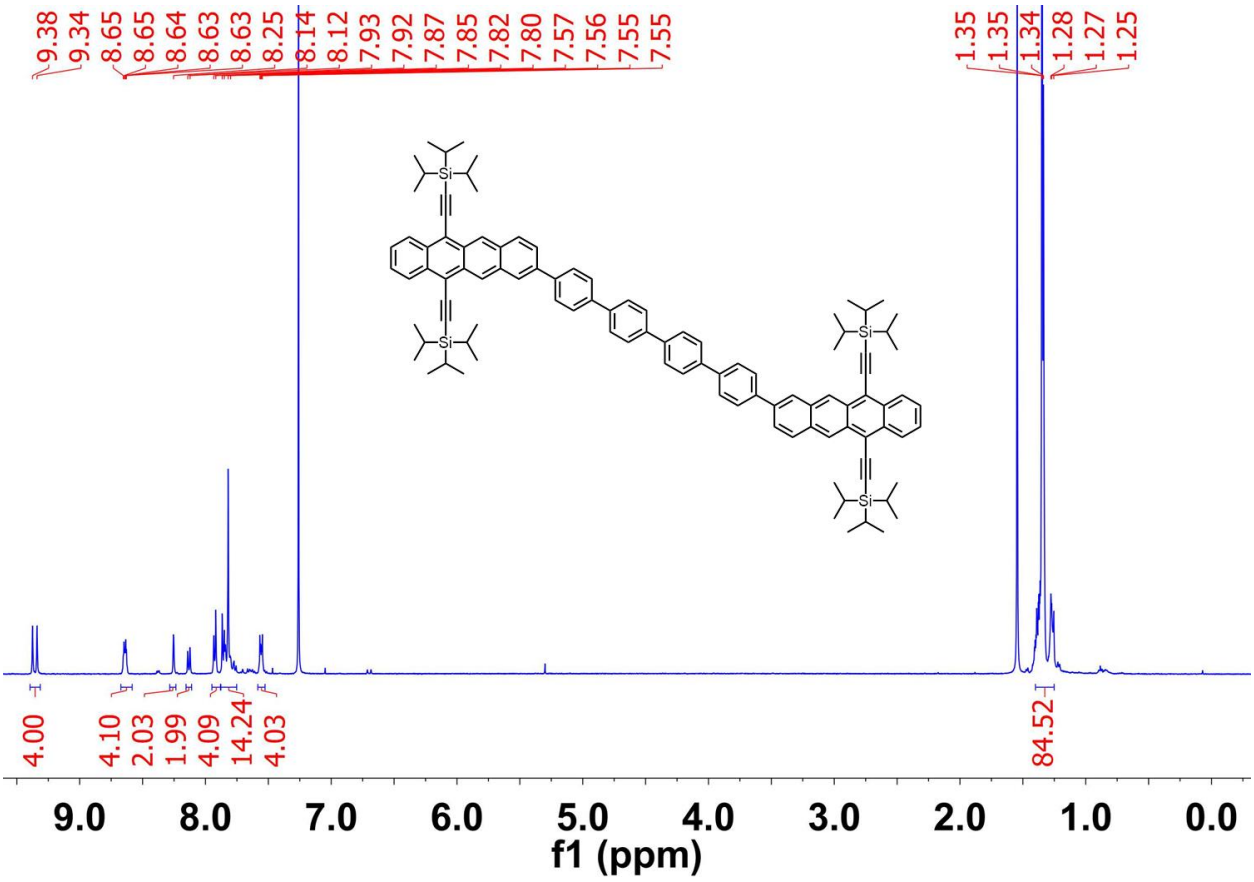

5.15 Outlook

One of the largest challenges that this project faced is conclusively proving that iTF is occurring. We were able to show it with deductive reasoning, demonstrating that our enhanced upconversion was not being caused by factors such as triplet lifetime or rates of triplet energy transfer. This was backed up further by the kinetic modeling that Dan did. I am confident iTF is occurring in our materials, but it still would be nice to have an individual experiment that demonstrates that it is occurring. Any attempts to design a molecule that makes xTF more difficult would also reduce the efficiency of the sensitization event. It could be possible to get around this by covalently linking an iTF annihilator to a sensitizer. The length of the covalent link between annihilator and sensitizer would need to be long enough to prevent the sensitizer from absorbing the photon the annihilator emits. Measuring this would still require a detector

sensitive enough to pick up the photons emitted from a single annihilator, and the singlet on the annihilator does not last long enough to observe via transient absorption.

On that note, nearly every time I have presented this material to a new audience, I get asked about covalently linking annihilators to sensitizers. This has been attempted by various groups (Yoan Simon, Ronald Steer) but there is no significant increase in UCPL seen when this is done. I believe you could observe enhanced UCPL by carefully designing a molecule as described above, with a long tether between a sensitizing chromophore and the annihilator chromophores. The tether would need to be tuned appropriately, as would the chromophores in all likelihood, but it seems like a problem that can be solved despite previous attempts.

Future work related to this project could involve further tuning the bridge between chromophores. One phenylene was the best we demonstrated, but that was only among comparing oligophenylenes. The length of the oligomer for TF upconversion could also be increased to observe if there is any effect. And while work with anthracene shows no significant enhancement to UCPL because the system is already so efficient, expanding iTF to other upconversion chromophores could be tried.

5.16 References

(1) Pun, A. B.; Sanders, S. N.; Sfeir, M. Y.; Campos, L. M.; Congreve, D. N. Annihilator Dimers Enhance Triplet Fusion Upconversion. *Chem. Sci.* **2019**, *10* (14), 3969–3975.

(2) Schulze, T. F.; Schmidt, T. W. Photochemical Upconversion: Present Status and Prospects for Its Application to Solar Energy Conversion. *Energy Environ. Sci.* **2015**, *8* (1), 103–125.

(3) Ravetz, B. D.; Pun, A. B.; Churchill, E. M.; Congreve, D. N.; Rovis, T.; Campos, L. M. Photoredox Catalysis Using Infrared Light via Triplet Fusion Upconversion. *Nature* **2019**, *565*, 343–346.

(4) Zhou, Y.; Han, S.-T.; Chen, X.; Wang, F.; Tang, Y.-B.; Roy, V. A. L. An Upconverted Photonic Nonvolatile Memory. *Nat. Commun.* **2014**, *5*, 4720.

(5) Liu, S.-W.; Lee, C.-C.; Yuan, C.-H.; Su, W.-C.; Lin, S.-Y.; Chang, W.-C.; Huang, B.-Y.; Lin, C.-F.; Lee, Y.-Z.; … Chen, K.-T. Transparent Organic Upconversion Devices for Near-Infrared Sensing. *Adv. Mater.* **2015**, *27* (7), 1217–1222.

(6) Park, Y. Il; Lee, K. T.; Suh, Y. D.; Hyeon, T. Upconverting Nanoparticles: A Versatile

Platform for Wide-Field Two-Photon Microscopy and Multi-Modal in Vivo Imaging. *Chem. Soc. Rev.* **2015**, *44* (6), 1302–1317.
(7) Schmidt, T. W.; Castellano, F. N. Photochemical Upconversion: The Primacy of Kinetics. *J. Phys. Chem. Lett.* **2014**, *5* (22), 4062–4072.
(8) Zhou, J.; Liu, Q.; Feng, W.; Sun, Y.; Li, F. Upconversion Luminescent Materials: Advances and Applications. *Chem. Rev.* **2015**, *115* (1), 395–465.
(9) Goldschmidt, J. C.; Fischer, S. Upconversion for Photovoltaics – a Review of Materials, Devices and Concepts for Performance Enhancement. *Adv. Opt. Mater.* **2015**, *3* (4), 510–535.
(10) Bharmoria, P.; Hisamitsu, S.; Nagatomi, H.; Ogawa, T.; Morikawa, M.; Yanai, N.; Kimizuka, N. Simple and Versatile Platform for Air-Tolerant Photon Upconverting Hydrogels by Biopolymer–Surfactant–Chromophore Co-Assembly. *J. Am. Chem. Soc.* **2018**.
(11) Agrawal, U.; Reilly, D. T.; Schroeder, C. M. Zooming in on Biological Processes with Fluorescence Nanoscopy. *Curr. Opin. Biotechnol.* **2013**, *24* (4), 646–653.
(12) Askes, S. H. C.; Bahreman, A.; Bonnet, S. Activation of a Photodissociative Ruthenium Complex by Triplet–Triplet Annihilation Upconversion in Liposomes. *Angew. Chem. Int. Ed.* **2014**, *53* (4), 1029–1033.
(13) Singh-Rachford, T. N.; Castellano, F. N. Photon Upconversion Based on Sensitized Triplet–triplet Annihilation. *Coord. Chem. Rev.* **2010**, *254* (21–22), 2560–2573.
(14) Baluschev, S.; Miteva, T.; Yakutkin, V.; Nelles, G.; Yasuda, A.; Wegner, G. Up-Conversion Fluorescence: Noncoherent Excitation by Sunlight. *Phys. Rev. Lett.* **2006**, *97* (14), 143903.
(15) Wu, M.; Congreve, D. N.; Wilson, M. W. B.; Jean, J.; Geva, N.; Welborn, M.; Van Voorhis, T.; Bulović, V.; Bawendi, M. G.; Baldo, M. A. Solid-State Infrared-to-Visible Upconversion Sensitized by Colloidal Nanocrystals. *Nat. Photonics* **2016**, *10* (1), 31–34.
(16) Huang, Z.; Li, X.; Mahboub, M.; Hanson, K. M.; Nichols, V. M.; Le, H.; Tang, M. L.; Bardeen, C. J. Hybrid Molecule-Nanocrystal Photon Upconversion Across the Visible and Near-Infrared. *Nano Lett.* **2015**, *15* (8), 5552–5557.
(17) Huang, Z.; Li, X.; Yip, B. D.; Rubalcava, J. M.; Bardeen, C. J.; Tang, M. L. Nanocrystal Size and Quantum Yield in the Upconversion of Green to Violet Light with CdSe and Anthracene Derivatives. *Chem. Mater.* **2015**, *27* (21), 7503–7507.
(18) Gray, V.; Xia, P.; Huang, Z.; Moses, E.; Fast, A.; Fishman, D. A.; Vullev, V. I.; Abrahamsson, M.; Moth-Poulsen, K.; Lee Tang, M. CdS/ZnS Core-Shell Nanocrystal Photosensitizers for Visible to UV Upconversion. *Chem. Sci.* **2017**, *8* (8), 5488–5496.
(19) Dzebo, D.; Börjesson, K.; Gray, V.; Moth-Poulsen, K.; Albinsson, B. Intramolecular Triplet–Triplet Annihilation Upconversion in 9,10-Diphenylanthracene Oligomers and Dendrimers. *J. Phys. Chem. C* **2016**, *120* (41), 23397–23406.
(20) Baluschev, S.; Yakutkin, V.; Miteva, T.; Avlasevich, Y.; Chernov, S.; Aleshchenkov, S.; Nelles, G.; Cheprakov, A.; Yasuda, A.; … Wegner, G. Blue-Green Up-Conversion: Noncoherent Excitation by NIR Light. *Angew. Chem. Int. Ed.* **2007**, *46* (40), 7693–7696.
(21) Thévenaz, D. C.; Lee, S. H.; Guignard, F.; Balog, S.; Lattuada, M.; Weder, C.; Simon, Y. C. Single-Component Upconverting Polymeric Nanoparticles. *Macromol. Rapid Commun.* **2016**, *37* (10), 826–832.
(22) Duan, P.; Yanai, N.; Nagatomi, H.; Kimizuka, N. Photon Upconversion in Supramolecular Gel Matrixes: Spontaneous Accumulation of Light-Harvesting Donor–Acceptor Arrays in

Nanofibers and Acquired Air Stability. *J. Am. Chem. Soc.* **2015**, *137* (5), 1887–1894.
(23) Mase, K.; Okumura, K.; Yanai, N.; Kimizuka, N. Triplet Sensitization by Perovskite Nanocrystals for Photon Upconversion. *Chem. Commun.* **2017**, *53* (59), 8261–8264.
(24) Di, D.; Yang, L.; Richter, J. M.; Meraldi, L.; Altamimi, R. M.; Alyamani, A. Y.; Credgington, D.; Musselman, K. P.; MacManus-Driscoll, J. L.; Friend, R. H. Efficient Triplet Exciton Fusion in Molecularly Doped Polymer Light-Emitting Diodes. *Adv. Mater.* **2017**, *29* (13), 1605987–n/a.
(25) Gray, V.; Dzebo, D.; Abrahamsson, M.; Albinsson, B.; Moth-Poulsen, K. Triplet-Triplet Annihilation Photon-Upconversion: Towards Solar Energy Applications. *Phys. Chem. Chem. Phys.* **2014**, *16* (22), 10345–10352.
(26) Cheng, Y. Y.; Fückel, B.; Khoury, T.; Clady, R. G. C. R.; Ekins-Daukes, N. J.; Crossley, M. J.; Schmidt, T. W. Entropically Driven Photochemical Upconversion. *J. Phys. Chem. A* **2011**, *115* (6), 1047–1053.
(27) Boutin, P. C.; Ghiggino, K. P.; Kelly, T. L.; Steer, R. P. Photon Upconversion by Triplet–Triplet Annihilation in Ru(Bpy)3- and DPA-Functionalized Polymers. *J. Phys. Chem. Lett.* **2013**, *4* (23), 4113–4118.
(28) Lee, S. H.; Thévenaz, D. C.; Weder, C.; Simon, Y. C. Glassy Poly(Methacrylate) Terpolymers with Covalently Attached Emitters and Sensitizers for Low-Power Light Upconversion. *J. Polym. Sci. Part A Polym. Chem.* **2015**, *53* (14), 1629–1639.
(29) Gray, V.; Moth-Poulsen, K.; Albinsson, B.; Abrahamsson, M. Towards Efficient Solid-State Triplet–triplet Annihilation Based Photon Upconversion: Supramolecular, Macromolecular and Self-Assembled Systems. *Coord. Chem. Rev.* **2018**, *362*, 54–71.
(30) de Mello, J. C.; Wittmann, H. F.; Friend, R. H. An Improved Experimental Determination of External Photoluminescence Quantum Efficiency. *Adv. Mater.* **1997**, *9* (3), 230–232.
(31) Sanders, S. N.; Kumarasamy, E.; Pun, A. B.; Trinh, M. T.; Choi, B.; Xia, J.; Taffet, E. J.; Low, J. Z.; Miller, J. R.; … Campos, L. M. Quantitative Intramolecular Singlet Fission in Bipentacenes. *J. Am. Chem. Soc.* **2015**, *137* (28), 8965–8972.
(32) Sanders, S. N.; Kumarasamy, E.; Pun, A. B.; Steigerwald, M. L.; Sfeir, M. Y.; Campos, L. M. Intramolecular Singlet Fission in Oligoacene Heterodimers. *Angew. Chem. Int. Ed.* **2016**, *55* (10), 3373–3377.
(33) Sanders, S. N.; Kumarasamy, E.; Pun, A. B.; Appavoo, K.; Steigerwald, M. L.; Campos, L. M.; Sfeir, M. Y. Exciton Correlations in Intramolecular Singlet Fission. *J. Am. Chem. Soc.* **2016**, *138* (23), 7289–7297.
(34) Kumarasamy, E.; Sanders, S. N.; Pun, A. B.; Vaselabadi, S. A.; Low, J. Z.; Sfeir, M. Y.; Steigerwald, M. L.; Stein, G. E.; Campos, L. M. Properties of Poly- and Oligopentacenes Synthesized from Modular Building Blocks. *Macromolecules* **2016**, *49* (4), 1279–1285.
(35) Singh-Rachford, T. N.; Castellano, F. N. Pd(II) Phthalocyanine-Sensitized Triplet−Triplet Annihilation from Rubrene. *J. Phys. Chem. A* **2008**, *112* (16), 3550–3556.
(36) Frisch, M. J.; Trucks, G. W.; Schlegel, H. B.; Scuseria, G. E.; Robb, M. A.; Cheeseman, J. R.; Scalmani, G.; Barone, V.; Mennucci, B.; … Fox, D. J. Gaussian 09, Revision D.01. *Gaussian 09, Revision D.01, Gaussian, Inc., Wallingford CT*. 2009.
(37) Korovina, N. V; Das, S.; Nett, Z.; Feng, X.; Joy, J.; Haiges, R.; Krylov, A. I.; Bradforth, S. E.; Thompson, M. E. Singlet Fission in a Covalently Linked Cofacial Alkynyltetracene Dimer. *J. Am. Chem. Soc.* **2016**, *138* (2), 617–627.
(38) Müller, A. M.; Avlasevich, Y. S.; Schoeller, W. W.; Müllen, K.; Bardeen, C. J. Exciton Fission and Fusion in Bis(Tetracene) Molecules with Different Covalent Linker

Structures. *J. Am. Chem. Soc.* **2007**, *129* (46), 14240–14250.
(39) McCusker, C. E.; Castellano, F. N. Efficient Visible to Near-UV Photochemical Upconversion Sensitized by a Long Lifetime Cu(I) MLCT Complex. *Inorg. Chem.* **2015**, *54* (12), 6035–6042.
(40) Zhao, J.; Xu, K.; Yang, W.; Wang, Z.; Zhong, F. The Triplet Excited State of Bodipy: Formation{,} Modulation and Application. *Chem. Soc. Rev.* **2015**, *44* (24), 8904–8939.
(41) Cheng, Y. Y.; Khoury, T.; Clady, R. G. C. R.; Tayebjee, M. J. Y.; Ekins-Daukes, N. J.; Crossley, M. J.; Schmidt, T. W. On the Efficiency Limit of Triplet-Triplet Annihilation for Photochemical Upconversion. *Phys. Chem. Chem. Phys.* **2010**, *12* (1), 66–71.
(42) Haefele, A.; Blumhoff, J.; Khnayzer, R. S.; Castellano, F. N. Getting to the (Square) Root of the Problem: How to Make Noncoherent Pumped Upconversion Linear. *J. Phys. Chem. Lett.* **2012**, *3* (3), 299–303.
(43) Soldatova, A. V; Kim, J.; Rizzoli, C.; Kenney, M. E.; Rodgers, M. A. J.; Rosa, A.; Ricciardi, G. Near-Infrared-Emitting Phthalocyanines. A Combined Experimental and Density Functional Theory Study of the Structural, Optical, and Photophysical Properties of Pd(II) and Pt(II) α-Butoxyphthalocyanines. *Inorg. Chem.* **2011**, *50* (3), 1135–1149.

Chapter 6: Diketopyrrolopyrrole Annihilators

6.1 Preface

This chapter is based on manuscript entitled "Tunable Emission from Triplet Fusion Upconversion in Diketopyrrolopyrroles" by Andrew B. Pun, Luis M. Campos, and Daniel N. Congreve published in The Journal of the American Chemical Society.[1]

I synthesized and characterized all the materials studied. I characterized the upconversion properties of these materials with help from Daniel N. Congreve.

6.2 Introduction

The ability to generate high-energy photons from low-energy irradiation can have a wide range of impact in therapeutics, synthetic chemistry, and optoelectronics, among other areas.[2–7] Triplet fusion (TF) upconversion is the process by which two or more low-energy photons are converted into one high energy photon.[8,9] This phenomenon has been widely studied recently for its wide variety of potential applications, ranging from night vision[10] to biological imaging[11] and photovoltaics.[12–15] TF upconversion requires two species: a sensitizer and an annihilator (Figure 6.1). Low-energy photons ($h\nu_1$) are absorbed by the sensitizer ([Sen], Figure 6.1), yielding an excited singlet state ^{1}[Sen]* that undergoes intersystem crossing (ISC) to the excited triplet state, ^{3}[Sen]*. In the next step, the sensitizer and annihilator ([An]) undergo triplet energy transfer, populating the annihilator into its excited triplet state ^{3}[An]*. The TF process takes place when two annihilators in the triplet state meet, yielding one annihilator in the excited-state singlet (^{1}[An]*) and another annihilator returning to the ground state. The ^{1}[An]* state then decays to the ground state, giving off a high-energy photon ($h\nu_2$) via fluorescence. The TF process is energetically allowed, so long as the singlet energy of the annihilator is less than two times its triplet energy. It is imperative to develop efficient sensitizers and annihilators to improve the

overall yield of upconversion throughout each step described above. More importantly, by expanding the number of available sensitizers and annihilators, it is possible to tune the input and output energy of light.

6.3 Results and Discussion

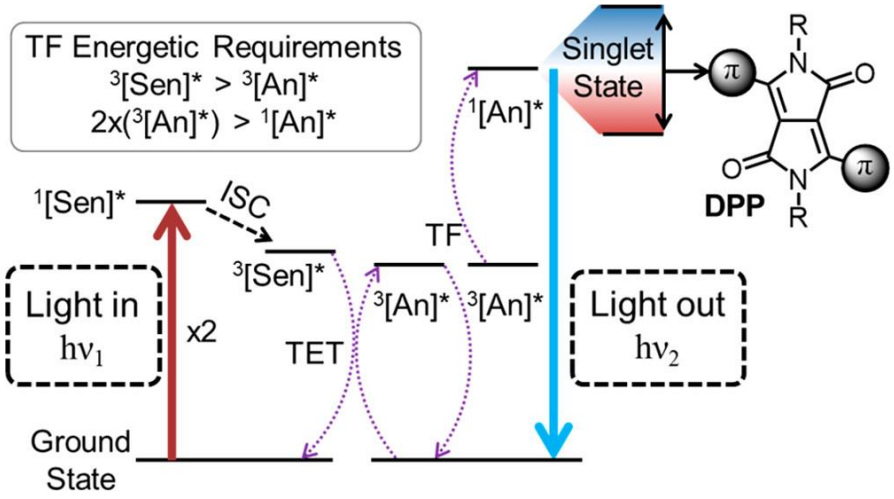

Figure 6.1 Schematic of the TF Upconversion Process. Sensitizer and annihilator species denoted by [Sen] and [An], respectively. Spin-state singlets and triplets denoted with superscript 1 and 3, respectively. Star denotes first excited state. Aryl substituents upon DPP core denoted by π.

To date, most efforts have focused on the search of novel sensitizers, with a number of new molecules and materials having been shown to be efficient in TF upconversion.[16–23] Interesting work has been done studying derivatives of known upconversion annihilators, such as acenes, but very little work has been done in the development of new families of upconversion annihilators.[16,24–28] Here, we investigate how a commonly used dye in organic electronics, diketopyrrolopyrrole (DPP), can be chemically modified to yield a series of novel upconversion annihilators. By altering the aromatic groups appended to the DPP core, we can modulate the energy difference between ground state and the ^{1}[An]* state of the DPP annihilator (Figure 6.1). This can be done without significantly changing the energy of the ^{3}[An]* state. In doing so, we find that the TF upconversion process can be suppressed and activated in these DPP derivatives.

Additionally, because the energy of ^{1}[An]* can be tuned, the energy of the upconverted emission can be adjusted to match the needs of a particular application. The findings reported here represent a leap toward understanding how chemical structure impacts the mechanism of TF upconversion, and recent studies from our team have shown the importance of these systems in photoredox catalysis.[29]

DPP has been widely explored as a building block in organic semiconductors, mainly for use in photovoltaics and transistors.[30,31] Besides its use as an excellent electron-deficient unit, DPP also meets most of the desirable criteria of a conjugated building block. It has strong absorption in the visible range and high fluorescence quantum yield.[32] DPP is also inexpensive, stable, and easy to derivatize.[33–35] Previous work has pegged the triplet excited-state energy of the DPP core at ∼1.15 eV, but the singlet energy can widely fluctuate based on the aryl substituents flanking the core (Figure 6.1).[36] These properties were previously noted in a study on the singlet fission properties of DPP-based materials.

In order to test how modulating the singlet energy impacts the light given off upon TF upconversion, we synthesized eight DPP derivatives, each with a different aryl group appended to the DPP core (Figure 6.2A). Due to the strong electron-withdrawing nature of DPP, compounds **1**–**8** are push–pull type chromophores, which are known to exhibit strong charge-transfer character. The rich chemistry of DPP made possible the rapid, divergent synthesis of the series of molecules reported here. For example, from compound **4**, a simple bromination with *N*-bromosuccinimide afforded compound **5**. In turn, **5** was converted to compounds **6**, **7**, and **8** by Suzuki and Stille cross-coupling reactions.

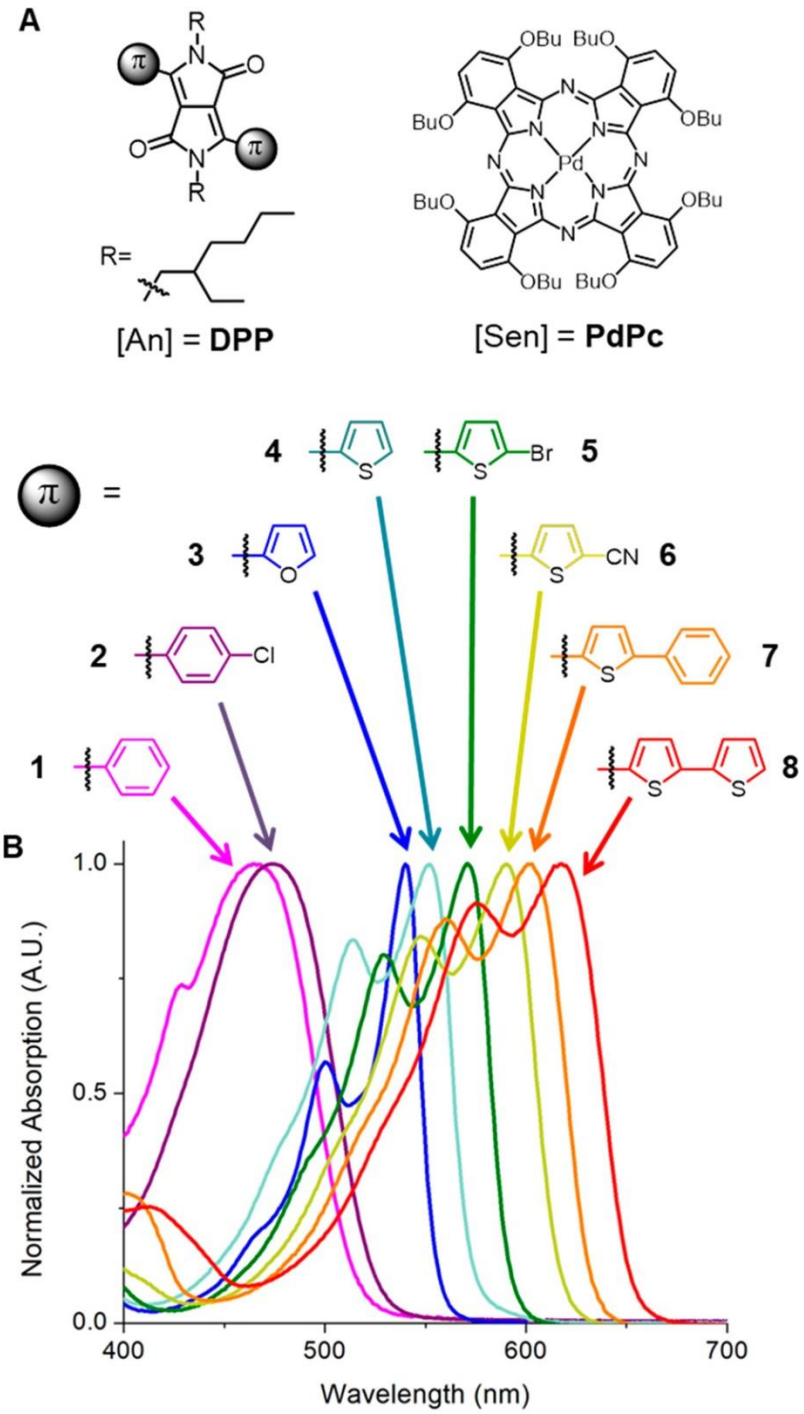

Figure 6.2 DPP Structures and Absorption A) Structures of the compounds used in this work. B) Normalized steady-state absorption of DPP derivatives **1**-**8** in toluene.

The DPP derivatives synthesized exhibit a steady decrease in the energy gap between the ground state and the ^{1}[An]* state. This can be observed by comparing the steady-state absorption

spectra of the eight derivatives, with the gradual red shift of the onset of absorption being indicative of a shrinking optical energy gap (Figure 6.2B). We then performed density functional theory (DFT) calculations which confirmed a DPP triplet energy of ~1.15 eV, with minimal changes between DPP derivatives (Table 6.2).[37] Given a DPP triplet energy of ~1.15 eV, it is expected that TF upconversion should not be possible for compounds **1** and **2**, but energetically allowed for compounds **3** through **8**. This is because the singlet energies of compounds **3** through **8** are below 2.3 eV (Table 6.1), values that are less than double the triplet energy of DPP. This strategy of turning upconversion on and off by altering ^{1}[An]* has been corroborated by theoretical work from other research groups. They have shown that TF upconversion can be either exothermic or endothermic for DPPs depending on the aryl substituents on the DPP core.[38]

Compound	Singlet Energy ^{1}[An]* (eV)	Upconversion Quantum Yield (%)
1	2.40	-
2	2.34	-
3	2.21	3.2
4	2.16	0.91
5	2.08	0.50
6	2.00	0.55
7	1.95	1.8
8	1.90	1.1

Table 6.1 DPP S_1 and UQY Summary of singlet energies and upconversion quantum yields of DPP derivatives.

In order to test the ability of these chromophores to undergo TF upconversion, various solutions of the DPP derivatives with PdPc (Figure 6.2A) were prepared in toluene. PdPc is a

known upconversion sensitizer that absorbs near-infrared radiation and undergoes ISC to generate a triplet with an energy of ~1.3 eV,[39] high enough to undergo triplet energy transfer to the DPPs. As predicted by the ^{1}[An]* energies given by their optical bandgaps, upon sensitization by PdPc, DPP derivatives **3**–**8** were able to undergo TF upconversion and generate a higher energy photon than the incident 730 nm input (Figure 6.3). Conversely, compounds **1** and **2** were not able to perform TF upconversion because the energy of their ^{1}[An]* states is greater than twice their ^{3}[An]* states.[38]

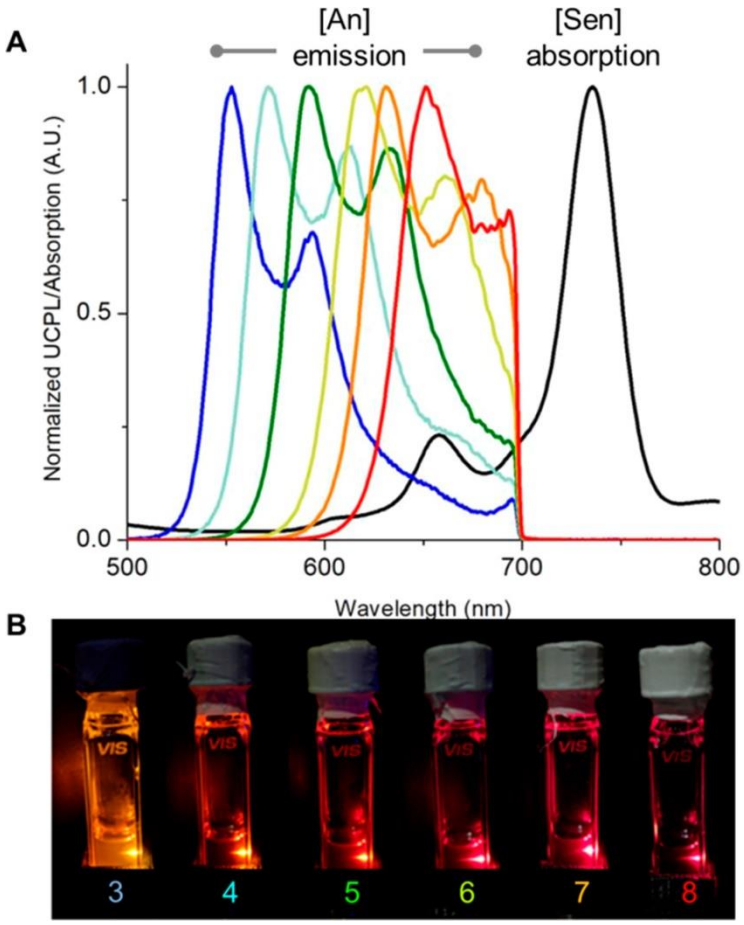

Figure 6.3 DPP Optical Upconversion A) Normalized UCPL of compounds **3**, **4**, **5**, **6**, **7**, and **8** (blue, cyan, green, yellow, orange, and red, respectively) in toluene, excited with a 730 nm laser diode, with a 700 nm short pass filter used. Normalized steady-state absorption of PdPc in toluene (black). B) Photographs of UCPL of derivatives **3**–**8**.

These results demonstrate DPPs as a new class of annihilator in TF upconversion, so long as the energetic criteria for TF are met in an individual DPP derivative. The ability to modulate the singlet energy of DPP without significantly changing its triplet energy means that the output wavelength of upconversion emission can be easily tuned. By altering the electron-donating ability of the aryl groups attached to the DPP core, the ^{1}[An]* energy of the annihilator can be tuned. A stronger electron-donating group leads to a smaller optical band gap, meaning a reduction in ^{1}[An]* energy and longer wavelength upconversion photoluminescence (UCPL). This stands in stark contrast to the commonly used IR-to-visible annihilator rubrene, where synthetic difficulties have prevented its derivatization.[40]

We then turned to evaluate the efficiency of the upconversion. Table 6.1 shows the upconversion quantum yield (UQY) values for the various DPPs, where UQY is defined as the number of absorbed low-energy photons that leads to a singlet on the annihilator. While we can control whether or not upconversion occurs, UQY varies greatly between compounds **3**–**8**. This is because besides the energetic requirement, that ^{1}[An]* < 2(^{3}[An]*), UQY is dependent on a variety of other processes. These include the rate of triplet energy transfer from sensitizer to annihilator and the efficiency of the TF process between annihilators. Owing to the synthetic modularity of DPP, these other processes can be further optimized to enhance UQY in DPP annihilators. Compound **3** showed the highest UQY, 3.2%. This value is lower than our measured UQY of rubrene (5.5%), a common annihilator for IR-to-yellow upconversion. However, DPPs offer the chemical modularity to tune the energy of the output light via straightforward chemical synthesis, something that is nearly impossible with rubrene. Moreover, DPPs are also much more robust than acenes, exhibiting better chemical stability in ambient conditions (Figures 6.4-6). These added benefits showcase DPPs as an attractive alternative to

rubrene in upconversion applications, in spite of the modest decrease in UQY of **3** relative to rubrene.

6.4 Conclusion

In this work, we have studied the impact of chemical structure on TF upconversion in a new class of annihilators. DPP has been widely studied in the past with an abundance of detailed chemical literature, making it amenable to facile and rapid derivatization, in stark contrast to the commonly used acene-based TF upconversion annihilators such as rubrene or diphenylanthracene. Importantly, understanding how DPP interacts with light has resulted in important observations of valuable photophysical phenomena, such as singlet fission[36] and TF upconversion (this work). The chemical modularity of DPP opened opportunities to explore intricate details on how structure affects the excited-state energy of the singlet state. Triplet fusion upconversion was observed in chromophores that meet the energetic requirement for TF (^{1}[An]* < 2(^{3}[An]*)). Importantly, the ability to replace highly oxygen-sensitive tetracene derivatives with extremely stable DPP derivatives will greatly increase the scope of potential applications for these TF upconversion chromophores.

6.5 Methods

Synthetic Methods: All reagents were used as received from Alfa Aesar, Sigma-Aldrich, Acros Organics, TCIAmerica, and Oakwood Products. PdPc was purchased from Frontier Scientific. DPP derivatives **1**–**8** were synthesized according to literature.[36,41–45]

Optical Characterization: Solutions of DPP derivatives (1×10^{-3} M) and PdPc (1×10^{-5} M) were prepared from anhydrous toluene in a nitrogen glovebox and mixed 1:1 by volume. Solutions were then placed in 1 cm × 1 cm cuvettes purchased from Spectrocell, degassed by sparging with nitrogen for 30 s, and then sealed before removing from glovebox for

measurement. Solutions were excited with a 730 nm laser diode purchased from Thorlabs, focused to a beam diameter of 0.15 mm. All upconverted PL spectra were measured with a QEPro spectrometer purchased from Ocean Optics through a 700 nm short-pass filter. Absorption spectra were obtained on an Agilent Technologies Cary 60 UV–vis spectrophotometer. Emission spectra were obtained on a Horiba Fluoromax-4.

UQY: Upconversion quantum yield was determined following the method from de Mello et al.[46] Briefly, a cuvette of the upconverting materials was placed at the center of the integrating sphere. The spectrum was recorded with an Ocean Optics QE Pro spectrometer in three conditions: with the cuvette in the beam, with the cuvette out of the beam, and with the cuvette out of the sphere. Using these spectra, a photoluminescence quantum yield (PLQY) can be determined. This measurement was repeated with both 730 and 445 nm excitation, allowing us to calculate the UQY, defined here as the percentage of absorbed photons that lead to a singlet state on the annihilator. The equation used to calculate UQY is as follows:

$$UQY = 2 * \frac{\Phi_{UC}}{\Phi_{PL}}$$

The factor of two is included such that this value is out of a maximum 100%. UQY represents the number of photons absorbed by the system that undergo intersystem crossing, energy transfer, and perform triplet fusion. Upconverted PLQY (Φ_{UC}) is defined as:

$$\Phi_{UC} = \Phi_{ISC}\Phi_{TET}\Phi_{TF}\Phi_{PL}$$

With Φ denoting efficiency of intersystem crossing (ISC), triplet energy transfer (TET), triplet fusion (TF) and photoluminescence (PL), where Φ_{TF} (and therefore Φ_{UC}) have a maximum efficiency of 50%. All optical equipment was calibrated against a calibrated Newport photodetector.

6.5 DPP Stability vs Rubrene

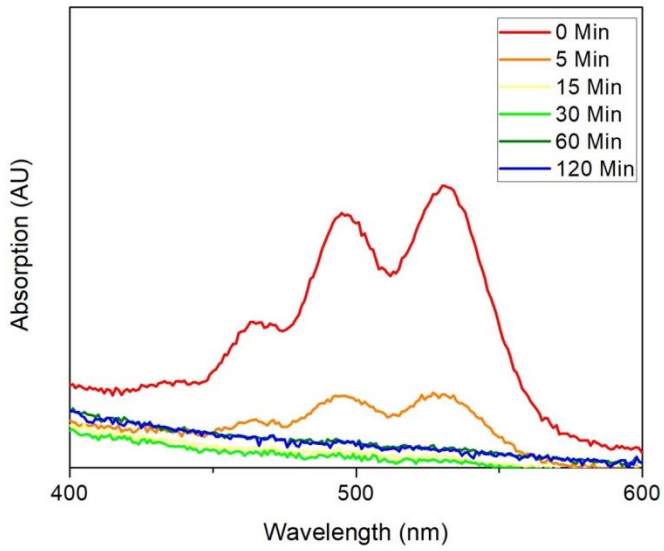

Figure 6.4 Rubrene Stability Evolution of the absorption spectrum of a thin film of rubrene exposed to ambient laboratory conditions. Film was cast on a glass substrate at 2000 RPM, from 4 mg/mL rubrene.

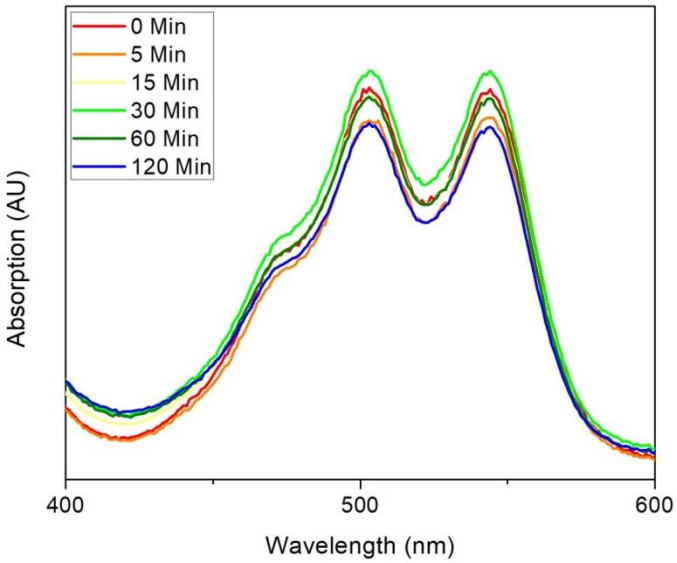

Figure 6.5 DPP Stability Evolution of the absorption spectrum of a thin film of compound **3** exposed to ambient laboratory conditions. Film was cast on a glass substrate at 2000 RPM, from 4 mg/mL **3**.

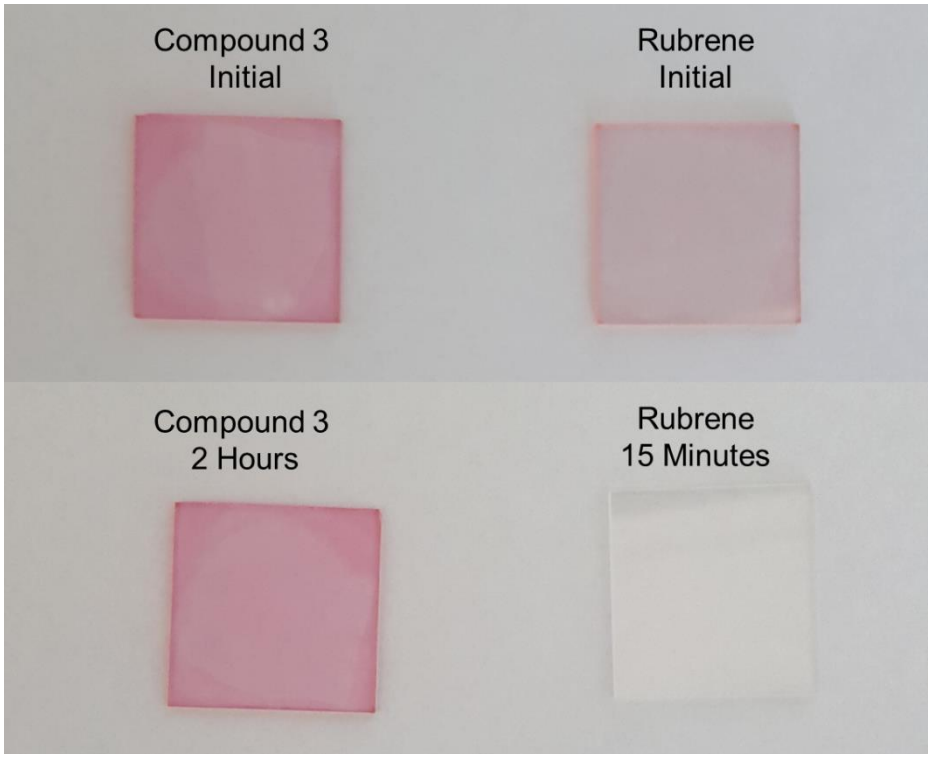

Figure 6.6 DPP vs Rubrene Film Stability Optical images of thin films of **3** and rubrene after exposure to ambient laboratory conditions. **3** maintains its color over two hours while rubrene rapidly decays.

6.6 DPP Power Dependence

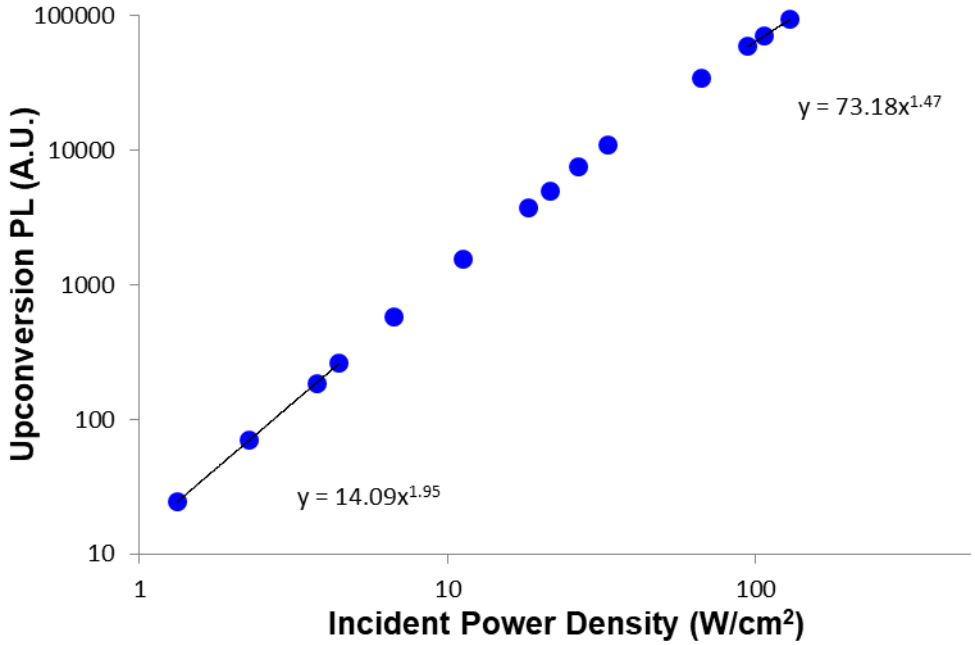

Figure 6.7 Power Dependence of 3 Dependence of upconverted PL on incident light intensity of **3** at $1x10^{-3}$ M mixed 1:1 with $1x10^{-5}$ M PdPC in toluene.

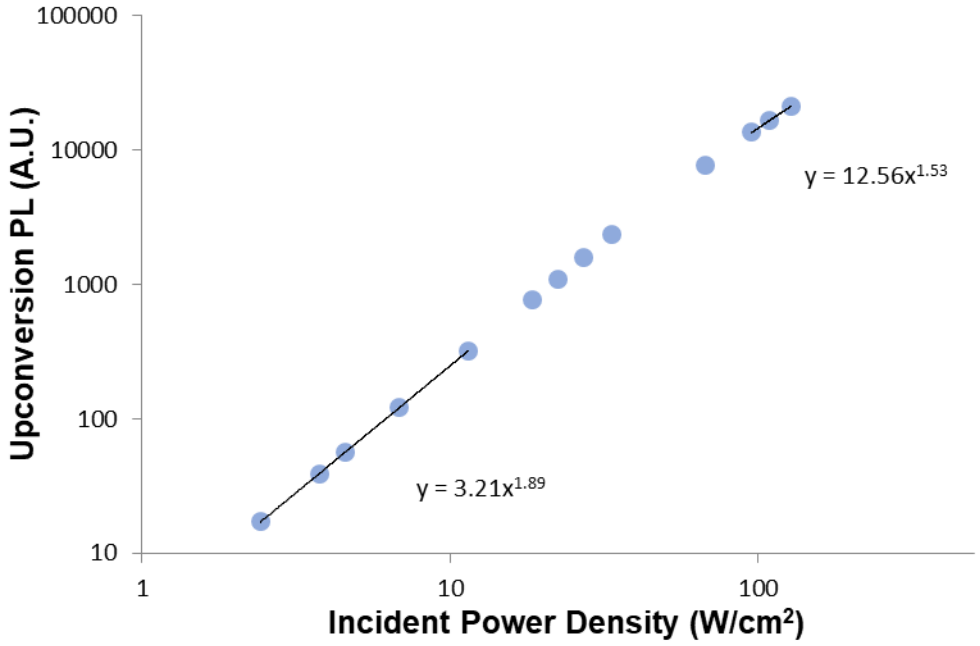

Figure 6.8 Power Dependence of 4 Dependence of upconverted PL on incident light intensity of **4** at $1x10^{-3}$ M mixed 1:1 with $1x10^{-5}$ M PdPC in toluene.

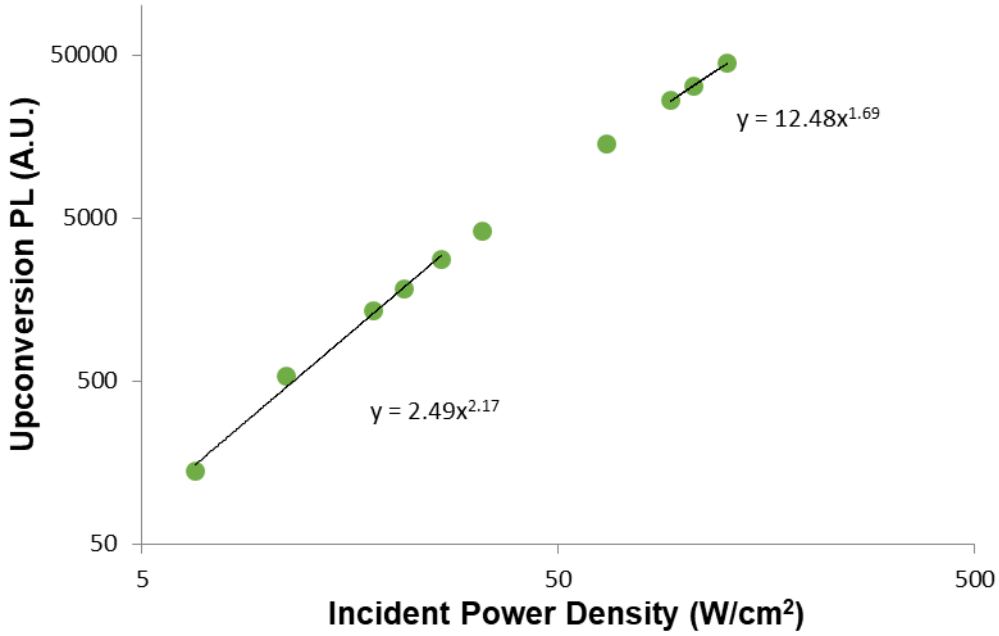

Figure 6.9 Power Dependence of 5 Dependence of upconverted PL on incident light intensity of **5** at $1x10^{-3}$ M mixed 1:1 with $1x10^{-5}$ M PdPC in toluene.

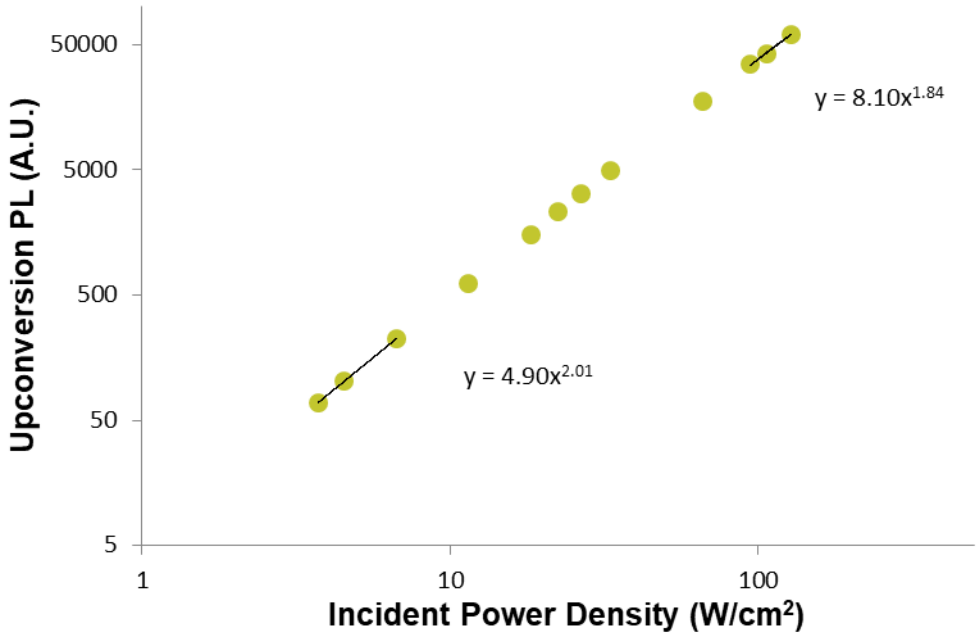

Figure 6.10 Power Dependence of 6 Dependence of upconverted PL on incident light intensity of **6** at $1x10^{-3}$ M mixed 1:1 with $1x10^{-5}$ M PdPC in toluene.

.

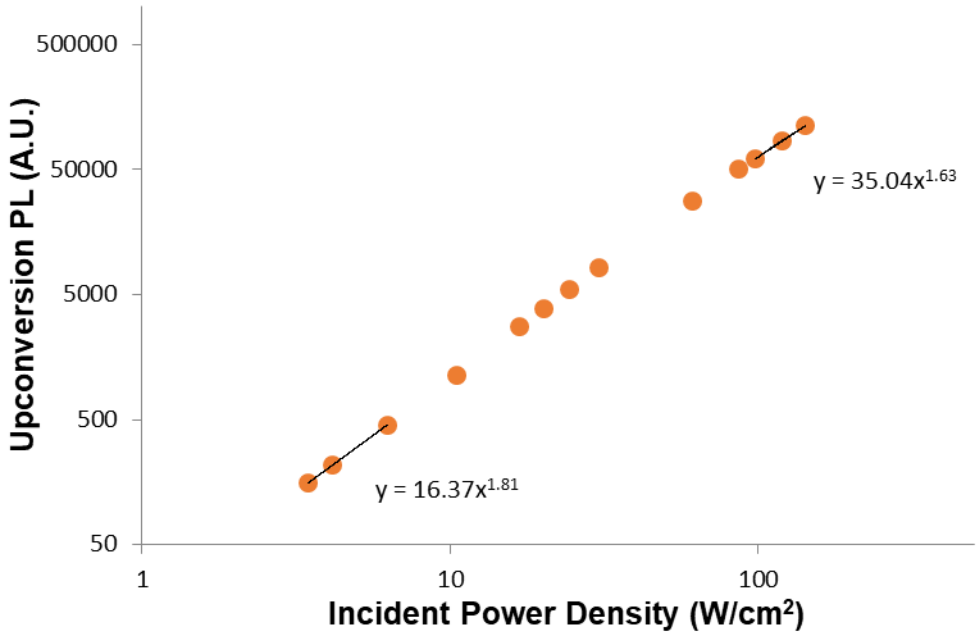

Figure 6.11 Power Dependence of 7 Dependence of upconverted PL on incident light intensity of **7** at $1x10^{-3}$ M mixed 1:1 with $1x10^{-5}$ M PdPC in toluene.

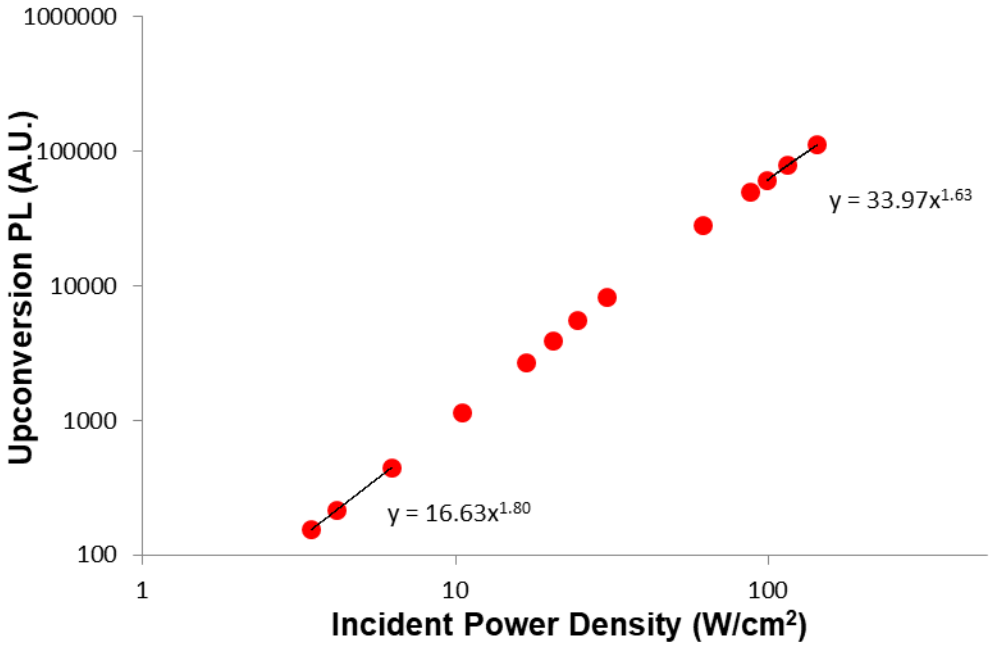

Figure 6.12 Power Dependence of 8 Dependence of upconverted PL on incident light intensity of **8** at $1x10^{-3}$ M mixed 1:1 with $1x10^{-5}$ M PdPC in toluene.

6.7 DPP Absorption Solvent Dependence

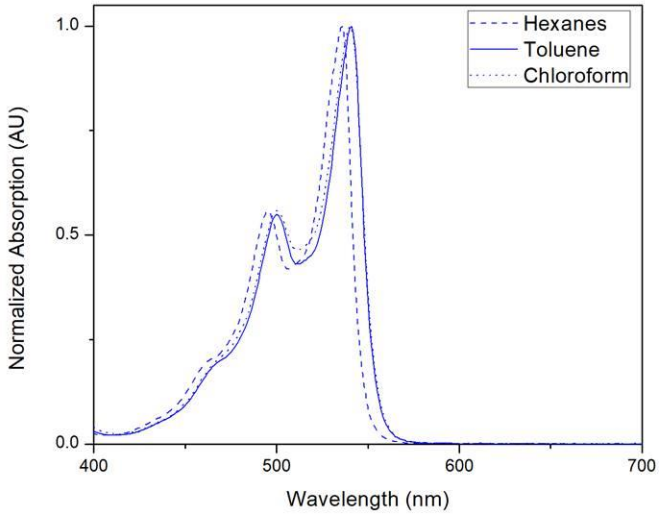

Figure 6.13 Solvent Dependence on UV/Vis of 3 Normalized steady state absorption of DPP derivative **3** measured in solvents of different polarities.

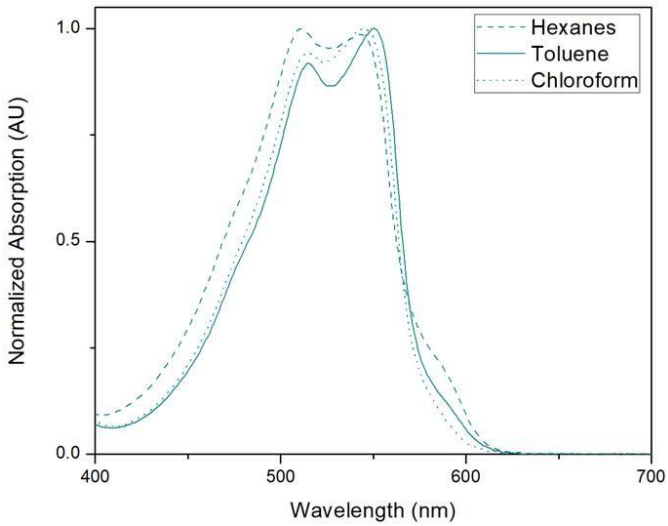

Figure 6.14 Solvent Dependence on UV/Vis of 4 Normalized steady state absorption of DPP derivative **4** measured in solvents of different polarities.

6.8 Computational Methods

Calculations were done using density functional theory (DFT) within the Gaussian 09 Suite, all geometries were optimized using the B3LYP functional and the 6-31G** basis set. To simplify the computation, the R groups on compounds **1**-**8** were set as methyl groups.

Compound	S_0 State Energy (Hartree)	T_1 State Energy (Hartree)	$E(T_1)_{vert}$ (eV)
1	-1031.757301	-1031.713668	1.19
2	-1950.945843	-1950.90311	1.16
3	-1027.303636	-1027.264778	1.06
4	-1673.262397	-1673.223073	1.07
5	-6815.457548	-6815.419489	1.04
6	-1857.739835	-1857.704935	0.95
7	-2135.395334	-2135.358957	0.99
8	-2776.900916	-2776.866558	0.93

Table 6.2 Summary of Computations Total energy of S_0 and T_1 states of compounds **1**-**8**, along with the difference between these energies in eV.

6.9 DFT Optimized Coordinates

Compound 1 S_0

Atom X Y Z

C	-0.60551	0.377822	0.149443
C	0.605537	-0.37779	0.149329
C	0.257728	-1.78648	0.124989
N	-1.1768	-1.78462	0.054419
C	-1.68723	-0.48508	0.064202
C	-0.2577	1.78653	0.125139
N	1.176813	1.78468	0.054565
C	1.68726	0.485153	0.064201
C	-3.10751	-0.14694	-0.04038
C	3.107524	0.146955	-0.04039
O	-0.91399	2.819145	0.202367
O	0.913953	-2.81914	0.202309
C	-1.88937	-3.04152	0.22332
C	1.889326	3.041655	0.223082
C	-4.04436	-0.98234	-0.68081
C	-5.38185	-0.60734	-0.77529
C	-5.81352	0.604664	-0.23421
C	-4.89112	1.450433	0.385706
C	-3.55182	1.086279	0.480018
C	4.044467	0.98233	-0.68074
C	5.381929	0.607249	-0.77519
C	5.8135	-0.60482	-0.23416
C	4.891031	-1.45055	0.385686
C	3.551754	-1.08631	0.479982
H	-1.17995	-3.74947	0.655151
H	-2.74415	-2.9144	0.890198
H	-2.23506	-3.45105	-0.73182
H	2.74391	2.914901	0.890294
H	2.235291	3.450765	-0.73213
H	1.179709	3.749733	0.654365
H	-3.7259	-1.91072	-1.13741
H	-6.08656	-1.26161	-1.27981
H	-6.85811	0.892774	-0.30577
H	-5.21446	2.402503	0.79542
H	-2.83714	1.763597	0.932505
H	3.72612	1.910752	-1.13732
H	6.086708	1.261486	-1.27966
H	6.858082	-0.893	-0.30571
H	5.214302	-2.40265	0.795384
H	2.837016	-1.7636	0.93244

Compound 1 T_1

Atom	X	Y	Z
C	-0.58219	0.372094	0.083508

C	0.582214	-0.37207	0.083491
C	0.218283	-1.78363	0.074104
N	-1.20398	-1.78573	0.038293
C	-1.73538	-0.50383	0.033407
C	-0.21827	1.78365	0.074102
N	1.203983	1.785766	0.038362
C	1.735405	0.503877	0.033406
C	-3.13086	-0.1484	-0.04121
C	3.130876	0.14842	-0.04122
O	-0.88571	2.818532	0.130534
O	0.885673	-2.81854	0.130585
C	-1.89843	-3.05595	0.192267
C	1.898395	3.056045	0.192058
C	-4.13875	-1.02762	-0.51537
C	-5.46977	-0.63174	-0.56033
C	-5.84749	0.647292	-0.14266
C	-4.86498	1.536323	0.30432
C	-3.531	1.155339	0.353576
C	4.13884	1.02767	-0.51517
C	5.469843	0.631726	-0.56013
C	5.847477	-0.6474	-0.14265
C	4.864899	-1.53644	0.304154
C	3.530944	-1.1554	0.353409
H	-1.1643	-3.77185	0.563385
H	-2.72129	-2.95704	0.902345
H	-2.28408	-3.42686	-0.76257
H	2.72122	2.957334	0.902218
H	2.284099	3.42669	-0.76286
H	1.164224	3.772013	0.562942
H	-3.87879	-2.00884	-0.88776
H	-6.21739	-1.32438	-0.93603
H	-6.88948	0.950158	-0.17753
H	-5.14064	2.539112	0.617077
H	-2.78228	1.867576	0.679491
H	3.878983	2.008967	-0.8874
H	6.217514	1.324386	-0.93567
H	6.889457	-0.95031	-0.17752
H	5.140503	-2.53929	0.616774
H	2.78218	-1.86764	0.679219

Compound 2 S_0

Atom	X	Y	Z
C	0.633989	0.326433	0.210675
C	-0.63399	-0.32661	0.210529

C	-0.40285	-1.75901	0.189255
N	1.026425	-1.87633	0.120349
C	1.64161	-0.62296	0.127331
C	0.402895	1.758843	0.189401
N	-1.02637	1.87619	0.120491
C	-1.6416	0.622838	0.127229
C	3.082671	-0.39951	0.018871
C	-3.08267	0.399432	0.018736
O	1.143499	2.732614	0.268568
O	-1.14336	-2.73287	0.268375
C	1.631242	-3.18851	0.292976
C	-1.63112	3.18845	0.292731
C	3.956824	-1.31967	-0.59284
C	5.31908	-1.05816	-0.69666
C	5.826155	0.135919	-0.18562
C	4.982809	1.076626	0.406366
C	3.622104	0.811077	0.502379
C	-3.95683	1.319763	-0.59272
C	-5.3191	1.058348	-0.69649
C	-5.8262	-0.13579	-0.18562
C	-4.98289	-1.07662	0.406195
C	-3.62216	-0.81117	0.502169
Cl	7.54531	0.464446	-0.30381
Cl	-7.54541	-0.46419	-0.30373
H	0.860443	-3.83624	0.713753
H	1.952476	-3.62308	-0.65958
H	2.484342	-3.13544	0.972073
H	-2.48385	3.135798	0.97235
H	-0.86004	3.836361	0.7127
H	-1.9529	3.622481	-0.65988
H	3.576061	-2.23563	-1.02495
H	5.981275	-1.76968	-1.17659
H	5.38727	2.008713	0.784132
H	2.964925	1.559281	0.93031
H	-3.57608	2.235792	-1.02467
H	-5.98131	1.769981	-1.17624
H	-5.3874	-2.00871	0.783893
H	-2.96502	-1.55946	0.930019

Compound 2 T_1

Atoms	X	Y	Z
C	0.611947	0.320167	0.116837
C	-0.61194	-0.32023	0.116927
C	-0.37111	-1.75795	0.110677

N	1.045204	-1.88395	0.075732
C	1.685139	-0.65235	0.068819
C	0.371061	1.757927	0.110547
N	-1.04517	1.883929	0.075617
C	-1.68515	0.65229	0.068931
C	3.103541	-0.41656	-0.00772
C	-3.10352	0.416521	-0.00772
O	1.126351	2.730022	0.168055
O	-1.12634	-2.73008	0.168243
C	1.625658	-3.21083	0.227232
C	-1.62561	3.210787	0.227494
C	4.040631	-1.38656	-0.44973
C	5.399717	-1.11005	-0.5008
C	5.863687	0.148863	-0.11477
C	4.968738	1.137796	0.301364
C	3.611105	0.860977	0.350538
C	-4.04059	1.386551	-0.44975
C	-5.39968	1.110069	-0.50086
C	-5.8637	-0.14882	-0.11481
C	-4.96878	-1.13777	0.30138
C	-3.61115	-0.86099	0.350588
Cl	7.582169	0.494045	-0.16987
Cl	-7.58219	-0.49395	-0.1699
H	0.826404	-3.86388	0.578931
H	1.993306	-3.60469	-0.72548
H	2.440472	-3.19124	0.953254
H	-2.44047	3.190957	0.953462
H	-0.82638	3.863738	0.579433
H	-1.99322	3.604933	-0.72511
H	3.709421	-2.3557	-0.79451
H	6.098182	-1.8623	-0.84978
H	5.335617	2.118192	0.58376
H	2.926313	1.645615	0.650858
H	-3.70935	2.355672	-0.79455
H	-6.09812	1.862337	-0.84987
H	-5.33571	-2.11814	0.583796
H	-2.92639	-1.64563	0.650975

Compound 3 S_0

Atom	X	Y	Z
C	0.598328	-0.38797	0.000003
C	-0.59833	0.387973	0.000003
C	-0.24213	1.797531	-1E-06
N	1.200137	1.773213	-2E-06

C	1.688841	0.472371	0
C	0.242127	-1.79753	-1E-06
N	-1.20014	-1.77321	-2E-06
C	-1.68884	-0.47237	0
C	3.085404	0.144023	0
C	-3.0854	-0.14402	-1E-06
O	0.879894	-2.83888	-1E-06
O	-0.87989	2.838882	-1E-06
C	4.269723	0.855306	-9E-06
C	5.321644	-0.10281	-6E-06
C	4.717802	-1.32768	0.000006
O	3.372189	-1.19732	0.000009
C	-4.26972	-0.85531	-0.00001
C	-5.32164	0.102809	-5E-06
C	-4.7178	1.327675	0.000006
O	-3.37219	1.197318	0.000008
C	1.945746	3.014457	0.000001
C	-1.94575	-3.01446	0.000001
H	4.381879	1.926845	-1.9E-05
H	6.383665	0.093552	-1.1E-05
H	5.090144	-2.34017	0.000013
H	-4.38188	-1.92685	-1.9E-05
H	-6.38367	-0.09355	-9E-06
H	-5.09014	2.340165	0.000012
H	1.202223	3.81322	0.000006
H	2.571719	3.10822	0.893603
H	2.571714	3.108227	-0.8936
H	-2.57172	-3.10822	0.893604
H	-2.57172	-3.10823	-0.8936
H	-1.20222	-3.81322	0.000006

Compound 3 T_1

Atom	X	Y	Z
C	0.57531	-0.38176	0.000001
C	-0.57531	0.381755	0.000001
C	-0.20812	1.796691	0
N	1.218968	1.776936	0.000001
C	1.727232	0.488138	0.000001
C	0.20812	-1.79669	0
N	-1.21897	-1.77694	0
C	-1.72723	-0.48814	0
C	3.093582	0.142534	-1E-06
C	-3.09358	-0.14253	-1E-06
O	0.863345	-2.83324	0.000002

O	-0.86335	2.833234	0.000001
C	4.301421	0.844271	-5E-06
C	5.334824	-0.12565	-6E-06
C	4.719865	-1.34792	0
O	3.370738	-1.20623	0.000002
C	-4.30142	-0.84427	-5E-06
C	-5.33482	0.125654	-5E-06
C	-4.71986	1.34792	0
O	-3.37074	1.206229	0.000002
C	1.964571	3.019375	0.000005
C	-1.96457	-3.01938	0.000004
H	4.42644	1.914423	-9E-06
H	6.399612	0.056849	-9E-06
H	5.083678	-2.3633	0.000002
H	-4.42644	-1.91442	-8E-06
H	-6.39961	-0.05685	-8E-06
H	-5.08368	2.363296	0.000001
H	1.226373	3.822352	0.000011
H	2.592129	3.104188	0.893007
H	2.592124	3.104197	-0.893
H	-2.59213	-3.10419	0.893007
H	-2.59213	-3.1042	-0.893
H	-1.22637	-3.82235	0.000009

Compound 4 S_0

Atom	X	Y	Z
C	-0.61929	0.34935	-0.02666
C	0.619287	-0.3493	-0.0267
C	0.340157	-1.76811	-0.01675
N	-1.09523	-1.83678	0.015584
C	-1.66936	-0.56309	0.01131
C	-0.3402	1.76816	-0.01653
N	1.095269	1.836822	0.015845
C	1.669361	0.563135	0.011281
C	-3.08937	-0.31152	0.053205
C	3.089377	0.31152	0.053161
O	-1.05203	2.765315	-0.05206
O	1.052035	-2.76525	-0.05236
C	-4.1437	-1.18193	0.299438
C	-5.41456	-0.55991	0.265911
C	-5.335	0.781869	-0.00678
S	-3.70996	1.31874	-0.21165
C	4.143728	1.181936	0.299236
C	5.414582	0.559879	0.265813

C	5.334983	-0.78193	-0.00668
S	3.709931	-1.31883	-0.21146
C	-1.73892	-3.1343	-0.06512
C	1.738924	3.134337	-0.06526
H	-4.01581	-2.23107	0.51857
H	-6.3461	-1.08542	0.439986
H	-6.1462	1.49255	-0.08912
H	4.015858	2.231126	0.5181
H	6.34613	1.085391	0.439818
H	6.146187	-1.49262	-0.08891
H	-0.94295	-3.85594	-0.25569
H	-2.23256	-3.40473	0.874396
H	-2.46527	-3.16603	-0.88159
H	2.464976	3.165983	-0.882
H	0.94287	3.855932	-0.25563
H	2.23291	3.404901	0.874031

Compound 4 T_1

Atom	X	Y	Z
C	-0.59717	0.34447	-6E-06
C	0.597157	-0.34442	-6.6E-05
C	0.305305	-1.77133	-0.00018
N	-1.11508	-1.84234	-0.0001
C	-1.70934	-0.58212	0.000025
C	-0.30526	1.771405	-6.8E-05
N	1.115087	1.842389	-0.00016
C	1.709346	0.582137	-0.00011
C	-3.09983	-0.31667	0.000131
C	3.099828	0.316653	0.000096
O	-1.03027	2.764398	-0.00012
O	1.030303	-2.76433	-0.00039
C	-4.19383	-1.20015	0.000447
C	-5.4463	-0.55558	0.000441
C	-5.34412	0.815148	0.000138
S	-3.70108	1.355701	-0.00021
C	4.193839	1.2001	0.000411
C	5.446303	0.5555	0.000506
C	5.344094	-0.81522	0.000205
S	3.701043	-1.35575	-0.00015
C	-1.75244	-3.14606	-0.00011
C	1.752454	3.146126	-0.00025
H	-4.09633	-2.27432	0.000736
H	-6.39175	-1.08571	0.000683
H	-6.14439	1.542428	0.000088

H	4.096375	2.274276	0.000734
H	6.39177	1.085614	0.000729
H	6.144353	-1.54251	0.000203
H	-0.94597	-3.88018	-0.00043
H	-2.36687	-3.28723	0.893883
H	-2.36735	-3.28698	-0.89381
H	2.367371	3.286961	-0.89395
H	0.945974	3.880216	-0.00065
H	2.366869	3.287368	0.893737

Compound 5 S_0

Atom	X	Y	Z
C	0.6793	0.205465	0.002134
C	-0.6793	-0.20545	0.002187
C	-0.71638	-1.64949	0.003095
N	0.668815	-2.0318	0.008579
C	1.507515	-0.91417	0.008365
C	0.716341	1.649504	0.002938
N	-0.66881	2.031809	0.008451
C	-1.50753	0.914175	0.008401
C	2.947548	-0.96785	0.015893
C	-2.94757	0.967821	0.016043
O	1.633001	2.463656	-0.00433
O	-1.63301	-2.46365	-0.00406
C	3.804303	-2.06087	0.056842
C	5.177529	-1.72311	0.052117
C	5.36423	-0.36632	0.007128
S	3.886365	0.533518	-0.027
C	-3.80431	2.060854	0.057471
C	-5.17753	1.723098	0.052711
C	-5.36425	0.366323	0.007238
S	-3.88636	-0.53348	-0.02727
C	1.007977	-3.44211	-0.00784
C	-1.00795	3.44213	-0.00834
Br	7.012427	0.537999	-0.01589
Br	-7.01242	-0.53802	-0.01601
H	3.468905	-3.08555	0.093445
H	5.986325	-2.44173	0.080863
H	-3.46891	3.085513	0.094486
H	-5.98633	2.441698	0.081793
H	0.058569	-3.97878	-0.04218
H	1.597644	-3.70325	-0.89171
H	1.548349	-3.73831	0.896682
H	-1.59794	3.70295	-0.89208

H	-1.54797	3.73867	0.896284
H	-0.05854	3.978745	-0.0432

Compound 5 T_1

Atom	X	Y	Z
C	0.656904	0.206666	-0.00011
C	-0.65691	-0.20665	-0.00012
C	-0.68233	-1.66241	-0.00014
N	0.687949	-2.04102	-0.00011
C	1.540807	-0.93795	-5.5E-05
C	0.682319	1.662444	-0.00023
N	-0.68792	2.041053	-0.00022
C	-1.54081	0.937979	-0.00013
C	2.953026	-0.97397	0.000061
C	-2.95302	0.974018	0.000089
O	1.608946	2.469994	-0.00034
O	-1.60893	-2.46998	-0.00025
C	3.833059	-2.07216	0.000317
C	5.195701	-1.72248	0.000363
C	5.380555	-0.36081	0.000134
S	3.894182	0.538848	-0.00016
C	-3.83309	2.072172	0.00062
C	-5.19573	1.722456	0.000648
C	-5.38055	0.360787	0.000166
S	-3.89418	-0.53887	-0.00034
C	1.028459	-3.45215	-9.2E-05
C	-1.02844	3.45219	-0.00034
Br	7.023893	0.548345	0.000102
Br	-7.0239	-0.54837	0.000067
H	3.506026	-3.1	0.000489
H	6.009962	-2.43594	0.000564
H	-3.50609	3.100023	0.001171
H	-6.01	2.435895	0.001012
H	0.082644	-3.99513	-0.00033
H	1.597632	-3.72283	-0.89427
H	1.597236	-3.72291	0.894311
H	-1.59785	3.722704	-0.8944
H	-1.59697	3.723101	0.894176
H	-0.08262	3.995156	-0.00089

Compound 6 S_0

Atom	X	Y	Z
C	-0.66395	-0.24624	-0.00644

C	0.663927	0.246256	-0.00644
C	0.611765	1.692742	-0.00399
N	-0.79361	1.988971	0.011347
C	-1.55869	0.821253	0.010842
C	-0.61176	-1.69272	-0.00402
N	0.79361	-1.98895	0.011281
C	1.558682	-0.82123	0.010839
C	-3.00081	0.78157	0.033625
C	3.000803	-0.78154	0.033633
O	-1.47833	-2.55731	-0.02389
O	1.478322	2.557334	-0.02386
C	-3.91874	1.822558	0.149171
C	-5.26062	1.401075	0.137984
C	-5.38461	0.03025	0.012894
S	-3.83731	-0.76399	-0.08458
C	3.918715	-1.82255	0.14916
C	5.260606	-1.40111	0.13797
C	5.384623	-0.03027	0.012907
S	3.837344	0.763984	-0.08454
C	-1.21936	3.376619	-0.03345
C	1.219343	-3.37662	-0.03338
C	-6.58871	-0.71355	-0.03142
N	-7.57988	-1.32471	-0.06882
C	6.588722	0.713509	-0.03144
N	7.579884	1.324687	-0.06886
H	-3.64227	2.860166	0.249429
H	-6.11109	2.066335	0.219766
H	3.642234	-2.86016	0.249394
H	6.11106	-2.06638	0.219732
H	-0.30792	3.968811	-0.12729
H	-1.86241	3.56877	-0.89677
H	-1.73422	3.671705	0.88608
H	1.862352	-3.56887	-0.89672
H	1.734239	-3.6716	0.886158
H	0.307891	-3.9688	-0.12714

Compound 6 T_1

Atom	X	Y	Z
C	-0.64161	0.246617	0.000329
C	0.641618	-0.24665	0.000367
C	0.575336	-1.70312	-3.9E-05
N	-0.8173	-1.99516	-0.00058
C	-1.59612	-0.84148	-0.00041
C	-0.57534	1.703097	-0.00023

N	0.817288	1.99514	-0.00051
C	1.596115	0.841455	-0.00027
C	-3.00745	-0.78469	-0.00084
C	3.007442	0.784694	-0.0007
O	-1.44823	2.564619	-0.00023
O	1.448205	-2.56466	0.000272
C	-3.95327	-1.83192	-0.00315
C	-5.28076	-1.39914	-0.00271
C	-5.40225	-0.01523	-1.9E-05
S	-3.84452	0.779108	0.001861
C	3.953255	1.831932	-0.00299
C	5.280754	1.39916	-0.00266
C	5.402258	0.015251	-3.6E-05
S	3.844535	-0.77909	0.001866
C	-1.24396	-3.38434	0.000317
C	1.243938	3.38432	0.000427
C	-6.60023	0.73093	0.001086
N	-7.59075	1.347136	0.002018
C	6.600248	-0.7309	0.000948
N	7.59077	-1.34709	0.001767
H	-3.68877	-2.87721	-0.0055
H	-6.13754	-2.06172	-0.00436
H	3.688752	2.877222	-0.00505
H	6.137523	2.061756	-0.00434
H	-0.33382	-3.98481	0.002416
H	-1.82869	-3.61742	0.894622
H	-1.82578	-3.61964	-0.89533
H	1.828641	3.617389	0.894764
H	1.82579	3.619634	-0.89519
H	0.333793	3.984781	0.002464

Compound 7 S_0

Atom	X	Y	Z
C	-0.6908	-0.16487	0.010197
C	0.690803	0.164823	-0.00952
C	0.814345	1.605141	0.009238
N	-0.54515	2.067913	0.044637
C	-1.45095	1.003386	0.048345
C	-0.81436	-1.6052	-0.00904
N	0.545153	-2.06796	-0.0447
C	1.450949	-1.00342	-0.04811
C	-2.88197	1.151466	0.089416
C	2.881956	-1.15147	-0.08932
O	-1.77476	-2.36772	-0.00136

O	1.774751	2.367656	0.001352
C	-3.66374	2.288383	0.268214
C	-5.0489	2.03464	0.261505
C	-5.36772	0.702105	0.07668
S	-3.92368	-0.26019	-0.09189
C	3.663764	-2.28835	-0.26823
C	5.048913	-2.03458	-0.26161
C	5.367707	-0.70204	-0.07674
S	3.923679	0.260211	0.091972
C	-0.8021	3.494748	0.018771
C	0.802093	-3.49479	-0.0189
C	-6.70049	0.092738	0.022595
C	6.700476	-0.0927	-0.02271
C	-7.81728	0.863532	-0.353
C	-9.08996	0.30139	-0.39308
C	-9.27677	-1.04459	-0.07065
C	-8.17694	-1.82298	0.294193
C	-6.90338	-1.26221	0.344249
C	6.903407	1.262217	-0.34447
C	8.176973	1.822963	-0.29444
C	9.276791	1.044589	0.070477
C	9.089944	-0.30136	0.393011
C	7.817247	-0.86347	0.352981
H	-3.25963	3.276232	0.427165
H	-5.79338	2.805233	0.422966
H	3.259662	-3.27623	-0.42703
H	5.793392	-2.80515	-0.42319
H	0.170048	3.973579	-0.10838
H	-1.45325	3.766799	-0.81678
H	-1.24386	3.846511	0.957012
H	1.244218	-3.84643	-0.957
H	1.452873	-3.767	0.816897
H	-0.17011	-3.97364	0.107798
H	-7.67979	1.902242	-0.63612
H	-9.93721	0.913604	-0.68793
H	-10.2696	-1.48277	-0.10638
H	-8.31089	-2.86991	0.549564
H	-6.0609	-1.8735	0.653858
H	6.060939	1.873493	-0.65413
H	8.31092	2.869883	-0.54987
H	10.26959	1.482752	0.106179
H	9.937171	-0.91359	0.687913
H	7.679737	-1.90214	0.636237

Compound 7 T_1

Atom	X	Y	Z
C	-0.66942	-0.16494	0.00206
C	0.669412	0.164934	-0.00221
C	0.787002	1.617268	0.026017
N	-0.55618	2.080067	0.055094
C	-1.47916	1.032484	0.040864
C	-0.78701	-1.61725	-0.02622
N	0.556229	-2.08006	-0.05526
C	1.479156	-1.03247	-0.04109
C	-2.88221	1.162193	0.061012
C	2.882216	-1.16214	-0.06132
O	-1.75987	-2.36809	-0.02504
O	1.759905	2.368058	0.024873
C	-3.68976	2.314956	0.157828
C	-5.06204	2.05111	0.146596
C	-5.38316	0.702908	0.042044
S	-3.92746	-0.2681	-0.05118
C	3.689725	-2.31488	-0.15858
C	5.062023	-2.05106	-0.14723
C	5.383149	-0.70291	-0.04213
S	3.927463	0.268084	0.051451
C	-0.80753	3.508901	0.063183
C	0.807568	-3.50889	-0.06353
C	-6.7082	0.091493	0.013417
C	6.708197	-0.0915	-0.01324
C	-7.84937	0.868761	-0.27618
C	-9.11719	0.297369	-0.29436
C	-9.28274	-1.06534	-0.0336
C	-8.16243	-1.85028	0.246555
C	-6.89246	-1.28205	0.272501
C	6.892477	1.282097	-0.27199
C	8.162447	1.850315	-0.2458
C	9.282728	1.065299	0.034272
C	9.117152	-0.29747	0.294688
C	7.849324	-0.86885	0.276262
H	-3.29546	3.314259	0.255444
H	-5.80975	2.829461	0.243946
H	3.295395	-3.31412	-0.25673
H	5.80973	-2.82937	-0.24491
H	0.168734	3.991629	0.005331
H	-1.41159	3.808467	-0.79806
H	-1.30471	3.822205	0.986396
H	1.304333	-3.82218	-0.98698
H	1.412029	-3.80848	0.797421

H	-0.16866	-3.99162	-0.00526
H	-7.73667	1.922788	-0.50821
H	-9.97983	0.916647	-0.52256
H	-10.273	-1.51002	-0.0516
H	-8.27776	-2.91023	0.452891
H	-6.03545	-1.90403	0.513229
H	6.035486	1.904136	-0.51265
H	8.277817	2.910308	-0.45188
H	10.27303	1.509967	0.052462
H	9.979761	-0.91681	0.522818
H	7.736577	-1.92293	0.508032

Compound 8 S_0

Atom	X	Y	Z
C	-0.68368	0.190543	-0.01781
C	0.683691	-0.19028	-0.01767
C	0.753166	-1.63409	-0.02316
N	-0.62199	-2.04671	-0.0426
C	-1.48827	-0.94895	-0.04046
C	-0.7532	1.634347	-0.02324
N	0.621993	2.046987	-0.04229
C	1.488288	0.94923	-0.03997
C	-2.92221	-1.04193	-0.06611
C	2.922234	1.042182	-0.06507
O	-1.68587	2.430764	-0.00105
O	1.685828	-2.43053	-0.00081
C	-3.74996	-2.15156	-0.21092
C	-5.12281	-1.84672	-0.2009
C	-5.38768	-0.49652	-0.04589
S	-3.90593	0.417179	0.089851
C	3.750187	2.151937	-0.20764
C	5.122997	1.846951	-0.1975
C	5.38769	0.496455	-0.04466
S	3.905784	-0.41734	0.088804
C	-0.93118	-3.46242	0.012644
C	0.931115	3.462723	0.012351
C	-6.67058	0.168319	0.003268
C	6.670515	-0.16852	0.004074
S	-8.16278	-0.75045	0.140448
C	-9.11644	0.696851	0.12468
C	-8.33626	1.81708	0.027657
C	-6.94795	1.519793	-0.04171
S	8.163155	0.750223	0.136868
C	9.116454	-0.69733	0.123133

C	8.335889	-1.8176	0.029788
C	6.947555	-1.52016	-0.03825
H	-3.38536	-3.15859	-0.34143
H	-5.89925	-2.59377	-0.3204
H	3.385807	3.15928	-0.33628
H	5.899527	2.594222	-0.31502
H	0.025055	-3.97504	0.128333
H	-1.57375	-3.69751	0.866008
H	-1.40525	-3.81177	-0.9105
H	1.57238	3.698521	0.866518
H	1.406572	3.81132	-0.91035
H	-0.02529	3.975414	0.126288
H	-10.1934	0.63083	0.189867
H	-8.73827	2.82308	0.001672
H	-6.17556	2.274958	-0.13492
H	10.19351	-0.6314	0.186652
H	8.73763	-2.82376	0.0056
H	6.174888	-2.27541	-0.12835

Compound 8 T_1

Atom	X	Y	Z
C	-0.66242	0.190697	-1E-06
C	0.662404	-0.1907	0.000033
C	0.723838	-1.64679	-0.00016
N	-0.63543	-2.05806	-0.00037
C	-1.51809	-0.97346	-0.00028
C	-0.72384	1.646801	-0.00012
N	0.635426	2.058063	-0.0001
C	1.518084	0.97344	-8E-06
C	-2.92185	-1.04594	-0.00028
C	2.921848	1.045914	-2.2E-05
O	-1.66853	2.432605	-0.00018
O	1.66853	-2.4326	-0.00011
C	-3.7766	-2.1721	-0.00055
C	-5.13422	-1.85862	-0.00044
C	-5.40209	-0.49089	-8.5E-05
S	-3.90941	0.43339	0.000133
C	3.776586	2.172082	-0.00016
C	5.13421	1.858621	-0.00007
C	5.402093	0.490888	0.000132
S	3.909415	-0.4334	0.000148
C	-0.94096	-3.4762	-0.00054
C	0.940971	3.476196	-1.2E-05
C	-6.67611	0.169821	0.000099

C	6.676114	-0.16981	0.000294
S	-8.18146	-0.74624	0.000285
C	-9.12664	0.708089	0.000424
C	-8.33699	1.827474	0.000348
C	-6.95005	1.527835	0.000174
S	8.181461	0.746255	-0.00074
C	9.126646	-0.70807	0.000113
C	8.337004	-1.82746	0.001089
C	6.950062	-1.52783	0.001206
H	-3.42024	-3.19003	-0.00085
H	-5.91581	-2.61039	-0.00064
H	3.420206	3.190001	-0.00028
H	5.915783	2.610396	-0.00009
H	0.018362	-3.99508	-0.00055
H	-1.50314	-3.76258	0.893441
H	-1.50305	-3.76237	-0.89463
H	1.503208	3.762381	0.893989
H	1.503005	3.762542	-0.89409
H	-0.01835	3.995088	0.000116
H	-10.2058	0.646482	0.000556
H	-8.73452	2.835668	0.000414
H	-6.17183	2.282587	0.000072
H	10.20578	-0.64645	-0.00017
H	8.734539	-2.83565	0.001733
H	6.171851	-2.28258	0.001987

6.10 Outlook

One question that I constantly get asked about this work, especially by Bruno, is if the materials that did not work as annihilators can be used for singlet fission. The Wasielewski group showed that the phenyl DPP that does not function as an annihilator also does not undergo singlet fission, at least in the solid state. It would be interesting to synthesize dimers of phenyl DPP, as they should undergo intramolecular singlet fission. The electronic coupling between DPP chromophores would be very interesting as well, if they are directly linked you would imagine you would see a significant redshift in the onset of absorption of these compounds; would that then make them suitable as annihilators? A longer bridge than a phenyl spacer might be needed to maintain a high enough singlet energy to undergo singlet fission.

Another loose end of this work is the exact triplet energies of these DPPs synthesized. We quote the energy as 1.15 eV, and DFT calculations show this value staying "relatively" constant, but it still looks like that triplet energy is slowly decreasing. If the triplet energy of compound **8** is really 0.93 eV, we could sensitize that with other materials than $PdPc(OBu)_8$. 0.93 eV is well below the bandgap of Si, and could potentially be sensitized by PbS nanocrystals, themselves excited by IR light of ~1.0 eV. Another minor issue I still have with this work is the lack of trend in UCQY for the DPPs synthesized, there has to be some reason underpinning this that could be explored.

Finally, I still have qualms about how triplet energies are measured or calculated, and reported, across singlet fission and upconversion papers in the field, it is hard to trust any number that is reported, and I just consider them +/- 0.2 eV. More accurate computation of singlet and triplet state energies would greatly increase the speed of discovery of new upconversion sensitizers, annihilators, and pairings of the two. I hope the Reichman group and other theorists are able to build on this in years to come.

6.11 References

(1) Pun, A. B.; Campos, L. M.; Congreve, D. N. Tunable Emission from Triplet Fusion Upconversion in Diketopyrrolopyrroles. *J. Am. Chem. Soc.* **2019**, *141* (9), 3777–3781.

(2) Park, Y. Il; Lee, K. T.; Suh, Y. D.; Hyeon, T. Upconverting Nanoparticles: A Versatile Platform for Wide-Field Two-Photon Microscopy and Multi-Modal in Vivo Imaging. *Chem. Soc. Rev.* **2015**, *44* (6), 1302–1317.

(3) Bhawalkar, J. D.; Kumar, N. D.; Zhao, C.-F.; Prasad, P. N. Two-Photon Photodynamic Therapy. *J. Clin. Laser Med. Surg.* **1997**, *15* (5), 201–204.

(4) Oliveira, S. L.; Corrêa, D. S.; Misoguti, L.; Constantino, C. J. L.; Aroca, R. F.; Zilio, S. C.; Mendonça, C. R. Perylene Derivatives with Large Two-Photon-Absorption Cross-Sections for Application in Optical Limiting and Upconversion Lasing. *Adv. Mater.* **2005**, *17* (15), 1890–1893.

(5) Singh-Rachford, T. N.; Castellano, F. N. Photon Upconversion Based on Sensitized Triplet–triplet Annihilation. *Coord. Chem. Rev.* **2010**, *254* (21–22), 2560–2573.

(6) Khnayzer, R. S.; Blumhoff, J.; Harrington, J. A.; Haefele, A.; Deng, F.; Castellano, F. N. Upconversion-Powered Photoelectrochemistry. *Chem. Commun.* **2012**, *48* (2), 209–211.

(7) Stolik, S.; Delgado, J. A.; Pérez, A.; Anasagasti, L. Measurement of the Penetration

Depths of Red and near Infrared Light in Human “Ex Vivo” Tissues. *J. Photochem. Photobiol. B Biol.* **2000**, *57* (2), 90–93.
(8) Zhou, J.; Liu, Q.; Feng, W.; Sun, Y.; Li, F. Upconversion Luminescent Materials: Advances and Applications. *Chem. Rev.* **2015**, *115* (1), 395–465.
(9) Schulze, T. F.; Schmidt, T. W. Photochemical Upconversion: Present Status and Prospects for Its Application to Solar Energy Conversion. *Energy Environ. Sci.* **2015**, *8* (1), 103–125.
(10) Liu, S.-W.; Lee, C.-C.; Yuan, C.-H.; Su, W.-C.; Lin, S.-Y.; Chang, W.-C.; Huang, B.-Y.; Lin, C.-F.; Lee, Y.-Z.; … Chen, K.-T. Transparent Organic Upconversion Devices for Near-Infrared Sensing. *Adv. Mater.* **2015**, *27* (7), 1217–1222.
(11) Kwon, O. S.; Song, H. S.; Conde, J.; Kim, H.; Artzi, N.; Kim, J.-H. Dual-Color Emissive Upconversion Nanocapsules for Differential Cancer Bioimaging In Vivo. *ACS Nano* **2016**, *10* (1), 1512–1521.
(12) Cheng, Y. Y.; Fuckel, B.; MacQueen, R. W.; Khoury, T.; Clady, R. G. C. R.; Schulze, T. F.; Ekins-Daukes, N. J.; Crossley, M. J.; Stannowski, B.; … Schmidt, T. W. Improving the Light-Harvesting of Amorphous Silicon Solar Cells with Photochemical Upconversion. *Energy Environ. Sci.* **2012**, *5* (5), 6953–6959.
(13) Goldschmidt, J. C.; Fischer, S. Upconversion for Photovoltaics – a Review of Materials, Devices and Concepts for Performance Enhancement. *Adv. Opt. Mater.* **2015**, *3* (4), 510–535.
(14) Green, M. A. Third Generation Photovoltaics: Ultra-High Conversion Efficiency at Low Cost. *Prog. Photovolt. Res. Appl.* **2001**, *9* (2), 123–135.
(15) Wu, M.; Congreve, D. N.; Wilson, M. W. B.; Jean, J.; Geva, N.; Welborn, M.; Van Voorhis, T.; Bulović, V.; Bawendi, M. G.; Baldo, M. A. Solid-State Infrared-to-Visible Upconversion Sensitized by Colloidal Nanocrystals. *Nat. Photonics* **2016**, *10* (1), 31–34.
(16) Amemori, S.; Yanai, N.; Kimizuka, N. Metallonaphthalocyanines as Triplet Sensitizers for Near-Infrared Photon Upconversion beyond 850 Nm. *Phys. Chem. Chem. Phys.* **2015**, *17* (35), 22557–22560.
(17) Sasaki, Y.; Amemori, S.; Kouno, H.; Yanai, N.; Kimizuka, N. Near Infrared-to-Blue Photon Upconversion by Exploiting Direct S-T Absorption of a Molecular Sensitizer. *J. Mater. Chem. C* **2017**, *5* (21), 5063–5067.
(18) Mase, K.; Okumura, K.; Yanai, N.; Kimizuka, N. Triplet Sensitization by Perovskite Nanocrystals for Photon Upconversion. *Chem. Commun.* **2017**, *53* (59), 8261–8264.
(19) Huang, Z.; Li, X.; Mahboub, M.; Hanson, K. M.; Nichols, V. M.; Le, H.; Tang, M. L.; Bardeen, C. J. Hybrid Molecule-Nanocrystal Photon Upconversion Across the Visible and Near-Infrared. *Nano Lett.* **2015**, *15* (8), 5552–5557.
(20) Mahboub, M.; Huang, Z.; Tang, M. L. Efficient Infrared-to-Visible Upconversion with Subsolar Irradiance. *Nano Lett.* **2016**, *16* (11), 7169–7175.
(21) Moor, K.; Kim, J.-H.; Snow, S.; Kim, J.-H. [C70] Fullerene-Sensitized Triplet-Triplet Annihilation Upconversion. *Chem. Commun.* **2013**, *49* (92), 10829–10831.
(22) Zhang, C.; Zhao, J.; Wu, S.; Wang, Z.; Wu, W.; Ma, J.; Guo, S.; Huang, L. Intramolecular RET Enhanced Visible Light-Absorbing Bodipy Organic Triplet Photosensitizers and Application in Photooxidation and Triplet–Triplet Annihilation Upconversion. *J. Am. Chem. Soc.* **2013**, *135* (28), 10566–10578.
(23) Oldenburg, M.; Turshatov, A.; Busko, D.; Wollgarten, S.; Adams, M.; Baroni, N.; Welle, A.; Redel, E.; Wöll, C.; … Howard, I. A. Photon Upconversion at Crystalline Organic–

Organic Heterojunctions. *Adv. Mater.* **2016**, *28* (38), 8477–8482.
(24) Baluschev, S.; Yakutkin, V.; Miteva, T.; Avlasevich, Y.; Chernov, S.; Aleshchenkov, S.; Nelles, G.; Cheprakov, A.; Yasuda, A.; … Wegner, G. Blue-Green Up-Conversion: Noncoherent Excitation by NIR Light. *Angew. Chem. Int. Ed.* **2007**, *46* (40), 7693–7696.
(25) Dzebo, D.; Börjesson, K.; Gray, V.; Moth-Poulsen, K.; Albinsson, B. Intramolecular Triplet–Triplet Annihilation Upconversion in 9,10-Diphenylanthracene Oligomers and Dendrimers. *J. Phys. Chem. C* **2016**, *120* (41), 23397–23406.
(26) Yu, X.; Cao, X.; Chen, X.; Ayres, N.; Zhang, P. Triplet-Triplet Annihilation Upconversion from Rationally Designed Polymeric Emitters with Tunable Inter-Chromophore Distances. *Chem. Commun.* **2015**, *51* (3), 588–591.
(27) Singh-Rachford, T. N.; Haefele, A.; Ziessel, R.; Castellano, F. N. Boron Dipyrromethene Chromophores: Next Generation Triplet Acceptors/Annihilators for Low Power Upconversion Schemes. *J. Am. Chem. Soc.* **2008**, *130* (48), 16164–16165.
(28) Sugunan, S. K.; Greenwald, C.; Paige, M. F.; Steer, R. P. Efficiency of Noncoherent Photon Upconversion by Triplet–Triplet Annihilation: The C60 Plus Anthanthrene System and the Importance of Tuning the Triplet Energies. *J. Phys. Chem. A* **2013**, *117* (26), 5419–5427.
(29) Ravetz, B. D.; Pun, A. B.; Churchill, E. M.; Congreve, D. N.; Rovis, T.; Campos, L. M. Photoredox Catalysis Using Infrared Light via Triplet Fusion Upconversion. *Nature* **2019**, *565*, 343–346.
(30) Zhou, E.; Yamakawa, S.; Tajima, K.; Yang, C.; Hashimoto, K. Synthesis and Photovoltaic Properties of Diketopyrrolopyrrole-Based Donor−Acceptor Copolymers. *Chem. Mater.* **2009**, *21* (17), 4055–4061.
(31) Chen, H.; Guo, Y.; Yu, G.; Zhao, Y.; Zhang, J.; Gao, D.; Liu, H.; Liu, Y. Highly π-Extended Copolymers with Diketopyrrolopyrrole Moieties for High-Performance Field-Effect Transistors. *Adv. Mater.* **2012**, *24* (34), 4618–4622.
(32) Kaur, M.; Choi, D. H. Diketopyrrolopyrrole: Brilliant Red Pigment Dye-Based Fluorescent Probes and Their Applications. *Chem. Soc. Rev.* **2015**, *44* (1), 58–77.
(33) Bijleveld, J. C.; Zoombelt, A. P.; Mathijssen, S. G. J.; Wienk, M. M.; Turbiez, M.; de Leeuw, D. M.; Janssen, R. A. J. Poly(Diketopyrrolopyrrole−terthiophene) for Ambipolar Logic and Photovoltaics. *J. Am. Chem. Soc.* **2009**, *131* (46), 16616–16617.
(34) Qu, S.; Tian, H. Diketopyrrolopyrrole (DPP)-Based Materials for Organic Photovoltaics. *Chem. Commun.* **2012**, *48* (25), 3039–3051.
(35) Li, W.; Hendriks, K. H.; Wienk, M. M.; Janssen, R. A. J. Diketopyrrolopyrrole Polymers for Organic Solar Cells. *Acc. Chem. Res.* **2016**, *49* (1), 78–85.
(36) Hartnett, P. E.; Margulies, E. A.; Mauck, C. M.; Miller, S. A.; Wu, Y.; Wu, Y.-L.; Marks, T. J.; Wasielewski, M. R. Effects of Crystal Morphology on Singlet Exciton Fission in Diketopyrrolopyrrole Thin Films. *J. Phys. Chem. B* **2016**, *120* (7), 1357–1366.
(37) Frisch, M. J.; Trucks, G. W.; Schlegel, H. B.; Scuseria, G. E.; Robb, M. A.; Cheeseman, J. R.; Scalmani, G.; Barone, V.; Mennucci, B.; … Fox, D. J. Gaussian 09, Revision D.01. *Gaussian 09, Revision D.01, Gaussian, Inc., Wallingford CT*. 2009.
(38) Shen, L.; Tang, Z.; Wang, X.; Liu, H.; Chen, Y.; Li, X. Effects of Aromatic Substituents on Electronic Structure and Excited State Energy Levels of Diketopyrrolopyrrole Derivatives for Singlet Fission. *Phys. Chem. Chem. Phys.* **2018**, *20* (35), 22997–23006.
(39) Singh-Rachford, T. N.; Castellano, F. N. Pd(II) Phthalocyanine-Sensitized Triplet−Triplet Annihilation from Rubrene. *J. Phys. Chem. A* **2008**, *112* (16), 3550–3556.

(40) Daniele, B.; Abdelhafid, J.; Luciano, M.; Massimo, M.; Silvia, R.; Antonio, P.; Abderrahim, Y. The Rubrenic Synthesis: The Delicate Equilibrium between Tetracene and Cyclobutene. *Eur. J. Org. Chem.* **2011**, *2011* (22), 4160–4169.
(41) Data, P.; Kurowska, A.; Pluczyk, S.; Zassowski, P.; Pander, P.; Jedrysiak, R.; Czwartosz, M.; Otulakowski, L.; Suwinski, J.; … Monkman, A. P. Exciplex Enhancement as a Tool to Increase OLED Device Efficiency. *J. Phys. Chem. C* **2016**, *120* (4), 2070–2078.
(42) Ying, S.; Chen, M.; Liu, Z.; Zheng, M.; Zhang, H.; Xue, S.; Yang, W. Unusual Mechanohypsochromic Luminescence and Unique Bidirectional Thermofluorochromism of Long-Alkylated Simple DPP Dyes. *J. Mater. Chem. C* **2017**, *5* (24), 5994–5998.
(43) J., M. C.; R., S. C.; Martina, F.; Sven, H.; Mukundan, T. High Bulk Electron Mobility Diketopyrrolopyrrole Copolymers with Perfluorothiophene. *Adv. Funct. Mater.* **2015**, *25* (18), 2725–2736.
(44) Suraru, S.-L.; Zschieschang, U.; Klauk, H.; Wurthner, F. Diketopyrrolopyrrole as a P-Channel Organic Semiconductor for High Performance OTFTs. *Chem. Commun.* **2011**, *47* (6), 1767–1769.
(45) Bürckstümmer, H.; Weissenstein, A.; Bialas, D.; Würthner, F. Synthesis and Characterization of Optical and Redox Properties of Bithiophene-Functionalized Diketopyrrolopyrrole Chromophores. *J. Org. Chem.* **2011**, *76* (8), 2426–2432.
(46) de Mello, J. C.; Wittmann, H. F.; Friend, R. H. An Improved Experimental Determination of External Photoluminescence Quantum Efficiency. *Adv. Mater.* **1997**, *9* (3), 230–232.

Chapter 7: Upconversion and Photoredox

7.1 Preface

This chapter is based on manuscript entitled "Photoredox Catalysis using Infrared Light via Triplet Fusion Upconversion" by Benjamin D. Ravetz, Andrew B. Pun, Emily M. Churchill, Daniel N. Congreve, Tomislav Rovis, and Luis M. Campos published in Nature.[1]

I characterized the upconversion properties of these materials with help from Daniel N. Congreve. I performed and analyzed the photoredox and materials penetration experiments with Benjamin D. Ravetz and Emily M. Churchill. Equal contributions to this paper were made by Benjamin D. Ravetz and myself.

7.2 Introduction

Existing photocatalysts must be excited with either ultraviolet or visible light, translating to an initial excited-state energy of 50–80 kcal mol^{-1}.[2,3] This energy is then transferred to the substrate of interest, leading to the desired reactivity. Near-infrared (NIR) light can generate only low-energy excited states (around 35 kcal mol^{-1}), which fall short of the energy required to achieve the majority of desired transformations.

The photophysical process of triplet fusion upconversion—the conversion of low-energy photons into high-energy excited states—has gained increased attention in recent years,[4] in large part due to its potential to increase the efficiency of photovoltaics.[5] Although the solar applications of triplet fusion upconversion have received the most attention, it can be applied in various other fields ranging from biological imaging[6] to data storage.[7]

NIR light can be harnessed for chemical transformations by using lanthanide-containing nanoparticles or by upconversion via triplet fusion; however, these approaches are limited to the direct activation of substrates.[8–11] This shortcoming limits the methodology to

substrates bearing photocleavable bonds and can be addressed by the activation of a catalyst in place of the substrate. Organic chromophores have great potential for triplet fusion upconversion, especially because of their tunable electronic structure (Figure 7.1A).[12] We show that it is possible to use low-energy NIR light to access the complex synthetic toolbox enabled by photoredox catalysis. This strategy is highly modular, as it is possible to match components of the upconversion and photoredox systems to promote various chemical transformations in one pot.[13,14]

7.3 Results and Discussion

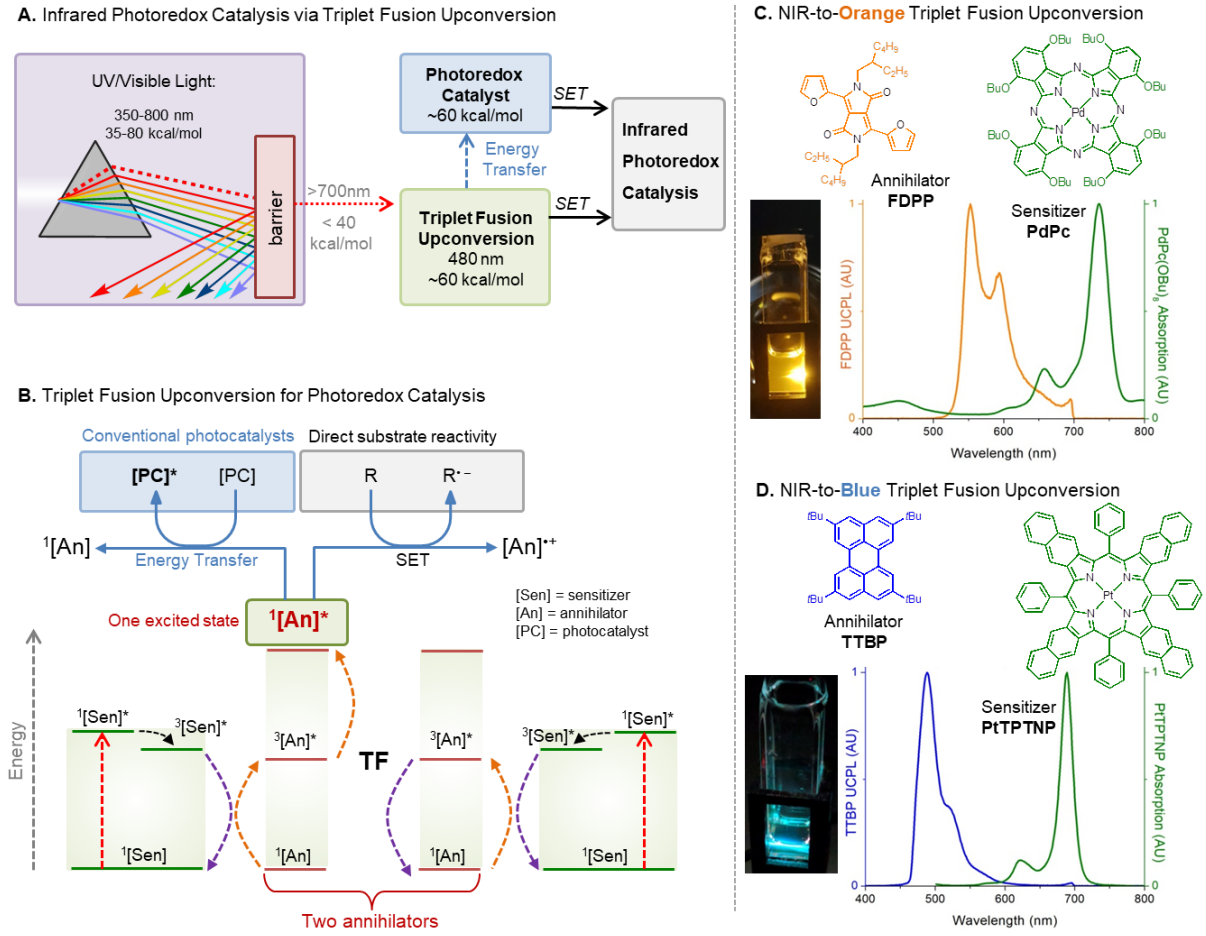

Figure 7.1 The NIR-to-Orange and NIR-to-Blue Upconversion Strategy A) A schematic of infrared photoredox catalysis via triplet fusion upconversion. SET, single-electron transfer. B) A Jablonski description of triplet fusion upconversion and its adaptation to photoredox catalysis. Energy transfer from ^{1}[An]* to the photocatalyst may occur by resonance transfer or

by photon emission or absorption. PC, photocatalyst; R, an organic compound; $R^{\bullet-}$, excited substrate radical anion; TF, triplet fusion. C) NIR-to-orange upconversion photoluminescence using FDPP and PdPc. D) NIR-to-blue upconversion photoluminescence using tetratertbutylperylene (TTBP) and platinum(II) tetraphenyltetranaphthoporphyrin (PtTPTNP).

The process of triplet fusion upconversion involves two species: an annihilator and a sensitizer (Figure 7.1B).[15,16] The sensitizer absorbs a low-energy photon, initially generating a singlet excited sensitizer, ^{1}[Sen]*, which decays into a triplet excited sensitizer, ^{3}[Sen]*. This energy is then transferred to the annihilators, forming ^{3}[An]*. Two ^{3}[An]* molecules can then undergo triplet fusion, which leads to the generation of a higher-energy singlet exciton on one of the annihilators, ^{1}[An]*. This then decays via fluorescence, giving off a high-energy photon.

In considering the energetic requirements of a new infrared–visible triplet fusion upconversion system, we became aware of a recent study that showed it is possible to vary the singlet energy levels of diketopyrrolopyrrole derivatives for singlet fission without altering the triplet energy.[17] We leveraged this finding to adjust the singlet energy until it was slightly less than double the triplet energy, and in doing so we observed triplet fusion upconversion. We used furanyldiketopyrrolopyrrole (FDPP) as an annihilator with palladium(II) octabutoxyphthalocyanine (PdPc) as the sensitizer;[18] this system absorbs NIR photons (λ_{max} = 730 nm) and has an emission that extends to around 530 nm (Figure 7.1C). The FDPP:PdPc system has an upconversion yield of 3.2%, while the fluorescence quantum yields of common photoredox catalysts such as $[Ru(bpy)_3]^{2+}$ (bpy, bipyridyl) and Rose Bengal are 9.5%[2] and 9%[19], respectively (see below for full details). When combining the upconversion system with hydrodehalogenation conditions,[20] we observed the dehalogenated product in 61% yield (Figure 7.2A). In this initial example, we established the ability of triplet fusion upconversion to enable low-energy NIR light to activate a catalyst, Eosin Y, that is capable of reducing a C–

Br bond. Control reactions, in which the photocatalyst or upconversion components are removed, show only trace yields. These results suggest that the external NIR radiation is converted inside the reaction vessel to visible light, which is then absorbed by Eosin Y. As a direct comparison, an identical reaction was irradiated with a 40-W blue Kessil lamp instead of an NIR diode; a 78% yield was obtained in a similar reaction time. It is notable that the 0.040-W NIR diode is orders of magnitude weaker than the blue light source. We thus propose that the light emitted from upconversion is generated deep within the reaction vessel, leading to a large number of 'lightbulbs' inside the flask. In turn, the net surface area of illumination by these lightbulbs is orders of magnitude greater than that possible with light sources on the outside. For this reason, we can maintain similar yields with a light source that is 1,000 times less powerful than the photoredox standard.

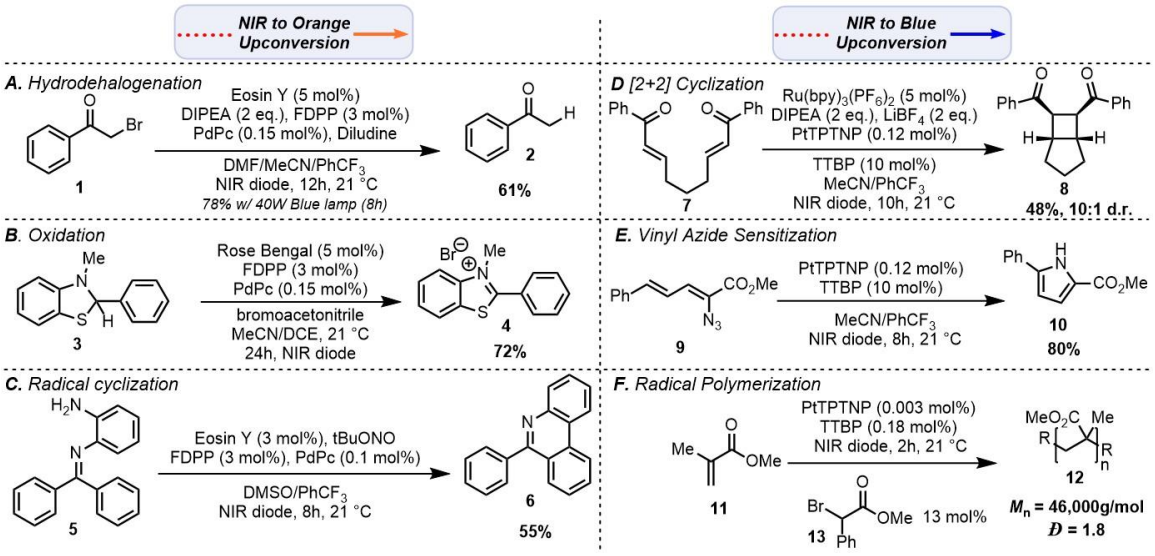

Figure 7.2 Selected Examples of Reactions Driven by NIR Light A) Hydrodehalogenation reaction catalyzed by Eosin Y. B) Amine oxidation catalyzed by Rose Bengal. C) Reductive radical cyclization yielding a phenanthridine product. D) Intramolecular [2+2] cyclization. E) Pyrrole formation via vinyl azide reduction. F) Polymerization of methyl methacrylate

To test the generality of this system towards other reactions, we pursued two other transformations. In a similar manner, we found that Rose Bengal could be excited by NIR-

light triplet fusion upconversion to catalyze amine oxidation in 72% yield (Figure 7.2B).[21] Further, this system was adapted to a C–N bond activation catalyzed by Eosin Y to yield phenanthridine products (Figure 7.2C).[22]

This FDPP:PdPc system enables the use of NIR light to promote reactions that require photocatalysts that absorb green or yellow light. However, most organometallic photocatalysts absorb higher-energy blue or ultraviolet light.[4] We found thatgoo it is possible to use the NIR-absorbing sensitizer platinum(II) tetraphenyltetranaphthoporphyrin (PtTPTNP),[23,24] together with a simple blue-emitting annihilator, tetratertbutylperylene (TTBP), to generate NIR-to-blue photon upconversion. This system generates a large anti-Stokes shift (around 1.0 eV)[25] and provides an upconversion yield of up to 2.0% (Figure 7.1D) (see below for full details).

We adapted this upconversion system to a prototypical $[Ru(bpy)_3]^{2+}$-catalyzed reaction: the intramolecular [2+2] cyclization of enones (Figure 7.2D).[26] Adding TTBP and PtTPTNP to the standard reaction conditions provided the cyclobutane product in moderate yield and excellent diastereomeric ratio. Control reactions revealed that the removal of $Ru(bpy)_3(PF_6)_2$ still results in a 38% yield of cyclobutane product, which suggests that the ^{1}[An]* of TTBP is capable of performing photoredox catalysis on its own; this reduces the three-component system to a two-component system and streamlines the catalysis.

To test whether the ^{1}[An]* state of TTBP could be applied directly for catalysis, we investigated the photoredox-catalyzed cyclization of dienyl azides to pyrroles (Figure 7.2E). Upon NIR (730 nm) irradiation of the sensitizer, annihilator and substrate, the pyrrole product was formed in 80% yield.

After observing the strong reducing nature of the ^{1}[An]* state of TTBP, we attempted to use NIR radiation to initiate the polymerization of methyl methacrylate (MMA) via C–Br bond reduction (Figure 7.2F). Simply irradiating the sensitizer, annihilator and initiator in neat MMA provided poly(methyl methacrylate) (PMMA; M_n = 46,000 g mol^{-1}; dispersity ($Đ$) = 1.80). The polymerization of MMA has previously been demonstrated with perylene as a photocatalyst under visible-light irradiation;[27] however, here we have enabled deep-penetrating NIR light to stimulate the photocatalyst, providing avenues for the integration of photoredox catalysis into new materials.

To demonstrate the ability of NIR light to penetrate a range of media, we performed the MMA polymerization with 5% ethylene glycol dimethacrylate as a crosslinker to generate a freestanding gel, while using several visible-light-absorbing materials to disrupt the path of the incident laser (Figure 7.3A,C). A PMMA gel was synthesized with an NIR light source through various different barriers; meanwhile, a gel was not formed when the 450-nm blue light source was used, presumably owing to its limited penetrating ability (Figure 7.3B). Notably, the NIR light showed excellent penetrating power through hemoglobin, a component of human blood that absorbs visible light. In addition to the gelation reaction, the [2+2] cyclization reaction shown in Figure 7.2D was performed through a barrier of 0.2 mM hemoglobin solution. The product yield with the NIR laser was 46%—identical to that of the reaction conducted without a barrier—whereas the blue laser gave a 1% yield.

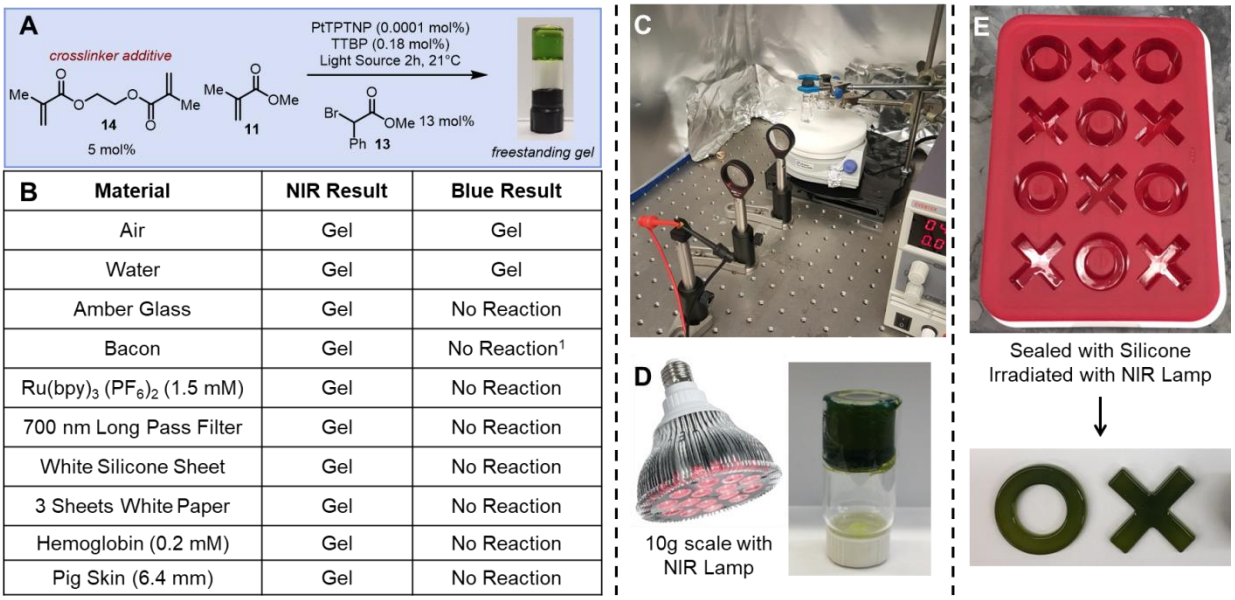

B Material	NIR Result	Blue Result
Air	Gel	Gel
Water	Gel	Gel
Amber Glass	Gel	No Reaction
Bacon	Gel	No Reaction[1]
$Ru(bpy)_3(PF_6)_2$ (1.5 mM)	Gel	No Reaction
700 nm Long Pass Filter	Gel	No Reaction
White Silicone Sheet	Gel	No Reaction
3 Sheets White Paper	Gel	No Reaction
Hemoglobin (0.2 mM)	Gel	No Reaction
Pig Skin (6.4 mm)	Gel	No Reaction

Figure 7.3 Material Penetration Experiments A) The reaction to form a crosslinked PMMA gel, used to test the penetration of NIR (730 nm) compared with blue (450 nm) light through various media. Reactions that bypass the barrier generate a gel. B) Table showing the results obtained when different materials are used as a light barrier in the reaction in A). [1]Experiment halted after 15 minutes owing to fire hazard, as the bacon began to burn upon irradiation. C) Experimental set-up using a laser diode, with water as the barrier. D) PMMA gel (right) prepared by performing the reaction on a 10-g scale using the NIR lamp shown (left). E) The silicone mold used, together with the PMMA shapes that were synthesized through a 7-mm white silicone pad.

7.4 Conclusion

The scale-up of visible-light photoredox reactions suffers from shallow light absorption, as evidenced by slow reaction rates. In addition, increasing the size of the reaction vessel decreases the relative surface area, thus reducing photon exposure[28,29] and fundamentally limiting photocatalyst excitation. Infrared photoredox can overcome both of these challenges. For example, the penetration of infrared light through the [2+2] cyclization reaction mixture (Figure 7.2D) is 304 times deeper than that of blue light, based on concentration and extinction coefficients (Figure 7.4). By the same analysis, we found that infrared light penetrates 293 times further than blue light through the polymerization reaction mixture (Figure 7.2F), thus rendering this chemistry scalable (Figure 7.3D). This reaction also

demonstrates that a laser is not necessary to perform upconversion, suggesting that this technique could be broadly applied. Scalability and improved penetration through materials were demonstrated by performing polymerization on a multi-gram scale in an opaque silicone mold (Figure 7.3E). The sealed mold is resistant to visible light, while the NIR photons pass through uninhibited. As predicted, the defined shapes were achieved only with the NIR lamp and not with the blue lamp. With this proof-of-principle experiment it is possible to observe the effects of the penetration of infrared radiation through various barriers, and studies to characterize the materials properties of various gels will follow.

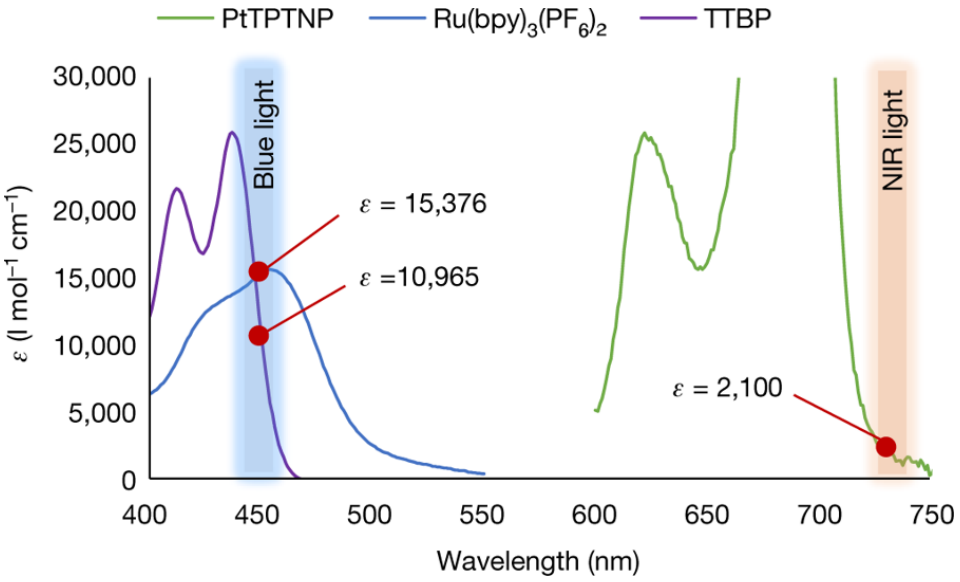

Figure 7.4 Application of the Beer-Lambert Law to Blue and NIR Light Comparison of extinction coefficients and concentrations of $Ru(bpy)_3(PF_6)_2$ and TTBP with those of PtTPTNP reveals a large increase in reaction penetration by infrared light compared to blue light, according to the Beer–Lambert relation $A = \varepsilon cl$ (A, absorbance; ε, molar extinction coefficient; c, concentration; l, path length). For $[Ru(bpy)_3]^{2+}$, ε is 7.29 times larger and c is 41.7 times larger than for PtTPTNP; infrared light (730 nm) thus penetrates 304 times further than blue light (450 nm) through the reaction solution in Figure 7.2D. For TTBP, ε is 5.17 times larger and c is 56.7 times larger than for PtTPTNP; the penetration of infrared light (730 nm) is therefore 293 times greater than that of blue light (450 nm) through the reaction solution in Figure 7.2F.

7.5 Materials and Methods

Unless noted, all reactions were performed in oven-dried glassware and carried out under

an atmosphere of argon or nitrogen with magnetic stirring. The reactions in the general procedures section are tolerant of non flame-dried vials. All column chromatography was performed using general flash techniques on SiliCycle® SilicaFlash® P60, 40-63 μm 60 Å. For particularly difficult separations, on Teledyne Isco Combiflash using CombiFlash gold pre-packed columns. Thin layer chromatography was performed on SiliCycle® 250 μm 60 Å plates. Visualization was accomplished with 254 nm UV light, $KMnO_4$ stain, or I_2.

NMR spectra were recorded on Varian 300 or 400 MHz spectrometers, and Bruker 400 or 500 MHz spectrometers at ambient temperature. Chemical shifts (δ) are reported in parts per million (ppm) from $CDCl_3$ (^{1}H: 7.26 ppm, ^{13}C: 77.16 ppm), CD_2Cl_2 (^{1}H: 5.32 ppm, ^{13}C: 54.0 ppm), CD_3OD (^{1}H: 4.78, 3.31 ppm, ^{13}C: 49.15 ppm) or CD_3CN (^{1}H: 1.94 ppm, ^{13}C: 1.32 ppm) with multiplicity (*s* = singlet, br. *s* = broad singlet, *d* = doublet, *t* = triplet, *q* = quartet, and *m* = multiplet) and coupling constants (in Hz). Diastereomer ratios for all compounds were determined by ^{1}H NMR analysis of the unpurified reaction mixtures. Mass spectra were recorded on a Waters Acquity H UPLC-MS. Infrared spectra were collected on a Perkin Elmer Spectrum Two FT-IR spectrometer. Gel permeation chromatography was performed using a Waters 1515 isocratic HPLC pump with a 2990 photodiode array detector and 2414 refractive index detector.

Solutions of FDPP, TTBP, PdPc, and PtTPTNP were prepared from anhydrous toluene in a nitrogen glovebox. Solutions were made in 1 cm x 1 cm quartz cuvettes from Spectrocell and were degassed by sparging with nitrogen for 30 seconds then sealed before removing from glovebox for measurement. Solutions were excited with a 730 nm laser diode purchased from Thorlabs, focused to a beam diameter of 0.15 mm. All upconverted PL spectra were measured with a QEPro spectrometer purchased from Ocean Optics through a 700 nm shortpass filter.

Absorption spectra were obtained on an Agilent Technologies Cary 60 UV-Vis spectrophotometer.

730nm and 450 nm laser diodes were purchased from Thorlabs. 700-800 nm LED lamp was purchased from powerPAR via Amazon. The Blue lamp is an H150 Kessil 35W LED lamp. Reactions were placed approximately 10 cm from lamps, and at the focal point of lasers

Unless otherwise stated, all starting materials were obtained from commercial sources including Sigma-Aldrich, TCI, Matrix, Alfa-Aesar, and Oakwood Scientific. FDPP and PtTPTNP were synthesized according to previously described procedures. PdPc was purchased from Frontier Scientific and was used without further purification. TTBP was purchased from TCI and used without further purification.

7.6 Starting Materials Preparation

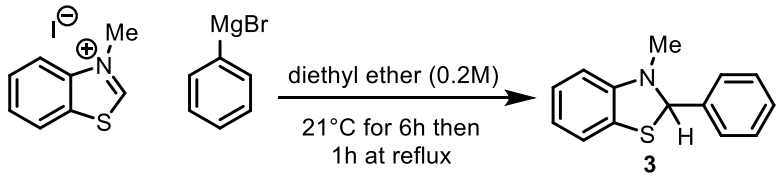

3

Compound 3 was isolated according to published procedure and the product spectra are identical to the known compound.[30]

^{1}H-NMR (400 MHz, $CDCl_3$): δ 7.56 (dd, J = 7.7, 1.8 Hz, 2H), 7.42 – 7.33 (m, 3H), 7.06 – 6.99 (m, 2H), 6.72 (td, J = 7.5, 1.0 Hz, 1H), 6.41 (d, J = 7.8 Hz, 1H), 5.99 (s, 1H), 2.64 (s, 3H) ppm.

^{13}C-NMR (101 MHz, $CDCl_3$): δ 148.3, 139.5, 129.1, 128.9, 127.8, 125.9, 121.5, 119.4, 33.8 ppm.

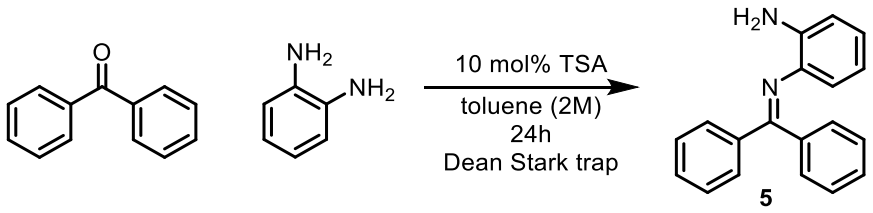

Compound 5 was isolated according to published procedure and the product spectra are identical to the known compound (ii).[31]

^{1}H-NMR (400 MHz, $CDCl_3$): δ 7.78 (*d*, *J* = 1.5 Hz, 2H), 7.51 – 7.44 (*m*, 1H), 7.44 – 7.38 (*m*, 2H), 7.36 – 7.27 (*m*, 3H), 7.22 – 7.14 (*m*, 2H), 6.81 (*td*, *J* = 7.8, 1.4 Hz, 1H), 6.71 (*dd*, *J* = 7.9, 1.3 Hz, 1H), 6.40 (*td*, *J* = 7.7, 1.4 Hz, 1H), 6.18 (*dd*, *J* = 7.8, 1.3 Hz, 1H), 3.92 (*s*, 2H) ppm.

^{13}C-NMR (101 MHz, $CDCl_3$): δ 168.7, 140.3, 139.9, 137.8, 136.5, 130.8, 129.5, 129.2, 129.0, 128.2, 125.0, 120.0, 118.1, 115.0 ppm.

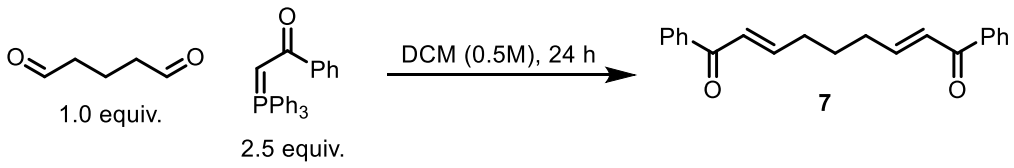

Compound 7 was isolated according to published procedure and the product spectra are identical to the known compound.[32]

^{1}H-NMR (400 MHz, $CDCl_3$): δ 7.95 – 7.91 (m, 4H), 7.59 – 7.53 (m, 2H), 7.50 – 7.44 (m, 4H), 7.06 (dt, *J* = 15.3, 6.8 Hz, 2H), 6.92 (dt, *J* = 15.4, 1.3 Hz, 2H), 2.45 – 2.37 (m, 4H), 1.80 (m, 2H). ppm.

^{13}C-NMR (101 MHz, $CDCl_3$): δ 190.8, 148.6, 138.0, 132.9, 128.7, 128.7, 126.7, 32.3, 26.9 ppm.

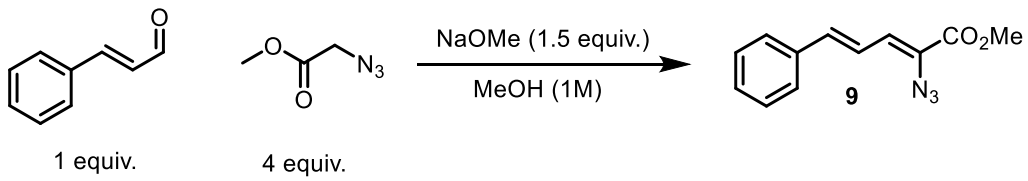

Compound 9 was isolated according to published procedure and the product spectra are identical to the known compound.[33]

^{1}H-NMR (400 MHz, $CDCl_3$): δ 7.51 – 7.46 (*m*, 2H), 7.39 – 7.27 (*m*, 3H), 7.17 (*dd*, *J* = 15.7, 11.2 Hz, 1H), 6.85 – 6.73 (*m*, 2H), 3.88 (*s*, 3H) ppm.

^{13}C-NMR (101 MHz, $CDCl_3$): δ 163.7, 139.3, 136.5, 129.1 (d, *J* = 18.6 Hz), 127.4 (d, *J* = 13.0 Hz), 125.6, 122.4, 52.8.ppm.

FDPP was isolated according to published procedure and the product spectra are identical to the known compound.[34]

^{1}H-NMR (400 MHz, $CDCl_3$): δ 8.32 (d, 2H), 7.61 (d, 2H), 6.69 (m, 2H), 4.04 (d, 4H), 1.76 (m, 2H), 1.38 – 1.24 (d, 16H), 0.93-0.84 (m, 12H). ppm.

^{13}C-NMR (101 MHz, $CDCl_3$): δ 161.4, 145.0, 144.8, 134.1, 120.3, 113.6,106.6, 46.3, 40.1, 30.1, 28.8, 24.0, 23.2, 14.2, 10.9 ppm.

PtTPTNP was isolated according to published procedure and the product spectra are identical to the known compound.[23] The ^{1}H-NMR (400 MHz, $CDCl_3$) of the non-metallated macrocycle precursor has been provided below.

7.7 General Procedures

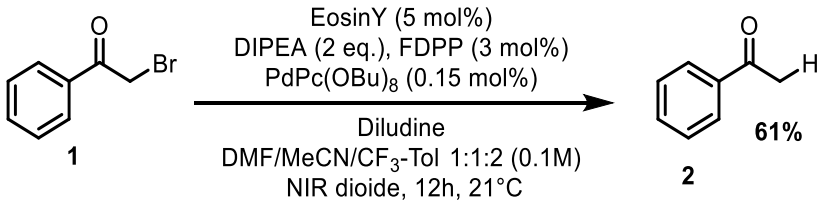

To a flame dried 1 dram vial containing a stir-bar was added 50.0 mg **1** (0.25 mmol), 70 mg diludine (0.28 mmol), 8.1 mg Eosin Y (0.0125 mmol), and 3.5 mg FDPP (0.007 mmol). The vial was then pumped into a glove-box under argon atmosphere. After, 0.625 mL anhydrous DMF, 0.625 mL anhydrous acetonitrile, and 0.8 mL trifluorotoluene was added followed by 0.45 mg (0.000375 mmol) $PdPc(OBu)_8$ (stored as a 1 mg/mL solution in trifluorotoluene). Finally, 89 µl DIPEA (0.50 mmol) was added, the reaction was sealed, and transferred to the IR light source under the shield of aluminum foil. After, the reaction was irradiated for 12 h at 21°C. Upon completion, the vial was wrapped in aluminum foil and was concentrated under reduced pressure to remove the acetonitrile. The crude mixture was subjected to column chromatography on silica gel using pentane/ethyl acetate as eluent. The combined fractions were concentrated under reduced pressure and the product spectra are identical to the known compound **2**.[20]

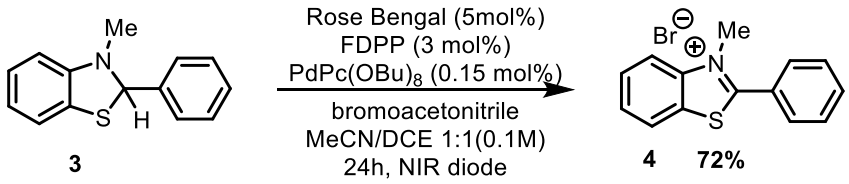

To a flame dried 1 dram vial containing a stir-bar was added 57.0 mg **3** (0.25 mmol), 12.2 mg Rose Bengal (0.0125 mmol), and 3.5 mg FDPP (0.007 mmol). The vial was then pumped into a glove-box under argon atmosphere. After, 1.03 mL anhydrous DCE, 20 µL bromoacetonitrile (0.28 mmol), and 1.03 mL anhydrous MeCN were added followed by 0.45 mg (0.0004 mmol) $PdPc(OBu)_8$ (stored as a 1 mg/mL solution in trifluorotoluene). Afterward, the reaction was sealed, and transferred to the IR light source under a shield of aluminum foil. After, the reaction was irradiated for 24 h at 21°C. Upon completion, the vial was wrapped in aluminum foil and was concentrated under reduced pressure to remove all solvent. To the crude mixture was added 3 mL diethyl ether which produced a white precipitate. The solid was filtered and washed with 5 mL diethyl ether. Then, the solid was washed with acetonitrile and the filtrate was concentrated and re-precipitated with diethyl ether. This process was repeated 4 times to remove Rose Bengal to yield 72% product **4**.

^{1}H-NMR (400 MHz, CD_3CN): δ 8.44 (d, J = 8.2 Hz, 1H), 8.22 (d, J = 8.5 Hz, 1H), 7.98 (ddd, J = 8.5, 7.3, 1.1 Hz, 1H), 7.91 – 7.83 (m, 4H), 7.82 – 7.72 (m, 2H), 4.23 (s, 3H). ppm.

^{13}C-NMR (101 MHz, CD_3OD): δ 176.4, 144.1, 135.3, 131.5, 131.5, 131.4, 131.1, 130.3, 126.7, 125.2, 118.6, 38.6. ppm. IR (neat): ν 3397 (*s*), 3061 (*s*), 2924 (*s*), 1630 (*s*), 1596 (*s*), 1446 (*s*), 1334 (*m*), 1246 (*s*), 760 (*s*) cm^{-1}.

HRMS-ASAP (positive): M = $C_{14}H_{12}BrNS$; expected $(M+)^+$ *m/z* 226.0690, observed $(M+H)^+$ *m/z* 226.0695; expected $(NaBr_2)^-$ *m/z* 180.8264, observed $(NaBr_2)^-$ *m/z* 180.8287.

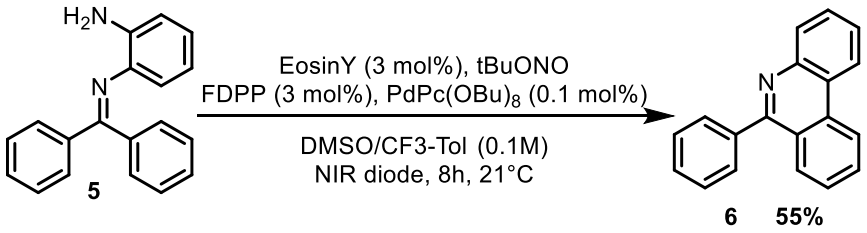

To a flame dried 1 dram vial containing a stir-bar was added 68.8 mg **5** (0.25 mmol), 5.2 mg Eosin Y (0.008 mmol), and 3.5 mg FDPP (0.007 mmol). The vial was then pumped into a glove-box under argon atmosphere. After, 0.95 mL anhydrous trifluorotoluene and 1.25 mL anhydrous DMSO were added followed by 0.30 mg (0.0003 mmol) $PdPc(OBu)_8$ (stored as a 1 mg/mL solution in trifluorotoluene) and 45 µl tert-butyl nitrite (0.38 mmol). Afterward, the reaction was sealed, and transferred to the IR light source under the shield of aluminum foil. After, the reaction was irradiated for 8 h at 21°C. Upon completion, the vial was wrapped in aluminum foil and was concentrated under reduced pressure to remove all solvent. The product was purified via column chromatography of silica eluting 20% ethyl acetate in hexanes. The combined fractions were concentrated revealing a yellow solid product. The product spectra are identical to the known compound **6**.[22]

^{1}H-NMR (400 MHz, $CDCl_3$): δ 8.72 (*d*, *J* = 8.3 Hz, 1H), 8.63 (*dd*, *J* = 8.1, 1.4 Hz, 1H), 8.25 (*dd*, *J* = 7.9, 1.2 Hz, 1H), 8.13 – 8.09 (*m*, 1H), 7.87 (*ddd*, *J* = 8.3, 7.0, 1.3 Hz, 1H), 7.81 – 7.67 (*m*, 4H), 7.65 – 7.52 (*m*, 4H) ppm.

^{13}C-NMR (101 MHz, $CDCl_3$): δ 161.4, 144.0, 140.0, 133.6, 130.7, 130.5, 129.9, 129.1, 129.0, 128.8, 128.6, 127.3, 127.1, 125.4, 123.9, 122.4, 122.1 ppm.

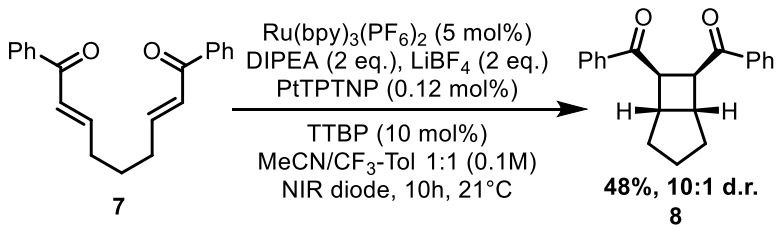

7 **8**

To a flame dried 1 dram vial containing a stir-bar was added 76.0 mg **7** (0.25 mmol), 46.9 mg $LiBF_4$ (0.50 mmol), 10.7 mg $Ru(bpy)_3(PF_6)_2$ (0.0125 mmol), and 11.9 mg TTBP (0.0025 mmol). The vial was then pumped into a glove-box under argon atmosphere. After, 1.25 mL anhydrous MeCN and 0.89 mL anhydrous trifluorotoluene were added followed by 0.36 mg (0.0003 mmol) PtTPTNP (stored as a 1 mg/mL solution in trifluorotoluene). Finally, 87 µl DIPEA (0.50 mmol) was added to the reaction mixture. Afterward, the reaction was sealed, and transferred to the IR light source under the shield of aluminum foil. After, the reaction was irradiated for 2 h at 21°C. Upon completion, the vial was wrapped in aluminum foil and was concentrated under reduced pressure to remove all solvent. The product was purified via column chromatography of silica eluting 20% ethyl acetate in hexanes. The combined fractions were concentrated revealing a white crystalline product. The product spectra are identical to the known compound **8**.[26]

^{1}H-NMR (400 MHz, $CDCl_3$): 7.76 (*dt*, *J* = 8.5, 1.6 Hz, 4H), 7.47 – 7.41 (*m*, 2H), 7.38 – 7.32 (*m*, 4H), 3.87 (*d*, *J* = 4.1 Hz, 2H), 3.21 (*dq*, *J* = 4.2, 2.5 Hz, 2H), 2.09 – 1.99 (*m*, 2H), 1.89 – 1.82 (*m*, 2H), 1.76 – 1.65 (*m*, 2H) ppm.

^{13}C-NMR (101 MHz, $CDCl_3$): δ 198.7, 136.5, 132.6, 128.6, 127.9, 48.4, 39.2, 32.6, 25.4 ppm.

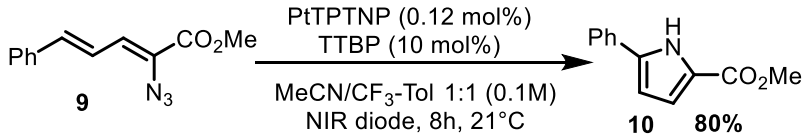

To a flame dried 1 dram vial containing a stir-bar was added 57.3 mg **9** (0.25 mmol) and 11.9 mg TTBP (0.0025 mmol). The vial was then pumped into a glove-box under argon atmosphere. After, 1.25 mL anhydrous MeCN and 0.89 mL anhydrous trifluorotoluene were added followed by 0.36 mg (0.0003 mmol) PtTPTNP (stored as a 1 mg/mL solution in trifluorotoluene). Afterward, the reaction was sealed, and transferred to the IR light source under the shield of aluminum foil. After, the reaction was irradiated for 24 h at 21°C. Upon completion, the vial was wrapped in aluminum foil and was concentrated under reduced pressure to remove all solvent. The product was purified via column chromatography with silica eluting 20% ethyl acetate in hexanes. The combined fractions were concentrated revealing a white, solid product. The product spectra are identical to the known compound.[35] Note: We propose the mechanism involves TTBP's $^{1}[An]^{*}$ reducing the dienyl azide to the radical-anion which subsequently releases nitrogen gas and cyclizes onto the pendant alkene. The resulting radical can be oxidized by the radical cation, $^{2}A^{\bullet+}$, to turn the photocatalyst over and yield product. Notably, the $^{3}[An]^{*}$ (~35 kcal/mol, $E_{1/2}$ ($PC^{\bullet+}/PC^{*}$) = -0.78 V) is too low energy to perform energy transfer or SET with the substrate ($^{3}Sub^{*}$~45 kcal/mol, $E_{1/2}(Sub/Sub^{-\bullet})$ = -1.55 V vs Ag/AgCl in MeCN), which justifies the requirement of TF upconversion for catalysis.[18]

^{1}H-NMR (400 MHz, $CDCl_3$): 9.46 (br. s, 1H), 7.58 (dd, *J* = 8.4, 1.2 Hz, 2H), 7.41 (td, *J* = 7.0, 1.7 Hz, 2H), 7.33 – 7.28 (m, 1H), 6.97 (dd, *J* = 3.9, 2.4 Hz, 1H), 6.55 (dd, *J* = 3.9, 2.7 Hz, 1H), 3.88 (s, 3H) ppm.

^{13}C-NMR (101 MHz, $CDCl_3$): δ 161.8, 137.0, 131.5, 129.2, 127.9, 124.9, 123.2, 117.0, 108.2, 51.7 ppm.

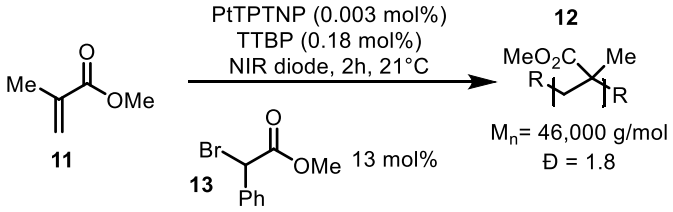

To a flame dried 1 dram vial containing a stir-bar was added 8 mg TTBP (0.017 mmol). The vial was then pumped into a glove-box under argon atmosphere. After, 1 mL methyl methacrylate **11** (9.35 mmol), 200 μL amethyl α-bromophenyl acetate **13** (1.27 mmol) and 0.36 mg (0.0003 mmol) PtTPTNP (stored as a 1 mg/mL solution in trifluorotoluene) were added to the vial. Afterward, the reaction was sealed, and transferred to the IR light source under the shield of aluminum foil. After, the reaction was irradiated for 2 h at 21°C. Upon completion, the reaction solution was precipitated from methanol. The product was collected as a white solid. GPC analysis reveals the molecular weight and dispersity of our polymer **12**. Note: the ($E_{1/2}(13/13^{\bullet-})$ = -1.58 V vs Ag/AgCl in MeCN.

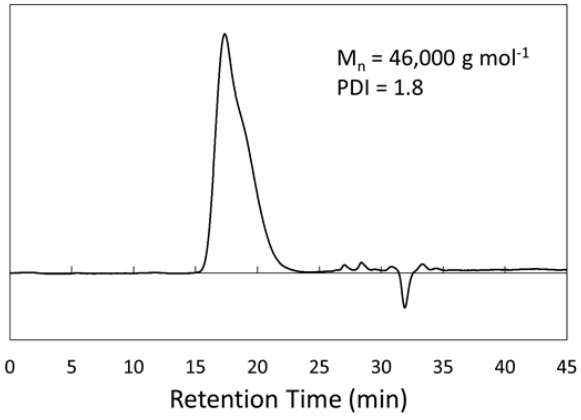

Figure 7.5 Gel Permeation Chromatograph of Methyl Methacrylate Polymer

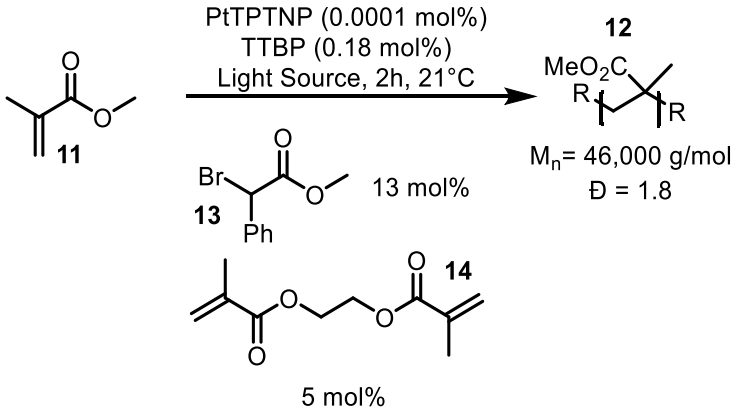

To a flame dried 1 dram vial containing a stir-bar was added 8 mg TTBP (0.017 mmol). The vial was then pumped into a glove-box under argon atmosphere. After, 1 mL methyl methacrylate **11** (9.35 mmol), 200 µL methyl α-bromophenyl acetate **13** (1.27 mmol), 88 µl ethylene glycol dimethacrylate **14** (0.47 mmol) and 0.36 mg (0.0003 mmol) PtTPTNP (stored as a 0.1 mg/mL solution in trifluorotoluene) were added to the vial. Afterward, the reaction was sealed, and transferred to the light source under the shield of aluminum foil. After, the reaction was irradiated for 4 h at 21°C. Upon completion, the reaction solution became a freestanding gel, indicative of the formation of a crosslinked PMMA if the light source is able to penetrate the barrier. The reaction mixture remaining as a liquid is indicative of a failed reaction.

7.8 Barrier Penetration

Light sources used were:

Thorlabs 730 nm 40 mW laser diode (NIR)
Thorlabs 450 nm 1.6 W laser diode (Blue)
powerPAR 700-800 nm 15W LED lamp (NIR)
H150 Kessil 35W LED lamp (400-520 nm, Blue).

LEDs were used when the barrier could be physically wrapped around the reaction vial, otherwise lasers were used in order to fix the barrier in the path of the incident light. The NIR light source was not capable of forming a gel with either a spinach leaf or tripe as a barrier.

Barrier	LED or Laser	Blue Result	NIR-Result
Air	Laser	Gel	Gel
Water (1 cm path length cuvette)	Laser	Gel	Gel
Amber Glass Vial	Lamp	No Gel	Gel
Bacon (3.2 mm thick)	Laser	No Gel[a]	Gel
$Ru(bpy)_3 (PF_6)_2$ solution (1.5 mM in DCM) (1 cm path length cuvette)	Laser	No Gel	Gel
700 nm long pass filter	Laser	No Gel	Gel
3 Sheets white printer paper	LED	No Gel	Gel
Silicone Sheet (7 mm thick)	Lamp	No Gel	Gel
Spinach leaf	Lamp	No Gel	No Gel
Hemoglobin (0.2mM)[b]	Laser	No Gel	Gel
Tripe (14.3 mm thick)	Laser	No Gel	No Gel
Pig Skin (6.4 mm thick)	Laser	No Gel	Gel

Table 7.1 Barrier Penetration Details [a]Reaction halted due to bacon burning where laser was focused. [b]In addition to the gelation reaction, the [2+2] in Fig. 2D was performed under the shield of 0.2 mM hemoglobin solution. The yield with the NIR laser is 46% while the blue laser provides 1% yield.

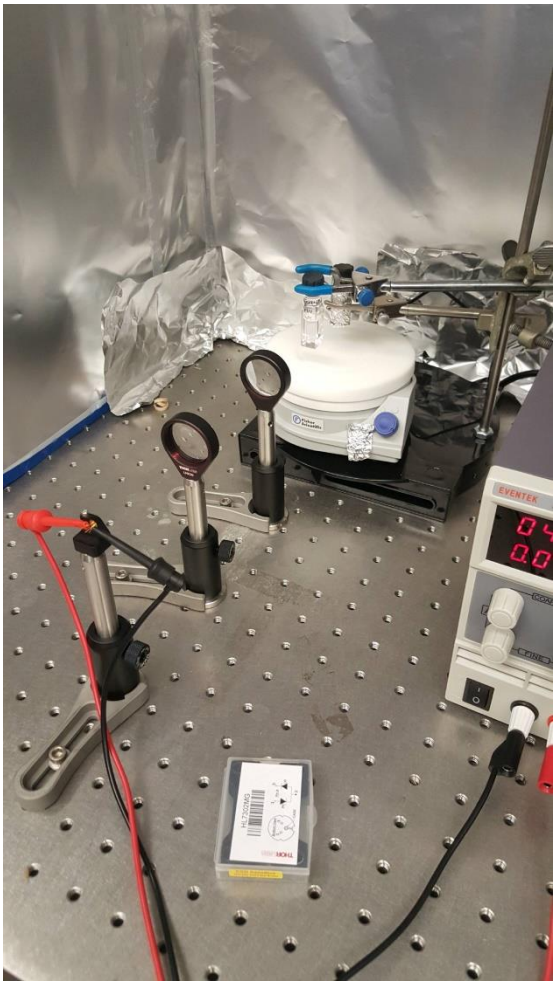

Figure 7.6 Experimental Set Up for Materials Barrier Penetration Shown here with 730 nm laser on, with 1 cm path length quartz cuvette filled with water as the barrier. Reaction wrapped with foil to prevent visible light excitation while taking picture

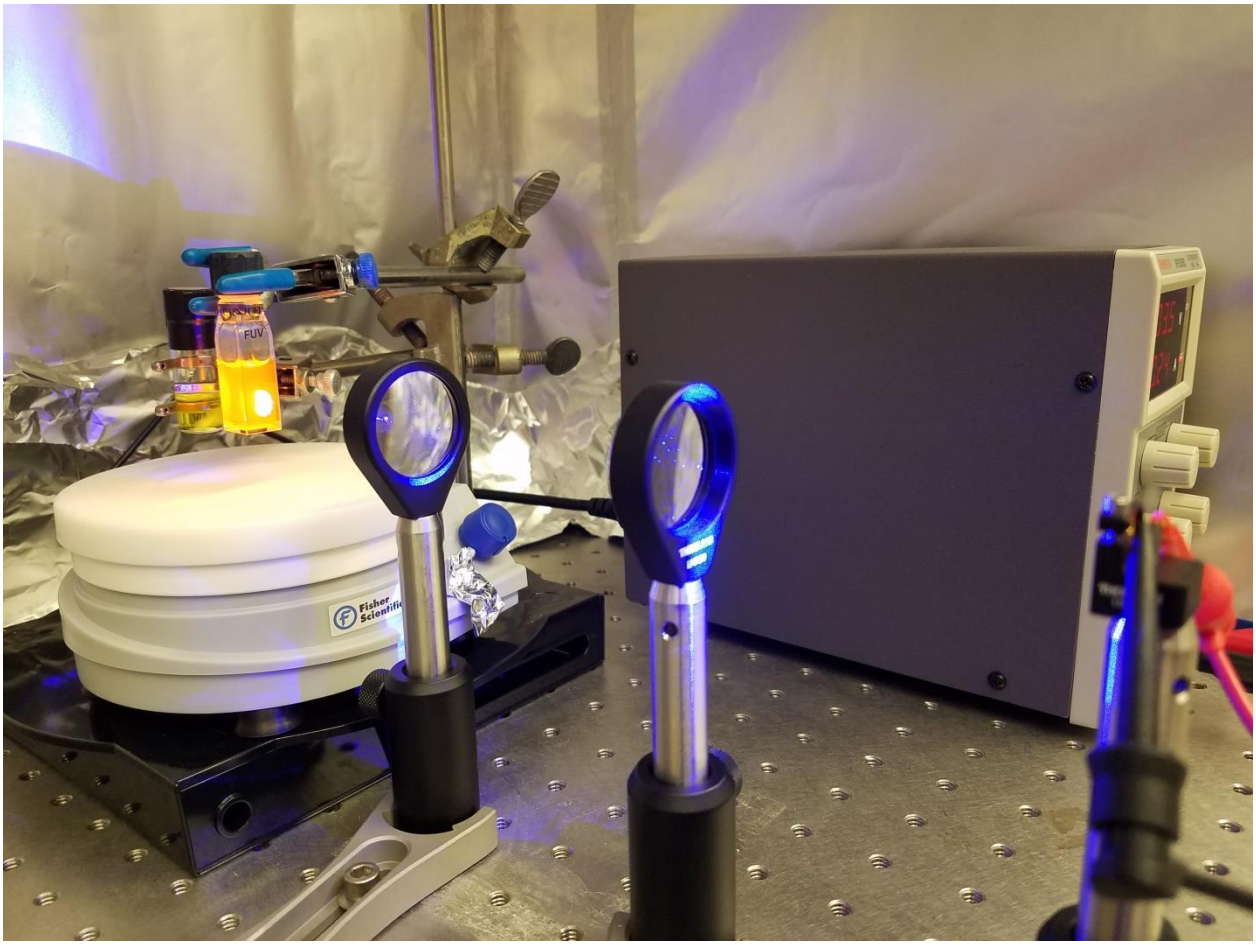

Figure 7.7 Experimental Set Up for Materials Barrier Penetration Experimental set up for materials barrier penetration. Shown here with 450 nm laser on, with 1.5mM Ru(bpy)3(PF6)2 solution in DCM as the barrier. Note that the barrier completely blocks the reaction vial behind it from absorbing any visible light.

Figure 7.8 Silicone Mold Barrier Penetration Filled with gel reaction mixture, irradiated with NIR lamp through silicone barrier, yielded defined X and O PMMA gels.

7.9 Additional Upconversion Details

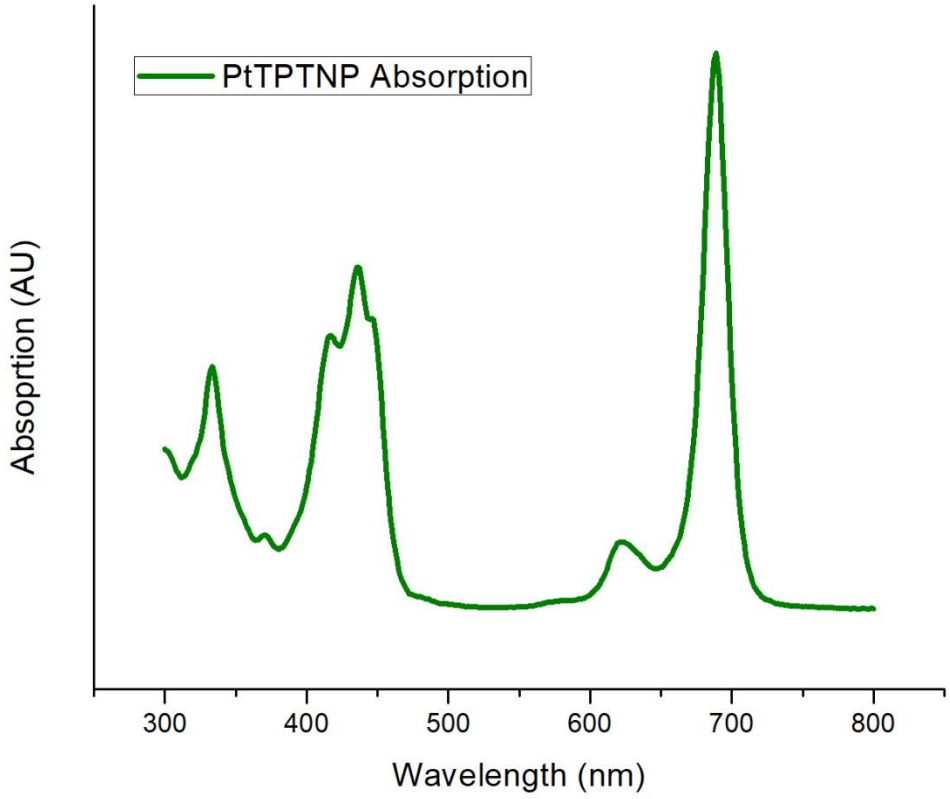

Figure 7.9 Absorption Spectrum of PtTPTNP in toluene.

A.

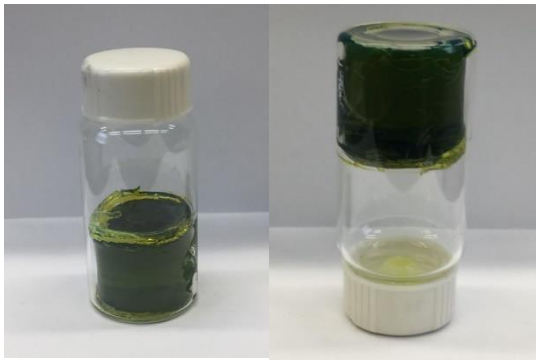

B. NIR Blue

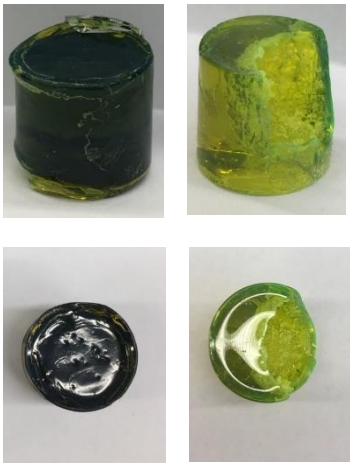

Figure 7.10 Barrier Penetration Scale Up (A) 10g scale cross-linked polymerization flip-experiment with IR lamp; (B) Resulting plastic obtained from IR lamp irradiation (left) and blue lamp irradiation (right).

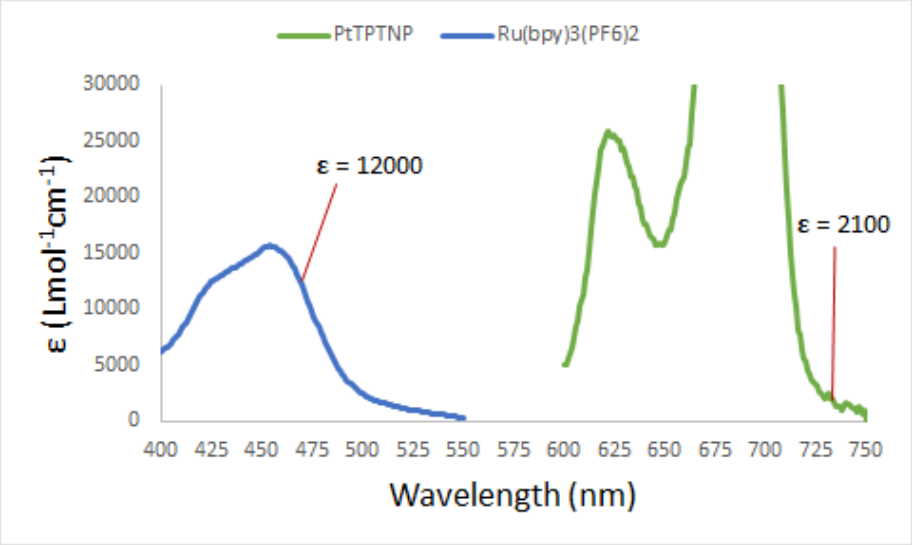

Figure 7.11 Absorbance Depth Penetration for IR vs Blue Light

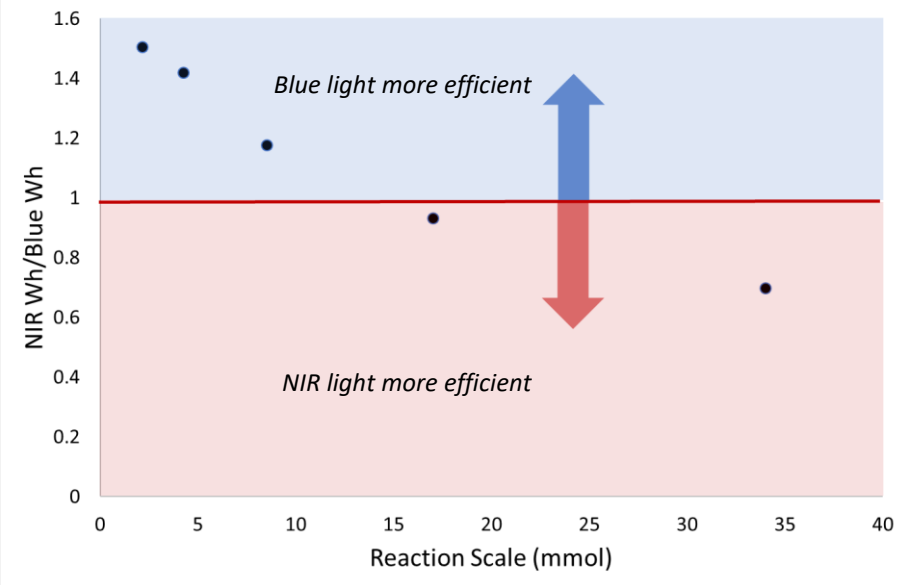

Figure 7.12 A Comparison of Power Efficiency with Reaction Scale (Procedure: See procedure for Figure 7.2F. The reaction was monitored by GCMS with mesitylene as a standard. The time of the reaction to reach 50% monomer conversion at various scales was measured. Multiplying the reaction time (h) by the power (W) of the beam provides the Wh necessary to perform the reaction. The NIR Wh/Blue Wh is >1 at lower scales and <1 at larger scales.)

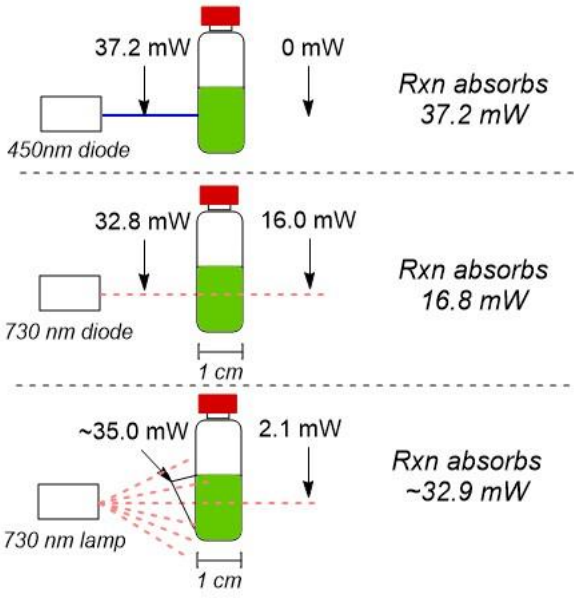

Figure 7.13 Schematic of How Laser Power was Measured Reactions were conducted in 1 cm path length quartz cuvettes. Laser power was measured using a Newport 818-SL Si photodetector, which was placed directly in front of and behind the cuvette in order to measure the amount of power absorbed by the reaction. In the case of the 450 nm blue laser diode, no photocurrent was measured by the Si diode behind the cuvette, indicating full absorption of 37.2 mW. In the case of the 730 nm NIR diode, we measured significant photocurrent penetrating the cuvette, withed only 16.8 mW absorbed. The laser fluence was measured periodically throughout the experiment and remained constant. 450 nm 80 mW diode was attenuated to achieve a similar power to the 730 nm 40 mW diode. The NIR lamp delivers 35 mW of relatively diffuse photons. As a quantitative comparison of the two light sources, the polymerization in Fig. 2F was performed with each light source and the energy required to reach 50% monomer conversion was measured. The NIR laser requires 0.168 Wh while the NIR lamp requires 0.1925 Wh, indicating comparable reaction efficiencies.

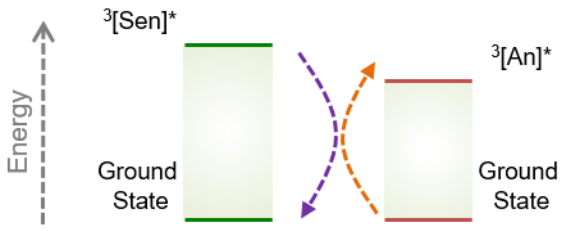

^{3}[Sen]* Energy	^{3}[An]* Energy
PtTNTP: >1.53 eV	TTBP: 1.53 eV
PdPc: 1.24 eV	FDPP: 1.1 eV

Figure 7.14 Simplified Jablonski Diagram TET from triplet excited sensitizer ^{3}[Sen]* to triplet excited state annihilator ^{3}[An]*, as well as these triplet energies for the sensitizers and annihilators used in this work. It is necessary that the energy of ^{3}[Sen]* be greater than that of ^{3}[An]* in order for TET to occur. These energies informed our choice of sensitizer and annihilator pairs. Triplet energies for PdPc[18] and FDPP[17] have been reported. We denote the triplet energy of PtTPTNP as greater than 1.53 eV, because in the past it has been reported as

lower,[24] but the observation of optical upconversion when combined with TTBP indicates that it must have a higher triplet energy than the reported 1.53 eV of TTBP. Previous studies have shown it is possible to use TTBP as an annihilator with 730 nm excitation.[25]

Upconversion Yield Measurements

Upconversion yield (upconversion yield is defined as the percentage of absorbed photons that participate in generating a singlet on the annihilator) measurements were taken following the procedure below:

Samples were mixed in an air and moisture-free glovebox and bubbled with N2 for 60 seconds before being tightly sealed and transferred to an integrating sphere. The upconversion yields were measured following de Mello,[36] where the luminescence with the sample in the beam, out of the beam, and out of the sphere were measured. With this information, the upconversion yield can be calculated. The measurement was performed with both blue 445 nm excitation and NIR excitation; two times the ratio of these two measurements gives the upconversion yield.[37]

15 mg/mL TTBP, 0.01 mg/mL PtTPTNP excited at 690 nm in toluene → 2.0% upconversion yield.

2 mg/mL FDPP, 0.03 mg/mL PdPc excited at 730 nm in toluene → 3.2% upconversion yield.

7.10 NMR Spectra

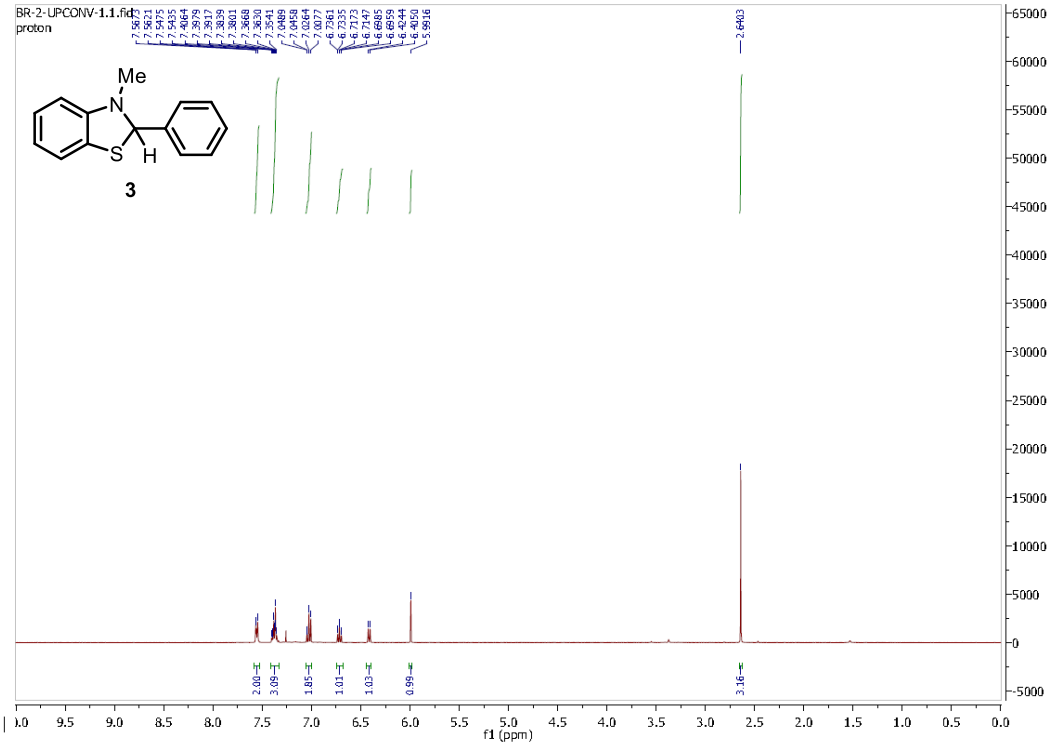
BR-2-UPCONV-1.1.fid
proton
Me
N
S
H
3
f1 (ppm)

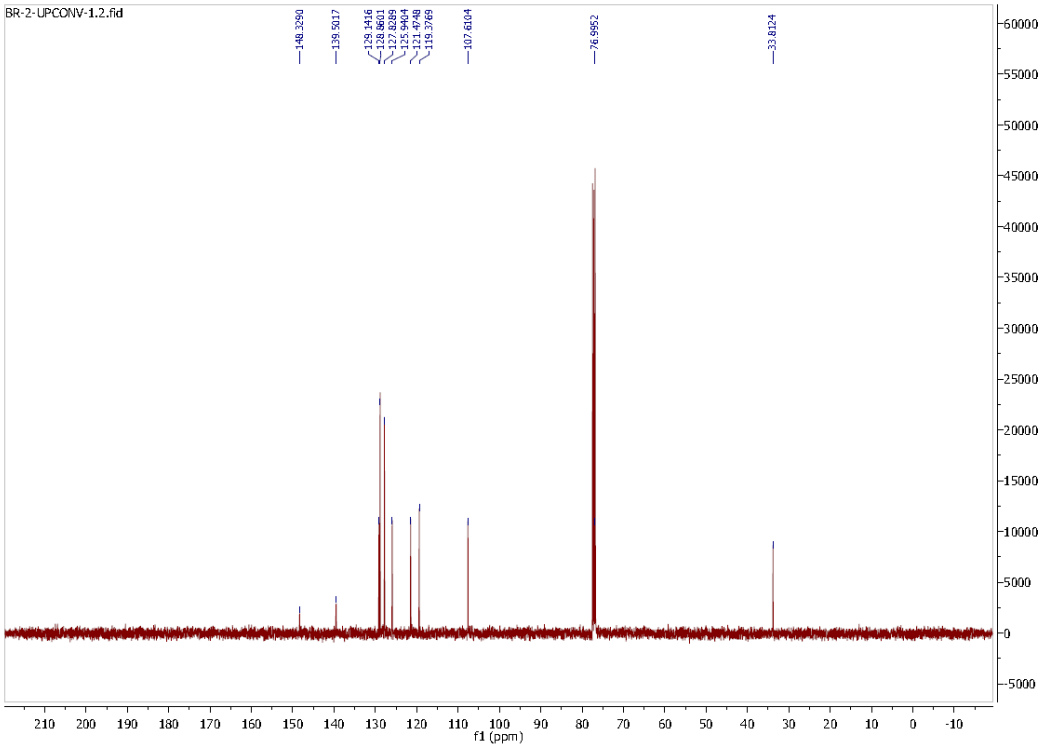
BR-2-UPCONV-1.2.fid
148.3290
139.5017
129.1416
128.8601
127.8289
125.9464
121.4748
119.3769
107.6104
76.9952
33.8124
f1 (ppm)

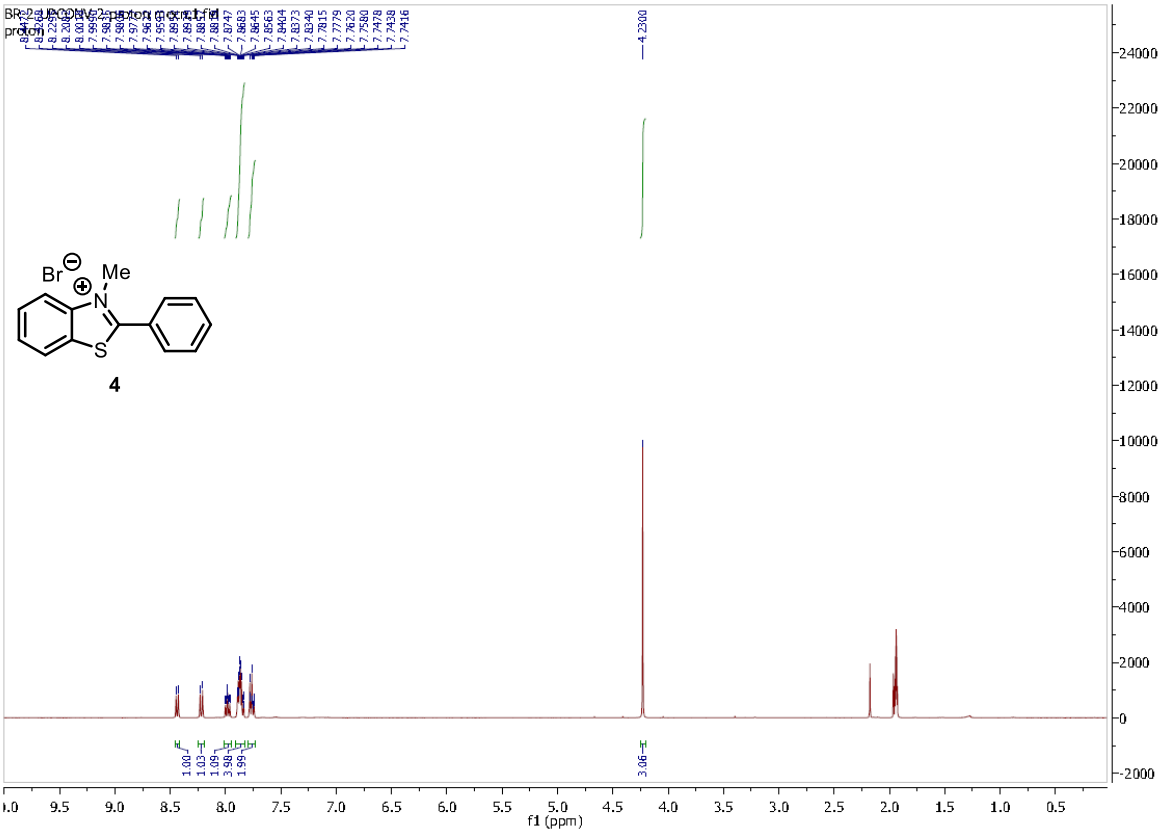
Br
Me
N
S
4
f1 (ppm)

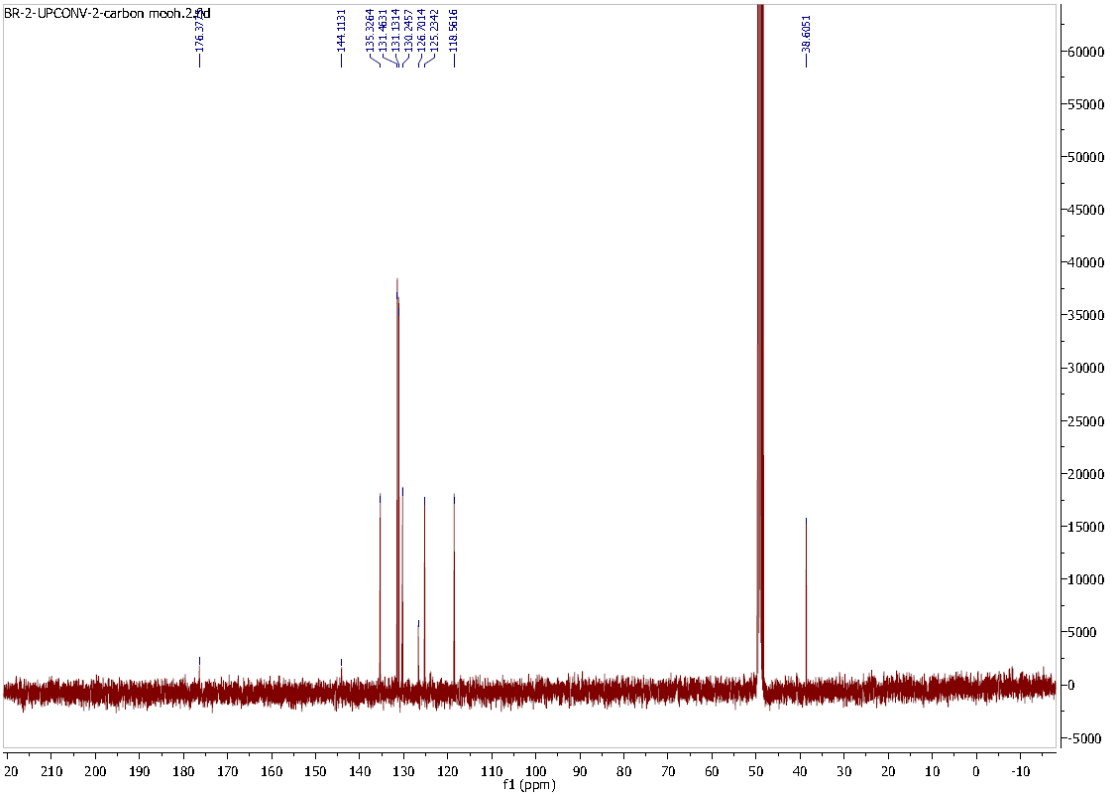
BR-2-UPCONV-2-carbon mooh.2.fid
176.3774
144.1131
135.3264
131.4631
131.1314
130.2457
126.7014
125.2342
118.9616
38.6051
f1 (ppm)

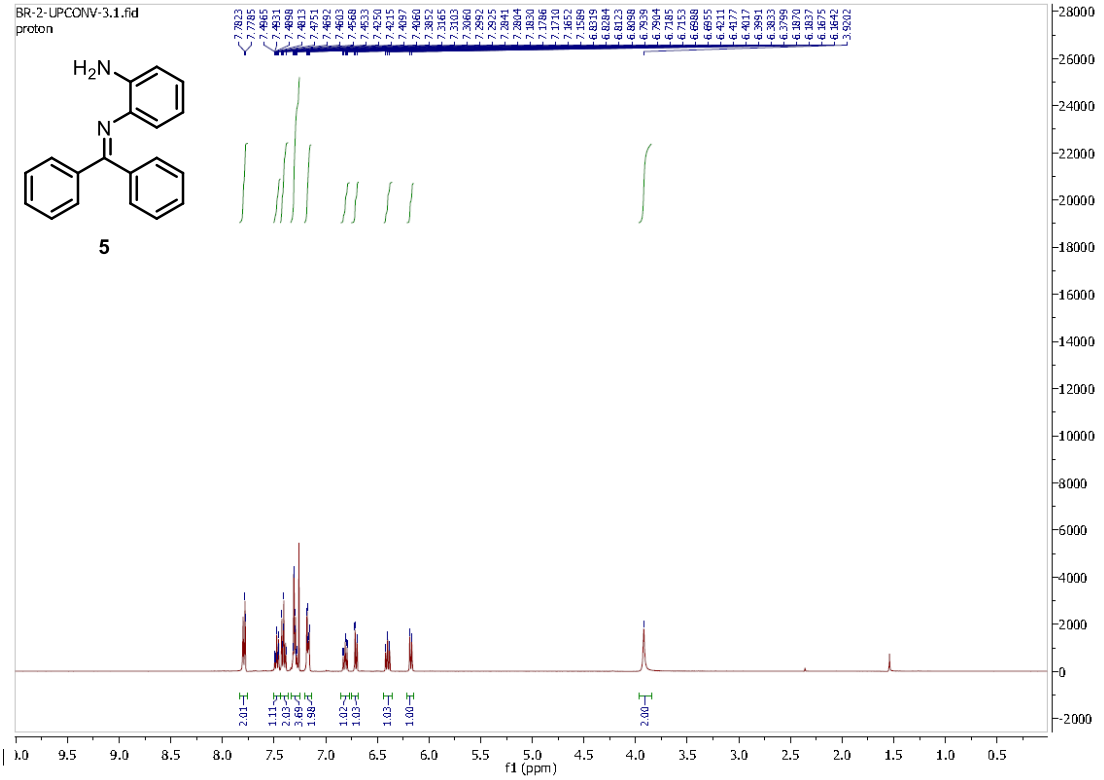
BR-2-UPCONV-3.1.fid
proton
5
f1 (ppm)

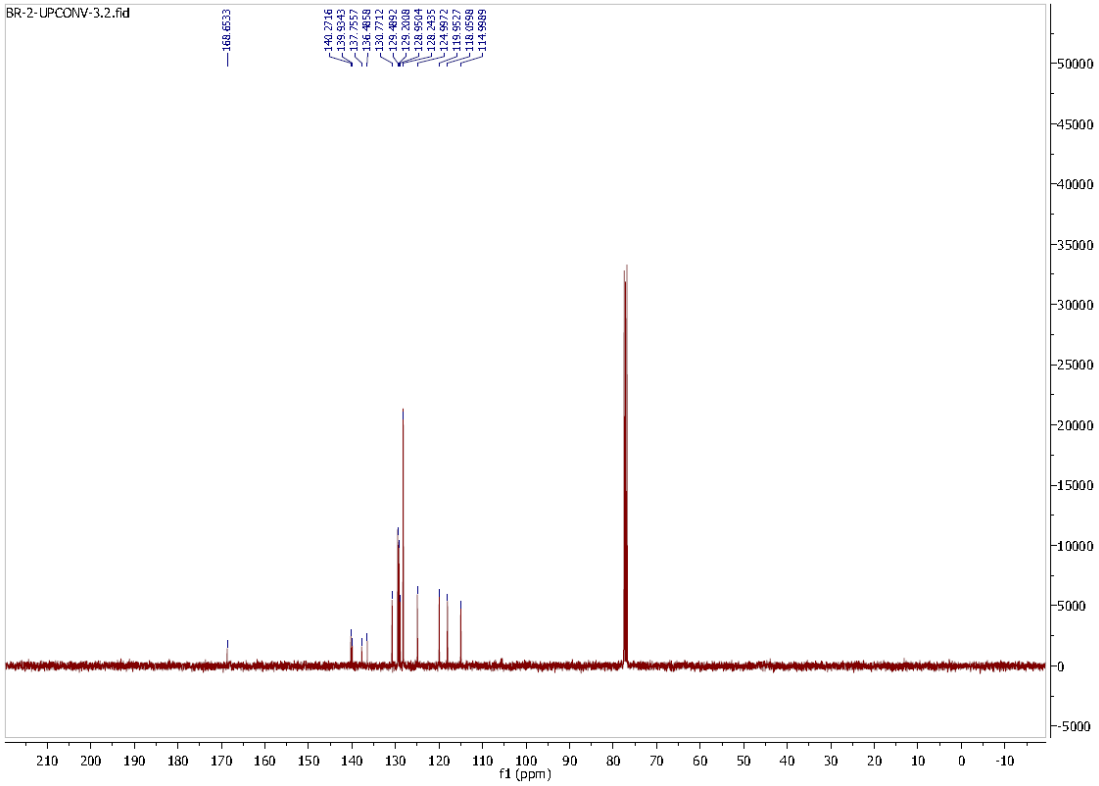
BR-2-UPCONV-3.2.fid
f1 (ppm)

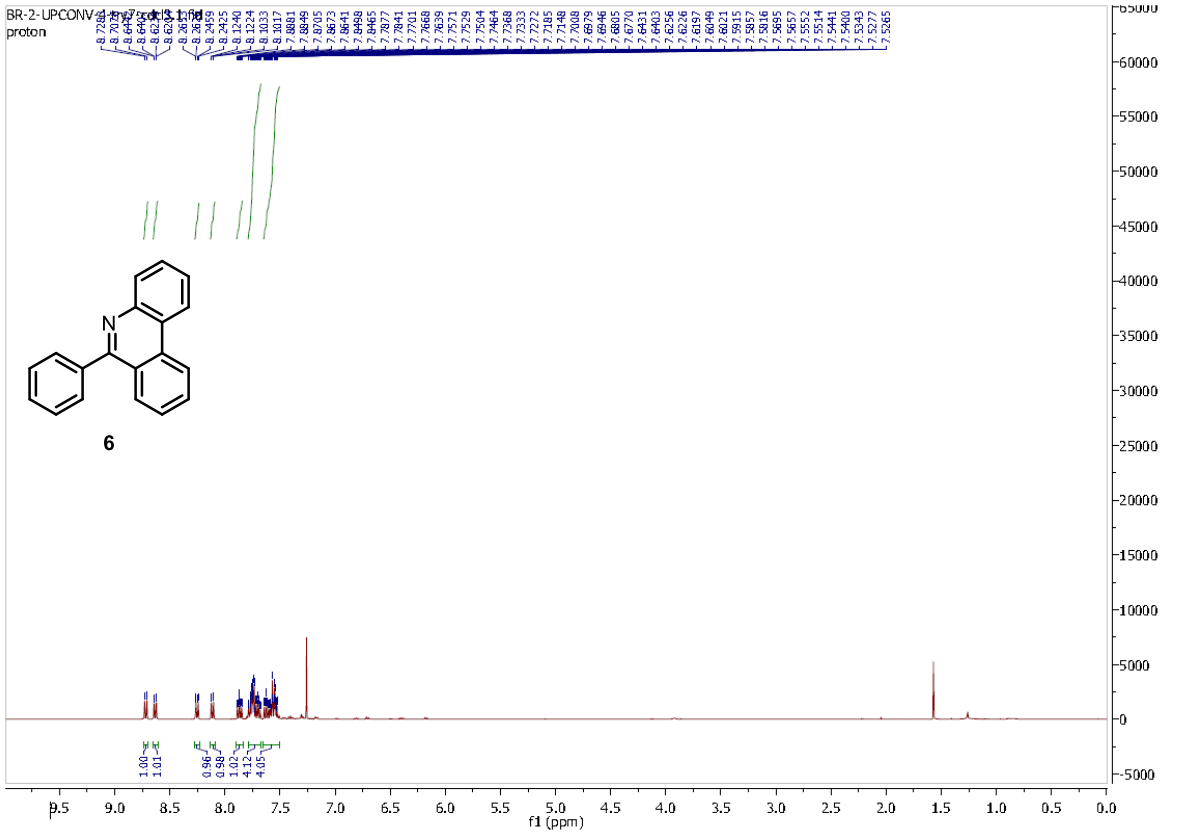
BR-2-UPCONV-4-try7-cdcl3.1.fid
proton
6
f1 (ppm)

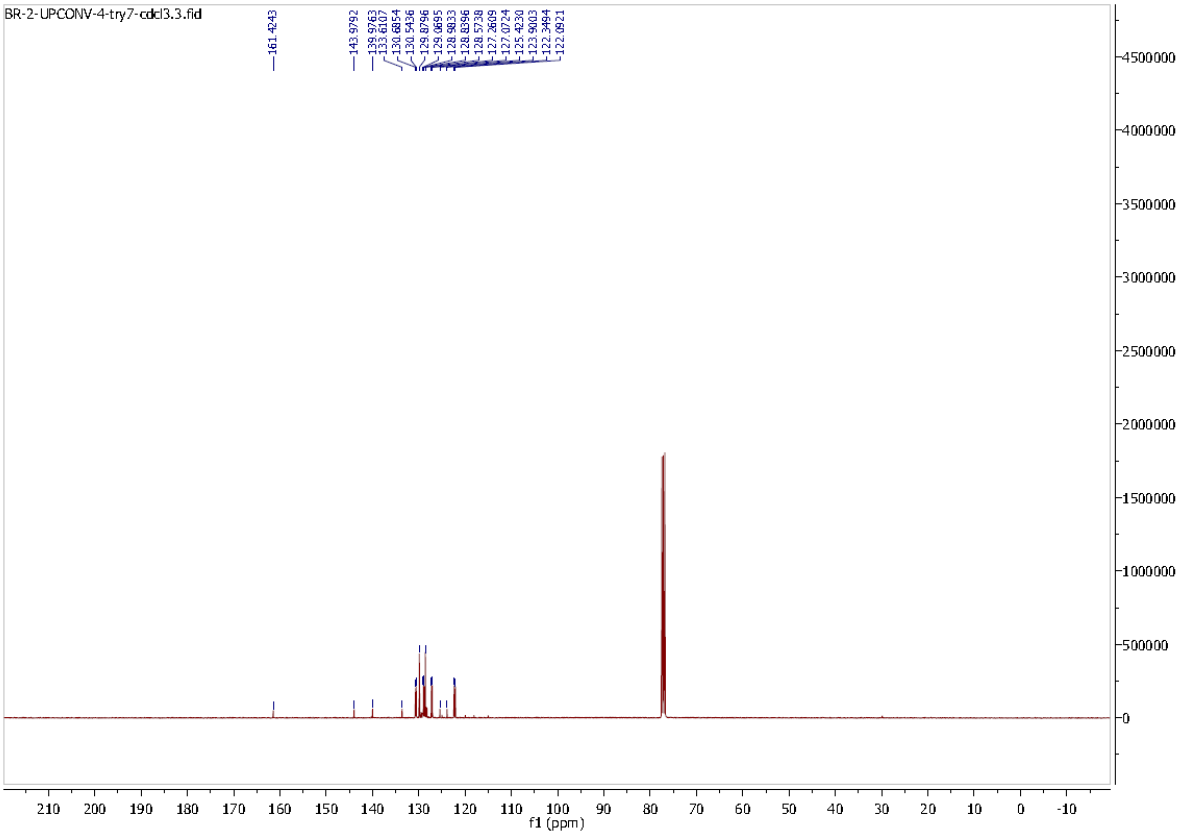
BR-2-UPCONV-4-try7-cdcl3.3.fid
f1 (ppm)

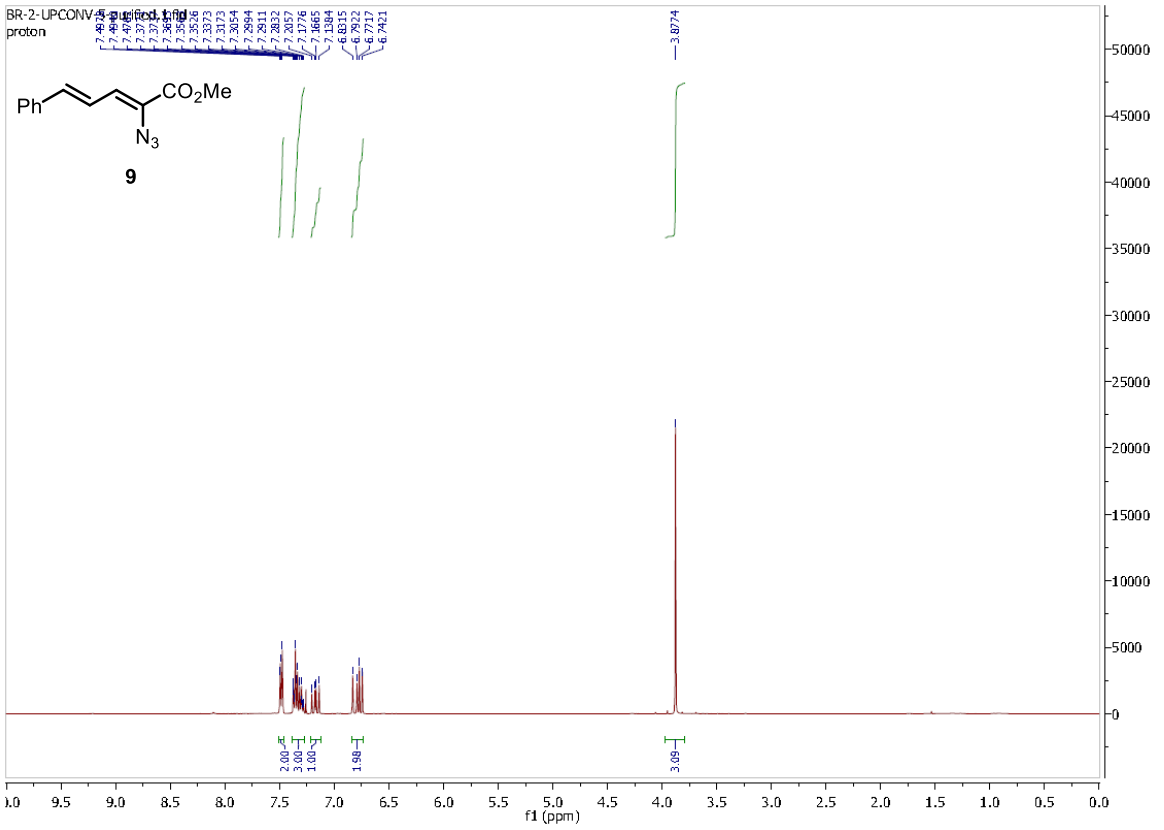
proton
Ph
CO2Me
N3
9
3.8774
2.00
3.00
1.00
1.98
3.09
f1 (ppm)

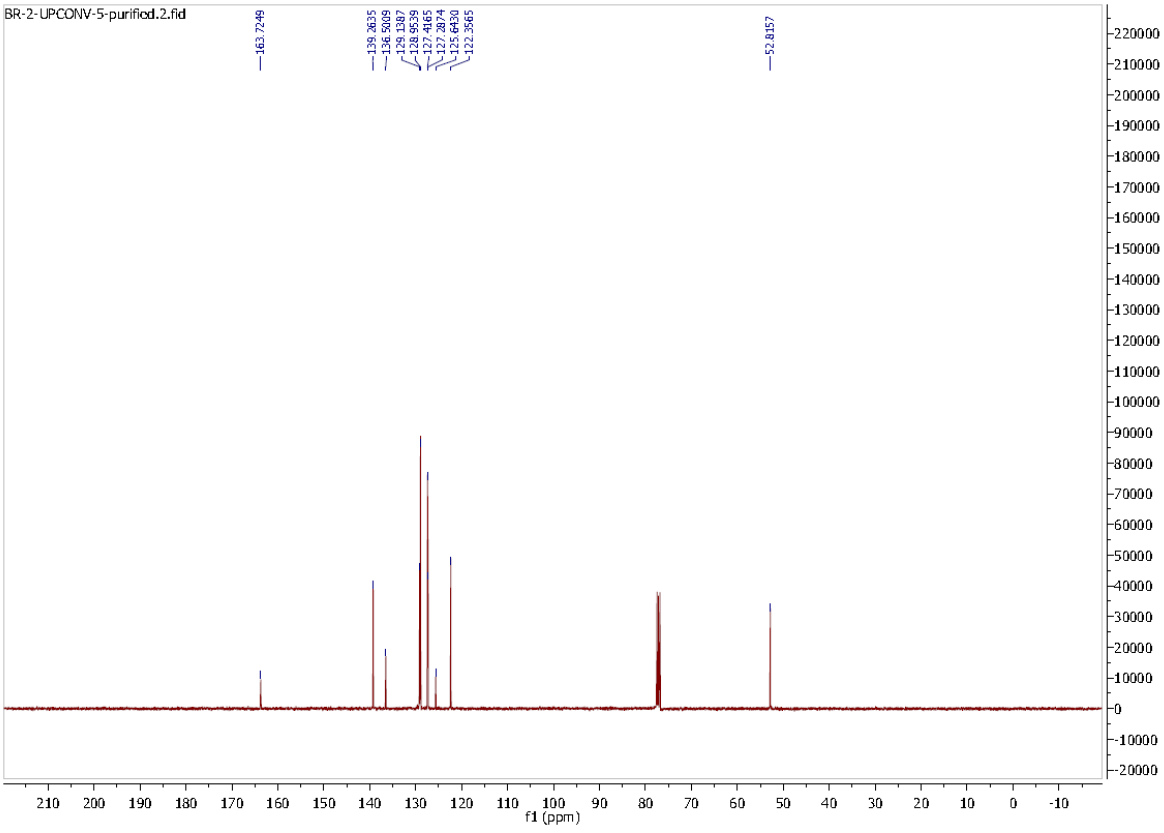
BR-2-UPCONV-5-purified.2.fid
163.7249
139.3635
136.5009
129.1387
128.9539
127.4165
127.2874
125.6430
122.3565
52.8157
f1 (ppm)

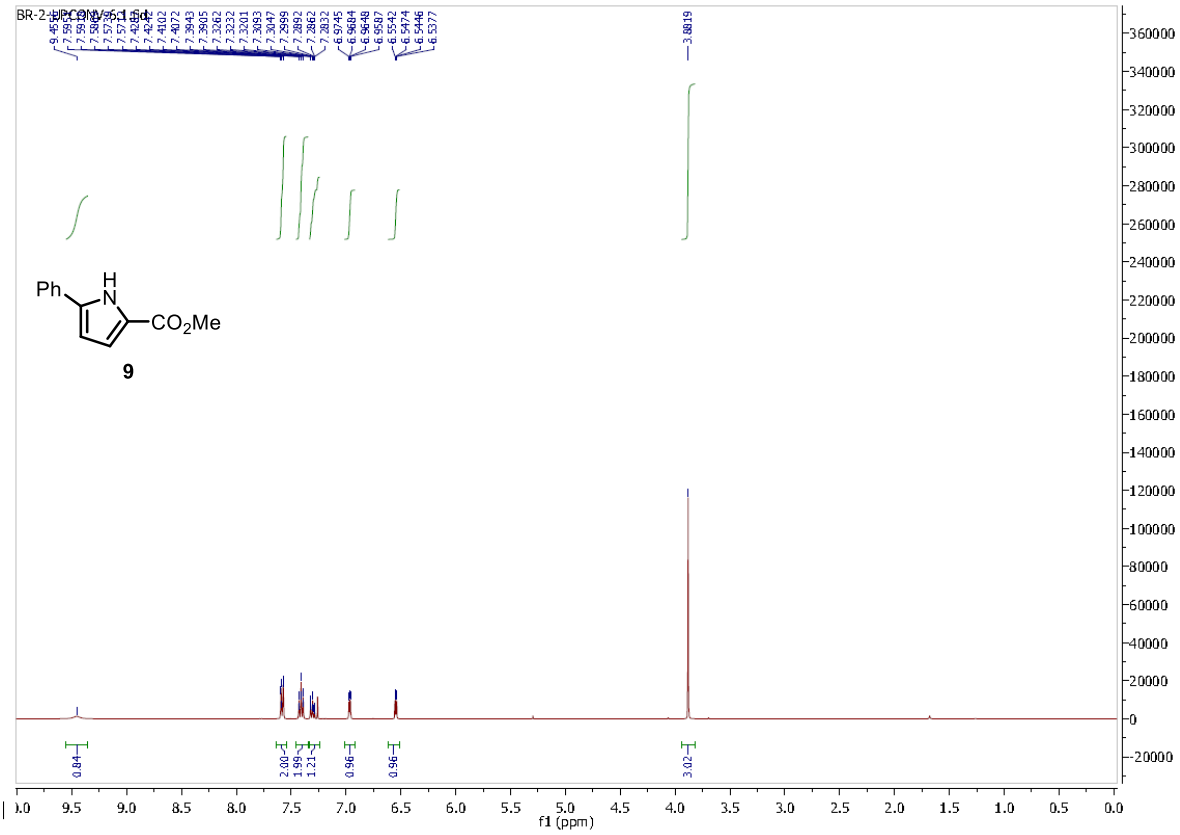
Ph
H
N
CO2Me
9
f1 (ppm)

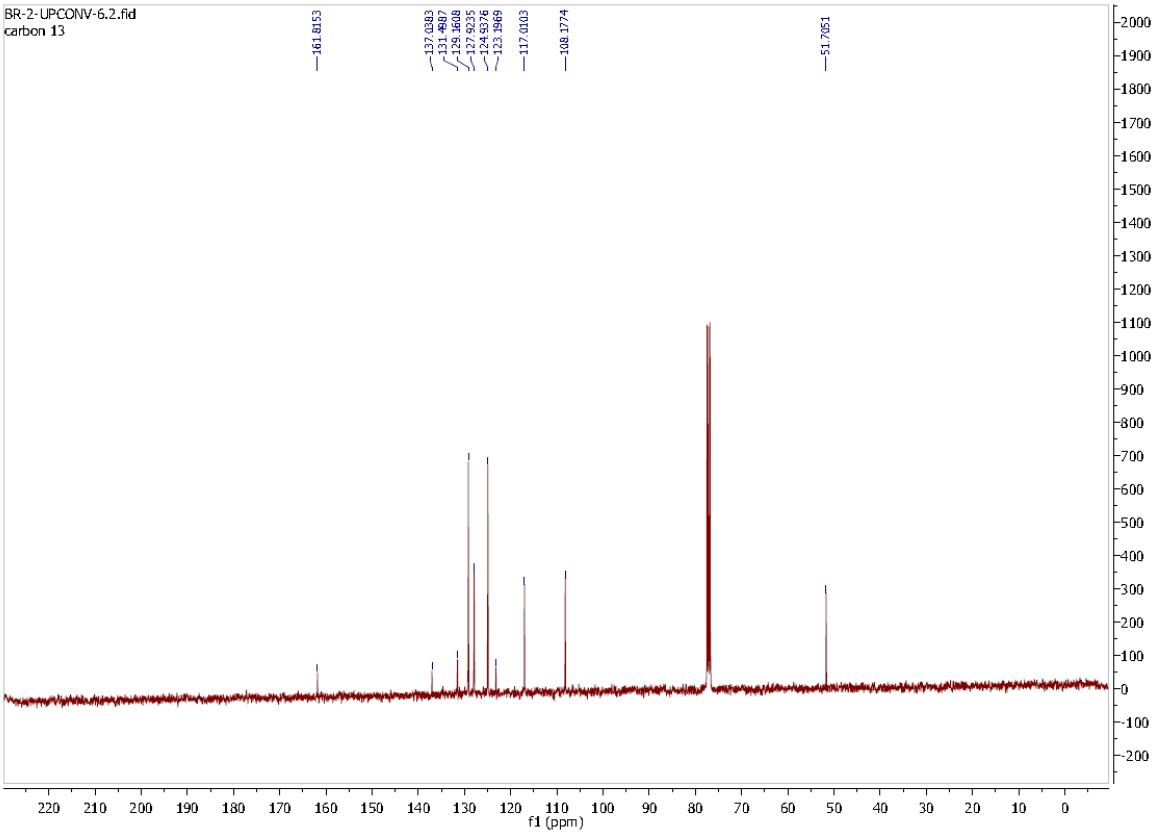
BR-2-UPCONV-6.2.fid
carbon 13
f1 (ppm)

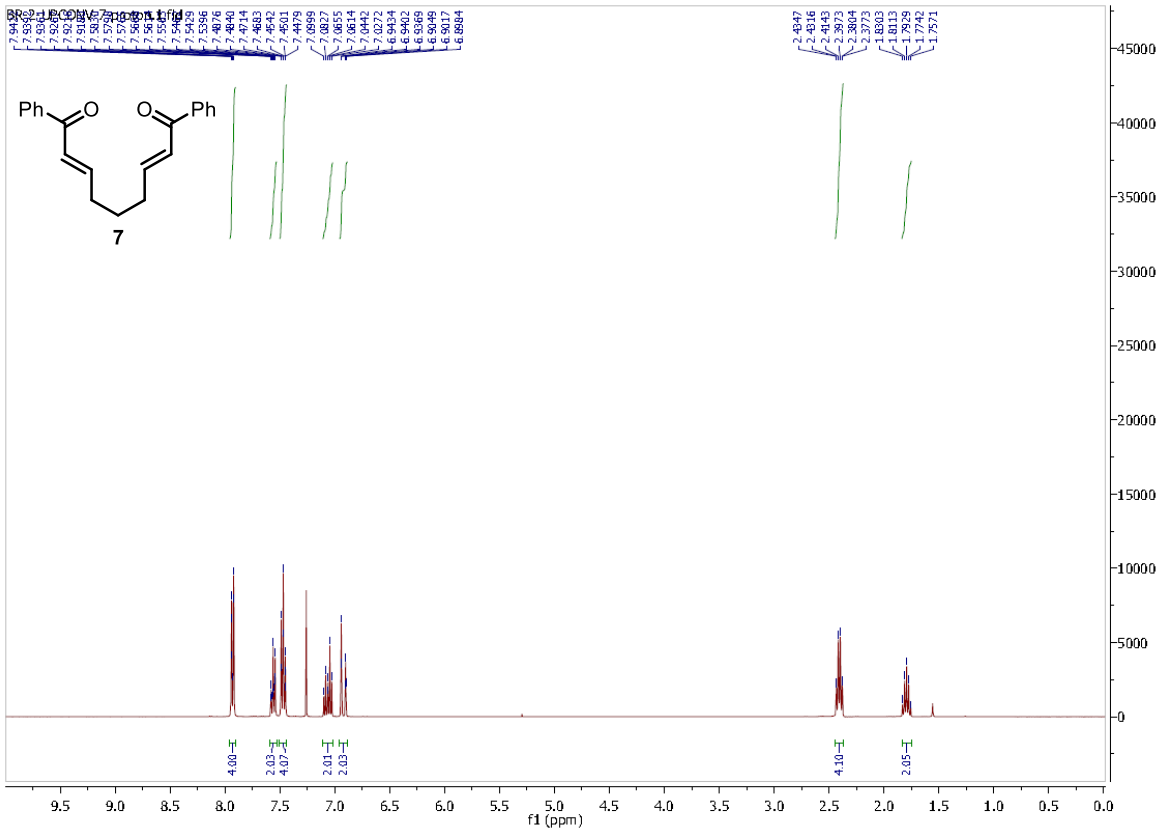
Ph
O
O
Ph
7
f1 (ppm)

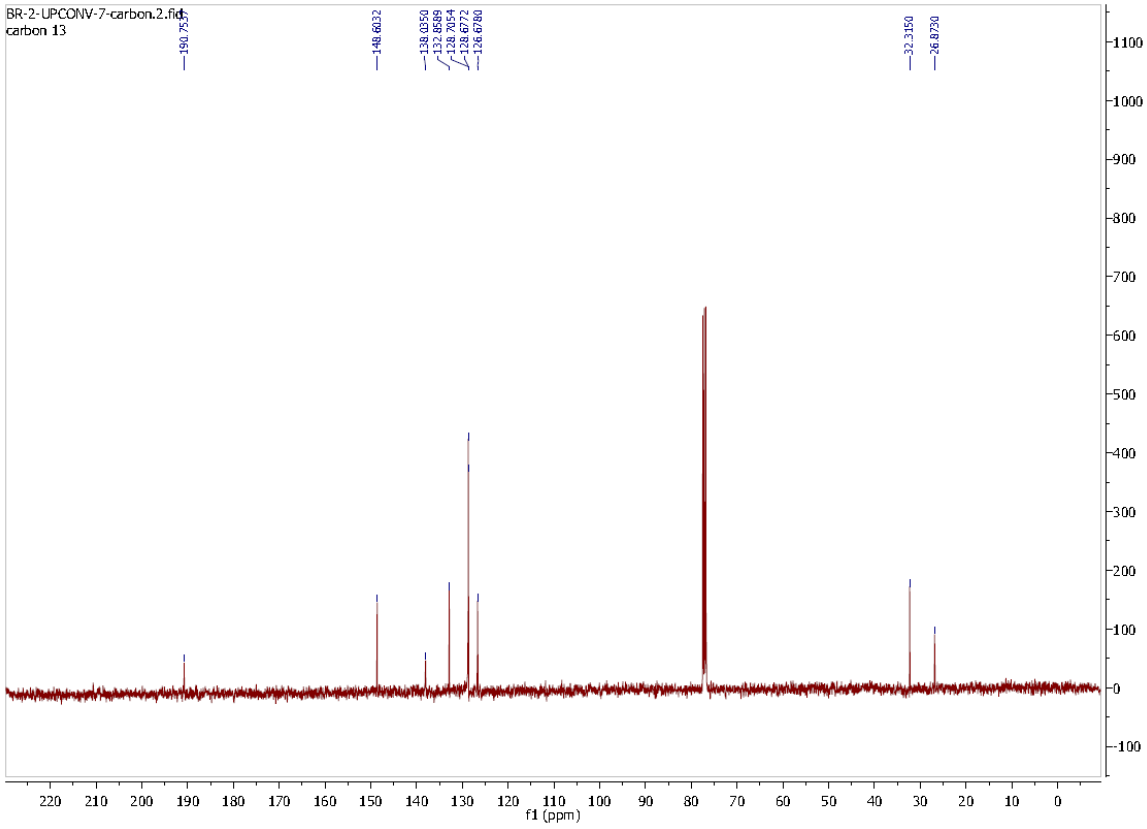
BR-2-UPCONV-7-carbon.2.fid
carbon 13
190.7537
146.6032
138.0350
132.8589
128.7054
128.6772
126.6780
32.3150
26.8730
f1 (ppm)

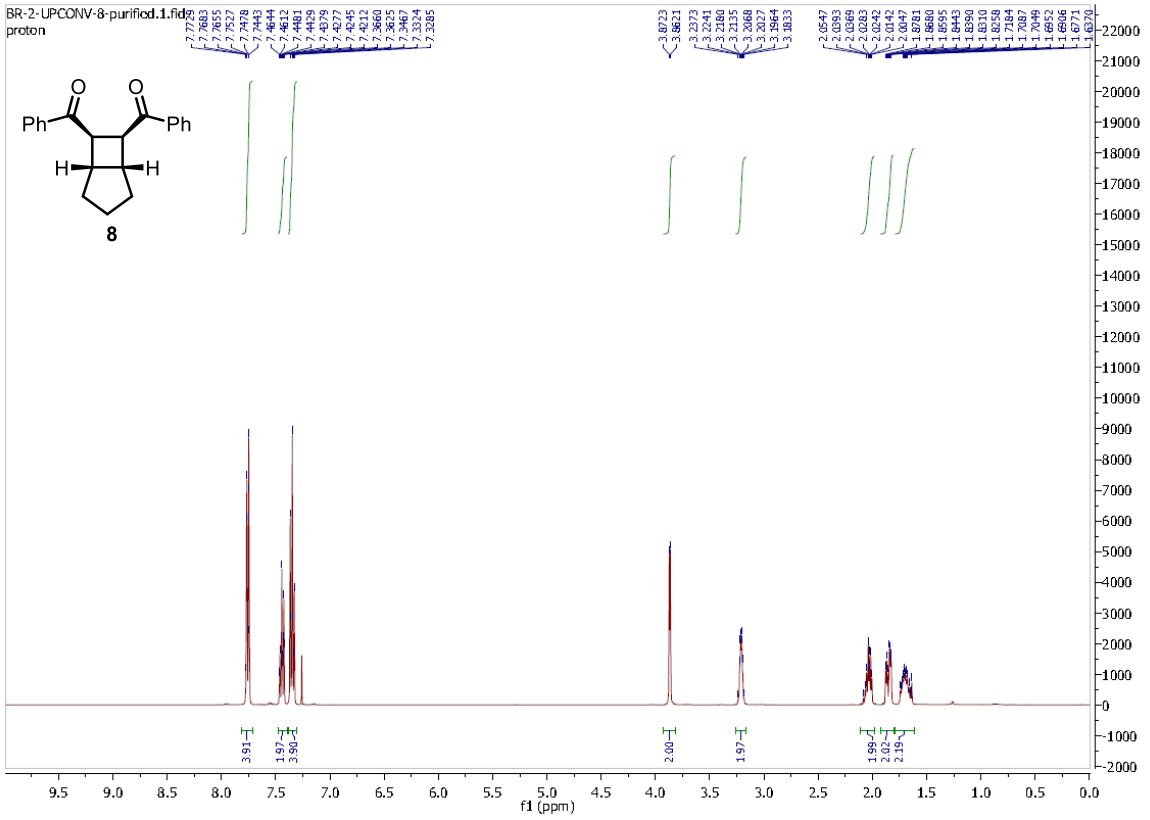
BR-2-UPCONV-8-purified.1.fid
proton
Ph
Ph
H
H
8
f1 (ppm)

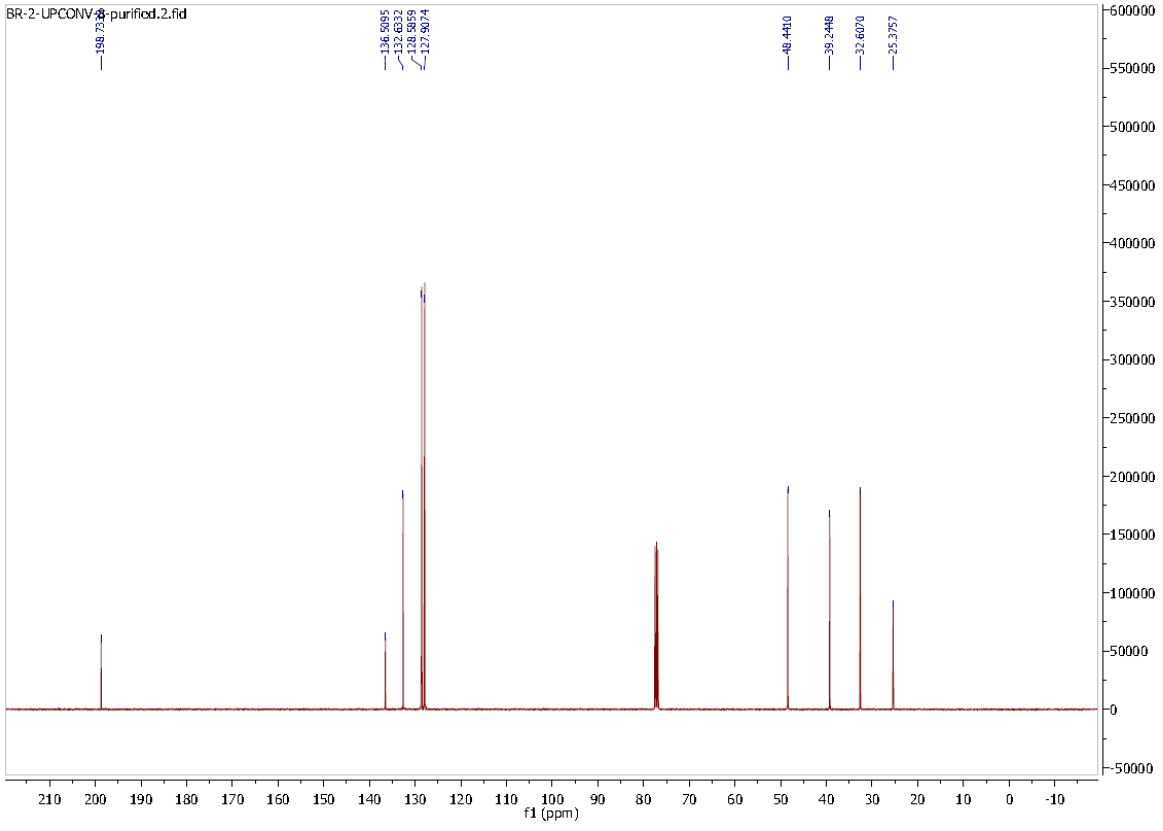
BR-2-UPCONV-8-purified.2.fid
198.7338
136.5095
132.6332
128.5859
127.9074
48.4410
39.2448
32.6070
25.3757
f1 (ppm)

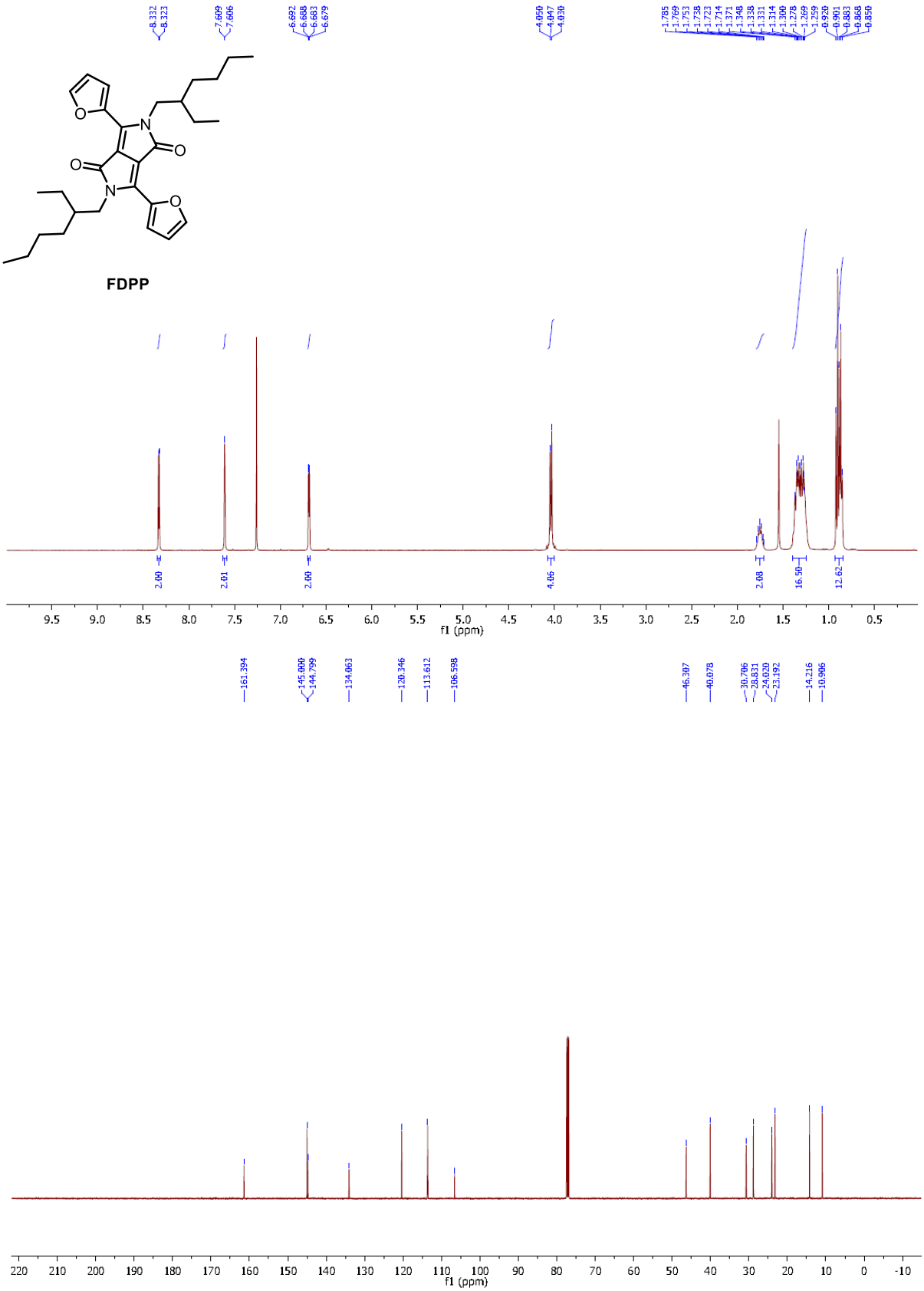
FDPP
f1 (ppm)
f1 (ppm)

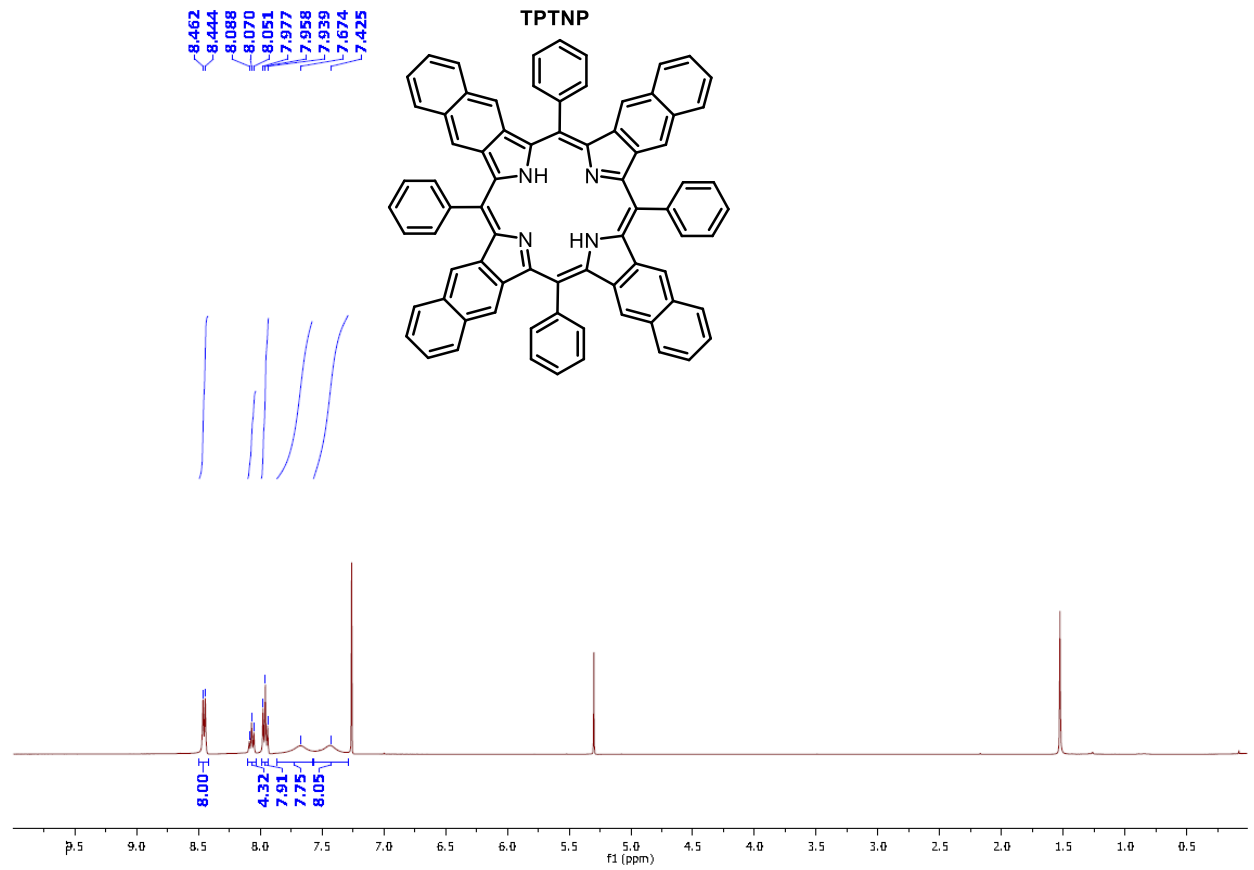

7.11 Outlook

The work in this chapter demonstrates how powerful collaborative research can be, and a project I'm proud to be a part of. If you read any paper about singlet fission or upconversion it will start off talking about how these processes can be used to make solar cells more efficient, and use this to frame why the research is being done. This chapter shows what's possible when we start thinking outside the box, and combine expertise from different disciplines to do something new. In my most honest opinion, I'm not sure singlet fission will ever be used in large area solar energy. Silicon is just too cheap of a material, where the boost from SF is too small given how much they would cost. That being said, this work demonstrates why researching these materials is absolutely worth doing. As we learn more about these processes, our deeper

understanding allows us to apply them to things we hadn't thought about before. I'm excited to see what new applications researchers will discover for SF and upconversion in the coming years.

In terms of building off the results from this chapter, using this technique for targeted photodynamic therapy is the next big jump. In order to do that the system needs to work in aqueous environments and be non-toxic, two issues that are currently being worked on by the Campos, Congreve, and Rovis groups.

Further expanding the upconversion systems that we use needs to be done as well. Our NIR-to-blue system has an excellent anti-Stokes shift, but the system is quite inefficient because of how little of the sensitizer absorption we actually excite with the NIR laser. Efficiently generating UV light from visible light, or even IR, with a considerable anti-Stokes shift would be ideal as well. This would allow us to access further photoredox catalysts based on iridium, as well as perform a variety of chemical transformations which just need UV irradiation to occur. An idea to do this would be an upconversion cascade. Upconverting upconverted light would allow for two anti-Stokes shifts, possibly allowing us to convert NIR to UV light. There is so much work to be done in upconversion and it's a field that I hope I'll be able to contribute to in the years to come.

7.12 References

(1) Ravetz, B. D.; Pun, A. B.; Churchill, E. M.; Congreve, D. N.; Rovis, T.; Campos, L. M. Photoredox Catalysis Using Infrared Light via Triplet Fusion Upconversion. *Nature* **2019**, *565*, 343–346.

(2) Arias-Rotondo, D. M.; McCusker, J. K. The Photophysics of Photoredox Catalysis: A Roadmap for Catalyst Design. *Chem. Soc. Rev.* **2016**, *45* (21), 5803–5820.

(3) Le, C. "Chip"; Wismer, M. K.; Shi, Z.-C.; Zhang, R.; Conway, D. V; Li, G.; Vachal, P.; Davies, I. W.; MacMillan, D. W. C. A General Small-Scale Reactor To Enable Standardization and Acceleration of Photocatalytic Reactions. *ACS Cent. Sci.* **2017**, *3* (6), 647–653.

(4) Zhou, J.; Liu, Q.; Feng, W.; Sun, Y.; Li, F. Upconversion Luminescent Materials:

Advances and Applications. *Chem. Rev.* **2015**, *115* (1), 395–465.
(5) Schulze, T. F.; Schmidt, T. W. Photochemical Upconversion: Present Status and Prospects for Its Application to Solar Energy Conversion. *Energy Environ. Sci.* **2015**, *8* (1), 103–125.
(6) Park, Y. Il; Lee, K. T.; Suh, Y. D.; Hyeon, T. Upconverting Nanoparticles: A Versatile Platform for Wide-Field Two-Photon Microscopy and Multi-Modal in Vivo Imaging. *Chem. Soc. Rev.* **2015**, *44* (6), 1302–1317.
(7) Zhou, Y.; Han, S.-T.; Chen, X.; Wang, F.; Tang, Y.-B.; Roy, V. A. L. An Upconverted Photonic Nonvolatile Memory. *Nat. Commun.* **2014**, *5*, 4720.
(8) Viger, M. L.; Grossman, M.; Fomina, N.; Almutairi, A. Low Power Upconverted Near-IR Light for Efficient Polymeric Nanoparticle Degradation and Cargo Release. *Adv. Mater.* **2013**, *25* (27), 3733–3738.
(9) He, S.; Krippes, K.; Ritz, S.; Chen, Z.; Best, A.; Butt, H.-J.; Mailander, V.; Wu, S. Ultralow-Intensity near-Infrared Light Induces Drug Delivery by Upconverting Nanoparticles. *Chem. Commun.* **2015**, *51* (2), 431–434.
(10) Chen, Z.; Sun, W.; Butt, H.-J.; Wu, S. Upconverting-Nanoparticle-Assisted Photochemistry Induced by Low-Intensity Near-Infrared Light: How Low Can We Go? *Chem. – A Eur. J.* **2015**, *21* (25), 9165–9170.
(11) Askes, S. H. C.; Bahreman, A.; Bonnet, S. Activation of a Photodissociative Ruthenium Complex by Triplet–Triplet Annihilation Upconversion in Liposomes. *Angew. Chem. Int. Ed.* **2014**, *53* (4), 1029–1033.
(12) Mahboub, M.; Huang, Z.; Tang, M. L. Efficient Infrared-to-Visible Upconversion with Subsolar Irradiance. *Nano Lett.* **2016**, *16* (11), 7169–7175.
(13) Majek, M.; Faltermeier, U.; Dick, B.; Pérez-Ruiz, R.; Jacobi von Wangelin, A. Application of Visible-to-UV Photon Upconversion to Photoredox Catalysis: The Activation of Aryl Bromides. *Chem. – A Eur. J.* **2015**, *21* (44), 15496–15501.
(14) Häring, M.; Pérez-Ruiz, R.; Jacobi von Wangelin, A.; Díaz, D. D. Intragel Photoreduction of Aryl Halides by Green-to-Blue Upconversion under Aerobic Conditions. *Chem. Commun.* **2015**, *51* (94), 16848–16851.
(15) Singh-Rachford, T. N.; Castellano, F. N. Low Power Visible-to-UV Upconversion. *J. Phys. Chem. A* **2009**, *113* (20), 5912–5917.
(16) Singh-Rachford, T. N.; Castellano, F. N. Photon Upconversion Based on Sensitized Triplet–triplet Annihilation. *Coord. Chem. Rev.* **2010**, *254* (21–22), 2560–2573.
(17) Hartnett, P. E.; Margulies, E. A.; Mauck, C. M.; Miller, S. A.; Wu, Y.; Wu, Y.-L.; Marks, T. J.; Wasielewski, M. R. Effects of Crystal Morphology on Singlet Exciton Fission in Diketopyrrolopyrrole Thin Films. *J. Phys. Chem. B* **2016**, *120* (7), 1357–1366.
(18) Singh-Rachford, T. N.; Castellano, F. N. Pd(II) Phthalocyanine-Sensitized Triplet−Triplet Annihilation from Rubrene. *J. Phys. Chem. A* **2008**, *112* (16), 3550–3556.
(19) Romero, N. A.; Nicewicz, D. A. Organic Photoredox Catalysis. *Chem. Rev.* **2016**, *116* (17), 10075–10166.
(20) Neumann, M.; Füldner, S.; König, B.; Zeitler, K. Metal-Free, Cooperative Asymmetric Organophotoredox Catalysis with Visible Light. *Angew. Chem. Int. Ed.* **2011**, *50* (4), 951–954.
(21) Mashraqui, S. H.; Kellogg, R. M. 3-Methyl-2,3-Dihydrobenzothiazoles as Reducing Agent. Dye Enhanced Photoreactions. *Tetrahedron Lett.* **1985**, *26* (11), 1453–1456.
(22) Natarajan, P.; Kumar, N.; Sharma, M. Visible Light-Mediated Intramolecular C-H

Arylation of Diazonium Salts of N-(2-Aminoaryl)Benzoimines: A Facile Synthesis of 6-Arylphenanthridines. *Org. Chem. Front.* **2016**, *3* (10), 1265–1270.
(23) Sommer, J. R.; Shelton, A. H.; Parthasarathy, A.; Ghiviriga, I.; Reynolds, J. R.; Schanze, K. S. Photophysical Properties of Near-Infrared Phosphorescent π-Extended Platinum Porphyrins. *Chem. Mater.* **2011**, *23* (24), 5296–5304.
(24) Deng, F.; Sommer, J. R.; Myahkostupov, M.; Schanze, K. S.; Castellano, F. N. Near-IR Phosphorescent Metalloporphyrin as a Photochemical Upconversion Sensitizer. *Chem. Commun.* **2013**, *49* (67), 7406–7408.
(25) Sasaki, Y.; Amemori, S.; Kouno, H.; Yanai, N.; Kimizuka, N. Near Infrared-to-Blue Photon Upconversion by Exploiting Direct S-T Absorption of a Molecular Sensitizer. *J. Mater. Chem. C* **2017**, *5* (21), 5063–5067.
(26) Ischay, M. A.; Anzovino, M. E.; Du, J.; Yoon, T. P. Efficient Visible Light Photocatalysis of [2+2] Enone Cycloadditions. *J. Am. Chem. Soc.* **2008**, *130* (39), 12886–12887.
(27) Miyake, G. M.; Theriot, J. C. Perylene as an Organic Photocatalyst for the Radical Polymerization of Functionalized Vinyl Monomers through Oxidative Quenching with Alkyl Bromides and Visible Light. *Macromolecules* **2014**, *47* (23), 8255–8261.
(28) Cambié, D.; Bottecchia, C.; Straathof, N. J. W.; Hessel, V.; Noël, T. Applications of Continuous-Flow Photochemistry in Organic Synthesis, Material Science, and Water Treatment. *Chem. Rev.* **2016**, *116* (17), 10276–10341.
(29) Tucker, J. W.; Zhang, Y.; Jamison, T. F.; Stephenson, C. R. J. Visible-Light Photoredox Catalysis in Flow. *Angew. Chem. Int. Ed.* **2012**, *51* (17), 4144–4147.
(30) Akiba, K.; Ohara, Y.; Inamoto, N. Alkylation of Benzothiazolines and the Stevens Rearrangement of the Resulting 2,3,3-Trisubstituted Benzothiazolinium Salts. *Bull. Chem. Soc. Jpn.* **1982**, *55* (9), 2976–2983.
(31) Dalla Cort, A.; Mandolini, L.; Palmieri, G.; Pasquini, C.; Schiaffino, L. Unprecedented Detection of Inherent Chirality in Uranyl–salophen Complexes. *Chem. Commun.* **2003**, No. 17, 2178–2179.
(32) Li, K.; Alexakis, A. Copper-Catalyzed Enantioselective Intramolecular Conjugate Addition/Trapping Reactions: Synthesis of Cyclic Compounds with Multichiral Centers. *Chem. – A Eur. J.* **2007**, *13* (13), 3765–3771.
(33) Chen, L.; Yang, T.; Cui, H.; Cai, T.; Zhang, L.; Su, C.-Y. A Porous Metal–organic Cage Constructed from Dirhodium Paddle-Wheels: Synthesis, Structure and Catalysis. *J. Mater. Chem. A* **2015**, *3* (40), 20201–20209.
(34) Sivakumar, G.; Sasikumar, M.; Rao, V. J. Synthesis and Characterization of Diketopyrrolopyrrole-Based D-π-A-π-D Small Molecules for Organic Solar Cell Applications. *J. Heterocycl. Chem.* **2017**, *54* (3), 1983–1994.
(35) Farney, E. P.; Yoon, T. P. Visible-Light Sensitization of Vinyl Azides by Transition-Metal Photocatalysis. *Angew. Chem. Int. Ed.* **2014**, *53* (3), 793–797.
(36) de Mello, J. C.; Wittmann, H. F.; Friend, R. H. An Improved Experimental Determination of External Photoluminescence Quantum Efficiency. *Adv. Mater.* **1997**, *9* (3), 230–232.
(37) Wu, M.; Congreve, D. N.; Wilson, M. W. B.; Jean, J.; Geva, N.; Welborn, M.; Van Voorhis, T.; Bulović, V.; Bawendi, M. G.; Baldo, M. A. Solid-State Infrared-to-Visible Upconversion Sensitized by Colloidal Nanocrystals. *Nat. Photonics* **2016**, *10* (1), 31–34.